ACTA CHIMICA

ACADEMIAE SCIENTIARUM HUNGARICAE

ADIUVANTIBUS

V. BRUCKNER, GY. DEÁK, K. POLINSZKY,
E. PUNGOR, G. SCHAY, Z. G. SZABÓ

REDIGIT

B. LENGYEL

TOMUS 69 FASCICULUS 1

AKADÉMIAI KIADÓ, BUDAPEST

1971

ACTA CHIMICA

A MAGYAR TUDOMÁNYOS AKADÉMIA KÉMIAI TUDOMÁNYOK OSZTÁLYÁNAK IDEGEN NYELVŰ KÖZLEMÉNYEI

SZERKESZTI

LENGYEL BÉLA

TECHNIKAI SZERKESZTŐK

DEÁK GYULA és HARASZTHY-PAPP MELINDA

Az Acta Chimica német, angol, francia és orosz nyelven közöl értekezéseket a kémiai tudományok köréből.

Az Acta Chimica változó terjedelmű füzetekben jelenik meg, egy-egy kötet négy füzetből áll. Évente átlag négy kötet jelenik meg.

A közlésre szánt kéziratok a szerkesztőség címére (Budapest 112/91 Műegyetem) küldendők.

Ugyanerre a címre küldendő minden szerkesztőségi levelezés. A szerkesztőség kéziratokat nem ad vissza.

Megrendelhető a belföld számára az „Akadémiai Kiadó"-nál (Budapest V., Alkotmány utca 21. Bankszámla 05-915-111-46), a külföld számára pedig a „Kultúra" Könyv- és Hírlap Külkereskedelmi Vállalatnál (Budapest I., Fő utca 32. Bankszámla: 43-790-057-181) vagy annak külföldi képviseleteinél és bizományosainál.

Die Acta Chimica veröffentlichen Abhandlungen aus dem Bereiche der chemischen Wissenschaften in deutscher, englischer, französischer und russischer Sprache.

Die Acta Chimica erscheinen in Heften wechselnden Umfanges. Vier Hefte bilden einen Band. Jährlich erscheinen 4 Bände.

Die zur Veröffentlichung bestimmten Manuskripte sind an folgende Adresse zu senden:

Acta Chimica
Budapest 112/91 Műegyetem

An die gleiche Anschrift ist auch jede für die Redaktion bestimmte Korrespondenz zu richten. Abonnementspreis pro Band: $16.00.

Bestellbar bei dem Buch- und Zeitungs-Außenhandels-Unternehmen »*Kultúra*« (Budapest I., Fő utca 32. Bankkonto No. 43-790-057-181) oder bei seinen Auslandsvertretungen und Kommissionären.

ACTA CHIMICA

ACADEMIAE SCIENTIARUM HUNGARICAE

ADIUVANTIBUS

V. BRUCKNER, GY. DEÁK, K. POLINSZKY,
E. PUNGOR, G. SCHAY, Z. G. SZABÓ

REDIGIT

B. LENGYEL

TOMUS 69

AKADÉMIAI KIADÓ, BUDAPEST

1971

ACTA CHIM. (BUDAPEST)

ACTA CHIMICA

ТОМ 69 — ВЫП. 4

РЕЗЮМЕ

Ректификация многокомпонентных смесей, I

Топологический анализ диаграмм фазового равновесия жидкость-пар

Л. А. СЕРАФИМОВ, В. Т. ЖАРОВ и В. С. ТИМОФЕЕВ

В статье рассмотрены основные вопросы классификации диаграмм фазового равновесия жидкость-пар на основе правил азеотропии. Показано, что каждый из типов диаграмм характеризуется специфическим поведением компонентов при осуществлении фазовых процессов. Дано понятие об областях дистилляции и ректификации и рассмотрены основные принципы построения технологических схем ректификации многокомпонентных неидеальных смесей на основе качественного термодинамико-топологического анализа структуры диаграммы фазового равновесия жидкость-пар. В статье также изложены основные положения принципа перераспределения полей концентраций между областями ректификации и приведен пример разделения гетероазеотропной смеси.

Изучение молекулярного строения алкил- и арилалкоксисиланов, II

Диэлектрические исследования моно-, ди- и триалкоксисиланов

Й. НАДЬ, Ш. ФЕРЕНЦИ-ГРЕС, Р. ФАРКАШ, И. БАРТА и А. БОРБЕЙ-КУСМАН

1. Методом Онсагера были определены величины дипольных моментов гомологических рядов метилалкоксисиланов общей формулы $(CH_3)_nSi(OR)_{4-n}$ (где $n = 1,2,3$ и $R = C_2H_5$, C_3H_7, *изо*-C_3H , C_4H_9, *втор*-C_4H_9, C_6H_{13}).

2. Сравнительным методом расчета Карапетянца была найдена линейная корреляция между дипольными моментами отдельных членов гомологических рядов метилалкоксисланов с различной функциональностью. На основе этого были рассчитаны значения регрессированных дипольных моментов.

3. Было установлено, что в случае алкильной группы небольшого объема у монофункциональных силанов наблюдается свободное вращение, в то время как вращение дитри- и тетрафункциональных алкоксисиланов является заторможенным и степень торможения возрастает в направлении тетрафункциональных соединений.

Исследование дипольных моментов и ИК спекторов феноксисиланов

Й. НАДЬ, П. ХЕНЧЕИ, Ш. ФЕРЕНЦИ-ГРЕС и Т. ГАБОР

Были определены дипольные моменты и снимались ИК спектры различных феноксисиланов. Был рассчитан момент связи m_{SiO} и было установлено, что молекулы триметилфеноксисилана и *п*-бис-(триметилсилокси)-бензола обладают свободным вращением, в то время как вращение в молекулах других феноксисиланов является заторможенным.

На основе ИК спектров было установлено, что величина ν_{SiO} в феноксисиланах выше, чем в алкоксисиланах. Отсюда было сделано заключение, что в феноксисиланах между кремнием и кислородом образуется связь $d\pi-p\pi$, что оказывает свое влияние и на фенильную группу.

Коэффициенты самодиффузии системы метанол—вода—хлористый калий

Т. ЭРДЕИ-ГРУЗ, П. ЧАНЬИ-ФОДОР, Б. ЛЕВАИ и Э. ДЬЁРИ-СИЛАДЬИ

Зависимость коэффициента самодиффузии метанола от состава в системах метанол—вода—хлористый калий и метанол—вода—соляная кислота обладает минимумом при содержании метанола 15—20 мол.%. Произведение же $D^*\eta_r$ проходит через максимум при 45 мол.%, а при пониженных температурах обладает также небольшим минимумом при 8 мол.%-ах.

Энергия активации самодиффузии имеет максимум в прибл. 15 мол.%-ной смеси.

Коэффициенты самодиффузии двух различных ионов хлористого калия, растворенного в смеси метанол-вода, различаются весьма мало. Коэффициент самодиффузии ионов, исходя из воды или метанола, уменьшается под влиянием другого компонента и при 35—40 мол.%-ах обладает плоским минимумом. Величина произведения $D^*\eta_r$, относящаяся к ионам K^+ и C_1^-, не имеет граничного значения: монотонно возрастает с увеличением содержания воды.

Зависимость перенапряжения кислорода от активности воды, III

Влияние pH в сульфатных растворах

Т. ЭРДЕИ-ГРУЗ, М. ГАЙАШ и З. СЕТЕИ

Изучалось перенапряжение при анодном выделении кислорода в водных растворах с 0,1 N концентрацией сульфатного иона при приблизительно одинаковых ионных силах. Измерения проводились при различных плотностях тока и в зависимости от pH и активности воды.

В чистых водных растворах ($a_w = 0{,}998$), в случае постоянной плотности тока перенапряжение растет линейно с увеличением pH, в присутствии ионов Na^+ до pH = 12, а ионов K^+ до pH = 10. С дальнейшим увеличением pH перенапряжение линейно падает, В кислой области, в присутсвии K^+, $\frac{d\eta}{d\,\mathrm{pH}}$ 0,006—0,009 в зависимости от плотности тока. в присутствии ионов Na^+, $\frac{d\eta}{d\,\mathrm{pH}}$ — 0,002—0,003, а в щелочной области $\frac{d\eta}{d\,\mathrm{pH}}$ почти не зависит от катиона.

В растворах с меньшей активностью воды ($a_w = 0{,}906$, 0,0778, 0,738) перенапряжение в интервале pH = 1—10 также растет линейно с возрастанием pH, однако прямая $\eta = f(\mathrm{pH})$ имеет излом при pH = 7, величина $\frac{d\eta}{d\,\mathrm{pH}}$ становится большей. Это изменение является самым значительным при активностях воды $a_w = 0{,}906$ и самым меньшим при $a_w = 0{,}738$.

Химические свойства производных 4H-1,3-бензтиазина, II

Кватернизация производных 2-арил-4H-1,3-бензтиазина

Й. САБО, И. ВАРГА, Э. ВИНКЛЕР и Е. БАРТОШ

При нагревании 2-арил-4H-1,3-бензтиазинов с алкильными и аралкильными галогенидами образуются соответствующие 3-аралкил- и 3-аралкил-4H-1,3-бензтиазиниевые галогенистые производные.

ACTA CHIMICA

TOMUS 69

Fasciculus 1: 1971
Fasciculus 2: 1971
Fasciculus 3: 1971
Fasciculus 4: 1971

INDEX

ABOU-OUF, A. A., YOUSEF, A. F. and EL-GENDY, M. A.: Synthesis of Certain New Salicylisulfonylurea Derivatives 81

АПЬОК, Й., БАРТОК, М. и КОВАЧ, К: Химия 1,3-Бифункциональных систем, X. (APJOK, J., BARTÓK, M. and KOVÁCS, K.: Chemistry of 1,3-Bifunctional Systems, X. Catalytic Transformation of 4-Substituted 1,3-Dioxanes, Cyclic Acetals and Ketals 445

BARTA, I. s. CSÁSZÁR, J.

BARTA, I. s. NAGY, J.

BARTHOS, É. s. SZABÓ, J.

BARTÓK, M. s. APJOK, J.

BENDE, Z. s. CSŰRÖS, Z.

BERKES, R. s. UJHIDY, A.

BITTER, I. s. CSŰRÖS, Z.

Book Reviews 117, 243

BORBÉLY-KUSZMANN, A. s. NAGY, J.

BÖRÖCZ, SZ.: Derivation of the Transport Equations of Non-Isothermal Hydrodynamics from the Gyarmati Principle in Different Pictures 329

CSÁSZÁR, J. und BARTA, I.: Über Komplexe vom Bis-(Salicyl-aldimin-N-R)Nickel(II)-typ)(Kurze Mitteilung). [On the Complexes of Bis-(Salicyl-aldimine-N-R) Nickel(II)-type (Short Communication)] 77

CSŰRÖS, Z., SOÓS, R., BITTER, I., BENDE, Z. and ECET, M.: Thermal Dissociation of Urea Derivatives, II 373

CSŰRÖS, Z., SOÓS, R., BITTER, I. and PÁLINKÁS, J.: The Use of Amide Chlorides in Ring Closure Reactions, III. Synthesis and Ring Closure of Noval Amidrazones 361

DOBOS, S.: Der Bindungszustand der Alkaliionen in der Oberflächenschicht von Natriumoxydhaltigen Gläsern. (The Bonding State of the Alkali Ions in the Surface Layer of Glass Containing Sodium Oxide) 49

DOBOS, S.: Strukturumwandlungen des Silikatnetzwerkes im Laufe der Ausbildung der Oberflächenschicht bei Natriumoxydhaltigen Gläsern. (Changes in the Structure of Silicate Skeletons During the Development of the Surface Layer of Glasses Containing Sodium Oxide) 43

ECET, M. s. CSŰRÖS, Z.

EL-GENDHY, M. A. s. ABOU-OUF, A. A.

ERDEY-GRÚZ, T., FODOR-CSÁNYI, P., LÉVAY, B. und SZILÁGYI-GYŐRI, E.: Selbstdiffusionskoeffizienten des Systems Methanol–Wasser–Kaliumchlorid. (Self-Diffusion Coefficients of the System Methanol–Water–Potassium Chloride) 423

ERDEY-GRÚZ, T., GALLYAS, M. und SZETEY, É.: Abhängigkeit der Sauerstoffüberspannung von der Aktivität des Wassers, II. Wirkung der Alkalimetallionen in schwefelsaurer

Lösung. (Dependence of the Oxygen Overvoltage on the Activity of Water, II. The Effect of Alkali Metal Ions in Sulfuric Acid Solution) 203

ERDEY-GRÚZ, T., GALLYAS, M. und SZETEY, É.: Abhängigkeit der Sauerstoffüberspannung von der Aktivität des Wassers, III. Wirkung der Alkalimetallionen in schwefelsauer Lösung. (Dependence of the Oxygen Overvoltage on the Activity of Water, III. The Effect of Alkali Metal Ions in Sulfuric Acid Solution) 433

ERDEY-GRÚZ, T. und LÉVAY, B.: Bestimmung des Selbstdiffusionskoeffizienten des Dioxans in den Systemen Dioxan–Wasser und Dioxan–Methanol. (Determination of the Self-Diffusion Coefficient of Dioxane in the Systems Dioxane–Water and Dioxane–Methanol) 215

ERDEY, L. s. INCZÉDY, J.

FARKAS, J. s. KISS, L.

FARKAS, R. s. NAGY, J.

FEJES, P. s. WOJNÁROVITS, L.

FERENCZI-GRESZ, S. s. NAGY, J.

FIDLER, A. s. HAVÍŘ, J.

FLÓRA, T.: Einfluß des Materials der derivatographischen Probenbehälter auf die thermische Zersetzung von Ammoniumnitrat. (Effect of the Derivatographic Sample Holders of Various Nature on the Thermal Decomposition of Ammonium Nitrate) 1

FLÓRA, T. und MENYHÁRT, M.: Untersuchung der beim Erhitzen zwischen den Komponenten von N–P–K-Düngern verlaufenden Vorgänge, I. Im System Ammoniumnitrat–Kalciumchlorid verlaufende Prozesse. (Investigation of the Processes Occurring on Heating between the Components of N–P–K-Fertilizers, I. Processes Proceeding in the System Ammonium Nitrate–Potassium Chloride) 145

FLÓRA, T. und MENYHÁRT, M.: Untersuchung der beim Erhitzen zwischen den Komponenten von N–P–K-Düngern Verlaufenden Vorgänge, II. Systeme: Ammoniumnitrat–Ammoniumdihydrophosphat, Ammoniumnitrat–Calciumhydrophosphat, Ammoniumdihydrophosphat–Calciumhydrophosphat, Ammoniumdihydrophosphat–Kaliumchlorid und Calciumhydrophosphat–Kaliumchlorid. (Investigation of the Processes Occurring on Heating between the Components of N–P–K-Fertilizers, II. Systems: Ammonium Nitrate–Ammonium Dihydrogen Phosphate, Ammonium Nitrate–Calcium Hydrogen Phosphate, Ammonium Dihydrogen Phosphate–Calcium Hydrogen Phosphate, Ammonium Dihydrogen Phosphate–Potassium Chloride and Calcium Hydrogen Phosphate–Potassium Chloride) 301

FODOR-CSÁNYI, P. s. ERDEY-GRÚZ, T.

GALLYAS, M. s. ERDEY-GRÚZ, T.

GARZÓ, J., TAMÁS, J., SZÉKELY, T. and UJSZÁSZI, K.: Thermal Decomposition of Branched-Chain Methylpolysiloxanes, II. Separation and Identification of the Pyrolysis Products by Gas Chromatography and Mass Spectrometry 273

GÁBOR, T. s. NAGY, J.

HAUFFE, K. und HEGEDÜS, A. J.: Über die Beeinflussung der Verdampfungsgeschwindigkeit von Zinkoxid durch kurzwelliges Licht. (The Effect of Shortwave Light on the Volatility of ZnO) 123

HAVÍŘ, J. and FIDLER, A.: The Reaction of Ferrocyanide Ion with Silver Nitrate (Short Communication) 163

HEGEDÜS, A. J. s. HAUFFE, K.

HENCSEI, P. s. NAGY, J.

HORÁNYI, GY., RIZMAYER, E. M. and NAGY, F.: Investigation of Adsorption Phenomena on Platinized Pt Electrodes by Tracer Methods, IX. Measurement of Adsorption on Platinum Powder 35

HORÁNYI, R. and NÉMETH, J.: Theoretical Investigation of the Clarification Process in a Tube Centrifuge 59

HORÁNYI, GY. s. VÉRTES, GY.

INCZÉDY, J., KLATSMÁNYI-GÁBOR, P. and ERDEY, L. †.: The Use of Complex Forming Agents in Ion Exchange Chromatography, V. Adsorption of Metal Ions Cation Exchange Resin in the Presence of Pyridine, Ethylenediamine and Triethanolamine 137

Inczédy, J.: The Use of Complex Forming Agents in Ion Exchange Chromatography, VI. Separation of Organic Bases on a Cation-Exchange Column 265

Jodál, M. s. Lipták, A.

Kajtár, J. s. Vajda, T.

Kaposi, O. and Riedel, M.: Experimental Study of Positive Ion Emission from Tungsten, II 19

Kaposi, P. s. Zsadon, B.

Kiss, L. und Farkas, J.: Untersuchung der Ionisation von Metallen und Metallionen-Neutralisation mit der rotierenden Ring-Scheibenelektrode, VIII. Allgemeine Behandlung der an der Ringelektrode meßbaren Parameter. (Investigation of the Ionisation of Metals and the Neutralisation of Metal Ions at the Rotary Ring and Disc Electrode, VIII. General Discussion of the Parameters Measurable at the Ring Electrode) 167

Klatsmányi-Gábor, P. s. Inczédy, J.

Klivényi, F. s. Vinkler, P.

К. И Кучкова, А. А. Семенов и И. В. Терентьева: Карболины, II. Полный синтез алкалоида бревикарина и его низшего гомолога

(Kuchkova, K. I., Semenov, A. A., Terentjeva, I. V.: Carbolines, II. Total Synthesis of Alkaloide Brevicarine and its Inferior Homologue) 367

Kocka, I. s. Toldy, L.

Kovács, K. s. Apjok, J.

Kozmutza, K. s. Schneer-Erdey, A.

Légrádi, L.: Mechanism of an Adsorption Indication, IX. Phthaleins as Adsorption Indicators 157

Lévay, B. s. Erdey-Grúz, T.

Lipták, A. and Jodál, N.: Carbohydrate Methyl Ethers, III. Thin-Layer Chromatographic Separation and Quantitative Determination of Glucose Methyl Ethers 103

Magyar, M. s. Ujhidy, A.

Menyhárt, M. s. Flóra, T.

Nagy, F. s. Horányi, Gy.

Nagy, F. s. Vértes, Gy.

Nagy, J., Ferenczi-Gresz, S., Farkas, R., Barta, I. and Borbély-Kuszmann, A.: Study of the Molecular Structure of Alkyl- and Aryl-Alkoxysilanes, II. Dielectric Study of Mono-, Di-, and Trialkoxysilanes 397

Nagy, J., Hencsei, P., Ferenczi-Gresz, S. and Gábor, T.: Investigation of the Dipole Moments and Infrared Spectra of Phenoxysilanes 411

Németh, J. s. Horányi, R.

Otta, K. s. Zsadon, B.

Pálinkás, J. s. Csűrös, Z.

Répásy, O. s. Ujhidy, A.

Riedel, M. s. Kaposi, O.

Rizmayer, E. M. s. Horányi, Gy.

Ruff, F. s. Vajda, T.

Schneer-Erdey, A. and Kozmutza, K.: Xenon Difluoride as an Analytical Reagent, I. Determination of Iodine 9

Semenov, A. A. s. Kuchkova, K. I.

Serafimov, L. A., Zharov, V. T. and Timofeyev, V. S.: Rectification of Multicomponent Mixtures, I. Topological Analysis of Liquid–Vapour Phase Equilibrium Diagrams 383

Soós, R. s. Csűrös, Z.

Sólyom, S. s. Toldy, L.

Stájer, G. s. Vinkler, P.

Szabó, A. E. s. Vinkler, P.

Szabó, J., Varga, E., Vinkler, E. and Barthos, É.: Chemistry of 4*H*-1,3-Benzothiazine Derivatives, II. Quaternization of 2-Aryl-4*H*-1,3-Benzothiazine Derivatives 459

Szetey, Z. s. Erdey-Grúz, T.

Székely, T. s. Garzó, J.

Szilágyi-Győri, E. s. Erdey-Grúz, T.

Szirtes, L. s. Zsinka, L.

Takács, J. s. Ujhidy, A.

Tamás, J. s. Garzó, J.

Terentjeva, I. V. s. Kuchkova, K. I.

Timofeyev, V. S. s. Serafimov, L. A.

Toldy, L., Sólyom, S., Kocka, I., Tóth, G. und Tóth, I.: Thiocarbamidderivate mit tuberkulostatischer Wirkung, II. Acylthiocarbamide. (Thiourea Derivatives with Tuberculostatic Action, II. Acyl Thiourea) 221

Tóth, G. s. Toldy, L.

Tóth, I. s. Toldy, L.

Tóth, J.: State Equations of the Solid–Gas Interface Layers 311

Ujhidy, A., Magyar, M. und Berkes, R.: Einfluß der Schwefelsäurekonzentration auf die Nitrierungsgeschwindigkeit von Nitrobenzol untersucht in einem Dünnschichtreaktor. (The Effect of the Sulfuric Acid Concentration on the Nitration Rate of Nitrobenzene in a Film Reactor) 107

Ujhidy, A., Répásy, O. and Takács, J.: The Competitive Nitration of Some Aromatic Compounds 349

Ujszászi, K. s. Garzó, J.

Vajda, T., Kajtár, J. and Ruff, F.: The Reaction of Ammonium Thiocyanate with Dicyclohexylcarbodiimide 97

Varga, E. s. Szabó, J.

Vértes, Gy., Horányi, Gy. and Nagy, F.: Oxidation on the Nickel Hydroxide Electrode, IV. Kinctics of Oxidation of Primary Alcohols 341

Vijay Mohan Bhatnagar: Preparation and Unit Cell Dimensions of Lead Apatites (Short Communication) 15

Vinkler, E. s. Szabó, J.

Vinkler, E. s. Vinkler, P.

Vinkler, P., Klivényi, F., Vinkler, E., Stájer, G. und Szabó, A. E.: Untersuchungen über aromatische Sulfenylchloride, II. Reaktionen des Sulfenylchlorids mit Thiocarbamiden und Thiosemicarbaziden. (Investigations in the Field of Aromatic Sulfenyl Chlorides, II. The Reaction of Sulfenyl Chloride with Thioureas and Semi-Thioureas) 229

Wojnárovits, L. and Fejes, P.: Radiation Chemistry of Saturated–Unsaturated Hydrocarbon Systems, III. Kinetic Study of Hydrogen Formation 177

Zharov, V. T. s. Serafimov, L. A.

Zsadon, B. and Kaposi, P.: Tabersonine from Ripen Seeds of *Vinca rosea* L. (Preliminary Communication) 241

Zsadon, B. and Otta, K.: Indole and Indole Derivatives, X. Saponification, Acid Hydrolysis and Decarboxylation of (−)-Vincadifformine and Tabersonine 87

Zsinka, L. and Szirtes, L.: Investigations on a Chromium Phosphate Ion Exchanger.... 249

Yousef, A. F. s. Abou-Ouf, A. A.

Acta Chimica Academiae Scientiarum Hungaricae, Tomus 69 (1), pp. 1—7 (1971)

EINFLUSS DES MATERIALS DER DERIVATOGRAPHISCHEN PROBENBEHÄLTER AUF DIE THERMISCHE ZERSETZUNG VON AMMONIUMNITRAT

T. FLÓRA

(Forschungsinstitut für Chemische Schwerindustrie, Veszprém)

Eingegangen am 10. Februar 1970

Die thermische Zersetzung des Ammoniumnitrats wurde derivatographisch in Probebehältern aus verschiedenen Materialien (Platin, Nickel, oxydiertes Nickel, rostfreier Stahl, Graphit, Korund) untersucht. Es wurde gefunden, daß die Zersetzung nur in den Tiegeln aus Metall bzw. Metalloxyd heftig, explosionsartig exotherm verläuft, vermutlich, weil das Material dieser Tiegel die Oxydation der aus der Dissoziation des Ammoniumnitrats stammenden Zersetzungsprodukte katalysiert. Bei der Zersetzung in Tiegeln aus Graphit und Korund spielt sich in erster Reihe die endotherme thermische Dissoziation des Ammoniumnitrats ab.

Aus den derivatographischen Kurven wurde die Reaktionsordnung und Aktivierungsenergie der thermischen Zersetzung des Ammoniumnitrats in den verschiedenen Tiegeln bestimmt. In Tiegeln aus Platin, Nickel und oxydiertem Nickel ergab sich eine Zersetzungsreaktion nullter bzw. negativer Ordnung. In Tiegeln aus rostfreiem Stahl, Graphit und Korund gelangt — nach den anfänglichen Reaktionen nullter Ordnung — die thermische Dissoziationsreaktion erster Ordnung des Ammoniumnitrats zur Geltung. Die Brutto-Aktivierungsenergie der erstgenannten Reaktionen nullter Ordnung ist wesentlich geringer, als jene der Reaktion erster Ordnung, die in den rostfreien Stahl-Graphit- und Korundtiegeln verläuft.

Die thermischen Eigenschaften des Ammoniumnitrats wurden von vielen Verfassern untersucht; seine Umwandlungstemperaturen sind mit verschiedenen Verfahren bestimmt worden [1—8].

Nach den Umwandlungspunkten schmilzt die Verbindung — laut verschiedener Literaturangaben — bei 166 °C [1], 169 °C [9] bzw. 170 °C [10]. Ihre Zersetzung beginnt — je nach den Bedingungen — bei 150 °C [1], 175 °C [11] bzw. 190 °C [12] und kann nach mehreren Reaktionsmechanismen verlaufen. Einige Verfasser [11—16] beschreiben die Zersetzung des Ammoniumnitrats mit folgender Reaktionsgleichung:

$$NH_4NO_3 \longrightarrow N_2O + 2H_2O \qquad (1)$$

Nach DAVIS und ABRAMS [17] handelt es sich um einen zweistufigen Zersetzungsmechanismus unter Bildung von Nitramid, wobei N_2O und Wasserdampf entsteht:

$$NH_4NO_3 \xrightarrow{\text{langsam}} NH_2NO_2 + H_2O$$
$$NH_2NO_2 \xrightarrow{\text{schnell}} N_2O + H_2O \qquad (2)$$

Je nach den Zersetzungsbedingungen berichten die Mitteilungen über den Zersetzungsmechanismus des Ammoniumnitrats [10—14], [18], [19] noch über die Bildung von Sauerstoff, Stickstoff, Stickstoffdioxyd, Stickstoffmonoxyd und Salpetersäure als Zersetzungsprodukte.

SAUNDERS [14], SHAH [15] sowie FEICK und HAINER [20] erklären die Dissoziation des Ammoniumnitrats mit der Gegenwart von Ammoniak in den gasförmigen Zersetzungsprodukten:

$$NH_4NO_3 \longrightarrow NH_3 + HNO_3 \qquad (3)$$

Andere Verfasser [12, 13] teilen im Zusammenhang mit den Änderungen des Wärmeinhalts mit, daß letztere Reaktion — im Gegensatz zu den vorangehenden — endotherm ist.

Außer dieser Feststellung berichten die angeführten Mitteilungen über die explosionsartige Zersetzung des Ammoniumnitrats um 260 °C.

Die durch verschiedene Verfasser beschriebenen verschiedenartigen Mechanismen der Zersetzung des Ammoniumnitrats zeigen, daß die Versuchsbedingungen einen wesentlichen Einfluß auf die thermische Zersetzung ausüben. Um diese Wirkung zu untersuchen, prüften wir die Rolle des Probenbehältermaterials auf die thermischen Vorgänge des Ammoniumnitrats auf derivatographischen Weg.

Dazu wurde das Ammoniumnitrat in Tiegel aus Platin, Nickel, oxydiertem Nickel, rostfreiem Stahl, Graphit und Korund eingewogen. Die Derivatogramme wurden auf einem Derivatographen GYEM 676, System PAULIK—PAULIK—ERDEY [21] bei einer Aufheizgeschwindigkeit von 2,6 °C/Minute in Gegenwart von Luft aufgenommen. Die Einwaage betrug in sämtlichen Fällen 500 mg. Die Galvanometerempfindlichkeit für die DTG-Kurven betrug 1/20, für die DTA-Kurven 1/10.

Die Ordnungen und Aktivierungsenergien der in den verschiedenen Tiegeln verlaufenden Reaktionen wurden auf Grund der TG- und DTG-Kurven berechnet [22], ausgehend aus dem auf den Angaben der TG-Kurve beruhenden Verfahren von FREEMAN und CAROLL [23].

Versuchsergebnisse und Diskussion

Die in Tiegeln aus verschiedenem Material erhaltenen DTA-Kurven sind in Abb. 1, die TG- und DTG-Kurven in Abb. 2 dargestellt.

Die durch die DTA-Kurven angezeigten Phasenumwandlungen, die bei drei verschiedenen Temperaturen verlaufen (IV—III, III—II, II—I), sind in Tabelle 1 angeführt, wobei vergleichshalber auch die mit verschiedenen Methoden erhaltenen Ergebnisse anderer Verfasser angegeben sind.

Nach den Phasenumwandlungen erfolgt das Schmelzen (Abb. 1) und danach die Zersetzung des Ammoniumnitrats (Abb. 2). Im Platintiegel erfolgt die Zersetzung bei 240 °C in einer einzigen Stufe explosionsartig, in einem heftigen exothermen Vorgang (Kurve 1, Abb. 1). Im Nickeltiegel zersetzt sich das Ammoniumnitrat in zwei Stufen, bei Spitzentemperaturen von 210 und 300 °C. Beide Stufen werden von Wärmeentwicklung begleitet (Kurve 2, Abb. 1). Im bereits einmal benützten, mit einer Oxydschicht überzogenen Nickeltiegel verläuft die Zersetzung in einer einzigen Stufe mit maximaler Geschwindigkeit bei 283 °C Spitzentemperatur, ebenfalls exotherm (Kurve 3, Abb. 1). Im rostfreien Chromstahltiegel spielt sich wieder ein Zweistufenvorgang (bei 258 und 287 °C) ab, der von einer langsamen Wärmeentwicklung begleitet ist (Kurve 4, Abb. 1). Während die Zersetzung des Ammoniumnitrats — in Übereinstimmung mit den Literaturangaben — in Metalltiegeln

Tabelle I

Phasenumwandlungen anzeigende DTA-Spitzentemperaturen verglichen mit Literaturangabeu

Prüfverfahren	Phasenumwandlung			Literaturhinweis
	IV—III °C	III—II °C	II—I °C	
	32	83	125	[3]
	32	86	126	[4]
Optisch	32	82	125	[5]
Mikroskopisch	32,3	84,2	125,2	[7]
DTA	32	82	125	[8]
Dilatometrisch	32	83	126	[6]
Derivativ-dilatometrische DTA-Kurve	31	84	122	[2]
Derivativ-dilatometrische Kurve	31	82	115 128	[2]
Derivatographische DTA-Kurve	45	84	130	[1]
Derivatographische DTA-Kurve				
im Platintiegel	52	87	125	Eigene Ergebnisse
im Nickeltiegel	49	87	126	Eigene Ergebnisse
im oxydierten Nickeltiegel	55	92	131	Eigene Ergebnisse
im rostfreien Stahltiegel	56	89	128	Eigene Ergebnisse
im Graphittiegel	54	90	128	Eigene Ergebnisse
im Korundtiegel	47	85	123	Eigene Ergebnisse

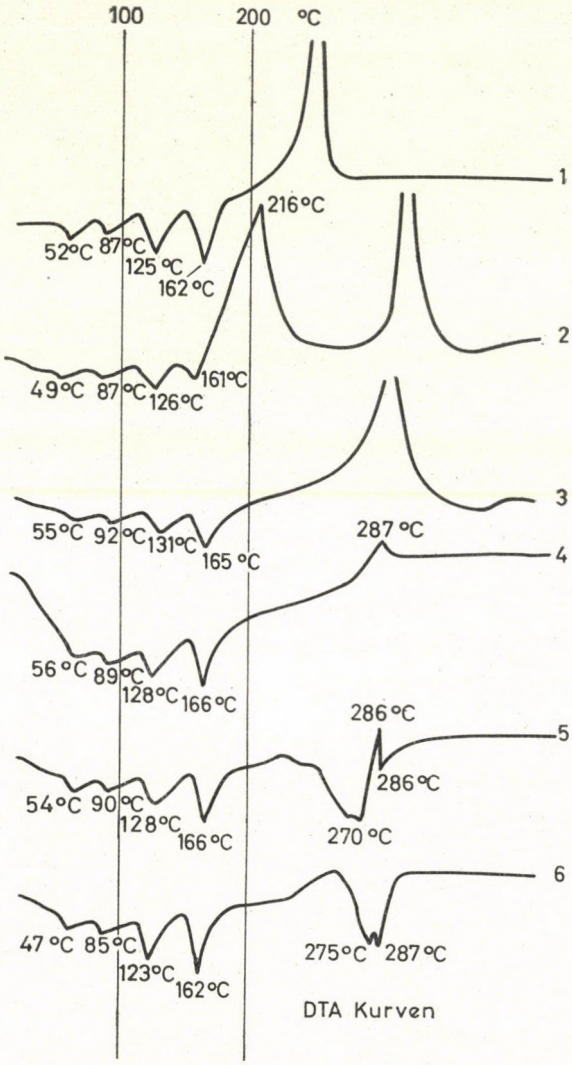


Abb. 1. DTA-Kurven von Ammoniumnitrat. 1 — im Platintiegel, 2 — im Nickeltiegel, 3 — im mit einer Oxydschicht überzogenen Nickeltiegel, 4 — im Chromstahltiegel, 5 — im Graphittiegel, 6 — im Korundtiegel

meist in Form einer heftigen exothermen Reaktion verläuft, spielt sie sich in Graphit- und Korundtiegeln, abgesehen von geringen exothermen Abschnitten zu Beginn und am Ende der Reaktion, praktisch als endothermer Vorgang ab (Kurven 5 und 6 in Abb. 1). Daraus kann gefolgert werden, daß beim Erhitzen in nichtmetallischen Tiegeln in erster Reihe mit der von Wärmeabsorption begleiteten thermischen Dissoziation des Ammoniumnitrats, während in Metalltiegeln daneben mit dem Verlauf von sekundären Reaktionen gerechnet werden muß.

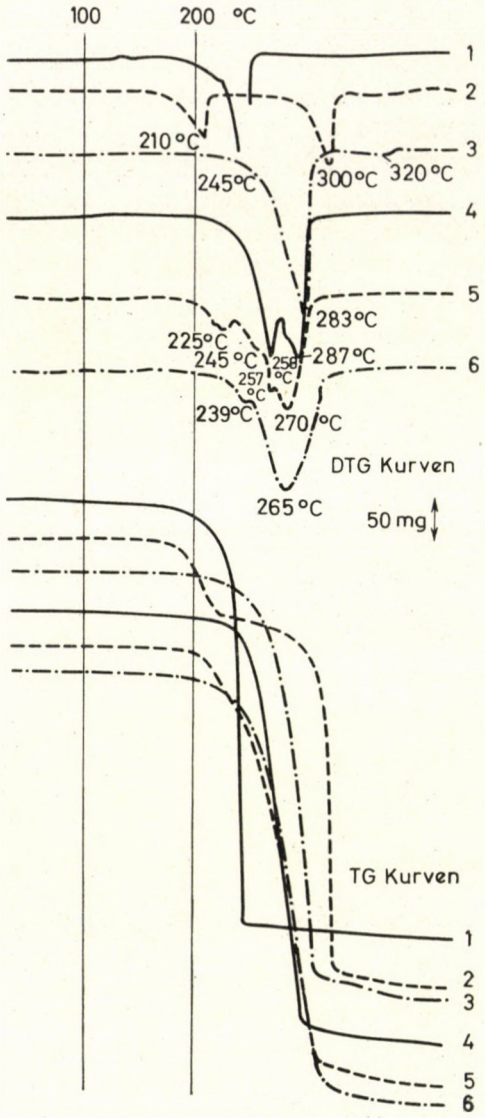


Abb. 2. DTG- und TG-Kurven von Ammoniumnitrat. 1 — im Platintiegel, 2 — im Nickeltiegel, 3 — im mit einer Oxydschicht überzogenen Nickeltiegel, 4 — im Chromstahltiegel, 5 — im Graphittiegel, 6 — im Korundtiegel

NÁRAY erwähnt in seinem Buch [9], daß Nickel in der Ammoniumnitratschmelze unter Bildung von Nickelnitrat gelöst wird; Nebenprodukte der Reaktion sind Ammoniak, Stickstoff und Wasserdampf. Außerdem berichtet er, daß Ammoniumnitrat beim Erhitzen mit Metalloxyden, u.a. mit Nickel(II)oxyd unter Bildung von Nickelnitrat, Ammoniak und Wasserdampf reagiert. Eisen, Chrom und ihre Oxyde werden von der Ammoniumnitratschmelze nicht angegriffen.

Wir konnten keinen Literaturhinweis darüber finden, ob sich zwischen Ammoniumnitratschmelze und Platin beim Erhitzen eine Reaktion abspielt.

Bei der Zersetzung im Nickeltiegel könnte die bei 210 °C verlaufende exotherme Reaktion aus der Wechselwirkung des metallischen Nickels und des Ammoniumnitrats stammen (Kurve 2, Abb. 1), da diese Reaktion — nach unseren Rechnungen auf Grund des Gesetzes von Hess — exotherm ist. Die Reaktion zwischen dem oxydierten Nickel und dem Ammoniumnitrat (Kurve 3, Abb. 1) kann jedoch keine Enthalpieänderung exothermer Art hervorrufen, da diese Reaktion nach unseren Berechnungen endotherm ist. Auch im Fall des Platintiegels und Chromstahltiegels kann nicht von einer Reaktion des Metalls mit dem Ammoniumnitrat gesprochen werden. Daß die Zersetzung des Ammoniumnitrats in diesen Metalltiegeln bzw. oxydierten Metalltiegeln dennoch exotherm verläuft, könnte seinen Grund darin haben, daß die sekundäre Reaktion der bei der Dissoziation des Ammoniumnitrats entstehenden Zersetzungsprodukte unter sich bzw. die Oxydation des Ammoniaks durch das Metall des Tiegels katalysiert wird. Platin und Nickel wirken auch auf den Beginn der Zersetzung des Ammoniumnitrats katalytisch. In den Zersetzungsversuchen mit Platin- und Nickeltiegeln wurden bis zu 200 °C Gewichtsverluste von 3,6—6,6% gemessen, während in den übrigen Tiegeln bis zu dieser Temperatur nur Gewichtsverluste von 1—2% beobachtet wurden.

Die zu den einzelnen Zersetzungsstufen gehörenden Gewichtsverluste und die Gestaltung des Gewichtsverlustes 200 und 300 °C sind in Tabelle II zusammengestellt. Wie ersichtlich, nimmt die Zersetzungsgeschwindigkeit im Nickeltiegel nach dem schnellen Beginn ab; bis zu 250 °C ist der Gewichtsverlust im Nickeltiegel fast der niedrigste unter allen. Über 250 °C verlangsamt sich auch die Zersetzung im Platintiegel. Bis 275 °C war der Gewichtsverlust im Korundtiegel am höchsten, ihm folgten die Werte im Graphittiegel und im rostfreien Stahltiegel.

Aus den Derivatogrammen wurden die Ordnungen und Aktivierungsenergien der in den verschiedenen Tiegeln verlaufenden Reaktionen bestimmt; diese Werte sind ebenfalls in Tabelle II enthalten. Im Platin-, Nickel- und oxydierten Nickeltiegel ergab sich eine Reaktion nullter bzw. negativer Ordnung. Bei der Zersetzung in Tiegeln aus rostfreiem Stahl, Graphit und Korund gelangte — nach der anfänglich auftretenden Reaktion nullter Ordnung — die thermische Dissoziationsreaktion erster Ordnung des Ammoniumnitrats zur Geltung. Die Brutto-Aktivierungsenergien der in den Platin-, Nickel- und oxydiertem Nickeltiegeln verlaufenden Reaktionen nullter Ordnung sind kleiner, als die Aktivierungsenergie der Reaktion erster Ordnung, die sich in den Tiegeln aus rostfreiem Stahl, Graphit und Korund abspielt.

Tabelle II

Tiegelmaterial	DTG Spitzen-temp. °C	Gew. Verlust %	Aktivie-rungs-energie Kcal/Mol	Ordnung der Reak-tion	Gewichtsverlust bis				
					200 °C	225 °C	250 °C	275 °C	300 °C
Platin	245	100	—38,3	0	3,6	11,6	45,0	57,0	100,0
Nickel	210	14,0	—31,7	0					
	300	86,0	— 0,34	—1,2	6,6	14,5	17,5	24,5	93,3
Oxydiertes Nickel	283	96,0	—21,7	0					
	320	4,0			1,2	3,5	12,0	45,5	96,0
Rostfreier Stahl	258	50,0	—51,4	0					
	287	50,6	—56,2	1	0,8	2,5	18,6	71,0	99,0
Graphit	225	14,0	—41,0	0					
	245	18,0	—30,8						
	257	23,5	—26,5	0					
	270	45,0	—53,3	1	1,6	10,5	35,0	85,0	98,9
Korund	239	12,8	—21,2	—0,3					
	265	87,2	—48,6	1	1,6	5,0	18,4	86,0	99,6

LITERATUR

1. ERDEY, L., GÁL, S., LIPTAY, G.: Talanta, **11,** 913 (1964)
2. PAULIK, F., PAULIK, J., ERDEY, L.: Microchim. Acta **1966,** 894
3. BRITSKE, E. W., KAPUSTINSKY, A. F.: Termitscheskie konstanty neorganitscheskich weschtsestw. Isd. Akad. Nauk S.S.S.R., Moskau—Leningrad, 1949
4. BROWN, R. N., MCLAREN, A. C.: Proc. Roy. Soc. **266** A, 329 (1962)
5. WALLERANT: Bull. Soc. Min. **28,** 315 (1905); C. R. Acad. Sci. **142,** 217 (1900)
6. BEHN: Proc. Roy. Soc. **80** A, 448 (1908)
7. HENDRICKS, POSNJACK, KRACEK: J. Am. Chem. Soc. **54,** 2766 (1932)
8. MORAND, J.: Ann. Chim. **12,** 1018 (1955)
9. NÁRAY-SZABÓ, I.: Anorganische Chemie. Verlag der Ung. Akad. der Wiss., Budapest, 1962. Akademie-Verlag, Berlin, 1962
10. SOLOMON, C. H., BARCLAY, K. S.: Broschüre der Firma Fisons Fertilizers Ltd., Levington. London, 1965
11. BARCLAY, K. S., CREVE, J. M.: J. Appl. Chem. **17,** 21 (1967)
12. MARINELA MAN: Revista de Chimie, **18,** 145 (1967)
13. WATERS, CH. W., SMITH, J. A., NOVOTNY, J.: J. Agr. Food Chem., **8,** 475 (1960)
14. SAUNDERS, J. L.: J. Chem. Soc. **121,** 698 (1922)
15. SHAH, M. S., OZA, R. M.: J. Chem. Soc. **1932,** 725
16. BESSON, M., ROSSET, M.: Compt. Rend. **142,** 633 (1906)
17. DAVIS, T. L., ABRAMS, A. J. J.: J. Am. Chem. Soc. **47,** 1043 (1925)
18. KNOP, W.: Zbl. für Arbeitsmedizin und Arbeitschutz, **12,** 122 (1962)
19. KAISER, R.: Angew. Chem. **48,** 149 (1935)
20. FEICK, G., HAINER, R. M.: J. Am. Chem. Soc., **76,** 5860 (1954)
21. PAULIK, F., PAULIK, J.: Termoanalízis. Műszaki Könyvkiadó, Budapest, 1963
22. FLÓRA, T.: Acta Chim. Hung. **48,** 225 (1966)
23. FREEMAN, E. S., CAROLL, B.: J. Phys. Chem. **62,** 394 (1958)

Teréz FLÓRA; Veszprém, Wartha V. u. 1—3. Hungary.

Acta Chimica Academiae Scientiarum Hungaricae, Tomus 69 (1), pp. 9—13 (1971)

XENON DIFLUORIDE AS AN ANALYTICAL REAGENT, I

DETERMINATION OF IODINE

A. SCHNEER-ERDEY and K. KOZMUTZA

(Inorganic Chemical Research Group of the Hungarian Academy of Sciences, and Institute of General and Inorganic Chemistry, L. Eötvös University, Budapest)

Received February 15, 1970

Solid xenon difluoride, a strongly oxidizing reagent, has unlimited storability, and is easy to handle. Its use is very convenient for the detection and determination of very small amounts of iodine and iodide based on the oxidation of iodine to periodate.

Xenon difluoride is the most simple xenon compound, prepared also in Hungary [1]. According to our studies, this substance can be conveniently used for qualitative and quantitative analytical purposes, owing to its strong oxidizing power, almost unlimited storeability, and easy handling and dosing of the solid compound. The reactions which can be performed with this reagent can be carried out only in a very complicated way with other reagents under normal conditions.

In our preliminary report [2] we stated that in acid medium xenon difluoride oxidizes iodide ions to periodate within a few minutes through the intermediate stages of iodine and iodate.

$$4\,XeF_2 + HI + 4\,H_2O = 4\,Xe + HIO_4 + 4\,H_2F_2$$

In our experiments, plastic beakers, spatulas and stirrers were used (polyethylene or polyvinyl chloride). According to our recent observations, upon the addition of excess xenon difluoride to an aqueous solution, there is no difference between the use of plastic or glass equipment. The samples were weighed by means of an automatic semimicro balance (Type WP 11). After a longer period, the inner surface of the stoppered glass vessel used for weighing the xenon difluoride, became opaque. Its weight loss was nearly 100 mg after use for a few months in a laboratory atmosphere of about 50% relative humidity.

Experimental

In our experiments calibrated volumetric flasks, pipettes, semimicro burettes, redistilled water and reagents of analytical grade were used. In order to determine the conditions of the analysis, several parallels were carried out in plastic and glass beakers containing a few mg of potassium iodide dissolved in 5—40 ml of 1 *N* sulfuric acid. Xenon difluoride was added to the solutions in an amount sufficient to ensure abundant excess of the reagent for oxidation

of the iodide to periodate. The oxidation of 1 mg of potassium iodide to periodate requires 8.4648 mg of xenon difluoride. Immediate liberation of iodine was observed and the brown solution lost its colour within a few minutes. The effervescent solutions were heated on a water-bath for 10—60 minutes to complete the reaction and decompose and remove excess xenon difluoride. About half of the solutions in plastic beakers were kept for titration. All the other solutions were washed into glass titration flasks and kept slowly boiling on a sand bath for 5—30 minutes, with small funnels placed into their necks. The colourless solutions in glass beakers were also placed on a sand bath in a similar manner. 2 *N* hydrochloric acid was added to each solution after cooling and some solid potassium iodide was added immediately before titration. The iodine formed was titrated with 0.01 *N* $Na_2S_2O_3$ solution against starch indicator. The obtained results, as shown in Table I, indicate oxidation to the periodate state.

Table I

Oxidation of potassium iodide by xenon difluoride

Weighed KI mg	Weighed XeF_2 mg	Consumption of 0.01 *N* $Na_2S_2O_3$ ml	Found KI mg	Deviation	
				mg	%
6.08	43.39	27.55	5.72	—0.36	—5.9
1.67	18.07	8.15	1.69	+0.02	+1.3
1.52	22.98	7.60	1.58	+0.06	+3.7
1.00	11.02	4.76	0.99	—0.01	—1.0
0,95	9.22	4.40	0.91	—0.04	—3.8
0.90	15.66	4.23	0.88	—0.02	—2.3
0.45	13.07	2.13	0.44	—0.01	—1.8

In order to check the completeness of oxidation, the determination of periodate and iodate in the presence of each other was carried out and also the measurement of a known amount of potassium iodide was performed after the reduction of periodate to iodate in two different manners. These experiments also reveal whether or not the intervals prescribed for standing or heating are sufficient to ensure the completeness of oxidation and the removal of the excess reagent without residue. Determination of periodate and iodate ions in the presence of each other was carried out with the stock solution too. The results of these measurements are given in Table II; in this case potassium iodide was used for the reduction of periodate to iodate [3].

Iodine formed in slightly alkaline media buffered with sodium hydrogen carbonate in the course of reduction of periodate ions to iodate by potassium iodide may oxidize the thiosulfate ions partially beyond the tetrathionate stage, to sulfate. Being aware of this fact, thiosulfate was used only for the reduction of iodine formed in the course of the reaction. After acidification with excess hydrochloric acid and addition of a new portion of potassium iodide, the freshly liberated iodine was titrated with sodium thiosulfate and the amount of the potassium iodide was calculated from this (Table II).

Table II

Determination of the amount of KI in the stock solution, based on the measurement of KIO_3 and KIO_4 (reduction by KI) [3]

Weighed KI	0.1 *N* $Na_2S_2O_3$ consumed by iodine liberated by		KI found in the titration of		Deviation			
	KIO_3	KIO_4	KIO_3	KIO_4	KIO_3		KIO_4	
mg	ml	ml	mg	mg	mg	%	mg	%
1.67	6.30	8.15	1.74	1.69	+0.07	+4.2	+0.02	+1.2
1.52	5.80	7.60	1.61	1.58	+0.09	+5.9	+0.06	+3.9
1.00	3.61	4.76	1.00	0.99	±0.00	±0.0	—0.01	—1.0
0.95	3.26	4.30	0.90	0.89	—0.05	—5.2	—0.06	—6.3
0.90	3.25	4.23	0.90	0.88	±0.00	±0.0	—0.02	—2.2

Periodate was also reduced to iodate with hydrogen peroxide according to the following equation:

$$HIO_4 + H_2O_2 = HIO_3 + H_2O + 1/2\ O_2,$$

without liberation of iodine. After accomplishment of the reaction, the excess hydrogen peroxide was decomposed followed by acidification and the amount of iodine formed representing six equivalents, was determined iodometrically [4]. Some results obtained by the two different methods of reduction are given in Tables II and III.

Table III

Determination of KI with KIO_3 obtained by the reduction of KIO_4 with hydrogen peroxide

Weighed KI	Weighed XeF_2	Consumed 0.01 *N* $Na_2S_2O_3$	Found KI	Deviation	
mg	mg	ml	mg	mg	%
1.32	17.52	4.83	1.33	+0.01	+1.2
1.62	19.80	5.71	1.58	—0.04	—2.5
1.62	22.60	5.94	1.64	+0.02	+1.5
1.78	20.20	6.42	1.77	—0.01	—0.2

The decomposition of excess hydrogen peroxide by simple boiling is not satisfactory. Thus the solution was evaporated to dryness in the presence of excess sodium carbonate in a platinum crucible. Under these conditions the iodate loss is avoided and the decomposition of xenon difluoride and hydrogen peroxide is securely accomplished. Fluoride ions remaining in the solution will not interfere with the iodometric measurement in accordance with the

observations of other authors [5]. Small quantities of chloride ion — disregarding the consumption of some xenon difluoride — does not interfere in the determination since the chlorine formed is removed on heating.

In addition to this the determination of the weighed potassium iodide sample was also carried out by means of the direct measurement of periodate ions (Table I). The present method permits a more accurate determination of the amount of iodide appearing in the cooling water of nuclear reactors than it was possible with earlier procedures [6].

The present studies proved that:

1. the oxidation proceeds to periodate, involving eight equivalents;
2. heating for 30 minutes on a water-bath or slow boiling for 20 min. on a sand bath after disappearance of the colour is sufficient;
3. there is no difference between the use of plastic and glass vessels;
4. too great excesses of xenon difluoride have no influence on the process

Procedure

1—20 ml of the solution to be analyzed, containing iodine or iodide ions is acidified to about 1 *N* with sulfuric acid in a beaker or titrating flask and xenon difluoride is added in excess. After disappearance of the colour the solution is allowed to stand for 30 min. at about 100 °C. Further handling of the cooled solution depends on the expected iodine content.

a) The solution is titrated with 0.1 or 0.01 *N* $Na_2S_2O_3$ solution against starch indicator after adding a few ml of 2 *N* hydrochloric acid and a few tenths of a gram of potassium iodide. 1 ml of 0.01 *N* $Na_2S_2O_3$ is equivalent to 0.2075 mg of KI.

b) A few potassium iodide crystals are added to the solution buffered with a small excess of solid $NaHCO_3$ and the liberated iodine is reduced with 0.01 *N* $Na_2S_2O_3$ in the presence of starch. 2 *N* hydrochloric acid is added to the solution in excess and after adding a small amount of potassium iodide the liberated iodine is titrated with 0.1 *N* or 0.01 *N* $Na_2S_2O_3$. 1 ml of 0.01 *N* $Na_2S_2O_3$ solution is equivalent to 0.2767 mg of potassium iodide.

Table II shows the results obtained with a stock solution.

These data also support the statement that iodine or iodide can be determined both in the form of I (V) and I (VII).

A separate series of measurements was carried out with the potassium iodide stock solution in order to determine the error of the method. These results are summarized in Table IV.

These data indicate reproducible oxidation of iodine to periodate with xenon difluoride. In the case of volumetric measurement, the standard deviation is $\pm$ 0.0208 mg or $\pm$ 2.1%.

Table IV

Determination of 0.9986 mg of KI after oxidation to periodate

Consumed 0.01 *N* $Na_2S_2O_3$	Found KI	Deviation		Standard deviation	
ml	mg	mg	%	mg	%
4.67	0.9688				
4.72	0.9786				
4.74	0.9830				
4.74	0.9842				
4.85	1.0060				
4.87	1.0112				
4.88	1.0135				
mean 4.79	0.9922	—0.0064	—0.64	±0.0208	±2.1

The sensitivity of the reaction can be further increased by using non-volumetric method for the determination of the iodine [7]. Very small amounts of iodine or idodide ions can be detected and measured directly or photometrically [8], by means of the strongly oxidizing xenon difluoride reagent.

*

The authors thank Dr. P. Gróz (Department of Chemistry, Central Research Institute for Physics, Hungarian Academy of Sciences) for supplying the valuable xenon difluoride preparate.

REFERENCES

1. Theis, E.: MTA Kém. Tud. Oszt. Közl. **24,** 215 (1965)
Gróz, P., Kiss, I., Révész, A., Sipos, T.: J. Inorg. Nucl. Chem. **28,** 909 (1966)
2. Schneer-Erdey, A., Kozmutza, K.: Magy. Kém. Foly. **75,** 378 (1969)
Schneer-Erdey, A., Kozmutza, K.: Acta Chim. Acad. Sci. Hung. **61,** 325 (1969)
3. Barbaby, O. L.: Am. Soc. **38,** 33 (1916)
Pascal, P.: Nouveau Traité de Chimie Minéral, Tome XVI. pp. 626. Masson et Cie, Paris, 1960
4. Schwicker, A.: Z. Anal. Chem. **110,** 182 (1937)
Szekeres, L.: Magy. Kém. Foly. **63,** 273 (1957)
5. Jaselskis, B., Warriner, J. P.: Anal. Chem. **38,** 963 (1966)
6. Csada, I., Schneer-Erdey, A.: KFKI Közl. **16,** 53 (1968)
7. Morrison, G. H.: Trace Analysis, p. 10. Interscience, New York, 1965
8. Erdey, L., Szabadváry, F.: Magy. Kém. Foly. **61,** 341 (1955)
Z. Anal. Chem. **155,** 90 (1957)

Anna Schneer-Erdey
Kornélia Kozmutza
Budapest VIII., Múzeum-krt. 6—8.

Acta Chimica Academiae Scientiarum Hungaricae, Tomus 69 (1), pp. 15—17 (1971)

PREPARATION AND UNIT CELL DIMENSIONS OF LEAD APATITES

(SHORT COMMUNICATION)

VIJAY MOHAN BHATNAGAR*

(Department of Chemistry, University of New Brunswick, Fredericton, Canada)

Received September 2, 1970

The apatites are a group of inorganic compounds which can be represented by the general formula $X_{10}(YO_4)_6Z_2$ where X = Al, Ba, Ca, Cd, Mg, Mn, Sr, and Pb; Y = As, P, S, Si, and V; Z = Cl, Br, F, and OH. They have a hexagonal structure with space group $P6_3/m$. From the general formula it follows that the unit cell of an apatite has 42 sites. In the complete apatite, 10 of these sites are occupied by X atoms, 6 by Y atoms, 24 by oxygen atoms, and 2 by Z atoms. In all the apatites reported so far it is presumably necessary for the X and Z sites to be occupied. However, WONDRATSCHEK [1] and BHATNAGAR [2] have described a series of lead apatites which range from those in which the Z site is fully occupied to those where this site is partially or completely vacant. These 'vacant' or 'non-stoichiometric' apatites also satisfy the condition for electroneutrality, *i.e.* the sum of all the ionic charges is equal to zero. It seems that some of the ions of these apatites are replaced or substituted by ions that have different charges. Evidently, the electroneutrality is obtained only if some of the former halogen sites remain unoccupied. One example is $[Pb_4^{2+}K^{1+}](PO_4)_3^{3-}$.

We have recently studied a number of mineralogical and synthetic lead apatites where the Z sites are completely occupied, partially or completely empty. We wish to report here on several lead apatites which have been synthesized in our laboratory. Only one 'non-stoichiometric' lead apatite is reported here. This is a commercial sample of lead phosphate from the Matheson, Coleman, and Bell Company. A sample purified in 1962 was listed in the chemical catalogue as $Pb_3(PO_4)_2$ but no formula or molecular weight appeared on the label. The X-ray pattern was that of a 'vacant' apatite and the major peaks in the infrared spectra were: 530 vs, 542 sho., 572 vs ($\nu_4PO_4^{3-}$), 960 to 1055 vs, br ($\nu_3PO_4^{3-}$). The analysis of this compound given by BLOOD [3] is Pb = 73.5, PO_4 = 21.8, Pb/P = 1.54. The calculated analyses for $Pb^3(PO_4)_2$

* This work was carried out at Faculté des Sciences de Toulouse, École Nationale Supérieure de Chimie, 38 rue des 36 Ponts, Toulouse, France

and $Pb_{10}(PO_4)_6(OH)_2$, respectively, are: Pb = 76.7, PO_4 = 23.3, Pb/P = 1.50, and Pb = 77.4, PO_4 = 21.3, Pb/P = 1.67. The powder diffraction pattern shows that this water-stable compound has the apatite structure.

Lead hydroxyapatite, $Pb_{10}(PO_4)_6(OH)_2$: The apatite was prepared by dropwise addition of Na_2HPO_4 (3.6 g/150 ml) to a continuously stirred solution of $Pb(CH_3COO)_2$ (7.5 g/250 ml) at 100 °C. The mixture was stirred for about 24 hours, then filtered, washed with distilled water and dried at about 100 °C. The unit cell dimensions are: a = 9.88 Å, c = 7.42 Å, c/a = 0.751.

Lead hydroxyapatite, $Pb_{10}(PO_4)_6(OH)_2$: Na_2HPO_4 (4.25 g/300 ml) and NaOH (0.40 g/100 ml) were mixed and added dropwise with constant stirring to a $Pb(CH_3COO)_2$ solution (16.26 g/300 ml) at about 100 °C. The stirring was continued for about 2 hours. The product was filtered, washed with distilled water and dried at 100 °C. The X-ray results of this apatite are: a = 9.88 Å, c = 7.41 Å, c/a = 0.750.

Lead fluorapatite, $Pb_{10}(PO_4)_6F_2$: A solution of Na_2HPO_4 (5.76 g/200 ml) and NaF (1.00 g/200 ml) was added dropwise with stirring to a solution of $Pb(CH_3COO)_2$ in distilled water (2.56 g/200 ml). The temperature of the reaction was held at 100 °C. The reaction soon set in and the stirring was continued for about 7 hours. The lead fluorapatite formed was removed by filtration and washed with several portions of distilled water. The product was dried at 100 °C. The cell parameters are: a = 9.77 Å, c = 7.27 Å, c/a = 0.744.

Lead fluorapatite, $Pb_{10}(PO_4)_6F_2$: K_2HPO_4 (1.80 g/100 ml) and NaF (0.14 g/50 ml) were mixed and added slowly — dropwise — to a stirred solution of 5.40 g of $Pb(CH_3COO)_2$ in 100 ml of distilled water. The reacting mixture was kept at about 100 °C and stirred for about 3 hours. The milky white compound was filtered, washed with distilled water and dried at 100 °C. The X-ray powder pattern was that of an apatite. The unit cell dimensions are: a = 9.77 Å, c = 7.30 Å, c/a = 0.747.

Lead fluorapatite, $Pb_{10}(PO_4)_6F_2$: Ammonium solutions [$(NH_4)_2HPO_4$, 3.96 g/250 ml, NH_4F, 0.37 g/100 ml] were mixed together and added dropwise to a lead acetate solution, 16.26 g/250 ml, at room temperature (23 °C). The mixture was stirred for about 2 hours, and the product was filtered, washed with distilled water and dried at about 100 °C. The lengths of the a and c axes are: a = 9.78 Å, c = 7.30 Å, c/a = 0.746.

Lead fluorapatite, $Pb_{10}(PO_4)_6F_2$: A solution (2.56 g/200 ml) of lead acetate was added dropwise to a solution of PbF_2 (1.75 g/200 ml) and Na_2HPO_4 (5.76 g/200 ml) at about 100 °C. The reacting mixture was stirred for about 4 hours, filtered, washed with distilled water and dried at 100 °C. The unit cell dimensions are: a = 9.76 Å, c = 7.25 Å, c/a = 0.742.

Lead phosphate, $Pb_3(PO_4)_2$: This was a commercial sample as described earlier. The unit cell dimensions of the specimen were found to be: a = 9.81 Å, c = 7.25 Å, c/a = 0.739. This may be a defect lead hydroxyapatite.

Lead chlorapatite, $Pb_{10}(PO_4)_6Cl_2$: A solution of $(NH_4)_2HPO_4$ (3.96 g/100 ml) was mixed with a solution of NH_4Cl (0.53 g/100 ml). The ammonium solutions were then added dropwise to a continuously stirred solution of $Pb(CH_3COO)_2$ (16.26 g/300 ml) at about 100 °C. The stirring was continued for about 4 hours then the solution was filtered, washed with distilled water, and dried at 100 °C. The cell parameters are: $a = 9.99$ Å, $c = 7.34$ Å, $c/a = 0.734$.

Lead chlorapatite, $Pb_{10}(PO_4)_6Cl_2$: A 1 : 1 mixture of $Pb_9(PO_4)_6$ [2] and $PbCl_2$ was thoroughly ground in an agate mortar as acetone slurry. The mixture was carefully transferred to a platinum tube and slowly heated to 400 °C. Then the materials were thoroughly reground and refired at the sintering temperature. The whole process took about 1 hour. The unit cell dimensions are: $a = 9.97$ Å, $c = 7.32$ Å, $c/a = 0.734$.

Lead bromapatite, $Pb_{10}(PO_4)_6Br_2$: Stoichiometric amounts of $PbBr_2$ and $Pb_9(PO_4)_6$ were thoroughly mixed in an agate mortar for about half an hour and heated in a platinum tube at about 250 °C for 5 hours. The lengths of a and c axes are: $a = 10.05$ Å, $c = 7.33$ Å, $c/a = 0.729$.

Lead-sodium apatite, $Pb_8Na_2(PO_4)_6$: This compound was prepared by a slight variation of the method described by RATHJE [4]. The solutions of KH_2PO_4 (4.08 g/300 ml) and NaOH (2.40 g/200 ml) were mixed together and added dropwise to a stirred solution of $Pb(CH_3COO)_2$ (13.01 g/300 ml) at about 100 °C. The reacting mixture was stirred for about 24 hours, filtered, washed with distilled water, and dried at 100 °C. The unit cell dimensions are: a 9.77 Å, $c = 7.24$ Å, $c/a = 0.741$.

Mixed fluor-chlorapatite of lead, $Pb_{10}(PO_4)_6(F, Cl)_2$: The solutions of NH_4Cl (0.27 g/100 ml) and NH_4F (0.19 g/100 ml) were mixed together, then this solution and a solution of $(NH_4)_2HPO_4$ (3.96 g/300 ml) were taken in two separate containers (separating funnels) and added dropwise to a lead acetate solution (16.26 g/300 ml) at about 100 °C. The reacting mixture was stirred for about 24 hours, filtered, washed with distilled water and dried at 100 °C. The cell parameters are: $a = 9.92$ Å, $c = 7.34$ Å, $c/a = 0.739$.

*

This work was supported by the Office National de l'Azote (France). I am grateful to Prof. G. MONTEL for helpful discussions and interest in lead apatite investigation.

REFERENCES

1. WONDRATSCHEK, H.: N. Jb. Miner. Abh. **99**, 113 (1963)
2. BHATNAGAR, V. M.: Arch. Oral. Biol. (London) **15**, 469 (1970)
3. BLOOD, F. H.: Ph. D. Thesis, Indiana Univ. (1963)
4. RATHJE, W.: Ber. deutsch. chem. Ges. **74**, 357 (1941)

VIJAY MOHAN BHATNAGAR; Iroquois Chemicals Limited, P. O. Box 399, Cornwall, Ontario, Canada.

Acta Chimica Academiae Scientiarum Hungaricae, Tomus 69 (1), pp. 19—34 (1971)

EXPERIMENTAL STUDY OF POSITIVE ION EMISSION FROM TUNGSTEN, II*

O. KAPOSI and M. RIEDEL

(Department of Physical Chemistry and Radiology, L. Eötvös University, Budapest)

Received December 2, 1969

A study was made of the temperature dependence of the ion emission of tungsten wires prepared with various additives. Two maxima were found on the emission curves. It was concluded from the values of the activation energies calculated from the curves that the first maximum is caused by desorption of the surface alkali metal impurities, while the reason for the renewed increase in ion emission above 2000 °K is the increased grain boundary diffusion due to recrystallization of the tungsten. During annealing of thermally treated, recrystallized tungsten, an ion current was obtained which was smaller by an order of magnitude than the previous ones, and the temperature dependence of the emission was also different. In this case transient maxima were observed in the regions of 1800 and 2100 °K; measurements showed that these are caused by anion emission increasing effect of the residual gases. As a result of the further elevation of temperature, at above 2500 °K the ion current again increases with temperature. On the basis of the value of the ion emission activation energy (ca. 120 Kcal·mole^{-1}), this phenomenon points to the volume diffusion of the alkali metals.

Introduction

From a comparison of our earlier experiments [1—3] with other results of tungsten research, the mechanism on the spontaneous thermal ion emission of tungsten can be interpreted in its main outlines. Recent results support our concepts concerning the processes involved in ion emission, and also permit the interpretation of emission phenomena (transient emission peaks of thermally treated filaments [2, 3]) for which the previous experimental data were not sufficient. At the same time the present results are new proof that emission experiments form an important part of research into the 'life' within the metal of foreign material traces which decisively determine the properties of tungsten.

Traces of foreign materials have long been known to play an important role in the formation of a crystal structure which meets the high requirements set for tungsten (used for vacuum technical purposes) [4, 5]. However, it is still not known how these additives are arranged in the tungsten, how they behave during thermal treatment, or how they regulate the recrystallization of tungsten. We approach these problems in a different manner from the

* O. KAPOSI, M. RIEDEL: Experimental Study of PositiveIon Emission from Tungsten, I. Acta Chim. Acad. Sci. Hung., 61, 349 (1969)

previous routes, with ion emission studies, hoping that our results together with those of other metallurgical studies will bring nearer an understanding of the phenomena and will contribute with new points of view to the elucidation of the problems.

The new results of our emission experiments carried out with the above objectives are reported under the following headings:

1. Study of the correlation between the recrystallization of tungsten and ion emission.

2. Dependence of ion emission on the gas pressure.

3. Determination of the activation energies of processes involved in the emission.

The experimental techniques reported earlier [1—3, 6] were used for the measurements. We are indebted to the Tungsram Corp. for the tungsten samples used in the experiments.

Experimental

1. *Effect of the recrystallization of tungsten on ion emission*

When not-recrystallized GK filaments [7] were heated at not too high a rate to 2650 °K (*i.e.* over the operating temperature of the filaments of incandescent lamps), two more or less well distinct maxima were observed [1, 3] on the curves describing the variation of ion emission. The position of the second maximum for this type of filament corresponded to a good approximation with the temperature interval of the secondary recrystallization [8]. At the same time, second maximum did not appear on the emission curves during the heating of tungsten single crystals [2, 3]. It was concluded [2, 3] from these phenomena that the increased ion emission taking place in the recrystallization interval caused by substantial crystallite-boundary and dislocation motion results in a faster movement of foreign materials than in boundary diffusion. The occurrence of this process has also been pointed out experimentally by MILLNER *et al.* [7] on other models. Since the secondary recrystallization is the last phase which determines the ultimate technical properties of tungsten metal used for vacuum technical purposes, and since our knowledge regarding the chemical and physical causes of the relation of impurities and recrystallization is still very deficient, it appears worthwhile from this aspect too to study the ion emission of tungsten in detail.

It seems expedient to supplement our earlier emission measurements with experiments in which wires prepared with other additives are used, these recrystallizing at different temperatures than GK tungsten. At the same time, it is necessary in the interest of the verification of the relation presumed

between the rate of recrystallization and ion emission to study the variation of ion emission in time during the heating at different rates of wires of different diameters.

For the experiments the following samples were used: GK and UC helical tungsten filaments (diam. 30 μ), GK and UC wires and the same free of additives (diam. 80 μ) as well as sections of GK wires consisting of single crystals. GK tungsten is prepared with Na, K, Si and Al-containing additives, whilst in the UC product the Al-containing additive is absent [7]. Secondary recrystallization takes place in additive-free tungsten, UC tungsten and GK tungsten at about 1800 °K, 2100 °K and 2500 °K, respectively. In so far as our earlier supposition is correct, it is necessary in the case of various tungsten wires for the second maximum of the emission curves to appear roughly in the neighbourhood of these temperature values.

It is to be expected that the two maxima observed in the time-course of ion emission can only be distinguished if the heating is sufficiently slow and the processes producing them may be separated in time, and if the heating period is sufficient for the individual processes of emission to take place in succession. Since the greater the driving force, *i.e.* the number of dislocations, the greater is the recrystallization rate at the same temperature, this has the result that the rate of recrystallization (by which we mean the combined rate of nucleation and crystal growth) of thinner wires, subjected to more operations and hence containing more dislocations [5], is greater than that of thicker wires of the same quality. Therefore, it was expected that with thinner wires and with filaments subjected to more operations (drawing, whirling and so on) it would be possible to observe the appearance of the second maximum during heating at a higher rate too, if the time-resolution of the spectrometer is sufficiently high (filming at a suitable speed). Therefore, with rapid heating, when the filmaent temperature was increased by 8833 °K/s, the filming rate was 50 frames/s; with slower heating, the rate was 5 frames/s. With medium, slow or very slow heating rates the sample was heated in 331, 132 or 44 °K/s, respectively.

With rapid heating, a single sharp maximum was obtained on the emission curve, independently of the quality or thickness of the filament (Fig. 2 in Ref. [1] and Fig. 3 in Ref. [3]). During the heating of tungsten single crystals the ion emission varied with the temperature according to a curve of essentially the same form; in addition to 'ion eruptions' causing a jagged nature of the emission curves, the ion intensity was found to decrease exponentially after an initial maximum (Fig. 11 in Ref. [3]). If, however, not-recrystallized filaments of an identical thickness to that of the former (prepared from 30 μ wire) were heated to 2700 °K within the same time (331 °K/s), the emission curves obtained with the majority of samples were of a different form from those of the single crystals (Figs 1 and 2).

From Figs 1 and 2 it may be seen that in accordance with expectations based on our earlier experiments, with both the GK filaments and the UC filaments prepared with additives of various composition, after an initial emission maximum, during the continuous increase of temperature, the ion current decreases temporarily and then again increases. (In the Figs throughout this work the ion currents are displayed on an arbitrary but identical scale.) In our opinion the initiai large emission maximum is caused by alkali metals desorbing from the surface. The value of the ion-emission activation energy measured in this temperature interval supports this assumption (section 3). The cause of the second increase in ion emission observed after the temporary decrease may be either a change in surface ionization or, according to our earlier supposition [2, 3], the grain boundary diffusion increasing due to recrystallization.

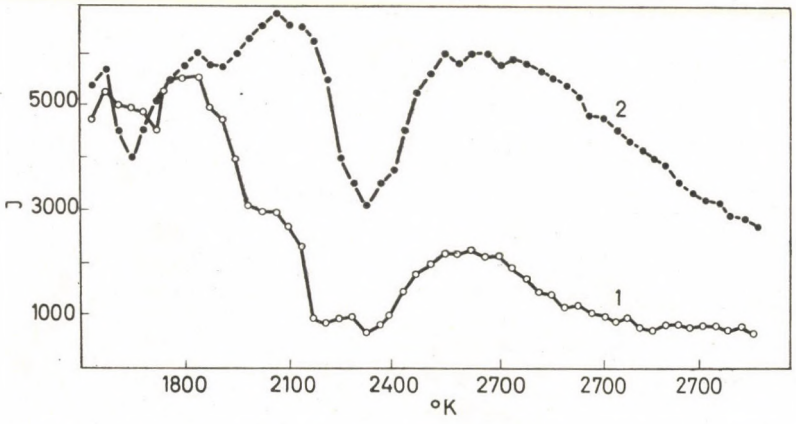


Fig. 1. Variation of ion emission from filaments prepared from 30 μ GK wire, as a function of temperature at a medium heating rate (331 °K/s). (Curves 1 and 2 refer to Na^+ and K^+, respectively.)

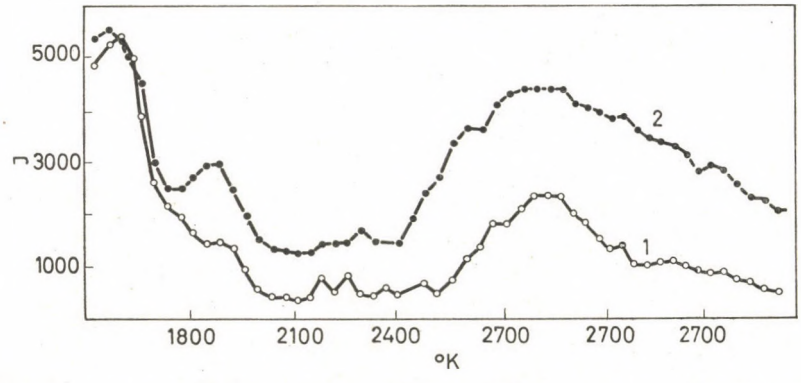


Fig. 2. Temperature dependence of the ion emission of a filament prepared from 30 μ diameter UC wire, at a medium heating rate (331 °K/s)

On the basis of the ion-emission activation energy values calculated from the increasing branch of the emission curves after the minimum, we regard as more essential the ion-emission increasing effect of grain boundary diffusion which is enhanced as a result of recrystallization. With UC and GK wires, the activation energy values for K^+ are about 100 Kcal · $mole^{-1}$, which is of the same order of magnitude as the normal value of the activation energy of grain boundary diffusion (*cf.* section 3 of this paper). At the same time, this value is close to the activation energy of crystal growth during recrystallization

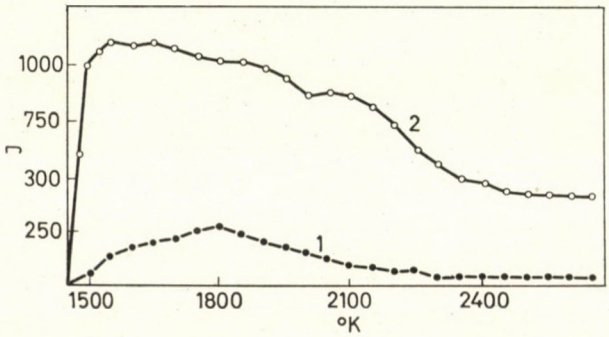


Fig. 3. Temperature dependence of the ion emission of additive-free, 80 μ diameter tungsten wire. Heating time: 1 min (44 °K/s)

determined by MILLNER *et al.* [8]. From this the conclusion may be drawn that in this temperature interval (2000—2500 °K) the process which affects ion emission to a decisive extent is recrystallization. This idea is supported by the shape of the ion-emission curve observed on heating tungsten wires which are additive-free and hence recrystallize at a different temperature (Fig. 3).

It may be seen from Fig. 3 that on heating additive-free tungsten, the repeated substantial increase of ion emission found with UC and GK filaments is not observed. It is known [4, 5] that the secondary recrystallization of additive-free tungsten wires takes place at such a low temperature compared with the GK and UC wires that the first desorption peak conceals the possible increase of ion emission. Because of the sudden removal of surface heterogeneities and impurity nuclei near the surface, the randomly appearing smaller peaks produced by 'ion eruptions' on the 'basic curve' (drawn with broken lines in Figs 4 and 5) superimpose; these make it more difficult to recognize and separate the effects systematically appearing in ion emission.

With thicker filaments, the processes affecting ion intensity to a large extent in the case of slow heating may be found to be separate from each other. As can be seen in Figs 4 and 5, when 80 μ diameter wires are heated for one minute (44 °K/s), in certain cases, despite the numerous smaller peaks, the already mentioned characteristic shape of the curve is also well discernible.

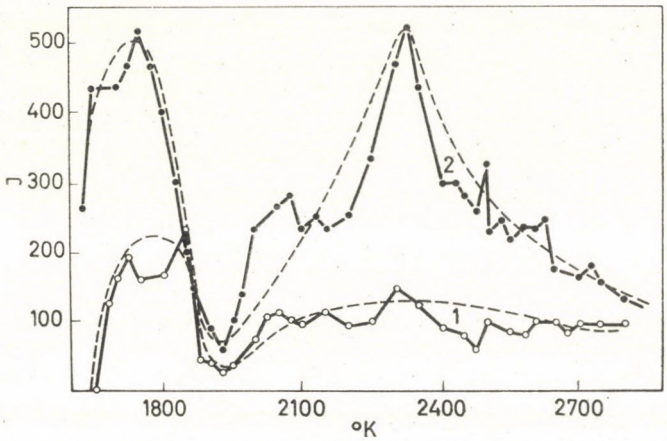


Fig. 4. Variation of the ion emission of 80 μ diameter GK wire in the case of 1 minute heating (44 °K/s)

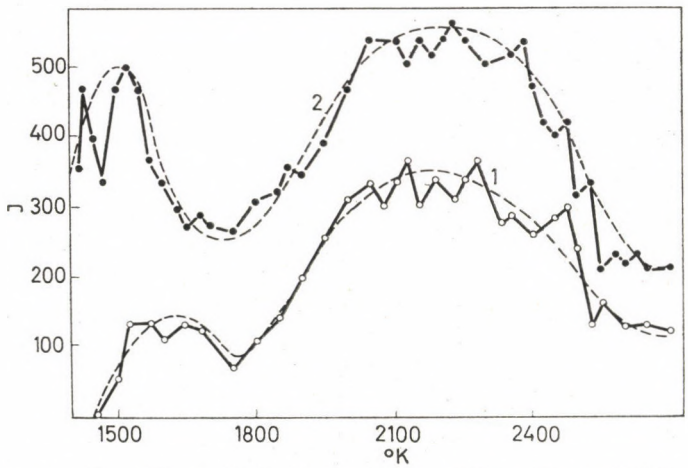


Fig. 5. Temperature dependence of the ion emission of 80 μ diameter GK wire with the application of 1 minute heating (44 °K/s)

From a comparison of Figs 4 and 5 it appears that at times it may also be gathered from the emission curves that the second maximum, attributed to the effect of secondary recrystallization, is, as expected, at a higher temperature for the GK wires than for the UC wires.

The experimentel results obtained on heating at different rates are in agreement with other data [8]. This proves that the rates of recrystallization of UC and GK wires are essentially the same. In other respects, it may be concluded from the shape of the emission curves found for wires of various thicknesses that the recrystallization of the thinner and coiled (and hence containing more dislocations) wires takes place in a shorter time than that of

less-worked thicker wires. From these conclusions it may be seen, that the study of the ion emission of tungsten wires prepared with various additives provides important data relating to the movement of alkali metals during recrystallization.

2. *Dependence of ion emission on the gas pressure*

The dependence of ion emission on the gas pressure was measured at various air and oxygen pressures in order to determine the cause of the appearance of the transient emission maxima found [1, 3] with thermally treated filaments. Heating was applied for one minute in which time the desired gas pressure, constant during the time of the experiment, was produced in the ion source, using the gas-introduction system shown in Fig. 6.

During the heating time the numbers of K^+ and Na^+ ion eruptions were counted continuously and separately, by means of the gating circuit shown in Fig. 7, and a GAMMA NK 109 single-channel energy-selective counter.

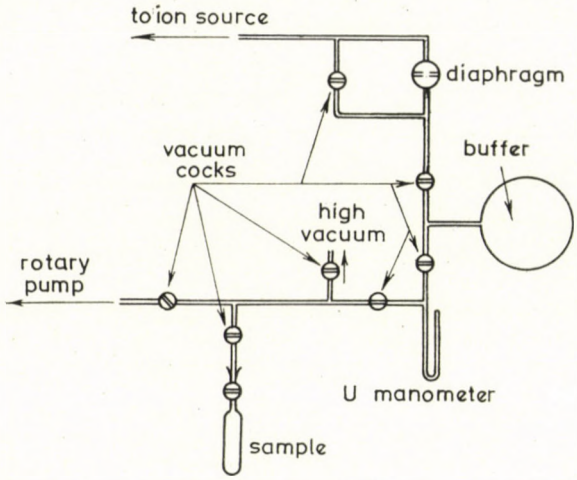


Fig. 6. The gas-introduction system of the mass spectrometer

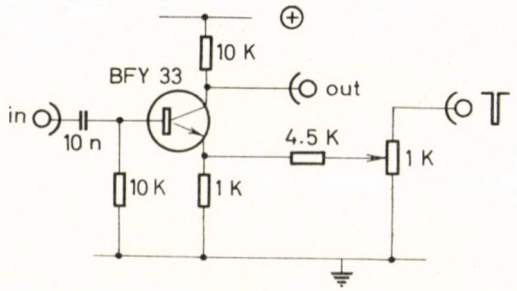


Fig. 7. Schematic diagram of the gating circuit

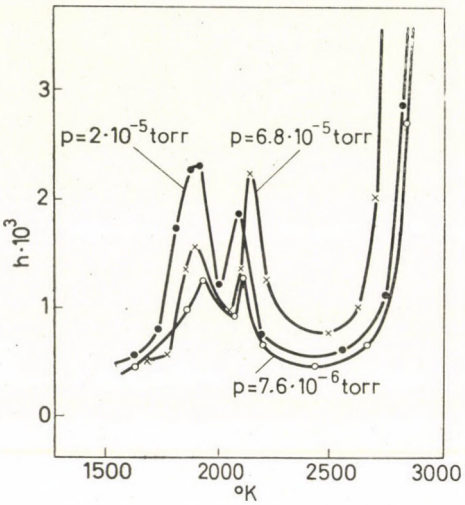


Fig. 8. Variation of the number of K^+ ion eruptions per second as a function of temperature for different air pressures

The decatron read-out of the analyzer was filmed at a rate of 5 frames/s. The numbers of glowing bulbs were read off from the individual film frames and hence the numbers of ion eruptions per second were obtained for the individual temperatures. A GK filament thermally treated at 2700 °K for one hour was used with each type of gas, and since the ion emission of the treated filaments changes only very slowly with time [3], the relative ion emission values pertaining to the different gas pressures can be compared. The experimental results are shown in Figs 8 and 9.

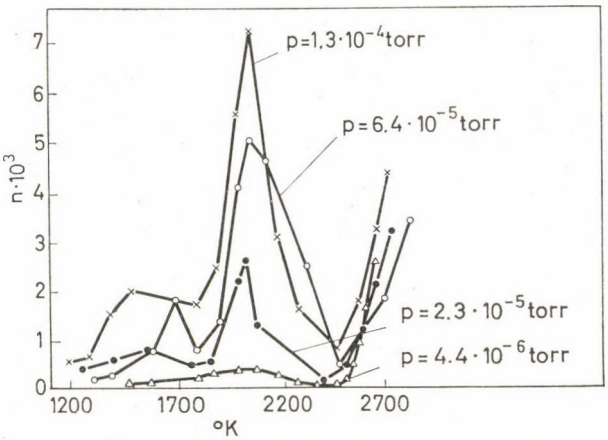


Fig. 9. Change of the number of K^+ ion eruptions per second as a function of temperature for different oxygen pressures

From Figs 8 and 9 it may be seen that in the cases of air and especially of oxygen the transient ion emission increases strongly with increase of the gas pressure and, in contrast to the earlier experimental results [1, 3] at higher pressures two emission maxima can be distinguished. A similar phenomenon was observed in the case of the ion current of Na^+ too. These experimental facts mean that in the temperature interval 1500—2400 °K the residual gases are in interaction with the tungsten, and as a result, a considerable alkali metal ion emission occurs. Two types of ion-emission increasing effects may be considered: 1. the ionization efficiency increases as a result of the interaction; 2. the number of alkali metal atoms arriving at the surface from within the metal increases suddenly.

The adsorbed residual gases (nitrogen and hydrogen, as well as carbon monoxide and carbon dioxide formed at high temperature from the carbon content of tungsten [10]) increase the work function of tungsten [11, 12], and as a consequence, the ionization efficiency increases in a manner given by the SAHA-LANGMUIR equation. From this point of view oxygen is particularly important; according to measurements it increases the work function by 1.9 eV [13]. Since the rate of oxygen chemisorption in the case of constant gas pressure shows a maximum in the temperature interval of transient emission maxima [14—19], the significant increase in ion emission due to the ionization efficiency may be understood. Depending on the temperature and oxygen coverage, tungsten oxides of various composition are formed; they evaporate from the surface and at a given oxygen pressure there is an equilibrium between chemisorption and desorption [16]. The concentration of desorption products measured in the gas phase is a maximum in the transient ion-emission temperature interval [14—16]; this results, because of the evaporation of tungsten in the form of oxides (according to other authors too [21—24]), in a considerable increase of ion emission because of the increasing diffusion of alkali metal atoms and at times even of the direct opening of impurity pockets. Understandably, in agreement with Figs 8 and 9, the two effects mentioned cause the greater ion emission increase the greater the coverage, that is, the background gas, and the oxygen pressure.

The oxide film formed as a result of chemisorption evaporates in the form of tungsten oxides (WO_2, WO_3, W_2O_6, W_3O_9), and also as atomic oxygen at higher temperatures. Differences may be observed between the data of individual authors relating to the composition of the desorbing products and to the temperature pertaining to the maximum concentrations of the individual products measured in the gas phases. In the literature data it is found in common that the most important components of tungsten evaporation, in part causing the increase of ion emission, are WO_3 and WO_2. According to the measurements [16], the formation of WO_3 and of WO_2 shows maxima at 1800 °K and 2200 °K, respectively; these coincide approximately with the

two transient emission maxima observed by us. The maximum formation rates of WO_3 and WO_2 are displaced towards lower temperatures with the increase of the oxygen pressure [16, 20]; this effect may be observed to a greater extent in the case of WO_3. Thus those suppositions are not unfounded that the two peaks of the transient emission (Figs 8 and 9) come about because of the tungsten evaporation corresponding to the formation and evaporation maxima of WO_3 and WO_2, and that with the increase of oxygen pressure not only does the separation of the two peaks become more pronounced but with pure oxygen (Fig. 9) the individual peaks are at somewhat lower temperatures than in the case of air as the background gas (Fig. 8). For a more accurate interpretation of the separation of the two maxima of transient emission there would be a need for the simultaneous analysis of spontaneous alkali metal emission and of other desorption products.

Everything considered, in our view the effect increasing the extent of ionization of the background gases causes the intense transient ion emission, and this is also contributed to by the fact that the number of alkali metal atoms coming out from the bulk of the filament in unit increases because of the evaporation taking place in the form of tungsten oxides.

3. *Determination of the activation energies of processes involved in the ion emission*

The temperature dependence of the thermal ion emission of tungsten suggests that the ion emission is composed by different parallel by-processes. The magnitude of the activation energies necessary for the individual by-processes may give an important basis to the physico-chemical characterization of the relevant process and to its mechanism.

The first maximum of the emission curve obtained on heating untreated filaments is explained by the desorption of alkali metals chemisorbed on the surface. If this is indeed so, then the activation energy calculated for the process must agree with the alkali ion desorption activation energy. The calculation is performed according to the following considerations.

The intensity of the ion current is proportional to the desorption rate constant (k) and to the surface alkali concentration (Θ):

$$I(\Theta) = A \cdot k \cdot \Theta \tag{1}$$

The surface alkali concentration decreases exponentially with time:

$$\Theta(t) = \Theta_0 \cdot \exp(-kt) \tag{2}$$

The rate constant is known to depend on the temperature as follows:

$$k(T) = B \cdot \exp\left(-\frac{E_d}{RT}\right) \tag{3}$$

In Eq. (3) E_d is the ion desorption activation energy and B is a constant.

From Eqs (1), (2) and (3):

$$I(t, T) = A \cdot B \cdot \exp\left(-\frac{E_d}{RT}\right) \cdot \Theta_0 \cdot \exp\left\{-B \cdot t \cdot \exp\left(-\frac{E_d}{RT}\right)\right\} \tag{4}$$

Eq. (4) gives the variation of ion emission as a function of time and temperature, and so the value of E_d may be calculated from the emission curve describing the maximum.

The complicated solution of the transcendent equation may be simplified if the initial, rising section of the emission curve is taken into consideration, assuming that the initial concentration undergoes but slight changes and thus it can be approximated by one constant:

$$\Theta(t) = C$$

Hence, from Eq. (4) we have:

$$I(t, T) = A \cdot B \cdot C \cdot \exp\left(-\frac{E_d}{RT}\right) \tag{5}$$

and taking logarithms we obtain the following expression:

$$\lg I = K_1 - K_2 \frac{1}{T} \tag{6}$$

Plotting lg I as a function of $1/T$ we obtain from the slope of $1/T$ the activation energy of the ion emission, *i.e.*:

$$E_d = 2.3\ R \cdot K_2 \tag{7}$$

With the aim of the experimental determination, on this basis, of the emission activation energy during the initial heating, the tungsten wire was heated for one minute and the spectrum was filmed with a rate of 96 frames/s. The change of ion emission with temperature during the initial part of the heating is shown in Fig. 10.

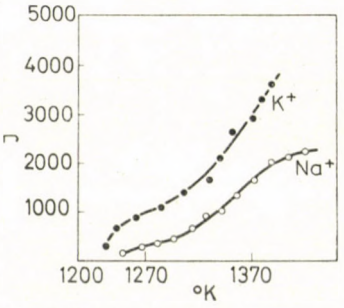


Fig. 10. Variation of the Na^+ and K^+ ion emissions of an untreated wire during the initial part of the heating

With the aim of comparing the literature and our own data, and of verifying the simplifying assumption used in the derivation, the activation energy for Cs^+ ion emission was also determined, in such a way that CsCl was placed on the surface of previously annealed tungsten and the temperature dependence of the Cs^+ ion emission was measured on heating (Fig. 11).

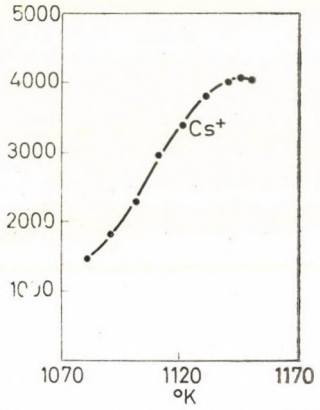


Fig. 11. Temperature dependence of Cs^+ ion emission on the surface of tungsten wire during the initial part of heating

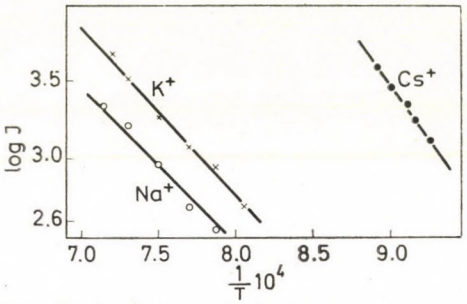


Fig. 12. Logarithm of the ion current as a function of the reciprocal of the absolute temperature

If the logarithm of the ion current is plotted as a function of the reciprocal of the absolute temperature, straight lines of different slopes are obtained for Na^+, K^+ and Cs^+ (Fig. 12).

Table I contains the desorption activation energy values calculated from the slopes according to Eq. (7), and the heats of adsorption found in the literature.

Considering that the chemisorption of alkali metals on tungsten is not an activated process, then according to the known relation $E_d = E_a - \Delta H_a$ [29], the desorption activation energy is equal to the value of the heat of adsorption, *i. e.* $E_d = \Delta H_a$. The activation energies (E_d) determined by us and the adsorp-

Table I

Desorption activation energies (E_d) and the measured and calculated heats of adsorption (ΔH_a) of alkali metals on tungsten taken from the literature

System	E_d (Kcal · mole^{-1}) measured in this work	ΔH_a (Kcal · mole^{-1}) literature	
		measured	calculated
Na—W	43.8	32.0 [25]	28.5 [28]
		63.0 [26]	
K—W	48.5	58.0 [26]	46.7 [28]
Cs—W	50.8	68.0 [27]	65.5 [28]

tion heat data (ΔH_a) found in the literature do agree approximately, although our data are systematically a little smaller than the literature values. The literature values of ΔH_a are given for $\Theta = 0$ in the Table. It is known that with increasing coverage (Θ), both E_d [30] and ΔH_a [31, 32] decrease. In our spontaneous ion emission measurements, however, the large ion current measured at the beginning of the heating is attributed to a certain degree of coverage of the surface, and this accounts for the difference in Table I. Thus, this experimental result is new proof of our earlier finding that the first maximum observed on heating the not annealed filaments is caused primarily by the alkali metal impurities desorbed from the surface, and in this temperature interval the alkali metals diffusing to the surface from within the filament play only a small role; this process requires an appreciably higher activation energy.

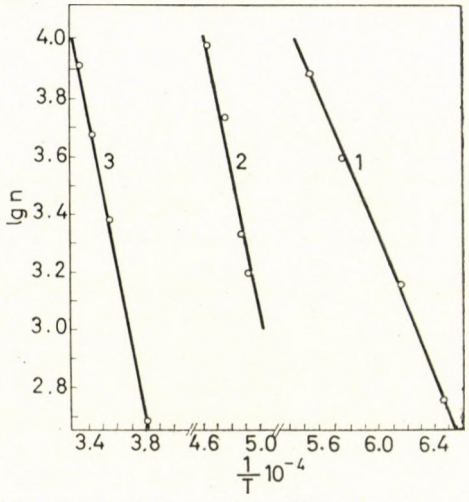


Fig. 13. Variation of the logarithm of the number of K^+ ion eruptions per second measured in different temperature intervals as a function of the reciprocal of the absolute temperature

The activation energy was also determined in the case of thermally treated filaments, the preliminary annealing of which had already removed the alkali metal layer adsorbed on the surface.

According to Figs 8 and 9, in the case of thermally treated filaments with a sufficiently high background gas pressure, after two emission maxima the ion current increases monotonously with the absolute temperature. If the number of ion eruptions per second on the three rising portions of the emission curve, for an air pressure of $6 \cdot 10^{-6}$ torr, is plotted as a function of the reciprocal of the absolute temperature, three lines of different slopes are obtained (Fig. 13).

The activation energy for K^+ ion emission was calculated from the slopes of the individual graphs using the SAHA-LANGMUIR equation [12]. The results are shown in Table II.

Table II

Activation energies for K^+ ion emission (E_i) measured in different temperature intervals

Temp. interval (°K)	E_i (eV · atom^{-1})	E_i (Kcal · mole^{-1})
1600—1800	2.4	55.4
2000—2200	4.8	110.7
2600—2900	5.4	124.6

Calculating from the ion current brought about by all the ions in the temperature interval 2700—3200 °K, HEGEDÜS *et al.* [24] obtained an emission activation energy of 7.54 eV · atom^{-1} (174 Kcal · mole^{-1}). According to them, this high value is caused by the W^+ ions present in large amount. RUETH and LICHTMANN [23] obtained a value of 3.3 eV · atom^{-1} (76 Kcal · mole^{-1}) for the activation energy of K^+ emission in the temperature interval 2200—2500 °K; according to them, this value is indicative of bulk diffusion. In contrast with this, on the basis of our results ion emission takes place according to different mechanisms in the individual temperature intervals. At lower temperatures (1600—2200 °K) the effect of high diffusivity paths requiring a lower activation energy (dislocations, grain boundaries) asserts itself; the magnitude of the ion current is determined by the surface phenomena acting from time to time to various extents (formation of tungsten oxides, adsorption and desorption of various gases). The experimental fact that at lower temperatures the activation energy values measured in parallel at various gas pressures are subject to some fluctuation may be explained by the strong heterogeneity of the tungsten surface. In contrast to this, at higher temperatures (above 2500 °K) a value of 120 Kcal · mole^{-1} was obtained to a good approximation for the ion emission activation energy in every case. This value agrees with the activation energy value obtained by DANNEBERG [33] for the self-diffusion of tungsten, takes place by a vacancy mechanism. It is known [34, 35] that in the case of very dilute alloys the activation energy of the diffusion of the metal present in low concentration is identical, to a good approximation, with the activation energy of the self-diffusion of the base metal. Since in the present case the condition of very low concentration obtains (according to the measurements of MILLNER *et al.* [8], the sintered GK bar contains 0.005% K), from the agreement of the activation energies it is possible to conclude on the potassium diffusion occurring by a lattice mechanism. At the same time, at such a high temperature the tungsten surface has already become clean, and hence the work function depends only on the temperature. For this reason the good agreement of the parallel emission activation energy data obtained at high temperature can be understood.

From the magnitude of the activation energies of the ion emission processes, an important conclusion may be drawn as to the arrangement and movement within the metal of foreign material traces in tungsten. The activation energy values obtained from a study of the temperature dependence of ion emission permit the conclusion, in agreement with the view of other authors [7, 8, 36, 37], that a part of the potassium, namely, those involved in the tungsten lattice, are present in an atom dispersed state. At the same time, however, according to the values measured for lower temperature intervals, a considerable proportion of the ions emitted originates from the atoms desorbing from the surface of the wire and diffusing out from the grain boundaries and crystal defects. The increase of emission observed during recrystallization also verifies the significance of grain boundary diffusion.

Our present diffusion experiments, in which the diffusion coefficients of the alkali metals in tungsten are determined by ion emission measurements at different temperatures, will serve to check these findings. The magnitude of the diffusion coefficients and their temperature dependence will allow even firmer conclusions as to the arrangement and movement of additives in tungsten.

REFERENCES

1. Kaposi, O., Riedel, M., Matus, L.: Magy. Kém. Foly., **74,** 429 (1968)
2. Kaposi, O., Riedel, M., Sztaniszláv, D.: Magy. Kém. Foly. **75,** 324 (1969)
3. Kaposi, O., Riedel, M.: Acta Chim. Acad. Sci. Hung. **61,** 349 (1969)
4. Neugebauer, J., Kerényi L.: Tungsten and Molybdenum Metal Bodies, Wires and Filaments (in Hungarian), No. 1, KGM, MTTI, Budapest, 1965
5. Rieck, G. D.: Tungsten and its Compounds, Pergamon Press, Oxford, 1967
6. Kaposi, O., Riedel, M., Törő, F.: Mérés és Automatika, **XVIII,** 177 (1969)
7. Millner, T.: MTA Műsz. Tud. Oszt. Közl. **34,** 55 (1964)
8. Millner, T.: MTA Műsz. Tud. Oszt. Közl. **XXI,** 349 (1957)
9. Neugebauer, J., Kerényi, L.: Properties, Production and Study of Tungsten (in Hungarian), Budapest, 1964
10. Young, J. R.: J. Appl. Phys. **30,** 1671 (1959)
11. Moesta, H.: Chemisorption und Ionisation in Metall-Metall Systemen. Springer Verlag, Berlin, 1968
12. Kaminsky, M.: Atomic and Ionic Impact Phenomena on Metal Surfaces. Springer Verlag, Berlin, 1965
13. Gomer, R., Hulm, J. K.: J. Chem. Phys. **27,** 1363 (1957)
14. Esinger, J.: J. Chem. Phys. **30,** 412 (1959)
15. Becker, J. A., Becker, E. J., Brandes, R. G.: J. Appl. Phys. **32,** 411 (1961)
16. Berkowitz-Mattuck, J. B., Büchler, A., Engelke, J. L., Goldstein, S. N.: J. Chem. Phys. **39,** 2722 (1963)
17. Singleton, J. H.: J. Chem. Phys. **45,** 2819 (1966)
18. Ptushinskii, Yu. G., Chuikov, B. A.: Surf. Sci. **6,** 42 (1967)
19. McCaroll, B.: J. Chem. Phys. **46,** 863 (1967)
20. Bartlett, R. W.: Transactions of the Metallurgical Society of AIME, **230,** 1097 (1964)
21. Minturn, R. E., Datz, S., Taylor, S. H.: J. Appl. Phys. **31,** 876 (1960)
22. Winters, H. F., Denison, D. R., Bills, D. G., Donaldson, E. E.: J. Appl. Phys. **34,** 1810 (1963)
23. Rueth, W. R., Lichtmann, D.: Surf. Sci. **12,** 96 (1968)
24. Hegedüs, J. A., Horváth, A., Kerek, L., Kürthy, J.: Magy. Kém. Foly. **74,** 218 (1968)
25. Bosworth, R. C. L.: Proc. Roy. Soc. (London) **A 162,** 32 (1937)
26. Starodubtsev, S. V.: J. exper. theor. Physics (USSR), **19,** 215 (1949)

27. TAYLOR, J., LANGMUIR, I.: Phys. Rev. **44**, 423 (1933)
28. HIGUSCHI, I., REE, T., EYRING, J.: J. Amer. Chem. Soc. **77**, 4969 (1955)
29. SZABÓ, Z.: Contact catalysis. Part II, FEJES P.: Adsorption, pp. 143—274 (in Hungarian). Akadémiai Kiadó, Budapest, 1966
30. SCHMIDT, L., GOMER, R.: J. Chem. Phys. **42**, 3573 (1965)
31. LANGMUIR, I.: J. Amer. Chem. Soc. **54**, 2798 (1932)
32. HIGUSCHI, I.: J. Amer. Chem. Soc. **79**, 1330 (1957)
33. DANNEBERG, W.: Metall, **15**, 977 (1961)
34. v. LIEMPT, J. A. M.: Rec. Trav. Chim. **64**, 239 (1945)
35. ZENER, C.: J. Appl. Phys. **22**, 372 (1951)
36. MANNERKOSKI, M.: J. Institute of Metals, **88**, 397 (1959—60)
37. MANNERKOSKI, M.: Acta Metallurgica, **10**, 982 (1962)

Olivér KAPOSI
Miklós RIEDEL
Budapest VIII., Puskin u. 11—13.

Acta Chimica Academiae Scientiarum Hungaricae, Tomus 69 (1), pp. 35—41 (1971)

INVESTIGATION OF ADSORPTION PHENOMENA ON PLATINIZED Pt ELECTRODES BY TRACER METHODS, IX

MEASUREMENT OF ADSORPTION ON PLATINUM POWDER

GY. HORÁNYI, E. M. RIZMAYER and F. NAGY

(Central Research Institute for Chemistry of the Hungarian Academy of Sciences, Budapest)

Received January 8, 1970

A method was elaborated for the study of the potential dependence of adsorption on Pt powder with the use of a tracer technique.

The reliability of the method was studied by means of the adsorption of hydrochloric acid labelled with ^{36}Cl.

In one group of adsorption measurements carried out with a tracer technique the adsorption is determined directly by the measurement of the activity originating from the adsorption phase [1]. The adsorption phase cannot usually be isolated from the liquid or gas phase in equilibrium with it without disturbing the equilibrium, and so, whatever may be the measurement set-up, the radiation due to the adsorption phase and its environment are observed simultaneously. One of the basic problems of the evaluation is the separation of these two quantities. As is easily seen, the accuracy and reliability of the measurements depend strongly on the ratio of the quantities mentioned. A decisive point in the practical performance of the measurements is whether the intensity of the radiation originating from the environment (I_e) can be neglected compared to the intensity of the radiation due to the adsorption phase (I_a), or whether it can be determined by measurement and calculation.

The essence of an earlier reported method can be understood on the basis of Fig. 1 [2].

The adsorbed substance of specific activity I_0 in concentration c in a medium of density ϱ_0 is situated above the plane l containing the adsorbent. The amount adsorbed per cm^2 is denoted by Γ and the detector by D.

In this measurement set-up it is possible to control the ratio of I_a and I_e by the magnitude of the roughness factor of the adsorption surface. To a first approximation the relation

$$I_t = \alpha I_0 \left(\frac{c}{\mu \varrho_0} + \gamma \Gamma \right) \tag{1}$$

may be considered valid for the intensity of radiation arriving from a 1 cm^2 surface (if the extent of the phase in the direction of x is greater than the range

of radiation). α is a proportionality factor, γ the roughness factor, and μ the mass absorption coefficient of the radiation. It follows from Eq. (1) that

$$I_e = \alpha I_0 \frac{c}{\mu \varrho_0}$$
$$I_a = \alpha I_0 \gamma \Gamma \tag{2}$$

The magnitude of γ was controlled by the platinization of a thin gold layer condensed on plane *l*. However, it must be kept in view that a large-scale increase of the roughness factor can only be achieved with the modification of the structure of the adsorbent, and with the increase of the quantity of adsorbent on a 1 cm^2 geometrical surface in the case of an adsorbent of a given structure. Under such conditions Eq. (1) may no longer be valid.

Let us consider the layer of platinum black as a granular aggregation. The studied system can be imagined as is shown in Fig. 2.

The system outlined in Fig. 2 consists of two parts: a disperse system of thickness k and a homogeneous system of thickness K.

Let us denote the density of the dispersed material by ϱ_m, that of the dispersion medium, similarly to the foregoing, by ϱ_0, the average density of the whole system by $\bar{\varrho}$, and the porosity of the system by ε ($0 \leq \varepsilon \leq 1$).

The intensity of radiation measurable on the surface q can be calculated on the basis of the following considerations.

In a volume element $q \cdot \mathrm{d}x$ of the layer, there is a volume of solution $\varepsilon \cdot q \cdot \mathrm{d}x$, in which the amount of adsorptive is $c \cdot \varepsilon \cdot q \cdot \mathrm{d}x$. In the volume element under consideration, the amount of adsorbed material is $(1 - \varepsilon)\varrho_m a_s q \cdot \Gamma \cdot \mathrm{d}x$ on an adsorbent of mass $(1 - \varepsilon)\varrho_m q \cdot \mathrm{d}x$ and of specific surface a_s. The intensity of radiation arriving into the detector from the volume element $q \cdot \mathrm{d}x$ located at site x is

$$\mathrm{d}I_s = \alpha I_0 [\varepsilon \cdot c + (1 - \varepsilon)\varrho_m a_s \Gamma] e^{-\mu \bar{\varrho} x} \cdot q \cdot \mathrm{d}x \tag{3}$$

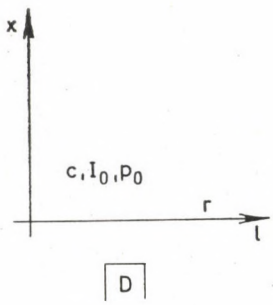


Fig. 1

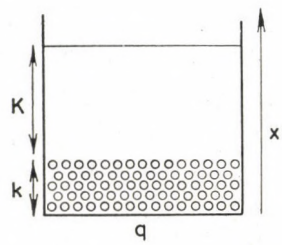


Fig. 2

Hence, after integration, the intensity of radiation arriving from the layer of thickness k is given by the relation

$$I_s = \frac{\alpha q I_0}{\mu\bar{\varrho}} [\varepsilon \cdot c + (1 - \varepsilon)\, \varrho_m\, a_s\, \Gamma] \,(1 - e^{-\mu\bar{\varrho}k}) \tag{4}$$

At the same time the intensity of the radiation arriving into the detector from the liquid layer of thickness K is

$$I'_e = \frac{\alpha q I_0 c}{\mu\varrho_0} (1 - e^{-\mu\varrho_0 K})\, e^{-\mu\bar{\varrho}k} \tag{5}$$

For the total intensity, we have from Eqs (4) and (5) the relation

$$I'_t = \frac{\alpha q I_0}{\mu} \left\{ c \left[\frac{\varepsilon}{\bar{\varrho}} \left(1 - e^{-\mu\bar{\varrho}k}\right) + \frac{1}{\varrho_0} (1 - e^{-\mu\varrho_0 K})\, e^{-\mu\bar{\varrho}k} \right] + \right.$$
$$\left. + \frac{\varrho_m}{\bar{\varrho}} (1 - \varepsilon)\, a_s \Gamma (1 - e^{-\mu\bar{\varrho}k}) \right\} \tag{6}$$

If a soft β-emitting isotope is used for the tracing and the thickness of the liquid layer is greater than the range of the radiation studied, then $\varrho_0 \mu K \gg$ $\gg 1$ and thus $1 - e^{-\mu\varrho_0 K} \approx 1$. Considering this, Eq. (6) assumes the form

$$I'_t = \frac{\alpha q I_0}{\mu\bar{\varrho}} \left\{ c \left[\varepsilon + \left(\frac{\bar{\varrho}}{\varrho_0} - \varepsilon \right) e^{-\mu\bar{\varrho}k} \right] + \varrho_m (1 - \varepsilon) a_s \Gamma (1 - e^{-\mu\bar{\varrho}k}) \right\} \tag{7}$$

From Eq. (7) it can be seen that with increasing thickness k of the layer of Pt-black, the measured intensity I becomes independent of the layer thickness, *i.e.* in the case of the fulfilment of the condition $\mu\bar{\varrho}k \gg 1$

$$I = \frac{\alpha q I_0}{\mu\bar{\varrho}} \varepsilon \left(c + \frac{1 - \varepsilon}{\varepsilon} \varrho_m a_s \Gamma \right) \tag{8}$$

Accordingly, the intensity arising from the adsorption on a geometrical surface q is

$$I'_a = \frac{\alpha q I_0 (1 - \varepsilon)}{\mu\bar{\varrho}} \varrho_m a_s \Gamma \tag{9}$$

while the intensity originating from the medium surrounding the granules is

$$I'_e = \frac{\alpha q I_0}{\mu\bar{\varrho}} \varepsilon \cdot c \tag{10}$$

It can be seen from Eq. (10) that the radiation originating from the environment will be much less than in the case given by Eq. (2), that is $\bar{\varrho} > \varrho_0$ and $\varepsilon < 1$. At the same time it can be shown that in the case of not too strong

coating, Eq. (1) can be considered valid. With the conditions $\mu\bar{\varrho}k \ll 1$ and $e^{-\mu\bar{\varrho}k} \sim 1 - \mu\bar{\varrho}k$, one obtains

$$I = \frac{\alpha q I_0}{\mu}\left\{\frac{c}{\varrho_0}\left[1 - \left(1 - \varepsilon\frac{\varrho_0}{\bar{\varrho}}\right)\mu\bar{\varrho}k\right] + (1-\varepsilon)\frac{\varrho_m}{\bar{\varrho}} a_s \Gamma \mu\bar{\varrho}k\right\} \quad (11)$$

since $\bar{\varrho} > \varrho_0$ and $0 \leqslant \varepsilon \leqslant 1$, thus $1 - \varepsilon\frac{\varrho_0}{\bar{\varrho}} < 1$, therefore, from Eq. (11) we obtain the relation

$$I = \alpha q I_0\left[\frac{c}{\mu\varrho_0} + (1-\varepsilon)\varrho_m a_s \Gamma k\right] \quad (12)$$

The amount of adsorbent $m = (1-\varepsilon)\varrho_m q k$. With a consideration of this, Eq. (12) can be written in the following form

$$I = \alpha q I_0\left[\frac{c}{\mu\varrho_0} + \frac{1}{q} m a_s \Gamma\right] \quad (13)$$

The total surface of Pt-black is ma_s, thus the roughness factor relating to surface q is given by $\gamma = \frac{ma_s}{q}$. Considering this, we obtain the relation

$$I = \alpha q I_0\left[\frac{c}{\mu\varrho_0} + \gamma\Gamma\right] \quad (14)$$

After division by q, Eq. (14) is identical with Eq. (1) and so the validity of of the latter equation can be considered verified in the case of not too strong coating.

The extension of the measurement method to Pt powders

On the basis of what has been written in the preceding part we must come to the conclusion that our method elaborated earlier can be used for the study of adsorption on a metal powder, and so also on Pt powder. In this case the high roughness factor was ensured not by platinization but by the scattering of a Pt-black on the surface. It can easily be seen that with the use of powder in the region of validity of Eqs (14) and (15) it is convenient working with a relatively large layer thickness. (It must be noted that in the case of a ^{14}C tracer and Pt powder the 'large' layer thickness amounts to only a few times 10^{-3} cm.)

For the proof of the usability of the measurement method the adsorption of hydrochloric acid labelled with ^{36}Cl was studied. The experimental set-up was exactly the same as that given in reference [2].

A sketch of the cell is shown in Fig. 3. The apparatus was charged with 1 N $HClO_4$, and the solution adjusted to a few times 10^{-3} M with ^{36}Cl-labelled hydrochloric acid of a specific activity of 0.1 mCi/mmole.

The dependence of the count rate on the mass of Pt powder taken was examined at 700 mV. The results are shown in Fig. 4.

As may be seen in the figure, with increasing amounts of the powder the intensity originating from the adsorption approaches a limiting value,

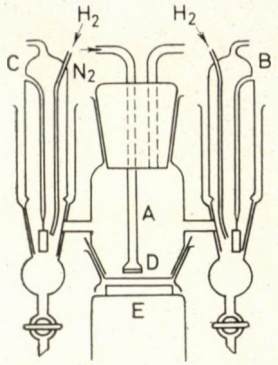


Fig. 3. A: cell compartment containing the studied solution, *B:* reference electrode, *C:* buxiliary electrode, *D:* gold-coated plastic foil, *E:* detector

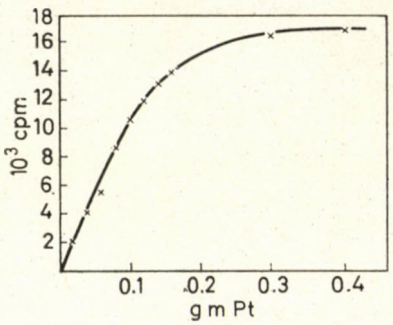


Fig. 4. Dependence of the count rate on the mass of Pt powder

in agreement with Eqs (8) and (9). The curve essentially demonstrates the self-absorption of β-radiation and fully agrees with the curve relating to the self-absorption of β-radiation found in the literature [3].

The extent of reproducibility of the results in the vicinity of the saturation value ($m > 0.3$ g) is an extremely important question.

Our results in this connection are given in Fig. 5.

The powder was stirred up at the times indicated by the arrows, stirring lasting for 1—2 minutes. After the stirring, as can be seen in the figure, exactly the same value was recovered, *i.e.* the measurement must be considered reproducible.

A few words must be said on the possibilities furnished by measurements on powder. If we consider $I_a = I_e$ as the worst case, then with a metal powder adsorbent ($\varrho_m \approx 10$ g $\cdot$ cm^{-3}; $a_s = 10^5$ cm^2 $\cdot$ g) the measurement of adsorption can also be realized for an adsorptive concentration of 10^{-1}—10^{-2} M in the case of values of $\Gamma \approx 10^{-10}$ cm^2, as follows from the relation $c = \dfrac{1-\varepsilon}{\varepsilon} \varrho_m a_s \Gamma$. $\left(\text{In the case of spherical granules } \dfrac{1-\varepsilon}{\varepsilon} \sim 1.\right)$ That is to say, adsorption can be measured up to substantially higher concentrations than in the case of thin layer platinization. In addition to this, the very large advantage of the measurements with powder is in relation to the reproducibility.

Platinization is commonly known to be of poor reproducibility and it is rare that two almost identical electrodes can successfully be produced. Dur-

ing measurements with electrodes the electrode deteriorates and so it is not possible to carry out several kinds of study with the same electrode. On the other hand, enough platinum powder can be prepared on one occasion to suffice for numerous experiments. If the time between experiments is not too

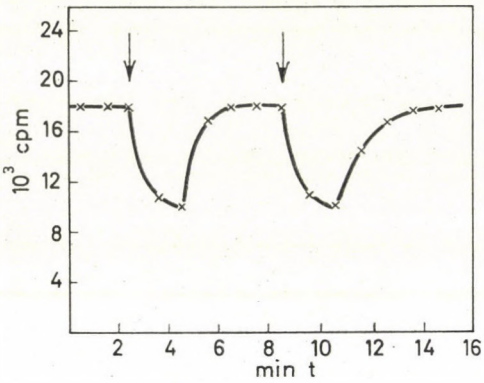


Fig. 5. Effect of stirring-up of the powder on the count rate

long, all portions of the powder from this preparation are completely equivalent.

From an electrochemical point of view there is no theoretical difference between a gold layer coated with platinum powder and a platinized electrode. The potential of the electrode can be adjusted without any particular difficulty. The capacity of the powder for hydrogen adsorption, as reported earlier [4], is easily determined and with the help of this the electrode and the powder can be compared.

In Fig. 6 we illustrate the equivalence of measurements on powder and on an electrode in the case of the potential dependence of the adsorption of chloride ions.

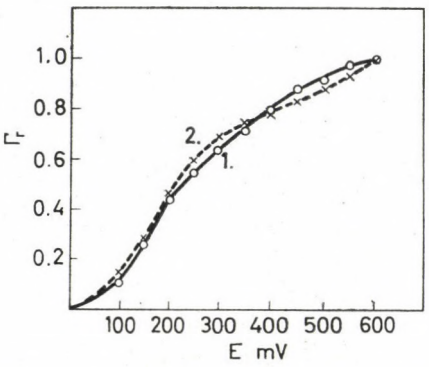


Fig. 6. Dependence of Γ_r on the potential in the case of (1) powder and (2) electrode

The values of Γ_r determined on 0.3 g of platinum powder and on a platinized electrode for a hydrochloric acid concentration of $3 \cdot 10^{-3}$ M are given in Fig. 6 as a function of the potential. The values of Γ_r were obtained by dividing the count rate relating to the individual potentials by the count rate relating to 600 mV (as we showed earlier [5], the Γ_r value is almost independent of concentration).

On the basis of this figure we may consider the agreement satisfactory.

Naturally, the reported method appears applicable to other adsorbents too, and it is absolutely unnecessary to use any electrochemical system.

It must be added of course that it is necessary to ensure that no significant change occurs in the concentration of the solution during adsorption on the powder. The method is particularly well applicable when, with a given amount of adsorbent, the change of concentration in the solution is so small that it is no longer possible to determine the adsorption from it.

REFERENCES

1. B. B. DAMASKIN *et al.*: Adsorbtsiya organicheskih soedinenii na elektrodah. Nauka, 1968, Moscow
2. SOLT, J., HORÁNYI, GY., NAGY, F.: Magy. Kém. Foly. **73,** 414 (1967)
3. M. HAISSINSKY: Nuclear chemistry and its uses (in Hungarian). Akadémiai Kiadó, 1963
4. CSERHEGYI, A., HORÁNYI, GY., NAGY, F.: Magy. Kém. Foly. **69,** 246 (1963)
5. SOLT, J., HORÁNYI, GY., NAGY, F.: Magy. Kém. Foly. **76,** 636 (1970)

György HORÁNYI
Edit M. RIZMAYER
Ferenc NAGY
Budapest II., Pusztaszeri út 57—69.

Acta Chimica Academiae Scientiarum Hungaricae. Tomus 69 (1), pp. 43—48 (1971)

STRUKTURUMWANDLUNGEN DES SILIKATNETZWERKES IM LAUFE DER AUSBILDUNG DER OBERFLÄCHENSCHICHT BEI NATRIUMOXIDHALTIGEN GLÄSERN

S. Dobos

(Forschungsgruppe für Anorganische Chemie der Ungarischen Akademie der Wissenschaften, Budapest)

Eingegangen am 30. Januar 1970

Es wurde die in Wasser ausgebildete Oberflächenschicht eines Glases der Zusammensetzung 28 Na_2O—4 BaO—68 SiO_2 untersucht. Aus der Bestimmung der Konzentrationsverteilung der Natriumionen, der Bariumionen, des »Wasserstoffs«, der Wasserstoffionen und des Wassers innerhalb der Schicht wird festgestellt, daß die Struktur des Silikatnetzwerkes bei der Ausbildung der Schicht eine sprunghafte Änderung erleidet. Der Primärvorgang dieser Änderung ist die Spaltung von $\geq$Si—O—Si$\leq$ Bindungen, welche durch die im Netzwerk erscheinenden Wassermoleküle verursacht wird. Es wird weiterhin festgestellt, daß die Protonen nicht nur in Form von Hydroxoniumionen, sondern auch — der Wanderungsfront der Wassermoleküle vorangehend — über die Sauerstoffatome des Netzwerkes wandern. Innerhalb der Oberflächenschicht sind zwei Abschnitte nachweisbar, ein dichterer Teil, in dem überhaupt keine Wassermoleküle mit den Protonen zusammenwandern und ein lockererer Teil, in dem die Wasserkonzentration in Richtung zur Grenzfläche Schicht—Wasser ansteigt. An dieser Grenzfläche ist die Konzentration der Wassermoleküle beträchtlich, die Schicht ist stark gequollen.

In unserer vorangehenden Mitteilung [1] wurde die Meinung ausgedrückt, daß bei der Ausbildung der Oberflächenschicht von Silikatgläsern außer dem Ionenaustausch und der Ablösung des Silikatnetzwerkes im allgemeinen noch mit einem dritten Vorgang, namentlich mit der Strukturänderung des Silikatnetzwerkes gerechnet werden muß. Es wurde ein Typ der möglichen Strukturänderungen an Hand eines weichen, kaliumoxidhaltigen Glases diskutiert. In anderen Arbeiten [2], [3] behandelten wir die Oberflächenschicht von natriumoxidhaltigen Gläsern; es wurde die Konzentrationsverteilung in der Oberflächenschicht von Gläsern mit der Zusammensetzung 28 Na_2O—4 MeO—68SiO_2 (mit Me = Ca, Sr, Ba) bzw. 20 Na_2O—12SrO—68 SiO_2 bestimmt. Aufgrund der Konzentrationsverteilung wurde festgestellt, daß zwei charakteristische Abschnitte innerhalb der Oberflächenschicht unterscheidbar sind, deren Struktur vermutlich verschiedenartig ist. Die Struktur verändert sich scharf bei einer bestimmten Konzentration der Natriumionen. Die Ursache der Strukturänderung suchten wir in der abweichenden Größe der beiden am Ionenaustausch teilnehmenden Partner, des Natriumions und des Hydroxoniumions.

Das Ziel der vorliegenden Arbeit war die eingehendere Untersuchung der Oberflächenschicht bei natriumoxidhaltigen Gläsern, die Charakterisie-

rung der Schicht mit Hilfe von weiteren Parametern außer der Konzentrationsverteilung der Alkaliionen, aufgrund der mehrseitigen Untersuchung der Struktur und ihrer Änderungen.

Versuchsmodell

Da unser Ziel die Klärung und Deutung jener grundlegenden Erscheinungen war, welche bei der Ausbildung der Oberflächenschicht eine Rolle spielen, wurde — um die Zahl der Variablen herabzusetzen — auf die Untersuchung der Wirkung der Glaszusammensetzung und der Temperatur verzichtet, ebenso, wie auch in unserer vorangehenden Arbeit [1]. Aufgrund der Konzentrationsverteilung der Natriumionen zeigten die in [2] und [3] behandelten natriumoxidhaltigen Gläser ein ähnliches Verhalten der Oberflächenschicht, es konnte also mit Recht angenommen werden, daß die an der Ausbildung der Oberflächenschicht eine Rolle spielenden grundlegenden Erscheinungen nur quantitative Abweichungen aufweisen. Wir wählten deshalb eines der in den erwähnten Arbeiten untersuchten Gläser, dessen Einwaagezusammensetzung 28 Na_2O—4 BaO—68 SiO_2 war.

Das Glas wurde aus analytisch reinem Na_2CO_3 und $Ba(NO_3)_2$ sowie aus präcipitiertem SiO_2 (BDH) geschmolzen. Letzteres wurde vorangehend 3 Stunden bei 900 °C entwässert. Das Glas wurde bei 1350±50 °C mit achtstündigem Schmelzen hergestellt und für unsere Versuche in Form von Stäben (Länge 6—7 cm, Durchmesser 2—3 mm) verwendet.

Experimenteller Teil

Die Vorbereitung und die Lagerung in Wasser der Proben wurde auf die bereits beschriebene Weise [1—3] durchgeführt, mit dem Unterschied, daß das Wasser, in dem die Stäbe gelagert wurden, mit Tritium — genauer gesagt mit HTO — markiert war (Aktivität 5 mC/g). Die Temperatur der Schichtausbildung betrug 40±0,2 °C, ihre Dauer 120 Stunden. Die Oberflächenschicht wurde in 15 Schritten mit 1%iger Fluorwasserstoffsäurelösung stufenweise abgelöst.

Dieses Ablösen erfolgte bei 20±0,2 °C; die Dauer der ersten zehn Ablösungen betrug je 5 Minuten, die der letzten fünf je 10 Minuten; zum Ablösen der gesamten Schicht wurden also insgesamt 100 Minuten benötigt. Es wurden der Natrium-, Barium- und Silikationengehalt der einzelnen Schichtfraktionen [1—3], sowie — durch Messung der Aktivität der Lösung mit einem Flüssigkeitscintillationsspektrometer Packard Typ 3003 und Einbeziehen des bekannten Verhältnisses H/T in das zur Lagerung der Probe verwendete Wasser — der »Wasserstoffgehalt« der einzelnen Schichtfraktionen bestimmt. Da die Protonen in der Schicht in sämtlichen möglichen Fällen (H_2O, H_3O^+, $\geq$Si—OH) an Sauerstoff gebunden vorliegen und der Austausch Wasserstoff-Tritium bei derartigen Bindungen — der Literatur gemäß — von keinem Isotopeneffekt begleitet wird, ist zu erwarten, daß unsere Bestimmung allein den Fehler enthält, welcher auch die an der Schicht durchgeführten Bestimmungen charakterisiert.

Sämtliche angeführten Meßdaten sind Durchschnittswerte aus dreimal reproduzierten Werten.

Die Bezeichnung der aus den Meßdaten berechneten Werte ist wie folgt:

c_{Na^+} Natriumionenkonzentration in der Oberflächenschicht, bezogen auf das Netzwerk-Silicium (m_{Na^+}/m_{Si}).

c_H »Wasserstoff«-Konzentration in der Oberflächenschicht, bezogen auf das Netzwerk Silicium (m_H/m_{Si}).

c_{H_2O} Wasserkonzentration in der Oberflächenschicht, bezogen auf das Netzwerk-Silicium (m_{H_2O}/m_{Si}). Auf die Berechnung dieser Größe wird weiter unten eingegangen.

c_{H^+} Wasserstoffionenkonzentration in der Oberflächenschicht, bezogen auf das Netzwerk-Silicium (m_{H^+}/m_{Si}). Auf die Berechnung dieser Größe wird weiter unten eingegangen.

$v_{HF,Si}$ Ablösungsgeschwindigkeit der Schicht mit Fluorwasserstoff. Die Dimension dieser Größe ist Grammatom $Si \cdot cm^{-2}\ min^{-1}$ [1].

g anstelle der Tiefenkoordinate der Schicht benützte Netzwerk-Siliciumkoordinate. Dimension: Grammatom $Si \cdot cm^{-2}$ [1—3].

$\Delta c_{Na^+}/\Delta g$ Konzentrationsgradient der Natriumionen, d. h. das auf graphischem Wege erhaltene Differential der Konzentrationsverteilungskurve.

Es soll bemerkt werden, daß wir uns an dieser Stelle mit der Bariumionenverteilung — obwohl sie ebenfalls bestimmt wurde — nicht befassen, da unsere Messungen unsere früheren Feststellungen [2, 3] nur bestätigten, ohne sie zu erweitern.

Versuchsergebnisse

Um die Diskussion über die Oberflächenschicht zu erleichtern, schien es zweckmässig zu sein, die Veränderungen der verschiedenen Parameter innerhalb der Schicht in Abhängigkeit von der Siliciumkoordinate g in kompakter und leicht vergleichbarer Form darzustellen. Unter den in Abb. 1 und 2 dargestellten Größen wurden c_{Na^+}, c_H und $v_{HF,Si}$ unmittelbar aus den Meßdaten berechnet, $\Delta c_{Na^+}/\Delta g$ ist eine ohne Vernachlässigung berechnete, mittelbare Größe. c_{H_2O} und c_{H^+} dagegen wurden unter Annahme bestimmter Vernachlässigungen berechnet, haben folglich nur halbquantitative Bedeutung. Die Grundlage zur Berechnung dieser Größen war einerseits die »Wasserstoff«-Konzentration der Schicht (c_H). Wasserstoff kann in der Schicht in Form von $\geqslant$Si—OH, H_2O oder H_3O^+ zugegen sein. Die Menge der in die Schicht *eingewanderten* Protonen (wobei davon abgesehen werden soll, ob sie an Wasser gebunden einwandern oder nicht), ist mit der durch die Protonen ausgetauschten und aus der Schicht herausdiffundierten Natriumionenmenge identisch. Es kann also angenommen werden, daß die Protonenkonzentration c_{H^+} an einer bestimmten Stelle der Schicht gleich dem Unterschied zwischen der ursprünglichen und der aktuellen Natriumionenkonzentration ist:

$$c_{H^+} \cong c_{Na^+Glas} - c_{Na^+}.$$

Wird nun die auf diese Weise erhaltene Wasserstoffionenkonzentration aus dem Wert der »Wasserstoffkonzentration« der Schicht in Abzug gebracht, so kann die Differenz nur aus in Form von Wasser in die Schicht eingewandertem »Wasserstoff« bestehen. (Eine andere Frage ist freilich, ob das Wasser dort auch weiterhin in molekularer Form zugegen ist.) Die »Wasserkonzentration« kann also berechnet werden, indem die Differenz zwischen der »Wasserstoffkonzentration« und der »Wasserstoffionenkonzentration« durch 2 dividiert wird:

$$c_{H_2O} \cong \frac{c_H - c_{H^+}}{2}.$$

Diskussion der Ergebnisse

Kurve I in Abb. 1, welche die Natriumionenkonzentrationsverteilung in der Schicht darstellt, weist zwei deutlich verschiedene Strecken auf. Rechts von dem engen Gebiet, in dem der Bruch im Verlauf der Natriumionenkonzentration erfolgt, d. h. in Richtung zum kompakten Glas, steigt die Konzentration scharf an, bis zu dem im kompakten Glas gemessenen Wert. Links von

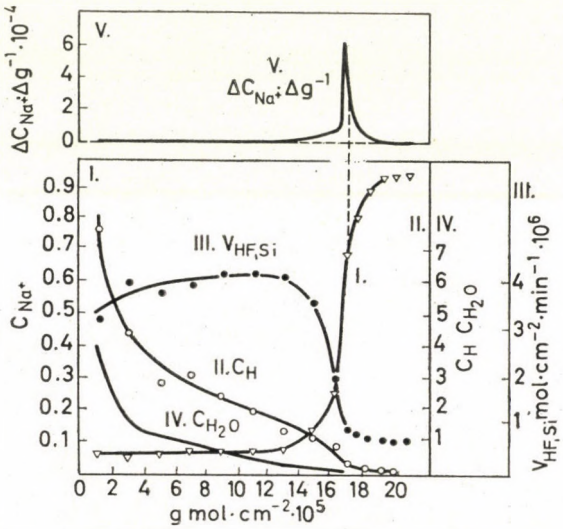


Abb. 1. Natriumkonzentration (I), Gradient der Natriumionenkonzentration (V), »Wasserstoffkonzentration« (II), Ablösungsgeschwindigkeit des Netzwerkes mit Fluorwasserstoffsäure (III) und Wasserkonzentration (IV) in Abhängigkeit von der mit dem Silikatgehalt der Schicht ausgedrückten Tiefenkoordinate

diesem Gebiet, in Richtung zur Wasserphase hin ist die Konzentration verhältnismäßig gering und ändert sich nur geringfügig; in der Nähe der Grenzfläche Schicht—Wasser ändert sich die Konzentration überhaupt nicht, der Konzentrationsgradient (Kurve V) ist gleich Null. Diese Strecke, in welcher auch ein geringer Konzentrationsgradient die Diffusion der Natriumionen aufrechterhalten kann, muß folglich eine lockerere, von der Struktur der Schicht in der Nähe des kompakten Glases wesentlich abweichende Struktur besitzen; diese Annahme wurde bereits in unseren früheren Arbeiten [2, 3] geäußert Die bezüglich der Ionendiffusion lockerere Struktur kann — wie in [1] an einem Beispiel gezeigt wurde — durch die spontane Umordnung des Silikatnetzes, durch die Spaltung von ≥Si—O—Si≤ Bindungen oder durch die Kombination beider Vorgänge erfolgen. Um zu entscheiden, welcher der beiden Vorgänge abläuft, bzw. welcher Vorgang als primär betrachtet werden soll, wurde die chemische Stabilität des Silikatnetzwerkes untersucht, indem die Verteilung der Geschwindigkeit der Ablösung der Schicht in Fluorwasser-

stoffsäure ($v_{HF,Si}$) in Abhängigkeit von der Koordinate g bestimmt wurde (Kurve III). Wie ersichtlich, ändert sich die Ablösungsgeschwindigkeit scharf an der Grenze der beiden Strecken der Schicht. In der dichteren Strecke weicht der Wert der Geschwindigkeit kaum von dem das kompakte Glas charakterisierenden Wert ab, während die Geschwindigkeit in dem lockereren Teil mehr als das Sechsfache beträgt. Eine derartige Zunahme der Geschwindigkeit der Ablösung kann nur damit erklärt werden, daß ein Teil der $\rangle$Si—O—Si$\langle$ Bindungen in diesem Teil der Schicht gespalten wird.

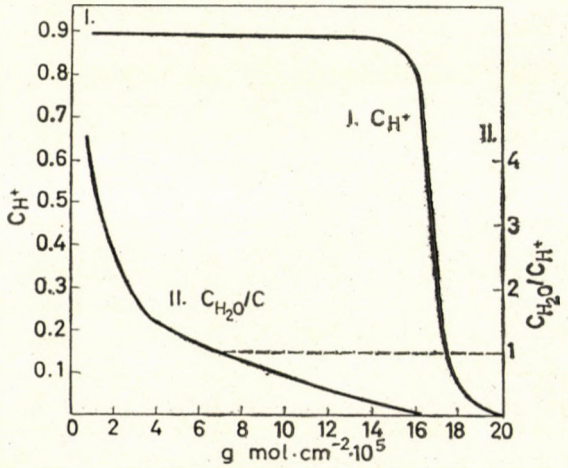


Abb. 2. Wasserstoffionenkonzentration (I) und Verhältnis der Wasserkonzentration zur Wasserstoffionenkonzentration (II) in Abhängigkeit von der mit dem Silikatgehalt der Schicht ausgedrückten Tiefenkoordinate

Die Ursache der Spaltung dieser Bindungen ist in den mit den Protonen zusammen wandernden Wassermolekülen zu suchen. Der Verlauf der Wasserkonzentrationsverteilung (Kurve IV) zeigt an, daß die Hydrolyse der $\rangle$Si—O—Si$\langle$ Bindungen mit dem Erscheinen der Wassermoleküle im Netzwerk zusammenfällt. Die Wanderungsfront der Wassermoleküle liegt an der Grenze der beiden Schichtstrecken, in der dichteren Schichtstrecke sind keine Wassermoleküle vorhanden. Der letztere Umstand scheint uns besonders interessant zu sein, da er im Gegensatz zu der bisherigen Auffassung steht, wonach die Protonen im Glas bei der Ausbildung der Oberflächenschicht in Form von Hydroxoniumionen an Wasser gebunden wandern. Gemäß unseren Feststellungen erfolgt der Protonentransport in dem dichteren Teil der Schicht ausschließlich unter Teilnahme der Sauerstoffatome des Silikatnetzwerkes und auch in einem wesentlichen Bruchteil der lockereren Schichtstrecke, von $g \simeq 7 \cdot 10^{-5}$ an liegt die Zahl der Wassermoleküle pro Proton unter 1 (Abb. 2, Kurve II).

Wie bereits aus dem Gesagten hervorgeht, ist die Struktur der »lockereren« Schichtstrecke keineswegs als einheitlich zu betrachten. Daß keine ein-

heitliche Struktur vorliegt, wird eigentlich bereits dadurch angezeigt, daß der Wert des Konzentrationsgradienten in der Nähe der Grenzfläche Schicht—Wasser gleich Null ist, da ja in einer unveränderten Struktur bei einem Konzentrationsgradienten von Null keine Diffusion erfolgt. Da jedoch die Diffusion auch in dieser Strecke verläuft, dürfte sich die Struktur parallel mit der Wasserkonzentration ändern und die Schicht in der Nähe der Grenzfläche Schicht—Wasser, wo 3—4 Wassermoleküle pro Siliciumatom vorhanden sind, stark gequollen sein. Hier hat es eingentlich keinen Sinn mehr, die Natriumionenkonzentration auf das Silicium des Netzwerkes zu beziehen. Es kann weiterhin angenommen werden, daß das Wasser in der Nähe der Grenzfläche in molekularer Form vorliegt, und daß die Natriumionen teilweise an diese Wassermoleküle gebunden, in hydratierter Form zugegen sind.

Zur Bestätigung der letzteren Annahme sollen in unserer nächsten Arbeit weitere Versuchsangaben veröffentlicht werden.

Endlich möchten wir erneut betonen, daß wir zwar den primären Grund für die Strukturänderung bei der Ausbildung der Oberflächenschicht in der hydrolytischen Spaltung der $\rightarrow$Si—O—Si$\leftarrow$ Bindungen sehen, jedoch keineswegs die Möglichkeit ausschließen, sondern es vielmehr für sehr wahrscheinlich halten, daß dieser Primärvorgang von einer Umordnung des Silikatnetzwerkes begleitet wird, bzw. daß eine Umordnung dem Primärvorgang folgt. Die Ablösungsgeschwindigkeit des Silikatnetzwerkes mit Fluorwasserstoff weist nämlich, obwohl die Schicht in Richtung zur äußeren Grenzfläche hin stets lockerer wird, keinen kontinuierlichen Anstieg auf, sondern nimmt nach einem flachen Maximum geringfügig ab.

Die Tatsache scheint auf eine, die Stabilität des Skeletts steigernde Umordnung hinzuweisen. Im Laufe dieser Umordnung kann eine Änderung in der Zahl der $\rightarrow$Si—O—Si$\leftarrow$ Bindungen auftreten, sie kann auch zunehmen, es kann also eine sekundäre Kondensation auftreten. Die an der Erscheinungsstelle des Wassers auftretende Strukturänderung wird durch die Hydrolyse wahrscheinlich nur eingeleitet; die angeführten Versuchsergebnisse sind jedoch nicht ausreichend, um die Natur der im weiteren verlaufenden Strukturänderungen bestimmen zu können. Auf diese Frage soll im späteren, in Verbindung mit der IR-spektroskopischen Untersuchung der Oberflächenschichten noch eingegangen werden.

LITERATUR

1. Dobos, S.: Acta Chim. Acad. Sci. Hung. **68**, 371 (1971)
2. Bouquet, G., Dobos, S., Boksay, Z.: Ann. Univ. Sci. Budapest, Sect. Chim. **6**, 5 (1964)
3. Boksay, Z., Bouquet, G., Dobos, S.: Physics and Chemistry of Glasses, **8**, 140 (1967)

Sándor Dobos; Budapest VIII., Múzeum-krt 6—8.

Acta Chimica Academiae Scientiarum Hungaricae, Tomus 69 (1), pp. 49—57 (1971)

DER BINDUNGSZUSTAND DER ALKALIIONEN IN DER OBERFLÄCHENSCHICHT VON NATRIUMOXIDHALTIGEN GLÄSERN

S. DOBOS

(Forschungsgruppe für Anorganische Chemie der Ungarischen Akademie der Wissenschaften Budapest)

Eingegangen am 30. Januar 1970

Es wurde die Verteilung der Alkaliionenkonzentration in der in Wasser, wäßriger Natriumchlorid- bzw. Lithiumchloridlösung ausgebildeten Oberflächenschicht eines Glases mit der Zusammensetzung 28 Na_2O—4 BaO—68 SiO_2 untersucht. Aus den Ergebnissen wurde gefolgert, daß der stark gequollene Teil der Oberflächenschicht mit hohem Wassergehalt eine mikroheterogene Struktur besitzt. In diesem Teil der Schicht diffundieren die Alkaliionen teilweise in den festen Mikrophasen an die $\rightarrow$Si—$\bar{O}$ Gruppen gebunden und teilweise in hydratiertem Zustand in den flüssigen Mikrophasen, welche molekulares Wasser enthalten. Weiterhin wird festgestellt, daß in Schichten, welche in neutralen Alkalichloridlösungen ausgebildet wurden, keine Chloridionen nachgewiesen werden können und daß zugleich die Geschwindigkeit der Ablösung des Netzwerkes ansteigt. Die Ursache dieser Erscheinung ist darin zu suchen, daß das Chloridion in neutralem (oder alkalischem) Medium die nukleophile Substitution am Siliciumatom katalysiert. Demzufolge führt sein Auftreten im Netzwerk unter solchen Bedingungen zu der völligen Zerstörung des Raumnetzes.

In unserer vorangehenden Arbeit [1] wurde bei der Diskussion der in Wasser ausgebildeten Oberflächenschicht von Glas der Zusammensetzung 28 Na_2O—4 BaO—68 SiO_2 festgestellt, daß in dem Teil der Schicht, der in der Nähe der Grenzfläche Schicht–Wasser liegt, der Gradient der Natriumionenkonzentration gleich Null ist und diese Konzentration, bezogen auf das Silicium des Netzwerkes, ziemlich hoch liegt ($\sim$0,065). Da in diesem Teil der Schicht auch die aufgrund des »Wasserstoffgehalts« berechnete Wasserkonzentration sehr hoch ist, nahmen wir die Gegenwart von molekularem Wasser und die teilweise Bindung der Natriumionen an diese Wassermoleküle, d. h. das Vorhandensein eines Teils der Natriumionen im hydratierten Zustand an.

In der vorliegenden Arbeit soll diese Annahme über den Bindungszustand der Alkaliionen nun untermauert werden.

Überlegungen

Die erste Bedingung für den hydratierten Zustand der Natriumionen ist die Gegenwart eines beträchtlichen Teils des in die Schicht eindiffundierten Wassers in molekularer Form. Wird bei der Ausbildung der Schicht mit der Spaltung von $\rightarrow$Si—O—Si$\leftarrow$ Bindungen des Silikatnetzwerkes gerechnet, so wird die Menge des molekularen Wassers durch diesen Vorgang herabgesetzt.

Es wurde gezeigt [1], daß die Hydrolyse bereits in Gegenwart von recht geringen Wassermengen erfolgt; die Geschwindigkeit der Ablösung des Silikat-Netzwerkes in Fluorwasserstoffsäurelösung nimmt in der Umgebung der Diffusionsfront des Wassers sprunghaft zu, steigt jedoch nicht parallel mit der weiteren Zunahme der Wasserkonzentration in Richtung zur Grenzfläche Schicht–Wasser an, sondern nimmt nach Durchlaufen eines flachen Maximums geringfügig ab (siehe Abb. 1, Kurve III in [1]). Diese Erscheinungen zeigen nicht an, daß die Hydrolyse nach der sprunghaften Veränderung beendet

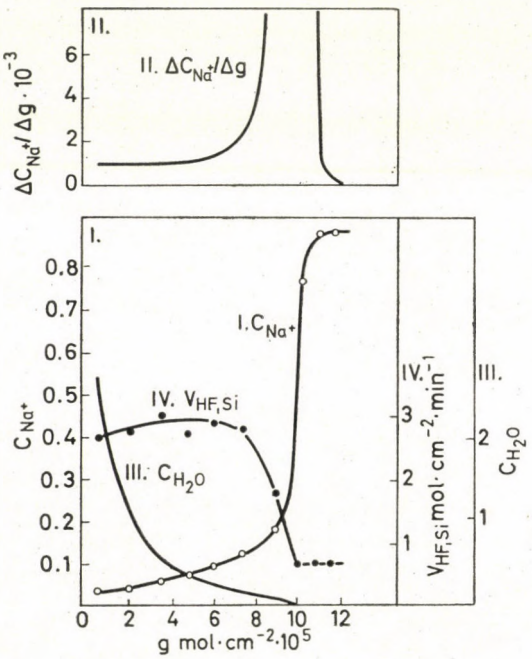


Abb. 1. Natriumionenkonzentration (I), Gradient der Natriumkonzentration (II), Wasserkonzentration (III) und Ablösungsgeschwindigkeit des Netzwerkes in Fluorwasserstoffsäure (IV) in Abhängigkeit von der mit dem Silikatgehalt der Schicht ausgedrückten Tiefenkoordinate der Schicht bei calciumoxidhaltigem Glas

wäre, sondern der Verlauf der Lösungsgeschwindigkeitskurve widerspiegelt wahrscheinlich den Einfluß einer Umordnung des Silikatnetzwerkes. Wird jedoch in Betracht gezogen, daß bei dem geprüften Modell bereits im kompakten Glas 0,64 kettenendständige Sauerstoffatome und in der Nähe Grenzfläche Schicht–Wasser 3—4 Wassermoleküle pro Siliciumatom vorliegen, so ist eine fortgeschrittene Hydrolyse, d. h. das Abreagieren eines wesentlichen Teiles der Wassermenge schlechthin unmöglich, da ein derartiger Vorgang zur völligen Zerstörung der Raumnetzstruktur führen würde.

Die Gegenwart von molekularem Wasser in der Netzwerkstruktur der Schicht ist noch kein genügender Grund zur Annahme, daß Alkaliionen im

hydratierten Zustand zugegen wären. Es muß außerdem angenommen werden, daß bei der Lockerung der Schicht im Laufe der Strukturänderung die Bildung von flüssigen Mikrophasen ermöglicht wird, in denen für mehr Wassermoleküle Platz vorhanden ist. Die Bildung derartiger Mikrophasen ist durch die partielle Hydrolyse der $\rightarrow$Si—O—Si$\leftarrow$ Bindungen allein nicht gesichert, sondern erst durch die Umordnung des Netzes nach der Hydrolyse, letzten Endes also durch die Bildung einer mikroheterogenen Struktur. Aus diesen Hypothesen ergibt sich ein vollständigeres Bild über den Mechanismus der in der Schicht erfolgenden »Quellung«.

Aufgrund der Annahme einer mikroheterogenen Struktur können sich die Alkaliionen teils in der festen Mikrophase an das Netzwerk, teils in der flüssigen Mikrophase an Wassermoleküle gebunden, in hydratiertem Zustand bewegen. An der Grenzfläche der beiden Mikrophasen kann ein Ionenaustausch-»Gleichgewicht« herrschen. Der Rücktritt der Natriumionen in die feste Mikrophase ist durch ihren hydratierten Zustand erschwert, demzufolge ist der Ionenaustausch zugunsten des Austritts der Natriumionen aus dem Netzwerk verschoben.

Das im vorangehenden skizzierte Bild gibt Aufschluß darüber, daß die Möglichkeit besteht, daß der Konzentrationsgradient der Natriumionen, bezogen auf das Netzwerk-Silicium, in der Nähe der Grenzfläche Schicht–Wasser gleich Null ist. Daß wir bei unserem Modell einen Gradientenwert von Null erhalten hatten, kann als günstiger Zufall betrachtet werden: es ergab sich dadurch ein Widerspruch, der letzten Endes zu der Formulierung des beschriebenen Bildes führte. Offensichtlich muß der molekulare Wassergehalt mit den darin gelösten Natriumionen zu einer Abnahme des Gradienten führen, aber in jedem Fall zu dem auffallenden Wert von Null. So ist z. B. in Abb. 1 das Verhalten der Oberflächenschicht eines Glases der Zusammensetzung 28 Na_2O—4 CaO—68 SiO_2 gezeigt, die im Laufe von 6 Tagen in mit HTO markiertem Wasser bei 40 °C ausgebildet wurde. Kurve I zeigt die Veränderung der Natriumionenkonzentration, Kurve II den Gradienten dieser Konzentration, Kurve III die Veränderung der Wasserkonzentration und Kurve IV die Veränderung der Geschwindigkeit der Ablösung des Netzwerkes in Fluorwasserstoffsäure. Diese Größen wurden nach [1] und [2] gemessen und berechnet. Wie ersichtlich, sind die Kurven charaktermäßig jenen Kurven ähnlich, die mit dem BaO-haltigen Modell erhalten wurden. Die Schichtausbildung ist also das Ergebnis ähnlicher Teilvorgänge. Jedoch nimmt der Gradient nicht bis zum Wert von Null in der Nähe der Grenzfläche Schicht–Wasser ab. Dagegen wurde bei dem Glas der Zusammensetzung 28 Na_2O—4 SrO—68 SiO_2 ebenfalls ein Gradient mit dem Wert von Null oder annähernd Null erhalten, wie in unseren früheren Mitteilungen aus den Abbildungen ersichtlich ist, welche die Verteilung der Natriumionenkonzentration bei diesem Glas darstellen [3, 4].

Experimenteller Teil

Zu dem bariumoxidhaltigen Versuchsmodell zurückkehrend, ergeben sich weitere experimentelle Möglichkeiten, um die Gegenwart von Alkaliionen in hydratierter Form in der Oberflächenschicht zu beweisen und unsere Hypothesen über die mikroheterogene Struktur des betreffenden Teiles der Schicht zu unterstützen.

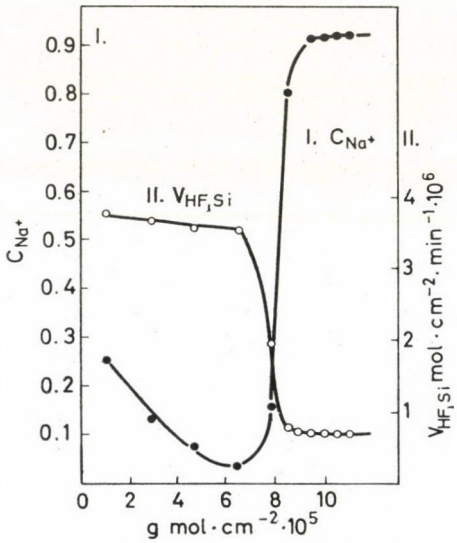


Abb. 2. Natriumionenkonzentration (I) und Ablösungsgeschwindigkeit des Netzwerkes in Fluorwasserstoffsäure (II) in Abhängigkeit von der mit dem Silikatgehalt der Schicht ausgedrückten Tiefenkoordinate bei einer in 0,1 *m* NaCl-Lösung ausgebildeten Oberflächenschicht

1. Ist der Konzentrationsgradient in reinem Wasser (dessen Natriumionenkonzentration zwar nicht Null, jedoch stets $< 10^{-4}$ Mol/Liter war) gleich Null, so muß der Konzentrationsgradient in Lösungen mit höheren Natriumionenkonzentrationen einen negativen Wert haben. Wird nämlich die Oberflächenschicht in einer Natriumionen enthaltenden Lösung ausgebildet, so erhöhen die in der Lösung befindlichen und bereits hydratierten Natriumionen die Konzentration der in den flüssigen Mikrophasen »gelösten« Natriumionen in beträchtlichem Maße, mit Rücksicht auf den »Quasi-Gleichgewichtszustand« des Ionenaustausches zwischen der Schicht und der Lösung.

In Abb. 2 ist die Natriumionenkonzentration (Kurve I) und die Ablösungsgeschwindigkeit des Netzwerkes in Fluorwasserstoffsäure (Kurve II) bei einer Oberflächenschicht dargestellt, die in 0,1 *m* NaCl-Lösung bei 40$\pm$ 0,2 °C im Laufe von 2 Tagen ausgebildet wurde. Die Natriumionenkonzentration nimmt in Richtung zur Grenzfläche Schicht–Wasser keineswegs ab, sondern sie nimmt zu (der Gradient nimmt also negative Werte an), obwohl die Diffusion der Natriumionen in allen Querschnitten der Schicht in Richtung

zur Grenzfläche Schicht–Wasser erfolgt. Die Diffusion der Natriumionen nach außen ist nämlich durch die Tatsache bedingt, daß die Schicht in Natriumchloridlösung ausgebildet wurde. Die hohe Natriumionenaktivität der wäßrigen Lösung steigert jedoch auch die Konzentration der in der Schicht befindlichen hydratierten Natriumionen. Natürlich wächst die Konzentration der hydratierten Natriumionen in Richtung zum Inneren der Schicht in den flüssigen Mikrophasen. Da aber die Konzentration des molekularen Wassers, d. h. der »flüssigen Mikrophasen« — bezogen auf das Netzwerk-Silicium — in Richtung zum Inneren der Schicht scharf abnimmt, nimmt die Menge der hydratierten Natriumionen in dieser Richtung ebenfalls ab. Wird die Konzentration der hydratierten Natriumionen auf das Netzwerk bezogen, so nimmt dieser Wert in Richtung zum Inneren der Schicht ebenfalls ab. Abb.2 zeigt, daß die Gesamtkonzentration der Natriumionen in Richtung zum kompakten Glas ein Minimum durchläuft. Dies ist die Folge der Tatsache, daß die Gesamtkonzentration der Natriumionen, bezogen auf das Netzwerk-Silicium, im Inneren der aufgelockerten Schicht durch die nichthydratierten, an das Netzwerk gebundenen Natriumionen, im äußeren Teil dagegen durch die hydratierten Natriumionen bestimmt wird.

2. Obwohl die Alkaliionenverteilung in der in 0,1 *m* NaCl-Lösung hergestellten Oberflächenschicht die Wahrscheinlichkeit der zweierlei Bindungen der Natriumionen innerhalb der Schicht wesentlich unterstützt, wäre doch ein vollständigerer Beweis unserer Hypothese dadurch ermöglicht, wenn die Konzentrationsänderungen der in zweierlei Bindungszuständen befindlichen Natriumionen innerhalb der Schicht auf irgendeine passende Art getrennt werden könnten. Hierzu bietet folgender Versuch eine Möglichkeit: die Ausbildung der Schicht wird nicht in Natriumchloridlösung, sondern in der Lösung eines anderen, leicht hydratierbaren Ions durchgeführt, wobei angenommen werden kann, daß das leicht hydratierbare Ion den Platz der hydratierten Natriumionen in der Schicht einnimmt. Ein derartiges Ion ist das Lithiumion.

In Abb. 3 ist die Alkaliionenkonzentrationsverteilung in der in 0,1 *m* LiCl-Lösung ausgebildeten Oberflächenschicht dargestellt. Kurve I stellt die Natriumionenkonzentration, Kurve II die Lithiumionenkonzentration dar.

Was zunächst auffällt, ist der gleichmäßige Anstieg der Natriumionenkonzentration in Richtung zum Inneren der Schicht. Der Gradient der Natriumionenkonzentration (Kurve III) ist klar unterscheidbar nicht gleich Null und positiv. Zugleich ist der Wert der Natriumionenkonzentrationen wesentlich niedriger als bei der entsprechenden Strecke der Schicht, die in reinem Wasser ausgebildet wurde. Bei letzterer beträgt ihr Wert 0,065, während bei der in Lithiumchloridlösung gebildeten Schicht der Wert zwischen 0,0072 und 0,014 liegt.

Vor allem wurde also derjenige Bruchteil der Natriumionen gefunden, der den durch die nach außen hin gerichtete Diffusion erforderten, von Null

abweichenden, positiven Konzentrationsgradienten aufweist und der in erster Reihe an die feste Mikrophase der Schicht gebunden vorstellbar ist. Zugleich nimmt die Lithiumionenkonzentration in Richtung zum Inneren der Schicht ab. Wahrscheinlich erfolgt also ein schneller Austausch zwischen den Lithiumionen und die hydratierten Natriumionen. Die Richtigkeit unserer Hypothese wird also durch den Versuch mit Lithiumchloridlösung kräftig unterstützt.

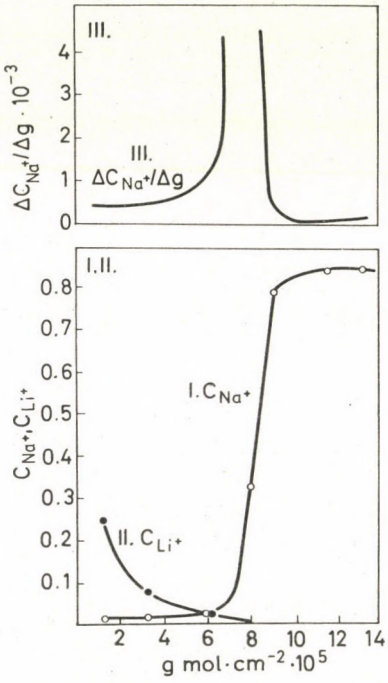


Abb. 3. Natriumionenkonzentration (I), Gradient der Natriumionenkonzentration (III) und Lithiumionenkonzentration (II) in Abhängigkeit von der mit dem Silikatgehalt der Schicht ausgedrückten Tiefenkoordinate bei einer in 0,1 *m* LiCl-Lösung ausgebildeten Oberflächenschicht

Zusammenfassend kann festgestellt werden, daß der gequollene, wasserhaltige Teil der Oberflächenschicht eine mikroheterogene Struktur besitzt. Diese mikroheterogene Struktur, die vermutlich durch die partielle Spaltung der $\rangle$Si—O—Si$\langle$ Bindungen und die anschließende Umordnung des Raumnetzes gebildet wird, besteht aus festen und flüssigen — molekulares Wasser enthaltenden — Mikrophasen. Die Alkaliionen befinden sich teils in den festen Mikrophasen, an die $\rangle$Si—$\bar{O}$ Gruppen des Netzwerkes gebunden und teils in den flüssigen Mikrophasen, in hydratiertem Zustand. Zwischen den beiden

Phasen muß ein Ionenaustausch bestehen. Im Kraftfeld des Netzwerkes sind die Wassermoleküle, welche die flüssige Phase bilden, wahrscheinlich stark polarisiert, der Bindungsabstand der Wasserstoffe nimmt zu, demzufolge ist es leicht vorstellbar, daß die von den Wassermolekülen der flüssigen Mikrophase abgespaltenen Protonen ebenfalls an der Wasserstoffionendiffusion, die in das Innere der festen Phase gerichtet ist, teilnehmen und die zurückbleibende negative Ladung durch die in die flüssige Phase eintretenden Natriumionen kompensiert wird. Ein Ionenaustausch tritt außerdem natürlich zwischen dem Wasser, in dem die Probe gelagert ist, und der Schicht auf: einerseits zwischen der flüssigen Makrophase und der flüssigen Mikrophase, andererseits zwischen der flüssigen Makrophase und der festen Mikrophase.

Die Rolle des Chloridions

Bei der Lagerung der Proben in Natriumchlorid- bzw. Lithiumchloridlösung taucht die Frage auf, ob und wie das Chloridion in diesen Fällen die Struktur der Schicht beeinflußt. Zunächst erhob sich die Frage, ob in Schichten, welche durch Lagerung in Alkalichloridlösung gebildet wurden, die hydratierten Alkaliionen nicht neben Hydroxylionen, sondern neben aus der Lösung eindiffundierten Chloridionen in der Schicht existieren. Um diese Frage zu beantworten, wurde der Chloridionengehalt der Schicht mit einer entsprechend empfindlichen Methode [5] untersucht. Es konnten jedoch keine Chloridionen in den einzelnen Schichtfraktionen nachgewiesen werden.

Während dieses negative Ergebnis einerseits die Annahme bestätigt, daß die Ladung der hydratierten Alkaliionen auch bei Lagerung in Alkalichloridlösung allein durch Hydroxylionen neutralisiert wird, kann das Ergebnis aber auch als merkwürdig bezeichnet werden, da — trotz des großen Durchmessers der Chloridionen — kein offensichtlicher Grund dafür vorliegt, warum diese Ionen, wenn auch wegen ihrer Abmessungen langsamer, nicht in die Schicht eindiffundieren sollten.

Eine Erklärung für diese Erscheinung kann mit Hilfe der Abb. 4 gegeben werden. In der Abbildung sind Meßergebnisse dargestellt, die mit Glasproben erhalten wurden, welche 2 Tage bei 40 °C in Natriumchloridlösungen verschiedener Konzentrationen gelagert wurden. Kurve I zeigt die Stelle der Front des die Schicht ausbildenden Ionenaustauschs, in Grammatom Silicium $\cdot$ cm^{-2} ausgedrückt (g_f). Mit anderen Worten ist g_f die Zahl der Grammatome Silicium, die in einem Prisma zwischen der »Grenzfläche« kompaktes Glas — Oberflächenschicht und der ursprünglichen Oberfläche des Glases, mit einer Grundfläche von 1 cm^2, enthalten sind. g_f wurde nach dem durch LENGYEL und DOBOS für die mechanische Abtrennung der Oberflächenschicht

entwickelten Verfahren [6] bestimmt.* Kurve II stellt die Zahl der Grammatome Silicium dar, die während der Lagerung der Probe in der Lösung von einem cm^2 der Probenoberfläche in die Lösung übergetreten sind ($m_{H_2O,Si}$). Die Dimension dieser Größe ist dieselbe wie die Dimension von g_f. Der Wert von g_f nimmt mit zunehmender Natriumchloridkonzentration ab, weil die Geschwindigkeit des die Oberflächenschicht ausbildenden Ionenaustausches durch die zunehmende Aktivität der Natriumionen in der Lösung herabgesetzt

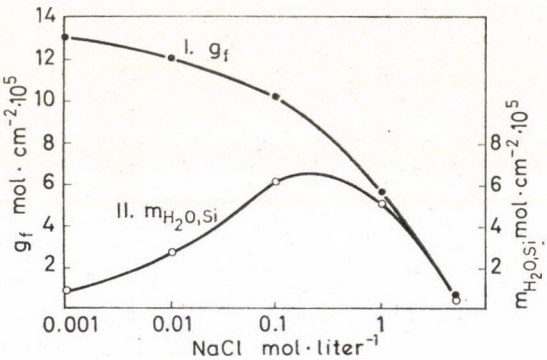
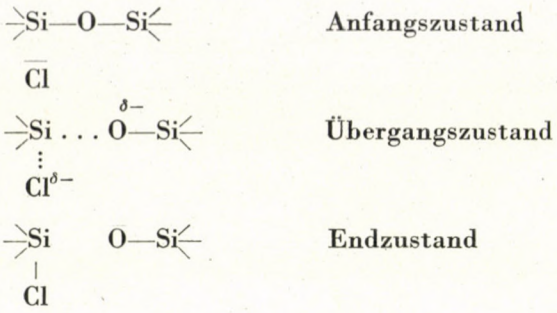


Abb. 4. Veränderung der Front des Ionenaustauschs (I) und der Menge der in Lösung gehenden Silikationen in Abhängigkeit von der NaCl-Konzentration der bei der Ausbildung der Schicht verwendeten Lösung

wird. Zugleich nimmt der Wert von $m_{H_2O,Si}$ solange zu, bis die Kurve g_f erreicht wird. Im weiteren fallen die beiden Kurven zusammen, d. h. dem Ionenaustausch folgt sofort der Abbau des Silikatnetzwerkes, eine Oberflächenschicht wird *praktisch* nicht gebildet. Der Anstieg der Abbaugeschwindigkeit des Silikatnetzwerkes mit der Konzentration des Natriumchlorids und die Abwesenheit des Chloridions in der Oberflächenschicht können miteinander durch einen logischen Zusammenhang verbunden werden, und zwar auf folgende Art: das Eindiffundieren der Chloridionen in die Schicht ist überhaupt nicht ausgeschlossen, nur — wie bereits erwähnt — verläuft sie am langsamsten unter allen Diffusionsvorgängen, da die Abmessungen der Chloridionen unter allen Komponenten am größten sind. Für die Tatsache, daß dennoch keine Chloridionen im Netzwerk zugegen sind, kann — unter Einbeziehung der in Kurve II ($m_{H_2O,Si}$) dargestellten Versuchsangaben — nur eine einzige Erklärung gegeben werden, daß nämlich das Chloridion in neutralem oder

* Es soll bemerkt werden, daß es theoretisch nicht gestattet ist, irgendeine Grenzfläche zwischen der Schicht und dem kompakten Glas festzulegen, da ja die Schicht kontinuierlich in das kompakte Glas übergeht und die Protonenkonzentration den Wert von Null streng genommen im Unendlichen erreicht. Praktisch wird die Grenzfläche kompaktes Glas—Schicht derjenigen Stelle zugeordnet, wo die Schicht auf mechanisch-thermischem Wege vom Glas abgetrennt werden kann (siehe Abb. 3 in [3]). An der Stelle der Abtrennung ist die Protonenkonzentration endlich und gering.

alkalischem (d. h. nukleophilem) Medium äußerst geeignet ist, die nukleophile Substitution am Siliciumatom zu katalysieren. Die Reaktion kann nach folgendem Schema verlaufen:



Die Bindung $\rightarrow$Si—Cl wird durch Einwirkung des anwesenden Wassers hydrolytisch gespalten. Demgemäß katalysiert das Chloridion — zugleich mit seinem Eindiffundieren — die völlige Hydrolyse der $\rightarrow$Si—O—Si$\leftarrow$ Bindungen des Netzwerkes und Chloridionen sind deshalb in der Schicht nicht auffindbar, weil ihr Auftreten in der Schicht zu einem Zusammenbruch der Netzwerkstruktur führt.

LITERATUR

1. Dobos, S.: Acta Chim. Acad. Sci. Hung. **69**, 43 (1971)
2. Dobos, S.: Acta Chim. Acad. Sci. Hung. **68**, 37 (1971)
3. Bouquet, G., Dobos, S., Boksay, Z.: Ann. Univ. Sci. Budapest, Sect. Chim. **6**, 5 (1964)
4. Boksay, Z., Bouquet, G., Dobos, S.: Physics and Chemistry of Glasses, **8**, 140 (1967)
5. Boltz, D.: Colorimetric Determination of Non-Metals, p. 166. Interscience Publ. 1958
6. Lengyel, B., Dobos, S.: Proceedings of the Sixth Conference on the Silicate Industry, Budapest, 1961. p. 279. Akadémiai Kiadó, 1963

Sándor Dobos; Budapest VIII., Múzeum-krt. 6—8

Acta Chimica Academiae Scientiarum Hungaricae, Tomus 69 (1), pp. 59—75 (1971)

THEORETICAL INVESTIGATION OF THE CLARIFICATION PROCESS IN A TUBE CENTRIFUGE

R. HORÁNYI* and J. NÉMETH**

(Factory for Chemical Machinery, Budapest, Research Institute for Technical Chemistry,** Hungarian Academy of Sciences, Budapest)*

Received February 10, 1970

The authors attempt to give a theoretical description of the steps of sediment formation. On the basis of theoretical conclusions it is proposed that for convenient treatment, sediment formation be broken up into steps. This permits to distinguish first and second steps, efficient from the aspect of clarifying techniques, and an inefficient filling-up as third step. In the discussion of these steps, the introduction and application of new concepts, necessary for the discussion of the processes, are proposed. The equations derived permit a more realistic and, from the physical aspect, a more reasonable design of centrifugal clarifying in the case of retentive suspensions than has been proved experimentally for a model suspension.

Clarification operations for which vertical shaft tube centrifuges of high speed of rotation are most often used are the settling of solid particles from suspensions and the breaking of emulsions. Out of these two operations settling is carried out more frequently in tube centrifuges, and therefore, our investigations concern primarily the clarification of suspensions. Naturally, available results from the borderland of chemical engineering operations (fluid mechanics, physical chemistry of disperse systems, hydrology, mathematics) have been applied in these studies. Under consideration of these results, LAMB-flow was assumed in the clarifying tube centrifuge, and conditions of free settling for the suspension. It should be noted that the assumption of LAMB-flow in the tube centrifuge is to be considered as a new concept, since up to the present uniform plug flow was used primarily in practice for the description of axial velocities.

Our objective in the field of operation studies was the determination of the actual performance of the tube centrifuge. Every design method used so far presumes a sediment-free clarifying rotor in the determination of the performance. However, this state is characteristic only of the first instant of clarifying. The shape of the effective clarifying volume changes as the sediment settles out, and the sediment proper, due to its sticky, hardening or free flowing properties, can influence the concentration of the suspension flowing from the drum, and hereby the quantity of the possible suspension flow per unit time, *i.e.* the performance. Investigations reported in our present work concern therefore primarily the pattern of arrangement of the sludges in the sediment volume of the rotor, and its influence on the efficiency of clarification.

The axial flow determines unequivocally the performance of a clarifying centrifuge of a given diameter. For the study of the dispersion medium flowing in axial direction in the tube centrifuge, the drum of the tube centrifuge is considered as a tube of infinite length rotating at an angular velocity ω about its longitudinal axis (Fig. 1). The inflowing liquid gets between the blades

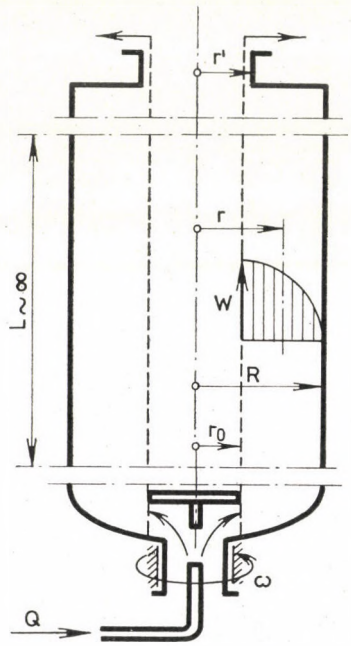


Fig. 1. Schematic diagram of the clarifying tube centrifuge

arranged at the lower end of the drum. The blades accelerate the liquid, and from here on it is assumed that each liquid particle flows already at the angular velocity of the drum.

The centrifugal force field of the rotating tube is several thousand times stronger than the gravitational field of force, so that the effect of the latter can be neglected.

The clarified liquid leaves the drum at its upper part, through the overflow weir of radius r'. Under the action of the centrifugal field of force and the overflow weir, the liquid forms a specific annular segment, for which the radius of the annulus is R, and its internal radius the free surface of radius r_0, determined by the centrifugal field of force. In first approximation, the value of r_0 can be taken as identical with r', the radius of the overflow weir. At the radius R, the axial component of the liquid velocity is zero. The description of flow under these assumed conditions is due according to some authors to LAMB, who published his relevant considerations in 1906, before the operation

of the first tube centrifuge [1]. Since in our case the internal flow of free surface in the annular liquid segment is due to the centrifugal field of force, the integration constants of the original relationship had to be determined for the new boundary conditions [2]. This resulted for the radial distribution of the axial velocity the following equation:

$$W = \frac{\Delta p}{4\eta L}\left(R^2 - r^2 - 2r_0^2 \ln \frac{R}{r}\right) \tag{1}$$

An analysis of Eq. (1) shows that there is a difference between the parabolic velocity distribution prevailing in a straight tube of circular cross-section and the flow pattern established in the annular segment. Presuming an identical radius r, the axial velocity is always lower in the annular segment, than in the case of plug flow.

The difference is

$$\Delta W = -\frac{r_0^2 \Delta p}{2\eta L} \ln \frac{R}{r} \tag{2}$$

Expediently, the term

$$\frac{\Delta p}{L\eta} = A$$

in the relationship obtained for the radial change in velocity will be expressed in analogy to the Hagen-Poiseuille equation in terms of the quantity of the suspension feed. Let us determine the quantity of suspension flowing through the annular segment of free surface in unit time, under consideration of Eq. (3):

$$Q = 2\pi \int_{r_0}^{R} W r \, dr \tag{3}$$

Substituting velocity W for relationship (1) obtained for the annular flow:

$$Q = \frac{A\pi}{2} \int_{r_0}^{R} \left(R^2 - r^2 - 2r_0^2 \ln \frac{R}{r}\right) r \, dr \tag{4}$$

Integration and rearrangement of the equation yields

$$Q = \frac{A\pi}{2}\left(\frac{R^4}{4} + \frac{3}{4} r_0^4 - R^2 r_0^2 + r_0^4 \ln \frac{R}{r_0}\right) \tag{5}$$

whence

$$A = \frac{2Q}{\pi} \cdot \frac{1}{\frac{R^4 + 3r_0^4}{4} - R^2 r_0^2 + r_0^4 \ln \frac{R}{r^0}} \tag{6}$$

and

$$\frac{\Delta p}{L\eta} = \frac{2Q}{\pi\alpha} \tag{7}$$

The substitution of this expression into Eq. (1) gives the axial velocity distribution in dependence on the radius r, expressed in terms of the throughput Q:

$$W = \frac{Q}{2\pi\alpha}\left(R^2 - r^2 - 2r_0^2 \ln\frac{R}{r}\right) \tag{8}$$

Let us determine now the path of the settling particle.

In a first approximation, the effect of the sediment, centrifuged out on the walls of the drum, on the axial flow of the dispersion medium is neglected. In the theoretical study of particle movement the following assumptions are made:

the dispersion medium is Newtonian;

the effect of the radial and Coriolis accelerations is not taken into account for the settling particle;

the settling particle follows slip-free at every point and time the movement of the liquid flow;

the movement of the particle in the dispersion medium is laminar in both radial and axial directions;

the physico-chemical conditions of free settling are ensured.

Using the notations of Fig. 2, let us write for an arbitrary point of the path of the particle the ratio of axial and radial velocities:

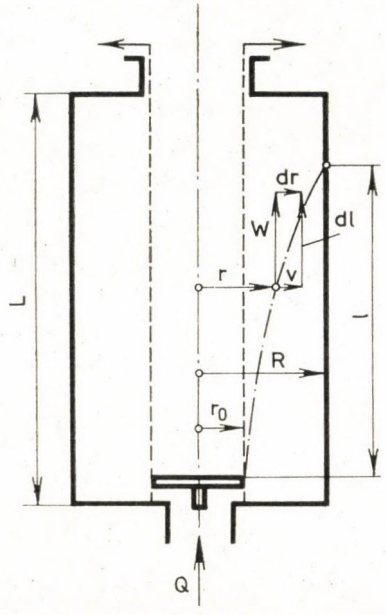


Fig. 2. The path of a particle in the clarifying tube centrifuge

$$\left[\frac{W}{v}\right]_r = \frac{\left[\frac{dl}{dt}\right]_r}{\left[\frac{dr}{dt}\right]_r} = \left[\frac{dl}{dr}\right]_r \tag{9}$$

On substituting the expressions of axial and radial velocity into Eq. (9) we have:

$$\left[\frac{dl}{dr}\right]_r = \frac{\frac{Q}{2\pi\alpha}\left(R^2 - r^2 - 2r_0^2 \ln\frac{R}{r}\right)}{\frac{D^2 r\omega^2 \Delta\varrho}{18\eta}} \tag{10}$$

As can be seen, the numerator is the right side of Eq. (8), while the denominator is Stokes' velocity written for a particle of diameter D, settling in the centrifugal field of force. After rearrangement, and separation of the variables, Eq. (11) can be integrated, to yield a solution to our problem

$$\int_0^l dl = \frac{9Q\eta}{D^2\pi\alpha\omega^2\Delta\varrho}\int_{r_0}^{R}\left(R^2 - r^2 - 2r_0^2 \ln\frac{R}{r}\right)\frac{dr}{r} \tag{11}$$

On performing the integration, that axial distance measured at the mantle is obtained, at which the particle of diameter D, starting from radius r_0, reaches the internal radius R of the drum.

$$l = \frac{\alpha_1}{D^2}\left[\frac{R^2}{2}\ln\frac{R}{r_0} - \frac{R^2 - r_0^2}{4} - \frac{r_0^2}{2}\ln^2\frac{R}{r_0}\right] \tag{12}$$

where

$$\alpha_1 = \frac{18Q\eta}{\pi\alpha\omega^2\Delta\varrho} \tag{13}$$

With the aid of Eqs (8) and (12) the conditions of movement in axial direction can be elucidated for the dispersion medium and the dispersed phase within the limits set by our starting assumptions. The performance of a sediment-free drum can be determined in this way by the substitutions $D = D_h^x$ and $l = L$. We wish to mention that D_h^x is the maximum grain size permissible in the fugate [5]. However, the drum of the clarifying tube centrifuge becomes filled up with sediment during its operation. Depending on the concentration of the suspension and its amount at which it is passed through the clarifying tube centrifuge, the process of sediment formation can be analyzed according to our investigations by subdivision into three subsequent steps.

The first step of sediment formation

Sediment formation of unimportant quantity is thought to be characteristic of the first step. Therefore, in the investigation of the first step, the determination of the real clarification of a monodisperse suspension is aimed at as first approximation besides the investigation of the quantity of sediment separated. According to the classical concept of clarification techniques, the centrifuge cannot separate particles, if the theoretical path-length of the particle is greater than the drum length of the clarifying centrifuge. This assumption is proved erroneous already by the consideration of the fact that the suspension has a homogeneous distribution also at the bottom part of the rotary drum, so that a great number of particles start from 'wall vicinity'. Preconditions for the separation for the centrifuging out of these particles are thus given.

Let us investigate the proportion of the solid phase of a monodisperse substance of concentration C_0 and diameter D_m, which can be separated at a given throughput Q.

The sedimentation time of a particle starting from radius r_0 and arriving without acceleration at the internal radius of the drum [3] is

$$t_0 = \frac{18\eta}{D_m^2 \omega^2 \Delta\varrho} \ln \frac{R}{r_0} \tag{14}$$

Applying Eq. (14), it can be stated that all those particles reach the internal wall of the rotary drum, the distance of which from the rotational axis is greater than

$$r_0 = R \exp\left(-\frac{\Delta\varrho\omega^2 D_m^2}{18\eta} t_0\right) \tag{15}$$

and their radial settling time is equal or smaller than the average residence time due to the axial movement determined by the quantity of the suspension introduced into the drum.

The average residence time is

$$\bar{t} = \frac{L}{\overline{W}} \tag{16}$$

where, owing to LAMB's velocity distribution

$$\overline{W} = \frac{1}{R - r_0} \int_{r_0}^{R} W dr = \frac{Q}{6\pi\alpha} [2R^2 - Rr_0 - 4r_0^2 + 3r_0^2 \ln R(R-1) - 3r^3 \ln r_0] \tag{17}$$

Under consideration of the radius characterized by the expression

$$r_i \geq R \exp\left[- \frac{D_m^2 \omega^2 \Delta\varrho}{18 \eta} \bar{t} \right] \tag{18}$$

the quantity Q flowing in axial direction in the rotating drum can be divided into two parts.

That quantity of suspension, which flows between the limits $R - r_i$ in the rotating drum is called Q_1. The particles flowing in this annular segment are considered on the basis of Eq. (18) as separated.

The quantity of suspension flowing in the clarifying tube centrifuge between the limits $r_i - r_0$ contains suspended particles which cannot be considered as separated. This quantity is called Q_2.

Under consideration of the average axial velocity:

$$Q_1 = Q \frac{R^2 - r_i^2}{R^2 - r_0^2} \tag{19}$$

and

$$Q_2 = Q \frac{r_i^2 - r_0^2}{R^2 - r_0^2} \tag{20}$$

Let us write now the mass of the solid phase separated along the drum length L from the monodisperse suspension of concentration C_0 and particle diameter D_m, passed through the centrifuge in time $\bar{t}$:

$$M_1 = Q_1 \bar{t} C_0 = \bar{t} C_0 Q \frac{R^2 - r_i^2}{R^2 - r_0^2} \tag{21}$$

On substituting expressions (18) and (16) into (21), and differentiating with respect to L, one obtains

$$\frac{dM_1}{dL} = \frac{C_0 Q}{\overline{W}} \cdot \frac{R^2}{R^2 - r_0^2} [1 - \exp(-BL) + BL \cdot \exp(-BL)] \tag{22}$$

where

$$B = \frac{D_m^2 \omega^2 \Delta\varrho}{9 \eta \overline{W}} .$$

From Eq. (22) for the mass of sediment per unit length of the drum, the conclusion can be drawn that the mass of the heavy phase separated decreases exponentially in the case of sticky sediments along the drum generator even in the case of a monodisperse suspension. Thus, the earlier design concept, according to which grains of identical dimension settle out in a heap at a well defined axis distance l, is erroneous.

According to the law of mass conservation, the mass of the non-separated particles in the outflowing suspension will be

$$M_1' = M_{\text{total}} - M_1 = \bar{t} C_0 Q \left[1 - \frac{R^2 - r_i^2}{R^2 - r_0^2}\right] \tag{23}$$

The expressions (21) and (23) hold true also with polydisperse suspensions, but will be modified by the integral of the particle distribution with

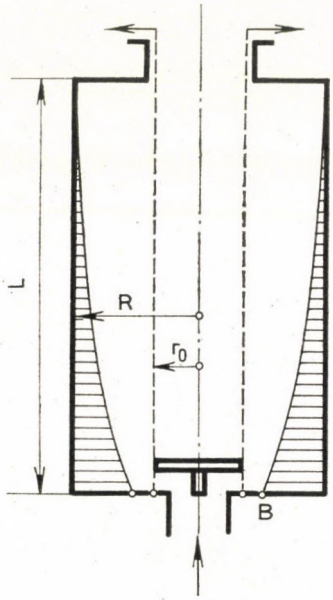


Fig. 3. The first step of sediment formation

respect to a given grain size [2]. The quantity separated consists in this case of two parts:

— the mass of particles above the given grain size, and

— the mass of particles below the given grain size, starting from the vicinity of the wall.

It has been assumed for the beginning of the first step of sediment formation that the quantity of sediment, separating on the internal wall of the drum does not attain in function of time the value, which would disturb the development of LAMB's velocity distribution. However, at the end of the first step of sediment formation, already such quantity of heavy phase is taken into consideration in the sediment volume of the drum, at which the point B in Fig. 3 approaches the radius r_0 of the flowing disperse medium. In the schematic picture shown in Fig. 3, the separation of the sediment along the generator has been realized through the full drum length L. In this case:

$$\frac{18\,\eta}{D^2\,\omega^2\,\Delta\varrho}\ln\frac{R}{r_0}=\frac{L}{\overline{W}} \tag{24}$$

Relationship (24) gives simultaneously the *maximum value of the grains* which can be separated. However, in the majority of practical cases only a part of the full length of the drum becomes covered with the heavy phase of the suspension during the first step. The operative drum length is therefore

$$l_m < L$$

Under consideration of relationships (15) and (16) l_m will be obtained for a predetermined grain size D_h with the aid of Eq. (24):

$$l_m=\frac{18\eta\,\overline{W}}{D_n^2\,\omega^2\,\Delta\varrho}\ln\frac{R}{r_0} \tag{25}$$

The end of the first step can be calculated on the basis of the following considerations. The settling curve of the suspension is a starting data. Consequently, the $F(D)$ granulometric curve, constructed by the Oden method, is also known [3]. On the granulometric curve, an $F(D_h) = F_1$ value belongs to the grain of diameter D_h, which gives the percentage value of the quantity of grains remaining in the sediment. For the end of the first step it can be written therefore that

$$QC_0F_1t_1 = V_1\bar{\varrho} \tag{26}$$

and

$$t_1=\frac{V_1\,\bar{\varrho}}{QC_0\,F_1} \tag{27}$$

The sediment volume V_1, filled out after the termination of the first step, can be determined from the l_m and $R - r_0$ data, under consideration of the inner rotational surface. The inner rotational surface of the sediment is obtained from Eq. (22), but in first approximation, point B belonging to the entrance radius r_0 can be connected with a straight line with the mantle length l_m and L, respectively, measured on the radius R. Thus

$$V_1=(R^2-r_0^2)\,\pi\,\frac{l_m}{2} \tag{28}$$

The beginning, course and termination of the first step of sediment formation can be characterized therefore as follows.

The suspension introduced into the rotary drum enters through a segment decreasing with time. This phenomenon is caused by the annular separation, sedimentation of the heavy phase in the function of time. With increasing quantity of the separated solid phase, the initially cylindrical mantle of the drum is transformed into a surface of revolution determined by the kine-

tics of sediment deposition, characterized by Eq. (22). Presumably, the separated sediment surface terminates the LAMB-flow of axial direction. However, our knowledge is still insufficient for the characterization of the new flow pattern, so that a LAMB-type velocity distribution is assumed also further as approximation. The first step of sediment formation is considered as terminated, when point B according to Fig. 3 reaches the internal surface of the liquid annulus.

In dependence on the design, the sediment deposition can be realized along the full length of the drum or only on part of the mantle lengthof the drum. From the operational aspect, this latter case is of importance.

The second step of sediment formation

If the process of centrifugal clarifying is continued after the termination of the first step, the filling up in axial direction of the sediment volume of the clarifying tube centrifuge begins. This process represents the second step of sediment formation.

Under consideration of the possible maximum path length of grain settling in radial direction, the same grouping can be used in the discussion of the second step as has been used in the first step:

the radial settling time of the grain investigated is less than the axial residence time;

$$t_0 = t_r < \bar{t}, \qquad l_m < L;$$

the radial settling time and the axial residence time of the grain investigated are the same in the rotary drum;

$$t_0 = t_r = \bar{t}, \qquad L = l_m.$$

In the discussion of the second step of sediment formation, the earlier assumptions and neglections are used. Moreover, the settling of the solid phase separated by the rotary drum is assumed in approximation to be similar to a piston movement (*cf.* Fig. 4). Above the filling-up of the piston-like sediment of the cross-section $(R^2 - r_0^2)\pi$, the sediment profile formed in the first step is proceeding.

Let us investigate first the increase in quantity of the heavy phase of the polydisperse suspension in the sediment volume.

$$QC_0F(D)dt = (R^2 - r_0^2)\pi\bar{\varrho}dl$$

$$\left(QC_0\,F(D) = (R^2 - r_0^2)\,\pi\bar{\varrho}\,\frac{dl}{dt}\right) \tag{29}$$

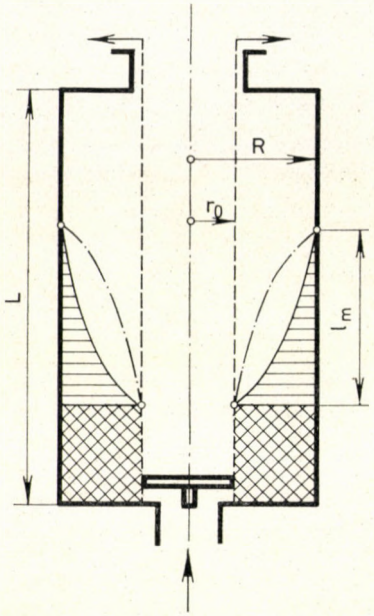


Fig. 4. The second step of sediment formation

To obtain the required relationship, Eq. (29) is rearranged and integrated

$$\int_{t_1}^{t_2} dt = \frac{(R^2 - r_0^2)\,\pi\bar{\varrho}}{QC_0} \int_{l_m}^{L} \frac{dl}{F(D)} \tag{30}$$

Unfortunately, the integration can be performed only partly without difficulties, because $F(D)$ is a function determined by measurement. It is a very rare case, when the particle distribution function can be expressed in a mathematical form, and integrated. However, for a given grain the function $F(D)$ is constant, and hence, Eq. (30) becomes

$$t_2 - t_1 = \frac{(R^2 - r_0^2)\,\pi\bar{\varrho}}{Q\,C_0\,F_1} (L - l_m) \tag{31}$$

If it is taken into account that the clarifying surface, determined by the settling length l_m still takes up some heavy phase in the last operational step, the sediment volume available from the operational aspect can be increased by this quantity. Thus,

$$t_2 \cong \frac{(R^2 - r_0^2)\,\pi\bar{\varrho}}{Q\,C_0\,F_1} (L - 0.5\,l_m) \tag{32}$$

Owing to the piston-like filling-up of the sediment volume, the clarifying surface of the centrifuge remains constant during the second step. It follows from this that the velocity of sediment separation, *i.e.* the quantity of the heavy phase settled, is also constant:

$$M = QC_0F_1t = \text{const} \times t \tag{33}$$

The total quantity of substance settled up to the end of the second step is:

$$M_2 = QC_0F_1t_2 = (R^2 - r_0^2)\pi\bar{\varrho}(L - 0.5\, l_m) \tag{34}$$

Accordingly, the sediment volume is

$$V_0 = V_1 + V_2 \tag{35}$$

where V_1 can be calculated from Eq. (28), while V_2 is

$$V_2 = (R^2 - r_0^2)\pi(L - l_m) \tag{36}$$

It can be stated as an approximation that the solid phase concentration of the fugate is also constant in this time interval:

$$C_2 = C_0(1 - F_1) \tag{37}$$

In summary, the second step of sediment formation can be characterized by the following.

The sediment profile developed at the end of the first step shifts parallel to itself. The annulus $(R^2 - r_0^2)\pi$ between the shifted sediment profile and the feed is filled up piston-like along its height. Thus, the quantity of sediment settled in unit time, that is to say, the velocity of the piston-like filling-up of the sediment, is constant also during the second step. Hence, the concentration of the fugate is also constant. The end of the second step is characterized by the fact that the height of the piston-like sediment filling-up becomes $(L - l_m)$ along the drum generator.

The third step of sediment formation

The total filling-up of the centrifuge drum after time t_2 is the third step. Practically, it is of minor importance, so that the discussion of this time interval will be limited here to qualitative statements.

Since at the end of the second step the surface of rotation characteristic of the termination of the first step has developed also in the upper l_m section of the drum (Fig. 5), the concentration of the fugate increases rapidly in the third step from C_2 to C_0. This is due to the complete filling-up of the sediment volume of the drum. The liquid feed flows through along the cylindrical mantle surface of radius r_0 in form of a thin annular film at an unchanged concentration. From the viewpoint of clarifying techniques, this state is inefficient.

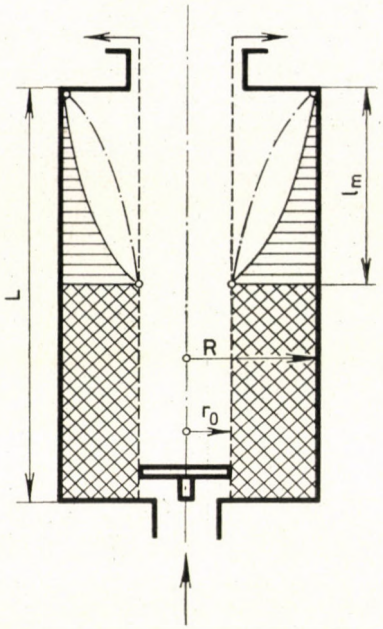


Fig. 5. Termination of the second step and beginning of the third step of sediment formation

Experimental verification

A tube centrifuge Model FC-45 of Hungarian manufacture was used for the experiments (Fig. 6). As shown by Fig. 7, feeding was undertaken at a constant level difference h_0. The speed of rotation of motor (4) could be changed with a regulating transformer (5). The tachometer consisted of the electric transmitter (3) arranged around the rotor (2), in a combination with an oscilloscope (6) and an audio frequency generator (7). The suspension used was Para Red dye suspended in water. The purity of the clarified substance was checked with an UVIFOT photometer, by microscopic particle count and by microphotography. The concentration of solids in the clarified substance was determined by evaporation. Fig. 8 shows the average results of 10 measurement series plotted against the time of operation. The ordinate is the concentration of the outflowing clarified suspension. Sections of the curve marked by 1, 2 and 3 correspond to the subsequent steps of clarification.

The sediment settled in the drum after 10 minutes of operation has been measured, and it was found that the sediment settled came close to r_0, the radius of the free surface. On the basis of Eq. (27), the calculated value is

$$t_1 = \frac{0.433\,(2.55^2 - 1.0^2)3.14}{15 \times 2.55 \times 10^{-3} \times 0.7}\,0.5 \times 6.6 = 680\,s \simeq 11.4\ \text{min}.$$

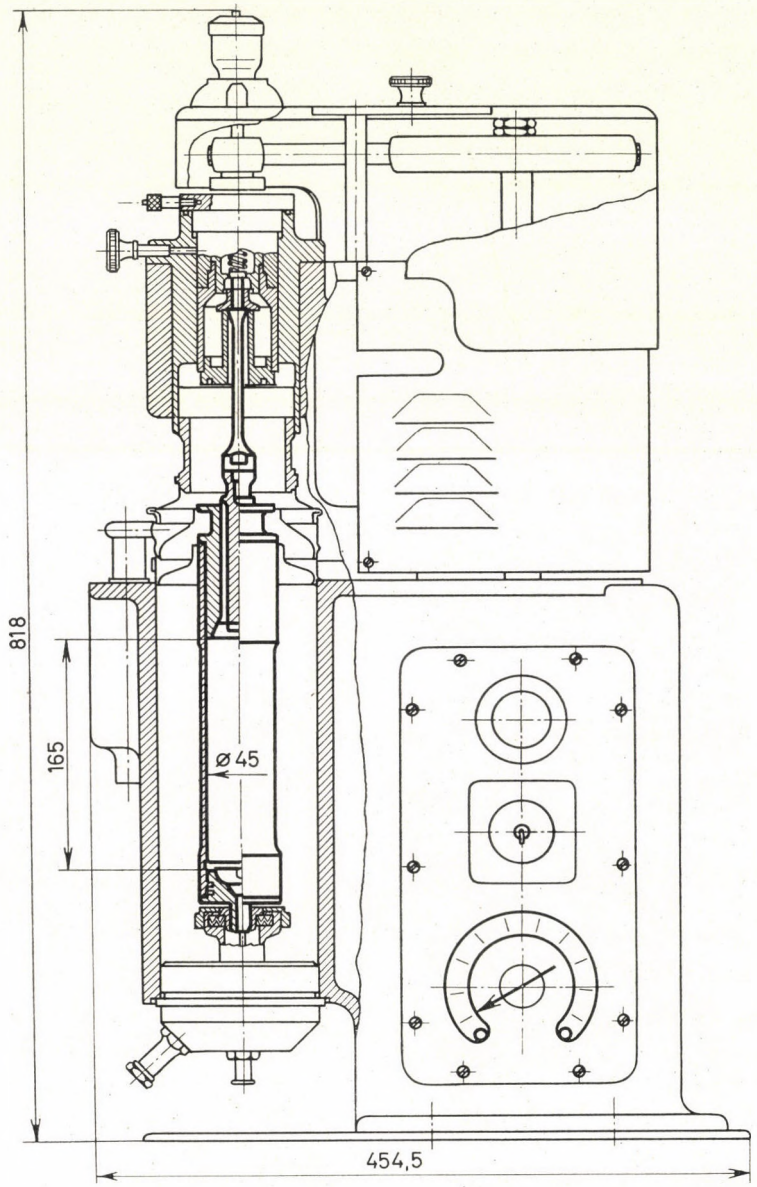


Fig. 6. The Model FC-45 supercentrifuge used for the investigation of sediment formation

which is in good agreement with the experiment. The grain diameter taken for the model suspension was 4.75 microns, the corresponding F_1 value was 0.7, and the l_m value 6.6 cm [2]. In our experiments, the values of the throughput, $Q = 15$ cm^3/s, and of the feed concentration, $C_0 = 2.55 \times 10^{-3}$ g/cm^3, were kept constant.

In accordance with our theoretical considerations, in zone 2, *i.e.* in the second step, the velocity of the filling-up of the sediment is constant

$$M = QC_0F_1t = 15\times2.55\times10^{-3}\times0.7\ t \cong 0.027\ t$$

Fig. 9 shows the change in mass of the sediment measured as a function of time. The initial slope of the curve is

$$\frac{M}{T_m} = 0.033$$

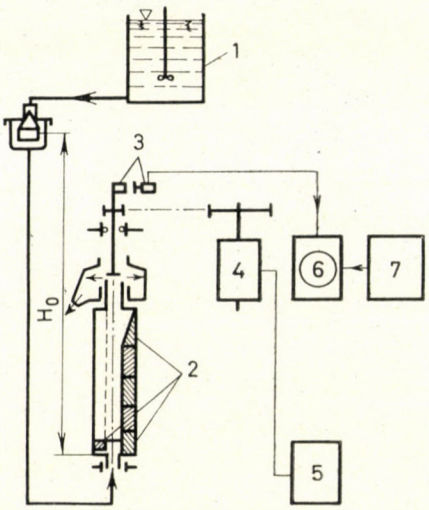


Fig. 7. Measuring system used for the investigation of sediment formation

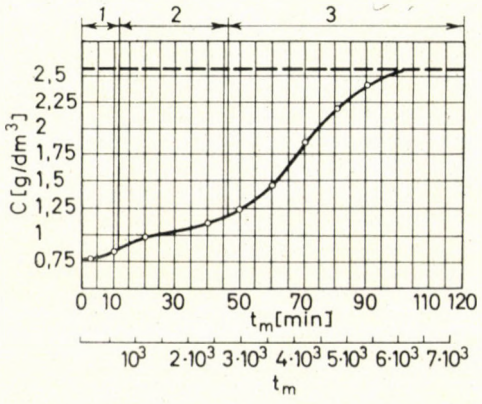


Fig. 8. Increase in concentration of the centrifuged suspension as a function of the operation time

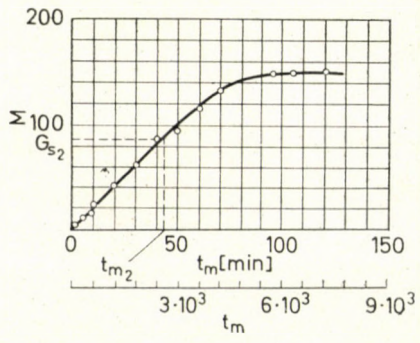


Fig. 9. Quantity of sediment separated in the sediment volume of the centrifuge as a function of the operation time

which is somewhat larger than the calculated value. This deviation is probably due to a difference between the theoretical D_h value and the actual grain size D_h [5].

The end of the second step on the basis of Eq. (32) is:

$$t_2 = \frac{0.433(2.55^2 - 1)\,3.14}{15 \times 2.55 \times 10^{-3} \times 0.7}(16.5 - 0.5 \times 6.6) = 2730\ s = 45.5\ \text{min}.$$

Up to time t_2, the solids content of the fugate is theoretically constant:

$$C = C_0(1 - F_1) = 2.55 \times 10^{-3}(1 - 0.7) = 7.65 \times 10^{-6}\ \text{g/cm}^3$$

As can be seen from Fig. 8, the constant $C = 7.65 \times 10^{-6}$ remains with the exception of the first 5 minutes below the concentration values measured. According to our opinion, the slow increase in concentration up to the end of the second step can be explained, besides the differences in the characteristic grain size mentioned already, by the design of the rotary drum (low number of outlets), and by a certain degree of swirling up and carrying out of sediment. This assumption is supported also by Fig. 10, showing the turbidity ratios of the fugate, measured with a nephelometer, as a function of the clarifying time. It should be mentioned that the greater numbers belong to the purer liquid. It can be seen from Fig. 10 that in the first 15 minutes the fugate becomes rapidly turbid. Subsequently, when the near optimal internal surface of rotation belonging to the flow pattern has been developed by the settling of the sediment, the turbidity changes only slightly in the following 50 to 55 minutes.

Section 3 of Fig. 8 shows the complete filling-up of the drum. The solids content of the fugate increases rapidly to the starting C_0 value. The same can be seen from Fig. 10, indeed, the turbidity value of the fugate attains already in the 75th minute the nephelometric ratio of the suspension feed.

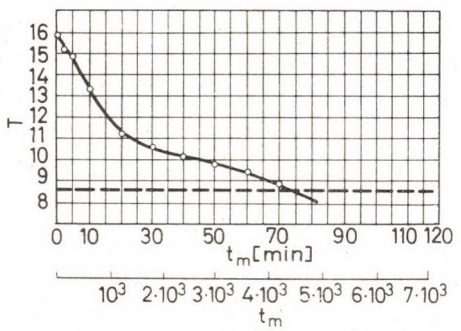


Fig. 10. Change in turbidity of the centrifuged suspension as a function of the operation time

List of symbols

C_0 — concentration of the suspension before centrifugation, g/cm³, g/dm³;
C, C_1, C_2 — concentration of the solid phase in the outflowing suspension, g/cm³;
D — the equivalent diameter of the particle, cm;
D_h^x — characteristic grain size, cm;
D_m — grain diameter of the monodisperse system, cm;
D_h — particle diameter of the so-called limit grain, cm;
$F(D)$ — ordinate of the granulometric curve, %;
M_{total} — mass of the grains in the suspension, g;
M, M_1, M_2 — mass of the grains centrifuged into the sediment volume, g;
L — complete drum length, cm;
l — changing drum length, cm;
ΔP — pressure drop on flow, g cm/s²;
Q — throughput, cm³/s;
r_0 — radius of the internal liquid surface, cm;
r, r_i — the changing radius, cm;
R — internal radius of the drum, cm;
T — turbidity, %;
t — time, s;
t_0 — settling time, s;
$\bar{t}$ — average residence time, s;
t_m — centrifuging (operational) time, s, min;
v — radial settling velocity in a centrifugal force field, cm/s;
V_0, V_1, V_2 — sediment volume, cm³;
W — axial flow velocity, cm/s;
$\bar{W}$ — average flow velocity, cm/s;
$\bar{\varrho}$ — average density of the sediment; g/cm³;
η — dynamic viscosity factor, g/cm.s;
$\Delta\varrho$ — difference in density of the settling particle and of the dispersion medium, g/cm³;
ω — angular velocity of the drum, 1/s.

REFERENCES

1. LAMB, H.: Hydrodynamics of Fluids. Pergamon Press, 1906
2. HORÁNYI, R.: Ph. D. Thesis, 1968
3. HORÁNYI, R., NÉMETH, J.: Periodica Polytechnica, **14**, 183, 1970
4. HORÁNYI, R., NÉMETH, J.: CHISA Congress, 1969

Róbert HORÁNYI; Budapest III., Árpád fejedelem út 60.
Jenő NÉMETH; Budapest XI., Budafoki út 47.

Acta Chimica Academiae Scientiarum Hungaricae, Tomus 69 (1), pp. 77—80 (1971)

ÜBER KOMPLEXE VOM BIS-(SALICYLALDIMIN-N-R)NICKEL(II)-TYP

(KURZE MITTEILUNG)

J. CSÁSZÁR und I. BARTA

(Institut für Allgemeine und Physikalische Chemie der József Attila Universität, Szeged)

Eingegangen am 6. Mai 1970

Es wurden die Viskositäten der Lösungen von Komplexen vom Typ bis-(Salicylaldimin-N-alkyl)Nickel(II) und die Molvolumina der Komplexe im festen und gelösten Zustand bestimmt. Die Ergebnisse werden durch Einbeziehung der Hyperkonjugationswirkung und besonders der sterischen Wirkung der Alkylsubstituenten gedeutet.

In früheren Mitteilungen [1—4] haben wir über die magnetischen und spektralen Eigenschaften von Komplexen vom bis-(Salicylaldimin-N-alkyl) Nickel(II)-Typ (im weiteren Ni(Hsai-N-R)$_2$) berichtet. In der Literatur liegen zahlreiche andere Arbeiten über diesen Themenkreis vor, über die Viskosität von Lösungen solcher Komplexe [5—8] und über die Molvolumenwerte der Verbindungen [9, 10] stehen jedoch nur wenige Angaben zu Verfügung.

In Tabelle I sind die Viskositäten der Lösungen in Toluol und Pyridin für verschiedene Komplexe sowie ihre Molvolumenwerte angeführt.

Tabelle I

Viskositäts- und Molvolumenwerte von Komplexen vom Typ Ni(Hsai—N—R)$_2$

No.	R	$\eta_{red.}$		Molvolumen		Para %[e]
		in Toluol	in Pyridin	fest[d]	in Toluol	
1.	Methyl	0,62[a]	1,15[c]	205	210[b]	34
2.	Äthyl	0,70	1,17[c]	243	245	8
3.	*n*-Propyl	0,77[c]	1,27[c]	269	283	14
4.	*i*-Propyl	1,54	1,27	284	375	42
5.	*n*-Butyl	0,86[c]	1,33[c]	304	324	7
6.	*i*-Butyl	0,97	1,43	333	381	36
7.	*n*-Amyl	0,97[c]	1,44[c]	351	353	10
8.	*i*-Amyl	0,80	1,43	368	384	10
9.	*n*-Hexyl	1,06[c]	1,50[c]	383	395	15
10.	*n*-Oktyl	1,29[c]	1,71[c]	447	480	3
11.	*n*-Decyl	1,59[c]	2,00[c]	—	550	10
12.	*n*-Dodecyl	1,94[c]	2,38[c]	602	610	14

[a,b] Extrapolierte Werte; [c] siehe [8]; [d] siehe Dichtewerte in [17]; [e] Para% $= 100(\mu^2_{BM}/3$

Wie ersichtlich, nimmt der Wert von $\eta_{red.}$* mit der Zahl der C-Atome zu; der Zusammenhang kann mit der Formel

$$\log (\eta_{red.}) = a + bn$$

beschrieben werden [8], wo n die Zahl der C-Atome, a und b für das Lösungsmittel charakteristische Konstanten sind (Abb. 1). Ähnlich zu Beobachtung bei anderen homologen Reihen [11, 12] zeigen die Ergebnisse, daß die Werte

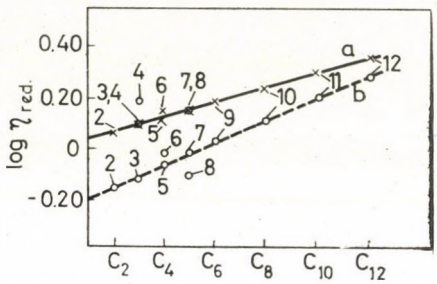


Abb. 1. Viskositätswerte der Lösungen in Pyridin (a) und in Toluol (b), gemessen bei 30°C, in Abhängigkeit von der Zahl der C-Atome in der N-Alkylgruppe

von $\eta_{red.}$ komplizierte Kombinationen der Wechselwirkungen zwischen Komplex und Komplex bzw. zwischen Komplex und Lösungsmittel widerspiegeln. Dies ist verständlich, da ja bekannt ist, daß in Lösungen die *n*-Alkylkomplexe in indifferenten Lösungsmitteln planar-quadratisch und assoziiert sind, während bei *i*-Alkylkomplexen ein planar-quadratisch-tetraedrisches Gleichgewicht vorliegt (siehe z. B. [13—15]).

Die *n*-Alkylverbindungen sind trans-planar [16], ihr Dipolmoment μD beträgt $\sim$0—1. Wären diese Verbindungen *cis*-planar oder quasi-tetraedrisch, so würden sie ein bedeutendes permanentes Dipolmoment besitzen, welches auch in einer gesteigerten Wechselwirkung mit dem Lösungsmittel in Erscheinung treten würde. Diese Wirkung liegt bei den i-Propyl-, i-Butyl und i-Amylderivaten tatsächlich vor; im Gegensatz zu den *n*-Alkylderivaten nehmen die $\eta_{red.}$-Werte in der Reihe C_3—C_4—C_5 ab. Aufgrund des Gesagten bedeutet dies, daß die Abweichung von der planaren Struktur bei dem i-Propylkomplex am stärksten und bei der i-Amylverbindung am geringsten ist. In voller Übereinstimmung mit dieser Feststellung ist, daß aus dem magnetischen Moment berechnete Para%-Werte, ebenfalls in dieser Reihenfolge abnehmen (42, 36, 10%). Wahrscheinlich spielen — neben der Hyperkonjugationswirkung der N-Alkylgruppen — die sterischen Faktoren eine wesentlichere Rolle in der Ausbildung dieser Tendenz. Die sterische Wirkung ist bei der

* $\eta_{sp} = (\eta_{Lösung}/\eta_{Lösungsmittel}) - 1$; die reduzierte Viskosität $\eta_{red.} = \eta_{sp}/c$. Die Messungen wurden bei 30 °C durchgeführt.

α-verzweigten i-Propylverbindung am stärksten, während sie bei den β-verzweigten i-Butyl- und i-Amylverbindungen wesentlich geringer ist.

In Pyridin werden sehr hohe Werte für $\eta_{red.}$ erhalten. Dies entspricht der Erwartung, da in der Lösung sechsfach koordinierte, infolge der recht geringen Symmetrie (D_{2h}) stark verzerrte Oktaeder-Species vorliegen. Die Werte für *n*- bzw. i-Verbindungen weisen keine oder nur recht geringe Unterschiede auf; es zeigt sich also, daß die Bildung des bis-Pyridin-Addukts unter solchen Bedingungen nicht davon abhängt, ob die Alkylgruppen geradkettig oder verzweigt sind. Diese Feststellungen stehen auch mit den Ergebnissen unserer Spektraluntersuchungen in Einklang.

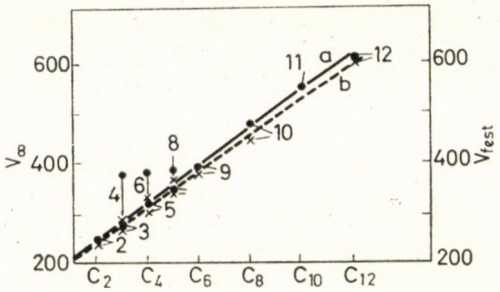


Abb. 2. Berechnete Molvolumenwerte der Komplexe, in Toluol gelöst (a) bzw. in festem Zustand (b), in Abhängigkeit von der Zahl der C-Atome im Alkylsubstituenten. (Die Zahlbezeichnungen der Meßpunkte in beiden Abbildungen sind mit den laufenden Nummern in Tab. I identisch)

Aus Abb. 2 geht hervor, daß die Molvolumina der Komplexe mit der Zahl der C-Atome linear verändert werden, sowohl im festen,* als auch im gelösten** Zustand. Auch hier ergeben sich höhere Werte bei den i-Alkylkomplexen; dies ist auf Grund der sterischen Struktur der Moleküle verständlich. Das Molvolumen der festen Probe ist immer kleiner als der auf unendlich verdünnte Lösungen extrapolierte Wert. Der verhältnismäßig geringe Unterschied weist darauf hin, daß die Wechselwirkungen in der Lösung nicht bedeutend sind. Der Unterschied zwischen den Molvolumina in festem und gelöstem Zustand nimmt — in Übereinstimmung mit den vorangehenden Feststellungen über die Struktur — ebenfalls in der Reihenfolge i-Propyl, i-Butyl, i-Amyl ab.

Weitere Untersuchungen sind im Gange.

* V_{fest} = Mol. Gew./s_{fest}.

** $V_{Lösung}$ = Mol. Gew./d_0 — $1000(d - d_0)/c \cdot d_0$, wo d bzw. d_0 die Dichte der Lösung bzw. des Lösungsmittels und c die Konzentration in Mol/Liter ist. Die V_∞-Werte in Tab. I wurden durch Extrapolierung aus dem Diagramm $V_{Lösung} - \sqrt{c}$ erhalten. Sämtliche Messungen wurden bei 25 °C durchgeführt.

LITERATUR

1. CSÁSZÁR, J.: MTA Kém. Oszt. Közl. **19**, 25 (1963); Magy. Kém. Foly. **68**, 440 (1962)
2. CSÁSZÁR, J.: Acta Chim. Acad. Sci. Hung. **34**, 389 (1962); **32**, 343 (1962)
3. CSÁSZÁR, J., SZEGHALMI, J.: Acta Phys. et Chem. Szeged, XII., 117 (1966)
4. CSÁSZÁR, J., BARTA, I.: Acta Chim. Acad. Sci. Hung. (unter Druck)
5. IRVING, H. M. N. H., SMITH, J. S.: J. Inorg. Nucl. Chem. **31**, 2895 (1969)
6. IRVING, H. M. N. H., SMITH, J. S.: J. Inorg. Nucl. Chem. **30**, 1873 (1968)
7. IRVING, H. M. N. H., SMITH, J. S.: J. Inorg. Nucl. Chem., **31**, 1212 (1969)
8. CHARLES, R. G.: J. Am. Chem. Soc., **81**, 1793 (1959)
9. FAJANS, K., JOHNSON, O.: J. Am. Chem. Soc. **64**, 668 (1942)
10. BILTZ, W.: Raumchemie der festen Stoffe. Verlag L. Vess, Leipzig 1934
11. STAUDINGER, H.: Die hochmolekularen organischen Verbindungen. Springer Verlag, Berlin, 1932
12. STAUDINGER, H.: Trans. Faraday Soc. **29**, 18 (1933)
13. SACCONI, L., CIAMPOLINI, M., NARDI, N.: J. Am. Chem. Soc. **86**, 819 (1964)
14. SACCONI, L., PAOLETTI, P., CIAMPOLINI, M.: J. Am. Chem. Soc. **85**, 411 (1963)
15. HOLM, R. H., SWAMINATHAN, K.: Inorg. Chem., **2**, 181 (1963)
16. SACCONI, L., PAOLETTI, P., DEL RE, G.: J. Am. Chem. Soc. **79**, 4062 (1967) und die dort angeführte Literatur
17. EWALD, A. H., SINN, E.: Inorg. Chem. **6**, 40 (1967)

József CSÁSZÁR
István BARTA
Szeged, Rerrich B. tér, Hungary.

Acta Chimica Academiae Scientiarum Hungaricae, Tomus 69 (1), pp. 81—86 (1971)

SYNTHESIS OF CERTAIN NEW SALICYLSULFONYLUREA DERIVATIVES

A. A. ABOU-OUF, A. F. YOUSEF* and M. A. EL-GENDY

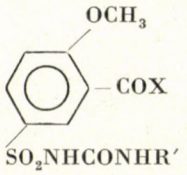
(Pharmaceutical Chemistry Department, Assiut University, Assiut, Egypt, UAR)

Received February 10, 1970

In extension of a previous work, three new series of salicylsulfonylureas have been prepared. They are mainly derived from N-(3-carboxy-4-methoxy-benzenesulfonyl)urea, N-(3-carbalkoxy-4-methoxy-benzenesulfonyl)urea and N-(3-carboxamido-4-methoxy-benzenesulfonyl)urea. The N′-substituents were mostly isopropyl, *p*-tolyl, *p*-chlorophenyl or antipyryl groups. The ethyl carbamate residue in the ethyl-N-(3-carbalkoxy-4-methoxy-benzenesulfonyl) carbamate is more readily attacked by aliphatic amines than the carbalkoxy group situated in position 3. Under certain conditions this carbalkoxy group can be converted into a substituted amide group with aliphatic amines, but not with aromatic amines.

Extensive work in the domain of antidiabetic sulfonylureas was done in our laboratories [1—6]. Some of these products proved to be highly active in pharmacological studies. Recently, it has been reported that salicylates could affect glucosuria and hyperglycemia in fairly large doses in diabetes of both the adult and juvenile type [7]. This inspired the synthesis of certain salicylic acid derivatives containing the sulfonylurea moiety, in the hope to initiate a series of compounds which may appear more active by synergism of the salicylate and sulfonylurea residues.

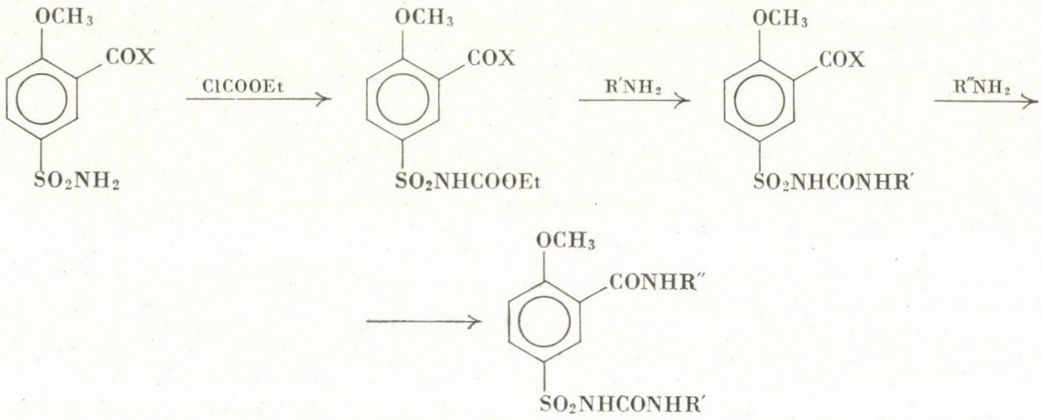
In view of the different mechanisms by which the two residues are effective, it seems of interest to study their combined effect when they occur together in one molecule. The following general structure was adopted as the parent compound from which the designed compounds presented in this work were derived.



X = OH, OR, HNR″

The synthesis of these compounds was carried out according to Scheme I.

* All correspondence should be addressed to Dr. A. F. Yousef.



Experimental

Melting points are uncorrected. Microanalyses were determined by the El-Naser Company, U. A. R. IR spectra were obtained in 300 mg KBr disks containing 1 mg of the sample, on a Perkin-Elmer Model 21 Spectrophotometer.

The following compounds were synthesized by the methods stated below:

Methyl o-methoxybenzoate, in 75% yield, according to COHEN [8].

o-Methoxybenzoic acid in 60% yield, by refluxing methyl *o*-methoxybenzoate with 10% sodium hydroxide.

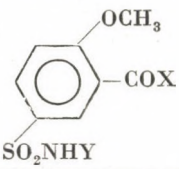
3-Carboxy-4-methoxybenzenesulfonamide (II) from *o*-methoxybenzoic acid [9].

3-Carbalkoxy-4-methoxybenzenesulfonamides (III, IV) by refluxing **II** with an excess of the corresponding absolute alcohol in the presence of conc. H_2SO_4. Table I shows the analytical data of the esters prepared.

Ethyl-N-(3-carboxy-4-methoxybenzenesulfonyl) carbamate (V). The synthesis and isolation were carried out as given by MUKHERJEE [10]. For analytical data see Table I.

Table I

Esters of salicylsulfonamide and carbamates



Compound	Y	X	Yield %	M.p. °C	Analysis	
					Calcd.	Found
III	H	OCH_3	88	176 (a)	N, 5.71	N, 5.94
IV	H	OC_2H_5	84	150 (a)	N, 5.41	N, 5.90
V	$COOC_2H_5$	OH	60	152—4 (b)	C, 43.56	C, 43.61
					H, 4.29	H, 4.87
VI	$COOC_2H_5$	OCH_3	74	137 (a)	N, 4.42	N, 4.88
VII	$COOC_2H_5$	OC_2H_5	78	101 (a)	N, 4.23	N, 4.36

(a) Recrystallized from 45% EtOH. (b) Recrystallized from water.

Ethyl-N-(3-carbalkoxy-4-methoxybenzenesulfonyl) carbamate (VI, VII)

The synthesis and isolation were carried out according to MARSHALL and SIGAL [11]. For analytical data see Table I.

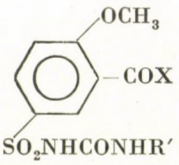
N-(3-Carboxy-4-methoxybenzenesulfonyl)-N′-alkyl-(or aryl-) ureas (VIII, XII)

These compounds were synthesized by the following general procedure. Compound **V** (0.01 mole) was dissolved in dry toluene (20 ml), then treated with the appropriate amine (0.01—0.02 mole). The reaction mixture was then refluxed in an oil bath at 120—130 °C for 3—5 hrs. The solvent was evaporated under reduced pressure, and the residue dissolved in 5% ammonium hydroxide solution. The unchanged amine was extracted with a small amount of ether and the aqueous layer filtered. The filtrate was acidified with dilute HCl and the mixture was cooled thoroughly, filtered and the residue crystallized from aqueous alcohol to give colourless needles.

In the case of N-(3-carbalkoxy-4-methoxybenzenesulfonyl)4N′-alkyl-(or aryl-) ureas (**XIII—XXII**) the corresponding starting compounds, either **VI** or **VII**, are used. The analytical data are shown in Table II.

Table II

N′-Substituted salicylsulfonylureas



Compound	X	R′	Yield %	M.p., °C	Analysis			
					Calcd.		Found	
VIII	OH	i-C_3H_7	65	181—2 (b)	N,	8.86	N,	9.18
IV	OH	C_6H_5	69	206 (b)	N,	8.00	N,	7.89
X	OH	*p*-$C_6H_4CH_3$	71	205 (b)	N,	7.69	N,	7.88
XI	OH	*p*-C_6H_4Cl	69	205 (b)	N,	7.28	N,	7.07
XII	OH	4-antipyryl	68	204—5 (b)	N,	12.17	N,	12.16
XIII	OCH_3	i-C_3H_7	71	160 (b)	N,	8.48	N,	8.46
XIV	OCH_3	C_6H_5	73	157—8 (b)	N,	7.69	N,	7.17
XV	OCH_3	*p*-$C_6H_4CH_3$	69	168—9 (b)	N,	7.41	N,	7.68
XVI	OCH_3	*p*-C_6H_4Cl	74	197 (b)	N,	7.30	N,	7.33
XVII	OCH_3	4-antipyryl	71	193 (c)	N,	11.81	N,	11.78
XVIII	OC_2H_5	i-C_3H_7	70	153—5 (b)	N,	8.14	N,	8.20
XIX	OC_2H_5	-C_6H_5	72	142—3 (b)	N,	7.41	N,	7.73
XX	OC_2H_5	*p*-$C_6H_4CH_3$	71	184—5 (b)	N,	7.14	N,	7.22
XXI	OC_2H_5	*p*-C_6H_4Cl	72	162 (b)	N,	6.79	N,	6.84
XXII	OC_2H_5	4-antipyryl	73	184 (c)	N,	11.79	N,	11.79
XXIII (a)	NH-i-C_3H_5	i-C_3H_7	72	208 (b)	N,	11.76	N,	12.03

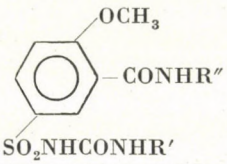
(a) The starting material is compound **VI** or **VII**, and the quantity of isopropylamine used is 3—4 times more than that used to prepare the corresponding R′-substituted compound.
(b) From 45% alcohol.
(c) From 65% alcohol.

N-(3-Carboxamido-4-methoxybenzenesulfonyl)-N′-substituted ureas (XXIV—XXXIX)

The following procedure was used for the preparation of the compounds of this series. Compound **XIII** (0.01 mole) was dissolved in 25% ammonium hydroxide (50 ml). The mixture was allowed to stand in a stoppered flask for 24 hrs. at room temperature, then the solution was filtered to remove any undissolved matter. The clear filtrate was acidified with dilute HCl and the product which separated was filtered and washed with water. After recrystallization from 45% alcohol compound **XXIV** was obtained. For analytical data, see Table III.

Table III

3-Carboxamido derivatives of N′-substituted salicylsulfonylureas



Compound	R′	R″		Yield %	M.p.[e] °C	Analysis			
						Calcd.		Found	
XXIV	i-C_3H_7	H	(a)	74	218	N,	13.33	N,	13.80
XXV	C_6H_5	H	(a)	68	191—2	N,	12.03	N,	11.99
XXVI	*p*-$C_6H_4CH_3$	H	(a)	70	203	N,	11.57	N,	11.65
XXVII	i-C_3H_7	CH_3	(b)	79	213	N,	12.76	N,	12.67
XXVIII	C_6H_5	CH_3		78	194	N,	11.57	N,	11.73
XXIX	*p*-$C_6H_4CH_3$	CH_3	(b)	80	215—6	N,	11.14	N,	11.03
XXX	*p*-C_6H_4Cl	CH_3	(b)	76	205	N,	10.57	N,	10.66
XXXI	4-antipyryl	CH_3	(b)	75	201	N,	14.80	N,	14.60
XXXII	i-C_3H_7	C_2H_5	(c)	63	202—3	N,	12.24	N,	12.36
XXXIII	C_6H_5	C_2H_5	(c)	67	187	N,	11.14	N,	11.30
XXXIV	*p*-C_6H_4Cl	C_2H_5	(c)	68	186	N,	10.21	N,	10.23
XXXV	4-antipyryl	C_2H_5	(c)	65	178	N,	14.37	N,	13.84
XXXVI	i-C_3H_7	C_2H_4OH	(d)	70	191—2	N,	11.69	N,	11.89
XXXVII	C_6H_5	C_2H_4OH	(d)	72	169—170	N,	10.69	N,	10.46
XXXVIII	*p*-$C_6H_4CH_3$	C_2H_4OH	(d)	69	176	N,	10.32	N,	10.41
XXXIX	*p*-C_6H_4Cl	C_2H_4OH	(d)	71	162	N,	9.82	N,	9.98

(a) 25% ammonium hydroxide solution.
(b) 33% aqueous solution of methylamine.
(c) 33% aqueous solution of ethylamine
(d) 50% aqueous solution of ethanolamine.
(e) From 45% alcohol.

Results and discussion

The series of compounds prepared in this work are regarded as sulfonylurea derivatives of salicylates. The salicylate residue was introduced in the form of certain derivatives such as ethers, esters, amides or their combinations attached to the substituted sulfonylurea segment. The preparation of salicyl-

sulfonyl carbamate *via* the interaction of salicylsulfonamide and ethylchloroformate required previous protection of the free hydroxyl group of the salicylic acid residue [12]. Methylation appeared to be suitable to protect the OH group, since it does not reduce the activity of the parent compounds [13, 14].

Sulfonylureas can be prepared by allowing alkyl isocyanates to react with free sulfonamides [15, 16], and by other methods [12, 17]. In this work, the required sulfonylureas were obtained by the interaction of the appropriate amine with the ethyl carbamate derivatives **V**—**VII**. In an attempted preparation of ethyl-N-(3-carboxy-4-methoxybenzenesulfonyl) carbamate (**V**) by MARSHALL's method [11], it was found very difficult to isolate the unchanged sulfonamide(**II**) due to the formation of a mixture of potassium salts derived either from the free carboxylic group, or the amide residue, or both. The formation of the potassium salts reduced the solubility in the reaction medium sued (acetone). The preparation of **V** was therefore carried out in aqueous medium, in the presence of sodium hydroxide, by applying MUKHERJEE and DAVIS's process [10]. The acetone medium used in MARSHALL's method was found suitable in the case of esters **III** and **IV** which gave ethyl--N-(3-carbmethoxy-4-methoxybenzenesulfonyl) carbamate **VI** and ethyl-N-(3-carbethoxybenzenesulfonyl) carbamate (**VII**), respectively. The amines $R'NH_2$ used in the reactions with the ethyl carbamates **V**—**VII** were alkyl, aryl, haloaryl or heterocyclic primary amines.

The sulfonylureas were obtained by heating an arylsulfonylurethane with the primary amine in the presence of dioxan, xylene, or toluene [18, 19]. When more than three molar equivalents of isopropylamine were used, the sulfonylurea was formed together with the corresponding 3-carboxamide (**XXIII**; Table II). This phenomenon was not observed in the case of aromatic

Table IV

Stretching vibrations (ν') of the functional groups

Compound	SO_2 (a) Sulfonamide (cm^{-1})	C=O (b) Urethane (cm^{-1})	C=O (c) Urea (cm^{-1})	C=O (e) Amide (cm^{-1})
VII	1350, 1170	1745	—	—
XIII	1350, 1170	—	1655	—
XIV	1350, 1170	—	1685 (d)	—
XXIII	1350, 1170	—	1660	1680

(a) Ref. [20], p. 308.
(b) Ref. [20], p. 266.
(c) Ref. [20], p. 265.
(d) The relatively increased ν' value may be attributed to the electron withdrawing effect of the phenyl group on the nitrogen atom [21].
(e) Ref. [20], p. 264.

amines which only attacked the carbamate residue giving no carboxamide under these conditions.

Compounds **VII, XIII, XIV** and **XXIII** were examined by IR spectrometry. Compound **VII** is the starting sulfonyl carbamate; compounds **XIII** and **XIV** represent N′-aliphatic and N′-aromatic substituted sulfonylureas, respectively, and the structure of compound **XXIII** was inferred on the basis of microanalytical data.

Table IV shows that besides the carbonyl absorption band at 1660 cm^{-1} of urea, the spectrum of compound **XXIII** has another band at 1680 cm^{-1} which can be due to the C=O group of a secondary amide. This band is not observed in the spectra of the other compounds.

On the basis of the structure of compound **XXIII** established IR spectrometry and microanalysis, it can be said that, under the conditions employed the site preferred which reacts first with the aliphatic amine is the carbamate residue. This can be attributed to the ortho effect of the methoxyl group, and further, to the presence of the sulfonamido group which reduces the electron density on the carbon atom of the carbonyl group in $SO_2NHCOOEt$, thus rendering it more sensitive to attack by strong nucleophilic amines.

All derivatives prepared in this work are under preliminary pharmacological screening.

REFERENCES

1. Abou-Zeid, Y. M., Abou-Ouf, A. A., Mussa, Y.: Bull. Faculty of Pharmacy, Cairo University, I. 59 (1966)
2. Abou-Ouf, A. A., Abou-Zeid, Y. M., Mussa, Y.: Drug Research C. O. P. C. A., U. A. R., **I**, 163 (1968)
3. Moustafa, A., Abou-Ouf, A. A., Mohtady, M. M.: *ibid.*
4. Farghaly, H. M.: Thesis, Cairo University, 1969
5. Abou-Ouf, A. A., El-Kerdawy, M. M., Abdulla, W. A., Selim, H. A.: To be published
6. Abou-Ouf, A. A., El-Kerdawy, M. M., Selim, H. A.: To be published
7. Fang, V., Foye O., Robinson, S. M., Jenkins, H. J.: J. Pharm. Sci. **57,** 2111 (1968)
8. Cohen, J. B., Dudley, H. W.: J. Chem. Soc. 1732. (1910)
9. Vogel, A. I.: Pract. Org. Chem., 3rd Ed., p. 820, Longmans, London, 1964
10. Mukherjee, S. L., David, A.: Indian Pat. 59097; C. A. **52,** 13791 (1958)
11. Marshall, F. J., Sigal, J.: Org. Chem. **23,** 927 (1958)
12. Kurzer, F.: Chem. Rev. **50,** 1 (1952)
13. McCell *et al.*: Canad. Med. Assoc. J. **77,** 624 (1957)
14. Shapiro, S. L., Parrino, V. A., Rogow, E., Freedman, L.: J. Am. Chem. Soc. **81,** 3725 (1959)
15. Farbwerke Hoechst, A. G.: Neth. Pat. 6 400 975; C. A. **62,** 16131 (1965)
16. Farbwerke Hoechst, A. G.: Neth. Pat. 6 504 975: C. A. **64,** 11129 (1966)
17. J. R. Geigy A. G.: Brit. Pat. 604 259; C. A. **43,** 1061 (1949)
18. Farbwerke Hoechst, A. G.: Neth. Pat. 6 509 757; C. A. **65,** 7106 (1966)
19. Mills, J., Marshall, F. J.: U. S. Pat. 3 155 721; C. A. **62,** 3978 (1965)
20. Colthup, N. B., Daly, L. H., Wiberley, S. E.: Introduction to Infrared and Raman Spectroscopy, Acad. Press, New York, 1964
21. Hoyer, H.: Chem. Ber. **89,** 2677 (1956)

A. A. Abou-Ouf
A. F. Yousef
M. A. El-Gendy

Pharmaceutical Chemistry Department, Assiut University, Assiut, Egypt, UAR.

Acta Chimica Academiae Scientiarum Hungaricae, Tomus 69 (1), pp. 87—95 (1971)

INDOLE AND INDOLE DERIVATIVES, X*

SAPONIFICATION, ACID HYDROLYSIS AND DECARBOXYLATION OF (—)-VINCADIFFORMINE AND TABERSONINE

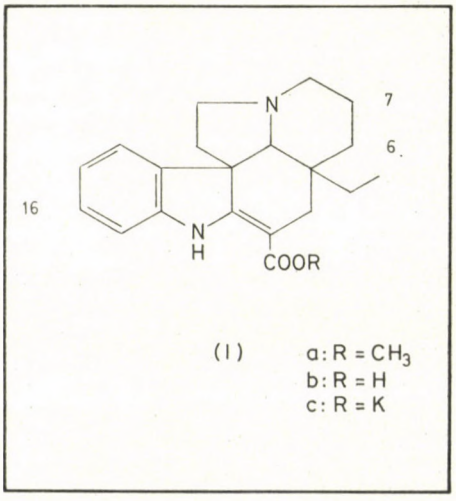
B. ZSADON and K. OTTA

(Department of Chemical Technology, L. Eötvös University, Budapest)

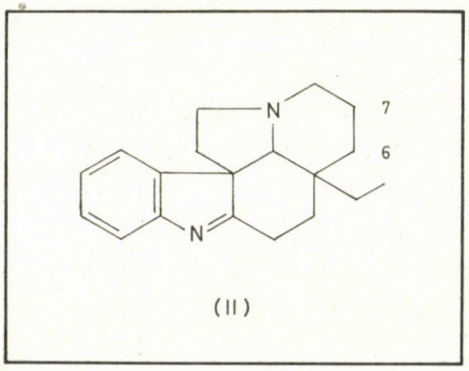
Received February 10, 1970

The acid hydrolysis and decarboxylation of (—)-vincadifformine (**Ia**) and tabersonine (6,7-dehydro-**Ia**) were investigated. (—)-1,2-Dehydroaspidospermidine (**II**) was prepared from (—)-vincadifformine in almost quantitative yield and decarbomethoxytabersonine (6,7-dehydro-**II**) was obtained from tabersonine in good yields under milder conditions than described in the literature. Studies on the saponification of vincadifformine and tabersonine revealed that both alkaloids can readily be saponified with 0.5 *N* potassium hydroxide in ethanol. The unstable (—)-vincadifformic acid (**Ib**) and tabersonic acid (6,7-dehydro-**Ib**) were prepared in almost quantitative yields; their physical constants and ultraviolet spectra are reported. The stability of these acids was examined and the rate of their decarboxylation was measured.

In the course of an investigation on the chemical properties of tabersonine (6,7-dehydro-**Ia**) JANOT, LE MEN and FAN [1] attempted the saponification of this alkaloid, but their experiment failed to give the expected product. Later on, DJERASSI, LE MEN, JANOT, PLAT and associates [2, 3, 4] subjected vincadifformine (**Ia**) and tabersonine to hydrolysis with hydrochloric acid. However, instead of the corresponding carboxylic acids (**Ib** and 6,7-dehydro-**Ib**) they obtained the indoline bases, 1,2-dehydroaspidospermidine (**II**) and



(I) a: R = CH_3
b: R = H
c: R = K



(II)

* Part IX. T. TÓTH, Á. GERECS, Acta Chim. Acad. Sci. Hung. **67**, 229 (1971)

decarbomethoxytabersonine (6,7-dehydro-**II**), respectively, because the hydrolysis of the above starting materials was accompanied by decarboxylation and this resulted in the formation of **II** and 6,7-dehydro-**II**. (A similar reaction was described for the first time in connection with the structure elucidation of akuammicine [5, 6]).

The authors, mentioned above, accomplished the acid hydrolysis under rather vigorous conditions (105 and 110 °C, in sealed tubes with 2 *N* and 4 *N* HCl for 6 and 2.5 hrs., respectively). Under such conditions the yields of the decarboxylation products were 47% with vincadifformine and 53% with tabersonine [4]. Recently PYUSKYULEV *et al.* [7] hydrolyzed 16-methoxytabersonine by refluxing it for 5 hrs. with 5 *N* hydrochloric acid. According to the published data, the corresponding indolenine derivate (6,7-dehydro-16-methoxy-**II**) was obtained in about 61% yield.

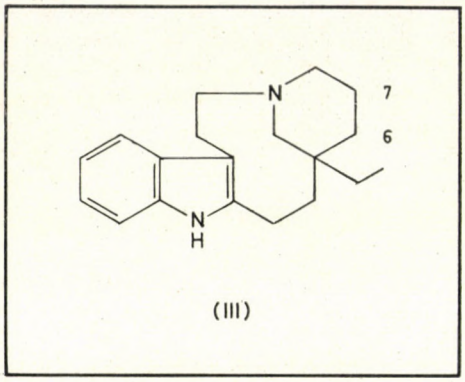
Thus neither the supposed vincadifformic acid nor tabersonic acid could be prepared hitherto, there are no available data concerning their stability, furthermore, the saponification of vincadifformine and tabersonine, too, requires further examination.

Results

The acid hydrolysis and decarboxylation of (—)-vincadifformine (**Ia**) and tabersonine (6,7-dehydro-**Ia**) were investigated, in order to find the optimum conditions for acid hydrolysis and to attain maximum yields of (—)-1,2-dehydroaspidospermidine (**II**) and decarbomethoxytabersonine (6,7-dehydro-**II**), respectively, as far as possible with complete elimination of side-reactions. The progress of the reaction was followed by measurement of the CO_2 evolved. It was found that the vigorous conditions reported in the literature are unnecessary, as both alkaloids undergo hydrolysis and decarboxylation at satisfactory rates already in 1 *N* hydrochloric acid at 100 °C. Both the product and the unreacted starting material were isolated from the reaction mixture in each case. Almost no by-product was formed in the hydrolysis of (—)-vincadifformine and only relatively little was formed in the analogous hydrolysis of tabersonine, provided that the reaction was carried out in 1 *N* hydrochloric acid at 100 °C and total conversion was not forced. Thus the hydrolysis of (—)-vincadifformine gave 71% (—)-1,2-dehydroaspidospermidine (**II**) and 26% unreacted (—)-vincadifformine in 6 hrs. (Accordingly, the yield is 96%.) Under similar conditions, but with a reaction time of 5 hrs., tabersonine gave 78% decarbomethoxytabersonine (6,7-dehydro-II) and 5% unreacted tabersonine (yield 82%).

For identification purposes, the products of acid hydrolysis and concomitant decarboxylation were reduced with complex metal hydrides. (See references [2, 3, 4].) Thus, (—)-1,2-dehydroaspidospermidine gave (—)-aspido-

spermidine and (+)-quebrachamine (**III**), while decarbomethoxytabersonine resulted in (—)-6,7-dehydroaspidospermidine and (+)-6,7-dehydroquebrachamine, prepared in crystalline form. (Physical constants are given in the experimental part, the ultraviolet spectra are shown in Fig. 1.)



(III)

In order to prepare (—)-vincadifformic acid (**Ib**) and tabersonic acid (6,7-dehydro-**Ib**), experiments were carried out for the saponification of (—)-vincadifformine (**Ia**) and tabersonine (6,7-dehydro-**Ia**) with potassium hydroxide in ethanol. It was found that in contrast to previous statements, both alkaloids can be saponified. The reaction proceeds at a satisfactory rate even with 0.5 *N* potassium hydroxide in ethanol at reflux temperature. The resulting carboxylic acids could be isolated in almost quantitative yields, provided that decomposition could be avoided. Thus, (—)-vincadifformine gave 74% (—)-vincadifformic acid on refluxing for 30 min. with 0.5 *N* potassium hydroxide in ethanol, and 22% (—)-vincadifformine could be recovered. (Accordingly, the yield is 95%.) After refluxing for one hr., 92% (—)-vincadifformic acid and 4% unreacted (—)-vincadifformine were isolated. (In this case the yield is 96%). Saponification of tabersonine gave 84% tabersonic acid and 15% unreacted tabersonine in one hr. (yield 99%). The physical constants of these compounds are given in the experimental part, the ultraviolet spectra are shown in Fig. 2.

All attempts to crystallize these compounds have failed heretofore.

Both (—)-vincadifformic acid and tabersonic acid are unstable compounds. In solution both compounds undergo spontaneous decarboxylation to give (—)-1,2-dehydroaspidospermidine (**II**) and decarbomethoxytabersonine (6,7-dehydro-**II**), respectively. They can be stored in alkaline solution at low temperatures for months. The free acids are storable in organic solvents (*e.g.* ether) for shorter periods, but undergo rapid decomposition in aqueous solutions containing strong acids. The rate of decomposition of (—)-vincadifformic acid was measured under various conditions. The results are shown in the experimental part.

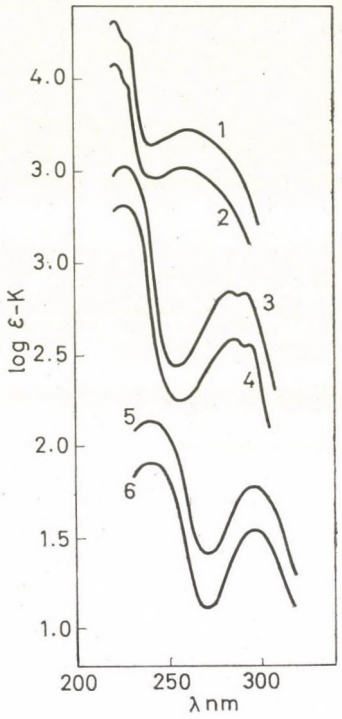


Fig. 1. Ultraviolet spectra, *1*, (—)-1,2-dehydroaspidospermidine ($K = 0$), *2*, decarbomethoxytabersonine ($K = 0.2$), *3*, (+)-quebrachamine ($K = 1$), *4*, (+)-6,7-dehydroquebrachamine ($K = 1.3$), *5*, (—)-aspidospermidine ($K = 1.7$), *6*, (—)-6,7-dehydroaspidospermidine ($K = 1.9$)

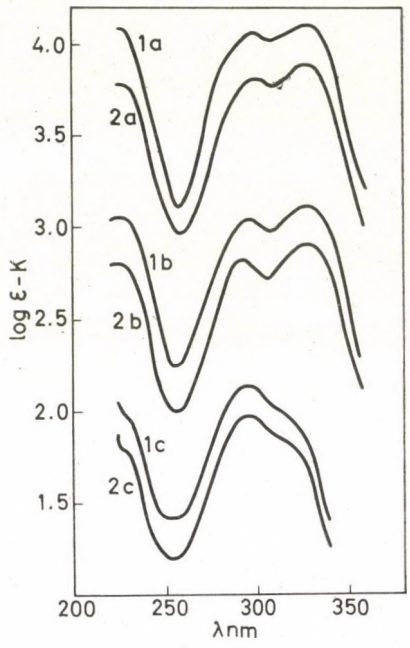


Fig. 2. Ultraviolet spectra. *1*, (—)-vincadifformic acid: *a*, in methanol ($K = 0$), *b*, in 0.1 *N* HCl in methanol ($K = 1$), *c*, in 0.01 *N* NaOH in methanol ($K = 2$), *2*, tabersonic acid: *a*, in methanol ($K = 0.2$), *b*, in 0,1 *N* HCl in methanol ($K = 1.2$), *c*, in 0.01 *N* NaOH in methanol ($K = 2.2$)

Experimental part

The experiments were carried out with tabersonine (m.p. 88 °C, $[\alpha]_D$ —360° in ethanol) obtained from seeds of *Amsonia tabernaemontana* [8], and with (—)-vincadifformine (m.p 96 °C, $[\alpha]_D$ —600° in ethanol) obtained by catalytic hydration of tabersonine [8]. The alkaloid components in various mixtures were detected by thin-layer chromatography. (Method *A*: aluminium oxide G and benzene as eluent; method *B*: silica gel G and a mixture of methanol, chloroform and toluene 50 : 36 : 80.) The optical rotatory power was measured with a Schmidt-Haensch polarimeter, the ultraviolet spectra were recorded on an Optica Milano CF-4R spectrophotometer.

Acid hydrolysis of (—)-vincadifformine (Ia)

5.1 g (15 mmoles) of (—)-vincadifformine were dissolved in 500 ml *N* HCl in a flask equipped with a reflux condenser and a gas inlet tube. The solution was heated for 6 hrs. on the water bath under a continuous stream of nitrogen. The exit gases leaving at the top of the condenser were passed through a $Ba(OH)_2$ solution in order to trap their CO_2 content. The $BaCO_3$ precipitate was filtered from time to time and its weight measured (Table I). After starting the reaction an induction period of about 20 min was observed. During this time the

reaction mixture was greenish and no CO_2 evolved. At the end of this period the evolution of CO_2 commenced and the colour of the solution changed to brownish-yellow. Altogether 2.1 g of $BaCO_3$ precipitated during the 6-hour reaction time, which is equivalent to 10.7 mmoles (71%) of CO_2.

At the end of the 6-hour reaction time the solution was cooled, alkalized and the alkaloids were extracted with ether. The ether extract (300 ml) contained, according to thin-layer chromatographic analysis, vincadifformine, 1,2-dehydroaspidospermidine (**II**) and some by-products. The two main components could be separated by counter-current distribution with

Table I

Reaction time (hrs.)	$BaCO_3$ precipitate (g)
0.5	0.10
1	0.37
2	0.91
3	1.50
5	1.85
6	2.10

150—150 ml of 1% citric acid and 300—300 ml of ether in 5 steps, so that vincadifformine remained in the organic phase and 1,2-dehydroaspidospermidine, together with the by-products, appeared in the aqueous phase. Evaporation to dryness of the ethereal phase gave 1.34 g (4 mmoles, 26%) of unreacted (—)-vincadifformine (**Ia**), which was identified on the basis of its R_f value, rotatory power and UV spectrum.

The aqueous phase was alkalized, extracted with benzene and the brownish-yellow benzene solution obtained was chromatographed on 40 g aluminium oxide (activity **II**) column. Elution was done with 600 ml of a 1 : 1 benzene–petroleum ether mixture. The combined eluates were evaporated to dryness to give 3.02 g (10.8 mmoles, 71%) of (—)-1,2-dehydroaspidospermidine (**II**), a colourless viscous oil, $[\alpha]_D$ —244° (in ethanol, c = 0.25). UV spectrum (Fig. 1) λ_{max} (in methanol) 222, 228 (shoulder) and 263 nm; log ε 4.34, 4.20 and 3.71, respectively.

$C_{19}H_{24}N_2$ (280.42). Calcd. N 9.99. Found N 9.98%.

Reduction of (—)-1,2-dehydroaspidospermidine (II) with complex metal hydrides

The reduction was carried out with $NaBH_4$ and $LiAlH_4$ as described earlier [8].

(a) (+)-Quebrachamine (III). 1.48 g (5.3 mmoles) of (—)-1,2-dehydroaspidospermidine (**II**) was reduced with $NaBH_4$ under refluxing in abs. ethanol. Subsequent work-up of the reaction mixture gave 1.20 g (4.3 mmoles, 80%) of (+)-quebrachamine as the main product. It was crystallized from heptane, m.p. 146—147 °C, $[\alpha]_D$ +114° (in $CHCl_3$, c = 0.5). UV spectrum (Fig. 1, curve 3) λ_{max} (in methanol) 228, 286 and 292 nm; log ε 4.53, 3.85 and 3.83, respectively.

$C_{19}H_{26}N_2$ (282.43). Calcd. N 9.92. Found N 9.95%.

(b) (—)-Aspidospermidine. 1.40 g (5 mmoles) of (—)-1,2-dehydroaspidospermidine (**II**) was reduced with $LiAlH_4$ in ether. The crude product was chromatographed on aluminium oxide to give 1.25 g (4.4 mmoles, 88%) of pure (—)-aspidospermidine. It was crystallized from heptane for analytical purposes, m.p. 120—121 °C, $[\alpha]_D$ —17° (in ethanol, c = 1.5). UV spectrum (Fig. 1, curve 5) λ_{max} (in methanol) 244 and 297 nm; log ε 3.82 and 3.48, respectively.

$C_{19}H_{26}N_2$ (282.43). Calcd. N 9.92. Found N 9.89%.

Acid hydrolysis of tabersonine (6,7-dehydro-Ia)

The hydrolysis of tabersonine was achieved similarly to that of vincadifformine. 2.02 g (6 mmoles) of tabersonine base were dissolved in 300 ml *N* HCl and the solution was heated for 5 hrs. on the water bath. The CO_2 evolved was measured similarly as above, by passing the exit gases through $Ba(OH)_2$ solution and weighing the $BaCO_3$ precipitate from time to time (Table II). A similar short induction period was observed after initiation of the reaction, as with vincadifformine. Altogether 0.95 g of $BaCO_3$ was precipitated during the 5 hour reaction time, which is equivalent to 4.8 mmoles (80%) of CO_2.

Table II

Reaction time (hrs.)	$BaCO_3$ precipitate (g)
0.5	0.10
1	0.26
2	0.62
3	0.80
5	0.95

After the 5-hour reaction period the solution contained decarbomethoxytabersonine, unreacted tabersonine and some by-products. This alkaloid mixture was separated just as in the case of the acid hydrolysis of vincadifformine, and 0.1 g (0.3 mmoles, 5%) of unreacted tabersonine, identified on the basis of its R_f value, rotatory power and UV spectrum, and 1.3 g (4.68 mmoles, 78%) of decarbomethoxytabersonine (6,7-dehydro-**II**), $[\alpha]_D$ —142° (in ethanol, $c = 0.25$), were obtained. The UV spectrum of decarbomethoxytabersonine obtained is shown in Fig. 1 (curve 2): λ_{max} (in methanol) 222, 228 (shoulder) and 264 nm; log ε 4.28, 4.17 and 3.65, respectively.

$C_{19}H_{22}N_2$ (278.40). Calcd. N 10.06. Found N 9.95%.

Reduction of (—)-decarbomethoxytabersonine (6,7-dehydro-II) with complex metal hydrides

The reduction was accomplished both with $NaBH_4$ and $LiAlH_4$, in the manner described earlier [8], similarly to the case of (—)-1,2-dehydroaspidospermidine.

(a) (+)-6,7-dehydroquebrachamine (6,7-dehydro-III). The reduction of decarbomethoxytabersonine with $NaBH_4$ in boiling ethanol gave (+)-6,7-dehydroquebrachamine as the main product, which was purified by chromatography on aluminium oxide column (as described above for quebrachamine) and subsequent crystallization from heptane. Colourless small plates, m.p. 124 °C, $[\alpha]_D$ +120° (in methanol, $c = 0.25$). UV spectrum (Fig. 1, curve 4) λ_{max} (in methanol) 228, 285 and 293 nm; log ε 4.60, 3.87 and 3.84, respectively.

$C_{19}H_{24}N_2$ (280.42). Calcd. C 81.38, H 8.63, N 9.99. Found C 81.30, H 8.67, N 9.95%.

(b) (—)-6,7-Dehydroaspidospermidine. Decarbomethoxytabersonine (6,7-dehydro-**II**) was reduced with $LiAlH_4$ in ether solution to give (—)-6,7-dehydroaspidospermidine in practically quantitative yield, which was then purified as described for aspidospermidine, *i.e.* by chromatography on aluminium oxide with elution with ether, followed by crystallization from heptane. Colourless small plates, m.p. 110—111 °C, $[\alpha]_D$ —16° (in methanol, $c = 1.5$). UV spectrum (Fig. 1, curve 6) λ_{max} (in methanol) 243 and 296 nm; log ε 3.82 and 3.46, respectively.

$C_{19}H_{24}N_2$ (280.42). Calcd. C 81.38, H 8.63, N 9.99. Found C 81.40, H 8.63, N 9.93%.

Saponification of (—)-vincadifformine (Ia) with KOH in ethanol in 0.5 hr: (—)-vincadifformic acid (Ib)

0.338 g (1 mmole) of (—)-vincadifformine base was dissolved in 6 ml of 0.5 *N* KOH in ethanol and the solution was refluxed for 30 min. After cooling a clear solution was obtained, which was diluted with 50 ml of 0.1 *N* aqueous KOH and extracted with ether. The ether extract was evaporated to dryness to give a 88 mg residue, which was dissolved in 50 ml of ether and subjected to counter-current distribution with 50—50 ml of ether and 50—50 ml of 1% aqueous citric acid solution in 5 steps. Upon evaporation, the combined ether extract gave 75 mg (0.22 mmoles, 22%) of unreacted (—)-vincadifformine, which was identified on the basis of its R_f value, rotatory power and UV spectrum.

The product of the saponification reaction (**Ic**) remained in the alkaline aqueous solution. The solution was cooled to —10 °C, neutralized with dilute acetic acid and immediately extracted with 5×50 ml of ether. The combined organic phase was dried over anhydrous Na_2SO_4 overnight in the refrigerator and evaporated to dryness in vacuum to give 0.24 g (0.74 mmoles, 74%) of (—)-vincadifformic acid (**Ib**), a colourless oil, which solidified on standing. This substance is soluble in organic solvents and alkaline aqueous media. It also dissolved in acidic aqueous solutions, but with simultaneous loss of CO_2. Mainly due to the instability of the compound, our attempts to crystallize the product have been fruitless hitherto. According to thin-layer chromatographic analysis, the freshly prepared substance was homogeneous, but decomposed soon on standing at room temperature. The physical constants of the material were measured with freshly prepared samples. $C_{20}H_{24}N_2O_2$ (324.4). $[\alpha]_D$ —520° (in methanol, $c = 0.25$) and —460° (in 0.01 *N* NaOH in methanol, $c = 0.25$).

The UV spectrum of (—)-vincadifformic acid was recorded in methanol, 0.1 *N* HCl in methanol and 0.01 *N* NaOH in methanol (Fig. 2, curves 1a, 1b and 1c). λ_{max} (in methanol) 224, 298 and 328 nm; log ε 4.08, 4.06 and 4.09, respectively. λ_{max} (0.1 *N* HCl in methanol) 226, 296 and 328 nm; log ε 4.06, 4.04 and 4.12, respectively. λ_{max} (0.01 *N* NaOH in methanol) 228, 296 and 310 (infl.) nm; log ε 3.98, 4.14 and 4.02, respectively.

Saponification of (—)-vincadifformine (Ia) with KOH in ethanol in 1 hour

1.52 g (4.5 mmoles) of (—)-vincadifformine base was dissolved in 27 ml of 0.5 *N* KOH in ethanol and the solution refluxed for 1 hour. A clear solution was obtained again, which was diluted with 0.1 *N* aqueous KOH and extracted with ether. The ethereal phase was evaporated to dryness and the residue (135 mg) fractionated between ether and 1% aqueous citric acid solution to give 61 mg (4%) of unreacted (—)-vincadifformine. The alkaline aqueous phase contained (—)-vincadifformic acid as the only alkaloid. From this solution 1.33 g (4.14 mmoles, 92%) of (—)-vincadifformic acid (**Ib**) was isolated similarly as above, the product was identified by means of its R_f value, optical activity and UV spectrum, and it was found to be identical with the product obtained in the 30 min saponification.

324 mg (1 mmole) of (—)-vincadifformic acid obtained was dissolved in 30 ml of 1 *N* HCl and refluxed for 20 min to achieve decarboxylation. The CO_2 evolved was trapped in $Ba(OH)_2$ solution to obtain 0.195 g of $BaCO_3$, which is equivalent to 0.98 mmoles of CO_2. The solution was then alkalized and extracted with ether. The ethereal phase was evaporated to give 274 mg (0.98 mmoles, 98%) of (—)-1,2-dehydroaspidospermidine (**II**), identical in every respect with the product obtained by acid hydrolysis of (—)-vincadifformine.

Attempts were made to prepare the crystalline salts of (—)-vincadifformic acid, but they failed heretofore.

Saponification of tabersonine with KOH in ethanol: tabersonic acid (6,7-dehydro-Ib)

0.67 g (2 mmoles) of tabersonine base was dissolved in 12 ml of 0.5 *N* KOH in ethanol and the solution was refluxed for one hour to give a clear solution, which was worked up similarly as in the case of vincadifformine. 0.10 g (0.3 mmoles, 15%) of unreacted tabersonine was recovered, which was identified on the basis of its R_f value, optical activity and UV spectrum.

As main product, 0.54 g (1.68 mmoles, 84%) of tabersonic acid (6,7-dehydro-**Ia**) was isolated in form of a colourless, viscous oil, which solidified on standing. This substance is

soluble in organic solvents and alkaline aqueous media. It also dissolves in acids with the evolution of CO_2 and the decomposition process goes to completion on heating the solution. The main product of the decomposition reaction is decarbomethoxytabersonine (6,7-dehydro-**II**), but by-products are also formed. The decarbomethoxytabersonine formed in the decarboxylation of tabersonic acid was identical with the product obtained in the acid hydrolysis of tabersonine.

Attempts to crystallize tabersonic acid or to prepare crystalline salts thereof have failed so far. The physical constants of these compounds were determined with freshly prepared samples of chromatographic purity. $C_{20}H_{22}N_2O_2$ (322.4). $[\alpha]_D$ —280° (0.01 *N* NaOH in methanol, $c = 0.2$). The UV spectrum of tabersonic acid was recorded in methanol, 0.1 *N* HCl in methanol and 0.01 *N* NaOH in methanol (Fig. 2, curves 2a, 2b and 2c). λ_{max} (in methanol) 224, 298 and 328 nm; log ε 3.97, 4.00 and 4.08, respectively. λ_{max} (0.1 *N* HCl in methanol) 226, 294 and 328 nm; log ε 4.00, 4.02 and 4.08. λ_{max} (0.01 *N* NaOH in methanol) 228, 296 and 310 (infl.) nm; log ε 3.98, 4.17 and 4.06, respectively.

Stability of (—)-vincadifformic acid (Ib)

(a) Rate of decarboxylation in acid solution. 15—15 ml portions of a standard solution of (—)-vincadifformic acid in 0.1 *N* NaOH were placed in an ultrathermostat and heated to the desired temperature. The initial vincadifformic acid content (c_0) of each sample was 45 mg. The samples were acidified with 2—2 ml of 5 *N* HCl at the temperature of measurement and after the reaction period was over, the decarboxylation reaction was stopped by addition of alkali. The vincadifformic acid content (c) of the samples was determined indirectly: the obtained 1,2-dehydroaspidospermidine (**II**) was extracted with ether from the alkaline solution, and the evaporation residue of the ether extract was measured by weight. Fig. 3 shows the log c_0/c *vs.* time (t) function at 20 °C, under the conditions given.

Similar measurements were carried out at 50, 0 and 10 °C. Table III shows the rate constants (k) calculated on the basis of these measurements, as well as the half-life time ($t_{1/2}$) of vincadifformic acid.

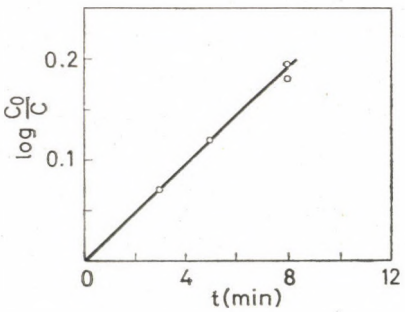


Fig. 3

Table III

Temperature (°C)	k (min^{-1})	$t_{1/2}$ (min)
—10	4×10^{-3}	173
0	1.1×10^{-2}	63
20	5.5×10^{-2}	12.5
50	5.1×10^{-1}	1.3

(b) Stability in alkaline medium. The stability of (—)-vincadifformic acid in 0.1 *N* NaOH solution was examined similarly as above at 0 °C. No decomposition was observed during a 2-month period.

(c) Rate of decarboxylation in ethereal solution. In ethereal solution the initial concentration (c_0) of (—)-vincadifformic acid decreased to its half in about 3 hrs. and 20 days at reflux temperature and at 0 °C, respectively. In this case, too, the determination was carried out indirectly. The unchanged (—)-vincadifformic acid was extracted with an alkaline aqueous solution and the ethereal phase was evaporated to dryness to give the decarboxylation product, which was weighed.

*

The authors are indebted to Prof. Á. Gerecs for his valuable comments during this work. The microanalyses were carried out by Mrs. M. Balogh, for which the authors are thankful.

REFERENCES

1. Janot, M-M., Le Men, J., Fan, Ch.: Compt. Rend. Acad. Sci. Paris, **248,** 3005 (1959)
2. Djerassi, C., Budzikiewicz, H., Wilson, J. M., Gosset, J., Le Men, J., Janot, M-M.: Tetrahedron Letters, **1962,** 235
3. Plat, M., Le Men, J., Janot, M-M., Wilson, J. M., Budzikiewicz, H., Durham, L. J., Nakagawa, Y., Djerassi, C.: Tetrahedron Letters, **1962,** 271
4. Plat, M.: Theses, **1963,** Paris, Série A, № 4043
5. Aghoramurthy, K., Robinson, R.: Tetrahedron **1,** 172 (1957)
6. Smith, G. F., Wróbel, J. T.: J. Chem. Soc. **1960,** 792
7. Pyuskyulev, B., Kompis, J., Ognyanov, J., Spiteller, G.: Coll. Czechoslov. Chem. Commun. **32,** 1289 (1967)
8. Zsadon, B., Hubay R., Egry, É., Rákli, M., Sárközi, M.: Magy. Kém. Foly. **76,** 466 (1970); Zsadon, B., Rákli, M., Hubay, R.: Acta Chim. Acad. Sci. Hung. **67,** 71 (1971)

Béla Zsadon
Klára Otta
Budapest VIII., Múzeum krt. 6—8.

Acta Chimica Academiae Scientiarum Hungaricae, Tomus 69 (1), pp. 97—102 (1971)

THE REACTION OF AMMONIUM THIOCYANATE WITH DICYCLOHEXYLCARBODIIMIDE

T. VAJDA, J. KAJTÁR and F. RUFF

(Institute of Organic Chemistry, L. Eötvös University, Budapest)

Received February 10, 1970

Equimolecular amounts of ammonium thiocyanate and dicyclohexylcarbodiimide in acetonitrile solution yield an equimolecular mixture of dicyclohexylthiourea and 1,2-dicyclohexyl-3-cyanoguanidine. The stoichiometry of the reaction and the composition of the recrystallized product have been studied.

The addition of compounds containing very different kinds of functional groups to the double bond system of carbodiimides has been studied in many cases [1]. Some of the studies dealt with the reaction between compounds containing heterocumulative bonds and dicyclohexylcarbodiimide [2]. To obtain a more general insight into these addition type reactions, it seemed to be interesting to investigate the behaviour of a compound having the allene-like bond system only as a resonance structure. For this purpose ammonium thiocyanate has been chosen whose anion exhibits an 'ambident' nature, *i.e.* it can be characterized by the following two resonance structures [3]:

$$^{-}S—C\equiv N \longleftrightarrow S=C=N^{-}$$

On the addition of an equimolecular amount of DCCI* to a 0.5 molar solution of NH_4SCN, within a few minutes after the dissolution of the DCCI, a mildly exothermicd reaction starts. The reaction is accompanied by the deposition of a considerable amount of colourless crystalline product.** The crude product (m.p. 150—151 °C) was recrystallized from 85% methanol (loss: 15%, m.p. 154—156 °C). The melting points did not change on further recrystallization.

As given in the following, the investigations of the recrystallized product — based primarily on mass spectroscopy — confirmed the formation of an equimolecular mixture of DCS and DCGN. Formally the reaction might be

* The following abbreviations are used: DCCI, dicyclohexylcarbodiimide; DCG, dicyclohexylguanidine; DCGN, 1,2-dicyclohexyl-3-cyanoguanidine; DCS, dicyclohexylthiourea; DCU, dicyclohexylurea.

** If the concentrations of the reacting components in acetonitrile are changed from 0.5 to 0.05 molar, the reaction proceeds without the deposition of crystals. After concentration of this solution it gave the same product in a similar yield as above.

considered as the addition of the "elements" of NH_4SCN (H_2S and NH_2CN) to two molecules of DCCI:*

$$NH_4SCN + 2\ C_6H_{11}N{=}C{=}NC_6H_{11} \rightarrow C_6H_{11}NHC(S)NHC_6H_{11} + C_6H_{11}NHC(NCN)NHC_6H_{11} \quad (1)$$

I (DCS) **II**(DCGN)

The composition of the reaction product purified by crystallization was proved with the following experimental results.

1. Mass spectroscopic data

Intense peaks in the mass spectrum of the reaction product were observed at *m/e* 55, 125, 207, 240, 248, corresponding to species **III—VII**, respectively, from which the first one is characteristic of the cyclohexyl group, while the last two are the molecular peaks of the reaction products (**I** and **II**).

$(CH_2{=}CHCH_2CH_2)^+$ **III**, *m/e* 55

$(C_6H_{11}NHC{=}NH)^+$ **IV**, *m/e* 125

$(C_6H_{11}NHC{=}NC_6H_{11})^+$ **V**, *m/e* 207

$(C_6H_{11}NHC(S)NHC_6H_{11})^+$ **VI**, *m/e* 240

$(C_6H_{11}NHC(NCN)NHC_6H_{11})^+$ **VII**, *m/e* 248

The relative intensities of the peaks of **VI** and **VII** depend on the time of scanning, because substance **VI** evaporates 10 times faster than **VII**.

The appearance of the peaks at *m/e* 240, 248 is consistent with the presence of **I** and **II** among the reaction products but, in principle, it might also be related to a product with an original molecular weight of 488. This ambiguity is involved in the explanation of the microanalytical data too. Namely, the per cent amounts of N and S (17.2 and 6.7) found for the crystallized product are in agreement with both the compound $C_{27}H_{48}N_6S$ (MW: 488.8) and the equimolecular mixture of compounds $C_{13}H_{24}N_2S$ (DCS: MW 240.4) and $C_{14}H_{24}N_4$ (DCGN: MW 248.4). (Calcd. N and S: 17.2 and 6.6%.) The possibility of the uniform product with a molecular weight of 488.8 is excluded by the results given in paragraphs 2—4.

* Considering this equation, the yield calculated for DCCI was 63% for the recrystallized material.

2. Thin layer chromatography

The thin layer chromatography of the recrystallized reaction product resulted two spots and the R_f data were similar to those of the authentic samples of DCS and DCGN.

3. Melting point diagram

The melting point diagram drawn on the basis of the melting points of authentic DCS and DCGN samples (Fig. 1) shows a characteristic eutectic point at the composition of 50—50% (m.p. 154—157 °C). The melting point

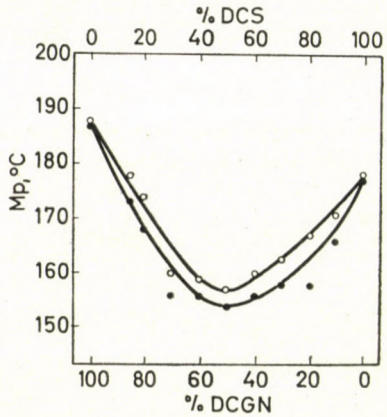


Fig. 1. Melting point diagram of the mixtures of DCS and DCGN. The composition is given in mole%. The melting point data are shown for the beginning ● and the end ○ of melting

of this eutectic mixture is almost identical with the value for the recrystallized reaction mixture. Upon mixing the eutectic material with the pure reaction product, there is no melting point depression, *i.e.* the two products are identical.

It should be mentioned that the composition was not changed upon recrystallization from aqueous methanol of a sample of the eutectic mixture (m.p. identically 154—156 °C). This shows also that the DCS—DCGN composition in per cent of the crystallized reaction product is characteristic of the crude product too.

4. IR spectroscopic data

The IR spectrum (Fig. 2) of the recrystallized reaction product is the same as that of the mixture containing 50—50% of authentic DCS and DCGN. Significant are the δNH bands (1562, 1512 cm^{-1}) characteristic of DCS and the νCN band (2162 cm^{-1}) characteristic of DCGN (Figs 3 and 4).

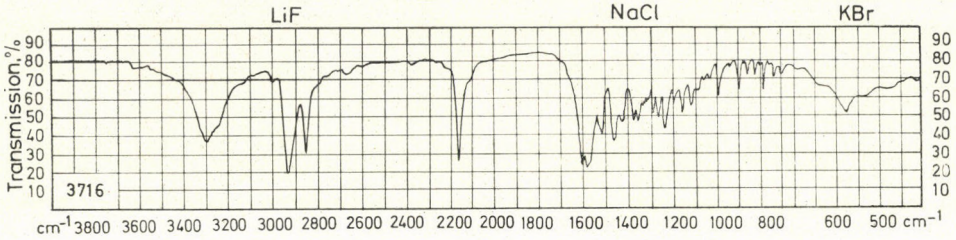


Fig. 2. Infrared spectrum of the reaction product in KBr pellet

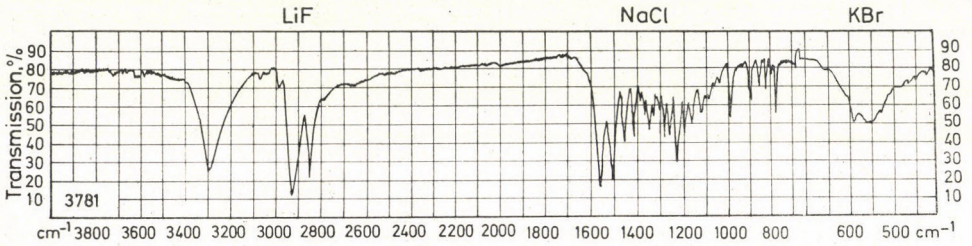


Fig. 3. Infrared spectrum of dicyclohexylthiourea in KBr pellet

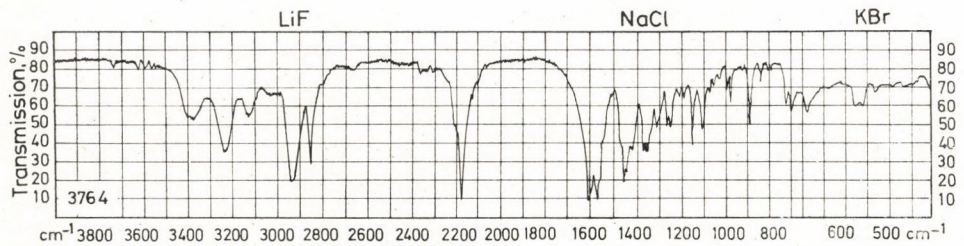


Fig. 4. Infrared spectrum of 1,2-dicyclohexyl-3-cyanoguanidine in KBr pellet

In some cases the relative intensities of the δNH and νCN bands allowed qualitative or nearly quantitative conclusions concerning the composition of crystalline mixtures of DCS and DCGN. Thus, it was concluded *e.g.* that the crude material produced in the reaction could not be resolved into components by fractional crystallization. Depending on the solvent, the composition either remains unchanged (chloroform–petroleum ether, aqueous ethanol, aqueous methanol, aqueous dioxane) or the mixture becomes slightly enriched in DCS (benzene).

The reaction of NH_4SCN with DCCI carried out in acetone instead of acetonitrile results in a crystalline product enriched in DCGN.* The slightly higher melting point of the product is in agreement with this (m.p. 156—158 °C).

* The amount of the deposited crystals is much smaller as compared to the acetonitrile solution.

Investigation of the reaction stoichiometry by preparative methods

NH_4SCN has been reacted with DCCI in different mole ratios. The compositions 3 : 1, 2 : 1, and 1 : 1 resulted in a similar amount of crystalline product, while the 1 : 2 ratio led only to one-half yield calculated for DCCI. This means that instead of the 1 : 2 stoichiometry shown in the formal Eq. (1), an equimolecular amount of ammonium thiocyanate is necessary for the conversion of dicyclohexylcarbodiimide with good yield.

Investigation of the consumption of SCN ions by an analytical method

The consumption of SCN ions has been measured iodometrically.* The determination of the reaction rate at the investigated dilutions was unsuccessful, because the concentration of SCN ions dropped below 40% already within 1 minute. Afterwards the reaction became very slow. The experiment carried out at a concentration of 0.1 *M* gave 25% of SCN ion in the equilibrium mixture obtained after the reaction. This indicates the incorporation of 75% of the SCN into covalent bonds, showing also an NH_4SCN to DCCI ratio of at least 1.5 : 2 required by the reaction.

Experimental

Melting points were determined in capillary tubes without correction. The errors of the m.p. determinations are around ± 2 °C. Samples for microanalyses were dried at 100 °C over P_2O_5 in vacuum (20 Torr) for 16 hrs. Thin layer chromatography (tlc) was carried out on silica gel G (Merck AG) using the following solvent systems: *A*, chloroform–petroleum ether, 10 : 20; *B*, chloroform–petroleum ether, 10 : 30; *C* [4], benzene–pyridine–acetic acid, 80 : 20 : : 2. The spots were detected by the chlorine–potassium iodide–toluidine method [4]. The spot of DCGN was greenish-yellow and that of DCS faint yellow. The composition of solvent mixtures used for thin layer chromatography and for recrystallization are given in % v/v.

Infrared spectra were recorded in KBr pellets with a Zeiss UR 10 instrument. Mass spectra were determined with an MX-1303 instrument furnished with a direct inlet system, at 50—150 °C and at an ionization energy of 70 eV.

Reaction of NH_4SCN with DCCI in acetonitrile

A crystalline powder of dicyclohexylcarbodiimide (103.2 g; 500 mmoles) was added, without external cooling, to a solution of ammonium thiocyanate (38.0 g; 500 mmoles) in 1000 ml of acetonitrile. In a few minutes a mildly exothermic reaction ensued (the temperature of the solution increased to 33—36 °C) accompanied by the evolution of ammonia.** After about half an hour the deposition of colourless crystals started. The mixture was left standing for 3 hrs.

* The concentration of the acetonitrile solution was for NH_4SCN and DCCI identical; 0.1 and 0.05 *M*, respectively.

** In some experiments carried out in more dilute (0.01 *M*) solution the ammonia has been determined quantitatively, the result being 3% of the total amount of ammonium thiocyanate. The evolved ammonia was expelled with N_2 from the acetonitrile solution and collected in 0.1 *N* H_2SO_4. The excess of the acid was measured with 0.1 *N* NaOH. The procedure was continued at least for 3 hrs.

at room temperature, occasionally shaken thoroughly, and then it was kept in the refrigerator during the night. The product (see Eq. (1): **I** and **II**) has been isolated by filtration, yielding 91.5 g (75%; calculated with 2 moles of DCCI for 1 mole of product) of colourless crystals, m.p. 150—151 °C. Recrystallization from aqueous methanol (1200 ml; 85%) gave 77.6 g (63%) of the material with a m.p. of 154—156 °C. Upon the addition of more water (around 200 ml) the mother liquor yielded another 7.7 g (6%) m.p. 156—157 °C. Tlc: *A*, R_f 0.4 and 0.1; *B*, R_f 0.5 and 0.1; *C*, R_f 0.9 and 0.8. The mixture of the authentic samples of DCS and DCGN [5] showed the following tlc spots: *A*, R_f 0.4 and 0.1; *B*, R_f 0.5 and 0.1; *C*, R_f 0.9 and 0.8.

$C_{13}H_{24}N_2S$ and $C_{14}H_{24}N_4$ (240.4 and 248.4). Calcd. N 17.2; S 6.6. Found N 17.2; S 6.7%.

Reaction of NH_4SCN with DCCI in acetone

The reaction was carried out in acetone (50 ml) with 25 mmoles of both components. The mixture was worked up in the usual way and afforded 3.3 g (54%) of the crude product which melted at 146—155 °C. The first recrystallization from aqueous methanol (55 ml; 80%) gave 2.4 g material with m.p. 154—157 °C while the second one (30 ml; 85%) yielded 1.7 g (28%) of product with a m.p. of 156—158 °C. Found: N 17.3; S 5.8%. Based on the IR peaks, the proportion of the components was roughly 40% DCS and 60% DCGN.

Determination of the SCN ion consumption

The determination of SCN ions has been carried out in a similar manner as given in the literature [6]. 2—5 ml samples of the 0.1 or 0.05 *M* acetonitrile mixtures were investigated 24 hrs after the mixing. After the addition of 20 ml water and 2 ml of a 20% phosphoric acid solution to the sample, bromine water was added dropwise until the yellow colour persisted. The sample was left standing for 5 min and then the excess bromine was removed with a 5% solution of phenol. After standing for 15 min, the developed bromocyanide was measured iodometrically with 0.02 *N* $Na_2S_2O_3$.

It was also attempted to determine the rate of disappearance of SCN ions. The acetonitrile solutions of NH_4SCN and DCCI were kept separately at 20° or 10 °C in a thermostat. The first sample was taken in 1 min after mixing the reaction partners. The sample removed from the reaction mixture was poured into 40 ml of cold 20% phosphoric acid. Then the procedure was the same as before.

*

The authors are indebted to Professor* V. BRUCKNER, the director of the Institute, for his interest and encouragement in this work. Thanks are due to Mr. I. VÁMOS for his technical assistance, to Miss Zs. PETRESS and Mrs. P. WITTMANN for recording the infrared spectra. The analyses were performed in the Analytical Laboratory of the Institute, supervised by Mrs. H. MEDZIHRADSZKY-SCHWEIGER. The authors would like to thank dr. J. TAMÁS (Hungarian Academy of Sciences, Chemical Structure Research Laboratory) for his valuable work regarding the mass spectroscopy.

This work was partly supported by the Chinoin Works which we acknowledge gratefully.

REFERENCES

1. For a review see, *e.g.*, KURZER, F., DOURAGHI-ZADEH, K.: Chem. Rev. **67,** 107 (1967); DETAR, D. F., SILVERSTEIN, R.: J. Am. Chem. Soc. **88,** 1013 (1966), and references therein
2. NEIDLEIN, R.: Arch. Pharm. **297,** 623 (1964); ULRICH, H., SAYIGH, A. A. R.: Angew. Chem. **77,** 545 (1965); MESSMER, A.: Lecture, presented at the Hungarian Academy of Sciences, January 28, 1969
3. BACON, R. G. R.: Organic Sulfur Compounds, N. Kharasch, Ed., Vol. 1, p. 306. Pergamon Press, New York, 1961
4. PATAKI, GY.: Dünnschichtchromatographie in der Aminosäure- und Peptid-Chemie. Walter de Gruyter and Co., Berlin, 1966
5. British Patent 643012 (1950); C. A. **45,** 5180 (1951)
6. SCHULEK, E.: Z. anal. Chem. **62,** 337 (1923); Z. anal. Chem. **65,** 332 (1925)

Tamás VAJDA
Judit KAJTÁR
Ferenc RUFF
Budapest VIII., Múzeum krt. 4/b.

Acta Chimica Academiae Scientiarum Hungaricae, Tomus 69 (1), pp. 103—106 (1971)

CARBOHYDRATE METHYL ETHERS, III*

THIN-LAYER CHROMATOGRAPHIC SEPARATION AND QUANTITATIVE DETERMINATION OF GLUCOSE METHYL ETHERS

A. LIPTÁK and I. N. JODÁL

(Biochemical Laboratory, L. Kossuth University, Debrecen)

Received February 27, 1970

2,3-Di-, 2,4-di-, 2,3,4-tri- and 2,3,4,6-tetramethyl-D-glucose liberated in the hydrolysis of methylated glucanes were separated by thin-layer chromatography, and their quantities were determined spectrophotometrically utilizing their colour reaction with aniline hydrogen phthalate. The method allows the quantitative determination of the above four glucose methyl ethers in the range 50—350 γ with an accuracy of $\pm 5\%$.

In the course of our studies on the structure of glucanes, the thin-layer chromatographic separation and quantitative determination of glucose methyl ethers have been achieved. The separation of the mixture of 2,3,4,6-tetramethyl-D-glucose, 2,3,4-trimethyl-D-glucose, 2,3-dimethyl-D-glucose and 2,4-dimethyl-D-glucose obtained on hydrolysis of methylated glucanes was effected on Kieselgel G adsorbent in methyl ethyl ketone saturated with water. The R_f values of the various methyl ethers are, in the above order, the following: 0.76, 0.63, 0.39 and 0.21.

A modified VAN CLEVE—SCHAEFFER method [1] was used for the quantitative determination. The detection of the substances was carried out directly on the chromatographic plates, the chromophore compound being developed on the plates under standard conditions, and the coloured substances were eluted from the adsorbent. Thus pre-detection and preliminary localization of the substances used in the VAN CLEVE—SCHAEFFER method could be avoided. Further on, the completion of the process could more easily be observed, owing to the elution of coloured substances; the evaporation required in the original method could also be omitted. This is an important advantage, since in the case of small quantities this operation can give rise to great errors.

The procedure developed by us is the following: after development of the chromatogram the plate was dried and sprayed uniformly with a detecting solution prepared from crystalline aniline hydrogen phthalate dissolved in butanol, then allowed to stand for 30 min at 98 ± 1 °C for accomplishment of the colour reaction. The detecting agent prepared from crystalline aniline

* Part II: A. LIPTÁK: Acta Chim. Acad. Sci. Hung. **66**, 315 (1970)

hydrogen phthalate [2] is superior to the usual butanol solution of aniline and phthalic acid, because it gives practically no 'background' on the plate.

A 2×2 cm area of the adsorbent containing and surrounding each detected spot was collected on a G5 sintered glass filter of 3 cm diameter, and the coloured substance was eluted with 96% ethanol of given volume. The light absorption of the solution was measured at 415 nm against 96% ethanol reference solution.

The spectra of the chromophores of the examined four methyl ethers formed with aniline hydrogen phthalate are very similar or nearly identical; however, their molar extinction coefficients show slight differences; they are nearly equal for the dimethyl ethers, and the highest in value; that of trimethyl-D-glucose is somewhat lower, and tetramethyl-D-glucose has the lowest extinction coefficient.

Calibration curves were constructed for the determination of these four substances. Each point of the calibration curves was obtained by averaging five measured values; thus the quantities of the four examined methyl ethers could be determined with $\pm 5\%$ accuracy in the 50—350 γ region.

For the purpose of our experiments, 2,3,4,6-tetramethyl-D-glucose was prepared according to WEST and HOLDEN [3]; 2,3,4-trimethyl-D-glucose was obtained by the method of IRVINE and OLDHAM [4]; the prescriptions of MCCLOSKEY and COLEMAN [5] were followed for the preparation of 2,3-dimethyl-D-glucose, and 2,4-dimethyl-D-glucose was obtained by a modified method of VAN CLEVE and SCHAEFFER [6, 7].

Dextran samples synthesized by two *Leuconostoc mesenteroides* cultures of different origin were examined. The polysaccharides were methylated three times with dimethyl sulfate in alkaline medium, according to HIBBERT *et al.* [8]. Three methylations made the polysaccharides soluble in chloroform and dimethylformamide, thus it could be methylated further with methyl iodide in dimethylformamide, repeated three times, according to KUHN [9]. After each procedure the progress of methylation was checked by infrared spectroscopy [10], measuring the decreasing intensity of the hydroxyl band. Six methylations resulted in complete disappearance of absorption in the 3600—3200 cm^{-1} region, and the methoxyl content of the substance was found to be 45 3%. Dimethylformamide was removed from the methylated polysaccharides by means of neutral aluminium oxide, according to DINER [11] except using chloroform for the elution.

The methylated polysaccharides were hydrolyzed with 90% formic acid [12], then with 0.5 *N* sulfuric acid. After neutralization, a stock solution of approx. 1% concentration was prepared from the hydrolysate. Suitable quantities of this solution were applied to the chromatographic plates, the actual volume depending on the glucose methyl ether to be determined, adjusting its quantity to fall in the optimum measuring region between 100 and 250 γ.

In the two examined polysaccharides the α (1—6) bond ratio was found to be 92—94%, based on the quantity of liberated formic acid and the periodate consumption; no data were available, however, concerning the nature of the other types of bonds present.

The oxidation with periodate was carried out in 0.015 *M* $NaIO_4$ solution with 100% excess of periodate at 20—22 °C, in total darkness, for 72 hrs. The periodate consumption was partly followed by means of spectrophotometry (decreased absorption at 222.5 nm) [13] and by iodometric titration [14]. The quantity of liberated formic acid was also measured iodometrically [15].

The periodate demand of the two polysaccharide samples, the quantity of liberated formic acid (moles), as well as the weight ratios of the various glucose methyl ethers and the molar ratios are summarized in Table I.

Table I

Periodate demand of dextranes produced by Leuconostoc mesenteroides and the quantity of formic acid liberated on oxidation

Weight- and molar ratios of the glucose methyl ethers obtained on methylation

Polysaccharide	Method									
	Periodate oxidation		Methylation							
	IO_4^-, mole	HCOOH, mole	2,3-dimethyl-D-glucose		2,4-dimethyl-D-glucose		2,3,4-trimethyl-D-glucose		2,3,4,6-tetramethyl-D-glucose	
			% by wt.	mole %	% by wt.	mole %	% by wt.	mole %	% by wt.	mole %
Dextrane I	1.90	0.92	5.5	5.9	1.8	1.9	84.3	84.3	8.4	7.9
Dextrane II	1.92	0.94	6.0	6.1	—	—	87.2	87.7	6.8	6.2

The results of periodate oxidation and methylation are in very good agreement. However, while the only difference between the two polysaccharide samples demonstrated by the periodate oxidation was the higher ratio of the α (1—6) bond in Sample 2, methylation indicated fundamental structural differences, such as the presence of α (1—4) branching in addition to the α (1—6) bonds forming the main chain in Sample 2; in Sample 1 the quantity of α (1—3) branching could also reliably be measured besides α (1—4) branching.

Experimental

Hydrolysis of methylated glucanes

0.5 g of methylated polysaccharide was dissolved in 25 ml of 90% formic acid and the solution was allowed to stand for 1 hr at 100 °C. It was concentrated to a syrup in vacuum, dissolved in 25 ml of 0.5 *N* sulfuric acid and heated at 100 °C for 14 hrs. After cooling, the solution was neutralized with barium carbonate and centrifuged. The precipitate was washed

with 2×10 ml of ethanol. The combined solutions were concentrated to a syrup in vacuum (0.50—0.52 g). After this, 10% solutions of this syrup were prepared in ethanol to be used in the chromatographic investigations.

Adsorbent: Kieselgel G (Merck), on 20×20 cm plates, according to Stahl's standard method.

Development: in a system containing methyl ethyl ketone saturated with water, up to 15 cm height on the plates.

Detecting agent: 1.608 g of crystalline aniline hydrogen phthalate was dissolved in *n*-butanol saturated with water and made up to 100 ml in a volumetric flask.

Colour development and elution: after development of the chromatogram, the plate was allowed to dry for half an hour at room temperature, then sprayed uniformly with the detecting agent. The plates were immediately placed into a drying oven of 98±1 °C for 30 min to promote the formation of the coloured compounds. They were allowed to cool to room temperature, then the adsorbent was collected from a 2×2 cm area around the spots on a G5 sintered glass filter. 2×5 ml of ethanol was pipetted to the collected adsorbent, stirred for 5 min in each case to ensure complete elution of the coloured compound, then the solution was sucked into a 10 ml volumetric flask and filled up to the mark.

The extinction of the solution was measured with a Unicam SP 800 ultraviolet spectrophotometer at 415 nm in a layer thickness of 10 mm, against a 96% ethanol reference solution, 5 min after the extraction.

For determination of the calibration curves, 1% methanolic solutions of the four glucose methyl ethers were prepared and 50, 100, 150, 200, 250, 300 and 350 γ quantities were applied to the plates by means of a CHROPA micropipette; the substances were chromatographed in the manner described above and, after formation of the coloured compounds and elution, the extinctions were measured.

For determination of the various glucose methyl ethers in the hydrolysate of the methylated polysaccharides, the volumes of the samples applied onto the plates for chromatography were chosen to contain 100—250 γ quantity of the methyl ether to be determined. In the case of trimethyl-D-glucose this was 0.02 ml, for the dimethyl-D-glucoses 0.2—0.4 ml and 0.05—0.08 ml for the tetramethyl-D-glucose.

*

The authors' thanks are due to Prof. Dr. P. NÁNÁSI for his interest in this work and for his useful advice.

REFERENCES

1. SCHAEFFER, W. C., VAN CLEVE, J. W.: Anal. Chem. **28,** 1290 (1956)
2. ANSCHÜTZ, R.: Ber. **20,** 3214 (1887)
3. WEST, E. S., HOLDEN, R. F.: Org. Synth. **20,** 97 (1940)
4. IRVINE, J. C., OLDHAM, J. W. H.: J. Chem. Soc. **1921,** 1744
5. MCCLOSKEY, C. M., COLEMAN, G. H.: J. Org. Chem. **10,** 184 (1945)
6. VAN CLEVE, J. W., SCHAEFFER W. C.; J. Am. Chem. Soc. 77, 5341 (1955).
7. NÁNÁSI, P., LIPTÁK, A., NAGY, G.: Acta Chim. Acad. Sci. Hung. **65,** 97 (1970)
8. LEVI, I., LINCOLN, H., HIBBERT, H.: J. Am. Chem. Soc. **64,** 1959 (1942)
9. KUHN, R., TRISCHMANN, H., LÖW, I.: Angew. Chem. **67,** 32 (1955)
10. REBERS, P. A., SMITH, F.: J. Am. Chem. Soc. **76,** 6097 (1954)
11. DINER, U. E., SWEET, F., BROWN, R. K.: Can. J. Chem. **44,** 1591 (1966)
12. BOUVENG, H. O., KIESSLING, H., LINDBERG, B., MCKAY, J. E.: Acta Chim. Scand. **16,** 615 (1962)
13. ASPINALL, G. O., FERRIER, R. J.: Chem. and Ind. **1957,** 1216
14. RANKIN, J. C., JEANES, A.: J. Am. Chem. Soc. **76,** 4435 (1954)
15. HALSALL, T. G., HIRST, E. L., JONES, J. K. N.: J. Chem. Soc. **1947,** 1427.

András LIPTÁK
Ildikó N. JODÁL } Debrecen 10. Hungary.

Acta Chimica Academiae Scientiarum Hungaricae, Tomus 69 (1), pp. 107—116 (1971)

EINFLUSS DER SCHWEFELSÄUREKONZENTRATION AUF DIE NITRIERUNGSGESCHWINDIGKEIT VON NITROBENZOL UNTERSUCHT IN EINEM DÜNNSCHICHTREAKTOR

A. UJHIDY*, M. MAGYAR** und R. BERKES*

(Forschungsinstitut für Technische Chemie der Ungarischen Akademie der Wissenschaften und Ungarisches Erdöl- und Erdgas-Forschungsinstitut**)*

Eingegangen am 16. Januar 1970

Es wird die Nitrierung von Nitrobenzol in einem Dünnschichtreaktor (Durchmesser: 53,3 mm) im Gebiet oberhalb der Grenzgeschwindigkeit durchgeführt. Die Änderung der Reaktionsgeschwindigkeit mit der Schwefelsäurekonzentration wurde auf Grund des Komponentstromes der Damköhler'schen Gleichung untersucht. Mit der Hilfe dieser Gleichung konnte das Quellenglied bestimmt werden und daraus konnten einige Folgerungen auf die Reaktionsgeschwindigkeit und auf den Reaktionsmechanismus gezogen werden.

Die Nitrierungsreaktion ein exothermer und praktisch meist in der heterogenen Phase durchführbarer Vorgang ist trotz ihrer Explosionsgefährlichkeit ein geeignetes Modell, um sie in einem Dünnschichtreaktor auszuführen, da diese Art von Reaktor zum Studium der Reaktion in vieler Hinsicht günstigere Verhältnisse schafft, als man in den bisherigen Untersuchungen angewandt hat [1]. Dies trifft auch auf zahlreiche Reaktionen anderer Art zu (z. B. Sulfonierung, Diazotierung, Oxydation usw.) [2—5].

Die Nitrierungsversuche wurden in einem vertikalen, zylindrischen, mit Rührwerken verschiedener Art (starre Flügeln, Wischer Typ von Samesreuther Müller Schuss GmbH) versehenen Rotationsdünnschichtreaktor von Laboratoriumsgröße (Durchmesser: 53,3 mm, aktive Fläche: 0,0578 m^2, Wandstärke: 1,5 mm) durchgeführt.

Die Versuche haben die Richtigkeit unserer früheren Annahme bestätigt, daß es zweckmäßiger ist, die in der heterogenen Phase vor sich gehenden Reaktionen in Flüssigkeitsfilmen mit erzwungener Strömung ablaufen zu lassen, da diese Methode hinsichtlich des Stoff- und Wärmetransports, ferner der Selektivität in vielen Fällen vorteilhafter ist, als sonstige herkömmliche Verfahren.

Zur Bestimmung der Grenze der Diffusionshemmung haben wir eine zu diesem Zweck bisher noch nicht gebrauchte konkurrierende (kompetitive) Prüfmethode eingeführt, bei welcher ein Vergleich der in der homogenen und heterogenen Phase gezeigten relativen Reaktionsfähigkeit von zwei chemischen Verbindungen zum Nachweis der Grenzgeschwindigkeit verwendet wird. Diese Methode ist einfacher, genauer und schneller, als die bisherigen üblichen Me-

thoden und scheint auch im Falle anderer Reaktorarten zum Nachweis der Grenzgeschwindigkeit von heterogenphasigen Reaktionen geeignet zu sein [6].

Im Laufe der Nitrierungsversuche haben wir nachgewiesen, daß die scheinbaren Aktivierungsenergien der Nitrierungsreaktionen der untersuchten aromatischen Verbindungen voneinander abweichen und auch von der Schwefelsäurekonzentration abhängig sind. Mit der Zunahme der Schwefelsäurekonzentration haben wir nämlich eine Abnahme der scheinbaren Aktivierungsenergien beobachtet [7].

In unserem Falle, zumal kein nennenswerter Druckabfall im Reaktor auftritt, kann der Impulsstrom unbeachtet bleiben. Da im Dünnschichtreaktor sehr günstige Wärmeübergangverhältnisse vorliegen und der Laboratoriumsreaktor isotherm gefahren werden kann, wird die Kenntnis des Wärmestromes so lange nicht benötigt, bis das Problem einer Vergrößerung der Abmessungen nicht auftaucht.

Die Änderung der Reaktionsgeschwindigkeit mit der Schwefelsäurekonzentration läßt sich auf Grund des Komponentenstromes der Damköhlerschen Gleichung prüfen [8], jedoch ist folgendes zu beachten:

1. Der Dünnschichtreaktor ist eine kontinuierlich betriebene Operationseinheit, und deshalb wird nach Erreichen des stationären Zustandes das die örtliche Konzentrationsänderung wiedergebende Glied im Komponentenstrom gleich Null.

2. Nach den Versuchsergebnissen kann das Diffusionsglied, da wir im turbulenten Gebiet arbeiten, nicht geschwindigkeitsbestimmend sein.

3. Da die Kinetik oberhalb der Grenzgeschwindigkeit gemessen wurde, konnte das Stofftransportglied gleich Null gesetzt werden, wonach:

$$V_R \nu_i r(c_i) = - G(c_{i0} - c_i) \frac{\text{Mol}}{\text{Zeit}}, \tag{1}$$

wo

V_R = Volumen des Reaktors, l;
ν_i = stöchiometrischer Koeffizient;
$r(c_i)$ = Reaktionsgeschwindigkeit, Mol/l · h;
G = Zuflußgeschwindigkeit, l/h;
c_{i0} = Anfangskonzentration der gewählten Komponenten, Mol/l;
c_i = die vorliegende Konzentration der gewählten Komponenten, Mol/l.

Beziehung (1) sagt aus, daß die Menge des durch den konvektiven Strom aus dem Reaktor herausgetragenen Produktes durch das Quellenglied bestimmt wird. Deshalb ist das Studium des Einflusses der Schwefelsäurekonzentration nur auf reaktionskinetischer Grundlage möglich.

Die reaktortechnische Prüfung eines technologischen Vorganges macht die Bestimmung des detailierten Reaktionsgeschehens nicht erforderlich, nur der Weg der Reaktion muß bekannt sein. Dieser besteht andererseits aus Schritten, die durch die Änderung der technologishen Parameter beeinflußt werden können. Zur Bestimmung des Reaktionsweges geben die mit dem Mechanismus zusammenhängenden theoretischen Erwägungen einen sehr brauchbaren Anhaltspunkt.

Die Nitrierung der aromatischen Kohlenwasserstoffe erfolgt offensichtlich durch ein labiles, doch stark reaktionsfähiges Zwischenprodukt (N), das auch eine Nitrogruppe enthält, dessen Struktur nicht bekannt zu sein braucht. Dieses Produkt soll durch die Aufeinanderwirkung von Schwefelsäure und Salpetersäure entstehen, in einer Gleichgewichtsreaktion, wobei noch die Entstehung eines Protonenakzeptor-Zwischenproduktes (S), das eine Sulfogruppe enthält, notwendig ist:

$$H_2SO_4 + HNO_3 \underset{k_2}{\overset{k_1}{\rightleftharpoons}} N^+ + S^- + (n\,H_2O). \tag{2}$$

Das im Laufe Reaktion (2) entstandene und eine Nitrogruppe enthaltende Zwischenprodukt reagiert mit dem aromatischen Kohlenwasserstoff und nachfolgend wird aus dem aromatischen Kern ein Proton abgespalten:

$$N^+ + Ar - H \xrightarrow{k_3} Ar - N + H^+. \tag{3}$$

Für das Abklingen des Vorganges muß die Regenerierung des als Protonenakzeptor vorliegenden Zwischenproduktes angenommen werden, das sich nur in folgender Form formulieren läßt:

$$S^- + H^+ \xrightarrow{k_4} H_2SO_4 + (n\,H_2O). \tag{4}$$

Die Reaktion (4) spielt sich zwischen einem Proton und einem reaktionsfähigen Produkt ab, deshalb verläuft sie sehr schnell und kann somit als geschwindigkeitsbestimmender Vorgang nicht in Frage kommen.

Auf Grund der Reaktionswege von (2), (3) und (4) ist die Bildungsgeschwindigkeit der Nitroverbindung:

$$\frac{d[Ar-N]}{dt} = k_3[N]\,[Ar-H]. \tag{5}$$

In einem kurzen Zeitabschnitt kann aber die Konzentration von [N] als die eines labilen Zwischenproduktes, als konstant betrachtet werden (Bodensteinsche Theorie):

$$\frac{d[N]}{dt} = k_1[HNO_3]\;[H_2SO_4] - k_2[N]\;[S] - k_3[N]\;[Ar-H] = 0 \tag{6}$$

woraus:

$$[N] = \frac{k_1 [HNO_3] [H_2SO_4]}{k_2 [S] + k_3 [Ar-H]} \tag{7}$$

Setzt man Gleichung (7) in die Beziehung (5) ein, so erhält man die Bruttogeschwindigkeitsgleichung:

$$\frac{d[Ar-N]}{dt} = k_3 \frac{k_1 [HNO_3][H_2SO_4]}{k_2 [S] + k_3 [Ar-H]} [Ar-H]. \tag{8}$$

In Gleichung (8) wird gesetzt:

$$k_1 [H_2SO_4] = k_{1HNO_3} \text{ und } k_2 [S] = k'.$$

Diese Vereinfachungen lassen sich durchführen, da die Schwefelsäure konzentration nach Gleichung (4) konstant ist, und [S] liegt ebenfalls als Zwischenprodukt vor, dessen Konzentration quasistationär ist.

Aus der Bruttogeschwindigkeitsgleichung (8) ist ersichtlich, daß die Kinetik durch die Konzentration der aromatischen Kohlenwasserstoffe stark beeinflußt wird:

A) Liegt die Konzentration der aromatischen Kohlenwasserstoffe relativ hoch, dann kann der Wert von k' im Nenner neben dem zweiten Glied vernachlässigt werden, und so wird die Reaktionsordnung für den aromatischen Kohlenwasserstoff Null sein.

$$\frac{d[Ar-N]}{dt} = k_{1HNO_3} [HNO_3]. \tag{9}$$

B) Im anderen Extremfall, sofern die Konzentration der aromatischen Kohlenwasserstoffe niedrig liegt, kann das Produkt $k_3[Ar - H]$ im Nenner vernachlässigt werden, und es gilt dann folgende Geschwindigkeitsgleichung:

$$\frac{d[Ar-N]}{dt} = \frac{k_3 k_{1HNO_3}}{k'} [HNO_3][Ar-H]. \tag{10}$$

Letzten Endes kann die Ordnung von [Ar — H] in Abhängigkeit von der Konzentration zwischen 0 und 1 jeden beliebigen Wert annehmen.

Die Messungen werden meistens in der Nähe der Variante B) durchgeführt. Zieht man $k_3 \cdot k_{1HNO_3}/k' = k_{II}$ zusammen, so wird man aus der für die Reaktionen zweiter Ordnung gültigen Differentialgleichung die zusammengezogene Konstante k_{II} berechnen können. Da in der Gleichung (10) die Konstanten erster und zweiter Ordnung gemischt vorkommen, stimmt man zweckmäßig ihre Dimensionen aufeinander ab [9, 10]. Hierzu bietet sich die Möglichkeit, die Konzentrationen in Molenbruch auszudrücken und auf diese

Weise die Dimension der Geschwindigkeitskonstanten von der Ordnung unabhängig (Zeit^{-1}) machen. Dies bringt auch den Vorteil mit sich, daß die Schwefelsäurekonzentration in Molenbruch ausgedrückt konstant wird. Von diesem Gesichtspunkt aus ist bei der klassischen Deutung des Mechanismus der Nitrierungsreaktion die Bezeichnung der Schwefelsäure als Katalysator begründet.

Der Einfluß der Schwefelsäurekonzentration auf die Nitrierungsgeschwindigkeit wird leichter verständlich, wenn wir auf Grund von Gleichung (10) die Bruttogeschwindigkeitskonstante zerlegen:

$$k_{II} = \frac{k_1 k_3 [H_2SO_4]}{k_2 [S]} . \tag{11}$$

In Gleichung (11) ist $k_1/k_2 = K_I$ eigentlich die Gleichgewichtskonstante der ersten Dissoziationsstufe der Schwefelsäure und gleich $1 \cdot 10^3$ [11].

Gleichung (11) wird also folgende geänderte Form aufnehmen:

$$k_{II} = \frac{k_3 K_I [H_2SO_4]}{[S]} . \tag{12}$$

Wenn also die Versuchsbedingungen so gewählt werden, daß sie der Variante A) entsprechen, wird man den Wert von k_{1HNO_3} aus Gleichung (9) berechnen können und nach Division durch den Molenbruch der Schwefelsäure erhält man k_1. Auf diese Weise läßt sich mit Hilfe von k_1 auch k_2 ermitteln.

Wird Quotient k_{II}/K_I als Funktion der Schwefelsäurekonzentration dargestellt, so erhalten wir eine Kurve, deren unterer Abschnitt als eine Gerade betrachtet werden kann. Auf Grund der Richtungstangente läßt sich aus der Beziehung (12) der Wert von k_3 berechnen, sofern wir den Wert von [S] im Konzentrationsbereich der Schwefelsäure, wo die Gerade ihre Gültigkeit noch beibehält, angeben können. Den Wert von [S] haben wir aus einem Diagramm anhand von Raman-Spektren geschätzt [11]. Danach wird [S] = 0,272.

Ist k_3 bekannt, so kann man den zu einer gegebenen Schwefelsäurekonzentration gehörigen Wert von [S] berechnen, der im Diagramm k_{II} gegen $[H_2SO_4]/[S]$ einen Punkt angibt. Da die Gleichung (12) die Gleichung einer Geraden ist, können wir den erhaltenen Punkt mit dem Koordinatenanfangspunkt zu einer Geraden verbinden, welche die Änderung von k_{II} in Abhängigkeit vom Verhältnis $[H_2SO_4]/[S]$ veranschaulicht. Wir benötigen aber die Funktion [S] gegen $[H_2SO_4]$, und dazu wird das auf Abb. 1 dargestellte Dreieckdiagramm gebraucht, welches den Zusammenhang zwischen NO_2^+ und der Schwefelsäurekonzentration zu erkennen gibt [12, 13, 14].

Aus den Tabellen I und II sind die zur gegebenen NO_2^+-Konzentration gehörigen k_{II}-Werte bekannt, und so läßt sich mit wiederholter Anwendung von Gleichung (12) der Wert von [S] von Punkt zu Punkt berechnen.

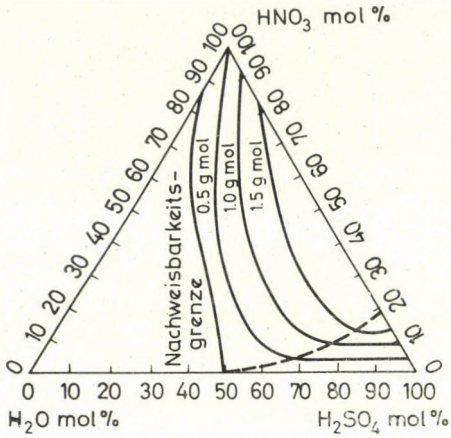


Abb. 1. Gehalt der Nitriersäure an NO_2^+-Ionen. Mol/1000 g Lösung

Tabelle I

Geschwindigkeitskonstanten k_{II} bei verschiedenen Temperaturen und verschiedenen DVS-Werten der Nitriersäure

Molenverhältnis von Salpetersäure—Nitrobenzol: 1,15

Versuchsnummer	DVS	H_2SO_4 %	Reaktionsdauer s	Temperatur °C	Nitrobenzolzufuhr g Mol/min	Umsatz %	R_a g Mol DNB / l.h	$k \times 10^6$ l / Mol.s	$k_{II} \times 10^3$ s^{-1}
D. 58	6,50	74,02	21,0	60	0,1960	68,80	603,00	2370,0	475,0
D. 112	5,75	72,80	27,1	59	0,0977	66,70	437,00	1710,0	335,50
D. 53	4,48	69,87	18,9	59	0,1860	40,80	388,00	895,0	200,40
D. 45	3,92	67,88	18,0	56	0,1960	0,51	5,05	9,4	1,93
D 28	3,15	62,20	16,7	59	0,1960	0,05	0,63	0,754	0,20
D. 59	6,50	74,02	18,9	78	0,1960	75,54	733,00	3540,00	697,00
D. 54	4,48	69,87	16,4	80	0,1860	54,85	600,00	1810,00	395,00
D. 46	3,92	67,88	17,8	80	0,1960	6,70	66,60	119,00	42,75
D. 29	3,15	62,20	16,1	80	0,1960	0,19	2,51	2,78	0,475
D 26	2,32	54,50	17,5	80	0,1960	0,10	1,44	1,21	0,459
D· 60	6,50	74,02	16,6	90	0,1960	76,07	873,00	4310,00	825,00
D. 115	5,75	72,80	20,0	88	0,0977	79,70	697,00	4120,00	817,50
D. 56	4,48	69,87	16,4	85	0,1860	63,85	695,00	2490,00	545,00
D. 48	3,92	67,88	14,7	90	0,1960	12,50	152,00	254,00	53,00
D. 30	3,15	62,20	15,9	90	0,1960	0,41	5,49	6,06	1,40
D. 37	2,32	54,50	17,0	90	0,1960	0,20	2,97	2,39	0,142

Tabelle II

Die Werte von [S] und die aus dem anhand der Versuchsergebnisse aufgenommenen Diagramm abgelesenen Werte

$k_{II} \times 10^3$	$\frac{[H_2SO_4]}{[S]}$	$\frac{NO_2^+ \text{ g Mol}}{1000 \text{ g}}$	$[H_2SO_4]$ Molenbruch	Temperatur °C	$[S] \times 10^4$ Molenbruch
600	3350	1,36	0,4725	60	1,41
500	2790	1,20	0,4550	60	1,63
400	2240	1,05	0,4375	60	1,95
300	1675	0,90	0,4200	60	2,50
200	1118	0,72	0,3975	60	3,56
100	560	0,58	0,3800	60	5,79
50	279	0,50	0,3625	60	13,35
700	3910	1,51	0,4900	60	1,251
800	4460	1,66	0,5080	60	1,138
900	5025	1,82	0,5275	60	1,045
1000	5580	1,96	0,5425	60	0,973
1200	6700	2,35	0,5900	60	0,880
1250	7000	2,45	0,6025	60	0,861
1300	7260	2,55	0,6150	60	0,846
1350	7550	2,65	0,6250	60	0,828
100	236	0,44	0,3650	78	15,48
200	460	0,56	0,3800	78	8,25
300	708	0,64	0,3900	78	5,51
400	940	0,72	0,3975	78	4,23
500	1180	0,80	0,4075	78	3,46
600	1410	0,88	0,4175	78	2,96
700	1645	0,96	0,4175	78	2,60
800	1880	1,04	0,4350	78	2,32
900	2120	1,12	0,4450	78	2,10
1000	2360	1,20	0,4550	78	1,93
1200	2830	1,40	0,4775	78	1,69
1400	3300	1,65	0,5075	78	1,54
1600	3780	1,89	0,5350	78	1,41
1800	4250	2,12	0,5625	78	1,32
2000	4720	2,35	0,5900	78	1,25
2200	5200	2,59	0,6175	78	1,19
2300	5440	2,70	0,6325	78	1,16
200	160	0,45	0,3675	90	23,0
300	240	0,52	0,3750	90	15,6
400	320	0,59	0,3825	90	11,95

Tabelle II (Forts.)

$k_{II} \times 10^3$	$\frac{[H_2SO_4]}{[S]}$	$\frac{NO_2^+ \text{ g Mol}}{1000 \text{ g}}$	$[H_2SO_4]$ Molenbruch	Temperatur °C	$[S] \times 10^4$ Molenbruch
500	400	0,66	0,3915	90	9,80
600	480	0,73	0,4000	90	8,34
700	560	0,80	0,4075	90	7,30
800	640	0,86	0,4150	90	6,50
900	720	0,94	0,4250	90	5,90
1000	800	1,00	0,4300	90	5,38
1200	960	1,25	0,4600	90	4,80
1400	1120	1,46	0,485	90	4,33
1600	1280	1,67	0,510	90	3,98
1800	1440	1,88	0,535	90	3,72
2000	1600	2,08	0,5575	90	3,48
2200	1760	2,29	0,5825	90	3,31
2400	1920	2,50	0,6075	90	3,16
2500	2000	2,60	0,6200	90	3,10
2550	2040	2,66	0,6275	90	3,08

Die Geschwindigkeitskonstanten der einzelnen, durch die Gleichungen (2) und (3) wiedergegebenen Reaktionsschnitte, sind in Tabelle III zusammengefaßt.

Tabelle III

Versuchsnummer	Temperatur °C	$k_1 \times 10^5$ s^{-1}	$k_2 \times 10^5$ s^{-1}	$k_3 \times 10^5$ s^{-1}
D. 58	60	9580	9,58	0,079
D. 59	80	12500	12,50	0,0424

Die Tabellendaten zeigen, daß der Wert von k_3 der kleinste ist. Unter den bei unseren Versuchen gegebenen Bedingungen wird der geschwindigkeitsbestimmende Faktor die Reaktion des aromatischen Kohlenwasserstoffs mit dem Zwischenprodukt (N), das auch ein Nitroniumion sein kann oder auch eine Vorverbindung dessen, z. B. das Nitrazidiumion. Diese Feststellung steht mit den Ergebnissen der Untersuchungen von MELANDER, BONNER, LAUER und OLÁH in Einklang [15, 16, 17, 18, 19].

Die vorher erwähnte Beziehung wird bei den gemessenen drei Temperaturen in Abb. 2 gezeigt. Auf Grund der Abbildung läßt sich folglich bei den gemessenen Temperaturen der zu einer beliebigen Schwefelsäurekonzentration

gehörige Wert von [S] ablesen, mit Hilfe dessen man die Bruttogeschwindigkeitskonstante berechnen kann. Daraus folgt, daß das Quellenglied des Komponentenstromes von Gleichung (1) ebenfalls ermittelt werden kann.

Die Verflachung der Kurven zeigt, daß der Wert von [S] oberhalb einem Schwefelsäure-Molenbruch von 0,6 praktisch konstant und sehr klein wird. Dies bedeutet nach Gleichung (11), daß in diesem Gebiet der Wert von k_{II},

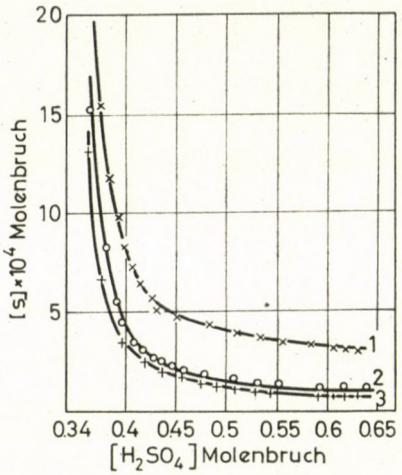


Abb. 2. Änderung von [S] in Abhängigkeit von der Schwefelsäurekonzentration bei verschiedenen Temperaturen. Reaktionstemperatur: 1 = 90°C; 2 = 78°C; 3 = 60°C

d. h. die Bruttogeschwindigkeit ihr Maximum erreicht, was auch mit den praktischen Erfahrungen übereinstimmt.

Wir müssen aber bemerken, daß wir die absoluten Werte der Konzentration [S] nicht für endgültig halten können. Die als Vergleichsbasis dienende Konzentration [S] konnten wir nämlich nur anhand der Raman-Spektren des Schwefelsäure–Wasser-Systems schätzen. Eine Änderung der absoluten Werte wird dadurch verursacht, daß im System sowohl Salpetersäure als auch aromatischer Kohlenwasserstoff enthalten ist, welche die H^+-Konzentration und damit das Dissoziationsgleichgewicht gemeinsam beeinflussen. Dies bedeutet aber nicht, daß die aus Abb. 2 gezogenen Folgerungen nicht zutreffend wären, sie rufen lediglich eine parallele Verschiebung der Kurven hervor.

Formelzeichen

c_i	Vorliegende Konzentration der gewählten Komponenten	$Mol \cdot l^{-1}$
c_{i_0}	Anfangskonzentration der gewählten Komponenten	$Mol \cdot l^{-1}$
DVS	Der aus dem prozentuellen Schwefelsäuregehalt der Nitriersäure und dem Wassergehalt der erschöpften Säure gebildete Quotient	
G	Zuflußgeschwindigkeit	$l \cdot h^{-1}$
k'; k_{II}	Reaktionsgeschwindigkeitskonstanten	s^{-1}
k_1—k_4	Reaktionsgeschwindigkeitskonstanten	s^{-1}

k_{1HNO_3}	Reaktionsgeschwindigkeitskonstante (auf die Salpetersäure bezogen)	s^{-1}
k	Geschwindigkeitskonstante der Reaktion zweiter Ordnung	$l \cdot Mol^{-1} \cdot s^{-1}$
K_I	Gleichgewichtskonstante	
N	Nitrogruppe enthaltendes Zwischenprodukt	
$r(c_i)$	in Molarität ausgedrückte Reaktionsgeschwindigkeit	$Mol \cdot l^{-1} \cdot h^{-1}$
R_a	Nitriergeschwindigkeit (auf die saure Phase bezogen)	$g\ Mol \cdot l^{-1} \cdot h^{-1}$
S	Sulfogruppe enthaltendes Zwischenprodukt	$g\ Mol \cdot l^{-1} \cdot h^{-1}$
V_R	Volumen des Reaktors	l
v_i	Stöchiometrischer Koeffizient	

LITERATUR

1. UJHIDY, A., BABOS, B.: Chem. Techn. **13,** 587 (1961)
2. UJHIDY, A., BABOS, B., HEIL, B.: Chem. Techn. **15,** 554 (1963)
3. UJHIDY, A., BABOS, B., FARÁDY, L.: Chem. Techn. **18,** 652 (1966)
4. BABOS, B., UJHIDY, A., FARÁDY, L.: Veszprémi Vegyipari Egyetem Közleményei, **6,** 289 (1962)
5. UJHIDY, A., MARKÓ, L., BABOS, B., HEIL, B.: Veszprémi Vegyipari Egyetem Közleményei, **8,** 49 (1964)
6. UJHIDY, A., BABOS, B., HEIL, B., MARKÓ, L.: Conference on Some Aspects of Physical Chemistry. Budapest. Vol. II. 179 (1966)
7. UJHIDY, A., BABOS, B., HEIL, B.: Chem. Techn. **22,** 744 (1970)
8. BENEDEK, P., LÁSZLÓ, A.: Grundlagen der Chemieingenieur Wissenschaft (ungarisch). (A vegyészmérnöki tudomány alapjai). Műszaki Könyvkiadó, Budapest, 1964
9. MAGYAR, M.: Magy. Kém. Lapja. **23,** 1 (1968)
10. MAGYAR, M.: Kém. Közl. **31,** 399 (1969)
11. Gmelins Handbuch der anorganischen Chemie, 9. Teil, Verlag Chemie, Weinheim, 1960 p. 739; 745
12. CHEDIN, J.: Ann. Chim. **8,** 243 (1937)
13. CHEDIN, J.: Mém. Serv. chim. de l'État. **31,** 113 (1944)
14. FENEANT, S., CHEDIN, J.: Mém. Serv. chim. de l'État. **40,** 292 (1955)
15. MELANDER, L.: Acta Chem. Scand. **3,** 95 (1949)
16. BONNER, T. G., BOWYER, F., WILLIAMS, G.: J. Chem. Soc. 3274 (1952)
17. BONNER, T. G., BOWYER, F., WILLIAMS, G.: J. Chem. Soc. 2650 (1953)
18. LAUER, W., M., NOLAND, W. E.: J. Amer. Chem. Soc. **75,** 3689 (1953)
19. OLÁH, G. S., KUHN, J. S., FOOD, S. H., EVANS, J. C.: J. Amer. Chem. Soc. **84,** 3687 (1962)

Aurél UJHIDY; Veszprém, Schönherz Zoltán u. 10. Hungary
Miklós MAGYAR; Veszprém, Wartha Vince u. 2/6. Hungary
Rudolf BERKES; Veszprém, Schönherz Zoltán u. 10. Hungary.

RECENSIONES

J. C. MAIRE and B. WAEGELL: *Structures, Mécanismes et Spectroscopie, 120 Problems, 60 Solutions.* Cours et Documents de Chimie, Vol. 2, pp. 300

Gordon et Breach. Paris, London, New York, 1969

The book is the second volume of a series, having the object to deal with all branches of chemistry, and in particular to discuss subjects which stand in the forefront of interest. A further aim of the series is to promote the education of university students learning chemistry. This second volume, treating the spectroscopic methods of the structural investigation of organic compounds, fits well into this latter object.

Chapter 1 (53 pages) presents problems concerned mainly with the evaluation of chemical shifts and coupling constants, and does not discuss stereochemical problems. This chapter treats the effect of a changing the solvent and the introduction of isotope atoms on the spectrum. In the second chapter (42 pages) the relationship between coupling constants and stereochemistry (Karplus' rule) is emphasized. The third chapter (17 pages) contains mainly examples indicative of the role of temperature. The fourth chapter (26 pages) discusses the spectra of compounds containing the most various atoms (^{11}B, ^{19}F, etc.). The fifth chapter (70 pages) comprises complex problems for exercise, involving spin decoupling, etc. The second part of the book contains the partial solution of the problems, bibliography and indexes.

As may be seen from the above listing of the contents, the book stresses primarily the NMR spectra. From this aspect, the book is at a disadvantage as compared to complex-task books, which present the most important spectra in their entity, and are therefore more instructive and stand closer to everyday's practice. On the other hand, the book has the great advantage of a vivid mode of discussion, true to life. The setting forth of the first task begins for example as follows: "Thorpe and Ingold, on condensing indanon-1 with ethylcyano acetate, obtained the ester I, etc." Thus, we get acquainted with the compounds feeling the atmosphere of the laboratory, and not stripped from their environment.

The book will be useful to all those organic chemists who want to deepen their knowledge in the interpretation of NMR spectra.

Cs. SZÁNTAY

V. BALZANI and V. CARASSITI: *Photochemistry of Coordination Compounds.* XVI + 432 pp.

Academic Press, London and New York, 1970

The last two decades have witnessed a spectacular development in our knowledge and understanding in the field of both photochemistry and coordination chemistry. There is an increasing interest in the photochemistry of coordination compounds. Although systematic investigations in this field began in the fifties, many sporadic studies and casual, but important, observations were made earlier and there was a demand for a monographic treatment of this branch of chemistry. The publication of BALZANI and CARASSITI's book therefore is very timely indeed.

The first, introductory Chapter gives an outline of the whole book. The following eighteen Chapters are grouped in two Parts. Part 1 (Chapters 2 to 6, pp. 6—78) gives briefly the background necessary to understand the photochemistry of coordination compounds. Neither the Chapters treating basic photochemical and photophysical principles, nor the Chapters

dealing with the spectroscopy and bonding problems of coordination compounds can be comprehensive; their inclusion is nevertheless useful and references are given to all of the important articles providing detailed information on each of the problems. A short Chapter on the characteristics of the electronically excited states of complexes is especially important to understand the photochemical behaviour of coordination compounds.

Chapters 7 to 17 deal with the photochemical behaviour of transition metal complexes in solution. (The titles of these Chapters: Chromium; Molybdenum and Tungsten; Manganese; Iron; Cobalt; Platinum; Copper, Silver and Gold; Zinc, Cadmium and Mercury; Uranyl compounds; Other elements; Carbonyl complexes, complexes containing π-bonding ligands, and dithizonato complexes.) The fact that the complexes of iron, cobalt and chromium are studied most thoroughly is reflected in the lengths of the corresponding Chapters (approximately 50 pages each). The problems of photography are not mentioned as such even in connection with silver compounds. It is regretted that the coordination chemistry aspect of photosynthesis is also omitted.

Chapter 18 gives an account on the studies of solid complexes. The concluding Chapter gives some generalizations on the types of photoreactions and their most characteristic features.

Each Chapter is followed by an exhaustive list of relevant papers; the total number of references (up to 1968) is near two thousand. Furthermore, some fifty papers which appeared in 1969 are listed as "additional references".

An especially helpful feature of the book is the highly informative Tables which give the most important data of the different reactions in condensed form. The Figures are very clear, the paper is excellent and the printing is very good, although a number of misprints have been found. (To the best of the reviewer's knowledge an error list will be provided.)

The authors of this excellent monograph are prolific workers in the field of the photochemistry of coordination compounds and their long experience with a great number of different systems qualified them to write a critical and authoritative book. The book is warmly recommended to coordination chemists and will undoubtedly contribute considerably to further progress in this exciting field.

M. T. Beck

J. O'M. Bockris and A. K. N. Reddy: *Modern Electrochemistry*, Vols 1, 2. pp. 1432 + Index

MacDonald, London 1970

The last two decades witnessed rapid advances in theoretical electrochemistry. Simultaneously, the practical importance of electrochemistry and its field of application have also increased. Scientists working in different branches of science, and practical experts in the most varied fields of industry are confronted with electrochemical phenomena and use in their everyday work.

Therefore, the book of Bockris and Reddy, Modern Electrochemistry, will be of immediate interest to a wide circle of readers. This expected interest is the more justified, as the authors' aim was to give to the readers a clearly written book of modern concept, which, in view of the special interdisciplinary character of electrochemistry, will be useful besides for electrochemists and college students learning this discipline, also to those engaged in work in various branches of science, where electrochemistry is used.

In the first chapter of the book, the authors define the subject of electrochemistry, and discuss its past and expected development. They show the relation of electrochemistry of other sciences, and its place and importance in the system of sciences. The authors are of the opinion that out of the two large branches of electrochemistry centering around "ionics" and "electrodics" the latter is to be considered the more important field (from the aspect of electrochemistry).

In accordance with the above division, the first volume (Chapters 2—6) of the book deals with the properties of solutions containing ions, while the second volume (Chapters 7—11) discusses the structure of the interface of electric and ionic conductors, and processes taking place at this interface.

The second chapter deals with the problems of ion-solvent interactions. The endeavour of the authors to give a clear presentation throughout the whole book is particularly conspic-

uous in this chapter, for example in making perceptible the difference between the model and the actual situation.

The third chapter, "Ion-Ion Interaction", discusses the Debye-Hückel theory, giving a detailed analysis of the domain of validity of this theory, and problems relevant to the activity coefficient and the formation of ion associates. This chapter discusses briefly also concentrated electrolytes, and describes methods, mainly spectroscopy, used for studying the structure of electrolyte solutions.

The fourth chapter of the book deals with ion transport in solutions. First, the case is discussed when ion migration is caused by a difference in chemical potentials, *i.e.* the case of diffusion, and subsequently the case when ion migration is caused by an electric potential gradient. The theoretical basis of these phenomena is also treated. A separate part of this chapter deals with the electric conductivity of non-aqueous solutions.

Protons play a special and important role in electrolyte solutions. Therefore, a separate chapter (Chapter 5) deals with the characteristics of protons exhibited in solutions. This chapter describes the solvation and transport of protons, and discusses acid–base theories.

The last chapter of the first volume deals with salt melts, called also ionic liquids. After a description of the models of ionic liquids, and transport processes characteristic of these systems, the authors discuss glasses, the ionic solution mixtures of practical importance, with a particular view to theoretical aspects.

The seventh chapter "The Electrified Interface" is the longest chapter in the book. This relatively large extent is justified by the basic importance of the substance summarized in this chapter. This chapter deals with the electrical double layer, the phase boundary potentials, the thermodynamics and the structure of electrified interfaces, electrokinetic phenomena, and certain colloid chemical aspects of the problems discussed. The adsorption on electrodes, which is of decisive importance from the viewpoint of electrode processes, is also discussed in this chapter.

The eighth chapter of the book deals with the electrode process proper, with the transition of the charged particles through the phase boundary. In connection with the relationships of transfer polarization, the authors discuss the Nernst equation pertinent to the current-free (equilibrium) electrode, the problems relative to the so-called symmetry factor. Charge transfer across non-metal (liquid) interfaces is also discussed (semiconductor, solution, biological membranes, etc.). A substantial part of this chapter is devoted to the presentation of the quantum chemical discussion of the charge transfer reaction.

The ninth chapter gives a survey of the complexity of electrode processes, and problems rising in connection with the elucidation of the mechanism of electrode processes, discussing multistep reactions, transient phenomena, diffusion polarization, theoretical and practical problems in the study of the process mechanism, and a few theoretical problems important from the viewpoint of chemical power sources. Reaction polarization is not discussed either here or in other chapters.

The tenth chapter describes a few electrode reactions, important from the theoretical and practical aspect, as for example problems of electrocatalysis, electrolytic metal deposition, hydrogen and oxygen overvoltage.

The last, eleventh chapter "Some Electrochemical Systems of Technological Interest", deals with the more important and electrochemical power sources.

It can be stated that the authors attained their purpose and made available an actually modern review to a large number of readers. It must be noticed, however, that the authors treat the rather voluminous material from time to time in a subjective manner. This book can be used as a textbook by university students, and as a handbook by specialists active in other fields, by plant engineers, corrosion specialists, biologists, analytical chemists, etc.

The publishing of this book of BOCKRIS and REDDY is an important event not only from the point of view of the development of electrochemistry, but, due to its modern concept, will contribute also to the development of other branches of science and industrial activity using (or "discovering" in the future) electrochemistry.

L. KISS

M. BECKE-GOEHRING and H. HOFFMANN: *Komplexchemie.* pp. 245

Springer-Verlag, Berlin, Heidelberg, New York, 1970

The book consists of five Chapters: 1. Introduction; 2. the phenomenological theory of complexes; 3. The structure of complexes of different coordination number; 4. The bonding between the central atom and the ligand; 5. Reactions of coordination compounds. Subject and author indexes are included.

The introduction is a fairly conventional one giving a good historical background. The second chapter amounts to more than half of the whole book and deals with such different topics as isomerism, carbonyl hydrides, and stabilities of complexes in solution. Some of the sub-chapters are as usually given in introductory texts, but some of them appear fairly uniquely treated in a short introduction. The authors treat the synthetic aspects very thoroughly and provide an up-to-date description of some interesting and important groups of coordination compounds such as the dinitrogen complexes. The reviewer feels, however, that such a detailed treatment is not necessary in an introductory text in all cases. For example, the mercury complexes of nitrogen-containing ligands are treated in a sub-chapter of comparable length with that on the stability of complexes. (Perhaps a title such as Introduction to Selected Topics of Coordination Chemistry would have been more correct.) On p. 19 some of the structural formulas of the ligands are misleading. The term autocomplex is not used in the same meaning as generally in the literature. The authors use it as a synonym of supercomplex (which refers to the formation of polynuclear complexes mainly in the solid state), while autocomplex formation is represented by an equilibrium in solution such as:

$$2\ CdI_2 = CdI^+ + CdI_-.$$

The short chapter dealing with the geometry of different complexes and the relatively long chapter on the bonding problems are very good. The concluding chapter deals with kinetic problems. The problems of substitution reactions are well treated, although the fundamentally important results obtained by relaxation methods should have not been omitted. It is also regretted that redox reactions are not mentioned at all.

Each chapter is followed by a list of references which enables the beginner to find deeper information.

The book is well printed, the paper is good, the figures are excellent.

As a whole, this text seems a little unbalanced and is recommended mainly to students who are interested particularly in the synthetic aspects of coordination chemistry.

M. T. BECK

J. FALBE: *Carbon Monoxide in Organic Synthesis.* pp. 219

Springer-Verlag, Berlin, Heidelberg, New York, 1970

This book is the revised and enlarged second edition of the German original, which appeared in 1967. (Synthesen mit Kohlenmonoxyd. Organische Chemie in Einzeldarstellungen, Band 10.) Especially the number of references has been greatly increased by adding the results published in the last 2—3 years.

The rapidly increasing importance of carbon monoxide as a basic raw material for the industrial synthesis of organic compounds is one of the most spectacular achievements of organometallic coordination chemistry, still often regarded as a curiosity by organic chemists. Despite the great number of review articles, this is the first comprehensive treatise of this important class of organic reactions from both the standpoint of the research chemist and the industrial expert. In this respect FALBE's book satisfies a need existing since a couple of years: those working in the academic aspects of this chemistry frequently hardly realize the advances made by industry, and people dealing with industrial organic chemistry are often reluctant to get acquainted with this rather new class of reactions.

This somewhat isolated situation of organometallic coordination catalysis is reflected by the fact that reactions of carbon monoxide are used on an industrial scale practically only for the conversion of hydrocarbons to produce simple, large tonnage "petrochemicals". J. FALBE

has done a lot of pioneering work in using carbon monoxide reactions to produce more complicated, valuable organic molecules and is surely one of the most competent specialists to call the attention of industry to this important and still neglected area of carbon monoxide chemistry. His book does excellent service in this respect.

The material is divided into four main chapters: Hydroformylation Reaction, Metal Carbonyl Catalyzed Carbonylation, Carbonylation with Acid Catalysts and Ring Closures with Carbon Monoxide. The book is complete with 1055 (!) references and a subject index.

The main emphasis is given to chapter I dealing with the hydroformylation reaction. This is in accordance with the industrial importance of "oxo synthesis", a reaction which now serves for the production of about 3 million tons of alcohols. This is surely the best part of the book, giving a clear picture of hydroformylation beginning with detailed problems of the mechanism and ending up with a good survey of technical and economical aspects.

The second chapter about metal carbonyl catalyzed reactions treats a less fruitful topic, since these reactions form a much more heterogeneous group. One also immediately feels the lack of basic research in this field. The author has devoted much effort to cover the patent literature and gives thus a good impression of what has been done up till now.

Chapter III is short but complete, a separate book as it is, since the reaction of carbon monoxide with carbonium ions has very little in common with the reactions catalyzed by metal carbonyls. It would have been perhaps better to put it as the last chapter. From the academic point of view it could have been even omitted, but if one regards the principal goal of the book, to serve as a handbook for those working in the organic chemical industry, its inclusion is completely justified.

The last chapter deals with a rather specialized subject, ring closure by incorporation of the carbon monoxide molecule. In contrast to the reactions treated in chapter II, the reactions covered in this section were investigated up till now apparently only by academic workers and industry has not yet realized the synthetic possibilities. Summarizing those reactions in a book like this will surely do a good job for the further development of this branch of chemistry.

The reviewer is greatly impressed by the huge number of references, proving the large amount of work done by the author in compiling this excellent book. A severe drawback has to be mentioned, however, in this respect: the references are given in a completely random manner, *i.e.* were not arranged alphabetically and also their numbering did not follow the text of the book. This greatly reduces the usefulness of the work as a handbook and at the same time leads sometimes to references appearing more than once under different numbers (*e.g.* 827 and 935, 808 and 927).

To summarize, this is a book which deserves attention and may be used by industrial and academic people with equal benefits. It should be on the shelf of every organic chemist.

L. MARKÓ

INDEX

INORGANIC AND ANALYTICAL CHEMISTRY – ANORGANISCHE UND ANALYTISCHE CHEMIE – НЕОРГАНИЧЕСКАЯ И АНАЛИТИЧЕСКАЯ ХИМИЯ

FLÓRA, T.: Einfluß des Materials der derivatographischen Probenbehälter auf die thermische Zersetzung von Ammoniumnitrat. (Effect of the Derivatographic Sample Holders of Various Nature on the Thermal Decomposition of Ammonium Nitrate) 1

SCHNEER-ERDEY, A. and KOZMUTZA, K.: Xenon Difluoride as an Analytical Reagent, I. Determination of Iodine 9

VIJAY MOHAN BHATNAGAR: Preparation and Unit Cell Dimensions of Lead Apatites (Short Communication) 15

PHYSICAL CHEMISTRY – PHYSIKALISCHE CHEMIE – ФИЗИЧЕСКАЯ ХИМИЯ

KAPOSI, O. and RIEDEL, M.: Experimental Study of Positive Ion Emission from Tungsten, II 19

HORÁNYI, GY., RIZMAYER, E. M. and NAGY, F.: Investigation of Adsorption Phenomena on Platinized Pt Electrodes by Tracer Methods, IX. Measurement of Adsorption on Platinum Powder 35

DOBOS, S.: Strukturumwandlungen des Silikatnetzwerkes im Laufe der Ausbildung der Oberflächenschicht bei natriumoxidhaltigen Gläsern. (Changes in the Structure of Silicate Skeletons During the Development of the Surface Layer of Glasses Containing Sodium Oxide) 43

DOBOS, S.: Der Bindungszustand der Alkaliionen in der Oberflächenschicht von natriumoxidhaltigen Gläsern. (The Bonding State of the Alkali Ions in the Surface Layer of Glasses Containing Sodium Oxide) 49

HORÁNYI, R., and NÉMETH, J.: Theoretical Investigation of the Clarification Process in a Tube Centrifuge 59

CSÁSZÁR, J. und BARTA, I.: Über Komplexe vom bis-(Salicylaldimin-N-R)Nickel(II)-typ (Kurzmitteilung) (On the Complexes of bis-(Salicyl-aldimine-N-R) Nickel(II)--type) (Short Communication) 77

ORGANIC CHEMISTRY – ORGANISCHE CHEMIE – ОРГАНИЧЕСКАЯ ХИМИЯ

ABOU-OUF, A. A., YOUSEF, A. F. and EL-GENDY, M. A.: Synthesis of Certain New Salicylsulfonylurea Derivatives 81

ZSADON, B. and OTTA, K.: Indole and Indole Derivatives, X. Saponification, Acid Hydrolysis and Decarboxylation of (—)-Vincadifformine and Tabersonine 87

VAJDA, T., KAJTÁR, J. and RUFF, F.: The Reaction of Ammonium Thiocyanate with Dicyclohexylcarbodiimide 97

LIPTÁK, A. and JODÁL, N.: Carbohydrate Methyl Ethers, III. Thin-Layer Chromatographic Separation and Quantitative Determination of Glucose Methyl Ethers 103

CHEMICAL TECHNOLOGY – CHEMISCHE TECHNOLOGIE – ХИМИЧЕСКАЯ ТЕХНОЛОГИЯ

UJHIDY, A., MAGYAR, M. und BERKES, R.: Einfluß der Schwefelsäurekonzentration auf die Nitrierungsgeschwindigkeit von Nitrobenzol untersucht in einem Dünnschichtreaktor. (The Effect of the Sulfuric Acid Concentration on the Nitration Rate of Nitrobenzene in a Film Reactor) 107

Recensiones 117

ACTA CHIMICA

ТОМ 69 — ВЫП. 1

РЕЗЮМЕ

Влияние дериватографических держателей образцов, изготовленных из различных материалов, на термическое разложение нитрата аммония

Т. ФЛОРА

Дериватографически изучалось термическое разложение нитрата аммония в тигелях, изготовленных из различных материалов (платина, никель, окисленный никель, нержавеющая сталь, графит и корунд). Было установлено, что разложение протекает бурно, как взрывоподобный экзотермический процесс лишь в металлических и окисно-металлических тигелях, где окисление продуктов разложения, образующихся при диссоциации нитрата аммония, катализируется, вероятно, материалом тигеля. При проведении разложения в графитных или корундовых тигелях протекает главным образом термическая диссоциация нитрата аммония эндотермического характера.

Из дериватографических кривых определялись порядок реакции и энергия активации терморазложения нитрата аммония, проводимого в тигелях из различных материалов. В тигелях из платины, никеля и окисленного никеля порядок реакции разложения был равен нулю или принимал отрицательное значение. При проведении разложения в тигелях из нержавеющей стали, графита и корунда, за начальной реакцией нулевого порядка следовала реакция термической диссоциации нитрата аммония первого порядка. Брутто энергия активации реакций нулевого порядка, протекающих в тигелях из платины, никеля и окисленного никеля, намного ниже, чем энергия активации реакции первого порядка, протекающей в тигелях из нержавеющей стали, графита и корунда.

Дифторид ксенона как аналитический реактив, I

Определение содержания йода

А. ШНЕЭР-ЭРДЕИ и К. КОЗМУЦА

Дифторид ксенона, обладающий сильными окислительными свойствами, легко дозируемый и легко хранимый в твердой фазе почти безграничное время, обладает большими преимуществами при качественном и количественном определении небольших количеств йода или йодистых ионов через окисление йода до перйодата.

Экспериментальное изучение эмиссии положительных ионов с вольфрама, II

О. КАПОШИ и М. РИДЕЛ

Изучалась температурная зависимость ионной эмиссии вольфрамовых спиралей, приготовленных с различными добавками. На кривых эмиссии наблюдалось два максимума. На основе энергий активации, рассчитанных из кривых, было сделано заключение, что появление первого максимума вызвано десорбцией поверхностных, щелочных примесей, в то время как повторное увеличение ионной эмиссии выше 2000° К вызвано повышенной диффузией на границе зерен, вследствие перекристаллизации вольфрама.

При накале вольфрама, подвергнутого термообработке и перекристаллизованного, измеряемые ионные токи были на порядок меньше, чем в предыдущем случае. Иной была и температурная зависимость эмиссии. В интервале температур 1800 и 2100° К наблю-

дались переходные максимумы, которые вызваны, по нашим измерениям, повышением ионной эмиссии —за счет остаточных газов. При дальнейшем повышении температур, выше 2500° К ионный ток вновь увеличивается. Это явление, исходя из величин энергии активации ионной эмиссии (прибл. 120 ккал/моль) приписывалось объёмной диффузии щелочных металлов.

Изучение адсорбционных явлений на платиновом электроде с помощью техники радиоактивной индикации, IX

Измерение адсорбции на платиновом порошке

ДЬ. ХОРАНИ, Э. РИЗМАЙЕР и Ф. НАДЬ

Был разработан метод изучения зависимости адсорбции на платиновом порошке от потенциала с помощью техники радиоактивной индикации. Надежность метода проверялась с исследованием адсорбции соляной кислоты, меченной изотопом Cl^{36}.

Структурные изменения в силикатном скелете при образовании поверхностного слоя в стеклах, содержащих окись натрия

Ш. ДОБОШ

Изучался возникающий в воде поверхностный слой стекол с составом $28Na_2O-4BaO-68SiO_2$. Определялось распределение ионов натрия, бария и водорода, а также «водорода» и воды в поверхностном слое. Было установлено, что при образовании поверхностного слоя происходит резкое изменение структуры силикатного скелета. Ступенью, инициирующей изменение, является разрыв связей $\geqslant Si-O-Si \leqslant$. Разрыв связей вызывают молекулы воды, появляющиеся в скелете. Было установлено также, что протон мигрирует не только как ион гидроксония, но и, опережая фронт миграции молекул воды, через кислороды скелета. В поверхностном слое может быть обнаружено два участка: один более компактный, на котором молекулы воды не мигрируют вместе с протонами, и другой более рыхлый, на котором наблюдается увеличение концентрации воды в направлении раздела фаз поверхностный слой — вода. На границе раздела фаз поверхностный слой — вода концентрация воды значительна, поверхность сильно набухшая.

Система связей щелочных ионов в поверхностном слое стекла, содержащего окись натрия

Ш. ДОБОШ

Изучалось распределение концентрации щелочных ионов в поверхностном слое стекла ($28Na_2O-4BaO-68SiO_2$), возникающем в водных растворах хлористого натрия и хлористого лития. Было установлено, что «набухший» участок поверхностного слоя с большим содержанием воды обладает микрогетерогенной структурой. Щелочные ионы на этом участке слоя диффундируют частично в твердой микрофазе, присоединяясь к группам $\geqslant Si-\overline{O}$ скелета, и частично в гидратированном состоянии в жидкой микрофазе, содержащей молекулярную воду. Было установлено также, что при приготовлении слоя в нейтральных растворах щелочных хлоридов хлористый ион не был обнаружен в поверхностном слое, в то время как скорость растворения скелета увеличилась. Причиной этого является способность хлористого иона к катализу нуклеофильного замещения на атоме кремния в нейтральных (или щелочных) средах, в результате чего появление его в скелете в данных условиях приводит разрушению скелета.

Теоретическое изучение процесса отстаивания в трубчатой центрифуге

Р. ХОРАНИ и Й. НЕМЕТ

Проводились попытки теоретического описания отдельных процессов образования седимента. По теоретическим соображениям предлагалось описание образования седимента с помощью составных процессов. Так разделялись эффективные с точки зрения оседания — первый и второй процесс и неэффективный — процесс заряжения частиц в качестве третьего составного процесса. При обсуждении этих составных процессов вводились и использовались новые — необходимые для обсуждения этих процессов — понятия. Выведенные уравнения позволяют проектирование центрифугального отстаивания в случае суспензий с сохраняющей формой, которое является более реалистическим и физически более обоснованным по сравнению с ранними известными попытками. Это подтверждалось на одной суспензионной модели.

О комплексах типа бис-(салицил-альдимин-N-R)никель (III)

Й. ЧАСАР и И. БАРТА

Измерялись величины вязкостей растворов комплексов типа бис-(салицил-альдимин-N-алкил)никель(II), а также величины молярных объемов твердых и растворенных комплексов. Результаты интерпретировались на основе эффекта сверхсопряжения и, главным образом, стерического эффекта заместителей.

Синтез некоторых новых производных салицилсульфониловых мочевины

А. А. Абу-УФ, А. Ф. ЮСЕФ и М. А. ЭЛЬ-ГЕНДИ

С целью расширения ранее проведенных исследований (1—6), были получены три новые серии салицилсульфониловых мочевин. В основном они были получены из N-(3-карбокси-4-метоксибензолсульфонил)мочевины, N-(3-карбалкокси-4-метоксибензолсульфонил) мочевины и N-(3-карбоксамидо-4-метоксибензолсульфонил)мочевины. N'-Заместителями являлись изопропильная, п-толильная, п-хлорфенильная и антипирильная группы. Этилкарбаматный остаток в этил-N-(3-карбалкокси-4-метоксибензосульфонил)карбамате взаимодействует с алифатическими аминами гораздо легче, чем карбалкокси-группа в положении 3. При некоторых определенных условиях эта карбалкокси-группа превращается в замещенный амидный сегмент под влиянием лишь алифатических, а не ароматических аминов. Это обсуждалось и доказывалось на основе физических и химических данных. Все полученные производные проходят сейчас фармакологическую проверку.

Индол и его производные, X

Изучение омыления, кислого гидролиза и декарбоксилирования (—)-винкадифформина и таберсонина

Б. ЖАДОН и К. ОТТА

Изучались кислый гидролиз и декарбоксилирование (—)-винкадифформина(1а) и таберсонина (6,7-дегидро-1а). При проведении реакции в более мягких условиях, нежели обычно, с почти полным исключением побочных реакций из (—)-винкадифформина был получен (—)-1,2-дегидроаспидоспермидин (11), а из таберсонина с хорошим выходом — декарбометокси-таберсонин (6,7-дегидро-11).

При исследовании возможностей омыления было установлено, что оба алкалоида быстро омыляются без протекания побочных реакций с помощью спиртового 0,5N КОН. Почти с количественным выходом были получены легко разлагающиеся (—)-винкадиф-

форминовая кислота (1b) и таберсониновая кислота (6,7-дегидро-1b); приводятся их физические постоянные и УФ-спектры. Измерялись их стабильность и скорость декарбоксилирования при различных условиях.

Реакция тиоцианата аммония с дициклогексилкарбодиимидом

Т. ВАЙДА, Й. КАЙТАР и Ф. РУФФ

Эквимолекулярные количества тиоцианата аммония и дициклогексилкарбодиимида в ацетонитрильном растворе приводят к образованию эквимолекулярной смеси дициклогексилтиокарбамида и 1,2-дициклогексил-3-цианогуанидина. Были определены стехиометрия реакции и состав кристаллического продукта.

Метиловые эфиры углеводов, III

Разделение метиловых ефиров глюкозы с помощью тонкослойной хроматографии и количественное определение их

А. ЛИПТАК и И. Н. ЙОДАЛ

Образующиеся в результате гидролиза метилированных глюканов 2,3-ди-, 2,4-ди-, 2,3,4-три- и 2,3,4,6-тетраметил-D-глюкозы разделялись с помощью тонкослойной хроматографии и их количества определялись спектрофотометрически на основе цветной реакции с анилингидрофталатом. Данный метод пригоден для определения четырех метиловых эфиров глюкозы с количествами в интервале 50—350 мкг и с точностью $\pm 5\%$.

Влияние концентрации серной кислоты на скорость нитрования нитробензола в случае использования пленочного реактора

А. УЙХИДИ, М. МАДЬЯР и Р. БЕРКЕШ

Нитрование нитробензола проводилось в пленочном реакторе (диаметром 53,3 мм) в области скоростей, превышающих предельную скорость.

Изменение скорости реакции с изменением концентрации серной кислоты изучалось на основе уравнения Дамкьёлера для потока компонента. С помощью этого уравнения может быть определен член источника, на основе которого могут быть сделаны заключения относительно механизма и скорости реакции.

J. HOLLÓ – É. KURUCZ – A. BORÓDI

THE APPLICATIONS OF MOLECULAR DISTILLATION

Molecular distillation is the only method for the separation of heat sensitive and slightly volatile materials of high molecular weight by means of distillation in which the decomposition of the materials can be avoided or reduced to a minimum rate. The development of chemistry and of chemical industry has implied the unavoidable fractionation and purification of a constantly increasing number of materials of the said characteristics. The work is destined to give a comprehensive survey of the definite fields of research and the applications of pilot-plant and unit operation character in which molecular distillation has been utilised as a technological method.

To this end, first a brief survey is presented concerning theoretical and apparatus-concentrated problems, and then the possibilities of the application of molecular distillation are described both in laboratory work and in industrial plants.

In English • Approx. 160 pages • 14×21 cm • Cloth

AKADÉMIAI KIADÓ

PUBLISHING HOUSE OF THE HUNGARIAN ACADEMY OF SCIENCES, BUDAPEST

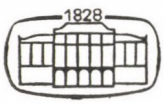
T. Erdey-Grúz

DIE CHEMISCHEN QUELLEN DER ENERGIE

Die ständige Entwicklung der menschlichen Kultur ist auch mit einem stets wachsenden Energieverbrauch verbunden, wodurch die höchst möglichste ökonomische Nutzung der Energiequellen erfordert wird. In der Gegenwart wird dieser Energiebedarf letztlich vorwiegend durch die Chemie bestritten. Die vorliegende Studie beschäftigt sich mit dem Ursprung der Energievorräte für die Menschheit, wobei das eigentliche Wesen der chemischen Energie, die besondere Natur der Wärme bzw. deren Verhältnis zur Arbeit, sowie das wichtige Problem der direkten Umwandlung chemischer in elektrische Energie in allgemein verständlicher Weise behandelt wird.

In deutscher Sprache • Etwa 320 Seiten • 14×21 cm • Ganzleinen

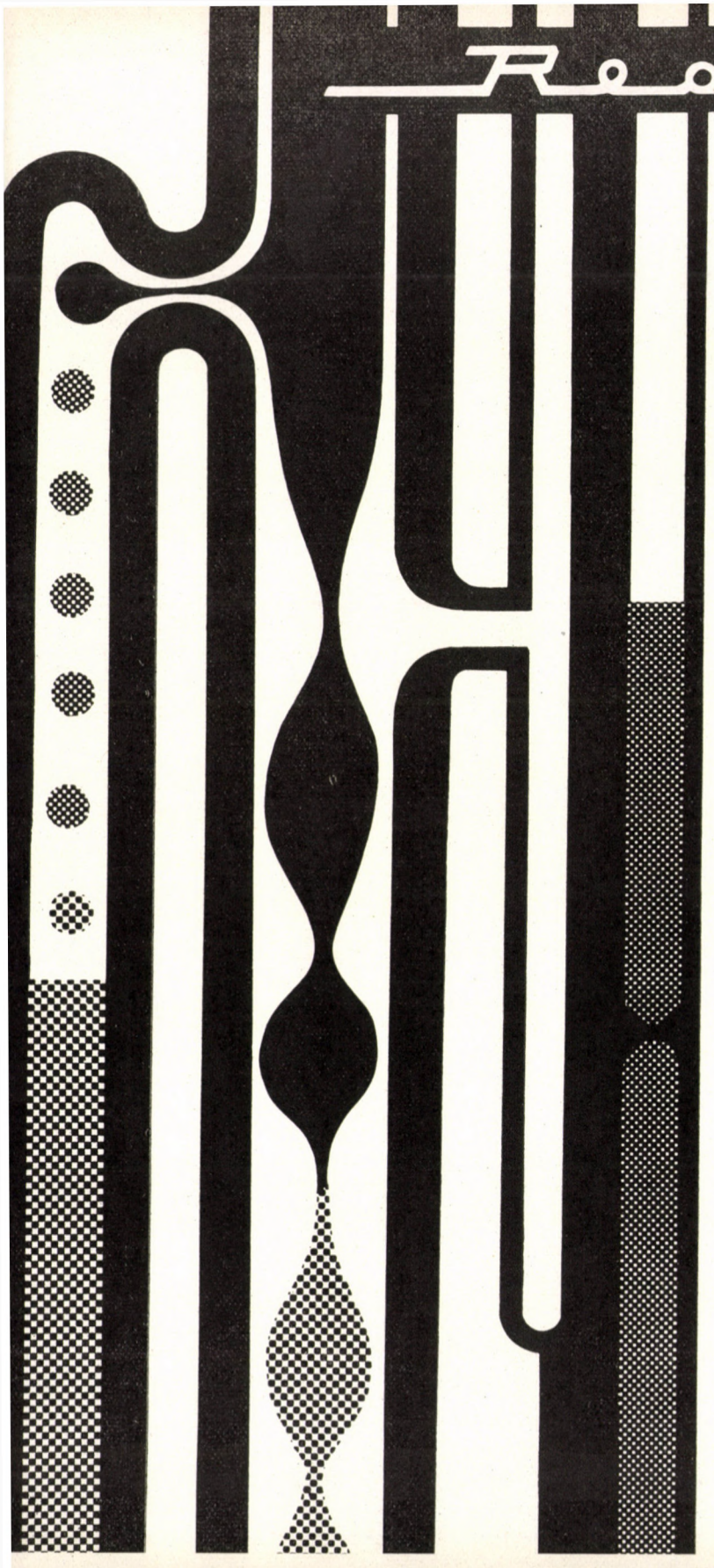
Eine Gemeinschaftsausgabe — vertrieben in den sozialistischen Ländern von KULTURA, Budapest, in allen anderen Ländern von VERLAG CHEMIE, Weinheim



AKADÉMIAI KIADÓ

VERLAG DER UNGARISCHEN AKADEMIE DER WISSENSCHAFTEN

Budapest



ANORGANISCHE UND ORGANISCHE FEINCHEMIKALIEN

Garantiert reine Reagenzien
für analytische Zwecke

Laboratoriumspräparate
für die Forschung
und Technik

Biochemikalien:
Aminosäuren und Derivate
Peptide und Derivate
Enzyme und Koenzyme
Nukleoproteide · Purine

Indikatoren
Tetrazoliumsalze
Präparate für Mikroskopie und Biologie
Kohlenhydrate

REANAL
FABRIK FÜR
FEINCHEMIKALIEN
Budapest · Ungarn

INFORMATION
UND LITERATUR
MEDIMPEX
BUDAPEST 5 · POSTFACH 126

Printed in Hungary

A kiadásért felel az Akadémiai Kiadó igazgatója — Műszaki szerkesztő: Várhelyi Tamás

A kézirat nyomdába érkezett: 1971. II. 15. — Terjedelem: 11,25 (A/5) ív, 51 ábra

71.71186 Akadémiai Nyomda, Budapest — Felelős vezető: Bernát György

The Acta Chimica publish papers on chemistry in English, German, French and Russian.

The Acta Chimica appear in volumes consisting of four parts of varying size, 4 volumes being published a year.

Manuscripts should be addressed to

Acta Chimica
Budapest 112/91 Műegyetem

Correspondence with the editors should be sent to the same address.

The rate of subscription is $16.00 a volume.

Orders may be placed with "*Kultúra*" Foreign Trade Company for Books and Newspapers (Budapest I., Fő utca 32. Account No. 43-790-057-181) or with representatives abroad.

Les Acta Chimica paraissent en français, allemand, anglais et russe et publient des mémoires du domaine des sciences chimiques.

Les Acta Chimica sont publiés sous forme de fascicules. Quatre fascicules seront réunis en un volume (4 volumes par an).

On est prié d'envoyer les manuscrits destinés à la rédaction à l'adresse suivante:

Acta Chimica
Budapest 112/91 Műegyetem

Toute correspondance doit être envoyée à cette même adresse.

Le prix de l'abonnement est de $16.00 par volume.

On peut s'abonner à l'Entreprise pour le Commerce Extérieur de Livres et Journaux «*Kultúra*» (Budapest I., Fő utca 32. Compte-courant No. 43-790-057-181) ou à l'étranger chez tous les représentants ou dépositaires.

«*Acta Chimica*» издают трактаты из области химической науки на русском, французском, английском и немецком языках.

«*Acta Chimica*» выходят отдельными выпусками разного объема. 4 выпуска составляют один том. 4 тома публикуются в год.

Предназначенные для публикации рукописи следует направлять по адресу:

Acta Chimica
Budapest 112/91 Műegyetem

По этому же адресу направлять всякую корреспонденцию для редакции.

Подписная цена — $16.00 за том.

Заказы принимает предприятие по внешней торговле книг и газет «*Kultúra*» (Budapest I., Fő utca 32. Текущий счет № 43-790-057-181) или его заграничные представительства и уполномоченные.

Reviews of the Hungarian Academy of Sciences are obtainable at the following addresses:

ALBANIA

Drejtorija Qändrone e Pärhapjes
dhe Propagandimit tä Librit
Kruga Konferenca e Päzes
Tirana

AUSTRALIA

A. Keesing
Box 4886, GPO
Sydney

AUSTRIA

Globus
Höchstädtplatz 3
A-1200 Wien XX

BELGIUM

Office International de Librairie
30, Avenue Marnix
Bruxelles 5
Du Monde Entier
5, Place St. Jean
Bruxelles

BULGARIA

Hemus
11 pl Slaveikov
Sofia

CANADA

Pannonia Books
2, Spadina Road
Toronto 4, Ont.

CHINA

Waiwen Shudian
Peking
P. O. B. 88

CZECHOSLOVAKIA

Artia
Ve Smečkách 30
Praha 2
Poštovní Novinová Služba
Dovoz tisku
Vinohradská 46
Praha 2
Mad'arská Kultura
Václavské nám. 2
Praha 1
Slovart A. G.
Gorkého
Bratislava

DENMARK

Ejnar Munksgaard
Nörregade 6
Copenhagen

FINLAND

Akateeminen Kirjakauppa
Keskuskatu 2
Helsinki

FRANCE

Office International de Documentation
et Librairie
48, rue Gay Lussac
Paris 5

GERMAN DEMOCRATIC REPUBLIC

Deutscher Buch-Export und Import
Leninstraße 16
Leipzig 701
Zeitungsvertriebsamt
Fruchtstraße 3—4
1004 Berlin

GERMAN FEDERAL REPUBLIC

Kunst und Wissen
Erich Bieber
Postfach 46
7 Stuttgart S.

GREAT BRITAIN

Blackwell's Periodicals
Oxenford House
Magdalen Street
Oxford
Collet's Subscription Import
Department
Dennington Estate
Wellingsborough. Northants.
Robert Maxwell and Co. Ltd.
4—5 Fitzroy Square
London W. 1

HOLLAND

Swetz and Zeitlinger
Keizersgracht 471—487
Amsterdam C.
Martinus Nijhof
Lange Voorhout 9
The Hague

INDIA

Hind Book House
66 Babar Road
New Delhi 1

ITALY

Santo Vanasia
Via M. Macchi 71
Milano
Libreria Commissionaria Sansoni
Via La Marmora 45
Firenze

JAPAN

Kinokuniya Book-Store Co. Ltd.
826 Tsunohazu 1-chome
Shinjuku-ku
Tokyo
Maruzen and Co. Ltd.
P. O. Box 605
Tokyo-Central

KOREA

Chulpanmul
Phenjan

NORWAY

Tanum-Cammermeyer
Karl Johansgt 41—43
Oslo 1

POLAND

Ruch
ul. Wronia 23
Warszawa

ROUMANIA

Cartimex
Str. Aristide Briand 14—18
Bucureşti

SOVIET UNION

Mezhdunarodnaya Kniga
Moscow G—200

SWEDEN

Almquist and Wiksell
Gamla Brogatan 26
S—101 20 Stockholm

USA

F. W. Faxon Co. Inc.
15 Southwest Park
Westwood Mass. 02090
Stechert Hafner Inc.
31. East 10th Street
New York, N. Y. 10003

VIETNAM

Xunhasaba
19, Tran Quoc Toan
Hanoi

YUGOSLAVIA

Forum
Vojvode Mišića bro 1
Novi Sad
Jugoslovenska Knjiga
Terazije 27
Beograd

27. VII. 1971 Index: 26.007

ACTA CHIMICA

ACADEMIAE SCIENTIARUM HUNGARICAE

ADIUVANTIBUS

V. BRUCKNER, GY. DEÁK, K. POLINSZKY,
E. PUNGOR, G. SCHAY, Z. G. SZABÓ

REDIGIT

B. LENGYEL

TOMUS 69 FASCICULUS 2

AKADÉMIAI KIADÓ, BUDAPEST

1971

ACTA CHIM. (BUDAPEST)

ACTA CHIMICA

A MAGYAR TUDOMÁNYOS AKADÉMIA KÉMIAI TUDOMÁNYOK OSZTÁLYÁNAK IDEGEN NYELVŰ KÖZLEMÉNYEI

SZERKESZTI

LENGYEL BÉLA

TECHNIKAI SZERKESZTŐK

DEÁK GYULA és HARASZTHY-PAPP MELINDA

Az Acta Chimica német, angol, francia és orosz nyelven közöl értekezéseket a kémia tudományok köréből.

Az Acta Chimica változó terjedelmű füzetekben jelenik meg, egy-egy kötet négy füzetből áll. Évente átlag négy kötet jelenik meg.

A közlésre szánt kéziratok a szerkesztőség címére (Budapest 112/91 Műegyetem) küldendők.

Ugyanerre a címre küldendő minden szerkesztőségi levelezés. A szerkesztőség kéziratokat nem ad vissza.

Megrendelhető a belföld számára az „Akadémiai Kiadó"-nál (Budapest V., Alkotmány utca 21. Bankszámla 05-915-111-46), a külföld számára pedig a „Kultúra" Könyv- és Hírlap Külkereskedelmi Vállalatnál (Budapest I., Fő utca 32. Bankszámla: 43-790-057-181) vagy annak külföldi képviseleteinél és bizományosainál.

Die Acta Chimica veröffentlichen Abhandlungen aus dem Bereiche der chemischen Wissenschaften in deutscher, englischer, französischer und russischer Sprache.

Die Acta Chimica erscheinen in Heften wechselnden Umfanges. Vier Hefte bilden einen Band. Jährlich erscheinen 4 Bände.

Die zur Veröffentlichung bestimmten Manuskripte sind an folgende Adresse zu senden:

Acta Chimica
Budapest 112/91 Műegyetem

An die gleiche Anschrift ist auch jede für die Redaktion bestimmte Korrespondenz zu richten. Abonnementspreis pro Band: $16.00.

Bestellbar bei dem Buch- und Zeitungs-Außenhandels-Unternehmen »*Kultúra*« (Budapest I., Fő utca 32. Bankkonto No. 43-790-057-181) oder bei seinen Auslandsvertretungen und Kommissionären.

Acta Chimica Academiae Scientiarum Hungaricae, Tomus 69 (2), pp. 123—135 (1971)

ÜBER DIE BEEINFLUSSUNG DER VERDAMPFUNGSGESCHWINDIGKEIT VON ZINKOXID DURCH KURZWELLIGES LICHT

K. HAUFFE* und A. J. HEGEDŰS**

*(*Institut für physikalische Chemie der Universität Göttingen und **TUNGSRAM-Forschungslaboratorien, Budapest-Újpest)*

Eingegangen am 17. Dezember 1969

Es wurde die Verdampfungsgeschwindigkeit von ZnO und Zn mit einer Vakuummikrowaage thermogravimetrisch gemessen. Der durch das Meßverfahren bedingte geeignetste Geschwindigkeitsbereich lag bei $1—2 \cdot 10^{-5}$ Torr im Falle von ZnO zwischen 450—525 und im Falle von Zn zwischen 140—200 °C. Über diesem Temperaturbereich kamen in beiden Fällen zu starke, störende Zn-Beschläge zustande. Auf die Geschwindigkeit der ZnO-Verdampfung konnte keine, auf die der Zn-Verdampfung jedoch eine starke UV-Lichteinwirkung mit Temperaturhysterese gemessen werden. ZnO- und Zn-Verdampfung, sowie ZnO + H_2-Reduktion haben praktisch gleiche Aktivierungsenergien. Die Gegenwart von H_2O-Dampf scheint die ZnO-Verdampfung zu beschleunigen.

1. Problemstellung

Es ist bekannt, daß Zinkoxid — insbesondere im Bereich niedriger Drucke — bei Einstrahlung von Licht mit einer Wellenlänge ≤ 380 nm ($\geq 3{,}2$ eV) nicht nur bei höheren Temperaturen sondern auch schon bei Zimmertemperatur Sauerstoff abgibt [1, 2]. Wie man heute auf Grund des vorliegenden experimentellen Materials annehmen darf, wird die Abgabe von Gas nicht nur durch eine Desorption eines elektronenaffinen, chemisorbierten Gases bewirkt, wie z. B.

$$O_2^-(\text{ads}) + \text{Licht} \rightarrow O_2(\text{gas}) + e' \tag{1}$$

oder

$$CO_2^-(\text{ads}) + \text{Licht} \rightarrow CO_2(\text{gas}) + e' \tag{2}$$

sondern auch durch eine Photolyse, wie z. B.

$$ZnO + \text{Licht} \rightarrow Zn^{\cdot} + e' + \frac{1}{2} O_2(\text{gas}) \tag{3}$$

verursacht, wobei insbesondere bei höheren Temperaturen auch mit einer Verdampfung von Zink gerechnet werden muß. Hierbei bedeutet e' ein freies Elektron und $Zn^{\cdot}$ ein Zinkion auf Zwischengitterplatz. Daß in der Tat bei Belichtung mit kurzwelligem Licht Desorptionsvorgänge gemäß Gleichung (1) und (2) und bei höheren Temperaturen besonders ausgeprägt photolytische Prozesse

gemäß Gleichung (3) ablaufen können, konnte einmal durch die Zunahme der Oberflächenleitfähigkeit [3, 4] und zum anderen durch die Abnahme der negativen Oberflächenladung (oft als positive DEMBER-Spannung bezeichnet) nachgewiesen werden [5, 6, 7]. Die Einwirkung von kurzwelligem Licht wurde auch auf die Auflösungsgeschwindigkeit von Zinkoxid in wässrigen Elektrolyten untersucht [8, 9], wobei eine deutliche Zunahme der Auflösungsgeschwindigkeit unter Licht gegenüber der im Dunkeln beobachtet werden konnte.

Die Kinetik der Verdampfung von II_B—VI_B Verbindungen, auch unter Lichteinwirkung, wurde kürzlich auf Grund der mit CdS erhaltenen Ergebnissen ausführlich behandelt [10], allerdings sind dabei keine Versuche mit polykristallinem Zinkoxid erwähnt worden. Umfassendes Material über die Verdampfung von Zinkoxid liegt ebenfalls vor [11], wobei jedoch die Frage der Lichteinwirkung unberührt blieb.

Auf Grund der bisher vorliegenden Versuchsergebnisse ist eine quantitative Ermittlung der vom Zinkoxid entweichenden Gasmenge je Oberflächeneinheit nicht möglich. Aus diesem Grunde erschien es reizvoll, einige Experimente über Geschwindigkeit und Ausmaß des Austritts von Sauerstoff und Zink neben der Desorption von elektronenaffinen Gasen, wie z.B. O_2 und CO_2, bei Lichteinstrahlung mittels einer empfindlichen Waage auszuführen. In dieser Arbeit möchten wir über die Ergebnisse unserer Verdampfungsversuche bei höheren Temperaturen berichten, während die Adsorption an unbelichtetem und UV-belichtetem Zinkoxid und die Photolyse des Zinkoxids an einer anderen Stelle besprochen werden soll. Über die Ergebnisse unserer Arbeit wurde unlängst kurz zusammenfassend an einer anderen Stelle berichtet [12].

2. Experimentelles

Die zeitliche Änderung der Masseabnahme von Zinkoxid infolge Desorption und Verdampfung wurde mittels einer elektronisch registrierenden Vakuum-Mikrowaage Typ 4102 der Firma Sartorius ermittelt [13, 14]. Der Aufbau der Versuchseinrichtung bestand gemäß dem in Abb. 1 dargestellten Schema aus einer Leybold-Vakuumanlage (Öldiffusionspumpe DO 121 mit normalem Diffelen-Öl, Quecksilber-Diffusionspumpe Quick 100, Gasballastpumpe D6 und Thermotron IV), dem Reaktionsrohr in Abb. 2 und der Mikrowaage. Direkt an die Waage war ein Penning III — Vakuummeter angeschlossen und darunter ein kurzer ($\approx$12 cm) Blindstutzen aus Glas. Unter dem anderen Ende des Waagebalkens befand sich ein etwa 100 cm langes Quarzrohr von 30 mm Außendurchmesser, das entsprechend Abb. 2 mit 38 Windungen aus Aluchrom 0 (0,8 mm $\varnothing$) direkt geheizt wurde. Die Anordnung der HBO-Höchstdrucklampe von 500 Watt [15] die als Lichtquelle diente, ist aus Abb. 2 zu entnehmen. Die Heizung wurde mit stabilisiertem Wechselstrom von 220 Volt betrieben. Die Ofentemperatur konnte mit einem Schiebetransformator und einem Hartmann und Braun Temperaturregler und Anzeigeinstrument Typ AAHT auf mindestens ± 2 °C genau eingestellt und geregelt werden. Bei laufender Diffusionspumpe betrug das erreichbare Höchstvakuum etwa $4 \cdot 10^{-6}$ Torr und das Arbeitsvakuum etwa $2 \cdot 10^{-5}$ Torr. Das Regelgerät der Waage war mit einem Leeds-Northrup Speedomax G-Schreiber verbunden, so daß die zeitliche Änderung der Masse der ZnO-Probe registriert werden konnte. Die Temperatur der Waage konnte mit einem Fakir Axiallüfter Thermomatic 202 S auf ± 3 °C konstant gehalten werden.

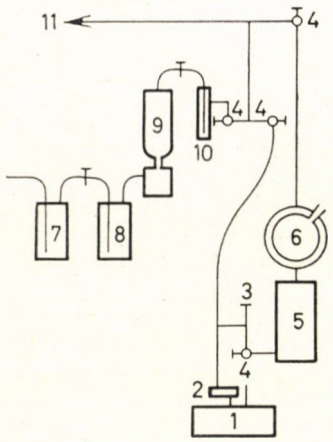


Abb. 1. Versuchsanordnung, Vakuumteil. 1. Ballastpumpe, 2. Automatische Belüftung, 3. Thermotron IV, 4. Ventile, 5. Diffusionspumpe, 6. Flüss. N_2-Falle, 7. cc. H_2SO_4-Falle, 8. Gran. KOH-Falle, 9. Silikagel-Falle, 10. Flüss. N_2-Falle, 11. Rezipient, Waage mit Penning III

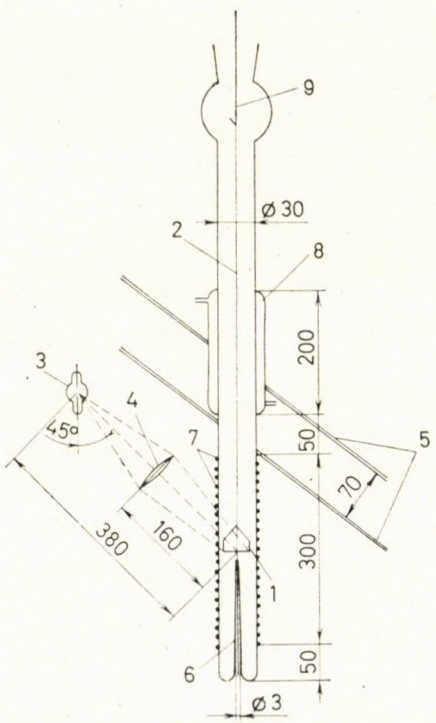


Abb. 2. Versuchsanordnung, Reaktionsrohr. 1. Quarzglastiegel, 2. Pt-Faden 0,05 mm ⌀ 3. OSRAM 500 W HBO Lampe, 4. Quarzglaslinse F = 125 mm ⌀ = 45 mm, 5. Asbestplatten ~ 40×50 cm, 6. Meßfinger für Thermoelement, 7. Heizspirale, 8. Angeschmolzener Quarzglasmantel, Liebig-Kühler, 9. Haken aus Glaskapillare oder Pt-Draht

Im Arbeitsvakuum konnte zwischen Tiegel und Temperatur-Meßfinger in der Reaktionszone nur ein kleiner Temperaturunterschied beobachtet werden, der bei 150 °C ein Maximum von 6,5 °C durchlief, bei 22 und 290 °C jedoch verschwand. Wie aus Abb. 3 entnommen werden kann, verursacht die Belichtung mit ungefiltertem Licht eine beachtliche Temperaturerhöhung des Tiegels, die durch Wärmefilter deutlich herabgesetzt werden konnte. Eine Beladung des Tiegels mit ZnO oder Zink hatte keinen Einfluß auf die durch Licht verursachte und in Abb. 3 angegebene Temperaturerhöhungen. Bei konstanter Lichtintensität ließen sich die Meßwerte recht gut reproduzieren.

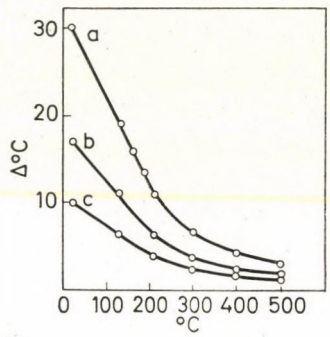


Abb. 3. Überhitzung der Probe (Δ °C) bei UV-Bestrahlung *a* ohne Wärmefilter, *b* durch Wärmefilter NG 11 oder 15 mm H_2O-Schicht, *c* durch 15 mm Schicht von 10% $CuSO_4$ in H_2O

Als Untersuchungsmaterialien dienten die folgenden Oxide und Metallbleche:

a) ZnO p. a. REANAL, Budapest (n-Typ-Halbleiter) mit einer Oberfläche von 3,9 m^2 per g (nach BET), der Reinheitsgrad war: Ag $\approx$ 0,00001, Al $\approx$ 0,00001, Cu $\approx$ 0,0001, Fe $\leq$ $\leq$ 0,0001, Mg $\approx$ 0,0001, Mn $\approx$ 0,0001, Pb $\leq$ 0,00001, Si $\approx$ 0,0006 und Ti $\leq$ 0,00001%.

b) ZnO Fotosiegel A/Fi 22(11) GRILLO, Oberhausen mit einer BET—Oberfläche von 3,8 m^2/g; Herstellung aus spektralreinem Zink. Wenn diese Probe vor der BET-Messung in Normalatmosphäre bei 400 °C 2 Stunden thermisch vorbehandelt wurde, erhielt man eine geringe Zunahme der spezifischen Oberfläche von 3,86 und 3,73 auf 3,89 und 3,98 m^2/g.

c) ZnO mit 0,27 Atom% Li/Mol ZnO dotiert (n-Typ-Halbleiter) wurde wie folgt hergestellt: 10 g ZnO REANAL (a) wurden in p. a. HNO_3 gelöst, 4,01 mg Li als $LiNO_3$-Lösung hinzugefügt, auf dem Wasserbad eingeengt, am Sandbad eingetrocknet und schließlich bei 1000 °C 2 Stunden in Luft von 1 atm geglüht. Die flammenphotometrische Li-Bestimmung nach dem Glühen ergab 216 μg Li/g ZnO. Die BET-Oberfläche war kleiner als 1 m^2/g und konnte daher mit der üblichen N_2-Adsorptionsmethode nicht exakt erfaßt werden. Durch den Lithiumgehalt erhielt das Zinkoxid eine deutlich gelbliche Anfärbung, die mit der Menge des Li-Gehaltes zunahm.

d) ZnO p. a. REANAL, 2 Stunden bei 1000 °C geglüht (*n*-Typ-Halbleiter). Die BET-Oberfläche schrumpfte auf weniger als 1 m^2/g zusammen und konnte aus den oben genannten Gründen nicht genau bestimmt werden. Ein 2stündiges Glühen bei 500 °C in Luft von 1 atm hat keine Veränderung der BET-Oberfläche zur Folge.

e) Feinzinkblech von 0,2 mm Dicke, Reinheitsgrad 99,995%.

3. Versuchsergebnisse und Diskussion

Ein Erhitzen von Zinkoxid-Pulver ist stets durch eine Gewichtsabnahme gekennzeichnet, da kondensiertes Wasser und die sowohl durch Physisorption als auch durch Chemisorption an der Oberfläche anwesenden Gase desorbieren.

Tabelle I

Verdampfungsgeschwindigkeiten des ZnO-Pulvers bei 450 °C, 1—2 · 10^{-5} Torr und 1,58 cm^2 geometrische Pulveroberfläche in µg/15 min, nach anfänglichen größeren Gewichtsabnahmen infolge Desorption von H_2O, CO_2 und O_2

Einwaagen: 185 (±5) mg ZnO

s.g.	g.	8,5	6	6	6	2,5	3												
s.g.	g.	7	4	5	2,5	2	2,5												
s.g.	g.	6	4	3,5	2,5	3	2												
s.g.	g.	6	3,5	3	2	3	2,5	3	3	3	2	1,5	1,5	2	2,5				
s.g.	g.	5,5	5	4	4	3,5	3,5												
s.g.	g.	4	2	4	1	1,5	3												
s.g.	g.	7	3																
s.g.**	g.	6,5	4	—	3														
s.g.*	g.	7	5	5	5	4	3												
Mittelwert in µg/h		*26*	*16*		*13*				*11*				*7,5*						

Einwaagen: 100 (±2) *mg ZnO*

s.g.	g.	9	5,5																
s.g.	g.	5	4	3	3	2,5	2,5												
s.g.	g.	4	3	—	4,5	3	3	—	3	4	2	—	1,5	1	2,5	—	2,5	2	1,5
s.g.**	g.	3,5	3,5	—	3,5														
s.g.**	g.	3	2	—	4	—	4	3,5	2	—	5	—	3	3	—	3			
Mittelwert in µg/h		*20*	*14*		*13*				*13*				*8*				*9*		

Bemerkungen: Untersuchtes Präparat, ZnO a) bei * ZnO b) s.g. = sehr groß; g = groß; ** Belüftung der Probe mit getrockneter Luft, statt normal Zimmerluft.

Der zeitliche Verlauf der Desorption und die desorbierte Gasmenge lassen sich mit Hilfe von Desorptionsgleichungen quantitativ formal erfassen. Während unterhalb von 400 °C die Desorptionsisothermen durch Grenzwerte gekennzeichnet sind, erhält man von 450 °C ab aufwärts bei niedrigstem Restgasdruck von etwa $1 \cdot 10^{-5}$ Torr und größter Empfindlichkeit (± 1 μg) der von uns verwandten Vakuum-Mikrowaage eine zeitlich konstante Gewichtsabnahme des ZnO-Pulvers. Es wurde beobachtet, daß diese zeitlich konstante Desorption nicht der spezifischen Oberfläche, sondern nur der geometrischen Oberfläche proportional war, ähnlich der Verdampfung einer Flüssigkeit. Den Übergang von der Desorption, die von der BET-Oberfläche und somit auch von der Einwaage des ZnO-Pulvers abhängig ist, zur Desorption, die nur von der geometrischen Oberfläche abhängt und demzufolge von der Einwaage unabhängig ist, kann man aus den Meßwerten in Tabelle I entnehmen. Verdampfungsversuche über 450 °C führten schon nach kurzer Zeit zu einem sichtbaren Niederschlag von metallischem Zink an den kühleren Stellen der Innenwand des Reaktionsrohres.

Eine Erwärmung im Vakuum führte stets zu einer grauen Anfärbung der Oberfläche des ZnO-Pulvers. Die Intensität der Graufärbung wuchs sowohl mit der Größe der spezifischen Oberfläche als auch mit der Höhe der Temperatur für die Wärmebehandlung. An den von uns verwandten ZnO-Proben mit einer spezifischen BET-Oberfläche von 3,9 m^2/g und einem Restgasdruck von $2 \cdot 10^{-5}$ Torr machte sich bereits ab 200 °C eine deutliche Graufärbung bemerkbar. Trägt man die Intensität der Graufärbung gegen die Temperatur auf, so durchläuft diese Kurve ein Maximum, weil mit steigender Temperatur nicht nur die Verdampfung gemäß

$$ZnO = Zn^{+}(ads) + O^{-}(ads) \tag{4}$$

und

$$Zn^{+}(ads) + O^{-}(ads) = Zn^{x}(ads) + \frac{1}{2} O_2(gas) \tag{5}$$

zunimmt, sondern auch die spezifische Oberfläche infolge Sinterung abnimmt. Diese graue Anfärbung, die auf eine fein verteilte Abscheidung von Zink beruht, blieb erhalten, wenn im Vakuum abgekühlt wurde. Sie verschwand hingegen, wenn in Luft bei einer Temperatur nachbehandelt wurde, die mindestens so hoch war wie die vorher bei der Wärmebehandlung im Vakuum. Das Innere der gröberen Pulveraggregate an der Oberfläche der im Tiegel befindlichen Pulverschicht sowie der unter der geometrischen Oberfläche liegende Teil der Pulverschicht blieb völlig weiß, was auf das Fehlen einer Zinkmetall-

Abscheidung zurückzuführen ist. Je dichter die Pulverschicht zusammengedrückt wurde, desto steiler nahm die Intensität der grauen Anfärbung in der Schicht nach dem Inneren hin ab, quasi auf die Geschehnisse eines Überganges von großer zu kleiner Oberfläche, bzw. von einer hochdispersen Form zum Einkristall hindeutend. Die graue Anfärbung, bzw. die Abscheidung von metallischem Zink, ist also eine Erscheinung, die in der Nähe der Oberfläche erfolgt und durch den p_{O_2}-Gradienten wesentlich bestimmt wird. Sie kommt, wie bereits erwähnt und in den Gleichungen (4) und (5) angedeutet, wegen thermischer Abspaltung von Oberflächen-Sauerstoff und demzufolge durch die hierdurch verursachte Anhäufung von Zn^+-Ionen, und Elektronen an der Oberfläche unter Ausscheidung von Zinkatomen zustande. Bei hinreichend großer spezifischer Oberfläche kann die Menge der überschüssigen Zn^+-Ionen bzw. der Zinkatome absorptionsspektroskopisch, gravimetrisch und/oder chemisch analytisch bestimmt und damit der Vorgang quantitativ erfaßt werden [16, 17]. Auch das mit Li_2O dotierte, gelblich gefärbte ZnO-Pulver zeigte unter gleichen Versuchsbedingungen ebenfalls einen Graustich. Das ZnO läßt sich bekanntlich durch Dotierung mit Li_2O zu einem n-Typ-Halbleiter mit hohem Widerstand umwandeln.

Zwecks Bestimmung der Verdampfungsgeschwindigkeit von ZnO-Pulver wurde nach Einstellung der oben erwähnten konstanten Gewichtsabnahme 30 bis 90 Minuten weiter erhitzt und aus den so registrierten stationären $\Delta\mu$g-Zeit-Geraden die Werte in Tabelle II erhalten. Beim Einwiegen wurde die Oberfläche des Pulvers im Tiegel vor Versuchsbeginn stets sanft glatt gedrückt. Neue Einwaagen lieferten anfangs höhere Werte, etwa von der Größenordnung der angekreuzten Daten in Tabelle II, die für die Berechnung der Durchschnittswerte nicht berücksichtigt wurden. Diese Anomalie konnte auf höhere Wasserdampfgehalte zurückgeführt werden, die bei den ersten Erwärmungen von frisch eingewogenen ZnO-Proben von der Probe und Innenwand der Apparatur abgesaugt wurden. Zur Beseitigung dieses unerwünschten Wassergehaltes wurde die Probe vor der Messung bei Zimmertemperatur einige Male mit hochgetrockneter Luft belüftet. Anschließend wurde die Meßreihe bei der höchsten Meßtemperatur begonnen. Hierdurch wurde auch gleichzeitig die schnellere Einstellung der notwendigen zeitlich konstanten Gewichtsabnahme erreicht. Für die Bestimmung der Verdampfungsgeschwindigkeit war es gleichgültig, ob die Meßtemperatur von einer höheren oder einer niedrigeren Temperatur kommend eingestellt wurde.

Aus den Zahlen der Tabelle II geht die Unabhängigkeit der Geschwindigkeit der Verdampfung von der Einwaage des ZnO-Pulvers und gleichzeitig ihre Abhängigkeit von der geometrischen Oberfläche des im Tiegel befindlichen Pulvers eindeutig hervor. Die Durchschnittswerte der Tabelle II wurden für die Konstruktion der in Abb. 4 dargestellten $\log k - 1/T$-Geraden verwandt. Die aus der Neigung ermittelte Aktivierungsenergie von 30,4 kcal/Mol

Tabelle II

Verdampfungsgeschwindigkeit des ZnO bei 1—2 · 10^{-5} Torr

Temperatur °C	450	475	500	525	
Einwaage 53,53 mg ZnO					
a), unbelichtet,	8	18	32	59	
	8	18	34	57	
belichtet	8	18	31	65*	
	7	17	32	62	
Einwaage 193,46 mg ZnO					
a), unbelichtet	10	20	40*	73*	
	4	14	32	63	
Einwaage 196, 31 mg ZnO					$\mu g \cdot h^{-1} \cdot 1{,}58\ cm^{-2}$
d), unbelichtet	10	27*	51*	71*	
	4	13	28	62	
Einwaage 222,76 mg ZnO					
c), unbelichtet,	11*	23*	37	60	
	11	15	35	58	
belichtet	9	19	33	62	
	9*	25*	29	57	
Durchschnittlich	8	17	32	60	
Einwaage 41,13 mg ZnO *a)*,					
unbelichtet	4	7	15	25	
	2	7	11	21	$\mu g \cdot h^{-1} \cdot 0{,}636\ cm^{-2}$
Durchschnittlich	3	7	13	23	
	4,89	10,89	20,35	37,07	$\mu g \cdot h^{-1} \cdot cm^{-2}$
	1,67	3,72	6,95	12,65	$\cdot 10^{-11}$ Mol $\cdot$ sec^{-1} $\cdot$ $\cdot$ cm^{-2}

stimmt auffallend gut sowohl mit der Aktivierungsenergie der Reaktion [18]

$$ZnO + H_2(gas) = Zn + H_2O(gas)$$

als auch mit der Verdampfungswärme des Zinks überein [19]. Auf Grund dieses Befundes ist der Schluß naheliegend, daß offenbar bei allen drei Prozessen die Verdampfung des Zinks der geschwindigkeitsbestimmende Schritt zu sein scheint.

Eine Beeinflussung der Verdampfungsgeschwindigkeit von Zinkoxid durch Einstrahlen von kurzwelligem Licht ($\leq$ 380 nm) konnte nicht nachgewiesen werden. Man müßte hierzu die Experimente bei niedrigeren Temperaturen und höherem Vakuum und auch mit größerer Lichtintensität wiederholen, wobei auch eine empfindlichere Meßtechnik zu empfehlen wäre.

Um die Richtigkeit der aus der erhaltenen Aktivierungsenergie gezogenen Folgerungen zu kontrollieren, wurde auch die Verdampfungsgeschwindigkeit von spektralreinen Zinkblechen ermittelt. Wenn man jedoch berücksichtigt, daß unter den hier vorliegenden Versuchsbedingungen das Zinkblech stets mit einer dünnen Zinkoxidschicht bedeckt ist, so sollte entweder die durch die Oxiddeckschicht erfolgende Diffusion von Zinkionen und Elektronen, die der Verdampfung vorausgeht, oder die Umladung der Ionen an der Oberfläche durch Einstrahlung von Licht beeinflußt werden können. Auf Grund dieser Möglichkeit erschien es wünschenswert, die Verdampfungsgeschwindigkeit von Zink auch unter Einstrahlung von ultraviolettem Licht zu studieren.

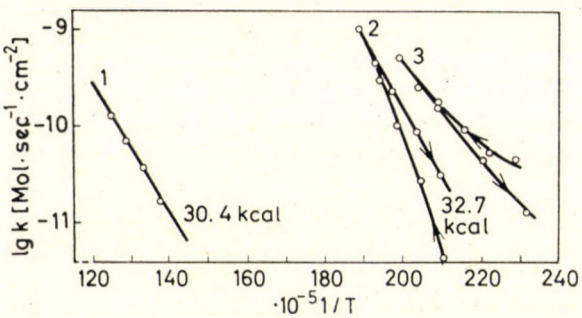


Abb. 4. Änderung der Verdampfungsgeschwindigkeit von ZnO (1) und der Verdampfungsgeschwindigkeit von Zn, unbelichtet (2), belichtet (3)

Zu diesem Zwecke wurden aus dem Feinzinkblech Scheiben von 13 mm ⌀ gestanzt, poliert und gereinigt und anschließend in den an der Waage hängenden Tiegel eingeführt. Die anschließenden Verdampfungsexperimente wurden in der gleichen Weise wie bei den ZnO-Pulverexperimenten durchgeführt. Infolge der hier wegfallenden Desorptionsperioden (wegen der kleinen Oberfläche unmeßbar klein) erübrigten sich lange Meßzeiten, da sich auch bei niedrigen Temperaturen schnell eine zeitlich konstante Verdampfungsgeschwindigkeit einstellte. Da eine Rekristallisation des gewalzten Zinkbleches bei den Versuchstemperaturen nicht zu vermeiden war und da diese aus thermochemischen Gründen zu der in Abb. 4 erkennbaren Änderung der Aktivierungsenergie beigetragen haben könnte (beständigere Form und niedrigere Verdampfungsgeschwindigkeit), wurde die Probe vor der Messung bei 280—300 °C rekristallisiert.

Die Versuchsergebnisse sind in Tabelle III und in den Kurven 2 und 3 der Abb. 4 wiedergegeben, wo in der üblichen Weise log k gegen $1/T$ aufgetragen ist. Während aus den mit ZnO erhaltenen Versuchsergebnissen hervorging, daß die Verdampfung von Zinkoxidpulver bei der Versuchstemperatur von 450—525 °C durch kurzwelliges Licht praktisch nicht beeinflußt wird,

Tabelle III

Verdampfungsgeschwindigkeit des Zn bei 1—2 · 10⁻⁵ Torr

C°	C° korrigiert nach Abb. 3	C° korrigiert nach Tabelle I	$10^5/T$	10^{-11} · g Atom · sec^{-1} · cm^{-2}	
				unbelichtet	belichtet
140	158	164	228,8	—	4,472
156	172	177,5	222,0	—	5,431
171	186	191	215,5	—	9,264
187	200	205	209,2	—	16,93
197	—	202	210,5	0,415	—
199	211	215,5	204,7	—	25,24
211	—	215,5	204,7	2,715	—
214	225	228,5	199,4	—	50,47
227	—	230,5	198,6	10,22	—
239	—	242,5	194,0	29,71	—
253	—	256	189,0	97,75	—
241	—	244,5	193,2	45,04	—
230	—	233,5	197,4	23,00	—
213	—	217,5	203,9	8,63	—
200	—	204,5	209,4	3,19	—
188	201	205,5	209,0	—	15,75
160	176	181	220,3	—	4,472
132	151	157,5	232,3	—	1,278

erfuhr zwischen 140—225 °C die Verdampfung von Zink aus einer Zinkmetallfolie, die mit einer dünnen Oxidschicht bedeckt ist, eine deutliche Beschleunigung durch Lichteinstrahlung. Mit steigender Temperatur nahm die beschleunigende Wirkung des Lichtes im Sinne der 3. Abbildung ab. Dieser auf den ersten Blick merkwürdige Befund wird verständlich, wenn man sich den möglichen Reaktionsablauf der durch Licht in dem dünnen ZnO-Film erzeugten Elektron-Lochpaare $e' \sim |e|^{\cdot}$ mit den Ionen an der Oberfläche klar macht.

Entsprechend der großen Zahl freier Elektronen, die in der dünnen im Kontakt mit Zink befindlichen ZnO-Schicht verfügbar sind, wird im Dunkeln stets eine starke Chemisorption von Sauerstoff vorhanden sein, so daß sich eine Verarmung an freien Elektronen und eine Anreicherung an Zinkionen auf Zwischengitterplatz eingestellt hat. Thermisch erfolgt nun eine Verdampfung von Zink ohne Lichteinwirkung in der Weise, daß Teilschritt (5) infolge des großen Reservoirs an Zink und der damit verfügbaren Elektronen nicht mehr nennenswert ablaufen kann, da nunmehr das gemäß

$$O^-(ads) + Zn^+(ads) \rightarrow O^\times(ads) + Zn^\times(ads) \qquad (6)$$

* Das liegende Kreuz an $Zn^\times$ oder $O^\times$ kennzeichnet den elektrisch neutralen Zustand

entladene Sauerstoffteilchen sofort ein Elektron aus dem großen Metall-Reservoir zurückerhält, so daß es unmittelbar umgeladen wird gemäß

$$O^{\times}(ads) + e' \rightarrow O^{-}(ads) \tag{7}$$

und demzufolge nicht entweichen kann, während das entladene Zinkatom die Oberfläche verläßt

$$Zn^{\times}(ads) \rightarrow Zn(gas) \tag{8}$$

Das an der Oberfläche fehlende $Zn^{+}(ads)$ wird infolge des starken Raumladungsfeldes, das in der dünnen ZnO-Schicht herrscht, offenbar relativ rasch von der Metalloberfläche ergänzt, indem es zur Oberfläche des Oxids gesaugt wird.

Infolge der Gleichheit der Aktivierungsenergien, ob für ZnO-Verdampfung oder ZnO + H_2–Reaktion oder Zinkmetall-Verdampfung über eine dünne ZnO-Schicht, kann man versuchsweise annehmen, daß der geschwindigkeitsbestimmende Schritt nicht der Antransport eines Zn-Ions aus der Metalloberfläche an die Phasengrenze ZnO|Vakuum ist sondern vielmehr der Umladungsschritt (6) verknüpft mit dem Teilschritt (8), der für den Austritt in das Vakuum verantwortlich ist. Wenn man jedoch berücksichtigt, daß durch Einstrahlung von Licht eine deutliche Erhöhung der Verdampfungsgeschwindigkeit registriert wird, so liegt es nahe, den Umladungsschritt (6) als den maßgebenden Teilschritt anzusehen, da der Desorptionsschritt (8) ein Neutralschritt ist. Das scheint auch mit den Verhältnissen beim CdS — gegebenenfalls bei allen II_B—VI_B Verbindungen — in Einklang zu stehen, weil dort gleichfalls der »charge transfer«-Schritt für maßgebend gefunden wurde [10]. Offenbar reagieren die durch Licht erzeugten Elektron-Lochpaare $e' \sim |e|^{\cdot}$ mit den an der Oberfläche befindlichen Zink- und Sauerstoffionen etwa in der folgenden Weise:

$$e' \sim |e|^{\cdot} + O^{-}(ads) \rightarrow O^{\times}(ads) + e' \tag{9}$$

mit der sich unmittelbar anschließenden Folgereaktion

$$Zn^{+}(ads) + e' \rightarrow Zn(gas) \tag{10}$$

und

$$O^{\times}(ads) + e'(Zn\text{-}Metall) \rightarrow O^{-}(ads) \tag{11}$$

Inwieweit auch eine merkliche Beteiligung einer Sauerstoff-Molekülbildung mit anschließender Desorption zu berücksichtigen ist gemäß

$$2\,O^{\times}(ads) \rightarrow O_2(gas) \tag{12}$$

kann aus den gegenwärtig verfügbaren Unterlagen nicht geschlossen werden.

Während die Verdampfungsgeschwindigkeit von ZnO stets gleiche Werte ergab unabhängig davon, ob man bei ansteigender oder abfallender Temperatur arbeitete, wurde für die Verdampfung von Zink aus der Metallfolie eine deutliche Hysterese mit ansteigender und abfallender Temperatur beobachtet. So ergab an unbelichteten Proben die Verdampfungsgeschwindigkeit von Zink bei steigender Temperatur kleinere Werte als bei fallender Temperatur. Eine Belichtung bewirkte gerade eine entgegengesetzt verlaufende Hysterese-Schleife. Bei unbelichteten Proben nimmt die Aktivierungsenergie mit steigender Temperatur solange ab, bis der Wert der Verdampfungs-Enthalpie des Zinks erreicht ist. Entsprechend nimmt die Aktivierungsenergie der Verdampfungsgeschwindigkeit einer belichteten Probe mit steigender Temperatur bis zur Verdampfungs-Enthalpie zu.

*

Für die Finanzierung dieser Arbeit sind wir der Deutschen Forschungsgemeinschaft zu großem Dank verbunden besonders dafür, daß hierdurch der Gast-Aufenthalt des einen von uns (A.J.H.) möglich wurde. Ferner sind wir auch dem Fonds der Chemischen Industrie für die Bereitstellung von Sachmitteln sehr dankbar.

LITERATUR

1. Myasnikov, I. A., Pshezhetskii.: Dokl. Akad. Nauk. UdSSR **99,** 125 (1954)
2. Melnick, D.: J. Chem. Phys. **26,** 1136 (1957)
   Medved, D.: J. Chem. Phys. **28,** 870 (1958)
3. Barry, T. I., Stone, F. S.: Proc. Roy. Soc. (A) **225,** 124 (1960)
   Haber, J., Kowalska, A.: Bull. Acad. Polon. Sci. Chim. **13,** 463 (1965)
4. Doerfeler, W., Hauffe, K.: J. Catalysis **3,** 156, 171 (1964)
5. Elder, T.: J. Apll. Phys. **33,** 2804 (1962)
   Williams, R.: J. Phys. Chem. Solids **23,** 1057 (1962)
6. Tashiro, I., Kimura, T., Endo, K.: Appl. Optics. Suppl. **3,** 180 (1969)
7. Hauffe, K., Schmidt, R.: Phys. Status Soldidi **3a,** 173 (1970)
8. Beranek, E., Barton, K., Smrcek, K., Sekerka, I.: Coll. Czechoslov. Chem. Commun. **25,** 358 (1960); **25,** 369 (1960)
9. Hauffe, K., Range, J., Volenik, K.: Ber. Bunsenges, phys. Chem. **74,** 286 (1970)
10. Somorjai, G. A., Lester, J. E.: Progr. solid state Chem. **4,** 1 (1967)
11. Stolze, F.: Kinetik der thermischen Dissoziation von Zinkoxid. Diss., T.U. Berlin, 1969
12. Hegedűs, A. J.: Über die vakuumthermomikrogravimetrische Messung der UV-Lichteinwirkung auf die Verdampfungsgeschwindigkeit von ZnO bzw. Zn und auf die Desorption und aktivierte Adsorption von Sauerstoff an ZnO. Vortrag gehalten an der IX. Konferenz über Mikrowägung im Vakuum, Berlin—West, 11. Juni, 1970
13. 1. Mitteilung aus der Entwicklungsabteilung der Sartorius-Werke Göttingen: Die elektronische Mikrowaage ELEKTRONO, Prinzip und Anwendungsmöglichkeiten. G-I-T Fachzeitschrift für das Laboratorium, Juni/Juli 1962
14. 2. Mitteilung aus der Entwicklungsabteilung der Sartorius-Werke, Göttingen: Aufstellung und Bedienungsanleitung zur Waage 4102, Göttingen 1967

15. OSRAM GmbH (8 München 90) Liste HBO, Quecksilberdampf-Höchstdrucklampen, 1966 und Druckschrift »Hinweise zur Ausgestaltung von Geräten für Quecksilberdampf-Höchstdrucklampen HBO«, 1966
16. Allsopp, H. J., Roberts, J. P.: Trans. Faraday Soc. **55,** 1386 (1959)
17. Norman, V. J.: Austr. J. Chem. **19,** 1133 (1966); **20,** 85 (1967)
18. Hegedűs, A. J., Kiss A. B.: Mikrochim. Acta **1966,** 813
19. Gmelin, L.: Handbuch der anorganischen Chemie, 8. Aufl., System Nr. 32, Zink u. Ergänzungsband, Leipzig — Berlin bzw. Weinheim/Bergstr. Verlag Chemie 1924 bzw. 1956.

Karl Hauffe; Göttingen, Bürgerstraße 50, BRD
Andreas J. Hegedűs; Budapest IV., Váci út 77.

Acta Chimica Academiae Scientiarium Hungaricae, Tomus 69 (2), pp. 137—143 (1971)

THE USE OF COMPLEX FORMING AGENTS IN ION EXCHANGE CHROMATOGRAPHY, V

ADSORPTION OF METAL IONS ON CATION EXCHANGE RESIN IN THE PRESENCE OF PYRIDINE, ETHYLENEDIAMINE AND TRIETHANOLAMINE

J. INCZÉDY, P. KLATSMÁNYI-GÁBOR and L. ERDEY

(Institute of General and Analytical Chemistry, Technical University, Budapest)

Received February 20, 1970

The distribution coefficients of some complex-forming divalent metal ions (Cu, Ni, Zn, Co, Cd) were determined on a cation exchange resin, from solutions containing various amounts of pyridine, triethanolamine and ethylenediamine. The ion exchange constants of the individual metal ions and complex species were estimated. On the basis of the results methods have been developed for the separation of copper and zinc.

In connection with the planning of chromatographic separation of metal ions the knowledge of the adsorption behaviour of certain divalent metal ions in the presence of organic bases was required [1, 2, 3].

Batch experiments were carried out to determine the distribution coefficients of the divalent metal ions from solutions containing the base in varying concentrations. The resin was used in the cation – form corresponding to the base (pyridinium, etc.) and the same amount of hydrochloric acid was added to each sample solution. In the experiments carried out with monoacidic bases, the constancy of the concentration of the competing cation was ensured by addition of the acid ($[BH^+] = 0.2\ M$). The total concentration of the metal ion was kept low compared to the resin capacity and to the total ion concentration of the solution. After equilibration of the resin with the solution, the liquid was analyzed and from the data the distribution coefficient of the metal ion was calculated. The latter are summarized in Figs. 1—3.

In the systems consisting of the cation exchange resin and a solution containing a monoacidic base, metal ion and hydrochloric acid, the following reactions take place:

$$B + H^+ \overset{K_1}{\rightleftharpoons} BH^+ \tag{1}$$

$$M^{2+} + n\,B \overset{\beta_n}{\rightleftharpoons} MB_n \tag{2}$$

$$MB_n^{2+} + 2\,R\text{–}BH \overset{K_n^x}{\rightleftharpoons} R_2\text{=}MB_n + 2\,BH^+ \tag{3}$$

K_1 is the protonation constant of base B; M^{2+} is the metal ion, β_n is the gross stability constant of the metal complex, and n may vary from 0 to 4 or 6.

Eq. (3) is the ion exchange reaction, where R represents the equivalent amount of the resin. K_n^x denotes the ion exchange equilibrium constant of the n-th complex.

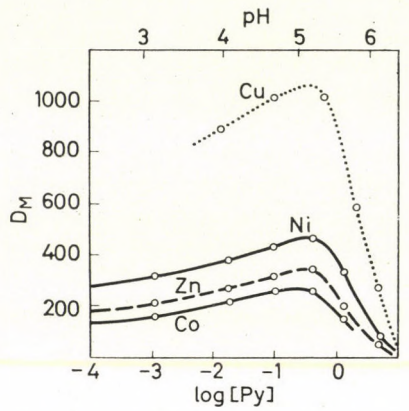


Fig. 1. Distribution coefficients of divalent metal ions on a Dowex 50×8 cation exchange resin of the pyridinium form as a function of the logarithm of free pyridine concentration, [pyH] = 0.2 *M*

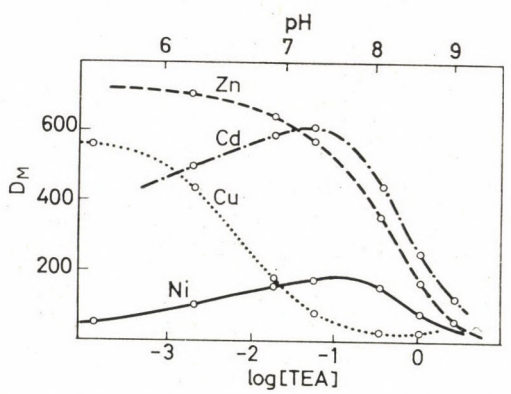


Fig. 2. Distribution coefficients of divalent metal ions on a Dowex 50×8 cation exchange resin of the triethanolammonium form as a function of the logarithm of free triethanolamine concentration, [teaH] = 0.2 *M*

The concentration of the protonated base in the solution was kept constant by addition of acid. The free ligand concentration also checked by pH measurements, and the mole fractions of the complex species at given ligand concentrations were calculated using literature complex stability data. Considering the calculated composition of the solution and the corresponding distribution coefficient, and assuming that the complex equilibria are the same in the resin and solution phase, the ion exchange equilibrium constants of the

individual species were estimated. The following equation was used:

$$K_n^x = \frac{(MB_n)\,[BH]^2}{[MB_n]\,(BH)^2} \approx D_M \frac{[BH]^2}{Q^2} \tag{4}$$

The terms in parentheses are concentrations in the resin phase (mole/l. column volume), while those in brackets are concentrations in the solution. D_M denotes the distribution coefficient of the metal and Q the volume capacity of the resin.

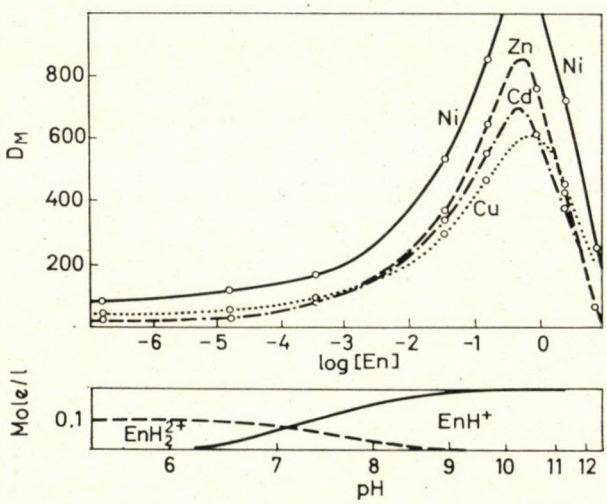


Fig. 3. Distribution coefficients of divalent metal ions on a Dowex 50×8 resin (ethylenediammonium form) as a function of the logarithm of free ethylenediamine concentration

In the presence of pyridine, copper exhibits the highest adsorption. There is no possibility for the six-coordinated species to be formed at the ligand concentration investigated (due to the low stabilities) and the order of adsorption strength of the metal ions corresponds to that of complex stabilities. The estimated exchange constants are summarized in Table I.

On the resin of the triethanolammonium form the complexed metal ions are bound more strongly than the aquo complexes. However, with increasing ligand concentration (*i.e.* with increasing pH of the solution) the formation of mixed hydroxo complexes becomes more pronounced and, upon decreasing the charge of the complexes, the distribution coefficient of the metal decreases. In the case of copper and zinc, the mixed complex is formed already at low ligand concentrations (due to the higher stability of the mixed complexes), while in the case of nickel and cadmium, there are ranges where the complexes of regular composition are predominant, and the weaker mixed complexes

form only at higher ligand concentrations. The curves of the distribution coefficient exhibit maxima.

The mole fractions of the copper and nickel complex species at varying pH and ligand concentration (corresponding to the compositions investigated) have been calculated from stability constant data and are presented in Fig. 4.

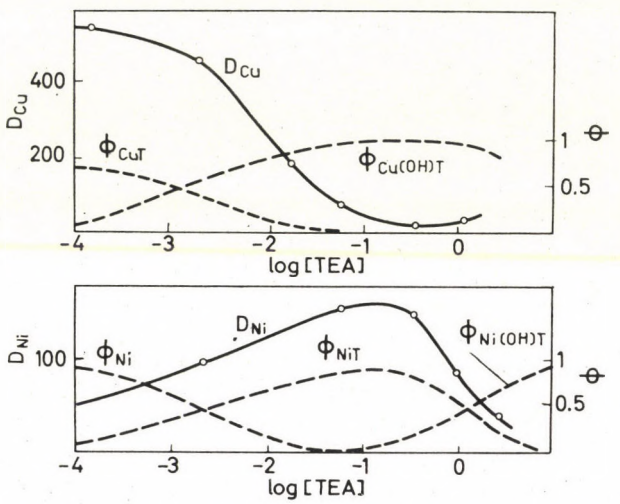


Fig. 4. Distribution coefficients of copper and nickel function of the logarithm of free triethanolamine concentration (solid lines). The dashed lines are calculated mole fractions of the complex species

As shown by the diagrams, the distribution coefficient values follow the mole fraction curves of the divalent complex ions. The estimated ion exchange equilibrium constants are summarized in Table I.

In systems consisting of the ethylenediammonium form of the resin and of a solution containing ethylenediamine, metal ion and hydrochloric acid,

Table I

Estimated volume ion exchange constants of metal ions and metal complexes on a cation exchange resin (Dowex 50 × 8) of the pyridinium and triethanol-ammonium form

Metal	PyH—form resin					TEAH — form resin		
	K_0^x	K_1^x	K_2^x	K_3^x	K_4^x	K_0^x	K_1^x	$K_{M(OH)T}^x$
Cu	—	—	—	14	(20)	—	12	2
Ni	3.3	5.1	6.2	—	—	0.3	3	—
Zn	2.5	3.3	(5.1)	—	—	—	6.6	—
Co^{II}	2.0	3.2	—	—	—	—	—	—

the following reactions take place:

$$\mathrm{En} + \mathrm{H}^+ \overset{\mathrm{K}_1}{\rightleftharpoons} \mathrm{EnH}^+ \tag{5}$$

$$\mathrm{EnH}^+ + \mathrm{H}^+ \overset{\mathrm{K}_2}{\rightleftharpoons} \mathrm{EnH}_2^{2+} \tag{6}$$

$$\mathrm{M}^{2+} + n\ \mathrm{En} \overset{\beta_n}{\rightleftharpoons} \mathrm{MEn}_n^{2+} \tag{7}$$

$$\mathrm{MEn}_n^{2+} + 2\ \mathrm{R{-}EnH} \overset{\mathrm{K}_n^{x(1)}}{\rightleftharpoons} \mathrm{R_2{=}MEn}_n + 2\ \mathrm{EnH}^+ \tag{8}$$

$$\mathrm{MEn}_n^{2+} + \mathrm{R_2{=}EnH_2} \overset{\mathrm{K}_n^{x(2)}}{\rightleftharpoons} \mathrm{R_2{=}MEn}_n + \mathrm{EnH}_2^{2+} \tag{9}$$

K_1 and K_2 are the protonation constants of ethylenediamine, n can vary from 0 to 2 or 3. $\mathrm{K}^{x(1)}$ and $\mathrm{K}^{x(2)}$ are the ion-exchange constants.

The concentrations of the protonated species in the range investigated have been calculated from the protonation constants ($\log \mathrm{K}_1 = 9.94$; $\log \mathrm{K}_2 = 7.14$ [I = 0.1]) and are presented in Fig. 3.

As seen from Fig. 3, the distribution coefficient of the metal ion increases with increasing ligand concentration (*i.e.* with increasing extent of complex formation). A sharp change appears in the curves at a certain ligand concentration, which is caused by the change in the nature of the competing cation since above pH 7 the univalent enH^+ predominates over the divalent enH_2^{2+} ion. The adsorption strength of univalent ions is much lower than that of divalent ones. The value of the ion exchange constant of the two ions is 5 according to STOKES and WALTON [4].

The order of adsorption strength of the metal ions, or rather metal complexes, corresponds to the order of the stability constants of the complexes for Ni, Zn and Cd. However, copper which does not form six-coordinated species but forms a very stable planar four-coordinated complex (of 1 : 2 composition),

Table II

Estimated volume ion exchange constants of metal ions and metal complexes on a resin of the ethylenediammonium form

(Dowex 50 × 8)

Metal	$\mathrm{K}_0^{x(2)}$	$\mathrm{K}_2^{x(2)}$	$\mathrm{K}_2^{x(1)}$	$\mathrm{K}_3^{x(1)}$
Cu	—	6.2	(7.7)	—
Ni	(2)	10	—	13
Zn	0.8	—	—	10.5
Cd	1.6	—	—	8.2

takes up water molecules in its inner sphere. On account of this behaviour its hydration ability is greater and its adsorption strength is lower, than those of metals forming saturated complexes. According to calculation, using the data of VINK [5] the formation of mixed hydroxo complexes is of very low degree in the range investigated. The estimated ion exchange equilibrium constants

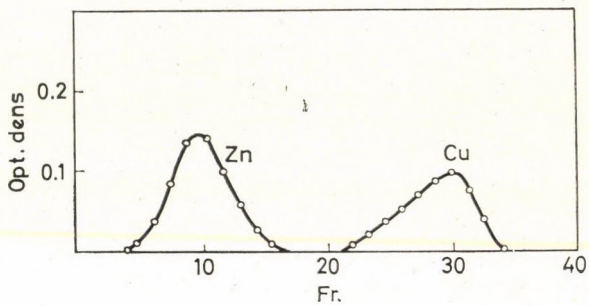


Fig. 5. Separation of zinc and copper on a cation exchange column of the pyH form (6.5×90 mm); 60 °C; Eluent: 1.2 *M* HCl + 1.3 *M* pyridine. Flow rate: 0.6 ml/min. Volume of fractions: 4.5 ml

are summarized in Table II. The steeply decreasing parts of the curves at high ligand concentrations in all diagrams can be accounted for by the rapid decrease in water activity and by shrinkage of the resin.

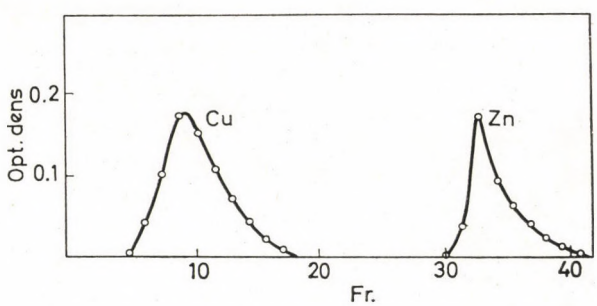


Fig. 6. Separation of copper and zinc on a resin column of the triethanolammonium form (6.5×60 mm); 80 °C; Eluent: 1.0 *M* HCl + 1.32 *M* triethanolamine. Flow rate: 0.6 ml/min. Volume of fractions: 4.5 ml

On the basis of the obtained ion exchange constant data, the separation of copper and zinc was planned and performed respectively, on a resin column of the pyridinium form, using an eluent containing a pyridinium salt and pyridine and on a resin column of the triethanolammonium form using a solution containing triethanolamine and its salt. In the former case zinc while in the latter case copper was eluted first. The separations were found sharp and quantitative (*cf.* Figs. 5 and 6).

Experimental

Reagents. In all experiments reagent grade chemicals, solvents (pyridine, ethylenediamine, triethanolamine) and deionized water were used.

For preparation of the metal stock solutions *cf.* Ref. [3].

Ion exchange resin. Dowex 50×8 resin of 50—100 mesh was treated and transformed first to H-form as usual. Thereafter the resin sample was converted to the required form using 1 *M* solution of the organic base. After loading and washing, the resin samples were dried in air and stored in glass-stoppered bottles. The capacities and column volumes of the air-dry resin samples were determined and found to be as follows: pyH-form resin: 3.26 mequ/g; 1.84 ml/g. teaH-form resin: 2.74 mequ/g; 1.49 ml/g. enH-form resin: 3.35 mequ/g; 1.76 ml/g. For the determination of the capacities, 0.5 g samples of air-dry were loaded with zinc ions and after elution, zinc was titrated chelatometrically.

The instruments and methods used for the determination of the metal ion distribution coefficients were the same as given earlier [3]. In one series, for the determination of the distribution coefficient of nickel in the presence of triethanolamine, the resin and not the solution was analyzed photometrically, after ignition of the resin samples in the presence of sulfuric acid.

Separation of copper and zinc. A glass column with a diameter of 6.5 mm, equipped with a heating jacket, was filled with cation exchange resin (of 100—200 mesh) in the required form and washed with water. 0.03 ml of each of the metal stock solutions were poured on the column and eluted. For the temperature, flow-rate and composition of the eluent used, *cf.* the legends of Fig. 5. and 6. The effluent was collected in 4.5 ml fractions by means of an automatic fraction collector (Fractomat Y-2, HAKO, GFR), and analyzed photometrically after extraction, using diphenylthiocarbazone as reagent. The complex stability data used in the calculations were taken from Refs. [6, 7, 8, 9].

REFERENCES

1. INCZÉDY, J., KLATSMÁNYI-GÁBOR, P., ERDEY, L.: Acta Chim. Acad. Sci. Hung. **61,** 261 (1969)
2. INCZÉDY, J., KLATSMÁNYI-GÁBOR, P., ERDEY, L.: Acta Chim. Acad. Sci. Hung. **62,** 1 (1969)
3. INCZÉDY, J.: Acta Chim. Acad. Sci. Hung. **62,** 131 (1969)
4. STOKES, R. H., WALTON, F.H.: J. Am. Chem. Soc. **76,** 3327 (1954)
5. VINK, H.: Arkiv kemi **11,** 5 (1957)
6. BJERRUM, J.: Chem. Rev. **46,** 381 (1950)
7. BJERRUM, J., REFN, S.: Soumen Kem. **29** *B*, 68 (1956)
8. BJERRUM, J.: Metal Ammine Formation in Aqueous Solution. P. Haase and Son, Copenhagen, 1941
9. CARLSON, G. A., MCREYNOLDS, J. P., VERHOECK, F. H.: J. Am. Chem. Soc. **67,** 1334 (1945)

János INCZÉDY; Veszprém, Schönherz Z. u. 12, Hungary.
Piroska KLATSMÁNYI-GÁBOR; Budapest XI., Gellért tér 4.

Acta Chimica Academiae Scientiarium Hungaricae, Tomus 69 (2), pp. 145—155 (1971)

UNTERSUCHUNG DER BEIM ERHITZEN ZWISCHEN DEN KOMPONENTEN VON N-P-K-DÜNGERN VERLAUFENDEN VORGÄNGE, I

IM SYSTEM AMMONIUMNITRAT–KALIUMCHLORID VERLAUFENDE PROZESSE

T. FLÓRA und M. MENYHÁRT

(Forschungsinstitut für die Chemische Schwerindustrie Veszprém)

Eingegangen am 25. Februar 1970

Die beim Erhitzen des Systems Ammoniumnitrat–Kaliumchlorid verlaufenden Vorgänge wurden derivatographisch untersucht. Die thermischen Untersuchungen wurden in einigen Fällen durch die Röntgenuntersuchung und Elementaranalyse der Rückstände ergänzt.

Auf Grund der Versuchsergebnisse wurde festgestellt, daß:

— beim mechanischen Verreiben bei Zimmertemperatur eine Austauschreaktion zwischen dem Ammoniumnitrat und Kaliumchlorid verläuft, die sich jedoch nicht quantitativ abspielt;

— ein Teil des unreagierten Ammoniumnitrats mit dem entstandenen Kaliumnitrat Mischkristalle bildet;

— ein anderer Teil des unreagierten Ammoniumnitrats mit dem entstandenen Ammoniumchlorid in eine thermische Wechselwirkung tritt;

— der Mischkristall Ammoniumnitrat–Kaliumnitrat um 90 °C mit dem noch unreagierten Kaliumchlorid in Reaktion tritt.

In den Dreinährstoffdüngern werden die für die Pflanzen lebenswichtigen Elemente Stickstoff, Phosphor und Kalium durch Ammoniumnitrat, Ammoniumdihydrophosphat, Calciumhydrophosphat und Kaliumchlorid geliefert.

In diesem zusammengesetzten System verlaufen beim Erhitzen verschiedene Reaktionen zwischen den Komponenten. Die Untersuchung dieser Reaktionen erschien uns deshalb wichtig, weil bei der Herstellung von N-P-K-Düngern das Produkt bei Temperaturen um 170 °C entwässert wird. Es ist also sowohl für den Verbraucher als für den Technologen interessant, zu wissen, wie sich die Zusammensetzung des Mischproduktes bei der genannten Temperatur verändert. Außerdem beginnt die Zersetzung des Ammoniumnitrats in der Nähe der Trocknungstemperatur, in Abhängigkeit von der Natur der Zusatzstoffe im Gemisch bei verschiedenen Temperaturen, wodurch gegebenenfalls eine Explosion hervorgerufen werden kann. Es ist deshalb äußerst wichtig, die Zersetzungstemperaturen der verschiedenen, Ammoniumnitrat enthaltenden Mischungen zu kennen.

Um die mannigfaltigen thermischen Vorgänge kennenzulernen, die sich im zusammengesetzten System abspielen, begannen wir mit der Untersuchung von binären Systemen. In der vorliegenden ersten Mitteilung berichten wir über die thermischen Vorgänge im System Ammoniumnitrat–Kaliumchlorid. Als Prüfverfahren wurde die Derivatographie angewendet. Die thermischen

Prüfungen wurden in einigen Fällen durch die Röntgen- und Elementaranalyse des Rückstandes nach dem Erhitzen ergänzt.

Die thermischen Eigenschaften des Ammoniumnitrats sind in zahlreichen Arbeiten untersucht worden. Es sollen hier nur derivatographische [1] und derivativ-dilatometrische [2] Ergebnisse erwähnt werden. Auch das Derivatogramm des Kaliumchlorids ist bekannt [3].

Röntgendiffraktometrisch wurde nachgewiesen, daß das Ammoniumnitrat und das Kaliumchlorid beim Granulieren des N-P-K-Düngers miteinander eine Austauschreaktion eingehen [4], die zu Selbsterhitzung führen kann [5]. Die thermischen Eigenschaften des im Laufe dieser Reaktion entstehenden Ammoniumchlorids und Kaliumnitrats sind ebenfalls bekannt [1, 6].

Es besteht auch die Möglichkeit der Bildung einer festen Lösung zwischen dem in Überschuß vorhandenen Ammoniumnitrat und dem Kaliumnitrat, mit einer zwischen $NH_4NO_3 \cdot KNO_3$ und $NH_4NO_3 \cdot 3KNO_3$ variierenden Zusammensetzung [5]. Dieses System wurde durch MORAND [7] und COATES [8] differentialthermoanalytisch und röntgenanalytisch untersucht. Die feste Lösung kann auch mit Kaliumchlorid gemäß folgender Reaktionsgleichung reagieren [5]:

$$NH_4NO_3 \cdot KNO_3 + KCl \rightarrow 2KNO_3 + NH_4Cl$$

Aus dem Gesagten geht hervor, daß die Ergebnisse über die thermischen Eigenschaften des Systems Ammoniumnitrat–Kaliumchlorid mittels DTA und Röntgenanalyse erhalten wurden. Der Verlauf von bestimmten thermischen Vorgängen zwischen den Komponenten wurde festgestellt, bzw. angenommen, jedoch wurde kein Anhaltspunkt hinsichtlich der Temperatur der Reaktionen erhalten. Die Derivatographie, die eine komplexe thermoanalytische Methode darstellt, bietet hierzu eine bessere Möglichkeit, als die Einzelverfahren, da sie die gleichzeitige Verfolgung der ohne Gewichtsverlust verlaufenden thermischen Vorgänge und der mit Gewichtsverlust verbundenen Zersetzungsreaktionen ermöglicht, wodurch ein besserer Einblick in die zwischen den Komponenten verlaufenden thermischen Vorgänge ermöglicht wird.

Versuchsbedingungen

Die Derivatogramme wurden mit dem durch die Firma MOM hergestellten Derivatograph, System PAULIK—PAULIK—ERDEY [9] unter zweierlei Versuchsbedingungen aufgenommen: bis 900 °C mit einer Aufheizgeschwindigkeit von 4 °C/Minute bzw. bis 200 °C mit einer Aufheizgeschwindigkeit von 1 °C/Minute, in Gegenwart von Luft. In den Platintiegel (oberer Durchmesser 9 mm) wurden bei sämtlichen Versuchen 500 mg Substanz eingewogen. Als Inertstoff wurde bei 1400 °C ausgeglühtes Aluminiumoxyd verwendet. Die DTG-Galvanometerempfindlichkeit betrug 1/5, die DTA-Galvanometerempfindlichkeit 1/2.

Die Röntgenogramme wurden mit dem Röntgendiffraktometer Müller-Micro 111 und einer Registriervorrichtung Phillips PW-1051 aufgenommen, unter folgenden Versuchsbedingungen: Strahlung Cu-K; Röhrenerregung 40 kW/18 mA; Spannung der GM-Röhre 1625V;

Detektiergeschwindigkeit 0,5 °C/Minute; Spaltsystem 1°—0,2°—1°; Teilung 16, 32, 64; Zeitkonstante 4 Sekunden; Papiergeschwindigkeit 400 mm/Stunde.

Die Gemische wurden durch 15 Minuten dauerndes Verreiben der Komponenten im Achatmörser hergestellt.

Versuchsergebnisse und Diskussion

In Abb. 1 sind die bis 900 °C aufgenommen Derivatogramme des Ammoniumnitrats, der Mischung von gleichen Gewichtsteilen Ammoniumnitrat und Kaliumchlorid und des Kaliumchlorids, in Abb. 2 die bis 160—200 °C auf-

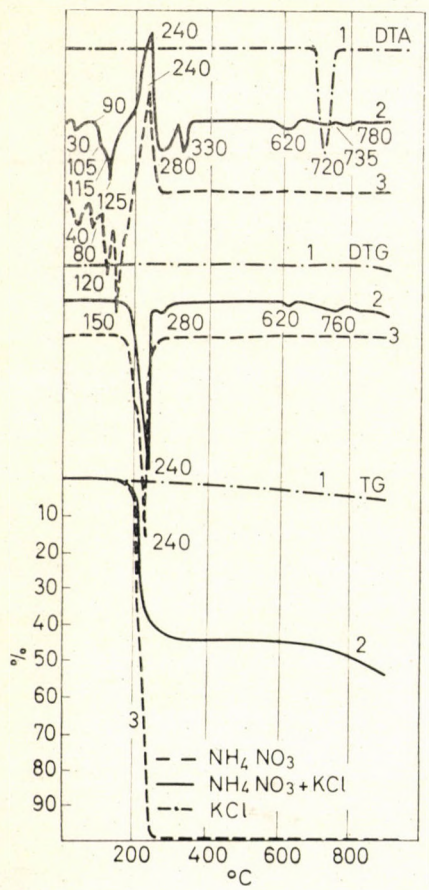


Abb. 1. Derivatographische Kurven des Systems Ammoniumnitrat–Kaliumchlorid. Aufheizgeschwindigkeit 4 °C/Minute. 1 — Kaliumchlorid; 2 — Gemisch aus gleichen Gewichtsteilen Ammoniumnitrat und Kaliumchlorid; 3 — Ammoniumnitrat

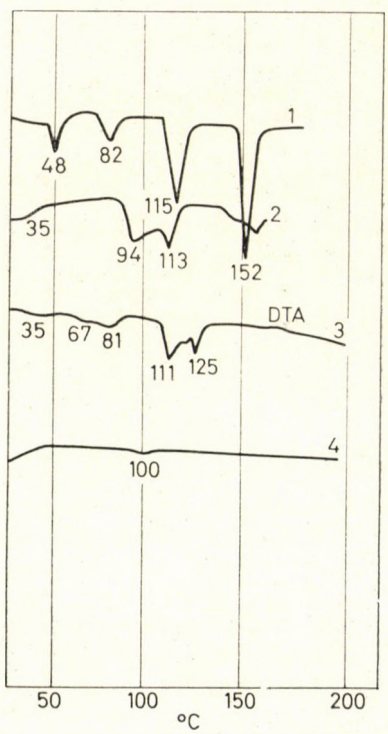


Abb. 2. DTA-Kurven des Systems Ammoniumnitrat–Kaliumchlorid. Aufheizgeschwindigkeit 1 °C/Minute. 1 — Ammoniumnitrat; 2 — Gemisch aus gleichen Gewichtsteilen Ammoniumnitrat und Kaliumchlorid; 3 — das gleiche Gemisch, bis 160 °C thermisch vorbehandelt; 4 — Kaliumchlorid

genommenen DTA-Kurven der genannten Substanzen dargestellt. In Abb. 2 ist außerdem die DTA-Kurve eines Ammoniumnitrat–Kaliumchlorid-Gemisches (1 : 1) gezeigt, welches vorangehend bis 160 °C erhitzt wurde (Kurve 3). Beim Vergleich der thermischen Kurven des Ammoniumnitrat–Kaliumchlorid-Gemisches (Abb. 1, Kurve 2, Abb. 2, Kurve 2) mit jenen der Komponenten (Abb. 1, Kurven 1 und 3, Abb. 2, Kurven 1 und 4) kann sofort die Wechselwirkung der Komponenten bei Erhitzen erkannt werden: die für die einzelnen Komponenten charakteristischen Spitzen sind praktisch verschwunden und neue, thermische Veränderungen anzeigende Spitzen sind erschienen.

Die für die Änderungen im Derivatogramm des Gemisches verantwortlichen thermischen Reaktionen sind die folgenden:

a) Zwischen dem Ammoniumnitrat und dem Kaliumchlorid hat sich eine Austauschreaktion abgespielt. Der Beweis dafür ist der im Derivatogramm des Gemisches (Abb. 1, Kurve 2) bei 280 °C beobachtete, von einem Gewichtsverlust begleitete Vorgang, der die Sublimation des einen Reaktionsproduktes, des Ammoniumchlorids anzeigt [1]. Die DTA-Spitze bei 330 °C zeigt das Schmelzen des anderen Reaktionsproduktes, des Kaliumnitrats an.

Röntgenuntersuchungen zeigen, daß die Austauschreaktion bereits beim Verreiben der Komponenten bei Zimmertemperatur erfolgt: das Röntgenogramm der thermisch unbehandelten Probe (Abb. 3, Kurve 1) zeigt die Gegenwart sowohl von Ammoniumchlorid als auch von Kaliumnitrat an.

Um das Maß der Austauschreaktion festzustellen, wurde das Aufheizen des Gemisches bei 44% Gewichtsverlust (bei ungefähr 310 °C) nach der Sublimation des Ammoniumchlorids unterbrochen (Abb. 1, Kurve 2) und der Chloridgehalt des Rückstandes bestimmt. Es zeigte sich, daß die Reaktion unter unseren Versuchsbedingungen nicht vollständig verlief; der Rückstand enthielt beträchtliche Mengen Chlorid, d. h. unreagiertes Kaliumchlorid. Aus der Menge des unreagierten Kaliumchlorids wurde mit stöchiometrischen Berechnungen festgestellt, daß nur 32% des eingewogenen Ammoniumnitrats in der Reaktion umgesetzt wurden, während 68% unverändert blieben.

b) Ein Teil des unreagierten Ammoniumnitrats hat mit dem entstandenen Kaliumnitrat Mischkristalle gebildet.

Der Beweis der Mischkristallbildung ist, daß auf den unter verschiedenen Bedingungen aufgenommenen Kurven des Ammoniumnitrat–Kaliumchlorid-Gemisches (Abb. 1 und 2) die für den Mischkristall Ammoniumnitrat–Kaliumnitrat charakteristischen Spitzen beobachtbar sind. (Die zum Vergleich dienenden Kurven des Systems Ammoniumnitrat–Kaliumnitrat sind in Abb. 4 und 5 dargestellt.) So sind z. B. die Spitzen bei 35, 94 und 113 °C der bei langsamen Erhitzen bis 160 °C erhaltenen DTA-Kurve für das thermisch unvorbehandelte Ammoniumnitrat–Kaliumchlorid-Gemisch (Abb. 2, Kurve 2) für den Mischkristall Ammoniumnitrat–Kaliumnitrat charakteristisch (Abb. 5, Kurve 3). (Es soll bemerkt werden, daß die derivatographischen Spitzentemperaturen

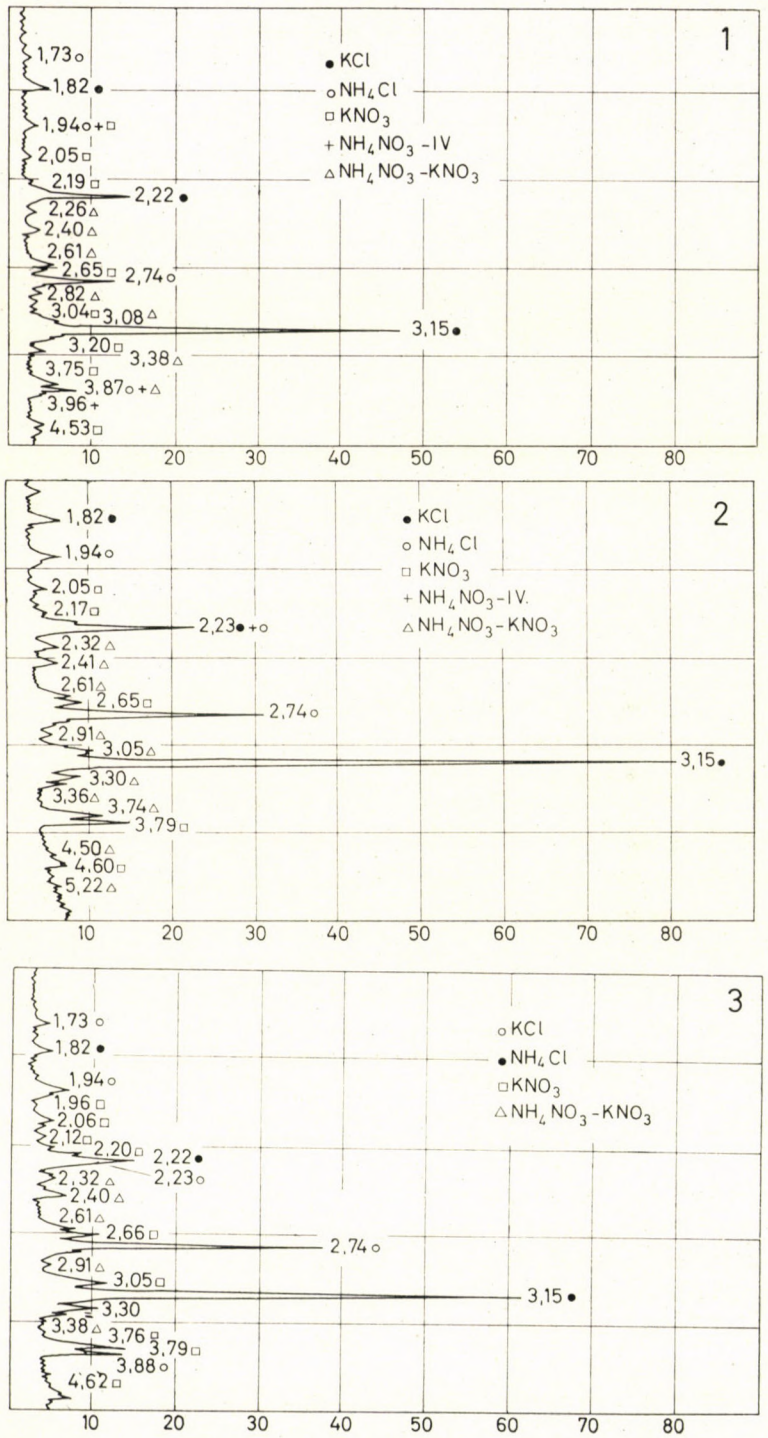


Abb. 3. Röntgenogramme des Systems Ammoniumnitrat–Kaliumchlorid. 1 — Thermisch unvorbehandeltes Gemisch (1 : 1); 2 — bis 85 °C thermisch vorbehandeltes Gemisch; 3 — bis 110 °C thermisch vorbehandeltes Gemisch

im allgemeinen mit einer Genauigkeit von 5 °C angegeben werden, jedoch in den vorliegenden Versuchen, wo mit einer hohen T-Empfindlichkeit gearbeitet wurde, mit einer Genauigkeit von 1 °C angegeben werden konnten.) Bei der DTA-Kurve des bis 160 °C thermisch vorbehandelten Ammoniumnitrat–Kaliumchlorid-Gemisches (Abb. 2, Kurve 3) können die Spitzen bei 67, 81 und 111 °C den Umwandlungspunkten des Systems Ammoniumnitrat–Kaliumnitrat (Abb. 5, Kurve 5) zugeordnet werden.

Auf dem Derivatogramm des Ammoniumnitrat–Kaliumnitrat-Gemisches 1 : 1, welches mit der höheren Aufheizgeschwindigkeit, d. h. mit 4 °C/Minute bis 900 °C, aufgenommen wurde (Abb. 1, Kurve 2), zeigen die DTA-Spitzen bei 30, 90, 105 und 115 °C die Mischkristallbildung Ammoniumnitrat–Kaliumchlorid an; die entsprechenden Vorgänge sind — mit einer geringen Temperaturverschiebung — auf der unter identischen Bedingungen aufgenommen DTA-Kurve des Ammoniumnitrat–Kaliumnitrat-Gemisches 1 : 1 erwartungsgemäß beobachtbar (Abb. 4, Kurve 2). Die DTA-Spitze bei 105 °C ist auch für das System Ammoniumnitrat–Ammoniumchlorid charakteristisch; hierauf kommen wir im weiteren noch zurück.

Aus dem Derivatogramm des Ammoniumnitrat–Kaliumnitrat-Gemisches (Abb. 4, Kurve 2) geht hervor, daß der Mischkristall — parallel mit dem Beginn der Zersetzung des Ammoniumnitrats — zerfällt. Bei 145 °C wird der herabgesetzte Schmelzpunkt des Ammoniumnitrats beobachtet; dann wird das Ammoniumnitrat bei einer etwas höheren Temperatur als erwartet (Abb. 4, Kurve 3, DTG-Maximum bei 240 °C), nämlich bei 260 °C völlig zersetzt (Abb. 4, DTG-Kurve 2); über 260 °C werden dann die für das Kaliumnitrat charakteristischen thermischen Vorgänge beobachtet. Demgemäß übt das infolge der Austauschreaktion zwischen Ammoniumnitrat und Kaliumchlorid entstehende Kaliumnitrat — abgesehen von der geringen zersetzungsverzögernden Wirkung — keinen wesentlichen Einfluß auf die thermische Zersetzung des unveränderten Ammoniumnitrats aus.

Der Mischkristallbildungsvorgang im System Ammoniumnitrat–Kaliumchlorid wurde auch durch Röntgenuntersuchungen bestätigt. Die Aufnahmen (Abb. 3, Kurve 1) zeigen, daß die Ammoniumnitrat–Kaliumnitrat-Mischkristallbildung, parallel mit der Austauschreaktion, bereits beim Verreiben der Komponenten bei Zimmertemperatur beginnt.

c) Der entstandene Ammoniumnitrat–Kaliumnitrat-Mischkristall tritt um 90 °C mit dem noch unreagierten Kaliumchlorid in Reaktion. Diese Reaktion wird durch den auf der DTA-Kurve der thermisch unvorbehandelten Ammoniumnitrat–Kaliumchlorid-Gemisches (Abb. 2, Kurve 2) bei 94 °C beobachtbaren endothermen Vorgang mit ziemlich hohem Wärmebedarf angezeigt. Eine Phasenumwandlung um 94 °C konnte auch beim Mischkristall Ammoniumnitrat–Kaliumnitrat beobachtet werden (Abb. 5, Kurve 5), ihr Wärmebedarf ist jedoch bei jeder Zusammensetzung geringer als der Wärme-

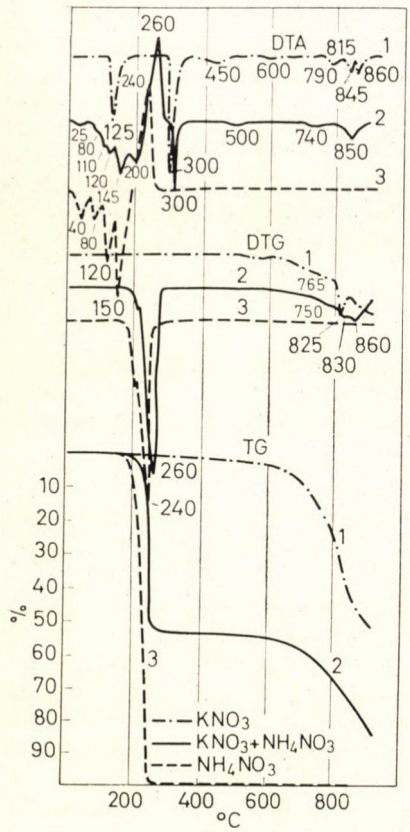


Abb. 4. Derivatographische Kurven des Systems Ammoniumnitrat–Kaliumnitrat. Aufheizgeschwindigkeit 4 °C/Minute. 1 — Kaliumnitrat; 2 — Gemisch aus gleichen Gewichtsteilen Ammoniumnitrat und Kaliumnitrat; 3 — Ammoniumnitrat

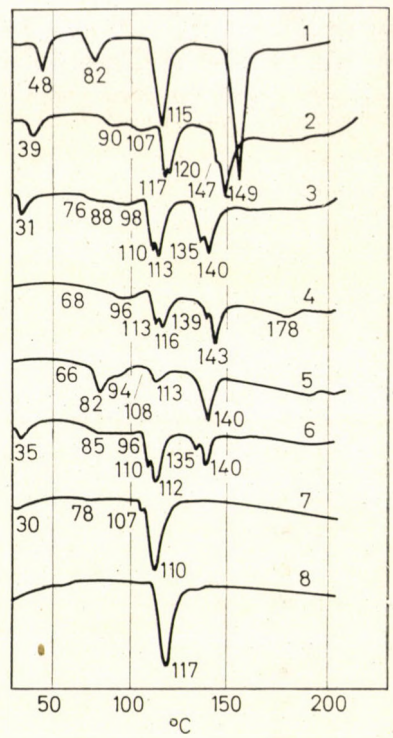


Abb. 5. DTA-Kurven des Systems Ammoniumnitrat–Kaliumnitrat. Aufheizgeschwindigkeit 1 °C/Minute. 1 — Ammoniumnitrat; 2 — 90% Ammoniumnitrat + 10% Kaliumnitrat; 3 — 50% Ammoniumnitrat + 50% Kaliumnitrat; 4 — Ammoniumnitrat–Kaliumnitrat (1:1), bis 120 °C vorbehandelt; 5 — Ammoniumnitrat–Kaliumnitrat (1:1), bis 150 °C vorbehandelt; 6 — 40% Ammoniumnitrat + 60% Kaliumnitrat; 7 — 10% Ammoniumnitrat + 90% Kaliumnitrat; 8 — Kaliumnitrat

bedarf der genannten Reaktion. Etwa bei der gleichen Temperatur (bei 97 °C) besitzt auch das System Ammoniumnitrat–Ammoniumchlorid einen Umwandlungspunkt; der letztere meldet sich jedoch auch nach der thermischen Vorbehandlung (Abb. 7, Kurve 3), verschwindet aber im untersuchten Fall (Abb. 2, Kurve 3). Der Verlauf der Reaktion wurde durch Röntgenuntersuchungen bestätigt.

Vor dem Beginn der Reaktion (bei 85 °C) und nach ihrem Ablauf (bei 110 °C) wurde das Aufheizen des Ammoniumnitrat–Kaliumchlorid-Gemisches

(1 : 1) bei zwei aufeinanderfolgenden Gelegenheiten unterbrochen und die Röntgenogramme der wärmebehandelten Proben wurden aufgenommen. Aus den Röntgenogrammen (Abb. 3, Kurven 2 und 3) ist ersichtlich, daß die bis 110 °C erwärmte Probe die gleichen Komponenten enthielt, wie die bis 85 °C erwärmte. Die beiden Röntgenogramme unterschieden sich allein in den Intensitätsverhältnissen der für die einzelnen Komponenten charakteristischen Linien: beim Erhitzen bis 110 °C nimmt die relative Menge des an der Reaktion teilnehmenden Kaliumchlorids ab, während die Menge des in der Reaktion entstehenden Ammoniumchlorids und Kaliumnitrats zunimmt.

d) Im Vorangehenden wurde bereits festgestellt, daß unter unseren Versuchsbedingungen nur ein Teil des Ammoniumnitrats mit dem Kaliumchlorid reagiert. Die Menge des Ammoniumnitratrückstandes im Vergleich zu dem in der Austauschreaktion gebildeten Kaliumnitrat in einem viel zu großen Überschuß vorhanden, um in seiner gesamten Menge mit dem letzteren Mischkristall zu bilden. Dennoch konnte in den bis 85 und 110 °C erhitzten Proben mittels Röntgenuntersuchungen (Abb. 3, Kurven 2 und 3) überhaupt kein Ammoniumnitrat nachgewiesen werden.

Wir nahmen an, daß der Überschuß des Ammoniumnitrats mit dem Ammoniumchlorid in eine thermische Wechselwirkung tritt. Um diese Annahme zu prüfen, wurden Derivatogramme von Ammoniumnitrat–Ammoniumchlorid-Mischungen in verschiedenen Konzentrationen bei verschiedenen Versuchsbedingungen aufgenommen. Von diesen sind in Abb. 6 und 7 die Kurven des 1 : 1-Gemisches gezeigt. Aus den Kurven geht eindeutig hervor, daß das Ammoniumnitrat und das Ammoniumchlorid beim Erhitzen tatsächlich in thermische Wechselwirkung treten. Die charakteristischen Merkmale des Systems Ammoniumnitrat–Ammoniumchlorid sind zugleich — in Übereinstimmung mit unserer Annahme — in den thermischen Kurven des Systems Ammoniumnitrat–Kaliumchlorid aufzufinden.

So wird z. B. der Schmelzpunkt des Ammoniumnitrats weder auf den DTA-Kurven des Gemisches aus Ammoniumnitrat und Kaliumchlorid (1 : 1) (Abb. 1 und 2, Kurve 2), noch auf den DTA-Kurven des Gemisches aus Ammoniumnitrat und Ammoniumchlorid (Abb. 6, Kurve 2, Abb. 7, Kurven 2 und 3) beobachtet, dagegen meldet sich eine neue DTA-Spitze bei niedrigeren Temperaturen, bei 113—125 °C, (Abb. 1 und 2, Kurve 2) dessen Temperatur bei Konzentrationsänderungen unverändert bleibt. Auf dem bei einer Aufheizgeschwindigkeit von 4 °C/Minute bis 900 °C aufgenommenen Derivatogramm der 1 : 1-Mischung von Ammoniumnitrat und Kaliumchlorid (Abb. 1, Kurve 2) ist die DTA-Spitze bei 105 °C ebenfalls für das System Ammoniumnitrat–Ammoniumchlorid charakteristisch (Abb. 6, Kurve 2). Es kann ferner beobachtet werden, daß nur ein Teil (etwa 60%) des Ammoniumchlorids bei der erwartungsgemäßen Temperatur um 300 °C aus 1 : 1-Gemisch aus Ammoniumnitrat und Ammoniumchlorid sublimiert (Abb. 6, Kurve 2), während ein anderer Teil — parallel mit der

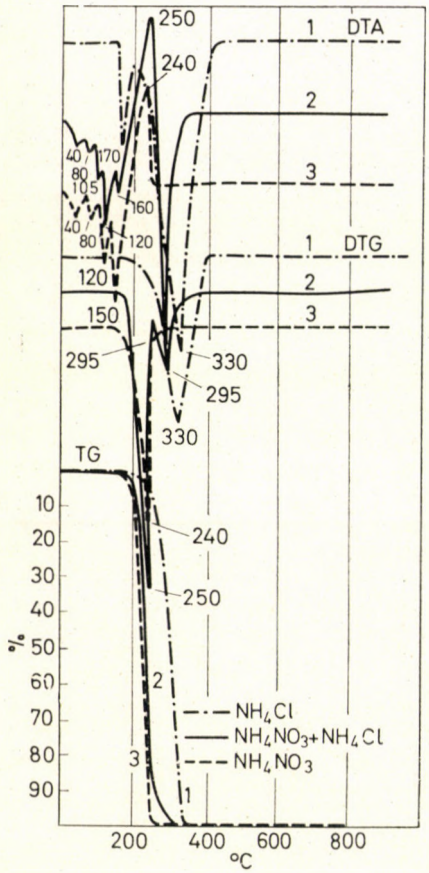


Abb. 6. Derivatographische Kurven des Systems Ammoniumnitrat–Ammoniumchlorid. Aufheizgeschwindigkeit 4 °C/Minute. 1 — Ammoniumchlorid; 2 — Gemisch aus gleichen Gewichtsteilen Ammoniumnitrat und Ammoniumchlorid; 3 — Ammoniumnitrat

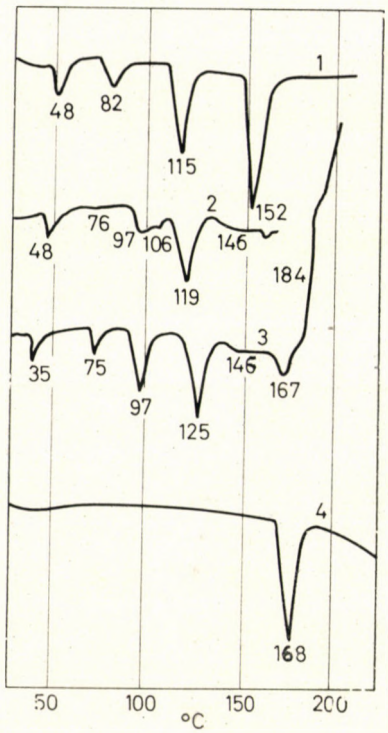


Abb. 7. DTA-Kurven des Systems Ammoniumnitrat–Ammoniumchlorid. Aufheizgeschwindigkeit 1 °C/Minute. 1 — Ammoniumnitrat; 2 — Gemisch aus gleichen Gewichtsteilen Ammoniumnitrat und Ammoniumchlorid; 3 — das gleiche Gemisch, bis 135 °C thermisch vorbehandelt; 4 — Ammoniumchlorid

Zersetzung des Ammoniumnitrats — bereits bei tieferen Temperaturen entweicht. Eine ähnliche Beobachtung wurde beim 1 : 1-Gemisch aus Ammoniumnitrat und Kaliumchlorid gemacht, wo nur 4,8% aus den entstandenen 10,5% Ammoniumchlorid bei 280 °C sublimierten, während der größere Teil bereits früher, parallel mit der Zersetzung des Ammoniumnitrats entwich (Abb. 1, Kurve 2).

Mit Hilfe der Derivatogramme konnte also festgestellt werden, daß eine thermische Wechselwirkung zwischen dem Ammoniumnitrat und dem Ammoniumchlorid verläuft; die Natur dieses Vorganges konnten wir jedoch mit den zur Verfügung stehenden Mitteln nicht klären. Die DTA-Kurven von Mischun-

gen aus Ammoniumnitrat und Ammoniumchlorid mit verschiedenen Konzentrationen zeigen keine Eutektikum-Bildung an. In dem 1 : 1-Gemisch konnte beim Aufheizen bis zu verschiedenen Temperaturen (115—140 °C) überhaupt keine neue Phase mittels Röntgenuntersuchungen entdeckt werden; eine Änderung zeigte sich allein darin, daß in dem Gemisch mit 50% Ammonium-

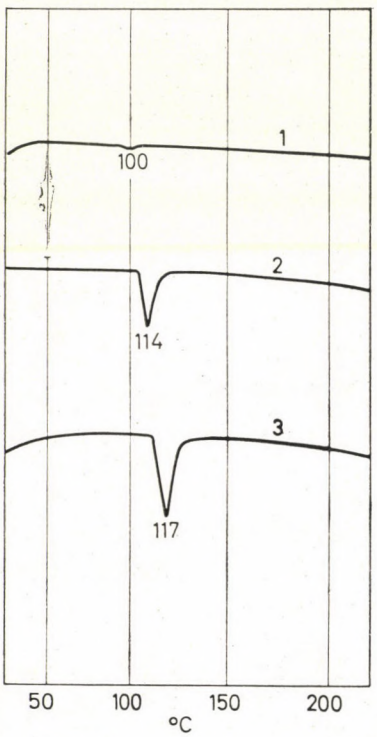


Abb. 8. DTA-Kurven des Systems Kaliumchlorid–Kaliumnitrat. Aufheizgeschwindigkeit 1 °C/Minute. 1 — Kaliumchlorid; 2 — Gemisch aus gleichen Gewichtsteilen Kaliumchlorid und Kaliumnitrat; 3 — Kaliumnitrat

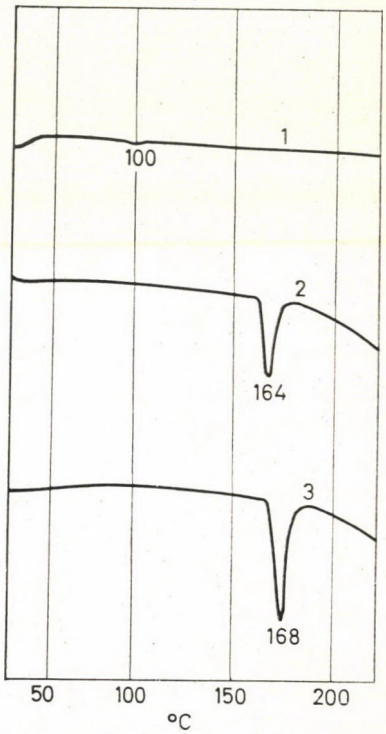


Abb. 9. DTA-Kurven des Systems Kaliumchlorid–Ammoniumchlorid. Aufheizgeschwindigkeit 1 °C/Minute. 1 — Kaliumchlorid; 2 — Gemisch aus gleichen Gewichtsteilen Kaliumchlorid und Ammoniumchlorid; 3 — Ammoniumchlorid

nitratgehalt das Röntgenogramm die Gegenwart von nur wenig Ammoniumnitrat neben viel Ammoniumchlorid anzeigte. Wie bereits erwähnt wurde, konnte in dem bis 85 °C aufgeheizten Gemisch aus Ammoniumnitrat und Kaliumchlorid röntgenographisch überhaupt kein Ammoniumnitrat nachgewiesen werden.

Im untersuchten System könnte auch der Ablauf von thermischen Reaktionen zwischen Kaliumchlorid und Kaliumnitrat, Kaliumchlorid und Ammoniumchlorid, Kaliumnitrat und Ammoniumchlorid angenommen werden, jedoch weisen die Derivatogramme dieser Systeme (Abb. 8, 9 und 10) auf keine

Wechselwirkung zwischen den genannten Komponenten hin. Die DTA-Kurve der Mischung aus Kaliumnitrat und Ammoniumchlorid zeigt wohl eine geringe Änderung im Vergleich zu den Kurven der reinen Komponenten; diese spielt jedoch — nach unseren Beobachtungen — eine nur unwesentliche Rolle in den thermischen Änderungen des Systems Ammoniumnitrat–Kaliumchlorid.

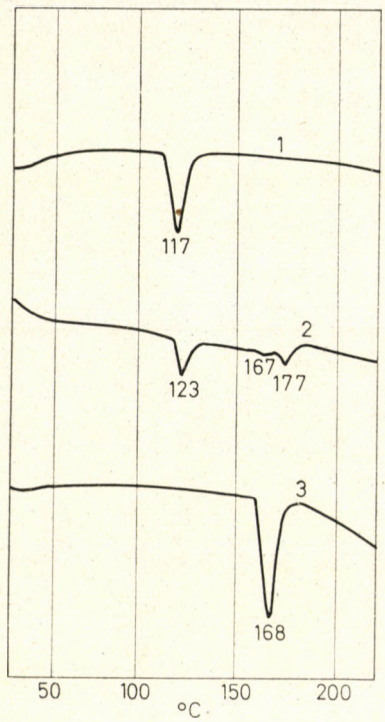


Abb. 10. DTA-Kurven des Systems Kaliumnitrat–Ammoniumchlorid. Aufheizgeschwindigkeit 1 °C/Minute. 1 — Kaliumnitrat; 2 — Gemisch aus gleichen Gewichtsteilen Kaliumnitrat und Ammoniumchlorid; 3 — Ammoniumchlorid

LITERATUR

1. Erdey, L., Gál, S., Liptay, G.: Talanta **11,** 913 (1964)
2. Paulik, F., Paulik, J., Erdey, L.: Michrochim. Acta **1966,** 894
3. Lóránt, B.: Z. für Ernährungswissenschaft, **8,** 258 (1967)
4. Coates, R. V., Woodard, G. D.: J. Sci. Td. Agric. **14,** 398 (1963)
5. Solomon, C. H., Barclay, K. S.: Fisons Fert. Ltd. Canada Technical Information 1965
6. Náray-Szabó, I.: Anorganische Chemie. Verlag der Ung. Akademie der Wissenschaften, Budapest 1962
7. Morand, J.: Ann. Chim. **12,** 1018 (1955)
8. Coates, R. V., Woodard, G.D. : J. Chem. Soc. **1965,** 2135
9. Paulik, F., Paulik, J.: Termoanalízis (Thermoanalysierung) Műszaki Könyvkiadó, Budapest, 1963

Teréz Flóra
Miklós Menyhárt } Veszprém, Wartha V. u. 1—3, Ungarn.

Acta Chimica Academiae Scientiarum Hungaricae, Tomus 69 (2), pp. 157–161 (1971)

MECHANISM OF ADSORPTION INDICATION, IX

PHTHALEINS AS ADSORPTION INDICATORS

L. LÉGRÁDI

(Nitrochemical Works, Fűzfőgyártelep)

Received January 22, 1970
In revised form April 27, 1970

Of phthalein indicators, α-naphthophthalein is suitable for the argentometric titration of chloride, bromide and thiocyanate ions; phenolphthalein for bromide and iodide ions; and thymolphthalein can be used for chloride, bromide and iodide ions. The mixtures of thymolphthalein and α-naphtophthalein or thymolphthalein and phenolphthalein also provide good adsorption indication. In the presence of these indicators, the titrations should be carried out in slightly alkaline medium (pH = 7—9), however, α-naphthophthalein can be used without making the solution alkaline. The phthalein indicators work on the surface precipitation principle. The silver salt of the dye can be detected on filter paper by means of a colour reaction and its isolation is also possible in the form of a precipitate.

In a previous work the possibilities of application of azo dyes as adsorption indicators were studied [1]. In the present paper phthalein indicators are considered for the same purpose. Of the phthalein indicators, α-naphthophthalein, phenolphthalein and thymolphthalein have been used in our experiments. In the literature argentometric applications of some sulfophthalein indicators (*e.g.* Bromophenol Blue) have been described [2, 3], but phthaleins with related structures have not yet been used in argentometry.

Experimental

Phthaleins are well-known indicator acids, their colour-change takes place in slightly alkaline pH range. Argentometric titrations were carried out with all the three phthalein compounds mentioned above. The results of these titrations are summarized in Table I. In the titrations, solutions of 50 ml initial volume were used. In each case, a 0.3 ml portion of the 0.1% alcoholic indicator solution was added. The relative error of the titration of anions with 0.1 *N* silver nitrate reagent solution was $\pm 0.15\%$. Phthalein indicators are not suitable for all kinds of argentometric titration. In argentometric titrations not included in Table I, colour changes could hardly be observed, and in the titration of cyanide ions no colour change occurred at all. Favourable results can be obtained by the use of mixed phthalein indicators.Thus thymolphthalein can be used together with α-naphthophthalein or phenolphthalein. Table II shows the possibilities of application of mixed indicators and also the indicators suitable for the titration of particular ions.

Studies of the mechanism of indication

In order to elucidate the mechanism of indication, the change of pH during the titrations and the decrease of the electrode potential due to the indicator were measured; further, the reaction between silver ions and the indicator was investigated.

Table I

Titration of anions with silver nitrate solution in the presence of phthalein indicators

Indicator	Ion	Medium	Colour change	$AgNO_3$ added, ml		Deviation	
				potentiometr.	ind.	ml	%
α-Naphtholphthalein	Cl^-	1 drop of 0.08*N* NaOH	greenish blue to violet	5.07	5.10	+0.03	0.6
α-Naphtholphthalein	Br^-	1 drop of 0.08*N* NaOH	greyish blue to violet	5.11	5.13	+0.02	0.4
α-Naphtholphthalein	SCN^-	1 drop of 0.08*N* NaOH	greyish blue to pink	5.10	5.12	+0.02	0.4
Phenolphthalein	Br^-	1 drop of 0.1*N* NaOH	pale rose to pink	5.11	5.10	—0.01	0.2
Phenolphthalein	I^-	1 drop of 0.1*N* NaOH	pale rose to pink	5.19	5.17	—0.02	0.4
Thymolphthalein	Cl^-	1 drop of 0.1*N* NaOH	blue to violet	5.28	5.29	+0.01	0.2
Thymolphthalein	Br^-	1 drop of 0.1*N* NaOH	pale blue to violet	5.11	5.09	—0.02	0.4
Thymolphthalein	I^-	1 drop of 0.1*N* NaOH	pale green to greenish blue	5.18	5.16	—0.02	0.4

1) *Change of pH during titration*

α-Naphthophthalein indicator, having the lowest pH range of colour change (pH = = 7.3—8.7), can be used without making the solution alkaline. In this case, in the titration of bromide ions with 0.1 *N* silver nitrate solution, the initial light orange colour turns to violet. In the titration of 5 ml of 0.1 *N* potassium bromide solution in the presence of α-naphthophthalein indicator, the pH value will drop from 6.20 to 5.80 in the range of the equivalence

Table II

Use of phthalein indicators in argentometric titrations

Ion to be titrated:	Chloride	Bromide	Iodide	Thiocyanate
Suitable indicators	α-naphtholphthalein	α-naphtholphthalein		α-naphtholphthalein
		phenolphthalein	phenolphthalein	
	thymolphthalein	thymolphthalein	thymolphthalein	
Mixed indicators		thymolphthalein + phenolphthalein (pink to bluish violet)	thymolphthalein + phenolphthalein (pink to blue)	
	thymolphthalein + α-naphtholphthalein (pale blue to violet)	thymolphthalein + α-naphtholphthalein (pale blue to violet)		

point; back-titration with potassium bromide produces a reverse change. A pH change of 0.2 units was observed in the absence of the indicator. When the titrations were accomplished in slightly alkaline medium, the changes of pH were smaller. *E.g.*, in the titration of 5 ml of 0.1 *N* potassium bromide solution with 0.1 *N* silver nitrate solution in the presence of α-naphthophthalein indicator and four drops of 0.08 *N* sodium hydroxide, the pH value decreased from 7.28 to 7.12 at the equivalence point. In the presence of phenolphthalein indicator and 1 drop of 0.1 *N* sodium hydroxide the pH changed from 8.30 to 8.15 in the titration of 5 ml of 0.1 *N* potassium iodide solution. No change of pH occurred when thymolphthalein indicator was used at pH 9.6.

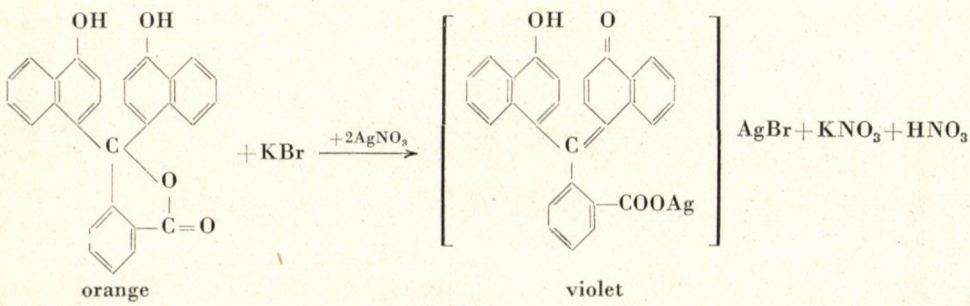
2) *The indicator-silver compound*

α-Naphthophthalein shows orange and greenish blue colour in acid and alkaline medium, respectively. Its reaction with silver ions can be demonstrated on filter paper by the addition of one drop of the indicator solution (1 drop of 0.1 *N* alkali is added to 10 ml of 0.1% alcoholic indicator solution) to one drop of 0.1 *N* silver nitrate solution, resulting in the appearance of a bluish violet colour. This colour cannot be obtained in solution. Further on, the following test was carried out to prove the existence of this silver compound: a 0.1% alcoholic solution of α-naphthophthalein was made alkaline with 0.05 *N* sodium hydroxide solution until the appearance of an olive green colour, followed by the addition of 0.1 *N* silver nitrate solution in about 1 : 1 ratio; the colour of the solution turned to violet and some precipitate of violet colour was formed. This precipitation was not quantitative. Accordingly, a reaction takes place between the indicator and the silver ions, but the compound formed is slightly soluble in this medium.

The reducing effect of the indicator on the electrode potential was also measured. One drop of 0.08 *N* sodium hydroxide solution was added to 5 ml of 0.1 *N* potassium iodide solution, and the mixture was titrated potentiometrically. At the equivalence point, the potential of the silver electrode (measured against standard calomel electrode) was 400 mV. After this 0.3 ml of 0.1% α-naphthophthalein indicator was added to the solution. Under continuous stirring the value of electrode potential gradually decreased to 200 mV.

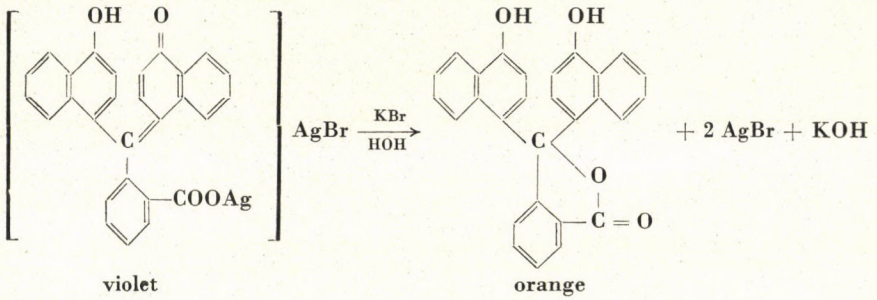
Results and discussion

The titration of potassium bromide with silver nitrate solution in the presence of α-naphthophthalein indicator can be carried out without making the solution alkaline; the colour change is from orange to violet. In this case two simultaneous processes take place. First, a quinoidal structure develops by loss of a proton, second, the silver ions are attached to the carboxyl ions:



The pH of the solution is reduced because of the nitric acid formed. This decrease of pH was demonstrated experimentally. In the presence of excess

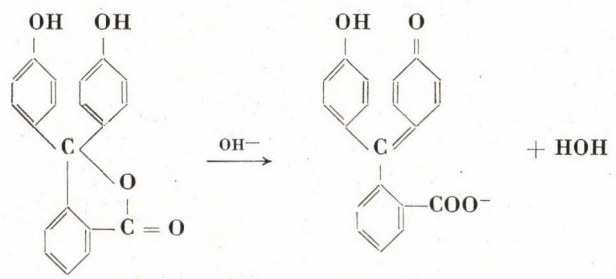
bromide ions the reaction is reversed:



violet orange

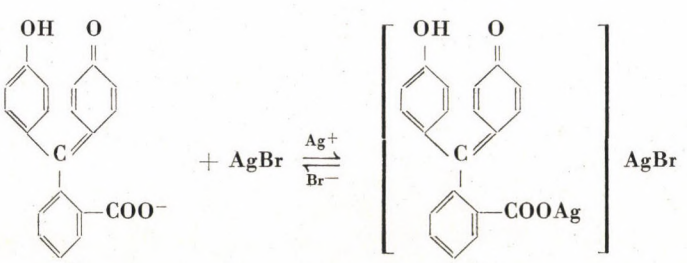
As a result, a suspension of light orange colour is obtained. Bromide ions decompose the coloured silver compound, to give a silver bromide precipitate. The dye is desorbed and takes up a proton thus liberating potassium hydroxide, which results in an increase of the pH of the solution. This pH rise was also observed experimentally.

No adsorption indication could be obtained with phenolphthalein and thymolphthalein indicators without making the solution alkaline. Here the quinoidal structure should — at least partly — already be developed in solution:



colourless red

The negatively charged dye will be adsorbed into the silver halide precipitate at the equivalence point only, then it gives a dye–silver salt with the excess of silver ions:



red violet

In the presence of excess bromide ions the reaction occurs in the reverse direction. The dye–silver salt is decomposed, and the negatively charged dye is desorbed.

Phthalein indicators are acid–base indicators though they work on the surface precipitate principle. Comparing them with the azo adsorption indicators working on the surface precipitate principle, certain differences can be noted. The former group of indicators includes dyes working exclusively on the surface precipitation principle and the latter working on both the surface precipitation and the acid–base principle. In this latter case two different colour changes can be observed: in acid medium, for the acid–base indication; and in neutral medium, for the surface precipitation indication. The phthalein indicators show only one colour change, thus they work either on the surface precipitation or the acid–base principle. The existence of the indicator–silver compound can be demonstrated, but the validity of the acid–base principle cannot be verified, since the change in the dissociation constant of the dye–adsorbate cannot be measured when precipitation or complex formation takes place. The small pH-change observed in the titrations is not a satisfactory evidence for the acid–base principle, since surface precipitation indication is also accompanied by a certain change of pH. Since the phthaleins must be in their alkaline form to make possible the formation of the indicator–silver compound, the pH of the solution should be adjusted to be near to the range of the colour change before starting the titration.

The mode of operation of phthalein indicators differ from that of azo surface precipitation indicators in one respect: in the latter case the proton loss occurring on the formation of the precipitate is independent of the acid–base functioning of these indicators; in the former case it can be attributed just to this process. In azo indicators the silver ion is supposed to substitute the proton of the sulfo- or carboxylic group, while acid–base indication is due to the proton attached to the nitrogen atom. In phthalein indicators the dissociation of the proton from the phenolic hydroxyl group is required for the formation of both the acid–base indicator and the indicator–silver compound.

REFERENCES

1. LÉGRÁDI, L.: Magy. Kém. Foly. **76**, 30 (1970)
2. KOLTHOFF, I. M.: Z. Anal. Chem. **70**, 395 (1927); **71**, 235 (1927)
3. MEHROTRA, R. C.: Anal. Chim. Acta, **3**, 69 (1949); **3**, 78 (1949); **4**, 38 (1950)

László LÉGRÁDI; Fűzfőgyártelep, Hungary.

Acta Chimica Academiae Scientiarum Hungaricae, Tomus 69 (2), pp. 163–166 (1971)

THE REACTION OF FERROCYANIDE ION WITH SILVER NITRATE

(SHORT COMMUNICATION)

J. HAVÍŘ and A. FIDLER

(A. Zápotocky Military Academy, Brno, Czechoslovakia)

Received December 1, 1969
In revised form August 28, 1970

Ferrocyanide ion reacts with silver ions forming sparingly soluble salts. The composition of these salts depends on the kind of ferrocyanide (potassium, sodium or lithium) used for precipitation. It is known that precipitation of sodium and lithium ferrocyanides by silver ions gives $Ag_4[Fe(CN)_6]$ directly while the precipitation of potassium ferrocyanide is rather complicated. NIEMZ [1], TREADWELL [2] and STEYER [3] found that the potentiometric titration of sodium and lithium ferrocyanides by silver nitrate gives a titration curve with one inflection only, corresponding to $Ag_4[Fe(CN)_6]$, but on the titration curve of potassium ferrocyanide there two clear inflections. The first inflection corresponds to the formation of $Ag_3K[Fe(CN)_6]$ and the second one indicates the end-point of titration when the total amount of potassium ferrocyanide is converted to $Ag_4[Fe(CN)_6]$.

Similar results were obtained by KOLTHOFF [4] applying conductimetric titration of potassium ferrocyanide with silver nitrate, and by KLEIBS [5] who used amperometric titration. ČIHALIK [6], using data by TOMICEK [7], determined the solubility product of $Ag_4[Fe(CN)_6]$($P_{Ag_4[Fe(CN)_6]} = 1.5 \times 10^{-41}$). The conductivity measurements of potassium ferrocyanide solutions reported by JAMES [8] showed that in aqueous solutions it is necessary to consider the formation of the intermediate ion $KFe(CN)_6^{3-}$ besides K^+ and $[Fe(CN)_6]^{4-}$. On the basis of conductivity measurements JAMES calculated the dissociation constant for the intermediate ion $[KFe(CN)_6]^{3-}$(4.3×10^{-3}).

By potentiometric titration of sodium ferrocyanide with silver nitrate in the presence of potassium ions, we determined the solubility product of $Ag_3K[Fe(CN)_6]$ and $Ag_4[Fe(CN)_6]$ and calculated the dissociation constant of $KFe(CN)_6^{3-}$.

Experimental

For the preparation of 0.025 *M* stock solutions, potassium ferrocyanide (Scherring-Kahlbaum) and potassiumfree sodium ferrocyanide were used. The molarity of stock solutions was determined by argentometric titration. For the potential measurements a Multoskop V apparatus was used. All titration were made at standard temperature and for the determinatio n of solubility products the temperature was kept at 25 ± 0.2 °C.

The data collected in Table I were obtained at a constant ionic strength equal 2.0 *M*, adjusted with potassium and sodium nitrate. The titration curve of 0.025 *M* sodium ferrocyanide has a sharp inflection at 0.150 V corresponding to $Ag_4Fe(CN)_6$. In the case of the addition of potassium nitrate to a sodium ferrocyanide solution, two inflections appeared on the titration curve. An increased concentration of potassium ions rises the height of the first inflection. Addition of rubidium, cesium and ammonium ions to sodium ferrocyanide solution causes the appearance of the first inflection too. In all the cases mentioned the position of the first inflection is at approximately 75% of the theoretical consumption of silver nitrate. An increased concentration of potassium ions in the sodium ferrocyanide solution reduces the height of the second inflection but its position remains unaltered.

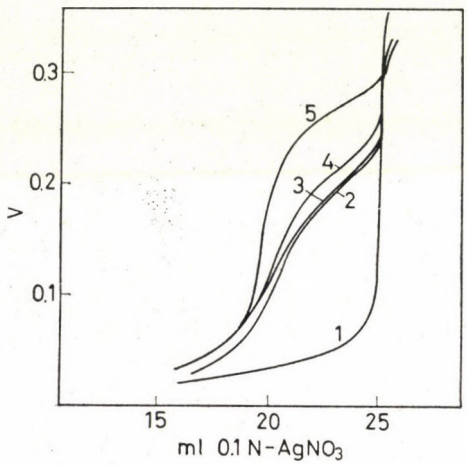


Fig. 1. The influence of potassium ions on titration of sodium ferrocyanide (25 ml of 0.025 *M* solution) by 0.1 *N* silver nitrate. 1 — without potassium ions; 2 — with 0.223 g KNO_3; 3 — with 0.456 g KNO_3; 4 — with 0.959 g KNO_3; 5 — with 10.0 g KNO_3

The titration curves with one and two inflections are shown in Fig. 1.

The mathematical evaluation of the titration curves of sodium ferrocyanide in the presence of potassium ions is possible with certain simplifications, *viz.* neglection of volume correction and use of concentrations instead of activities. The system is defined at constant pH with the activities or concentrations of Ag^+, K^+, Na^+, NO_3^-, $[Fe(CN)_6]^{4-}$, $[KFe(CN)_6]^{3-}$ and the concentration of precipitated $Ag_3K[Fe(CN)_6]$ and $Ag_4[Fe(CN)_6]$. If one chooses a region on the titration curve where the formal concentration of $Ag_3K[Fe(CN)_6]$ will be negligible in comparison with the concentration of $Ag_4[Fe(CN)_6]$, then the activity or concentration of potassium in the solution will be equal to its analytical concentration and the calculation will be much simplified.

$$P_{Ag_4Fe(CN)_6} = [Ag^+]^4[Fe(CN)_6^{4-}] \tag{1}$$

$$P_{Ag_3KFe(CN)_6} = [Ag^+]^3[KFe(CN)_6^{3-}] \tag{2}$$

$$K_{diss} = [K^+][Fe(CN)_6^{4-}][KFe(CN)_6^{3-}]^{-1} \tag{3}$$

from Eq. (1) and (2) one obtains

$$[Ag^+] = P_{Ag_4[Fe(CN)_6]}\ [KFe(CN)_6^{3-}][Fe(CN)_6^{4-}]^{-1}\ P^{-1}_{Ag_3KFe(CN)_6} \tag{4}$$

Combining this with Eq. (3) and (4) we have

$$[Ag^+] = [K^+]P_{Ag_4Fe(CN)_6}\ P^{-1}_{Ag_3KFe(CN)_6}\ K^{-1}_{diss} \tag{5}$$

The solubility products and the dissociation constant a be combined into a new constant A and then Eq. (5) becomes

$$[Ag^+][K^+]^{-1} = A \tag{6}$$

Constant A was determined by the following experiment. 25 ml of a 0.025 M sodium ferrocyanide solution was placed in a 100 ml volumetric flask, and potassium or sodium nitrate was added to adjust the ionic strength to be 2.0 M. The solution was diluted with water, 95% of the theoretical amount of silver nitrate was added and then diluted with water to 100 ml. The solution was stirred for 6 hrs and then left standing for 18 hrs. For the potential measurements we took the clear solution from the precipitate and performed the measurement with silver and saturated calomel electrodes. In Table I are summarized the data of measured potentials and the calculated values of constant A.

Table I

The determination of constant A

$A = [Ag^+]\,[K^+]^{-1}$

$[K^+]$	Potential *vs.* scE (V)	$[Ag^+]$	$A \times 10^6$
0.052	0.180	2.85×10^{-7}	5.51
0.180	0.185	4.89×10^{-7}	4.53
0.299	0.216	1.63×10^{-6}	4.46
0.504	0.230	2.82×10^{-6}	5.59
0.935	0.243	4.68×10^{-6}	5.75
0.990	0.248	5.69×10^{-6}	5.01
1.388	0.255	7.47×10^{-6}	5.38
1.582	0.262	9.55×10^{-6}	6.03
1.978	0.267	1.19×10^{-5}	6.02

Average: $A = 5.41\times10^{-6}$

Determination of the solubility product of $Ag_4[Fe(CN)_6]$ and $Ag_3K[Fe(CN)_6]$

The solubility product of $Ag_4[Fe(CN)_6]$ was determined by potential measurements with two silver electrodes; one immersed in a 0.025 M solution of sodium ferrocyanide (with a few drops of 0.1 M $AgNO_3$), the second in a 0.1 M solution of $AgNO_3$. The two solutions were connected with a saturated solution of potassium nitrate. A potential difference of 0.460 V corresponds to a silver ion activity of 1.55×10^{-9}. The solubility product of $Ag_4[Fe(CN)_6]$ is, according to (1), 1.43×10^{-37}.

To determine the solubility product of $Ag_3K[Fe(CN)_6]$, it is necessary to convert the ferrocyanide ion to $[KFe(CN)_6]^{3-}$ by an excess of potassium ions. If the concentration of potassium ions is 2.0 M, then as follows from (3), all $[Fe(CN)_6]^{4-}$ will be converted to $[KFe(CN)_6]^{3-}$. In this arrangement we measured the potential difference between two silver electrodes; one immersed in a 2.0 M solution of a potassium salt, 0.025 M in potassium ferrocyanide,

the other one in a 0.2 M solution of silver nitrate. The measured potential was 0.480 V, hence the solubility product $P_{Ag_3KFe(CN)_6} = 1{,}07 \times 10^{-29}$. Using solubility product data we calculated dissociation constant of $[KFe(CN)_6]^{3-}$ according to Eq. (5). From potential measurements the dissociation constant is $K_{diss} = 2.52 \times 10^{-3}$, in good agreement with the published by JAMES [8].

REFERENCES

1. NIEMZ, F.: Dissertation, Dresden 1920, ref. Müller, E.: Die Elektrometrische (Potentiometrische) Massanalyse, p. 140. Verlag v. Theodor Steinkopf, Dresden u. Leipzig, 1926
2. TREADWELL, W. D., CHERVET, D.: Helv. chim. Acta **5**, 633 (1922); **6**, 550 (1923)
3. STEYER, W.: Z. anal. Chem. **74**, 108 (1928)
4. KOLTHOFF, I. M.: Z. anal. Chem. **61**, 232 (1922)
5. KLEIBS, O.: Z. anal. Chim. **10**, 244 (1955)
6. ČIHALÍK, J.: Potenciometrie, p. 306. NČSAV, Praha, 1961
7. TOMIČEK, O., HUBROVÁ, K.: Coll. Czech. Chem. Comm. **8**, 293 (1936)
8. JAMES, J. C.: Trans. Faraday Soc. **45**, 855 (1949)

J. HAVÍŘ
Alois FIDLER
A. Zápotocky Military Academy Brno
Malinská 46. Brno 20. Czechoslovakia.

Acta Chimica Academiae Scientiarum Hungaricae, Tomus 69 (2), pp. 167—176 (1971)

UNTERSUCHUNG DER IONISATION VON METALLEN UND METALLIONEN-NEUTRALISATION MIT DER ROTIERENDEN RING-SCHEIBENELEKTRODE, VIII

ALLGEMEINE BEHANDLUNG DER AN DER RINGELEKTRODE MESSBAREN PARAMETER

L. KISS und J. FARKAS

(Lehrstuhl für Physikalische Chemie und Radiologie der Eötvös Loránd Universität, Budapest)

Eingegangen am 4. März 1970

Es wurde ein Zusammenhang für die Konzentrationen an der Oberfläche der Ringelektrode der an der rotierenden Scheibenelektrode in Reaktion tretenden bzw. entstehenden Ionen für den Fall angegeben, wenn kein Strom durch die Ringelektrode fließt und die Konzentration der betreffenden Ionen im Inneren der Lösung nicht vernachlässigbar ist. Es wurde die stromfreien Elektrodenpotentiale, die sich an der Ringelektrode einstellen, sowie die Zusammenhänge angegeben, welche die an der Ringelektrode meßbaren Grenzströme beschreiben.

In unseren vorangegangenen Veröffentlichungen [1, 2], wurde die Gleichung der Polarisationskurve für Elektrodenvorgänge abgeleitet, welche unter Teilnahme von zwei bzw. mehreren (N_m) Elektronen nach einem Mehrstufenmechanismus verlaufen. Die Konzentrationen der an der Scheibenelektrode in Reaktion tretenden bzw. entstehenden Ionen an der Oberfläche der Scheibe wurden ebenfalls angegeben. Der für den an der Ringelektrode meßbaren und durch die in der Reaktion teilnehmenden Ionen bestimmten Grenzstrom erhaltene Ausdruck war jedoch nur für jenen Fall gültig, wenn die Konzentration der entsprechenden Ionen in Inneren der Lösung Null war [1]. Bei der Ableitung des Zusammenhanges für das stromfreie Potential der Ringelektrode [1] wurde angenommen, daß die Konzentration an der Oberfläche des Ringes annähernd proportional der Konzentration an der Oberfläche der Scheibe ist. Diese Annahme ist nur dann richtig, wenn die Konzentration der betreffenden Ionen im Inneren der Lösung wesentlich niedriger ist, als an der Oberfläche der Scheibenelektrode bzw. wenn die Konzentration dieser potentialbestimmenden Ionen im Laufe der an der Oberfläche der Scheibenelektrode verlaufenden Reaktion nur wenig im Vergleich zur Konzentration im Inneren der Lösung verändert wird.

In der vorliegenden Arbeit sollen die Konzentrationen der an der Scheibenelektrode in Reaktion tretenden bzw. entstehenden Ionen an der Oberfläche der Ringelektrode für den Fall abgeleitet werden, wenn kein Strom durch die Ringelektrode fließt und die Konzentrationen der betreffenden Ionen im Inneren der Lösung nicht vernachlässigbar sind. In Kenntnis der Konzentrationen der potentialbestimmenden Ionen an der Oberfläche der Ringelektrode kann das an der Ringelektrode sich einstellende stromfreie

Potential angegeben werden und — unter Berücksichtigung der gegebenen Grenzbedingungen — der an der Ringelektrode meßbare Oxydations-, bzw. Reduktionsgrenzstrom der betreffenden Ionen bestimmt werden. Das an der Ringelektrode meßbare stromfreie Potential, sowie der Grenzstrom können von der Stromstärke durch die Scheibenelektrode, von der Geschwindigkeit der an der Scheibenelektrode verlaufenden Vorgänge, von der Drehzahl der Scheibenelektrode, von den Konzentrationen der betreffenden Ionenarten im Inneren der Lösung und von den hydrodynamischen Konstanten abhängig sein.

Um den Ausdruck für die *Konzentration der potentialbestimmenden Ionen an der Ringelektrode* angeben zu können muß das System von Differentialgleichungen der Konvektionsdiffusion für den in [2] behandelten Fall gelöst werden. In [2] wurde die Lösung für die Oberfläche der Scheibenelektrode angegeben [2], Gl. (9). Im weiteren wird — unter Anwendung dieser Lösung — die Konzentration (bzw. Durchschnittskonzentration) der Ionenart i an der Oberfläche der Ringelektrode aufgeschrieben. Die Differentialgleichung (in Zylinderkoordinaten), welche die Konzentrationsverteilung der Ionenart i beschreibt [3], ist

$$Ary \frac{\partial c_i}{\partial r} - Ay^2 \frac{\partial c_i}{\partial y} = D_i \frac{\partial^2 c_i}{\partial y^2} \tag{1}$$

wobei

$$\begin{aligned} r &= \text{Abstand von der Rotationsachse der Elektrode,} \\ y &= \text{Abstand von der Oberfläche der Elektrode,} \\ A &= 0{,}510\ \omega^{3/2}\ \nu^{-1/2} \\ \omega &= \text{Winkelgeschwindigkeit der rotierenden Elektrode,} \\ \nu &= \text{kinematische Viskosität der Lösung,} \\ D_i &= \text{Diffusionskoeffizient der Ionenart } i^* \text{ sind.} \end{aligned} \tag{2}$$

Die Randbedingungen sind:

$$\lim_{y \to \infty} c_i(r, y) = c_{i\infty} \tag{3}$$

$$\lim_{\substack{r \to r_1 \\ r < r_1}} c_i(r, y) = \lim_{\substack{r \to r_1 \\ r > r_1}} c_i(r, y) \tag{4}$$

wobei r_1 den Radius der Scheibenelektrode bedeutet

$$\left.\frac{\partial c_i(r, y)}{\partial y}\right|_{\substack{y=0 \\ r>r_1}} = 0$$

* Auch im weiteren werden die Bezeichnungen der vorangegangenen Publikationen [1], [2] verwendet.

In der Zone unter der Scheibe ($r < r_1$) sind die Randbedingungen die gleichen wie in [2], mit dem Unterschied, daß die Oberfläche der Scheibe in weiteren nicht gleich der Einheit ist; demzufolge tritt in die Randbedingungen (und auch in die Lösungen) anstelle der durch die Scheibe fließenden Stromstärke i der Stromdichtewert $j = \frac{i}{r_1^2 \pi}$. Unter Berücksichtigung des Gesagten ist die Lösung von Gl. (1) in der Zone unter der Scheibe (2), (3), (4):

$$c_i(y) = c_{i_0} + \frac{X_i}{D_i F}(c_{i\infty} - c_{i_0}) \int_0^y \exp \cdot \left\{ - \frac{A}{3D_i} t^3 \right\} dt \tag{6}$$

wo die Konzentration der Ionenart i an der Oberfläche der Scheibe, c_{i_0} durch das Gleichungssystem (9) in der Publikation [2] bestimmt ist und

$$X_i = 0{,}62\, F D_i^{2/3} \omega^{1/2} \nu^{-1/6} \tag{7}$$

Für den Fall $r > r_1$ kann die Lösung von Gl. (1) — unter Berücksichtigung der Gleichungen (3), (4), (5), (6) und (7) und Anwendung des Verfahrens von ALBERY und Mitarbeiter [4—7] und ihrer Teilergebnis — in folgender Form aufgeschrieben werden (an der Stelle $y = 0$, $r > r_1$):

$$c_i(r, y = 0) = c_{i_0} + (c_{i\infty} - c_{i_0}) \frac{r_1}{r} \left(\frac{r^3}{r_1^3} - 1 \right)^{1/3} \tag{8}$$

Wie aus Gl. (8) hervorgeht ändert sich $c_i(r, y = 0)$ stark mit r. Demzufolge kann an der Oberfläche der Ringelektrode ($r_2 < r < r_3$, wo r_2 der innere, r_3 der äußere Radius der Ringelektrode ist) nur mit einer durchschnittlichen Konzentration $\bar{c}_i$ gerechnet werden:

$$\bar{c}_i = c_{i_0}(1 - \mathbf{R}) + c_{i\infty}\, \mathbf{R} \tag{9}$$

wobei

$$\mathbf{R} = \frac{2r_1}{r_3^2 - r_2^2} \int_{r_2}^{r_3} \left(\frac{r_3}{r_1^3} - 1 \right)^{1/3} dr \tag{10}$$

ist.

Der Wert des durch Gl. (10) definierten geometrischen Faktors bei Verschiedenen Verhältnissen der Radien ist in Tabelle I enthalten.

Als Beispiel sollen die Ausdrücke für einen Zweistufenvorgang, bestehend aus zwei Einelektronenvorgängen, angeführt werden. Es werden die in [1]

Tabelle I

Werte von **R** *in Abhängigkeit von* r_2/r_1 *und* r_3/r_2

r_3/r_2 \ r_2/r_1	1,02	1,03	1,04	1,05	1,06	1,07	1,08	1,09	1,10
1,02	0,0090	0,0100	0,0108	0,0115	0,0122	0,0128	0,0134	0,0139	0,0144*
1,03	0,0143	0,0156	0,0168	0,0178	0,0188	0,0196	0,0204	0,0212	0,0219
1,04	0,0199	0,0216	0,0230	0,0244	0,0256	0,0267	0,0278	0,0288	0,0297
1,05	0,0258	0,0278	0,0296	0,0312	0,0327	0,0341	1,0354	0,0366	0,0378
1,06	0,0321	0,0344	0,0365	0,0383	0,0401	0,0417	0,0432	0,0447	0,0460
1,07	0,0386	0,0412	0,0436	0,0457	0,0477	0,0495	0,0513	0,0529	0,0545
1,08	0,0455	0,0483	0,0509	0,0533	0,0555	0,0576	0,0595	0,0614	0,0632
1.09	0,0526	0,0557	0,0585	0,0611	0,0635	0,0658	0,0680	0,0700	0,0721
1,10	0,0599	0,0633	0,0663	0,0691	0,0718	0,0743	0,0766	0,0790	0,0811
1,12	0,0752	0,0791	0,0826	0,0859	0,0889	0,0918	0,0946	0,0973	0,0999
1,14	0,0914	0,0957	0,0997	0,1034	0,1068	0,1102	0,1133	0,1164	0,1193
1,16	0,1084	0,1131	0,1175	0,1216	0,1255	0,1292	0,1327	0,1362	0,1395
1,18	0,1262	0,1313	0,1361	0,1406	0,1449	0,1489	0,1529	0,1566	0,1603
1,20	0,1446	0,1502	0,1554	0,1603	0,1649	0,1694	0,1736	0,1777	0,1818
1,22	0,1638	0,1698	0,1753	0,1806	0,1856	0,1904	0,1951	0,1996	0,2040
1,24	0,1836	0,1900	0,1959	0,2016	0,2070	0,2121	0,2172	0,2220	0,2267
1,26	0,2041	0,2108	0,2172	0,2232	0,2289	0,2345	0,2398	0,2450	0,2501
1,28	0,2252	0,2323	0,2390	0,2454	0,2515	0,2574	0,2631	0,2687	0,2741
1,30	0,2469	0,2544	0,2615	0,2682	0,2747	0,2810	0,2870	0,2929	0,2987
1,32	0,2692	0,2771	0,2845	0,2916	0,2985	0,3051	0,3115	0,3178	0,3239
1,34	0,2921	0,3003	0,3081	0,3156	0,3228	0,3298	0,3365	0,3432	0,3496
1,36	0,3155	0,3241	0,3323	0,3401	0,3477	0,3550	0,3622	0,3691	0,3759
1,38	0,3395	0,3485	0,3570	0,3652	0,3732	0,3808	0,3883	0,3956	0,4028
1,40	0,3641	0,3734	0,3823	0,3909	0,3992	0,4072	0,4150	0,4227	0,4302

und [2] abgeleiteten Worte c_{i_0} für $i = 1$ bzw. 2 in Gl. (9) eingesetzt, wobei für $\bar{c}_{1_0}$ und $\bar{c}_{2_0}$, d. h. für die durchschnittliche Konzentration des Ions mit einer, mit zwei positiven Ladungen an der Oberfläche des Ringes folgende Ausdrücke erhalten werden:

$$\bar{c}_{1_0} = \frac{j + X_1 c_{1\infty} + 2c_{2\infty} \dfrac{1}{\dfrac{1}{X_2} + \dfrac{1}{k_{k_2}}}}{1 + \dfrac{2k_{a_2}}{1 + \dfrac{X_1}{X_2} k_{k_2}}} (1 - \mathbf{R}) + c_{1\infty}\mathbf{R} \qquad (11)$$

und

$$\bar{c}_{2_0} = \left(c_{2\infty} \frac{X_2}{X_2 + k_{k_2}} + \frac{k_{a_2}}{X_2 + k_{k_2}} \cdot \right.$$

$$\left. \cdot \frac{j + X_1 c_{1\infty} + 2c_{2\infty} \dfrac{1}{\dfrac{1}{X_2} + \dfrac{1}{k_{k_2}}}}{X_1 + \dfrac{2k_{a_2}}{1 + \dfrac{k_{k_2}}{X_2}}} \right) (1 - \mathbf{R}) + c_{2\infty} \mathbf{R} \quad (12)$$

die Bedeutung der Symbole ist die gleich wie in [1] und [2].

Es soll bemerkt werden, daß — wie aus (8) ersichtlich ist — die durchschnittliche Konzentration $\bar{c}_{1_0}$ bei Anwendung einer breiten Ringelektrode sich als Durchschnitt sehr verschiedener Oberflächenkonzentrationen ergibt. So ist z. B. das Verhältnis der Oberflächenkonzentration am inneren und äußeren Rand der Ringelektrode bei $c_{i\infty} = 0$

$$\frac{c_{i_0}(r_2)}{c_{i_0}(r_3)} = 4{,}6, \quad \text{wenn} \frac{r_2}{r_1} = 1{,}02 \text{ und } \frac{r_3}{r_2} = 1{,}40 .$$

Dagegen ist der Wert des genannten Verhältnisses 1,1, wenn $r_2/r_1 = 1{,}02$ und $r_3/r_2 = 1{,}02$.

An der Ringelektrode meßbare stromfreie Elektrodenpotentiale

Mit Hilfe der in Gl. (9) bestimmten Durchschnittskonzentrationen können die an der Ringelektrode meßbaren stromfreien Potentiale ausgedrückt werden. Durch geeignete Wahl des Materials der Ringelektrode können verschiedene stromfreie Potentiale erhalten werden.

a) Ist die Ringelektrode ionenselektiv und reagiert sie auf die Konzentrationsänderung der Ionenart i, so ist das Potential der Ringelektrode φ_R

$$\varphi_R = \varphi' + \frac{RT}{nF} \ln \bar{c}_{i_0} \quad (13)$$

wobei

φ' = Konstante

n = Zahl der im Laufe des potentialbestimmenden Reaktionsschrittes durch die Phasengrenze tretenden Ladungen,

$\bar{c}_{i_0}$ durchschnittliche Konzentration der Ionenart i an der Oberfläche der Ringelektrode und nun wird die durch Gl. (9) definierte durchschnittliche Konzentration in Gl. (13) eingesetzt:

$$\varphi_R = \varphi' + \frac{RT}{nF} \lg \left[c_{i_0} (1 - \mathbf{R}) + c_{i\infty} \mathbf{R} \right] \tag{14}$$

Handelt es sich um einen Zweistufenvorgang und ist das Ion mit einer positiven Ladung potentialbestimmend, so erhält man durch Einsetzen von $\bar{c}_{1_0}$ in Gl. (13) die Abhängigkeit des Potentials der Ringelektrode von den einzelnen Parametern für den gegebenen Fall.

Dieser Fall a) wird z. B. bei der Untersuchung der anodischen Auflösung einer Scheibenelektrode aus Indium mittels einer Ringelektrode aus Indium realisiert [8].

b) Verhält sich die Ringelektrode als indifferente Elektrode (z. B. Edelmetall- oder Kohlenpastenelektroden), so kann an ihr — bei genügend hohem Austauschstrom — ein Redoxpotential gemessen werden. Es seien die beiden Ionenarten, welche das Redoxpotential bestimmen, die i-te und i-te. In diesem Fall ist

$$\varphi_R = \varphi' + \frac{RT}{(N_j - N_i) F} \ln \frac{\bar{c}_{j_0}}{\bar{c}_{i_0}} \tag{15}$$

bzw. nach Einsetzen der beiden Konzentration aus Gl. (9):

$$\varphi_R = \varphi' + \frac{RT}{(N_j - N_i) F} \ln \frac{\bar{c}_{j_0} (1 - \mathbf{R}) + c_{j\infty} \mathbf{R}}{\bar{c}_{i_0} (1 - \mathbf{R}) + c_{i\infty} \mathbf{R}} \tag{16}$$

wo N_j, bzw. N_i die Ladungszahlen der betreffenden Ionen sind.

Auf analoge Weise wie bei Fall a), werden bei Zweistufenvorgängen die durchschnittlichen Werte der Konzentrationen aus Gl. (11) und Gl. (12) in Gl. (15) eingesetzt. Dieser Fall b) wird z. B. bei der Untersuchung der anodischen Auflösung einer Scheibenelektrode aus Kupfer in saurer chloridhaltiger Lösun g realisiert, wenn die Ringelektrode aus Kohlenpaste hergestellt wird [9].

c) An der Ringelektrode kann sich auch ein Mischpotential einstellen, wenn z. B. das Oxydationsmittel in der Lösung das an der Scheibe entstehende einwertige Metallionen an der indifferenten Ringelektrode zu einem höhewertigen Ion oxydiert. In diesem Fall wird das Potential des Rings mit dem folgenden Ausdruck angegeben:

$$\varphi_R = \varphi' + \frac{RT}{[n\alpha_2 + z_0(1 - \alpha_0)] F} \ln \frac{\bar{c}_{0_0}}{\bar{c}_{1_0}} \tag{17}$$

wobei

α_2 = Übertrittsfaktor der Oxydation des einwertigen Metallions zum $(n + 1)$-wertigen Ion,

α_0 = Übertrittsfaktor der unter Übertritt von z_0 Ladungen sich abspielenden Reduktion des Oxydationsmittels,

c_{0_0} = Konzentration des Oxydationsmittels an der Oberfläche der Elektrode sind.

Tabelle II

Werte von S in Abhängigkeit von r_2/r_1 und r_3/r_2

r_3/r_2 \ r_2/r_1	1,02	1,03	1,04	1,05	1,06	1,07	1,08	1,09	1,10
1,02	0,1616	0,1648	0,1680	0,1712	0,1745	0,1778	0,1812	0,1845	0,1879
1,03	0,2131	0,2173	0,2216	0,2259	0,2302	0,2346	0,2389	0,2434	0,2479
1,04	0,2599	0,2650	0,2702	0,2754	0,2807	0,2860	0,2914	0,2968	0,3022
1,05	0,3036	0,3096	0,3156	0,3217	0,3279	0,3341	0,3404	0,3467	0,3531
1,06	0,3451	0,3519	0,3587	0,3657	0,3727	0,3798	0,3869	0,3941	0,4013
1,07	0,3849	0,3925	0,4002	0,4079	0,4157	0,4236	0,4315	0,4396	0,4477
1,08	0,4235	0,4316	0,4403	0,4488	0,4574	0,4661	0,4748	0,4836	0,4926
1,09	0,4611	0,4702	0,4793	0,4886	0,4979	0,5074	0,5169	0,5265	0,5362
1,10	0,4978	0,5076	0,5176	0,5276	0,5377	0,5478	0,5581	0,5685	0,5790
1,12	0,5696	0,5807	0,5920	0,6034	0,6150	0,6266	0,6384	0,6503	0,6623
1,14	0,6392	0,6518	0,6645	0,6773	0,6903	0,7034	0,7166	0,7299	0,7434
1,16	0,7076	0,7215	0,7356	0,7498	0,7642	0,7787	0,7933	0,8081	0,8230
1,18	0,7751	0,7904	0,8058	0,8214	0,8371	0,8530	0,8690	0,8851	0,9015
1,20	0,8420	0,8585	0,8753	0,8922	0,9093	0,9265	0,9439	0,9615	0,9792
1,22	0,9084	0,9263	0,9444	0,9626	0,9810	0,9996	1,018	1,038	1,056
1,24	0,9746	0,9938	1,013	1,032	1,053	1,072	1,093	1,113	1,133
1,26	1,040	1,061	1,081	1,102	1,124	1,145	1,167	1,188	1,210
1,28	1,106	1,129	1,150	1,172	1,196	1,218	1,241	1,264	1,287
1,30	1,172	1,196	1,219	1,242	1,267	1,291	1,315	1,339	1,364
1,32	1,239	1,264	1,288	1,313	1,339	1,364	1,389	1,415	1,441
1,34	1,305	1,332	1,357	1,383	1,410	1,437	1,464	1,491	1,518
1,36	1,372	1,399	1,427	1,454	1,482	1,511	1,539	1,568	1,596
1,38	1,439	1,468	1,496	1,525	1,555	1,584	1,614	1,644	1,675
1,40	1,507	1,537	1,567	1,597	1,628	1,659	1,690	1,721	1,753

Dieser Fall c) wird z. B. bei der Untersuchung des Intermediärproduktes der anodischen Auflösung einer Indiumscheibe mittels einer Ringelektrode aus Platin realisiert [8, 10, 11].

An der Ringelektrode meßbare Grenzströme

Die an der Ringelektrode meßbaren Grenzströme werden ebenfalls aus Gl. (1) bestimmt, unter Einbeziehung des Randbedingungensystems

$$\lim_{\substack{r \to r_2 \\ r < r_2}} c_i(r, y) = \lim_{\substack{r \to r_2 \\ r > r_2}} c_i(r, y) \tag{18}$$

$$c_i(r, y) = 0,$$

$$y = 0 \tag{19}$$

$$r_2 < r < r_3$$

Tabelle III

Werte von N in Abhängigkeit von r_2/r_1 und r_3/r_2

r_3/r_2 \ r_2/r_1	1,02	1,03	1,04	1,05	1,06	1,07	1,08	1,09	1,10
1,02	0,1013	0,0976	0,0947	0,0922	0,0902	0,0884	0,0869	0,0855	0,0843
1,03	0,1293	0,1250	0,1215	0,1186	0,1162	0,1140	0,1121	0,1104	0,1089
1,04	0,1529	0,1485	0,1444	0,1412	0,1385	0,1360	0,1339	0,1320	0,1302
1,05	0,1737	0,1687	0,1647	0,1612	0,1582	0,1556	0,1533	0,1512	0,1493
1,06	0,1923	0,1872	0,1829	0,1793	0,1761	0,1733	0,1708	0,1686	0,1665
1,07	0,2092	0,2039	0,1996	0,1958	0,1925	0,1896	0,1869	0,1846	0,1824
1,08	0,2247	0,2194	0,2149	0,2110	0,2076	0,2046	0,2019	0,1994	0,1972
1,09	0,2392	0,2338	0,2292	0,2252	0,2217	0,2186	0,2158	0,2133	0,2110
1,10	0,2526	0,2472	0,2426	0,2385	0,2350	0,2318	0,2289	0,2263	0,2240
1,12	0,2272	0,2717	0,2670	0,2629	0,2593	0,2560	0,2530	0,2503	0,2479
1,14	0,2992	0,2938	0,2890	0,2849	0,2812	0,2778	0,2748	0,2720	0,2695
1,16	0,3192	0,3138	0,3090	0,3048	0,3011	0,2977	0,2947	0,2919	0,2893
1,18	0,3375	0,3321	0,3274	0,3232	0,3194	0,3161	0,3130	0,3101	0,3075
1,20	0,3544	0,3490	0,3443	0,3402	0,3364	0,3330	0,3290	0,3271	0,3245
1,22	0,3701	0,3648	0,3601	0,3560	0,3523	0,3489	0,3458	0,3429	0,3403
1,24	0,3848	0,3795	0,3749	0,3708	0,3671	0,3637	0,3606	0,3577	0,3551
1,26	0,3985	0,3933	0,3887	0,3847	0,3810	0,3776	0,3745	0,3717	0,3691
1,28	0,4115	0,4063	0,4018	0,3977	0,3941	0,3907	0,3877	0,3849	0,3822
1,30	0,4237	0,4186	0,4141	0,4101	0,4065	0,4032	0,4001	0,3973	0,3947
1,32	0,4353	0,4302	0,4258	0,4218	0,4183	0,4150	0,4119	0,4092	0,4066
1,34	0,4463	0,4413	0,4369	0,4330	0,4294	0,4262	0,4232	0,4204	0,4178
1,36	0,4567	0,4518	0,4475	0,4436	0,4401	0,4369	0,4339	0,4311	0,4286
1,38	0,4667	0,4619	0,4576	0,4538	0,4503	0,4471	0,4441	0,4414	0,4389
1,40	0,4762	0,4715	0,4673	0,4635	0,4600	0,4568	0,4539	0,4512	0,4487

und mit Gl. (3), (4), (5), (6) und (7). Aus der Lösung von Gl. (1) ergibt sich für den durch die i-te Komponente bestimmten Grenzstrom (wenn die Ladungszahländerung im Laufe des Vorgangs an der Ringelektrode z_i ist):

$$i_{hi} = r_1^2 \pi z_i \{NX_i c_{i0} + (S - N) X_i c_{i\infty}\} \tag{20}$$

N = der geometrische Faktor der rotierenden Elektrode [1, 2, 5, 6—8] und

$$S = \frac{(r_3^3 - r_2^3)^{2/3}}{r_1^2} . \tag{21}$$

Der Wert des Faktors S bei verschiedenen Verhältnissen der Radien ist in Tabelle II angeführt. Die Werte des Faktors N in Gl. (20) sind in [4] ange-

Tabelle IV

Werte von (S—N) in Abhängigkeit von r_2/r_1 und r_3/r_2

r_3/r_2 \ r_2/r_1	1,02	1,03	1,04	1,05	1,06	1,07	1,08	1,09	1,10
1,02	0,0603	0,0672	0,0733	0,0790	0,0843	0,0894	0,0943	0,0990	0,1036
1,03	0,0838	0,0923	0,1001	0,1073	0,1140	0,1206	0,1268	0,1330	0,1390
1,04	0,1070	0,1167	0,1258	0,1342	0,1422	0,1500	0,1575	0,1648	0,1720
1,05	0,1299	0,1409	0,1509	0,1605	0,1697	0,1785	0,1871	0,1955	0,2038
1,06	0,1528	0,1647	0,1758	0,1864	0,1966	0,2065	0,2161	0,2255	0,2348
1,07	0,1757	0,1886	0,2006	0,2121	0,2232	0,2340	0,2446	0,2550	0,2653
1,08	0,1988	0,2122	0,2254	0,2378	0,2498	0,2615	0,2729	0,2842	0,2954
1,09	0,2219	0,2364	0,2501	0,2634	0,2762	0,2888	0,3011	0,3132	0,3252
1,10	0,2452	0,2604	0,2750	0,2891	0,3027	0,3160	0,3292	0,3422	0,3520
1.12	0,2924	0,3090	0,3250	0,3405	0,3557	0,3706	0,3854	0,4000	0,4144
1,14	0,3400	0,3580	0,3755	0,3924	0,4091	0,4256	0,4418	0,4579	0,4739
1,16	0,3884	0,4077	0,4266	0,4450	0,4631	0,4810	0,4986	0,5162	0,5337
1,18	0,4376	0,4583	0,4784	0,4982	0,5177	0,5369	0,5560	0,5750	0,5940
1,20	0,4876	0,5095	0,5310	0,5520	0,5729	0,5935	0,6149	0,6344	0,6547
1,22	0,5383	0,5615	0,5843	0,6066	0,6287	0,6507	0,6722	0,6951	0,7157
1,24	0,5898	0,6143	0,6381	0,6612	0,6859	0,7083	0,7324	0,7553	0,7779
1,26	0,6415	0,6677	0,6923	0,7173	0,7430	0,7674	0,7925	0,8163	0,8409
1,28	0,6945	0,7227	0,7482	0,7743	0,8019	0,8273	0,8533	0,8791	0,9048
1,30	0,7483	0,774	0,8049	0,8319	0,8605	0,8878	0,9149	0,9417	0,9693
1,32	0,8037	0,8338	0,8622	0,8912	0,9207	0,9490	0,9771	1,006	1,034
1.34	0,8587	0,8907	0,9201	0,9500	0,9806	1,011	1,041	1,071	1,100
1,36	0,9153	0,9472	0,9795	1,010	1,042	1,074	1,105	1,137	1,167
1,38	0,9723	1,006	1,038	1,071	1,105	1,137	1,170	1,203	1,236
1,40	1,031	1,066	1,100	1,136	1,168	1,202	1,236	1,270	1,304

geben. Um die Anwendung von Gl. (20) zu erleichtern, wurden diese Werte aus [4] übernommen und in Tabelle III zusammengefaßt. In Tabelle IV sind die Werte von $(S - N)$ angeführt.

Wie aus den Angaben von Tabellen I—IV, sowie aus Gl. (9) und (20) ersichtlich ist, wird das an der Scheibenelektrode entstehende Produkt in jenem Fall einen wesentlichen Effekt an der Ringelektrode hervorrufen, wenn die Isolierung und die Ringelektrode dünn genug sind, d. h. $(r_2 - r_1)$ und $(r_3 - r_2)$ genügend klein sind und wenn die Konzentration des an der Scheibenelektrode entstehenden, elektrochemisch aktiven Produktes im Inneren der Lösung niedrig ist.

*

Es sei Herrn Prof. Dr. I. KÁTAI für die Berechnung der Angaben der Tabellen I und II mit dem Computer an dieser Stelle gedankt.

LITERATUR

1. KISS, L., FARKAS, J.: Acta Chim. Acad. Sci. Hung. **64**, 241 (1970)
2. KISS, L., FARKAS, J.: Acta Chim. Acad. Sci. Hung. **65**, 141 (1970)
3. LEWITSCH, W. G.: Fisiko-chimitscheskaja gidrodinamika, Fizmatgiz, 2. Auflage, 1959 p. 338.
4. ALBERY, W. J., BRUCKENSTEIN, S.: Trans. Farad. Soc., **62**, 1920 (1966)
5. ALBERY, W. J.: Trans. Farad. Soc., **62**, 1915 (1966)
6. ALBERY, W. J., BRUCKENSTEIN, S., NAPP, D. T.: Trans. Farad. Soc., **62**, 1932 (1966)
7. ALBERY, W. J., BRUCKENSTEIN, S.: Trans. Farad. Soc., **62**, 2596 (1966)
8. KISS, L., FARKAS, J., KÖRÖSI, A.: Magy. Kém. Foly. **75**, 66 (1969)
9. KISS, L., FARKAS, J., KÖRÖSI, A.: Acta Chim. Acad. Sci. Hung. **67**, 179 (1971)
10. KISS, L.: Magy. Kém. Foly., **72**, 191 (1966)
11. KISS, L., KÖRÖSI, A., FARKAS, J.: Annales Univ. Sci. Eötvös, Sect. Chim. **9**, 3 (1967); Magy. Kém. Foly., **73**, 551 (1967)

László KISS
József FARKAS
} Budapest VIII., Puskin u. 11—13.

Acta Chimica Academiae Scientiarum Hungaricae, Tomus 69 (2) pp. 177–201, (1971)

RADIATION CHEMISTRY OF SATURATED–UNSATURATED HYDROCARBON SYSTEMS, III

KINETIC STUDY OF HYDROGEN FORMATION

L. WOJNÁROVITS and P. FEJES

(Isotope Institute of the Hungarian Academy of Sciences, Budapest)

Received September 20, 1969

The reactions leading to radiation-chemical hydrogen evolution have been studied in saturated–unsaturated and in open-chain–branched-chain hydrocarbon mixtures. These investigations have shown that the great number of possible reaction steps can be divided into groups by drawing together kinetically indistinguishable processes of identical character and can be arranged in a reaction scheme suitable for kinetic investigations. This scheme includes reactions of the following types: initial absorption of energy, decomposition of saturated and unsaturated molecules leading to the formation of hydrogen atoms, arbitrary energy transfer from the saturated to the unsaturated molecule, possible energy loss by unsaturated molecules without decomposition leading to the formation of hydrogen atoms, 'bimolecular' hydrogen evolution from hydrogen atoms by the intervention of saturated and unsaturated molecules, and hydrogen atom capture by unsaturated molecules. With the aid of optimization programs, a few of the characteristic relative rate constants of the above reactions have been determined using a digital computer. These relative rate constants permit deeper understanding of the so-called protective effect. One of the relative rate constants can be used for the numerical characterization of the various bond types.

I. Introduction

In the mixtures of unsaturated and branched-chain saturated hydrocarbons with saturated open-chain and cyclic hydrocarbons, the number of hydrogen molecules produced upon the absorption of 100 eV radiation energy, the so-called G_{H_2} value, decreases to a greater extent than predicted from the known behaviour of the components of the mixture, assuming simple additivity. As evidenced by the literature, this so-called 'protective effect' is one of the most frequently investigated problems in radiation chemistry.

In an earlier work, numerous experimental results concerning the G_{H_2} values of various liquid binary C_6—C_8 hydrocarbon mixtures have been described [1]. By comparing the data on hydrogen formation in various mixture systems, it was established that in mixtures formed with open-chain and cyclic saturated hydrocarbons, it is the branched-chain hydrocarbons that cause the smallest decrease in the G_{H_2} values, while the effect of unsaturated hydrocarbons increases along the series monoalkene, isolated diene and cumulated diene, producing about the same effect, conjugated diene, cyclooctatetraene. The effect of benzene exceeds that of the other hydrocarbons investi-

gated only at high benzene concentrations otherwise it is smaller (and in each case it is smaller than the effect produced by cyclooctatetraene).

On the basis of the large number of data available, and assuming a probable reaction mechanism of rather general validity in the present work we make an attempt to establish the kinetic model of H_2 evolution brought about by ionizing radiation in various saturated–unsaturated (open-chain–branched-chain) mixture systems. We wish to use this kinetic model for the determination of the relative rate constants of the assumed reactions, for the purpose of later comparison and evaluation.

II. Reactions of hydrogen evolution

As reported earlier in detail [2], radiation-chemical hydrogen evolution in binary saturated–unsaturated (open-chain–branched-chain) hydrocarbon mixtures occurs predominantly *via* the reactions listed in Column 3 of Table I. The symbols for the individual reactants and reactions are the same as used earlier, *i.e.*:

A a saturated open-chain or cyclic hydrocarbon;
E an unsaturated hydrocarbon, or a branched-chain saturated hydrocarbon in open-chain–branched-chain mixtures;
A^*, E^* a saturated or unsaturated (branched-chain) molecule in an arbitrary state of excitation;
A^+, E^+ an ion formed by removing one electron from a saturated or unsaturated (branched-chain) hydrocarbon molecule;
A_1, A_2, E_1, E_2 the fragmentation products of saturated or unsaturated (branched-chain) molecules after the cleavage of one C—C bond;
$A^\cdot$, $E^\cdot$ hydrocarbon radicals formed by the abstraction of one hydrogen atom from A or E;
$EH^\cdot$ semi-hydrogenated unsaturated hydrocarbon;
A^X, E^X 'activated' molecules possessing an arbitrary excess of excitation or ionization energy;
P the dose rate of radiation;
λ_A, λ_E energy yield factors;
e_A, e_E electron fraction of a saturated or unsaturated molecule, respectively.

Reactions which lead to identical overall results and cannot be distinguished from each other by simple kinetic methods, are grouped into the horizontal rows of the table, divided by solid lines. For their collective characterization, the corresponding reactions are grouped in column 4, while column 6 of the table contains the letter symbols of these reactions, and column 5 the characteristic reaction rates proper. Concerning the reaction groups listed in the table, the following remarks should be made

Table I

Grouping of the reactions resulting in hydrogen formation

Type of reaction	No.	Detailed formulae	Group representant	Reaction rate	Symbol
Primary energy transfer	1 2	$A \rightarrow A^*$ $A \rightarrow A^+ + e^-$	$A \rightarrow A^X$	$W_{0A} = P\lambda_A e_A$	—
	3 4	$E \rightarrow E^*$ $E \rightarrow E^+ + e^-$	$E \rightarrow E^X$	$W_{0E} = P\lambda_E e_E$	—
Loss of energy without reactions leading to hydrogen formation	6 14	$A^* \rightarrow A$ $A^* \rightarrow A_1 + A_2$	$A^X \rightarrow A$	$W_p = k_p[A^X]$	p
	7 15	$E^* \rightarrow E$ $E^* \rightarrow E_1 + E_2$	$E^X \rightarrow E$	$W_q = k_q[E^X]$	q
Energy transfer	Resultant of processes 8 and 9 resultant of processes 10, 11 and 12	$A^* + E \rightarrow$ $\rightarrow E^* + A$ $A^+ + E \rightarrow$ $\rightarrow E^+ + A$ $E + e^- \rightarrow E^-$	$A^X + E \rightarrow$ $\rightarrow E^X + A$	$W_r = k_r[A^X][E]$	r
Hydrogen atom formation	16	$A^* \rightarrow A^\cdot + H^\cdot$	$A^X \rightarrow A^\cdot + H^\cdot$	$W_s = k_s[A^X]$	s
	17	$E^* \rightarrow E^\cdot + H^\cdot$	$E^X \rightarrow E^\cdot + H^\cdot$	$W_t = k_t[E^X]$	t
Hydrogen evolution	20	$H^\cdot + A \rightarrow$ $\rightarrow H_2 + A^\cdot$	$H^\cdot + A \rightarrow$ $\rightarrow H_2 + A^\cdot$	$W_u = k_u[H^\cdot][A]$	u
	21	$H^\cdot + E \rightarrow$ $\rightarrow H_2 + E^\cdot$	$H^\cdot + E \rightarrow$ $\rightarrow H_2 + E^\cdot$	$W_v = k_v[H^\cdot][E]$	v
Hydrogen atom capture	22	$H^\cdot + E \rightarrow EH^\cdot$	$H^\cdot + E \rightarrow EH^\cdot$	$W_z = k_z[H^\cdot][E]$	z

Primary energy transfer

According to a fairly general view the energy transmitted by radiation to the components of the mixture, which is used for excitation or ionization of the molecules, is proportional to the electron fraction of the components of the mixture and to the dose rate of the radiation [3—5].

Loss of energy without reactions leading to hydrogen evolution

'Activated' molecules, produced by radiation, lose their excess energy (excitation or ionization) partly in reactions which do not result in the evolution of hydrogen, such as, *e.g.*, photon emission, the transfer of excitation

energy to internal degrees of freedom, the cleavage of C—C bonds, etc [6, 7]. Since processes such as No. 6 in Table I presumably do not play an important role in the case of saturated molecules, and the frequency of C—C bond

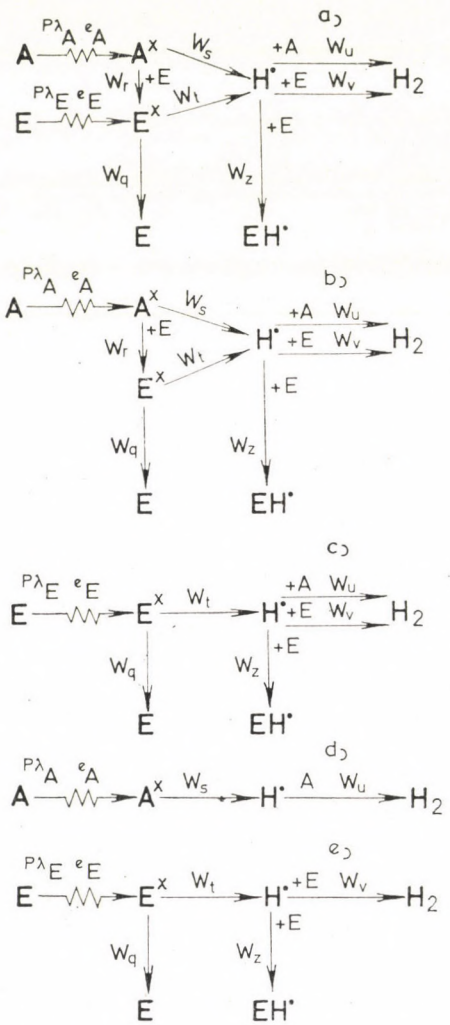


Fig. 1. Hydrogen evolution scheme used in the kinetic investigations

cleavage is lower than that of C—H bond fission these reactions of the saturated molecules have been disregarded in our further considerations. In doing this, the assumption has been made that the quasi steady-state concentrations of the reactants, to be considered from the viewpoint of hydrogen evolution, are not significantly influenced by these processes.

Energy transfer

One of the most important reactions involved in the processes leading to the 'protective effect' in binary hydrocarbon mixtures is energy transfer from the 'protected' to the 'protecting' molecule. This energy transfer may be charge transfer, transfer of excitation energy or electron capture [3, 4, 8, 11].

Hydrogen atom formation; reactions leading to hydrogen evolution

As evidenced by numerous works, the radiation-chemical evolution of hydrogen occurs predominantly *via* so-called 'hot' hydrogen atoms whose energy is considerably higher than the thermal value [12—16]. (For details, *cf.* the preceding paper in this series [2].)

Hydrogen atom capture

As a result of interaction between hydrogen atoms and unsaturated bonds, semi-hydrogenated radicals (EH') may be formed. This process is the basic reaction of the so-called chemical protection [12]. (Naturally, if E is a branched-chain hydrocarbon, this reaction is impossible.)

As already reported, the reactions brought about by irradiation of saturated–unsaturated hydrocarbon mixtures and resulting in the formation of hydrogen can be arranged in the scheme shown in Fig. 1/a.

III. Kinetic study of reactions leading to hydrogen evolution on the basis of data published in the literature

The mathematical description of the reactions leading to radiation-chemical hydrogen evolution in saturated and unsaturated hydrocarbon mixtures has been attempted by several authors with the aim of establishing the probable kinetics of the process, and to characterize numerically the so-called 'protective effect' of the unsaturated component.

In their pioneering work published in 1952, MANION and BURTON characterized the extent of 'protective effect' by a quantity called ϱ, which is the ratio of the calculated and measured radiation-chemical yields of hydrogen evolution from the saturated component [3] (*cf.* Fig. 2):

$$\varrho = \frac{G_{(H_2,A)\,\text{calcd.}}}{G_{(H_2,A)\,\text{measured}}} = \frac{e_A G_{H_2,A}}{G_{H_2} - e_E G_{H_2,E}} \tag{1}$$

where

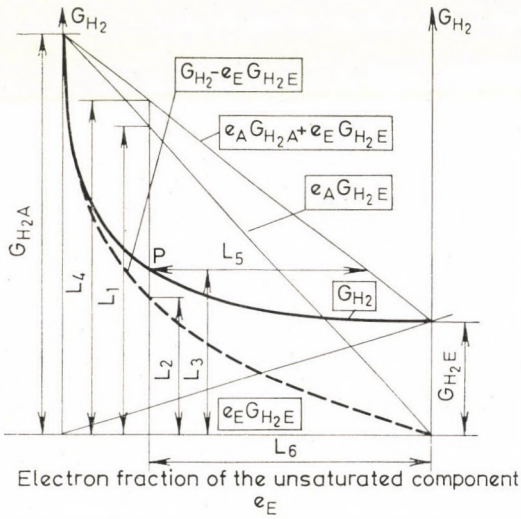
$G_{H_2,A}$ is the radiation-chemical yield of hydrogen formation from the more radiation-sensitive pure component A;

$G_{H_2,E}$ is the radiation-chemical yield of hydrogen formation from the more radiation-resistant pure component E;

$G_{(H_2,A)\,\text{calcd.}}$ is the calculated radiation-chemical yield of hydrogen evolution from component A of the mixture (according to the definition given by the authors mentioned, this equals the numerator of the right-hand side);

$G_{(H_2,A)\,\text{measured}}$ is the measured radiation-chemical yield of hydrogen evolution from component A of the mixture (by definition, the denumerator of the right-hand side);

e_A and e_E is the electron fraction of component A and E, respectively.



$$\varrho = \frac{e_A G_{H_2A}}{G_{H_2} - e_E G_{H_2E}} = \frac{L_1}{L_2}$$

$$\Theta = \frac{e_A G_{H_2A}}{G_{H_2}} = \frac{L_1}{L_3}$$

$$\Phi = \frac{e_A G_{H_2A} + e_E G_{H_2A}}{G_{H_2}} = \frac{L_4}{L_3}$$

$$\nu = \frac{e_A}{\Delta e_A} = \frac{L_6}{L_5}$$

Fig. 2. Schematic G_{H_2} *vs.* electron fraction curve of a saturated–unsaturated (open-chain–branched-chain) hydrocarbon mixture. The figure illustrates the calculation of the ϱ, Θ, Φ and ν values for an arbitrary point P

By plotting the values calculated from Eq. (1) for a small number of measured data as a function of the mole fraction of component E, they obtained a straight line. When deriving the kinetic equation

$$\varrho = 1 + \frac{k_r}{k_s}[C]\,x \tag{2}$$

corresponding to this straight line, they only considered energy transfer and the decomposition reactions of component A leading to hydrogen evolution, while possible hydrogen atom capture reactions are mentioned only in the discussion of the results. The k values are rate constants of the corresponding reactions, while x is the mole fraction of the unsaturated component. $[C]$ (mole/l) is the total volume concentration: $[C] = [A] + [E]$. The $\frac{k_r}{k_s}[C]$ value corresponding to Eq. (2) was found to be 11.9 for the cyclohexane–benzene system.

The evaluation of our own experimental results showed, however, that the plot of the ϱ-values against the mole fraction is not a straight line but a curve. Presumably, this is due to the fact that, besides simple energy transfer, other reaction steps also play a role in determining of the G_{H_2} values of the mixtures investigated.

By simultaneous consideration of processes (s), (u), (z) and (r), *i.e.* the possible reactions involving both energy transfer and radical capture, FREEMAN in his study on the cyclohexane–benzene system has derived the following expression for the function ϱ defined above:

$$\varrho = 1 + \frac{k_z}{k_u} + \frac{k_r}{k_s}[A] + \frac{k_r k_z}{k_u k_s}[E]\ \frac{[E]}{[A]} \tag{3}$$

where the values in square brackets, in accordance with the notations used earlier, represent volume concentrations of the given components in mole/l units [10].

FREEMAN assumed that the value of $\frac{k_r}{k_s}$ is considerably higher than those of $\frac{k_z}{k_u}$ and $\frac{k_r k_z}{k_u k_s}$, so that these can be neglected relative to $\frac{k_r}{k_s}$. With these neglections, FREEMAN obtained a value 0.74 l/mole for $\frac{k_r}{k_s}$.

Taking into consideration processes (p), (q), (s), (t) and a few possible reactions leading to the formation of molecular hydrogen, MERKLIN and LIPSKY have derived a relationship for the description of the mechanism of radiation-chemical hydrogen evolution in cycloalkane–benzene and aryl-cycloalkane–benzene mixtures [5]. Under consideration of these possible reactions, they found for the energy transfer coefficient $\frac{k_r}{k_s}$ of the system cyclohexane–benzene a value of 0.84 l/mole.

Several further publications discuss the kinetic description of hydrogen evolution [17—20]. Similarly to the examples discussed above, they have the

common characteristic of taking into account but a single effect, *i.e.* either only energy transfer, or only H-atom capture. The object of the present research work was to solve just this contradiction.

IV. Kinetic formulation of the problems

Let us consider again the reactions in Fig. 1/a. Even after the simplifications introduced, the reaction mechanism proposed here takes into account considerably more reaction steps, and is therefore more complicated, than reaction schemes proposed so far in the literature. Nevertheless, the rate of the processes leading to hydrogen formation can be calculated in a relatively simple way, if Bodenstein's principle of the steady-state radical concentration is applied to the intermediates, playing a role in radiolysis. (For the notation of the reactions, *cf.* Table I.)

If the difference between the rates of formation and subsequent reactions of 'active molecules' A^x is taken as approximately zero, one obtains

$$\frac{d[A^x]}{dt} = P\,\lambda_A\,e_A - k_s\,[A^x] - k_r[A^x]\,[E] \simeq 0.$$

Hence, the concentration (mole/l) of A^x in the steady state is:

$$[A^x]_{st} = \frac{P\lambda_A\,e_A}{k_s + k_r\,[E]}\,. \tag{4}$$

Similarly, the resultant reaction rates of the formation of E^x and $H^{\cdot}$ are:

$$\frac{d[E^x]}{dt} = P\,\lambda_E\,e_E + k_r\,[A^x]\,[E] - k_t\,[E^x] - k_q\,[E^x] \simeq 0, \tag{5}$$

$$\frac{d[H^{\cdot}]}{dt} = k_s\,[A^x] + k_t\,[E^x] - k_u\,[H^{\cdot}]\,[A] - k_v\,[H^{\cdot}]\,[E] - k_z\,[H^{\cdot}]\,[E] \simeq 0. \tag{6}$$

Upon inserting $[A^x]_{st}$ from Eq. (4), the concentration $[E^x]_{st}$ can be expressed from Eq. (5) as

$$[E^x]_{st} = \frac{P\lambda_E\,e_E + k_r\,[E]\,\dfrac{P\lambda_A\,e_A}{k_s + k_r\,[E]}}{k_q + k_t} \tag{7}$$

$[H^{\cdot}]$ can be easily calculated from Eq. (6) after substitution of $[A^x]_{st}$ and $[E^x]_{st}$ from Eqs. (4) and (7), respectively:

$$[H^{\cdot}]_{st} = \frac{k_s \dfrac{P\lambda_A e_A}{k_s + k_r[E]} + k_t \dfrac{P\lambda_E e_E + k_r[E] \dfrac{P\lambda_A e_A}{k_s + k_r[E]}}{k_q + k_t}}{k_u[A] + k_v[E] + k_z[E]} .$$

In the steady state, the rate of the processes leading to the formation of gaseous hydrogen can be written as:

$$\frac{d[H_2]}{dt} = k_u[H^{\cdot}][A] + k_v[H^{\cdot}][E] =$$

$$= (k_u[A] + k_v[E]) \frac{k_s \dfrac{P\lambda_A e_A}{k_s + k_r[E]} + k_t \dfrac{P\lambda_E e_E + k_r[E] \dfrac{P\lambda_A e_A}{k_s + k_r[E]}}{k_q + k_t}}{k_u[A] + k_v[E] + k_z[E]} \tag{8}$$

Eq. (8) can be reduced to a simpler form on the basis of the following considerations. From the viewpoint of the activation energy requirements of reactions (u) and (v), the H·-atoms can be regarded as 'hot' on the basis of what was said in the preceding chapter, *i.e.* it can be assumed that these processes do not need thermal activation. Therefore, their rate will be determined, among other factors, by the collision probabilities proportional to the relevant concentrations [2]. Furthermore, it follows from this that the ratio of the rate of process (u) producing hydrogen, to the sum of the rates of processes (v) and (z), producing hydrogen and semi-hydrogenated EH·-radicals, respectively, must be approximately the same as the ratio of the concentrations:

$$\frac{k_u[A][H^{\cdot}]_{st}}{(k_v + k_z)[E][H^{\cdot}]_{st}} \simeq \frac{[A]}{[E]} \tag{9}$$

since in the process of type (u) the only possible reaction of the H·-atom is radical exchange producing hydrogen, while of processes (v) and (z), either one or the other takes place, depending whether the H·-atom interacts with a part of the molecule containing no double-bond or with a part carrying a double-bond*. Using this simplification, and introducing the total molar concentration

* For details, *cf.* next chapter.

$[C]$ on the basis of the relationship $[A] + [E] = [C]$, or the mole fractions*, on the basis of relationships $\frac{[A]}{[C]} = 1 - x$ and $\frac{[E]}{[C]} = x$, Eq. (8) can be reduced to the following form:

$$\frac{d[H_2]}{dt} = \frac{P\left(1 - \frac{k_z}{k_u} x\right)}{k_s + k_r [C] x} \left\{\lambda_A e_A (k_s + f k_r [C] x) + \lambda_E e_E f (k_s + k_r [C] x)\right\} \quad (10)$$

where

$$f = \frac{k_t}{k_t + k_q} .$$

Denoting this latter form of the expression of $\frac{d[H_2]}{dt}$ by r_{H_2}, the G_{H_2}-value can be calculated from the following expression:

$$G_{H_2} = \frac{N \int_0^t r_{H_2}(\xi)\, d\xi}{1000\, P\omega t d} = \frac{N\, r_{H_2}}{1000\, P\omega d} \quad (11)$$

where

N is Avogadro's number,
ω is an energy conversion factor,
d is the density of the hydrocarbon mixture (g/cm^3),
t is the reaction time (sec).

If those parameters which are affected by the experimental conditions are varied in a wide interval, expression (11) permits, in principle, the determination of the reaction rate constants occurring in it, or at least some of them, from the experimental data. However, owing to the large number of parameters and to unavoidable experimental errors, it seems more appropriate to determine the relative rate constants, rather than their absolute values.

With this aim in mind, let us consider the following.

If we assume in accordance with Fig. 1/b that hydrogen evolution is to be attributed exclusively to the active molecular precursors A^x formed in the primary interaction between radiation and matter, then the rate of hydrogen formation, and the G-value characteristic of it (which corresponds to the quantity $G_{H_2,A\,\text{measured}}$, already discussed in connection with the ϱ-function defined by MANION and BURTON (*cf.* Eq. (1)), can be written in the following

* Owing to the difference in densities and molecular weights, the total concentration changes slightly in the full series of mixtures; in the calculations the arithmetic mean of the $[C]$ values referring to the pure A and E has been used.

form, repeating the considerations described when deriving Eq. (10):

$$\left[\frac{d[H_2]}{dt}\right]_A = \frac{P\lambda_A e_A\left(1 - \frac{k_z}{k_u}x\right)}{k_s + k_r[C]x}(k_s + k_r[C]fx) = r_{H_2,A}$$

$$G_{H_2,A\,\text{measured}} = \frac{Nr_{H_2,A}}{1000\,P\omega d} \tag{12}$$

On the other hand, if according to Fig. 1/c only the 'active' molecules E^x are considered as the precursors of hydrogen formation, the rate of hydrogen formation, and the G-value characteristic of it, can be calculated from the following equations:

$$\left[\frac{d[H_2]}{dt}\right]_E = P\lambda_E e_E f\left(1 - \frac{k_z}{k_u}x\right) = r_{H_2,E}$$

$$G_{H_2,E\,\text{measured}} = \frac{N r_{H_2,E}}{1000\,P\omega d} \tag{13}$$

It can be easily proved that in a hypothetic mixture, in which the electron concentration of A is e_A, and the only possible reaction of A, and of the radicals formed from it, is that according to (s) (*cf.* Fig. 1/d), the rate of hydrogen formation $r^0_{H_2,A}$ will be

$$r^0_{H_2,E} = P\lambda_A e_A,$$

and the G-value belonging to it, which corresponds to the quantity $G_{H_2,A\,\text{calcd.}}$ in Eq. (1) is

$$G_{(H_2,A)\,\text{calcd.}} = \frac{Nr^0_{H_2,A}}{1000\,P\omega d}. \tag{14}$$

Finally, in a hypothetical mixture, for which it is assumed that no kind of interaction exists between the components of the mixture (involving also that the H·-atoms having as precursors E^x formed in the primary processes, do not react with the saturated molecules 'A' according to (u) (*cf.* Fig. 1/e)), the rate of hydrogen formation attributable molecules E^x, and the corresponding G_{H_2} value ($G_{H_2,E\,\text{calcd.}}$) will be

$$r^0_{H_2,E} = P\lambda_E e_E f\frac{k_v}{k_v + k_z},$$

$$G_{H_2,E\,\text{calcd.}} = \frac{Nr^0_{H_2,E}}{1000\,P\omega d}. \tag{15}$$

After these preliminaries, we shall define a relative reaction rate for the formation of hydrogen which, similarly to the concept of selectivity used in reaction kinetics, is the ratio of suitably chosen rate expressions. The definition must be such that the relative rate could be easily calculated from the G_{H_2}-values obtained from the experimental data under various conditions, and an unequivocal correlation existed with the reaction rates defined above. Indeed, this is a prerequisite for the requirement stipulated earlier that the experimental data should permit to draw conclusions on the pertinent reaction rates.

Let us examine from this aspect first of all the ϱ-function defined by MANION and BURTON, which seems to fulfill the requirements mentioned.

Upon inserting the kinetic relationships corresponding to the quantities $G_{H_2,A\,\text{calcd.}}$ (Eq. (14)) and $G_{H_2,A\,\text{measured}}$ (Eq. (12)) into the equation defining ϱ, the following expression is obtained:

$$\varrho = \frac{G_{H_2,A\,\text{calcd.}}}{G_{H_2,A\,\text{measured}}} = \tag{16}$$

$$= \frac{1 + \dfrac{k_r}{k_s}[C]\,x}{1 + \left(\dfrac{k_r}{k_s} f[C] - \dfrac{k_z}{k_u}\right) x - \dfrac{k_r}{k_s} f \dfrac{k_z}{k_u}[C]\,x^2} = \frac{1 + bx}{1 + ax - cx^2}$$

It is easily seen that there is an inconsistency between kinetic expression (16) given for the ϱ-function on the basis of its definition (ratio of the calculated and measured radiation chemical yields of hydrogen formation from the same component) and the way of calculating the ϱ-values, since the latter does not take into account the fact that in the presence of type A molecules the G-value of hydrogen evolution from the E^x molecules formed in the primary processes increases because of the diminished possibility of the H·-atom capture reaction (due to lower concentration of the unsaturated hydrocarbon), so that $G_{H_2,A\,\text{measured}} \neq G_{H_2} - e_E G_{H_2,E}$ (*cf.* the right-hand side of Eq. (1)).

To eliminate this difficulty, it seems expedient to find a more natural definition for the relative rate of hydrogen formation than that proposed by MANION and BURTON, which, moreover, is unequivocal also from the kinetic point of view.

An obvious definition is reached by interpreting the relative reaction rate of hydrogen formation as the ratio of $G_{H_2,A\,\text{calcd.}}$, *i.e.* the G-value of hydrogen formed fictively at an electron fraction e_A from component A of the mixture, to the G_{H_2}-value measured for the mixture (Θ-function) (*cf.* Fig. 2.

and Eqs. (14) and (10)*):

$$\Theta = \frac{G_{H_2,A\,\text{calcd.}}}{G_{H_2}} = \frac{e_A G_{H_2,A}}{G_{H_2}} \tag{17}$$

$$\Theta = \frac{1 + \left(\frac{k_r}{k_s}[C] - 1\right)x - \frac{k_r}{k_s}[C]\,x^2}{1 + \left(\frac{k_r}{k_s}f[C] + f - \frac{k_z}{k_u} - 1\right)x - \left(\frac{k_r}{k_s}\,\frac{k_z}{k_u}f[C] + f\frac{k_z}{k_u} - \frac{k_z}{k_u}\right)x^2} =$$

$$= \frac{1 + (b-1)x - bx^2}{1 + dx - ex^2} \tag{18}$$

The relative reaction rate in question can be characterized also by the ratio of the calculated and measured hydrogen formation yields of the mixture of given composition (*cf.* Fig. 2 and Eqs. (14), (15), (10)*):

$$\Phi = \frac{G_{H_2,A\,\text{calcd.}} + G_{H_2,E\text{calcd.}}}{G_{H_2}} = \frac{e_A G_{H_2,A} + e_E G_{H_2,E}}{G_{H_2}} \tag{19}$$

$$\Phi = \frac{1 + \left\{\frac{k_r}{k_s}[C] + \left(1 - \frac{k_z}{k_u}\right)f - 1\right\}x - \left\{\frac{k_r}{k_s}[C]\left[1 - \left(1 - \frac{k_z}{k_u}\right)f\right]\right\}x^2}{1 + \left(\frac{k_r}{k_s}f[C] + f - \frac{k_z}{k_u} - 1\right)x - \left(\frac{k_r}{k_s}f\,\frac{k_z}{k_u}[C] + f\frac{k_z}{k_u} - \frac{k_z}{k_u}\right)x^2} =$$

$$= \frac{1 + gx - hx^2}{1 + dx - ex^2} \tag{20}$$

Constants a, b, c and b, d, e and g, h, d, e on the right-hand side of Eqs. (16), (18) and (20) can be determined by means of some appropriate method (*e.g.* method of least squares, optimization with a computer, etc.) from experimental data calculated using Eqs. (1), (17), and (19). If constants a, b, c, etc. are known, the relative rate constants can also be calculated on the basis of the corresponding definition equations.

* In the deduction of Eqs. (18) and (20) the following simplifications were made:

$$\lambda_E e_E \simeq Kx$$

$$\lambda_A e_A \simeq K(1 - x)$$

where K is constant. (Actually, this assumption is valid only in the case, when the electron numbers of the molecules A and E, EL_E and EL_A, and consequently the energy utilization factors λ_E and λ_A proper, characteristic of the absorption of primary radiation energy, differ only slightly from one another.

It should be mentioned here that a strict consistency can be established between the way of calculating the ϱ-function of MANION and BURTON, used repeatedly above, and kinetic expression (16), if the effect mentioned in connection with H·-radical capture is taken into account by a correction term $K(x)$ in the denominator of Eq. (1) comprising the instruction for the calculation:

$$\varrho^* = \frac{e_A G_{H_2,A}}{G_{H_2} - e_E G_{H_2,E} - K(x)} \tag{21}$$

where $K(x)$ can be given by the following function, utilizing the corresponding reaction rate expressions:

$$K(x) = e_E G_{H_2,E} \frac{\frac{k_z}{k_u}}{1 - \frac{k_z}{k_u}} (1 - x) \tag{22}$$

We wish to mention in connection with Eqs. (16), (18), and (20) that in those cases, where E is a branched-chain hydrocarbon, reaction step (z) is absent, since the capture of the H·-atom is not possible. In such cases, the formal substitution $k_z = 0$ may be made, and the above expressions will be reduced to the following form:

$$\varrho = \frac{1 + \frac{k_r}{k_s}[C]\,x}{1 + \frac{k_r}{k_s}[C] f x} \tag{23}$$

$$\Theta = \frac{1 + \left(\frac{k_r}{k_s}[C] - 1\right) x + \frac{k_r}{k_s}[C]\,x^2}{1 + \left(\frac{k_r}{k_s}[C] f + f - 1\right) x} \tag{24}$$

$$\Phi = \frac{1 + \left(\frac{k_r}{k_s}[C] + f - 1\right) x - \frac{k_r}{k_s}[C](1 - f)\,x^2}{1 + \left(\frac{k_r}{k_s}[C] f + f - 1\right) x} \tag{25}$$

For mixtures containing open-chain and branched-chain hydrocarbons there is also a simpler possibility for the determination of the relative rate constant $\frac{k_r}{k_s}[C]$ than the use of the above functions. On the basis of simple

quantitative considerations, HARDWICK has shown in one of his papers [12] that the fraction of primarily activated, open-chain molecules, which transfers its energy to branched-chain hydrocarbons is equal to $\frac{\Delta e_A}{e_A}$, where the meaning of Δe_A is shown in Fig. 2. Using this expression, the above relative reaction rate constant can be calculated from the slope of the following function, linear with respect to $\frac{1}{x}$:

$$\nu = \frac{e_A}{\Delta e_A} = \frac{k_r[A^x][E] + k_s[A^x]}{k_r[A^x][E]} = 1 + \frac{k_s}{k_r}\,\frac{1}{[C]}\,\frac{1}{x} \tag{26}$$

V. Results of calculations

In the present work, the discussion of the experimental method and direct experimental results is omitted, as these can be found in our earlier communication [1]. As concerns the hydrocarbons used in the experiments, we wish to mention here only that these were preparations of analytical purity, and have been purified by distillation immediately before use. Irradiation was performed in the liquid state, at room temperature, without thermostating, applying relatively high (about 20 Mrad) doses.

In our experiments, the G_{H_2}-values have been determined for different mixtures (listed in Column 3 of Table II) formed by unsaturated hydrocarbons of various bond types (monoalkenes, isolated dienes, cumulated dienes, conjugated dienes, benzene and cyclooctatetraene) as well as 2,2-dimethylbutane, with the saturated hydrocarbons shown. The G_{H_2} values of the pure components have been determined in separate experiments. Utilizing these data, the values of the $\varrho(x)$, $\Theta(x)$ and $\Phi(x)$ functions have been calculated for different concentrations of the saturated component, which permitted the determination of constants a — e on the right-hand side of Eqs. (16), (18) and (20), and from these, the relative reaction rate constants $\frac{k_r}{k_s}$ [C], $f = \frac{k_t}{k_t + k_q}$, and $\frac{k_z}{k_u}$. For this purpose an optimization method based on the Gauss—Newton iteration procedure has been applied to the sum of squares functions. Another computer method gave also a confidence interval for the error of the relative rate constants calculated from constants a — e [21]. This made possible the comparison of data obtained by using the different definition equations. Relative reaction rate constants obtained in this way and their standard deviations are shown in columns 4 to 12 of Table II.

For the illustration of the fact that Eqs. (16), (18) and (20) with the calculated values of constants a, b, c, b, d, e and g, h, d, e actually give a good

Table II

Rate constant combinations determined by the use of the functions

No.	Type of mixture	Components of the mixture	ϱ	
			$\frac{k_r}{k_s}[C]$	$f=\frac{k_t}{k_t+k_q}$
1.	Alkane–-monoalkene	*n*-hexane–1-hexene	29.6 ± 1.4	0.43 ± 0.01
2.		*n*-heptane–1-heptene	28.3 ± 3.4	0.44 ± 0.02
3.		*n*-octane–1-octene	29.0 ± 6.4	0.49 ± 0.02
4.		cyclohexane–cyclohexene	29.1 ± 1.5	0.43 ± 0.01
5.	Alkane–-isolated diene	*n*-octane–1,7-octadiene	35.1 ± 5.0	0.41 ± 0.01
6.		cyclohexane–1,4-cyclohexadiene	38.1 ± 4.1	0.44 ± 0.01
7.	Alkane–-cumulated diene	*n*-heptane–1,2-heptadiene	34.5 ± 4.0	0.37 ± 0.04
8.	Alkane–-conjugated diene	*n*-hexane–1,3-cyclohexadiene	28.4 ± 2.8	0.20 ± 0.02
9.		*n*-octane–2,4-octadiene	28.5 ± 2.0	0.23 ± 0.01
10.		cyclohexane–1,3-cyclohexadiene	26.2 ± 3.1	0.16 ± 0.01
11.		*n*-octane–1,3-cyclooctadiene	23.9 ± 1.3	0.16 ± 0.01
12.	Alkane–-cyclooctatetraene	*n*-octane–cyclooctatetraene	31.2 ± 4.0	0.11 ± 0.01
13.	Alkane–-benzene	*n*-hexane–benzene	18.6 ± 4.0	0.19 ± 0.02
14.		cyclohexane–benzene	16.3 ± 6.0	0.17 ± 0.05
15.	Open-chain alkane–branched-chain alkane	*n*-hexane–2,2-dimethylbutane	4.7 ± 0.5	0.8 ± 0.3

* Error limits given for the single parameters are identical with the standard deviations of the same parameters.

approximation of the experimental $\varrho(x)$, $\Theta(x)$ and $\Phi(x)$ curves, a few of these calculated curves are presented in Figs. 3 and 4, together with the experimental points. It can be seen that the agreement is satisfactory in all cases investigated.

We wish to mention here that data of the system *n*-hexane–2,2-dimethylbutane have not been processed according to Eqs. (23)—(25), but by means of Eqs. (16), (18), and (20). Since we have measured only a few data on open- and branched-chain systems, experimental data published in the literature have also been used for the evaluation. For these, the relative reaction rate constants have been calculated from the function corresponding to Eq. (16).

$\varrho(x)$, $\Theta(x)$ and $\Phi(x)$ of the hydrocarbon pairs investigated

	Θ			Φ		
$\frac{k_z}{k_u}$	$\frac{k_r}{k_s}[C]$	$f=\frac{k_t}{k_t+k_q}$	$\frac{k_z}{k_u}$	$\frac{k_r}{k_s}[C]$	$f=\frac{k_t}{k_t+k_q}$	$\frac{k_z}{k_u}$
0.10±0.02	27.8±0.7	0.43 ±0.03	0.55±0.01	28.6±0.8	0.43±0.03	0.61±0.02
0.17±0.04	22.7±1.0	0.41 ±0.04	0.53±0.02	22.7±1.6	0.41±0.06	0.60±0.07
0.27±0.03	25.8±4.2	0.47 ±0.11	0.57±0.03	28.0±4.7	0.49±0.11	0.78±0.05
0.16±0.02	25.5±1.5	0.41 ±0.04	0.34±0.02	27.1±1.5	0.42±0.04	0.46±0.04
0.29±0.03	26.0±2.4	0.37 ±0.02	0.72±0.02	28.5±2.5	0.39±0.05	0.84±0.03
0.18±0.02	30.6±0.54	0.41 ±0.04	0.58±0.01	32.2±1.8	0.42±0.04	0.66±0.02
0.64±0.02	21.6±2.0	0.27 ±0.04	0.74±0.02	22.6±2.0	0.28±0.04	0.94±0.03
0.23±0.05	25.9±1.3	0.2 ±0.02	0.52±0.03	26.9±1.5	0.2 ±0.02	0.62±0.05
0.25±0.02	24.2±0.8	0.21 ±0.02	0.7 ±0.01	24.6±1	0.22±0.02	0.73±0.02
0.51±0.05	23 ±2	0.14 ±0.02	0.75±0.04	23.8±2.3	0.14±0.03	0.86±0.06
0.37±0.04	22.5±1	0.17 ±0.02	0.73±0.02	23 ±1.2	0.17±0.02	0.79±0.06
0.76±0.02	19.7±0.6	0.052±0.006	0.92±0.01	20.6±0.6	0.06±0.01	0.97±0.01
0.81±0.02	11.3±0.7	0.1 ±0.02	1.00±0.01	9.7±0.6	0.08±0.02	1.11±0.03
0.78±0.05	9.7±0.4	0.08 ±0.01	0.98±0.01	10.2±0.3	0.08±0.02	1.05±0.01
0.01±0.03	6.1±0.8	0.83 ±0.20	0.24±0.03	5.0±1.6	0.8 ± 0.4	—0.16±0.50

As seen from Tables II and III, for these systems $\frac{k_z}{k_u}$ was actually zero, in accordance with the expectation.

In connection with expression (26), it was mentioned already that a linear relationship exists between $\frac{1}{x}$ and $\frac{e_A}{\Delta e_A}$ in the case of open-chain–branched-chain hydrocarbon mixtures. Indeed, the slope of the $e_A/\Delta e_A = \mathrm{f}\left(\frac{1}{x}\right)$ straight line is actually the reciprocal of one of the relative rate constants. The $\frac{k_r}{k_s}[C]$ values obtained by means of this straight line are as follows: 2.2 for mixture No. 15, 2.2 for mixture No. 16, and 2 for mixture

Table III

Rate constant combinations for a few n-alkane–i-alkane mixtures determined by Eq. (16)

No.	Mixture	$\frac{k_r}{k_s}$ [C]	$f = \frac{k_t}{k_t + k_q}$	$\frac{k_z}{k_u}$	Reference
16	*n*-hexane–2,3-dimethylbutane	2.5±2.0	0.74±0.21	0.01±0.14	[8]
17	*n*-hexane–2-methylpentane	2.9±2.2	0.78±0.15	0.02±0.1	[22]

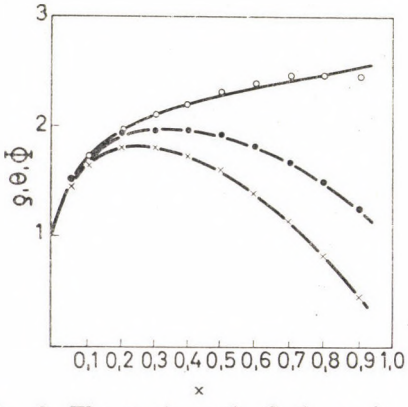


Fig. 3. The ϱ, (o–o–o), Θ, (×–×–×), and φ, (•–•–•) functions for *n*-heptane–1-heptene hydrocarbon mixtures calculated from the experimental data and the corresponding relationships (16), (18) and (20) defined by constants *a*—*e* determined previously (solid curves).

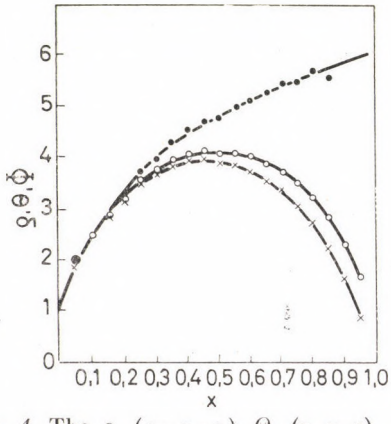


Fig. 4. The ϱ, (•–•–•), Θ, (×–×–×), and Φ, (o–o–o) functions of *n*oc-tane–1,3-cyclooctadiene mixtures calculated from the experimental data (points), and the corresponding relationships (16), (18) and (20) defined by constants *a*—*e* determined previously (solid curves).

Table IV

Rate constant combinations for a few saturated–unsaturated hydrocarbon mixtures, determined on the basis of ϱ^*, and the $k_z/k_u = j$ values used for the calculations in connection with Eqs. (21) and (22)

No.	$\frac{k_r}{k_s}$ [C]	$f = \frac{k_t}{k_t + k_q}$	$\frac{k_z}{k_u}$	j
2	23 ±1.2	0.4 ±0.01	0.29±0.02	0.29
4	27.2±1.5	0.43±0.01	0.33±0.02	0.25
5	30 ±4	0.4 ±0.02	0.57±0.02	0.5
14	12 ±1.7	0.12±0.02	0.86±0.03	0.9

No. 17. It can be seen that with the exception of the *n*-hexane–2,2-dimethylbutane mixture, the agreement between the values determined by the two approaches is satisfactory. It should be mentioned here that for these mixtures the relative rate constants can be determined in general only with a large error by means of expressions (16), (18) and (20) evidently owing to the characterless course of the curves.

If no neglections had been made in the derivation of Eqs. (16), (18) and (20) relevant to ϱ, Θ and Φ (*e.g.* in connection with ϱ: the reactions of the H˙ atom formed from E^x as precursor, produced, in turn, in the primary energy uptake; in connection with Θ and Φ: the simplifications $\lambda_E e_E = Kx$, and $\lambda_A e_A = K(1 - x)$), the three different definition equations should have resulted in practically identical relative reaction rate constants. However, as shown in Table II, strict agreement was found only in a few cases. If the standard deviations of the numerical values given are taken into consideration, the confidence intervals overlap in the majority of cases, *i.e.* the wider range of errors in the combined intervals comprises the points from all three methods. While the calculated $k_r/k_s[C]$ and f values differ noticeably only with systems 7, 12, 13 and 14, the standard deviation of the third rate constant, k_z/k_u practically do not overlap in any of the cases. It is remarkable that the k_z/k_u data calculated from the ϱ-function are in general considerably lower than those determined from the Θ and Φ functions.

As mentioned repeatedly in the preceding section in connection with Eqs. (21) and (22), the ϱ-function calculated from experimental data according to (1) and the exact kinetic expression (16) do not correspond strictly to one another, due to the H_2 evolution reactions of the E^x molecules formed in the primary processes. Using the method of calculation described, this error can be corrected by means of function ϱ^* proposed by us, inserting an acceptable average value for $k_z/k_u = j$ in (21)—(22). As seen from a few examples shown in Table IV, the relative rate constants given on the basis of the ϱ^* function are in much better agreement with the corresponding values of Θ and Φ, than those determined from the function ϱ. Among the constants appertaining to ϱ and ϱ^*, the greatest difference is exhibited just by the critical k_z/k_u values. This fact indicates that the differences in Table II between the constants k_z/k_u calculated from the ϱ, Θ and Φ functions, respectively, are caused predominantly by the neglection of the H˙ atom reactions mentioned.

Taking this into consideration, we have listed in Table V those values of the three relative rate constants, which we think are most probable. The table contains also numerical data for a few characteristics derived from the rate constants, as well as the average total molar concentration $[C]$ referred to room temperature.

When setting up Eq. (9), we endeavoured to accentuate the statistical characteristics of radical exchange according to (u) and (v), respectively, and

of the H·-atom capture reactions according to equation (*z*), and at the same time to utilize these characteristics for reducing the said equations. This was based on the idea that the probability of a 'hot' H· atom reacting with *A* according to scheme (*u*) is the same as that with *E* according to scheme (*v*) or (*z*). The magnitude of the 'cross-section of attack' exposed by *E* to the H· atoms will determine which one of the latter two possible reactions is

Table V

Combination of some characteristic average reaction rate constants for the hydrocarbon mixtures investigated, the average molar concentrations, [C], *and the* φ *values*

No.	$(k_r/k_s)[C]$	$f=\frac{k_t}{k_t+k_q}$	k_z/k_u	$\varphi=\frac{n_{E,C^=}}{n_{A,C^-}}$	[C] mole/l	k_r/k_s 1/mole	$k_q/k_t=\frac{1-f}{f}$	$1-f$
1.	28.5	0.43	0.4	0.33	8.0	3.5	1.3	0.57
2.	23	0.41	0.4	0.29	7.0	3.3	1.45	0.59
3.	27	0.48	0.4	0.25	6.4	4.2	1.1	0.52
4.	27	0.42	0.3	0.33	9.6	2.8	1.45	0.58
5.	31	0.40	0.6	0.50	7.6	4.1	1.5	0.60
6.	33	0.43	0.5	0.67	10.0	3.3	1.3	0.57
7.	30	0.34	0.7	0.43	7.3	4.1	1.9	0.66
8.	27	0.2	0.5	0.57	7.2	3.8	4.0	0.8
9.	25	0.22	0.6	0.50	—	—	3.5	0.78
10.	25	0.15	0.7	0.67	10.2	2.4	5.7	0.85
11.	23	0.16	0.5	0.50	—	—	5.2	0.84
12.	28	0.1	0.9	1.00	7.7	3.6	9	0.9
13.	13	0.13	0.9	1.00	9.4	1.4	6.7	0.87
14.	11	0.12	0.9	1.00	10.2	1.1	8.1	0.88
15.	5.0	0.82	0.00	0.00	7.2	0.7	0.22	0.18

actually realized. As a crude approximation, it may be assumed that part of the molecule *E* is involved in reaction (*z*), which carries the double bond. The magnitude of this part can be taken as proportional to the number of carbon atoms involved in the double bond. Similarly, in the case of (*v*) the 'cross-section of attack' can be taken as proportional to the number of carbon atoms which do not participate in the double bond. Evidently, these considerations do not apply to branched-chain hydrocarbons, regardless of the fact whether they participate in reactions of type *A* or *E*, because with these hydrocarbons the geometry of the molecule is more complicated, and varies with the actual hydrocarbon. However, with linear hydrocarbons it can be attempted according to the aforesaid, to regard *e.g.* k_z/k_u as equal to ratio of the 'cross-sections of attack' of the corresponding molecules. In the given case this is

the ratio of the number of carbon atoms participating in the double bond of E, $n_{E,C=}$, to the total number of the carbon atoms of A, $n_{A,C-}$, *i.e.*

$$\frac{k_z}{k_u} \simeq \frac{n_{E,C=}}{n_{A,C-}} = \varphi \tag{27}$$

Similarly, the following assumption may also be justified:

$$\frac{k_z}{k_v} \simeq \frac{n_{E,C=}}{n_{E,C-}} = \psi \tag{28}$$

where the meaning of $n_{E,C-}$ follows from the aforesaid. On comparing the k_z/k_u values in Table V with φ calculated according to (27), it may be seen that, with the exception of the systems No. 2, 3, 6 and 7, the agreement is very good or at least acceptable.

This train of thought can be concluded with the statement (which at the same time supports the reasoning used when simplifying Eq. (9)) that although the rate constant combination $\frac{k_u}{k_v+k_z}$ cannot be determined from the experimental data, here too, it can be assumed that:

$$1 + \psi \simeq \frac{k_v + k_z}{k_v} \qquad \text{and} \qquad \frac{\psi}{\varphi} \simeq \frac{k_u}{k_v}$$

from where

$$\frac{k_u}{k_v + k_z} \simeq \frac{\psi/\varphi}{1 + \psi} = \frac{n_{A,C-}}{n_{E,C-}} \cdot \frac{n_{E,C-}}{n_{E,C-} + n_{E,C=}} = 1,$$

since A and E contain an identical number of carbon atoms, so that

$$n_{A,C-} = n_{E,C-} + n_{E,C=} .$$

If the relative rate constants shown in Table IV and the concrete conditions of the irradiation experiments are known, there is a possibility for determining the actual values of the reaction rates in column 5 of Table I. These actual values help to provide a deeper understanding and evaluation of the protective processes occurring in the hydrocarbon mixtures investigated and, on the other hand, give a possibility to check the correctness of the computation scheme used.

Thus, knowing the amount of hydrogen gas formed upon irradiation (mole H_2/h), the quantity of the activated molecules A^x formed in the primary process of the interaction between radiation and matter, and subsequently undergoing reactions under hydrogen formation, has been calculated (mole

of activated molecule/h). Using this value, the $G_A x$-values have been calculated for the full series of mixtures. According to expectation, these values actually varied linearly as function of the electron fractions. The $G_A x$-values extrapolated to zero concentration of the unsaturated component agree, within experimental error, with the G_{H_2}-value of pure component A, supporting the assumption discussed earlier that in absence of unsaturated bonds, H_2 is formed quantitatively from the A^x molecules.

Table VI

The average k_r/k_s [C], f and k_z/k_u constants, the 1—f and $\Delta\varepsilon$ values for the types of hydrocarbon mixtures

No.	Type of mixture	$\frac{k_r}{k_s}$ [C]	$f = \frac{k_t}{k_t+k_q}$	$\frac{k_z}{k_u}$	$1-f$	$\Delta\varepsilon$ (eV)
1.	Branched-chain–open-chain	3.0	0.8	0.0	0.20	3—4
2.	Monoalkene–alkane	27.0	0.44	0.3	0.54	2.5
3.	Isolated diene–alkane	32.0	0.42	0.5	0.58	1.4
4.	Cumulated diene–alkane	30.0	0.34	0.7	0.66	1.1
5.	Conjugated diene–alkane	25.0	0.18	0.6	0.82	0.6
6.	Benzene–alkane	12.0	0.13	0.9	0.87	0.3
7.	Cyclooctatetraene–alkane	28.0	0.1	0.9	0.9	0.1

Fig. 5 shows the $G_A x$-values calculated in this manner for the *n*-heptane–*n*-heptene mixture as a function of the electron fractions (the G_{H_2}-value measured for pure *n*-heptane is 4.56).

To illustrate that the relative rate constants obtained from the experimental results are realistic, using the G_{H_2}-values for the mixtures of *n*-heptane with *n*-heptene, the $G_{H_2,A}$-values of hydrogen formed from the saturated hydrocarbon have been determined, on the one hand with the aid of the denominator of Eq. (21), and on the other hand, by means of the relative rate constants. As shown by Fig. 6, the G_{H_2}-values calculated by the two methods are in good agreement.

Our findings can be summarized as follows.

1) The first formal observation which can be made in connection with the constants $\frac{k_r}{k_z}$ [C], f and $\frac{k_z}{k_u}$ listed in Table IV is that the mixtures investigated can be arranged *on the basis of the constants characteristic of them* into groups, and these groups are characterized by the fact that each of them contains E-type components with double bonds of identical type. The average values of the constants $\frac{k_r}{k_z}$ [C], f and $\frac{k_z}{k_u}$ are listed in Table VI. We are of the opinion that this fact implies deeper correlations.

a) Our kinetic investigations on the saturated–unsaturated (open-chain–branched-chain) hydrocarbon mixtures lead to the conclusion that hydrogen evolution proceeds predominantly according to the reaction scheme shown in Fig. 1/a. Thus, the difference between the actual G_{H_2}-values of saturated–unsaturated hydrocarbon mixtures and the values calculated on the basis of the composition, is due to energy transfer from the more radiation-sensitive component to the less radiation-sensitive component, and from the 'capture' of the H· atoms formed.

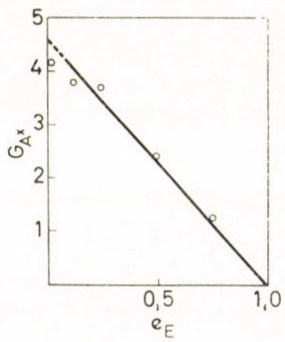


Fig. 5. Variation of the *G*-value of the 'active molecules' A^x formed in the initial process of interaction between radiation and matter as a function of the electron fraction of the unsaturated component, in *n*-heptane–1-heptene mixtures.

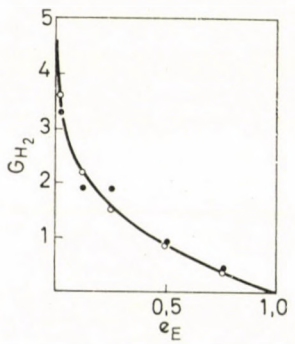


Fig. 6. G_{H_2}-values of *n*-heptane as a function of the electron fraction of *n*-heptene. ● = according to the denominator of Eq. (21). *o* = on the basis of the average rate constant combinations

b) We wish to add a further important supplement to the data in Table IV. By dividing the steady-state rates of the monomolecular decomposition of E^x according to the Eqs. (*t*) and (*t*) + (*q*), the value $f = \dfrac{k_t}{k_t + k_q}$ is obtained, which, in addition to the energy transfer factor, can serve as a number characteristic of the so called 'physical protective effect'. When changing the nature and the concentration of *E*, $(1 - f)$ will indicate the relative weight of those processes involving the E^x molecules, which do not result in H· atom formation (but give rise primarily to energy dissipation). According to Table VI, the smaller the energy difference $\Delta\varepsilon$ between the first electron excitation level and the C—H bond energy in the case of E^*, the more predominant the physical protective effect, *i.e.* the loss of energy by E^x without decomposition in processes (*t*) and (*q*) (*cf.* mixtures No. 2 to 7 in Table

* Excitation energies represent the average values of various data published in the literature. Dissociation energies were considered at a value of 4.2 eV = 97 kcal/mole.

VI). In straight–branched-chain hydrocarbon mixtures, the physical protective effect plays but a subordinate role, but nevertheless, in the given case this is the only likely reason causing deviation of the G_{H_2}-values of such mixtures from the calculated values (*cf.* mixtures No. 1 in Table VI).

The f values of monoalkenes and isolated dienes also merit some consideration. As evidenced by Tables IV and V, the agreement is very good, which is obviously due to the fact that the structure of the isolated double bonds does not differ significantly from that of the monoalkene double bonds. In view of what was said in the introductory part about the course of the G_{H_2} curves, it is not surprising that the f-values obtained for the mixture containing a cumulated diene is in fairly good agreement with the f value characteristic of the mixtures of monoalkenes with isolated dienes.

There is good agreement also between the f-value for cyclooctatetraene (with a conjugated bond system) and that for conjugated dienes (particularly for cyclic conjugated dienes).

It can be established from what was said so far that energy transfer is not the only important factor in the evaluation of the protective effect, but it is also essential to know how much energy transferred from the more radiation-sensitive to the less radiation-sensitive component is utilized for the production of H· atoms, and how much is lost in other (particularly physical) processes.

2) On the basis of our investigations, it seems reasonable to assume that statistical laws can be relied upon in the evaluation of the reaction possibilities of H·-atoms.

3) The relative rate constants, $k_r/k_s[C]$ and k_z/k_u, obtained by kinetic calculations, and f explain the fact mentioned in the introduction that the value of G_{H_2} diminishes in the hydrocarbon groups listed there. Though Table V is self-evident, it seems justified to point out the most interesting details.

a) The more pronounced G_{H_2}-diminishing effect of conjugated dienes relative to that of isolated and cumulated dienes can be ascribed to their higher ability to lose their excitation energy without decomposition leading to hydrogen radicals.

b) The fact that benzene at low concentrations has a weaker G_{H_2}-diminishing action than other unsaturated hydrocarbons, can be explained on the basis of the data in Tables II, IV and V by its relatively low energy transfer coefficient.

4) The present studies permitted the determination of the relative rate constants, characteristic of the individual steps of radiation-chemical hydrogen evolution in a variety of saturated–unsaturated (open-chain–branched-chain) hydrocarbon mixtures. Unfortunately, there was no possibility to compare these data with the results of other studies. We found data in the literature,

suitable for this purpose, only for the cyclohexane–benzene system. As shown by the numerical values given in Section 3 and the relevant data in Table V, there is a fairly good agreement between the k_r/k_S values published and those determined by us (1.15 l/mole [3], 0.74 l/mole [10], 0.84 l/mole [5], 1.1 l/mole).

REFERENCES

1. FÖLDIÁK, G., WOJNÁROVITS, L.: Acta Chim. Acad. Sci. Hung. **67**, 221 (1971)
2. FÖLDIÁK, G., WOJNÁROVITS, L.: Acta Chim. Acad. Sci. Hung. **67**, 209 (1971)
3. MANION, J. R., BURTON, M.: J. Phys. Chem. **56**, 560 (1952)
4. BURTON, M.: Proc. of the Sec. Tihany Symp. on Radiation Chemistry, p. 3. Akadémiai Kiadó, Budapest, 1967
5. MERKLIN, J. F., LYPSKY, S.: J. Phys. Chem. **68**, 3297 (1964)
6. L. S. POLAK: Physico-chemical Particularities of the Radiolysis of Hydrocarbons (in Russian), Proc. 2nd Federal Conf. Radiation Chem. Moscow, 1960, p. 262
7. VOEVODSKII, V. V., MOLIN, Yu. N.: Rad. Res. **17**, 366 (1962)
8. HARDWICK, T. J.: Phys. Chem. **66**, 2132 (1962)
9. YANG, J. Y., MARCUS, I.: J. Phys. Chem. **69**, 3113 (1965)
10. FREEMAN, G. R.: J. Chem. Phys. **33**, 71 (1960)
11. FREEMAN, G. R.: Rad. Res. Rev. **1**, 1 (1968)
12. HARDWICK, T. J.: J. Phys. Chem. **66**, 291 (1962)
13. HATANO, Y., SHIDA, S.: J. Chem. Phys. **46**, 4784 (1967)
14. HATANO, Y., SHIDA, S., SATO, S.: Bull. Chem. Soc. Japan **41**, 1120 (1968)
15. DYNE, O. J., JENKINSON, W. M.: Canad. J. Chem. **38**, 539 (1960)
16. DYNE, O. J., JENKINSON, W. M.: Canad. J. Chem. **39**, 2163 (1961)
17. FREEMAN, G. R.: Canad. J. Chem. **38**, 1043 (1960)
18. STONE, J. A., DYNE, P. J.: Rad. Res. **17**, 359 (1962)
19. RAJBENBACH, L. A., KALDOR, M.: J. Chem. Phys. **47**, 242 (1967)
20. HOROWITZ, A., RAJBENBACH, L. A.: J. Chem. Phys. **48**, 4278 (1968)
21. FEJES, P., VARGA, K.: Communications of the ACM (In press.)
22. DYNE, O. J., DENHARTOG, J., SMITH, D. R.: Discuss. Faraday Soc. **36**, 135 (1963)

László WOJNÁROVITS
Pál FEJES
Budapest XII., Konkoly Thege M. út.

Acta Chimica Academiae Scientiarum Hungaricae Tomus 69 (2), pp. 203–214 (1971)

ABHÄNGIGKEIT DER SAUERSTOFFÜBERSPANNUNG VON DER AKTIVITÄT DES WASSERS, II

WIRKUNG DER ALKALIMETALLIONEN IN SCHWEFELSAURER LÖSUNG

T. ERDEY-GRÚZ, M. GALLYAS und É. SZETEY

(Lehrstuhl für physikalische Chemie und Radiologie der Eötvös Loránd Universität, Budapest)

Eingegangen am 18. März 1970

Es wurde die Steigerung der Überspannung der elektrolytischen Sauerstoffentwicklung durch Li^+-, Na^+-, K^+- und Cs^+-Ionen in 0,1 *n* Schwefelsäurelösung untersucht, wobei die Aktivität des Wassers durch Auflösung von Kaprolaktam zwischen den Grenzen $a_w = 0{,}998$—0,738 verändert wurde. Die untersuchten Ionen erhöhen wohl die Überspannung, ändern jedoch die Form der Polarisationskurve nicht wesentlich und auch die Steilheit (die Konstante *b*) der Tafelschen Geraden wird nur wenig verändert.

In den Lösungen mit hoher Wasseraktivität ($a_w = 0{,}998$) ist die Reihenfolge der überspannungssteigernden Wirkung bei gleicher Ionenkonzentration $Cs^+ < Li^+ < Na^+ < K^+$, während die Reihenfolge in Lösungen mit verhältnismäßig geringen Wasseraktivitäten ($a_w = 0{,}778$ und 0,738) $K^+ < Na^+ < Li^+ < Cs^+$ ist.

In Lösungen mit $a_w = 0{,}906$ ist die Reihenfolge bei Ionenkonzentrationen von 0,005 *n* $Cs^+ < Na^+ < Li^+ < K^+$. Bei steigender Konzentration des K^+-Ions nimmt jedoch seine überspannungssteigernde Wirkung ab, und von der Konzentration 0,065 *n* an ist die Reihenfolge $K^+ < Cs^+ < Na^+ < Li^+$.

Diese Versuchsergebnisse weisen darauf hin, daß diejenigen Alkalimetallionen, die nicht größer als die Wassermoleküle sind, sich auch in dieser Beziehung anders verhalten, als die größeren Ionen und daß ihre Wirkung auch davon abhängig ist, ob die Zusammensetzung der Lösung in jenem Bereich liegt, wo der Aktivitätskoeffizient des Wassers mit zunehmender Wasserkonzentration zunimmt oder in jenem Bereich, wo dieser mit zunehmender Wasserkonzentration abnimmt.

Die elektrolytische Sauerstoffentwicklung ist sowohl in praktischer als auch in theoretischer Hinsicht von großer Bedeutung; ihr komplizierter und auch von den Bedingungen abhängiger Reaktionsmechanismus ist jedoch noch keineswegs eindeutig geklärt. Die Ergebnisse der zahlreichen diesbezüglichen Untersuchungen geben kein befriedigendes Bild über alle der Teilreaktionen des Anodenvorganges [1]. Dies ist hauptsächlich darauf zurückzuführen, daß je nach den Bedingungen der Reaktion vielerlei Intermediärprodukte entstehen können, von denen manche mit dem Anodenmetall verschiedene Oberflächenverbindungen bilden, am Metall adsorbiert bzw. darin gelöst werden können. Bezüglich der Kompliziertheit der Verhältnisse genügt es, z. B. auf die Arbeit von DAMJANOVIC, DEY und BOCKRIS [2] hinzuweisen und daran zu erinnern, daß — gemäß der theoretischen Untersuchung von MILNER [3] über aus konsekutiven Teilvorgängen zusammengesetzten Reaktionen — selbst dann 18 Elementarvorgänge möglich sind, wenn nur vier Intermediäre (OH, O, O_2H, O_2H^-) bei der anodischen Sauerstoffentwicklung aus alkalischer Lösung angenommen werden, und daß aus diesen 18 Teilvorgängen selbst

unter Berücksichtigung der beschränkenden Bedingungen 8568 Reihen von Simultangleichungssystemen aufgestellt werden können. Die Information über den Zusammenhang zwischen den unmittelbar meßbaren Parametern, die durch die Lösung dieser Gleichungssysteme geliefert werden könnte, würde es zur Zeit kaum ermöglichen, unter den reell vorstellbaren Alternativen die der Wirklichkeit entsprechende auszuwählen. Es ist also auch weiterhin wichtig, die Überspannung der elektrolytischen Sauerstoffentwicklung, d. h. eine der wichtigsten Offenbarungen des Elektrodenreaktionsmechanismus, unter gut definiert meßbaren und veränderbaren Bedingungen experimentell zu untersuchen. Solche Untersuchungen tragen selbst dann zu der Klärung der Verhältnisse bei, wenn ihre Ergebnisse zur Bestätigung eines der prinzipiell möglichen Reaktionsmechanismen nicht ausreichen, bzw. wenn sie zwar mit irgendeinem möglichen Mechanismus in Einklang stehen, jedoch keinen eindeutigen Beweis dafür liefern können, daß derselbe Zusammenhang zwischen den unmittelbar gemessenen Parametern innerhalb der Versuchsfehler nicht auch aus einem anderen Mechanismus abgeleitet werden könnte.

Als Fortsetzung unserer früheren Untersuchungen über die Abhängigkeit der Überspannung von der Aktivität des Wassers bei der elektrolytischen Sauerstoffentwicklung [4] wurde die Wirkung der Alkalimetallionen in Schwefelsäurelösungen bei verschiedenen Aktivitäten des Wassers untersucht.

Bezüglich der Alkalimetallionen haben ERDEY-GRÚZ und SAFARIK festgestellt [5], daß sie in Schwefelsäurelösungen die Überspannung der anodischen Sauerstoffentwicklung steigern. Diese Wirkung wurde dann eingehender durch FRUMKIN [6] und FRUMKIN, KAGANOWITSCH, JAKOWLEWA und SOBOL [7] untersucht. Als Erklärung nehmen sie an, daß der — durch die Chemisorption des Sauerstoffes an der Platinoberfläche entstehende — Oberflächenkomplex Pt—O einen Dipol bildet, dessen negativer Pol in Richtung zur Lösung orientiert ist, und daß Metallkationen an diesem Pol adsorbiert werden. Diese verstärken die Bindung der adsorbierten Anionen, wodurch die Stabilität der adsorbierten Schicht gesteigert und folglich die Sauerstoffentwicklung erschwert wird. In vorliegender Arbeit haben wir untersucht, wie weit die Veränderung der Aktivität des Wassers die Verhältnisse ändert.

Versuchsverfahren

Die Polarisationskurven, welche die Abhängigkeit der Überspannung von der Stromstärke beschreiben, sowie die Aktivität des Wassers wurden in der früher beschriebenen [4, 8] Versuchseinrichtung bei 25 °C in Sulfatlösungen mit verschiedenen pH-Werten bestimmt, in denen die Aktivität des Wassers (a_w) 0,998, 0,906, 0,778 und 0,738 betrug. Die Aktivität des Wassers wurde durch Auflösen von 5, 10 bzw. 15 Mol/Liter ε-Kaprolaktam eingestellt.

Zur Untersuchung der Wirkung von Alkalimetallionen wurden Li_2SO_4, Na_2SO_4, K_2SO_4 bzw. Cs_2SO_4 in Konzentrationen von 0,005—0,15 *n* in 0,1 *n* Schwefelsäurelösung gelöst, wodurch der pH nicht wesentlich verändert wurde. Höhere Salzkonzentrationen konnten nicht verwendet werden, da dabei der Nichtelektrolyt ausgesalzt wurde.

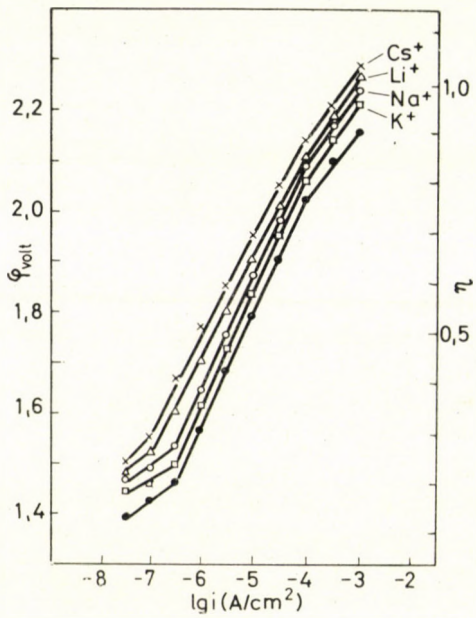


Abb. 1. Polarisationskurve einer 0,1 *n* Schwefelsäurelösung mit 0,05 *n* Alkalisulfatzusatz bei der Wasseraktivität $a_w = 0{,}778$. (Mit ● bezeichnet der in Lösung ohne Zusatz gemessene Wert.)

Versuchsergebnisse

Wirkung der Alkalimetallionen. In Abb. 1 ist die Abhängigkeit des Polarisationspotentials φ (gegenüber einer in derselben Lösung befindlichen Wasserstoffelektrode) bzw. der Überspannung η von der Stromdichte i in 0,1 *n* Schwefelsäurelösung, welche verschiedene Alkalimetallsulfate in gleicher Konzentration (0,05 *n*) enthielt, bei konstanter Wasseraktivität ($a_w = 0{,}778$) und pH = 1,65 dargestellt. In dem untersuchten Stromdichtebereich (10^{-8}—10^{-3} A/cm²) entspricht die Form der Überspannungskurve der Tafelschen Gleichung, setzt sich jedoch aus drei Teilen mit unterschiedlichen Neigungswinkeln zusammen. Die Änderung des Neigungswinkels erfolgt bei der Stromdichte von ungefähr 10^{-7} und 10^{-4} A/cm². Die Polarisationskurven in Lösungen mit anderen Wasseraktivitätswerten ergaben ein ähnliches Bild. Der erste und

dritte Teil ist im untersuchten Stromdichtebereich recht kurz und oft gar nicht vorhanden (siehe Tab. I, in der die Tafelsche Konstante $b = \frac{d\eta}{d \lg i}$ der Polarisationskurven angeführt ist, die bei Schwefelsäurelösungen mit verschiedenen Wasseraktivitäten und gleichen Konzentrationen des Alkalimetallsulfat-Zusatzes gemessen wurden).

Tabelle I

b-Werte der Tafelschen Gleichung in 0,1 n Schwefelsäurelösungen mit verschiedenen Werten der Wasseraktivität a_w und 0,05 n Alkalisulfatzusatz. (b_1, b_2 und b_3 entsprechen steigenden Stromdichtebereichen)

a_w	Li_2SO_4			Na_2SO_4			K_2SO_4			Cs_2SO_4		
	b_1	b_2	b_3	b_1	b_2	b_3	b_1	b_2	b_3	b_1	b_2	b_3
0,998	—	0,15	—	0,11	0,17	—	0,11	0,16	—	0,10	0,17	—
0,906	—	0,17	—	0,11	0,20	0,13	0,08	0,23	0,13	—	0,22	0,12
0,778	0,07	0,19	0,16	0,07	0,22	0,15	0,05	0,23	0,15	0,09	0,20	0,15
0,738	0,09	0,18	—	0,10	0,16	—	0,10	0,19	0,15	0,10	0,17	—

Aus der Tabelle ist ersichtlich, daß die Steilheit b_1 des ersten Teiles der Tafelschen Kurven ungefähr halb so groß ist, wie die Steilheit b_2 des mittleren Teiles, während die Steilheit des dritten Teiles b_3 zwischen diesen beiden Werten liegt. Die Abhängigkeit der Werte von der Art des Alkalimetallions ist gering. Mit abnehmender Aktivität des Wassers nimmt b_1 anfänglich ab und dann zu; b_2 nimmt anfänglich zu und dann ab; b_3 nimmt dagegen monoton zu. Der Inflexionspunkt der Veränderung von b_1 und b_2 liegt im Bereich $a_w = 0{,}906$—0,778, wo der Aktivitätskoeffizient des Wassers ein Minimum aufweist [4].

In Abb. 2 ist die Abhängigkeit des Polarisationspotentials φ bzw. der Überspannung η von der Konzentration des Salzzusatzes dargestellt, für drei verschiedene Stromdichtewerte, die den drei Teilen der Tafelschen Kurve entsprechen; diese Kurven wurden bei vier verschiedenen — jedoch jeweils konstanten — Wasseraktivitäten bestimmt. Wie ersichtlich, nimmt die Polarisationsspannung bzw. die Überspannung bei allen Alkalimetallionen und Stromstärken meistens linear mit der Konzentration der Alkalimetallionen zu. Die Reihenfolge der Wirkung der Alkalimetallionen ist jedoch in hohem Maße von der Aktivität des Wassers abhängig. Bei der höchsten Wasseraktivität (Abb. 2*a*, $a_w = 0{,}998$) ist die Reihenfolge der überspannungssteigernden Wirkung $Cs^+ < Li^+ < Na^+ < K^+$. In Lösungen in denem die Aktivität des Wassers durch Kaprolaktam auf den Wert von $a_w = 0{,}906$ herabgesetzt wurde (Abb. 2*b*), ist der Zusammenhang nur dann linear, wenn die Konzentration des Salzzusatzes c_{Ion} höher als 0,01 *n* ist. In verdünnteren Lösungen erfolgt durch die

Wirkung der Li^+- und Na^+-Ionen ein steilerer Anstieg der Überspannung. Bei K^+-Ionen nimmt die überspannungssteigernde Wirkung nur bis 0,01 *n* mit der Konzentration des Salzzusatzes zu; bei höheren Konzentrationen nimmt die Wirkung linear ab. Auch die Reihenfolge der übrigen Metallionen weicht von der für $a_w = 0{,}998$ gefundenen ab: es ist $Cs^+ < Na^+ < Li^+$. Bei den Lösungen mit $a_w = 0{,}906$ ist der Unterschied zwischen der Wirkung der ver-

Tabelle II

$\frac{\Delta\varphi}{\Delta c_{ion}}$ [*Steilheit der Kurven* $\varphi(\eta) - c$] *ausgedrückt in der Einheit V/Val/Liter für 0,1 n* H_2SO_4-*Lösungen mit Alkalisulfatzusatz, bei drei Stromdichten und verschiedenen Werten der Wasseraktivität*

(In Klammern die Steilheit der Strecke $c = 0{,}005$—$0{,}010$ Val/Liter)

a_w	10^{-3} A/cm²				10^{-5} A/cm²				10^{-7} A/cm²			
	Li_2SO_4	Na_2SO_4	K_2SO_4	Cs_2SO_4	Li_2SO_4	Na_2SO_4	K_2SO_4	Cs_2SO_4	Li_2SO_4	Na_2SO_4	K_2SO_4	Cs_2SO_4
0,998	1,5	1,6	1,7	1,7	1,3	1,5	1,5	1,2	1,1	0,7	0,8	1,2
0,906	(6,6)	(—)	(5,0)	(—)	(9,4)	(11,4)	(7,8)	(5,2)	(7,2)	(12,4)	(4,0)	(—)
	2,0	2,3	—2,0	2,2	2,3	2,1	—2,0	2,1	2,5	1,9	—1,3	1,6
0,778	1,8	1,7	1,7	1,8	1,3	1,3	1,2	1,1	1,1	1,1	1,1	1,3
0,738	0,5	0,5	0,7	0,5	0,4	0,8	0,7	0,3	0,9	0,7	0,7	0,7

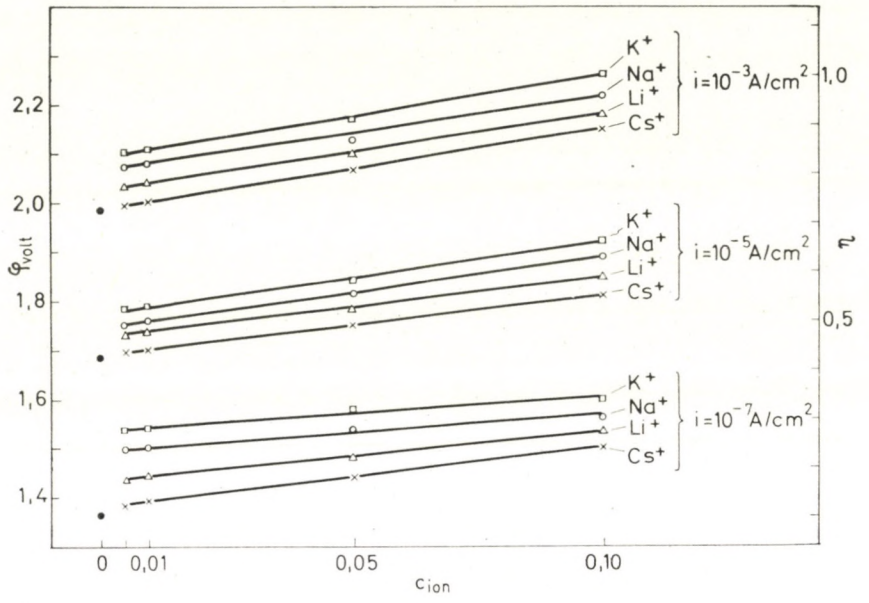
schiedenen Ionen höher als bei den übrigen untersuchten Lösungen mit höherer bzw. geringerer Wasseraktivität.

In den Lösungen mit geringerer Wasseraktivität (Abb. 2*c*, $a_w = 0{,}778$ und Abb. 2*d*, $a_w = 0{,}738$) ist die Reihenfolge der Wirkung der Ionen $K^+ < Na^+ < Li^+ < Cs^+$ und nimmt mit der Konzentration (zumindest in dem durch die Aussalzwirkung beschränkten Konzentrationsgebiet) linear zu.

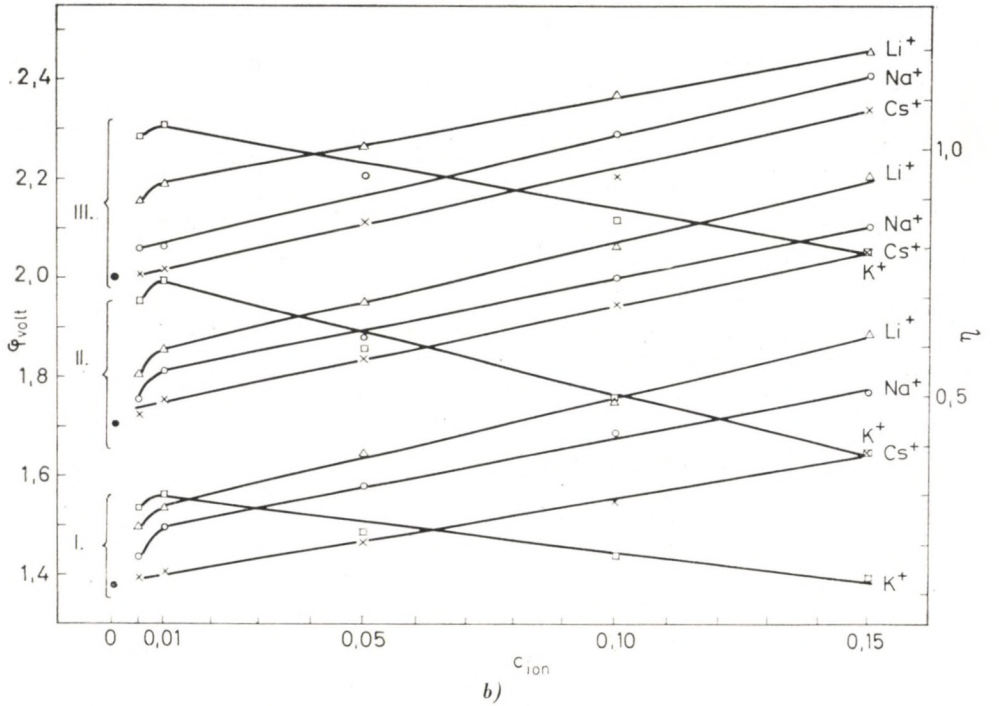
In Tab. II sind die Steilheiten der Kurven φ—c zusammengefaßt. Wie ersichtlich, werden die Kurven mit abnehmender Aktivität des Wassers in sämtlichen Fällen anfänglich steiler und dann flacher. Die Richtung der Veränderung wird in demselben Gebiet $a_w = 0{,}906$—$0{,}778$ umgekehrt, wie die Veränderung der Steilheit der Tafelschen Kurven. Die Werte für die verschiedenen Alkalimetallionen sind annähernd gleich und nehmen mit steigender Stromdichte in gleichem Maße zu, mit der Ausnahme der Wirkung des Lithiumions in Lösungen mit $a_w = 0{,}906$.

Die Abhängigkeit der Polarisationsspannung bzw. der Überspannung von der Aktivität des Wassers ist in Abb. 3 für drei verschiedene Ionenkonzentrationen (Abb. 3*a*, 3*b*, 3*c*) bei dreierlei Stromdichten dargestellt.

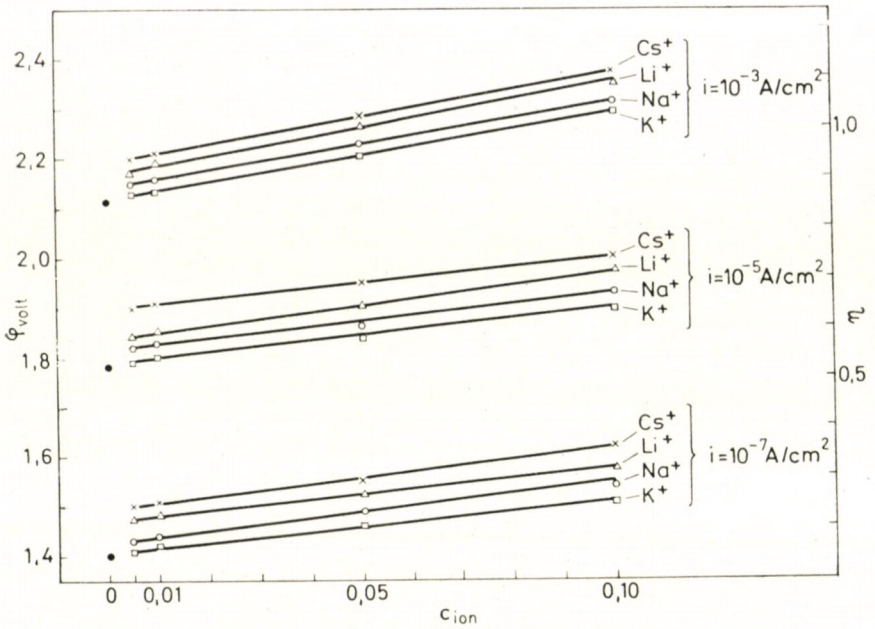
Wie ersichtlich, nimmt die Überspannung — abgesehen von einigen Ausnahmen — im Gebiet $a_w = 0{,}998$—$0{,}906$ zu und im Gebiet $a_w = 0{,}906$—$0{,}778$ zuerst ab und dann zu. Eine Ausnahme bilden die Caesiumionen enthaltenden


K+
Na+
Li+
Cs+
i=10⁻³A/cm²
i=10⁻⁵A/cm²
i=10⁻⁷A/cm²
2,2
2,0
1,8
1,6
1,4
φvolt
1,0
0,5
η
0
0,01
0,05
0,10
cion

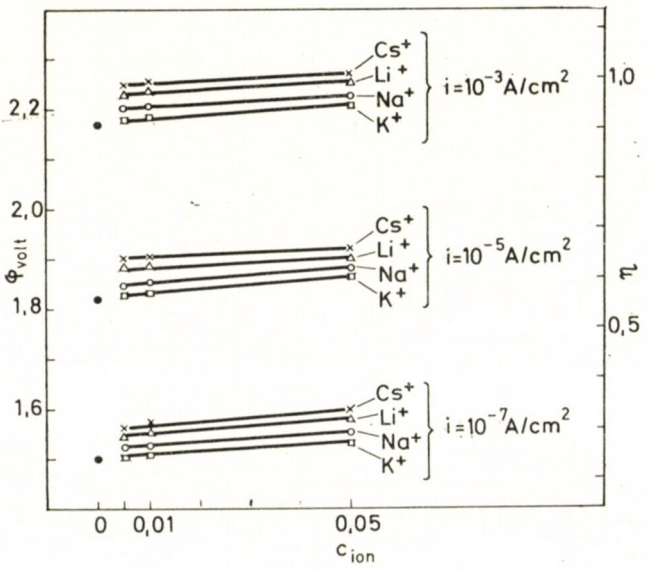
a)


2,4
2,2
2,0
1,8
1,6
1,4
φvolt
III.
II.
I.
Li+
Na+
Cs+
K+
1,0
0,5
η
0
0,01
0,05
0,10
0,15
cion

b)

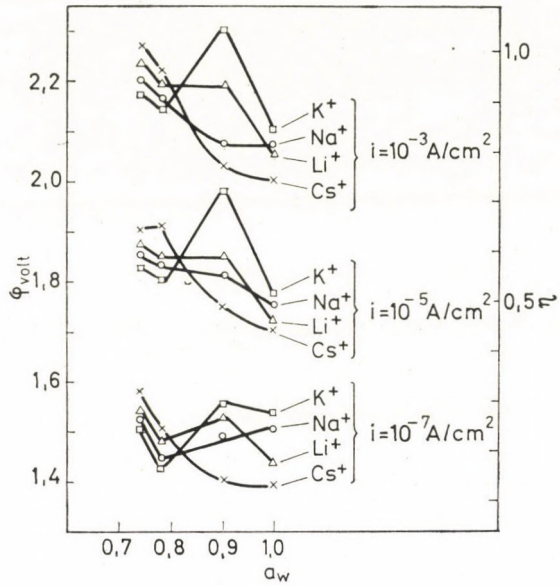


c)

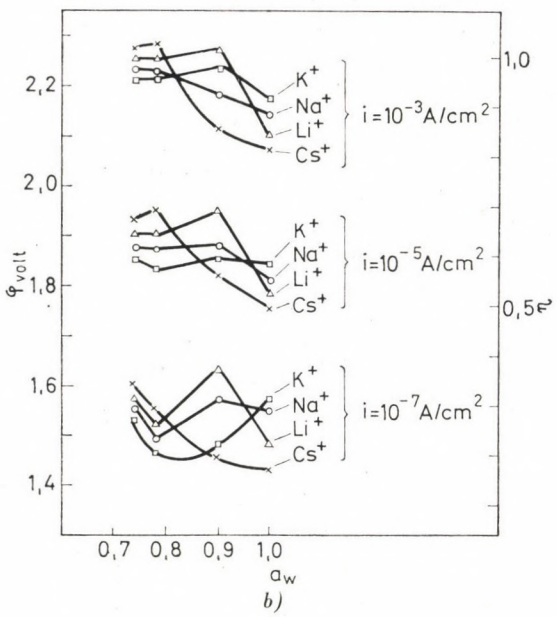


d)

Abb. 2. Veränderung des Polarisationspotentiales in Abhängigkeit von der Konzentration der Alkalimetallionen bei konstanter Stromdichte. (Mit ● bezeichnet der in der Lösung ohne Zusatz gemessene Wert.) *a)* Aktivität des Wassers $a_w = 0{,}998$. *b)* Aktivität des Wassers $a_w = 0{,}906$. (I: $i = 10^{-7}$ A/cm², II: $i = 10^{-5}$ A/cm², III: $i = 10^{-3}$ A/cm².) *c)* Aktivität des Wassers $a_w = 0{,}778$. *d)* Aktivität des Wassers $a_w = 0{,}738$


2,2
2,0
1,8
1,6
1,4
φvolt
1,0
0,5η
K+
Na+
Li+
Cs+
i=10⁻³A/cm²
i=10⁻⁵A/cm²
i=10⁻⁷A/cm²
0,7 0,8 0,9 1,0
aw

a)


2,2
2,0
1,8
1,6
1,4
φvolt
1,0
0,5η
K+
Na+
Li+
Cs+
i=10⁻³A/cm²
i=10⁻⁵A/cm²
i=10⁻⁷A/cm²
0,7 0,8 0,9 1,0
aw

b)

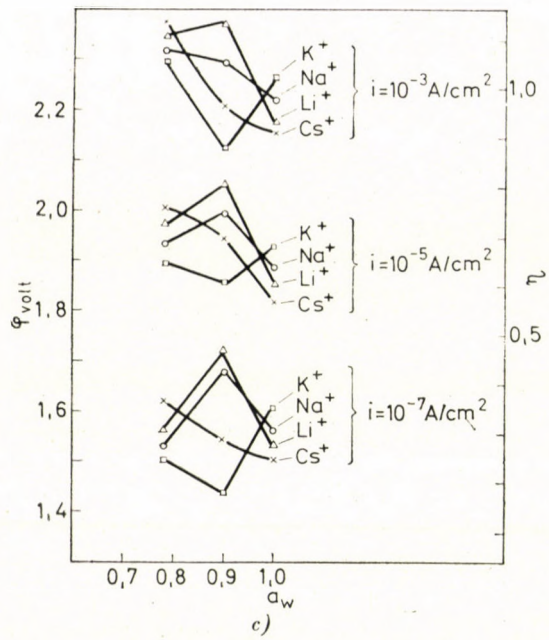


Abb. 3. Überspannungssteigernde Wirkung der Alkalimetallionen in Abhängigkeit von der Aktivität des Wassers in 0,1 *n* Schwefelsäurelösung. *a)* Konzentration des Alkalisulfats $c_{ion} = 0{,}01$ *n*. *b)* Konzentration des Alkalisulfats $c_{ion} = 0{,}05$ *n*. *c)* Konzentration des Alkalisulfats $c_{ion} = 0{,}10$ *n*

Lösungen, bei denen die Überspannung mit abnehmender Wasseraktivität beinahe in gesamten untersuchten Bereich zunimmt. Die Lösung mit 0,1 *n* Kaliumionengehalt weist ebenfalls ein abweichendes Verhalten auf: die Überspannung nimmt mit abnehmender Wasseraktivität im Bereich $a_w = 0{,}998$—0,906 ab und nimmt im weiteren, wie bei den übrigen Ionen, zu.

Diskussion der Ergebnisse

Anschließend an die Deutung unserer früheren Ergebnisse [4, 5] ist hinsichtlich der Wirkung der Alkalimetallionen besonders hervorzuheben, daß diese Ionen einerseits die Überspannung der elektrolytischen Sauerstoffentwicklung bereits bei äußerst geringen Konzentrationen (0,01 *n*) wesentlich steigern, und daß andererseits die Reihenfolge dieser Ionenwirkung durch die Änderung der Wasseraktivität verändert wird. Diesbezüglich muß freilich in Betracht gezogen werden, daß das im Wasser gelöste Kaprolaktam nicht nur die Aktivität des Wassers herabsetzt, sondern auch dessen Struktur verändern kann. Außerdem befindet sich nun ein neuer Stoff mit hoher Dielektrizitätskonstante in der Lösung, wodurch auch die auf der Anodenoberfläche gebildete Doppelschicht sicherlich geändert wird.

Bereits aus der Tatsache, daß die Überspannung durch Akalimetallionen in äußerst geringen Konzentrationen merklich verändert wird, kann gefolgert werden, daß die Wirkung dieser Ionen kaum auf einer Strukturveränderung im Inneren der Lösung beruht, sondern durch ihren Einbau in die Doppelschicht hervorgerufen wird. Die unmittelbare Adsorption an der — unter den gegebenen Versuchsbedingungen positiv geladenen — Platinoberfläche ist unwahrscheinlich, umsomehr als diese Oberfläche infolge der Vorbehandlung mit chemisorbiertem Sauerstoff bedeckt ist. Es ist jedoch wahrscheinlich, daß das in Richtung der Lösung befindliche Sauerstoffatom des auf der Oberfläche gebildeten Pt—O-Komplexes, zumindest partiell, negativ geladen ist. Die Alkalimetallionen werden dann auf sekundäre Art an diesen Sauerstoffatomen — eventuell auch an den primär adsorbierten SO_4^{2-}-Ionen — adsorbiert. Dadurch wird ein Teil der Wassermoleküle von der Anodenoberfläche verdrängt bzw. die verbleibenden Wassermoleküle werden derart deformiert, daß die Aktivierungsenergie der Sauerstoffentwicklung erhöht wird. (Daß der entwickelte Sauerstoff bei verdünnten sauren Lösungen und geringen Stromdichten aus Wasser stammt, ist eine allgemein akzeptierte Annahme [1, 6].)

Aus den Verhältnissen der überspannungssteigernden Wirkung der Alkalimetallionen meinen wir auf zwei Haupteffekte folgern zu können. Der erste steht mit den Abmessungen des Kations in Zusammenhang. Je größer der Ionenradius ist, desto mehr Platz nimmt das Ion an der Oberfläche ein, d. h. umso mehr Wassermoleküle werden verdrängt. Der zweite Haupteffekt stammt wohl von der Ladungsdichte des Ions: je höher die Ladungsdichte an der Ionengrenze ist, umso mehr werden dadurch die benachbarten Wassermoleküle polarisiert und ihre Wasserstoffbindungen mit weiteren benachbarten Wassermolekülen deformiert. Derartige Deformationen können allerdings durch Ionen, die größer als K^+-Ionen sind, auch bloß infolge ihrer Abmessungen hervorgerufen werden.

Aufgrund unserer Versuchsergebnisse scheint es, daß der entscheidende Effekt in Lösungen mit hoher Wasseraktivität (siehe Abb. 2*a*) im Falle der Li^+-, Na^+- und K^+-Ionen die Wasserverdrängung infolge des Ionenvolumens ist. Da jedoch diese Ionen nicht größer sind, als die Wassermoleküle und auch in den Strukturhohlräumen des Wassers Platz nehmen können, deformieren sie die Wasserstruktur in diesem Fall hauptsächlich nicht durch ihr Volumen, sondern durch ihr elektrisches Feld. Die Aktivierungsenergie der Sauerstoffentwicklung aus Wasser wird durch diese Ionen in der Reihenfolge ihrer Abmessungen erhöht. Das große Cs^+-Ion scheint dagegen infolge seiner Größe die Wasserstoffbindungen der Wassermoleküle und dadurch die Struktur des Wassers so zu deformieren, daß die Aktivierungsenergie der Sauerstoffentwicklung aus Wasser weniger ansteigt, als in Gegenwart der kleineren Ionen.

Bei Lösungen mit verhältnismäßig geringen Wasseraktivitäten (a_W = = 0,778 und 0,738, siehe Abb. 2*c* und 2*d*) wird die Reihenfolge der Wirkungen

umgekehrt: $K^+ < Na^+ < Li^+ < Cs^+$. Bei den drei Ionen, die nicht größer als das Wassermolekül sind, wird die Überspannung umso mehr gesteigert, je kleiner das Ion ist, d. h. je höher die Ladungsdichte an seiner Grenze ist. Das große Cs^+-Ion paßt auch in diesem Fall nicht in die Reihenfolge der Größen: seine überspannungssteigernde Wirkung ist stärker, als die des kleinen Li^+-Ions. In diesen Lösungen befinden sich infolge der herabgesetzten Aktivität des Wassers bzw. infolge der Gegenwart des Kaprolaktams mit höherem Dipolmoment als dasjenige des Wassers ($\mu_{Wasser} = 1{,}86$ Debye-Einheiten, $\mu_{Kaprolaktam} = 3{,}88$ Debye-Einheiten) verhältnismäßig wenig Wassermoleküle. Es scheint, daß in diesen Lösungen — infolge der Veränderungen der Flüssigkeitsstruktur und der Doppelschicht — die Aktivierungsenergie der Sauerstoffentwicklung durch die Kationen, die nicht größer als Wassermoleküle sind, umso mehr gesteigert wird, je stärker das elektrische Feld an der Ionengrenze ist. Bei dem Cs^+-Ion wird dagegen diese Wirkung durch seine — aus seinen Abmessungen sich ergebende — deformierende Wirkung auf die Struktur der Flüssigkeit übertroffen.

Die Lösungen mit $a_w = 0{,}906$ nehmen eine Übergangsstellung ein (siehe Abb. 2*b*). Hier nimmt die Überspannung im Ionenkonzentrationsbereich von 0,005—0,15 *n* allein mit steigender Cs^+-Ionenkonzentration linear zu. Durch Na^+- und Li^+-Ionen wird die Überspannung im Bereich 0,005—0,01 *n* sehr steil erhöht und nur über Konzentrationen von 0,01 *n* wird die Veränderung linear. Bei K^+ wächst die überspannungssteigernde Wirkung nur bis zur Konzentration von etwa 0,01 *n* mit der Ionenkonzentration und nimmt dann ab. Bereits von der Konzentration von etwa 0,065 *n* an ist die Wirkung des K^+-Ions geringer als die der übrigen Ionen. Es ist anzunehmen, daß bei diesem Wert der Wasseraktivität eine Umwandlung der Struktur der Flüssigkeit erfolgt, die es nach sich zieht, daß die Reihenfolge der überspannungssteigernden Wirkung der Alkalimetallionen umgekehrt wird. Es ist erwähnenswert, daß in diesem Bereich — gemäß unseren früheren Untersuchungen [4] — der Aktivitätskoeffizient des Wassers mit abnehmender Wasserkonzentration abnimmt, während im vorgenannten Bereich (bei $a_w = 0{,}778$ und 0,738) der Aktivitätskoeffizient mit abnehmender Wasserkonzentration zunimmt. Auch dieser Befund weist darauf hin, daß die Strukturverhältnisse in den beiden Bereichen verschieden sind. Die zu Verfügung stehenden Angaben reichen jedoch noch nicht aus, um ein ausführlicheres Bild über diese Verhältnisse zu erhalten.

LITERATUR

1. Siehe z. B. zusammenfassend HOARE, J. P.: Advances in Electrochemistry and Electrochemical Engineering (ed. P. Delahay) **6,** 201 (1967)
2. DAMJANOVIC, A., DEY, A., BOCKRIS, J. O'M.: Electrochim. Acta, **11,** 791 (1966)
3. MILNER, P. C.: J. Electrochem. Soc., **111,** 228 (1964)
4. ERDEY-GRÚZ, T., GOLOPENCZA-BAJOR, O., GALLYAS, M.: Acta Chim. Acad. Sci. Hung., **50,** 179 (1966)
5. ERDEY-GRÚZ, T., SAFARIK, I.: Trudy 4. Soweschtschanija po Elektrochimii, p. 263. Moskwa, 1959, Acta Chim. Acad. Sci. Hung., **13,** 159 (1957)
6. FRUMKIN, A. N.: Electrochim. Acta, **9,** 465 (1964)
7. FRUMKIN, A. N., KAGANOWITSCH, R. I., JAKOWLEWA, E. W., SOBOL, W. W.: Dokl. Akad. Nauk SSSR, **141,** 1416 (1961)
8. ERDEY-GRÚZ, T., GOLOPENCZA-BAJOR, O.: Acta Chim. Acad. Sci. Hung., **34,** 281 (1962)

Tibor ERDEY-GRÚZ
Miklós GALLYAS
Éva SZETEY
Budapest VIII., Puskin u. 11—13.

Acta Chimica Academiae Scientiarum Hungaricae, Tomus 69 (2), pp. 215—220 (1971)

BESTIMMUNG DES SELBSTDIFFUSIONSKOEFFIZIENTEN DES DIOXANS IN DEN SYSTEMEN DIOXAN–WASSER UND DIOXAN–METHANOL

T. ERDEY-GRÚZ und B. LÉVAY

(Lehrstuhl für physikalische Chemie und Radiologie, Eötvös Loránd Universität, Budapest)

Eingegangen am 24. März 1970

Es wurde der Selbstdiffusionskoeffizient des Dioxans in Dioxan–Wasser- bzw. Dioxan–Methanol-Gemischen bei 25 und 35 °C gemessen.

Im System Dioxan–Wasser besitzt der Selbstdiffusionskoeffizient bei 20 Mol% Dioxan ein Minimum, während die Aktivierungsenergie der Selbstdiffusion bei 15 Mol% Dioxan ein Maximum aufweist. Das Produkt $D^*\eta_r$ ist, vom reinen Dioxan ausgehend, bis zu etwa 40 Mol% annähernd konstant und nimmt bei höheren Wasserkonzentrationen ab.

Im System Dioxan–Methanol nimmt der Selbstdiffusionskoeffizient mit steigendem Methanolgehalt stark und monoton zu; dagegen ändert sich der Wert des Produktes $D^*\eta_r$ innerhalb verhältnismäßig enger Grenzen und besitzt ein flaches Minimum bei 40 Mol%. Die Aktivierungsenergie der Selbstdiffusion hat bei 20 Mol% ein Maximum.

In unserer Arbeit über das System Methanol–Wasser [1] wurde festgestellt, daß der Selbstdiffusionskoeffizient in Abhängigkeit von der Zusammensetzung ein Minimum aufweist, welches der relativ stärksten Flüssigkeitsstruktur entspricht. Um die Frage klären zu können, inwiefern andere Verhältnisse vorliegen, wenn die eine Komponente des Flüssigkeitsgemisches keine Hydroxylgruppen enthält, untersuchten wir den Selbstdiffusionskoeffizienten des Dioxans in Dioxan–Wasser- bzw. Dioxan–Methanol-Gemischen bei 25 und 35 °C.

Von den untersuchten Systemen fanden wir in der Literatur allein für Dioxan–Wasser-Gemische Selbstdiffusions-Daten vor [2—4]. Die Ergebnisse dieser Arbeiten weichen jedoch ziemlich voneinander ab; deshalb hielten wir es für begründet, den Selbstdiffusionskoeffizienten auch in Dioxan–Wasser-Gemischen erneut zu bestimmen, mit dem für die Bestimmung in Dioxan–Methanol-Gemischen angewendeten Verfahren.

Versuchsmethode

Der Selbstdiffusionskoeffizient wurde mit dem Kapillarenverfahren (mit offenem Ende) wie in [1] bestimmt.

Zur Markierung des Dioxans wurde das ^{14}C Isotop verwendet, dessen Aktivität — und somit die Konzentration des markierten Stoffes — nach dem Flüssigkeitsscintillationsverfahren [5, 6] bestimmt wurde.

Es wurden »pro anal.« Reagenzien verwendet; das Dioxan wurde nach dem Verfahren von EIGENBERGER [7] gereinigt. Die Gemische wurden durch Wägung hergestellt.

Die Diffusionsversuche wurden im Thermostaten durchgeführt, die Temperaturkonstanz war $\pm 0{,}01$ °C.

Der Fehler des Selbstdiffusionskoeffizienten beträgt etwa $\pm 0{,}05 \cdot 10^{-5}$ cm²/s.

Versuchsergebnisse

Der Selbstdiffusionskoeffizient D^* des Dioxans nimmt bei Zugabe von Wasser bis zu 20 Mol% Dioxan ab, durchläuft dann ein ziemlich scharfes Minimum und steigt dann verhältnismäßig steil an. In den wenig Dioxan enthaltenden Gemischen besitzt der Selbstdiffusionskoeffizient ungefähr denselben Wert, wie in reinem Dioxan (Abb. 1). Im Bereich von 25—35 °C ist der Ort des Minimums nicht merklich von der Temperatur abhängig. Da sich die Viskosität im System Dioxan–Wasser in Abhängigkeit von der Zusammensetzung nach einer Maximumkurve verändert [8] und die zum Maximum gehörende Konzentration sich kaum von jener Konzentration unterscheidet, bei der das Minimum des Selbstdiffusionskoeffizienten liegt, ändert sich das Produkt des Selbstdiffusionskoeffizienten und der relativen Viskosität $D^*\eta_r$ — welches unter den einfachsten Verhältnissen nach dem Stokesschen Gesetz konstant sein sollte — ohne einen ausgewägten Extremwert aufzuweisen mit der Konzentration (Abb. 1). Aus reinem Dioxan ausgehend ist das Produkt $D^*\eta_r$ bis zu ungefähr 40 Mol% Dioxangehalt annähernd konstant und nimmt dann mit steigendem Wasserhalt mäßig ab.

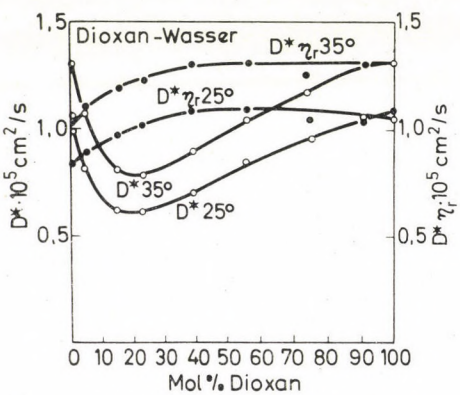


Abb. 1. Selbstdiffusionskoeffizient des Dioxans D^* und Produkt $D^*\eta_r$ in Gemischen aus Dioxan und Wasser bei 25 und 35 °C

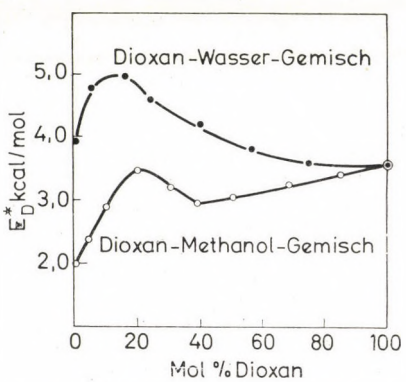


Abb. 2. Durchschnittliche Aktivierungsenergie der Selbstdiffusion des Dioxan E_D^* in Gemischen aus Dioxan–Wasser, bzw. Dioxan–Methanol

Unter der Annahme, daß die Anwendung der Gleichung

$$D^* = A \cdot e^{-E_D^*/RT} \tag{1}$$

im gegebenen Temperaturbereich gestattet ist, wurde aus der Temperaturabhängigkeit des Selbstdiffusionskoeffizienten die durchschnittliche Aktivierungsenergie der Selbstdiffusion E_{D^*} in Abhängigkeit von der Zusammensetzung des Gemisches berechnet. Die Ergebnisse dieser Berechnungen sind in Abb. 2 dargestellt. Aus reinem Dioxan ausgehend ändert sich die Aktivierungsenergie mit zunehmender Wasserkonzentration anfangs kaum, steigt dann etwas steiler an und durchläuft bei etwa 15 Mol% Dioxan ein ausgeprägtes Maximum.

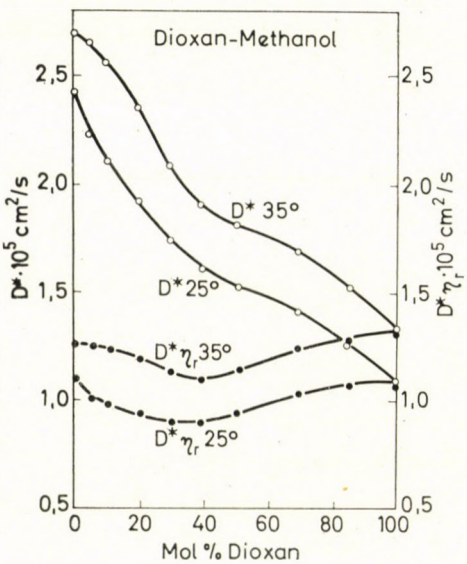


Abb. 3. Selbstdiffusionskoeffizient des Dioxans D^* und Produkt $D^*\eta_r$ in Gemischen auf Dioxan und Methanol bei 25 und 35 °C

Im System Dioxan–Methanol steigt der Selbstdiffusionskoeffizient bei beiden untersuchten Temperaturen mit zunehmender Methanolkonzentration stark und monoton an (Abb. 3). Das Produkt $D^*\eta_r$ ist jedoch wesentlich weniger konzentrationsabhängig als in wäßrigen Mischungen und durchläuft ein flaches Minimum, welches bei 25 °C ungefähr bei 30 Mol%, bei 35 °C ungefähr bei 40 Mol% Dioxan liegt. Dies weist darauf hin, daß die Änderung des Selbstdiffusionskoeffizienten mit der Zusammensetzung größtenteils die Folge der Viskositätsänderung ist [9].

Ausgehend von reinem Dioxan nimmt die Aktivierungsenergie der Selbstdiffusion bei Zugabe von Wasser bis zu ungefähr 40 Mol% ab, steigt dann an und durchläuft bei 20 Mol% Dioxan ein Maximum, wonach ihr Wert bis zum reinen Methanol steil abnimmt (Abb. 2).

Diskussion der Ergebnisse

In wäßrigen Lösungen kann aus dem bei etwa 20 Mol% Dioxan liegenden Minimum des Selbstdiffusionskoeffizienten und aus dem bei 15 Mol% liegenden Maximum der Aktivierungsenergie der Selbstdiffusion darauf gefolgert werden, daß das Dioxan — ähnlich wie Methanol [1] — in diesem Bereich die Struktur des Wassers verstärkt und daß diese Wirkung in beiden Fällen bei ungefähr gleicher Konzentration am stärksten ist. Dies steht in Einklang mit der Theorie von SAMOJLOW [10] über die Struktur von aus Wasser und Nichtelektrolyten bestehenden Systemen. Laut dieser Theorie füllen die Moleküle des zugefügten Nichtelektrolyten die Hohlräume in der eisartigen Struktur des Wassers aus und stabilisieren dadurch die Flüssigkeitsstruktur.

Die annähernde Konstanz des Produktes $D^*\eta_r$ in Gemischen mit mehr als 40 Mol% Dioxangehalt deutet darauf hin, daß das Wasser die Flüssigkeitsstruktur des Dioxans in diesem ziemlich breiten Konzentrationsbereich nicht wesentlich verändert, und daß die Wasserstruktur noch nicht merklich ausgebildet ist. Dies steht in Einklang mit den Ergebnissen von ERDEY-GRÚZ und NAGY-CZAKÓ [11] hinsichtlich der Überführungszahl des Wasserstoffions in diesen Gemischen.

Im Bereich hoher Wasserkonzentrationen hängt die beobachtete Abnahme des Produktes $D^*\eta_r$ wahrscheinlich mit der Ausbildung bzw. Verstärkung der Flüssigkeitsstruktur des Wassers zusammen. Daneben kann auch eine Komplexbildung zwischen Wasser und Dioxan eine Rolle spielen.

Die Ergebnisse von FRATIELLO und DOUGLASS [2] sowie CLEMETT [4], die die Diffusionskoeffizienten nach dem NMR Verfahren bestimmt hatten, stimmen im Falle von Gemischen mit höherem Dioxangehalt verhältnismäßig gut mit unseren Ergebnissen überein. Im Bereich höherer Wasserkonzentrationen liegen jedoch wesentliche Abweichungen vor; allerdings sind NMR-Messungen in diesem Bereich weniger genau. Deswegen sind auch die früheren Angaben für die Aktivierungsenergie gerade in der Umgebung des Maximums nicht genügend verläßlich. CLEMETT hat den Selbstdiffusionskoeffizienten des Wassers auch im System Dioxan–Wasser bestimmt. Die Aktivierungsenergie der Selbstdiffusion des Wassers zeigt bei 20—25 Mol% ebenfalls ein geringes Maximum.

Die von BRUN [3] in Gemischen mit hohen Wasserkonzentrationen nach einem dem unseren ähnlichen Verfahren gemessenen Selbstdiffusionskoeffizienten weichen in Gemischen mit hohen Wasserkonzentrationen ebenfalls von unseren Ergebnissen ab, jedoch ist der Verlauf der D^*-Kurve, der Ort des Minimums und der Verlauf der $D^*\eta_r$-Kurve dem von uns bestimmten ähnlich.

Auch andere Eigenschaften des Systems Dioxan–Wasser weisen in der Gegend von 15—20 Mol% Extremwerte auf. So liegt z. B. ein tiefes Minimum der Mischungswärme bei 14,3 Mol% Dioxan vor und das Minimum des Gefrier-

punktes und der Mischungsentropie befindet sich bei derselben Konzentration [12]. Die aus der Temperaturabhängigkeit der Viskosität berechnete Aktivierungsenergie weist bei 15—20 Mol% ein Maximum auf [13]. Einige Verfasser folgern aus dem um 20 Mol% beobachtbaren Extremum auf eine Komplexbildung des Dioxans mit vier Wassermolekülen [13].

Der Selbstdiffusionskoeffizient des Dioxans ändert sich in Gegenwart von Methanol ohne Extremum mit der Zusammensetzung des Gemisches, jedoch weist die Aktivierungsenergie auch hier ein Maximum bei 20 Mol% Dioxan — d. h. bei einer von System Dioxan–Wasser kaum abweichenden Konzentration — auf. Die Änderungen des Selbstdiffusionskoeffizienten weisen darauf hin, daß der Charakter der Wechselwirkung zwischen Dioxan und Methanol von dem System mit Wasser abweicht. Aus dem Maximum der Aktivierungsenergie kann vermutet werden, daß das Dioxan die Flüssigkeitsstruktur des Methanols ebenfalls verstärkt, jedoch wird diese Wirkung hinsichtlich des Selbstdiffusionskoeffizienten durch irgendeinen anderen Faktor — z. B. durch Umwandlungen von Methanol–Dioxan-Komplexen — verdeckt. Das bei etwa 40 Mol% Dioxan beobachtbare Minimum der Aktivierungsenergie zeigt sich auch als Minimum des Produkts $D^*\eta_r$. Es ist bemerkenswert, daß der Selbstdiffusionskoeffizient des Dioxans in Gemischen mit Methanol höhere Werte aufweist, als in den Gemischen entsprechender Konzentration mit Wasser, obwohl die Aktivierungsenergie kleiner ist. Das Produkt $D^*\eta_r$ ändert sich jedoch in beiden Systemen in etwa demselben Bereich.

Es soll noch bemerkt werden, daß die Aktivierungsenergie der Selbstdiffusion des Dioxans, auf die Dioxankonzentration Null extrapoliert, sowohl in Wasser als auch in Methanol annähernd mit der Aktivierungsenergie der Selbstdiffusion des reinen Wassers [14] bzw. des reinen Methanols [1] übereinstimmt. Ein ähnliches Ergebnis wurde auch beim System Methanol–Wasser gefunden [1], wo die Aktivierungsenergie der Selbstdiffusion des Methanols, auf eine Methanolkonzentration Null extrapoliert, ebenfalls ungefähr mit dem Wert für reines Wasser übereinstimmte. Diese Befunde zeigen, daß bei Spurenkonzentrationen der untersuchten Komponente in der Lösung die Eigenbewegung ihrer Moleküle eine etwa gleiche Aktivierungsenergie benötigt, wie die Bewegung der Moleküle des Lösungsmittels. Eine Erklärung hierfür wäre, daß unter diesen Bedingungen die energetische Verhältnisse für die Bewegung der in Spuren vorliegenden gelösten Moleküle identisch mit der energetischen Bedingungen für die Bewegung der Lösungsmittelmoleküle ist, da die Struktur der Flüssigkeit in beiden Fällen beinahe identisch ist.

*

Der Technikerin, Frau B. JANKÓ, sei auch an dieser Stelle für ihre Hilfe in der experimentellen Arbeit gedankt.

LITERATUR

1. ERDEY-GRÚZ, T., FODOR-CSÁNYI, P., LÉVAY, B., SZILÁGYI-GYŐRI, E.: Acta Chim. Acad. Sci. Hung (im Druck)
2. FRATIELLO, A., DOUGLAS, D. C.: J. Mol. Spectroscopy, **11,** 465 (1963)
3. BRUN, B.: Étude des interactions particulaires par mesure des coefficients de self-diffusion, (Thèse), 1967
4. CLEMETT, C. J.: J. Chem. Soc. (A), **1969,** 458
5. LÉVAY, B., FODOR-CSÁNYI, P.: Magy. Kém. Foly., **71,** 356 (1965)
6. FODOR-CSÁNYI, P., LÉVAY, B.: Acta Chim. Acad. Sci. Hung. **47,** 343 (1965)
7. EIGENBERGER, E.: J. Prakt. Chem., **75,** 130 (1931)
8. TIMMERMANS, J.: The Physico-Chemical Constants of Binary Systems in Concentrated Solutions, Vol. 4. p. 14. Interscience Publishers Inc., New York 1960
9. Loc. cit. [8], p. 432.
10. BULAEWA, M. N., SAMOJLOW, O. Ja.: Zh. strukt. chim. **4,** 502 (1963)
11. ERDEY-GRÚZ, T., NAGY-CZAKÓ, I.: Acta Chim. Acad. Sci. Hung. **67,** 283 (1971)
12. GOATES, J. R., SULLIVAN, R. J.: J. Phys. Chem. **62,** 188 (1958)
13. SCHKODIN, A. M., LEWITSKAJA, N. K., LOZHNIKOW, W. A.: Zh. strukt. chim. **38,** 1006 (1968)
14. WANG, J. H.: J. Am. Chem. Soc. **73,** 4181 (1951)

Tibor ERDEY-GRÚZ
Béla LÉVAY
Budapest VIII., Puskin u. 11—13.

Acta Chimica Academiae Scientiarum Hungaricae, Tomus 69 (2), pp. 221–227 (1971)

THIOCARBAMIDDERIVATE MIT TUBERKULOSTATISCHER WIRKUNG, II*

ACYLTHIOCARBAMIDE**

L. Toldy, S. Sólyom, I. Kocka, G. Tóth und I. Tóth

(Institut für Arzneimittelforschung, Budapest)

Eingegangen am 30. Januar 1970

Ausgehend aus den bei 2-Thiohidantoinen und N-Carbalkoxypiperazingruppen enthaltenden Thiocarbamidderivaten beobachteten Zusammenhängen zwischen Struktur und Wirkung wurden 1-Q-3-Acyl- und 1-Q-1-Acylthiocarbamide synthetisiert.

1-Q-3-Acylthiocarbamide entstehen eindeutig in der Reaktion der entsprechenden Amine und Acylisothiocyanate, während die 1-Q-1-Acylderivate durch Acylierung der S-Methoxymethylisothiocarbamide mit Säurehalogeniden und Hydrolyse der Schutzgruppe erhalten wurden. In der letzteren Reaktion wurde in bestimmten Fällen — je nach den Acylierungsmittel und den Substituenten des Thiocarbamids — eine 3-Acylierung beobachtet, deshalb wurden auch die Faktoren untersucht, die die Richtung der Acylierung beeinflussen.

Die 1-(4-Alkoxyphenyl)-3-carbalkoxythiocarbamide erwiesen sich sowohl *in vitro* als auch *in vivo* als stark tuberkulostatische und akut nicht toxische Verbindungen. Am wirksamsten war das 1-(4-Isoamyloxyphenyl)-3-carbäthoxythiocarbamid, dessen Resorptionseigenschaften ebenfalls günstig sind.

In unserer vorangegangenen Mitteilung [1] berichteten wir über *in vitro* wirksame, *in vivo* jedoch toxische 2-Thiohydantoine. Diese Verbindungen gaben den Anlaß zur Herstellung und biologischen Untersuchung von weiteren Verbindungen mit Thiocarbamid-Gerüst.

Unser Ziel war die Herstellung von neuen Derivaten, die strukturell mit den 2-Thiohidantoinen verwandt sind und von denen erwartet werden konnte, daß sie unter Beibehaltung der antituberkulotischen Aktivität weniger toxisch sind.

Bei der Auswahl der herzustellenden Verbindungstypen wurden zwei Ausgangspunkte in Betracht gezogen:

a) Die bereits untersuchten 2-Thiohidantoine [1] können auch als cyclische N-Aryl-N-acylthiocarbamide aufgefaßt werden.



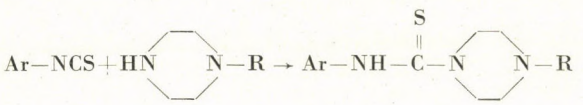
A

* I. Teil: Acta Chim. Acad. Sci. Hung. **68**, 93 (1971)

** Diese Arbeit ist ein Teil der Doktorarbeit von Sándor Sólyom (Eötvös Loránd Universität, Budapest 1969).

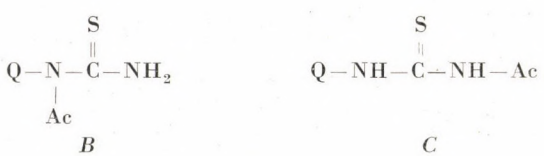
Demzufolge erschien es als begründet, bestimmte offenkettige 1-Aryl-1--acylthiocarbamide (Typ *A*) zu untersuchen; die tuberkulostatische Wirkung dieser Verbindungsgruppe ist bisher noch nicht untersucht worden.

b) Auch eine andere Tatsache lenkte unsere Aufmerksamkeit auf die Acylthiocarbamide, nämlich, daß wir aus Alkoxyphenylisothiocyanaten und N-substituierten Piperazinen einige Thiocarbamidderivate hergestellt hatten (Tabelle I), deren Mehrzahl inaktiv war.



Eine Ausnahme bildeten allein jene Verbindungen, die Carbalkoxy-Substituenten enthielten. Unter diesen war das Carbäthoxyderivat **VII** am aktivsten (6 μg/ml, Dubos). Aus dieser Tatsache konnte gefolgert werden, daß die Carbäthoxygruppe hinsichtlich der tuberkulostatischen Wirkung von Bedeutung sein kann.

Aus diesen beiden Ausgangspunkten ausgehend, erschien es als zweckmäßig, Verbindungen der Typen *B* und *C* zu untersuchen, die als Acylgruppen in erster Reihe Carbalkoxygruppen und als Gruppe Q den Substituenten 4-Alkoxyphenyl enthalten



Die Verbindungen des Types *C* können durch die Reaktion von Acylisothiocyanaten und den betreffenden Aminen eindeutig gewonnen werden (Tabelle II).

Um die Verbindungen des Typs *B* herzustellen, erschien die unmittelbare Acylierung von monosubstituierten Thiocarbamiden aufgrund von Literaturangaben [2, 3] aussichtsreich; bei dieser Reaktion können jedoch im Prinzip drei Acylisomeren entstehen:

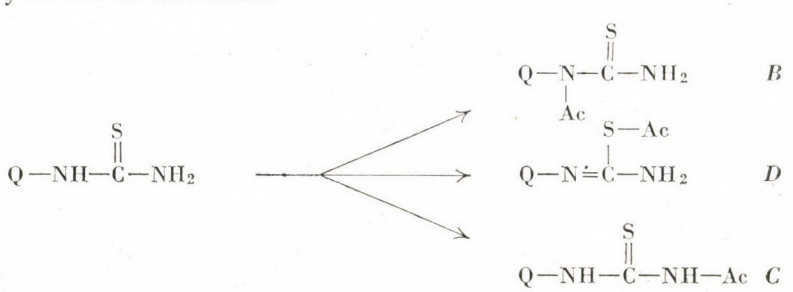
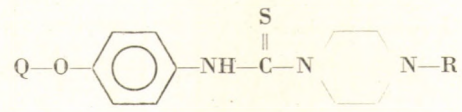
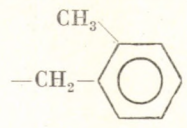
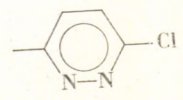
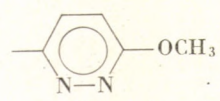
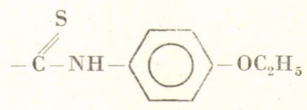
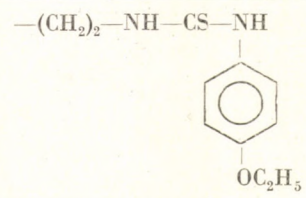
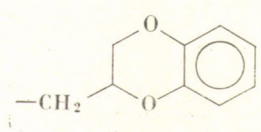
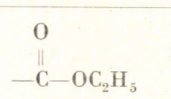
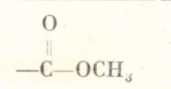
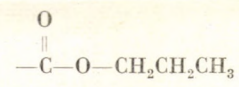
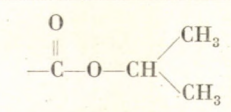
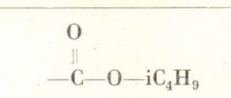
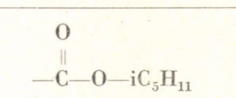
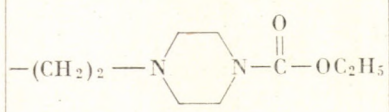
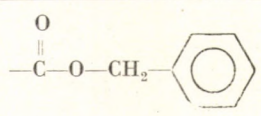
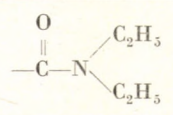
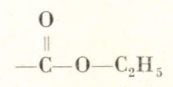
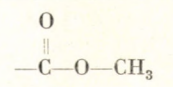
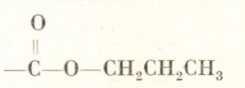
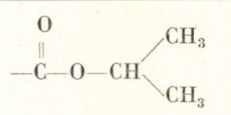
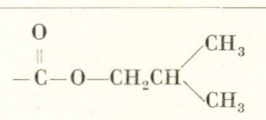
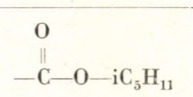


Tabelle I

1-(4-Alkoxyphenylthiocarbamyl)-4-R-piperazine

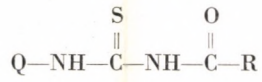


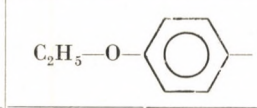
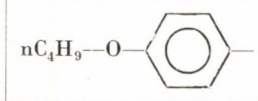
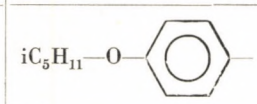
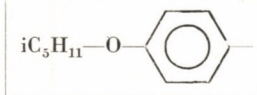
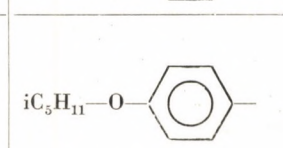
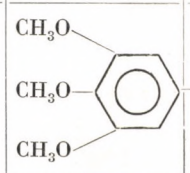
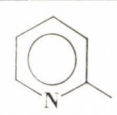
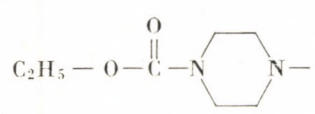
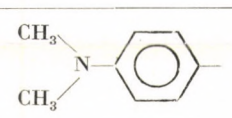
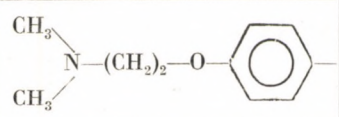
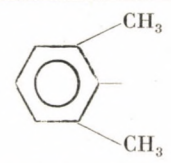
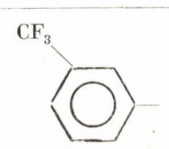
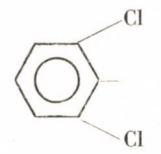
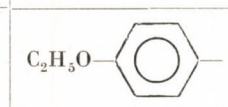
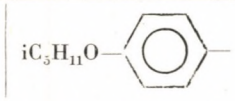
No.	Bezeichnung**	Q	R	Schmelzpunkt*	Analyse									Verfahren, Bemerkung
					Bruttoformel	Molekulargewicht	Berechnet				Gefunden			
							C	H	N	S	C	H	N	S	
I	T 424	C_2H_5—		140 °C	$C_{21}H_{27}N_3OS$	369,51	68,25	7,36	11,37	8,67	68,50	7,57	11,20	8,80	*A* Das verwendete Piperazinderivat nach [22]
II	T 432	C_2H_5—		220 °C	$C_{17}H_{20}ClN_3OS$	377,89	54,03	5,33	18,53	8,48 Cl: 9,38	54,16	5,54	18,53	8,34 Cl: 9,57	*A* Das verwendete Piperazinderivat nach [23]
III	T 433	C_2H_5—		165 °C	$C_{18}H_{23}N_5O_2S$	373,47	57,88	6,20	18,75	8,58	58,04	6,54	18,55	8,83	*A* Das verwendete Piperazinderivat nach [23]
IV	T 440	C_2H_5—		Kochen mit Alkohol 244 °C	$C_{22}H_{28}N_4O_2S_2$	444,60	59,43	6,34	12,60	14,42	59,23	6,25	12,69	14,70	*A* Ausgangsmaterial: Piperazin
V	T 425	C_2H_5		Kochen mit Alkohol 186 °C	$C_{24}H_{33}N_5O_2S_2$	487,66	59,10	6,82	14,36	13,15	59,11	6,48	14,40	13,44	*A* Ausgangsmaterial: N- (β-aminoäthyl)-piperazin
VI	T 434	C_2H_5		183 °C	$C_{22}H_{27}N_3O_3S$	413,52	63,89	6,58	10,16	7,75	63,79	6,77	9,93	7,80	*A* Das verwendete Piperazinderivat nach [24]
VII	T 361	C_2H_5—		134 °C	$C_{16}H_{23}N_3O_3S$	337,43	56,95	6,87	12,45	9,50	57,17	6,93	12,55	9,79	*A* Das verwendete Piperazinderivat nach [12]
VIII	T 472	C_2H_5—		Methanol 134—135°C	$C_{15}H_{21}N_3O_3S$	323,41	55,70	6,54	12,99	9,91	55,78	6,78	12,95	9,97	*A* Das verwendete Piperazinderivat nach [12]
IX	T 491	C_2H_5—		138 °C	$C_{17}H_{25}N_3O_3S$	351,46	58,09	7,17	11,96	9,12	58,30	7,20	12,06	9,22	*A*
X	T 495	C_2H_5—		168—169°C	$C_{17}H_{25}N_3O_3S$	351,46	58,09	7,17	11,96	9,12	58,18	7,29	11,79	9,23	*A*
XI	T 489	C_2H_5—		147 °C	$C_{18}H_{27}N_3O_3S$	365,48	59,15	7,44	11,50	8,77	59,11	7,12	11,46	8,87	*A* Das verwendete Piperazinderivat nach [12]
XII	T 494	C_2H_5—		130 °C	$C_{19}H_{29}N_3O_3S$	379,61	60,11	7,72	11,07	8,44	60,13	7,91	10,99	8,38	*A*
XIII	T 516	C_2H_5—		155 °C	$C_{22}H_{35}N_5O_3S$	449,61	58,76	7,84	15,58	7,13	58,89	7,79	15,64	7,29	*A* Das verwendete Piperazinderivat nach [25]
XIV	T 438	C_2H_5—		135 °C	$C_{21}H_{25}N_3O_3S$	399,50	63,13	6,30	10,52	8,01	63,20	6,52	10,66	8,11	*A* Das verwendete Piperazinderivat nach [26]
XV	T 439	C_2H_5—		Äthanol + Petroläther 106—107°C	$C_{18}H_{28}N_4O_2S$	364,50	59,31	7,74	15,37	8,79	59,44	7,61	15,30	8,77	*A* Ausgangsmaterial nach [27]
XVI	T 462	iC_5H_{11}—		168 °C	$C_{18}H_{27}N_3O_3S$	379,61	60,11	7,72	11,07	8,44	60,05	7,75	11,00	8,38	*A*
XVII	T 473	iC_5H_{11}—		175 °C	$C_{18}H_{27}N_3O_3S$	365,48	59,15	7,44	11,50	8,77	59,20	7,48	11,38	8,78	*A*
XVIII	T 492	iC_5H_{11}—		153 °C	$C_{20}H_{31}N_3O_3S$	393,54	61,03	7,94	10,68	8,14	61,21	8,17	10,54	8,26	*A*
XIX	T 496	iC_5H_{11}—		176—177°C	$C_{20}H_{31}N_3O_3S$	393,54	61,03	7,94	10,68	8,14	61,10	8,00	10,95	8,14	*A*
XX	T 490	iC_5H_{11}—		148—149°C	$C_{21}H_{33}N_3O_3S$	407,56	61,88	8,16	10,31	7,86	61,77	8,05	10,34	8,02	*A*
XXI	T 493	iC_5H_{11}—		139 °C	$C_{22}H_{35}N_3O_3S$	421,59	62,67	8,37	9,97	7,60	62,68	8,48	10,16	7,67	*A*

* Die Produkte wurden aus Äthanol kristallisiert; anderenfalls ist das Lösungsmittel in der Tabelle angeben.
** Im Institut für Arzneimittelforschung übliche Bezeichnungen.

Tabelle II

1-Q-3-*Acylthiocarbamide*

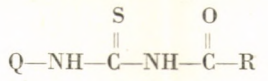


No.	Bezeichnung	Q	R	Schmelzpunkt*	Analyse									Verfahren, Bemerkung
					Bruttoformel	Molekulargewicht	Berechnet				Gefunden			
							C	H	N	S	C	H	N	S	
XXII	T 517		C_2H_5O—	141—142 °C	$C_{12}H_{16}N_2O_3S$	268,33	53,71	6,01	10,44	11,95	53,53	6,11	10,57	12,16	*C*
XXIII	T 548		C_2H_5O—	128 °C	$C_{14}H_{20}N_2O_3S$	296,38	56,73	6,80	9,45	10,82	56,91	7,02	9,50	10,95	*C*
XXIV	T 464		C_2H_5O—	121—122 °C	$C_{15}H_{22}N_2O_3S$	310,40	58,04	7,14	9,02	10,33	58,14	7,27	9,10	10,44	*C*
XXV	T 600		nC_3H_7O—	91 °C	$C_{16}H_{24}N_2O_3S$	324,43	59,23	7,45	8,63	9,88	59,37	7,53	8,84	10,10	*C*
XXVI	T 453			98 °C	$C_{22}H_{28}N_2O_5S$	432,52	61,09	6,52	6,48	7,41	61,13	6,66	6,52	7,53	*C*
XXVII	T 576		C_2H_5O—	102 °C	$C_9H_{11}N_3O_2S$	225,27	47,98	4,92	18,65	14,23	48,28	5,28	19,05	14,59	*C*
XXVIII	T 518		C_2H_5O—	114—115 °C	$C_{11}H_{19}N_3O_4S$	289,35	45,65	6,62	14,52	11,08	45,64	6,70	14,49	11,29	*C* Ausgangsamin nach [12]
XXIX	T 542		C_2H_5O—	193 °C (zersetzt) Benzol	$C_{12}H_{19}N_3O_2S$	267,34	53,91	6,40	15,72	11,99	53,76	6,67	15,89	12,08	*C* Ausgangsamin nach [28]
XXX	T 545		C_2H_5O—	125 °C	$C_{14}H_{21}N_3O_3S$	311,40	53,99	6,80	13,49	10,29	54,08	7,16	13,40	10,26	*C* Ausgangsamin nach [29]
XXXI	T 623		C_2H_5O—	204—205 °C Aceton	$C_{12}H_{16}N_2O_2S$	252,33	57,11	6,39	11,10	12,70	57,22	6,52	11,08	12,68	*C* Identisch mit **LIV** (Tab. III/b)
XXXII	T 635		C_2H_5O—	99 °C	$C_{11}H_{11}F_3N_2O_2S$	292,28	45,20	3,79	9,58	10,97	45,37	4,00	9,67	10,93	*C*
XXXIII	T 622		C_2H_5O—	205—206 °C Aceton	$2_{10}H_{10}Cl_2N_2O_2S$	293,16	40,96	3,44	9,55	10,93 Cl: 24,18	41,11	3.58	9,37	10,50 Cl: 24,38	*C*
XXXIV	20364			184—185 °C	$C_{18}H_{22}N_2OS$	314,43	68,75	7,05	8,91	10,19	68,87	7,08	8,75	10,20	*C*
XXXV	T 497		CH_3—	195—196 °C	$C_{11}H_{14}N_2O_2S$	238,30	55,44	5,92	11,76	13,45	55,82	6,02	11,84	13,56	*C* Identisch mit **XLVIII** (Tab. III/b)
XXXVI	T 549		CH_3—	137—138 °C	$C_{14}H_{20}N_2O_2S$	280,38	59,97	7,19	9,99	11,43	60,15	7,39	9,89	11,54	*C* Identisch mit **XLVII** (Tab. III/b)

* Die Produkte wurden aus Äthanol kristallisiert; anderenfalls ist das Lösungsmittel in der Tabelle angegeben.

Tabelle III/b

1-Q-3-*Acylthiocarbamide*



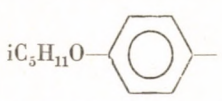
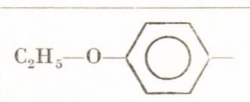
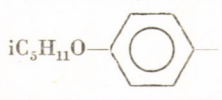
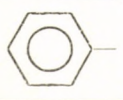
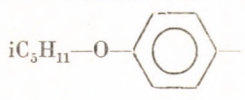
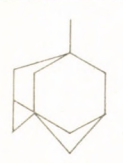
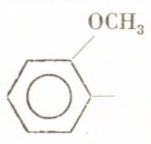
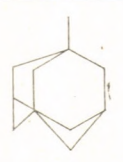
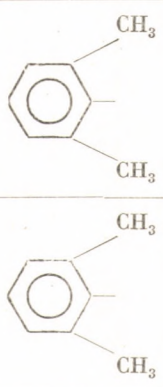
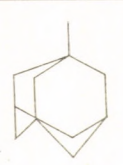
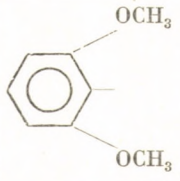
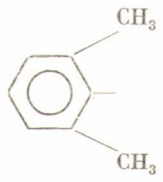
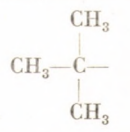
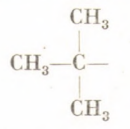
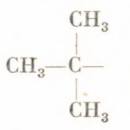
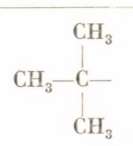
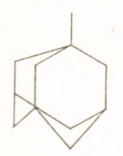
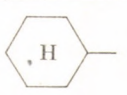
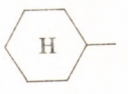
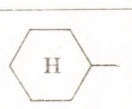
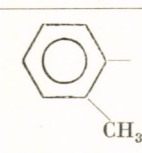
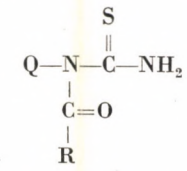
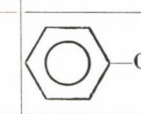
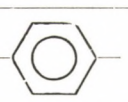
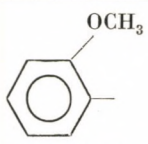
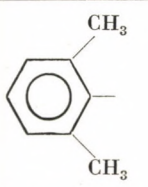
No.	Bezeichnung	Q	R	Schmelzpunkt	Analyse									Verfahren, Bemerkung
					Bruttoformel	Molekulargewicht	Berechnet				Gefunden			
							C	H	N	S	C	H	N	S	
XLVII	T 549		CH_3—	137—138 °C Äthanol	$C_{14}H_{20}N_2O_2S$	280,38	59,97	7,19	9,99	11,43	59,87	7,21	10,05	11,45	*B* Identisch mit **XXXVI** (Tabelle II)
XLVIII	T 497		CH_3—	196—197 °C Äthanol	$C_{11}H_{14}N_2O_3S$	238,30	55,44	5,92	11,76	13,45	55,63	6,18	11,80	13,35	*B* Diese Verbindung ist aus der Literatur bekannt [30] Identisch mit **XXXV** (Tabelle II)
XLIX	20369			133—134 °C Äthanol	$C_{19}H_{22}N_2O_2S$	342,44	66,63	6,47	8,18	9,36	66,75	6,50	7,93	9,26	*B*
L	20416			134—135 °C Äthanol	$C_{23}H_{32}N_2O_2S$	400,56	68,96	8,05	6,99	8,00	68,88	8,05	7,04	8,00	*B*
LI	20415			137—138 °C Äthanol	$C_{19}H_{24}N_2O_2S$	344,46	66,24	7,02	8,13	9,30	66,40	7,12	8,22	9,49	*B*
LII	20335			199 °C Äthanol	$C_{20}H_{16}N_2OS$	342,49	70,13	7,65	8,18	9,36	70,27	7,63	8,26	9,24	*B*
LIII	20433			233 °C Chloroform	$C_{18}H_{20}N_2O_3S$	344,42	62,76	5,85	8,13	9,31	62,64	5,83	8,16	9,38	*B*
LIV	T 623		C_2H_5—O—	204 °C Fraktionierte Kristallisation aus Äthanol	$C_{12}H_{16}N_2O_2S$	252,33	57,11	6,39	11,10	12,70	57,26	6,60	11,27	12,88	*B* Identisch mit **XXXI** (Tabelle II)
LV	20386		C_2H_5—O—	109—110 °C Äthanol	$C_{14}H_{22}N_2O_2S$	282,39	59,54	7,85	9,92	11,35	59,52	7,97	10,05	11,23	*B*
LVI	20387		iC_4H_9—O—	129 °C Äthanol	$C_{16}H_{26}N_2O_2S$	310,45	61,89	8,44	9,02	10,32	61,92	8,59	9,04	10,43	*B*
LVII	20417		CH_3—	211—213 °C (zersetzt) Äthanol	$C_{13}H_{20}N_2OS$	252,37	61,86	7,99	11,10	12,70	61,69	8,11	11,26	12,92	*B*
LVIII	20434		CH_3—	118—119 Äthanol	$C_7H_{14}N_2OS$	174,26	48,24	8,09	16,08	18,39	48,42	8,26	16,10	18,45	*B*
LIX	Só 510		C_2H_5—O—	58 °C Methanol + Fällen mit Wasser	$C_8H_{16}N_2O_2S$	204,29	47,03	7,89	13,71	15,69	47,13	8,11	13,90	15,53	*B*
LX	20419			131—132 °C Äthanol	$C_{12}H_{16}N_2OS$	236,33	60,98	6,82	11,85	13,56	61,24	7,02	11,79	13,67	*B*
LXI	20420			110 °C Äthanol	$C_{16}N_{26}N_2OS$	294,45	65,26	8,90	9,51	10,89	65,09	8,86	9,56	10,90	*B*
LXII	20421		—CH_3	103—104 °C Äthanol	$C_9H_{16}N_2OS$	200,30	53,96	8,05	13,99	16,00	54,23	8,14	13,96	16,15	*B* Diese Verbindung ist aus der Literatur bekannt [31]
LXIII	Só 540		C_2H_5—O—	65 °C Fraktionierte Kristallisation aus Äthanol–Petroläther	$C_{10}H_{18}N_2O_2S$	230,32	52,14	7,87	12,16	13,92	52,24	8,11	12,02	14,19	*B* Diese Verbindung ist aus der Literatur bekannt [32]
LXIV	20422			129—130 °C Äthanol	$C_{15}H_{20}N_2OS$	276,39	65,18	7,29	10,13	11,60	65,05	7,29	10,21	11,70	*B*
LXV	20435	nC_4H_9—		53 °C Petroläther	$C_{12}H_{16}N_2OS$	236,33	60,98	6,82	11,85	13,56	61,03	6,85	11,70	13,54	*B* Diese Verbindung ist aus der Literatur bekannt [33]. Das Reaktionsgemisch wird durch Säulenchromatographie auf Silikagel getrennt (Lösungsmittel Chloroform–Benzol 9 : 1)

Tabelle III/a

1-Q-1-*Acylthiocarbamide*



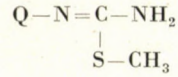
No.	Bezeichnung	Q	R	Schmelzpunkt*	Analyse									Verfahren, Bemerkung
					Bruttoformel	Molekulargewicht	Berechnet				Gefunden			
							C	H	N	S	C	H	N	S	
XXXVII	20280	iC_5H_{11}—O— 	C_2H_5O—	109—110 °C	$C_{15}H_{22}N_2O_3S$	310,40	58,04	7,14	9,02	10,33	57,89	7,13	9,15	10,29	*B*
XXXVIII	20324	iC_5H_{11}—O— 	nC_3H_7O—	128—129 °C	$C_{16}H_{24}N_2O_3S$	324,43	59,23	7,45	8,63	9,88	59,22	7,61	8,56	9,80	*B*
XXXIX	20323	iC_5H_{11}—O— 	iC_4H_9O—	129—130 °C	$C_{17}H_{26}N_2O_3S$	338,46	60,32	7,74	8,28	9,47	60,44	7,74	8,58	9,28	*B*
XL	20393	$iC_5H_{11}O$— 	 —CH_2—O—	140 °C	$C_{20}H_{24}N_2O_3S$	372, 47	64,49	6,49	7,52	8,60	64,35	6,54	7,58	8,55	*B*
XLI	20327	C_2H_5O— 	C_2H_5O—	161—162 °C	$C_{12}H_{16}N_2O_3S$	268,33	53,71	6,01	10,44	11,94	53,51	6,03	10,50	11,66	*B*
XLII	20367	C_2H_5O— 	nC_3H_7O—	170—171 °C	$C_{13}H_{18}N_2O_3S$	282,35	55,29	6,42	9,92	11,35	55,34	6,80	10,00	11,12	*B*
XLIII	20328	C_2H_5O— 	iC_4H_9O—	170 °C	$C_{14}H_{20}N_2O_3S$	296,38	56,73	6,80	9,45	10,81	56,60	6,82	9,30	10,81	*B*
XLIV	20287		C_2H_5O—	150—151 °C	$C_{11}H_{14}N_2O_3S$	254,30	51,95	5,55	11,02	12,60	51,69	5,56	10,97	12,58	*B*
XLV	20289		CH_3—	152—153 °C	$C_{11}H_{14}N_2OS$	222,30	59,43	6,34	12,60	14,42	59,57	6,37	12,60	14,18	*B*
XLVI	Só 542	nC_4H_9—	C_2H_5O—	92—93 °C	$C_8H_{16}N_2O_2S$	204,24	47,03	7,89	13,71	15,69	46,99	7,85	13,69	15,78	*B*

* Sämtliche Produkte wurden aus Äthanol kristallisiert.

In der ersten Stufe entsteht S-Acylisothiocarbamid (*D*), welches instabil ist und durch S → N Acylwanderung N-Acylthiocarbamid (*B* oder *C*) liefert.

Aus Phenylthiocarbamid und Acetylchlorid gelang es DIXON [2, 3], alle drei Acylisomeren, *B*, *D** und *C* herzustellen, aus Chlorkohlensäureäthylester ausgehend konnte jedoch nur das Derivat *B* isoliert werden.

Bei der erneuten Untersuchung der Struktur monosubstituierter S-Alkyl-isothiocarbamide [4] konnten wir feststellen, daß diese in gelöster Form z. B. die Struktur

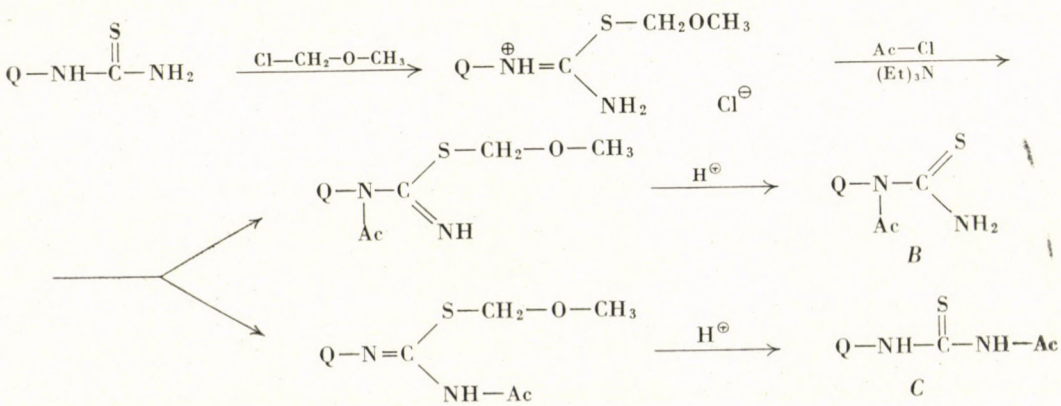


besitzen, und daß Stickstoffatom neben dem Substituenten basischer ist als das andere Stickstoffatom.

Demzufolge konnte erwartet werden, daß bei der Acylierung hauptsächlich das Isomere *B* entsteht. Die Verbindung *B* wünschten wir über Isothiocarbamide herzustellen, welche am S-Atom eine Schutzgruppe enthalten. Für diesen Zweck ist die Methylgruppe ungeeignet, da das bekannte Verfahren zur Spaltung der S-Methylgruppe bei N-Carbäthoxy-S-methyl-isothiocarbamiden nicht zum Ziel führt [5, 6].

Die Methoxymethyl-Schutzgruppe wurde durch FÖLDI und Mitarbeiter [7] mit Erfolg bei der Acylierung des Thiocarbamids mit Sulfonsäurechlorid verwendet. Dabei wurde das Thiocarbamid zuerst mit Chlordimethyläther zu S-Methoxymethyl-isothiocarbamidhydrochlorid umgesetzt und diese Verbindung mit Sulfonsäurechlorid acyliert. Das entstehende N-Sulfonyl-S-methoxymethylisothiocarbamid wurde mit katalytischen Säuremengen zu Sulfothiocarbamid umgesetzt.

Bei der Acylierung von monosubstituierten Thiocarbamiden bedienten wir uns im wesentlichen dieses Verfahrens:



* Das S-Acetylderivat (Typ *D*) existiert nur in Form von seinen Salzen.

In einigen Fällen versuchten wir, das primär entstehende S-Methoxymethylderivat zu isolieren, jedoch gelang es uns nicht, die Verbindung in reinem Zustand herzustellen, da sie allzu zersetzlich war. Deshalb wurde die Acylierung unmittelbar in der acetonischen Lösung des frisch hergestellten S-Methoxymethylisothiocarbamids bei —10 °C, in Gegenwart von Triäthylamin durchgeführt.

Aus den angegebenen Reaktionsgleichungen ist ersichtlich, daß bei der Acylierung auch in diesem Falle nicht allein das Acylthiocarbamid *B*, sondern auch das Isomere *C* entstehen kann. Durch passende Wahl des Substituenten Q und des Acyliermittels konnten beide Verbindungstypen hergestellt werden.

Obwohl die Annahme der höheren Basizität des Stickstoffatoms in Stellung 1 der monosubstituierten S-Alkylthiocarbamide durch das Entstehen des Acylisomeren *B* bestätigt wird, fördert der offensichtlich geringe Basizitätsunterschied zwischen den Stickstoffatomen in Stellung 1 und 3 auch das Entstehen des Isomeren *C*, und zwar besonders dann, wenn stark elektrophile Acylgruppen vorhanden sind. Q- und Acylgruppen mit hohem Raumbedarf wirken ebenfalls in dieser Richtung.

Es ist also verständlich, daß bei der Acylierung mit wenig elektrophilen Chlorkohlensäureestern und bei der Anwendung von verhältnismäßig kleinen Q-Gruppen (z. B. Q = 4-Alkoxyphenyl, Tab. IIIa) der Typ *B* entsteht, während bei Q-Gruppen oder Acylgruppen mit größerem Raumbedarf (z. B. 2,6-Dimethylphenyl, 1-Adamantyl, *terc.* Butyl, **LIV—LVI**, **LIX**, bzw. 1-Adamantoyl, 2,6-Dimethylbenzoyl, **L—LIII**) sowie auch bei stark elektrophilen Acylgruppen (z. B. Acetyl, Benzoyl, **XLVII—XLIX**, **LXII**, **LXV**) die Verbindung *C* gebildet wird. Eine Ausnahme bildet **XLV** (Tab. IIIa), wo trotz des 2,6-Dimethylphenyl-Substituenten mit verhältnismäßig hoher Raumausfüllung die Acylierung mit der stark elektrophilen Acetylgruppe am Stickstoffatom 1 erfolgt.

Die bei der Acylierung erhaltenen Isomeren wurden entweder durch Vergleich mit auf anderem Wege eindeutig herstellbaren 1-Q-3-Acylverbindungen oder — bei den Isomeren *B* — durch die NH_2-Banden im IR-Spektrum identifiziert.

Bei IR-Aufnahmen in fester Phase erscheinen im Bereich von 3400—3150 cm^{-1} die teilweise verschmolzenen monomeren und assoziierten Bandenpaare ν_{as} NH_2 und ν_s NH_2, während in verdünnten apolaren Lösungen allein das monomere Bandenpaar um 3490 und 3310 cm^{-1} auftritt. Demgemäß kann in Aufnahmen mit KBr die Ebene-Deformationsschwingungsband (βNH_2) um 1600 cm^{-1} gut identifiziert werden; diese verschiebt sich in den Aufnahmen mit Lösungsmittel in Richtung der niedrigeren Wellenzahlen [34].

Die hergestellten Verbindungen sind in Tab. IIIa und IIIb enthalten.

Biologische Versuchsergebnisse

a) Sowohl unter den 1-Acylverbindungen (Typ *B*) als auch unter den 3-Acylderivaten (Typ *C*) zeigten allein die mit 4-Alkoxy-, besonders die mit 4-i-Amyloxyphenyl und Carbäthoxygruppen substituierten Thiocarbamide (**XXXVII—XL, XXIV, XXV**) *in vitro* eine bemerkenswerte tuberkulostatische Wirkung (0,4—0,8 μg/ml, Dubos).

b) Die *in vitro* wirksamen 1-Acylderivate (**XXXVII—XLIII**, Tab. IIIa) sind — wie die Thiohidantoine [1] — bei Mäusen stark toxisch; dies ist vermutlich auf die analoge 1-Acylstruktur zurückzuführen.

c) Dagegen sind die 3-Acylverbindungen (**XXII—XXV**, Tab. II) akut nicht toxisch; es ist uns also gelungen, einen neuen antituberkulotischen Thiocarbamidtyp zu finden, der vorteilhafte Eigenschaften besitzt.

d) Als wirksamste Verbindung erwies sich das 1-(4-i-Amyloxyphenyl)-3-carbäthoxythiocarbamid (**XXIV**, Tab. II [8]), welches bei einer *in vitro* Aktivität von 0,8 μg/ml auch bei Mäusen und Meerschweinchen eine ausgesprochene antituberkulotische Wirkung zeigte.

e) Die Resorptionseigenschaften wurden mit der mit ^{35}S markierten Verbindung untersucht; dabei fanden wir einen Blutspiegel von 10 μg/ml, während der Blutspiegel bei Isoxyl (1,3-bis-(4-i-Amyloxyphenyl)-thiocarbamid), wie früher bestimmt [9] und durch uns von neuem untersucht wurde, nur 1—2 μg/ml beträgt.

Experimenteller Teil*

Verfahren A

1-(4-Alkoxyphenylthiocarbamyl)-4-R-piperazine, I—XXI (Tab. I.)

Äquivalente Mengen von 4-Alkoxyphenylisothiocyanat und N-R-Piperazin, in 5 bis 10fachen Alkoholvolumina gelöst, wurden nach Zusammengießen der Lösungen 10—30 Minuten lang im Sieden gehalten. Die gewünschten Produkte wurden aus dem Reaktionsgemisch — gegebenenfalls nach Einkonzentrieren — mit guter Ausbeute ausgeschieden.

Als Isothiocyanat-Komponente wurde das aus der Literatur bekannte 4-i-Amyloxyphenyl- bzw. das 4-Äthoxyphenylisothiocyanat verwendet [10, 11].

Die Literatur über die verwendeten N-R-Piperazine ist in Tab. I enthalten.

Drei, in der Literatur bisher nicht beschriebene N-Carbalkoxypiperazine wurden ähnlich wie das N-Carbäthoxypiperazin [12] hergestellt:

N-Carbo-*n*-propoxypiperazin,
Kp.: 108—110 °C/0,8—1 mm
Analyse: $C_8H_{16}N_2O_2$ (172,23)
N Ber. 16,27, N Gef. 16,05%

N-Carbo-i-propoxypiperazin,
Kp.: 90—92 °C/0,4 mm
Analyse: $C_8H_{16}N_2O_2$ (172,23)
N Ber. 16,27, N Gef. 16,42%

N-Carbo-i-amyloxypiperazin,
Kp.: 102 °C/0,1 mm
Analyse: $C_{10}H_{20}N_2O_2$ (200,28)
N Ber. 13,99, N Gef. 14,10%

* Unkorrigierte Temperaturen.

Verfahren B

Durch die Reaktion von Aminen und Acylisothiocyanaten erhaltene
1-Q-3-Acylthiocarbamide, XXII—XXXVI (Tab. II)

Zu der Lösung des Amins in Benzol oder Aceton wird — unter Rühren und gegebenenfalls unter Kühlung mit kaltem Wasser — die Lösung der äquivalenten Menge des Acylisothiocyanats in Benzol oder Aceton tropfenweise zugefügt. (Das vorangehende Isolieren des Acylisothiocyanats ist nicht notwendig, führt jedoch zu höheren Ausbeuten.) Aus dem Reaktionsgemisch wird das Acylthiocarbamid — gegebenenfalls nach Einkonzentrieren der Lösung — in kristalliner Form ausgeschieden.

Folgende Acylisothiocyanate wurden vor der Verwendung in reiner Form isoliert: Carbäthoxyisothiocyanat [13], 3,4,5-Trimethoxybenzoylisothiocyanat [14]. Die übrigen, nach [15] gewonnenen Acylisothiocyanate wurden zur Herstellung der in Tab. II angeführten Acylthiocarbamide in roher Form verwendet.

Verfahren C

Acylierung der **1-Q-S-Methoxymethylisothiocarbamide, XXXVII—XLVI** (Tab. IIIa) und **XLVII—LXV** (Tab. IIIb)

0,05 Mol monosubstituiertes Thiocarbamid werden in 50 ml abs. Aceton suspendiert; unter Rühren und Kühlen mit kaltem Wasser werden 4,3 g (0,05 Mol) Chlordimethyläther zugefügt. Anschließend wird eine Stunde lang bei Zimmertemperatur gerührt, wobei das Thiocarbamid in Lösung geht. Das Reaktionsgemisch wird mit Eis-Salz-Gemisch auf —10 °C abgekühlt und 14 ml (0,1 Mol) Triäthylamin sowie 0,05 Mol Säurechlorid werden gleichzeitig tropfenweise zugefügt, und zwar mit einer solchen Geschwindigkeit, daß die innere Temperatur nicht über —8 °C ansteigt. Nach Beendigung der Eintragung wird eine halbe Stunde lang unter 0° und weitere 2—3 Stunden lang bei Zimmertemperatur gerührt, das abgeschiedene Triäthylamin-hydrochlorid abfiltriert und mit 3×10 ml abs. Aceton gewaschen. Die acetonische Lösung wird bei 30—35 °C eingedampft und nach Zugabe von 1—2 ml mit Salzsäure angesäuertem abs. Äthanol 2—3 Minuten lang im Sieden gehalten. Das N-Acylthiocarbamid wird aus dem Reaktionsgemisch nach dem Abkühlen bzw. Eindampfen in kristalliner Form gewonnen. Bei diesen Acylierungen wurde stets nur eines der Isomeren erhalten.

Die verwendeten bekannten monosubstituierten Thiocarbamide waren 1-(4-i-Amyloxyphenyl)-thiocarbamid [16], 1-(4-Äthoxyphenyl)-thiocarbamid [17], 1-(2-Methoxyphenyl)-thiocarbamid [17], 1-(2,6-Dimethylphenyl)-thiocarbamid [17], 1-*terc.* Butylthiocarbamid [18], 1-*n*-Butylthiocarbamid [19], 1-Cyclohexylthiocarbamid [20]. Sie wurden nach einem in der Literatur beschriebenen anderen Verfahren [21] hergestellt.

Das 1-(Adamantyl-1)-thiocarbamid war bisher nicht bekannt. Diese Verbindung wurde auf analoge Weise nach [21] aus 1-Aminoadamantan hergestellt.

Schmp.: 173—174 °C
Analyse: $C_{11}H_{18}N_2S$ (210,33)
Ber.: C 62,81, H 8,62, N 13,32, S 15,24%
Gef.: C 62,80, H 8,62, N 13,32, S 15,09%

*

Die IR-Spektren wurden mit einem Zeiss Spektrophotometer IR-10 aufgenommen. Für die Mikroanalysen sei Frau Dr. Lenke Szabó an dieser Stelle gedankt.

LITERATUR

1. Sólyom, S., Koczka, I., Tóth, G., Toldy, L.: Acta Chim. Acad. Sci. Hung. **68,** 93 (1971)
2. Dixon, A. E., Hawthorne, J.: J. Chem. Soc. **91,** 122 (1907)
3. Dixon, A. E., Taylor, J.: J. Chem. Soc. **91,** 912 (1907)
4. Tóth, G., Tóth, I., Toldy, L.: Tetrahedron Letters. **1969,** 5299
5. Lakra, H., Dains, F. B.: J. Am. Chem. Soc. **51,** 2224 (1929)
6. Olin, J. F., Dains, F. B.: J. Am. Chem. Soc. **52,** 3322 (1930)
7. Földi, Z., Gerecs, Á., Demjén, I., Kőnig, R.: U.S. Patent: 2. 444. 926, C.A. **43,** 686 d

8. TOLDY, L., SÓLYOM, S., KOCZKA, I., TÓTH, I.: Ungarisches Patent 156. 045 (1967)
9. WALTER, A. M., HEILMEYER, L.: Antibiotika Fibel, 3. Aufl. G. Thieme Verlag, Stuttgart 1969. S. 564
10. DOUB, L. et al.: J. Am. Chem. Soc. **80,** 2205 (1958)
11. GALSTUCHOWA, N. B., SCHTSCHUKINA, M. N.: Zh. Obschtsch. Chim. **31,** 1090 (1961)
12. STEWART, H. W. et al.: J. Org. Chem. **13,** 134 (1948)
13. TAKAMIZAWA, A., HIRAI, K.: Bull. Chem. Soc. Japan. **36,** 1218 (1963)
14. SMITH, P. A. S., EMERSON, D. W.: J. Am. Chem. Soc. **82,** 3076 (1960)
15. HOUBEN, J., WEYL, TH.: Methoden der organischen Chemie. Band IX., G. Thieme Verlag, Stuttgart 1955. S. 878
16. SPIEGEL, L., SABBATH, S.: Ber. **34,** 1943 (1901)
17. DYSON, G. M., GEORGE, H. J., HUNTER, R. F.: J. Chem. Soc. **1927,** 436
18. SCHMIDT, E. *et al.:* Ann. **568,** 192 (1950)
19. HOFMANN, A. W.: Ber. **7,** 512 (1874)
20. SKITA, A,. ROLFES, H.: Ber. **53,** 1247 (1920)
21. DOUGLASS, J. B., DAINS, F. B.: J. Am. Chem. Soc. **56,** 1408 (1934)
22. STOCK, E. A.: J. Org. Chem. **27,** 308 (1962); Australisches Patent: 229. 238 (1960)
23. BOISSIER, J. P., RATOUIS, R., DUMONT, C.: J. Med. Chem. **6,** 541 (1963)
24. TOLDY, L., TÓTH, I., BORSY, J.: Acta Chim. Acad. Sci. Hung. **49,** 265 (1966)
25. TÓTH, I.: Acta Chim. Acad. Sci. Hung. (unter Druck)
26. GOLDMAN, L., WILLIAMS, J. H.: J. Org. Chem. **18,** 815 (1953)
27. KUSHNER, S. *et al.:* J. Org. Chem. **13,** 144 (1948)
28. GATTERMANN, L., WIELAND, H.: Die Praxis des organischen Chemikers. W. de Gruyter Co., Berlin 1953. S. 273
29. KAYE, I. A., BURLANT, W. J., PRICE, L.: J. Org. Chem. **16,** 1421 (1951)
30. HUGERSHOFF, A.: Ber. **32,** 3649 (1899)
31. ELMORE, D. T., OGLE, J. G., FLETCHER, W., TOSELAND, P. A.: J. Chem. Soc. **1956,** 4458
32. ELMORE, D. T., OGLE, J. G.: J. Chem. Soc. **1960,** 1961
33. ELMORE, D. T., OGLE, J. G.: J. Chem. Soc. **1958,** 1141
34. NAKANISHI, K.: Infrared Absorption Spectroscopy Holden-Day Inc., San Francisco, 1964. S. 38

Lajos TOLDY
Sándor SÓLYOM
István KOCZKA
Gábor TÓTH
István TÓTH

Budapest IV., Újpest, Szabadságharcosok útja 47—49.

Acta Chimica Academiae Scientiarum Hungaricae, Tomus 69 (2), pp. 229–239 (1971)

UNTERSUCHUNGEN ÜBER AROMATISCHE SULFENYLCHLORIDE, II**

REAKTIONEN DES SULFENYLCHLORIDS MIT THIOCARBAMIDEN UND THIOSEMICARBAZIDEN

P. VINKLER*, F. KLIVÉNYI, E. VINKLER, G. STÁJER und A. E. SZABÓ

*(*Zentralforschungsinstitut für Chemie der Ungarischen Akademie der Wissenschaften, Institut für pharmazeutische Chemie der Medizinischen Universität, Szeged)*

Eingegangen am 15. April, 1970

Es wurde die Struktur der in der Reaktion von Thiocarbamid, Thiosemicarbazid und einiger ihrer N-arylsubstituierten Derivate mit *p*-Toluylsulfenylchlorid entstehenden Verbindungen untersucht. Aufgrund IR-spektroskopischer Untersuchungen ergab sich, daß die Substitution in sämtlichen untersuchten Fällen am Schwefelatom erfolgt, und daß in der Reaktion eine Schwefel–Schwefel-Bindung gebildet wird.

Es wurde bewiesen, daß das basische Zentrum beim Thiosemicarbazid und seinen N^4-substituierten Derivaten das Stickstoffatom N^1 ist.

Theoretischer Teil

In der vorliegenden Mitteilung wird über Reaktionen mit Thiocarbamiden und Thiosemicarbaziden berichtet, die im Rahmen unserer Arbeit über die sog. »Sulfenylierungsreaktionen« der Sulfenylchloride mit verschiedenen schwefelhaltigen Verbindungen (siehe [1]) untersucht wurden.

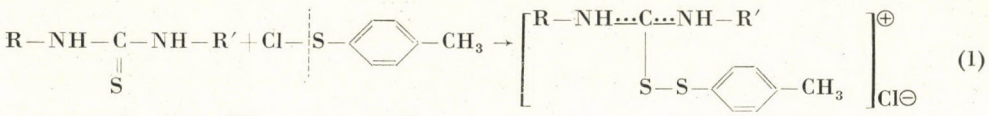
I. Reaktion mit Thiocarbamid

Die säurekatalysierte Reaktion des Thiocarbamids mit *n*-Butyl- bzw. Phenylsulfenylchlorid wurde von KOPYLOWA und FREIDLINA [2] sowie von FIELD und BUCKMAN [3] untersucht. Letztere stellten mit Röntgendiffraktionsmessungen fest, daß dabei das salzsaure Salz des S-Alkyl- bzw. -phenylsulfenylisothiocarbamids entsteht, daß also bei der Sulfenylierungsreaktion eine Schwefel–Schwefel-Bindung gebildet wird. Es schien interessant, diese Untersuchungen auf N-Aryl- bzw. N,N'-Diarylthiocarbamide auszudehnen.

In der Reaktion von Thiocarbamid (**I**), N-Phenylthiocarbamid (**II**) und N,N'-Diphenylthiocarbamid (**III**) mit 1 Mol *p*-Toluylsulfenylchlorid (**IV**) in wasserfreiem Medium (vorzugsweise Dioxan) entstanden — nach unserer Annahme — die salzsauren Salze der entsprechenden S-*p*-Toluylthioisothio-

** Vorgetragen auf der Vortragssitzung der Abteilung für chemische Wissenschaften der Ung. Akademie der Wissenschaften am 29. April 1969.

carbamid-Derivate **V**, **VI** und **VII** mit befriedigender Ausbeute (Gl. 1).



(1)

I, **II**, **III** **IV** **V**, **VI**, **VII**

1) In **I** und **V**: R = R' = H.
2) In **II** und **VI**: R = C_6H_5, R' = H.
3) In **III** und **VII**: R = R' = C_6H_5.

Die Verbindungen **V** und **VI** erwiesen sich als stabil, während **VII** nur im Kühlschrank längere Zeit haltbar war.

Derivate mit bestimmten Substituenten — z. B. N,N'-p-Chlorphenyl- und *p*-Nitrophenylthiocarbamid-Derivate gingen mit dem Sulfenylchlorid keine Reaktion ein. Das Ausbleiben der Reaktion ist vermutlich auf die bei diesen Verbindungen auftretenden Elektronenverschiebungserscheinungen zurückzuführen, da diese die Nukleophilität des Schwefelatoms verringern.

Um die Bindungsstelle der Arylsulfenylgruppe zu bestätigen, wurden die IR-Spektren der Ausgangsstoffe und der Reaktionsprodukte aufgenommen.

Jensen und Nielsen [4] berichten über das Vorkommen von zwei charakteristischen Banden im Bereich von 1400—1700 cm^{-1} (durch diese Verfasser Bande *A* und *B* genannt) in den Spektren von Thiocarbamide, Thiosemicarbaziden und ihren Derivaten. Die Bande *A*, die im wesentlichen von der symmetrischen Plandeformationsschwingung der Aminogruppe herrührt und mit der C—N-Valenzschwingung gekoppelt ist, kommt nur bei Verbindungen mit primären Aminogruppen vor. Bande *B* kann der antisymmetrischen Valenzschwingung der N—C—S-Kette zugeordnet werden, dabei tragen jedoch verschiedene Schwingungsarten von CS-, NH_2- und NH-Gruppen ebenfalls zur Bildung dieser Bande bei. Durch S-Substitution werden beide Banden — dem gesteigerten Doppelbindungscharakter der C—N-Bindung entsprechend — in Richtung höherer Wellenzahlen hin verschoben.

Bande *C* erscheint im Wellenzahlbereich von 1200—1400 cm^{-1}. Sie ist hauptsächlich das Ergebnis von N—C—N-Valenzschwingungen, die mit NH-Schwingungen gekoppelt sind. Durch S-Substitution wird die Bande *C* im allgemeinen in die Richtung der höheren Wellenzahlen verschoben, das Maß der Verschiebung ist jedoch bei verschiedenen Verbindungen recht abweichend [4].

Die Ergebnisse der genannten Verfasser bezüglich der Banden *A*, *B* und *C* wurden auch durch Hallam und Jones bestätigt [5].

Beim Vergleich der Spektren des Thiocarbamids **I** (Abb. 1) und des N-Phenylthiocarbamids **II** (Abb. 2) mit den Spektren ihrer Reaktionsprodukte **V** und **VI** (Abb. 3 und 4) zeigt sich, daß die Banden *A* und *B* der letzteren Verbindungen bei höheren Wellenzahlen liegen (Tab. I). Beim Thiocarbamidderi-

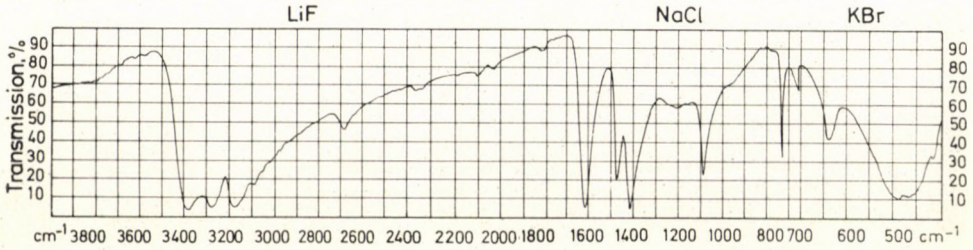


Abb. 1

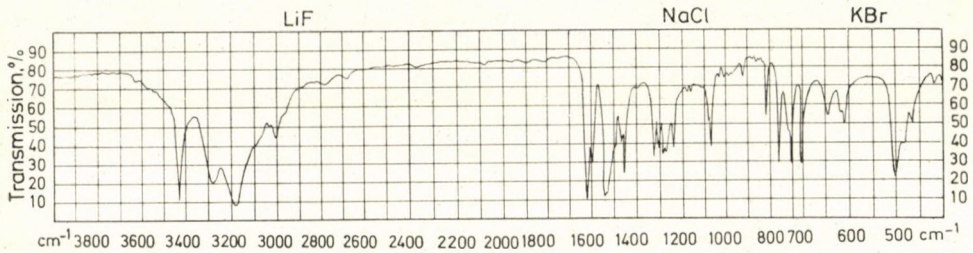


Abb. 2

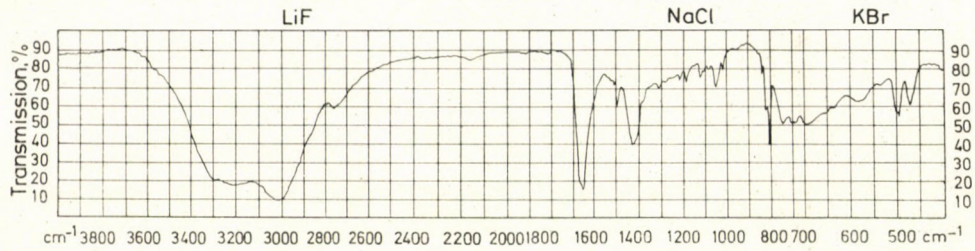


Abb. 3

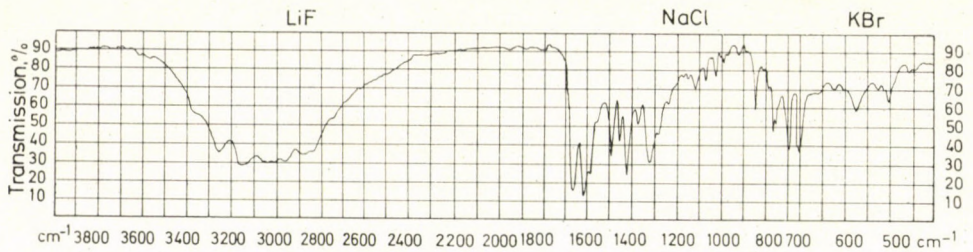


Abb. 4

vat **V** entspricht die schwache Absorption bei 1510 cm^{-1} vermutlich der Bande *B*, da diese im Fall von S-Methylthiuroniumchlorid bei 1520 cm^{-1} und im Fall von S-Benzylthiuroniumchlorid bei 1550 cm^{-1} liegt: in beiden Fällen ist sie sehr schwach [4]. Es kann aber auch angenommen werden, daß die bei 1648 cm^{-1} beobachtbare Schulter der Bande *B* der Verbindung **V** entspricht. Beim N,N'-Diphenylthiocarbamid **III** (Abb. 5) liegt selbstverständlich keine Bande *A* vor und Bande *B* ist bei dem Derivat **VII** in Richtung höherer Wellenzahlen verschoben (Abb. 6, Tab. I). Die NH-Valenzschwingungsbanden liegen

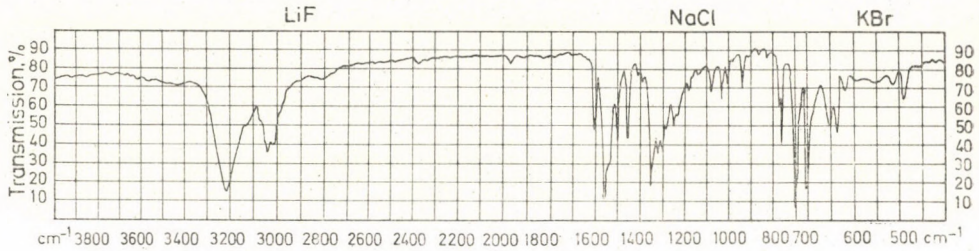


Abb. 5

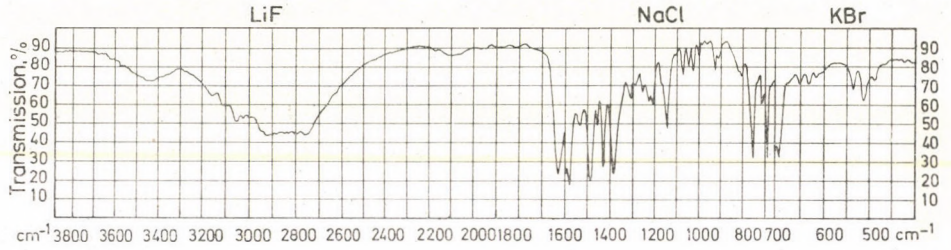
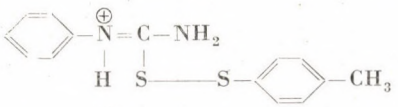


Abb. 6

bei niedrigeren Wellenzahlen und sind breiter, da die salzsauren Salze der Verbindungen vorliegen.

Bei den einzelnen Derivaten können verschiedenartige protonierte Formen zustandekommen. Diese wurden zwar hinsichtlich ihrer Struktur nicht untersucht, es soll jedoch bemerkt werden, daß die aus dem N-Phenylthiocarbamid **II** gewonnene Verbindung **VI** aufgrund der Banden bei 3400, 2600 und 1668 cm^{-1} in festem Zustand vermutlich folgende Struktur besitzt:



VI

Dies ist umsomehr wahrscheinlich, als die Struktur der 1-Aryl-S-methylisothiocarbamid-hydrochloride durch TÓTH und Mitarbeiter [6] aufgrund ihrer NMR- und IR-Spektren mit einer ähnlichen Formel beschrieben wurde.

Aus dem Gesagten ergibt sich, daß die Substitution in der Reaktion von Thiocarbamid und seinen N-substituierten Derivaten mit *p*-Toluylsulfenylchlorid am Schwefelatom verläuft, wobei die salzsauren Salze der S-(*p*-Toluylthio)-isothiocarbamid-Derivate entstehen.

II. Reaktion mit Thiosemicarbazid

In der Literatur konnten wir keine Hinweise über die Sulfenylierungsreaktion von Thiosemicarbazid und seinen N-substituierten Derivaten finden. In unserer Arbeit wurde die Reaktion von Thiosemicarbazid **VIII** und 1-Phenyl-

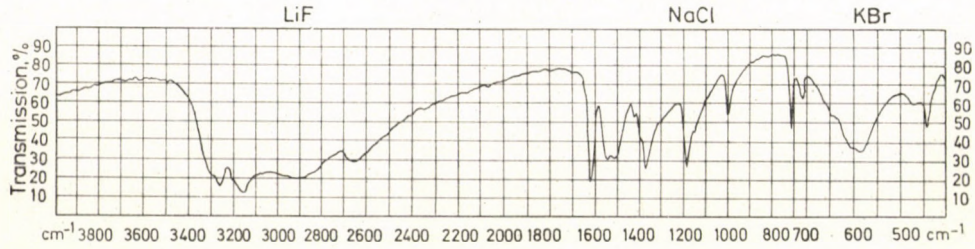


Abb. 7

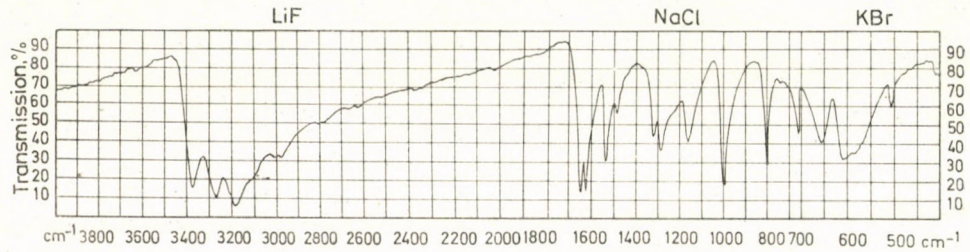


Abb. 8

thiosemicarbazid **IX** mit *p*-Toluyl-sulfenylchlorid **IV** in wasserfreiem Medium untersucht.

Auch in diesem Falle wünschten wir die Struktur der sulfenylierten Thiosemicarbazid-hydrochloride bzw. die Bindungstelle des Arylsulfenyl-Kations durch IR-spektroskopische Untersuchungen zu bestimmen.

Eine Vollanalyse der Spektren von Thiosemicarbaziden ist eine äußerst komplizierte Aufgabe. RAO und Mitarbeiter [7, 8] wiesen darauf hin, daß die Lösung dieser Aufgabe ohne Einbeziehung der Normalkoordinatenanalyse gar nicht möglich ist. Eine gründliche empirische Analyse der Spektren der genannten Verbindungen wurde durch MASHIMA [9], JENSEN und NIELSEN [4] sowie WILES und SUPRUNCHUK [10] angegeben. Die Normalkoordinatenanalyse von Thiosemicarbazid wurde durch VOLKA und HOLZBECHER [11] durchgeführt. Im Spektrum des salzsauren Salzes des Thiosemicarbazids **X** (Abb. 7) erscheinen die charakteristischen Banden der —$\overset{\oplus}{N}H_3$-Gruppe. Es fehlt dagegen die Absorption bei 1647 cm^{-1}, die im Spektrum der Base (Abb. 8) vorliegt und der Aminogruppe des Hydrazin-Teils zugeordnet werden kann. Daraus kann gefolgert werden, daß das Proton — ähnlich, wie bei dem durch MASHIMA [9] untersuchten Semicarbazid — an das Stickstoffatom 1 gebunden ist:

$$\left[\overset{+}{H_3N}-NH-\underset{\underset{S}{\|}}{C}-NH_2\right]Cl^{\ominus}$$

X

Das gleiche Ergebnis wurde bei den potentiometrischen Untersuchungen von BRAIBANTI und Mitarbeiter [12] festgestellt.

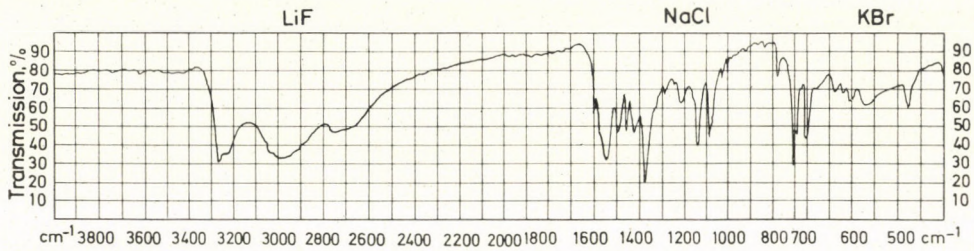


Abb. 9

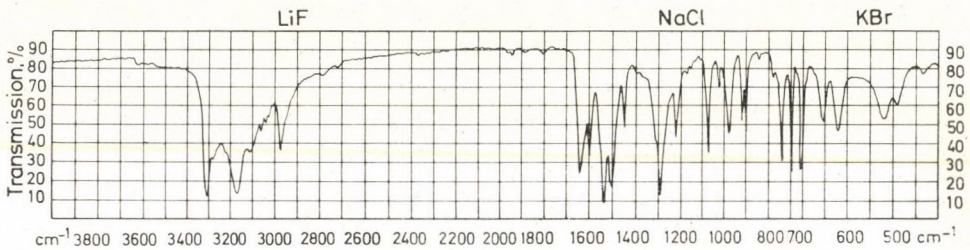
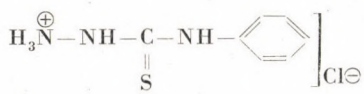


Abb. 10

Im Spektrum des salzsauren Salzes des N^4-Phenylthiosemicarbazids **XI** [13] (Abb. 9) sind die Verhältnisse im Vergleich zum Spektrum der freien Base (Abb. 10) ähnlich wie bei der vorangehenden Verbindung die Banden der $-\overset{\oplus}{N}H_3$-Gruppe sind vorhanden, während die Frequenzen der $-NH_2$-Gruppe fehlen. Die Struktur des salzsauren Salzes **XI** ist also:

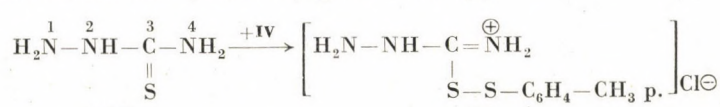


XI

Es ist bemerkenswert, daß die salzsauren Salze des Thiocarbamids und seiner N-substituierten Derivate am Schwefelatom protoniert sind, wie bereits von JANSSEN [14] sowie KUTZELNIGG und MECKE [15]festgestellt wurde, im Gegensatz zu den Thiosemicarbaziden, wo das Stickstoffatom N^1 das basische Zentrum ist.

Die salzsauren Salze des N^1-Phenylthiosemicarbazids **IX** und des $N^{1,4}$-Diphenylthiosemicarbazids können — wie aufgrund des Gesagten auch theoretisch zu erwarten ist — nicht hergestellt werden.

Das Thiosemicarbazid **VIII** liefert mit *p*-Toluylsulphenylchlorid **IV** unter Bildung einer Schwefel–Schwefel-Bindung S-(*p*-Toluylthiol)-isothiosemicarbazid-hydrochlorid **XII** (Abb. 11) gemäß Gl. (2):



VIII **XII** (2)

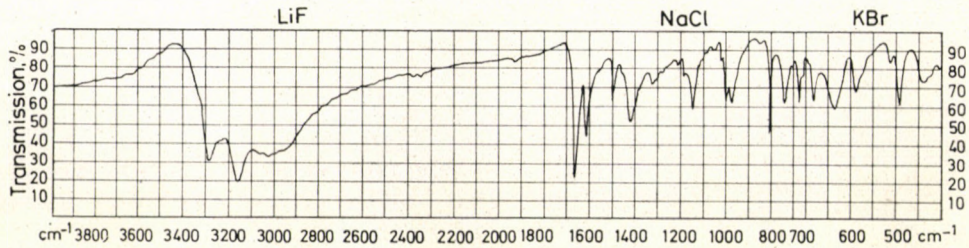


Abb. 11

Im IR-Spektrum der Verbindung **XII** (Abb. 11) weist die Bande *vcc* bei 1498 cm^{-1} und die Bande γ (= CH) bei 810 cm^{-1} auf den Einbau der *p*-Toluylsulfenylgruppe hin. Die bedeutende Zunahme der Wellenzahlen der Banden *A* und *B* (Tab. II) bestätigt, daß die Substitution bei der Sulfenylierung am S-Atom erfolgt. Die Banden *A* kann der NH_2-Gruppe zugeordnet werden, während die Bande *B* die Valenzschwingung der N—C—S-Kette ist: giese Valenzschwingung entspricht in dieser Verbindung — gemäß dem gesteiderten Doppelbindungscharakter der C—N-Bindung — der Valenzschwingung der Kette N=C—S. Daß tatsächlich dieser Fall vorliegt, wird auch durch das Spektrum der teilweise deuterisierten Verbindung (Abb. 12) bestätigt, worin

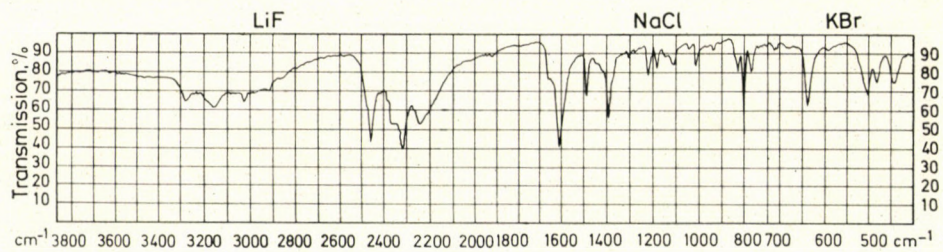


Abb. 12

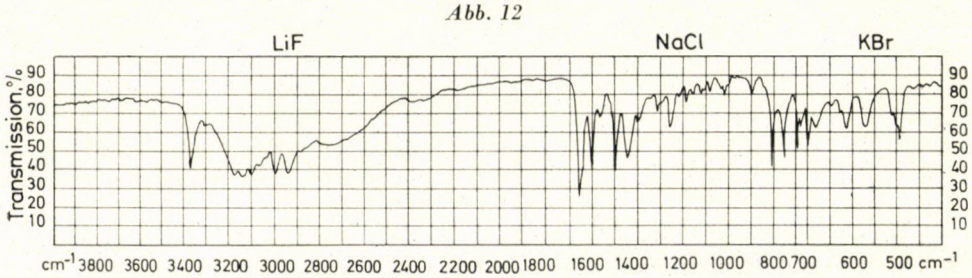


Abb. 13

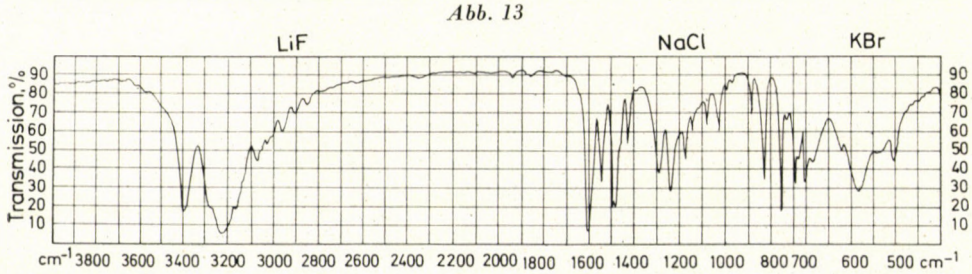
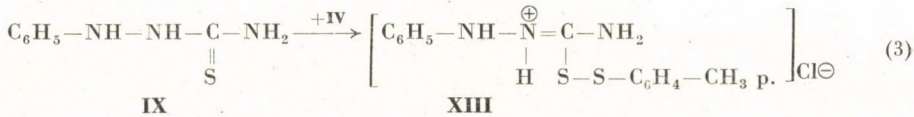


Abb. 14

die Bande *A* mit verringerter Intensität, die Bande *B* dagegen unverändert zu finden ist.

Im Spektrum des Reaktionsproduktes **XIII** (Abb. 13) des N^1-Phenylthiosemicarbazids **IX** mit *p*-Toluylsulfenylchlorid **IV** bekräftigt die Lage der Bande *A* im Vergleich zum Spektrum des Ausgangsstoffes (Abb. 14) ebenfalls die Substitution am Schwefelatom (Gl. 3).



(3)

IX **XIII**

Die Zuordnung der Bande *B* ist nicht eindeutig; es kann angenommen werden, daß sie in andere, intensivere Banden eingeschmolzen ist oder eventuell bei 1640 cm^{-1} in Form einer Schulter auftritt.

Der Beweis dafür, daß es sich tatsächlich um die angegebene Struktur handelt, wird durch das Ausschließen aller anderen Möglichkeiten geliefert. Die Möglichkeit der N^4-Substitution ist durch die Gegenwart der Banden bei 3370, 1658 und 570 cm^{-1} ausgeschlossen, da diese Banden die Gegenwart der NH_2-Gruppe anzeigen. Gegen die Substitution am Stickstoffatom N^1 spricht die Zunahme der Wellenzahl der Bande *A*. Die Bildung eines Isomeren mit der Bindung wie bei Thiosemicarbazid ist ebenfalls wegen den genannten, die Gegenwart der Aminogruppe anzeigenden Banden ausgeschlossen.

Obwohl im Spektrum von **XII** keine auf die Gegenwart von $-\overset{\oplus}{N}H_3$-Gruppen hinweisende Banden vorliegen, während im Spektrum von **XIII** die Bande *A* zugegen ist, kann angenommen werden, daß die Verbindungen im festen Zustand die aufgeschriebene Struktur besitzen. Die Existenz von anderen protonierten Formen kann jedoch keineswegs ausgeschlossen werden. Um diese Frage zu entscheiden, sollen im weiteren röntgenspektroskopische Untersuchungen durchgeführt werden.

Die sulfenylierten Thiocarbamid- und Thiosemicarbazidderivate zeigen eine mäßige antimikrobielle Aktivität gegen grampositive Bakterien [16].

Experimenteller Teil*

(Unkorrigierte Schmelzpunkte)

Die IR-Spektren wurden mit einem Spektrometer Typ Zeiss UR-10, in Kaliumbromidpastillen aufgenommen. Die Hydrochloride der Thiocarbamide und Thiosemicarbazide wurden aus der alkoholischen Lösung der Base durch Zufügen von mit Salzsäuregas gesättigtem Äther abgeschieden.

1. S-(p-Toluylthio)-isothiocarbamid-hydrochlorid (V)

Zu einer Suspension von 3,8 g (0,05 Mol) Thiocarbamid in 50 ml trockenem Dioxan werden unter Rühren 7,9 g (0,05 Mol) *p*-Toluylsulfenylchlorid in 50 ml Dioxan bei Raumtemperatur tropfenweise zugegeben. Die Temperatur des Reaktionsgemisches steigt dabei

* Unter Mitarbeit von Frl. E. Kiss.

Tabelle I

Characterische Banden des Thiocarbamids und seiner Derivate im Wellenzahlbereich 1400—1700cm^{-1}

	I	V	II	VI	III	VII
A	1618	1660	1613	1668		
B	1477	(1648) 1510	1533 (1520)	1618	1553 (1530)	1632
C	1418	1423	1320 1300	1325	1345	1390
*vcc**		1590	1590 1465 1450	1590 1495 1460	1600 1498 1453	1598 1582 1490 1438

* *vcc* = Skelettvalenzschwingung des aromatischen Ringes.

Tabelle II

Characterische Banden des Thiosemicarbazids und seiner Derivate im Wellenzahlbereich 1300—1700cm^{-1}

	VIII	XII	IX	XIII
A	1647 1618	1668	1605	1658
B	1535 1487	1618	1497 1487	(1640)
C	1320 1290	1422	1293	1440
*vcc**		1498	1550 1432	1602 1560 1498

* *vcc* = Skelettvalenzschwingung des aromatischen Ringes.

Tabelle III

Liste der IR-spektroskopisch untersuchten Verbindungen

Nr. des Spektrums	Benennung und Formelnummer der Verbindung
1.	Thiocarbamid **(I)**
2.	N-Phenylthiocarbamid **(II)**
3.	S-(*p*-Toluylthio)-isothiocarbamid-hydrochlorid **(V)**
4.	N-Phenyl-S-(*p*-toluylthio)-isothiocarbamid-hydrochlorid **(VI)**
5.	N,N'-Diphenylthiocarbamid **(III)**
6.	N,N'-Diphenyl-S-(*p*-toluylthio)-isothiocarbamid--hydrochlorid **(VII)**
7.	Thiosemicarbazid-hydrochlorid **(X)**
8.	Thiosemicarbazid **(VIII)**
9.	N^4-Phenylthiosemicarbazid-hydrochlorid **(XI)**
10.	N^4-Phenylthiosemicarbazid
11.	S-(*p*-Toluylthio)-isothiosemicarbazid-hydrochlorid **(XII)**
12.	Deuteriertes S-(*p*-Toluylthio)-isothiosemicarbazid-hydrochlorid
13.	N^1-Phenyl-S-(*p*-toluylthio)-isothiosemicarbazid-hydrochlorid **(XIII)**
14.	N^1-Phenylthiosemicarbazid **(IX)**

leicht an und die rote Farbe des Sulfenylchlorids verschwindet bald. Nach Abdestillieren des Lösungsmittels bei vermindertem Druck bleibt ein hellgelbes klebriges Rohrprodukt zurück, das in wenig Alkohol unter leichtem Erwärmen gelöst wird. Die Lösung wird filtriert und mit Salzsäuregas gesättigter trockener Äther wird zugegeben, wobei ein farbloses pulverartiges Produkt abgeschieden wird. Nach zweimaligem Wiederholen der Lösungs- und Fälloperation wird ein reines Produkt erhalten.

Schmp.: 91—92 °C. Ausbeute: 10,1 g (86,1%)
Analyse: $C_8H_{11}ClN_2S_2$ (234,77)
Berechnet N 11,9%; Gefunden N 11,5%

2. N-Phenyl-S-(p-toluylthio)-isothiocarbamid-Hydrochlorid (VI)

4,5 g (0,03 Mol) N-Phenylthiocarbamid [17] und 4,7 g (0,03 Mol) *p*-Toluylsulfenylchlorid werden wie unter Punkt 1. beschrieben in Reaktion gebracht und verarbeitet.

Schmp.: 145—146 °C unter Gasentwicklung. Ausbeute: 4,6 g (50%)
Analyse: $C_{14}H_{15}ClN_2S_2$ (310,71)
Berechnet C 54,07%, H 4,86%; Gefunden C 54,11%, H 4,88%

3. N,N'-Diphenyl-S(p-toluylthio)-isothiocarbamid-hydrochlorid (VII)

5,9 g (0,05 Mol) N,N'-Diphenylthiocarbamid [18] und 7,9 g (0,05 Mol) *p*-Toluylsulfenylchlorid werden wie unter Punkt 1. beschrieben in Reaktion gebracht und verarbeitet.

Das Produkt zersetzt sich über 80 °C unter Gasentwicklung.
Schmp.: 53—55 °C. Ausbeute: 9 g (46,6%)
Analyse: $C_{20}H_{19}ClN_2S_2$ (386,97)
Berechnet N 7,2%; Gefunden N 7,0%

4. S-(p-Toluylthio)-isothiosemicarbazid-hydrochlorid (XII)

2,7 g (0,03 Mol) fein pulverisiertes Thiosemicarbazid werden in 50 ml trockenem Dioxan suspendiert. 4,8 g (0,03 Mol) *p*-Toluylsulfenylchlorid werden unter Rühren tropfenweise zugefügt. Nach einer halben Stunde wird das Reaktionsprodukt abfiltriert. Nach mehrmaligem Umkristallisieren aus Alkohol werden farblose Prismen erhalten.

Schmp.: 151 °C unter Zersetzung. Ausbeute: 3,8 g (45%)
Analyse: $C_8H_{12}ClN_3S_2$ (250,8)
Berechnet C 38,4%, H 4,8%; Gefunden C 38,6%, H 4,8%

5. N¹-Phenyl-S-(p-toluylthio)-isothiosemicarbazid-hydrochlorid (XIII)

3,3 g (0,02 Mol) 1-Phenylthiosemicarbazid [19] und 3,2 g (0,02 Mol) *p*-Toluylsulfenylchlorid werden wie unter Punkt 4 beschrieben in Reaktion gebracht und verarbeitet. Aus Eisessig umkristallisiert werden gelblichweiße Nadeln erhalten.

Schmp.: 152—153 °C unter Zersetzung. Ausbeute: 2,7 g (42%)
Analyse: $C_{14}H_{16}ClN_3S_2$ (293,8)
Berechnet C 51,6%, H 4,9%, S 19,7%
Gefunden C 51,7%, H 4,9%, S 19,5%

LITERATUR

1. Klivényi, F., Vinkler, E., Stájer-Szabó, A. E.: Acta Chim. Acad. Sci. Hung. **63,** 435 (1970)
2. Kopylowa, B. W., Freidlina, R. Ch.: Dokl. Akad. Nauk SSSR, **159,** 138 (1964)
3. Field, L., Buckman, J. D.: J. Org. Chem. **33,** 3865 (1968)
4. Jensen, K. A., Nielsen, P. H.: Acta Chem. Scand. **20,** 597 (1966)
5. Hallam, H. E., Jones, Ch. M.: Spectrochim. Acta, **25,** 1791 (1969)
6. Tóth, G., Tóth, I., Toldy, L.: Tetrahedron Letters **60,** 5299 (1969)
7. Rao, C. N. R., Venkatarakhavan, R.: Spectrochim. Acta **18,** 541 (1962)
8. Rao, C. N. R., Venkatarakhavan, R., Kasturi, T. R.: Canad. J. Chem. **42,** 36 (1964)
9. Mashima, M.: Bull. Chem. Soc. Japan **37,** 974 (1964)
10. Wiles, D. M., Suprunchuk, T.: Canad. J. Chem. **47,** 1087 (1969)
11. Volka, K., Holzbecher, Z.: Coll. Czechoslov. Chem. Comm. **34,** 1353 (1969)
12. Braibanti, A., Leporati, D., Dallavalle, F., Fellinghelli, M. A.: Inorg. Chim. Acta **2,** 449 (1968)
13. Busch, M., Bauer, P.: Ber. **33,** 1061 (1900)
14. Janssen, M. J.: Spectrochim. Acta **17,** 475 (1961)
15. Kutzelnigg, W., Mecke, R.: Spectrochim. Acta **17,** 530 (1961)
16. Ferenczy, L.: Acta Biol. Hung. (unter Druck)
17. Org. Synth. Coll. Vol. III, p. 735
18. Houben-Weyl-Müller: Methoden der organischen Chemie, IV. Auflage, Band 9, s. 805, 1955
19. Fischer, E.: Annalen **212,** 324 (1882)

Péter Vinkler; Budapest II., Pusztaszeri út 57—69,
Ferenc Klivényi
Elemér Vinkler
Géza Stájer
Enikő A. Szabó
Szeged, POB 121. Ungarn

Acta Chimica Academiae Scientiarum Hungaricae, Tomus 69 (2), pp. 241—242, (1971)

TABERSONINE FROM RIPEN SEEDS OF *VINCA ROSEA L.*

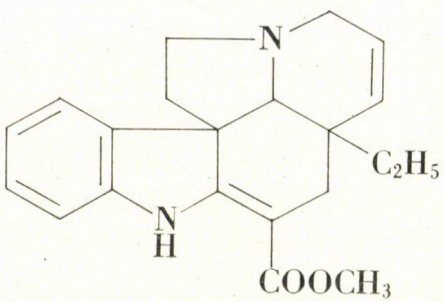
(PRELIMINARY COMMUNICATION)

B. ZSADON and P. KAPOSI*

*(Department of Chemical Technology of the L. Eötvös University, Budapest and *Research Institute for Medicinal Plants, Budapest)*

Received November 5, 1970

Tabersonine (**I**), first isolated from seeds of *Amsonia tabernaemontana* [1], has been found in a number of species, usually as the main alkaloid in the seeds [2a, 2b]. This alkaloid was isolated also by us from the leaves of *Amsonia tabernaemontana* [3], and it was found to be the main alkaloid in the seeds of *Rhazya orientalis*, too [4].



I

Some time ago, the sequence of alkaloid formation in *Vinca rosea* was studied by Qureshi and Scott [5], and among other results, tabersonine was first detected and isolated by thin-layer chromatography from the seedlings after 72 hours short-term germination of *Vinca rosea* seeds. As a consequence of the results of these investigations, tabersonine could be regarded as one of the probable intermediates in the biosynthesis of *Aspidosperma* and *Iboga* alkaloids. However, this alkaloid has not been detected in any part of mature *Vinca rosea* up to the present.

Recently, in the course of our investigations on *Aspidosperma* alkaloids, the alkaloid content of the ripen seeds of *Vinca rosea* was studied**, and tabersonine was isolated from those. According to the procedure given in a previous paper [6], 6.4 mg of tabersonine base of chromatographic purity was

** Our investigations were carried out on *Vinca rosea* plants grown in the Research Institute for Medicinal Plants, Budapest, in the year 1970.

obtained from 2.5 g of ripen seeds. Identification of the product was carried out by thin-layer chromatographic comparison with authentic tabersonine obtained from *Amsonia tabernaemontana* seeds [6]; also its physical characteristics were found to be identical with those given in the literature [1, 6]. UV-spectrum (in methanol) λ_{max} 226, 298 and 328 nm, $[\alpha]_D$ −360° (in ethanol, $c = 0.2$). The needle-shaped crystals of its hydrochloride melted at 195—198 °C (decomp.).

REFERENCES

1. Janot, M.-M., Pourrat, H., Le Men, J.: Bull. Soc. Chim. France, **1954**, 707, and Plat, M., Le Men, J., Janot, M.-M., Wilson, J. M., Budzikiewicz, H., Durham, L. J., Nakagawa, Y., Djerassi, C.: Tetrahedron Letters, **1962**, 271
2. (a) Hesse, M.: Indolalkaloide in Tabellen, Springer, 1964, Ergänzungswerk, 1968 (b) Kunesch, N., Miet, C., Troly, M., Poisson, J.: Ann. Pharm. Fr. **26**, 79 (1968)
3. Zsadon, B., Egry, É., Sárközi, M.: Acta Chim. Acad. Sci. Hung. **67**, 77 (1971)
4. Zsadon, B., Végh, Á., Hubay, R.: Magy. Kém. Foly. **77**, 52 (1971)
5. Quershi, A. A., Scott, A.: J. Chem. Comm. **1963**, 948
6. Zsadon, B., Rákli, M., Hubay, R.: Acta Chim. Acad. Sci. Hung. **67**, 71 (1971)

Béla Zsadon; Budapest VIII., Múzeum körút 6—8.
Pál Kaposi; Budapest XII., Dániel út 40.

RECENSIONES

Fortschritte der chemischen Forschung

(Topics in Current Chemistry 14/3) April, 1970. Preparative Organic Chemistry, pp. 235—365. Springer Verlag, Berlin—Heidelberg—New York

A systematic coverage of single, specialized aspects of the various branches of chemistry in reviews is a necessity nowadays, because of the enormous volume of information published in a very wide variety of sources. A lot of work can be saved for the practicing chemist if the new results of a single field are reviewed from time to time. "Topics in Current Chemistry" is one of the periodic publications dedicated exclusively to such reviews.

The issue reviewed here contains two papers. The first is the Acylation of Enamines (in German). It contains the following subjects: The scope and limit of the review; Synthetic methods for the preparation of enamines and subsequent reactions; Acylation of enamines with carboxylic acid derivatives (ketenes, diketenes, acid chlorides, anhydrides, Wilsmeier-reagents, etc.); Acylation with derivatives of carbon dioxide (alkylchlorocarbonates, ortho-esters, derivatives of cyanic acid, isocyanates and isothiocyanates, etc.).

The review summarizes both the mechanistic aspects and the preparative uses of the reaction in reasonable detail and is eminently readable also for those chemists who are not specialists in the field. 160 references are given, covering the subject up to 1969.

The second paper discusses nitrogen ylids (in English). After an introduction treating also the early development of the chemistry of nitrogen ylids, the review first gives data on reactions of the tetramethylammonium ion with organolithium compounds. After describing preparation and structural possibilities, decomposition reactions are dealt with. Separate sub-chapters discuss condensation reactions, adduct formation, transmetalation and dimetalation reactions. The reactions of the tetramethylammonium ion with other, strong and weak bases are discussed next and then ylid formation from other substituted quaternary ammonium salts is treated in the following order: phenyl substituted salts, benzyl and benzhydryl substituted salts (this latter chapter contains also the description of ion pair formation), other tetraalkylammonium salts and cyclic quaternary ammonium salts. Other synthetic approaches to nitrogen ylids are discussed, and finally a summary of the formation and decomposition of ylids is given. This last chapter is especially useful, as it is an attempt to give a unified approach to the subject, giving much food for thought and helping the non-specialist worker to put his knowledge in a usable form. 183 references — including literature coverage for 1969 — conclude the review.

The second review is also easily comprehended by non-specialists and helps in the understanding of a very interesting chapter of Nitrogen chemistry.

Although the papers reviewed here are in a single issue of a periodic publication, they should be taken as a sample of the whole. "Topics in Current Chemistry" is a well established periodical to which chemists can turn if their literature-search requires reviews on specific topics.

M. VAJDA

S. J. Ashcroft and C. T. Mortimer: *Thermochemistry of Transition Metal Complexes*

pp. 478. Academic Press, London, New York, 1970

Knowledge of the formation and chemical behaviour of transition metal complexes is of great importance both from the theoretical and practical points of view. Profound understanding of the energetical conditions of the formation of such complexes is of particular importance. Rapid development of direct calorimetric equilibrium measurements in recent years made possible the determination of truly reliable thermochemical data of these complexes, thus primarily their heat of formation.

The book of Ashcroft and Mortimer summarizes critically selected thermochemical data for more than 1500 complex systems. This is a valuable help to researchers in coordination chemistry. The book will be an indispensable handbook to all chemists working in this field.

With the exception of a short introduction of 20 pages, the whole book deals with the results of thermochemical investigation of the complexes. The subject is divided into chapters on the basis of ligand groups. (Two separate shorter chapters deal with the complexes of the platinum group and of the actinides.)

The thermodynamical data summarized in tables are also briefly interpreted for almost every system discussed by the authors, pointing out the main conclusions and relationships resulting from these data. A detailed bibliography is given at the end of the chapters. The nearly one thousand references afford great help not only to inorganic and coordination chemists, but also to researchers working in various related fields and to advanced students.

The use of the work as a handbook is facilitated by a detailed subject index, author index, and indexes listing the single complexes both according to the central atom and the ligands.

K. Burger

G. M. Bartanev: *The structure and mechanical properties of inorganic glasses*

246 pp. 116 figures. Welters-Noordhoff Publishing, Groningen, 1970

Bartanev's book begins with the discussion of the structure of liquids and melts (Chapter I). The author describes the structure of the liquids inclined to the glass formation, and points out that although the structure of melts and glasses is approximately the same at the temperature of glass formation, there are some considerable differences in the temperature dependences of properties.

The author of the book attaches particular importance to the time of molecular relaxation, which is used later on as a basis of some concepts. The statement saying "the viscosity of silicate glasses at softening temperature under the usual experimental conditions is approximately 10^{13} p" is presumably a misspelling. (Viscosity at softening temperature is $10^{7.6}$ p, at transformation temperature 10^{13} p.) This chapter deals further with the similarity of the structures of melts to those of crystals, the phase separation, polymerization and depolymerization processes in melts.

The views of the author on the structure of glass are set forth in detail in the second chapter, from which the reader gains the pleasant impression that the author of the book does not pledge himself to any the theories. The various theories have no absolute validity, but are considered by the author as useful approximations, which can be applied from certain aspects to certain glasses.

The author shows the notable difference in the behaviour of vitreous silicon dioxide and boron trioxide, which makes it probable that the latter contains polymeric chains.

The crystallite theory, which could not be proved unequivocally by X-ray investigations (at least not for common glasses), is valid according to the author for micro-crystalline glasses, the so called pyroceram substances. He establishes further that the crystal-chemical concept (Goldschmidt, Zachariasen), though capable of explaining several properties of glasses, owes its well known limitations to the fact that it takes into consideration only the hyperfine structure of glass, and pays no attention to the supramolecular structure. Bartanev

considers the silicon–oxygen rings and chains as fundamental elements of glass and emphasizes quoting many early observation that glass cannot be considered an ideally homogeneous body. The results of electron microscopic investigations and the problem of phase separation are discussed in details.

The third chapter is devoted to the elastic and visco-elastic properties of glass. Within this chapter, theories relevant to the time-dependence of deformation are discussed. A table of the formulae proposed by the various authors, facilitates the survey. The dependence of the modulus of elasticity on temperature and thermal treatments is discussed in detail, as well as the contribution of ion migration to the mechanical loss.

Under the title "Internal stress in glasses" the author describes and explains an interesting phenomenon: on slow heating, the glass rods investigated twists even in absence of any external force. The third chapter closes with the description of structural investigations by means of ultrasound techniques.

In Chapter IV, carrying the title "Strength and Failure of Glasses, the author points out that the strength calculated from interatomic bonding energy or from the Young module is always lower than the value found experimentally. He stresses the importance of the number, shape and magnitude of micro-cracks. In view of the poor reproducibility of the measurements, he attaches proper importance to the statistic evaluation of the results. Curves of strength distribution, exhibiting the maxima, illustrate the complexity of the phenomenon. Problems like the weight of the sample, or the effect of temperature and surface-active agents on strength are also considered. This chapter concludes with a detailed discussion of the theories pertinent to the problems treated.

One of the advantages of the book that BARTANEV makes frequent comparisons between inorganic glasses and organic polymers. From the order in which concepts are the author presumes that the reader is well versed in the theme. For example, transition temperature is mentioned already on page 22, while its definition, owing to the logical structure of the book, can be read only on pages 30–33. It should be mentioned here that the opinion of the author on problems concerning transition temperatures is very noteworthy. From the above, it is be clear that the book is a very useful for all those, who wish to deepen and systemize their knowledge in the field of glasses and the investigation of their mechanical properties. Ample bibliography, involving about 600 references, is given. It is a pity that results of the very last years are missing from this valuable work. An author and subject index and a list of notations would increase the merits of the book.

Z. BOKSAY

Proceedings of the 3rd Symposium on Coordination Chemistry

Edited by Prof. M. T. BECK. Vol. I, pp. 525. Akadémiai Kiadó, Budapest, 1970

The volume contains the text of 48 papers presented at the 3rd Symposium on Coordination Chemistry, organized under joint auspices of the Work-Committee for Coordination Chemistry of the Hungarian Academy of Sciences and the Section for Coordination Chemistry of the Hungarian Chemical Society. The Symposium dealt with three spheres of subjects of coordination chemistry, which are of particular interest at present: the chemistry of mixed ligand complexes, polynuclear complexes and complexes of the outer sphere type. Some of the authors deal extensively with the theoretical aspects of these topics, however, the predominant part of the papers reports on results of various experimental investigations of the complex systems.

The papers read by the authors of international renown pregnantly show the trends of development in coordination chemical research. In addition to equilibrium investigations, kinetic studies, the elucidation of reaction mechanisms and various structural investigations steadily gain in importance. In the evaluation of experimental data, graphical approximation methods are increasingly replaced by exact computerized procedures. The rapid development of experimental techniques and evaluation methods has made possible the successful investigation of systems of increasing complexity. Several papers included in the volume report on results of this kind.

Owing to the limited space of this review, it is impossible to discuss all the papers. The reviewer has to limit himself to calling attention to a few papers of particular interest to him; as every selection of this kind, this is, of course, a subjective one.

The paper presented by S. AHRLAND on the regularities of the formation of outer-sphere complexes produced a lively discussion. Great interest was shown in the paper of S KIRSCHNER dealing with the optical activity of outer-sphere complexes and the effect of solvents on this activity, and in the paper of M. BECK discussing the stability problems of outer-sphere cobalt(III) complexes.

Of the papers on the stability and structural characteristics of mixed complexes, the work of L. NEWMAN dealing with palladiumhalide mixed complexes, H. SIGEL's paper presenting the factors affecting the stability of copper(II) mixed complexes, the paper of N. YELLIN and Y. MARCUS discussing the Raman spectra of cadmiumhalide mixed complexes, and F. JURSIK's work on mixed amino acid complexes should be particularly mentioned.

The kinetic importance of mixed complex formation is well reflected by the papers of D. A. DURHAM and M. BECK dealing with the reduction of chromium(VI), H. HOFFMANN on the investigation of nickel–ethylene–diamine-tartrate mixed complexes, E. BRÜCHER on the formation of the terbium(III)-EDTA complex, and in the paper presented by J. ZSAKÓ on the kinetic investigation of mixed dioxime complexes.

U. BELLUCO reports on the catalytic effect of platinum–olefin complexes. The paper of L. CATTALINI deals with the kinetic investigation of the *cis*-effect in palladium complex systems.

A valuable paper presented by F. J. C. ROSSOTTI discusses the determination of the stability constants of protonated complexes; R. OSTERBERG points out the possible applications of potentiostatic EMF titration, a new method of equilibrium measurement.

The topic of several papers is the application of the Mössbauer effect in coordination chemistry. M. L. GOOD corroborates his data obtained by Mössbauer spectroscopy of iron and tin mixed halide complexes by the results of far-infrared studies. E. KÖNIG reports on a Mössbauer investigation of the low spin ↔ high spin electron configuration thermal equilibrium of iron(II) complexes. K. BURGER used the Mössbauer effect for structural investigation of the intermediate products of the thermal decomposition of iron–pyridine mixed complexes. A. VÉRTES followed the hydrolysis processes of iron(III) by a Mössbauer investigation of quick-frozen solutions.

The paper of K. B. YATSMIRSKII *et al.* reports the results of PMR investigations of mixed complexes; H. A. O. HILL present results obtained by NMR spectroscopy in mixed complex systems.

The paper of S. PAPP points out the possibilities of application of derivative thermal analysis in coordination chemistry.

Besides presenting new scientific results, most papers give a brief survey of the literature pertinent to the topic discussed, and almost all papers contain an extensive list of references. Therefore, this volume will also be useful as a source of literature to researchers.

The editor of the volume, Professor BECK prepares now the second volume of this publication which will comprise the papers presented at the plenary sessions of the Symposium and a full report of all the ensuing discussions. In view of the great success of the Symposium, the publication of the second volume of the Proceedings is expected with great interest.

K. BURGER

Corrosion Week

Akadémiai Kiadó, Budapest, 1970

The book published by Akadémiai Kiadó contains 128 papers presented of the meeting "Corrosion Week". Researchers engaged in the theoretical or practical investigation of corrosion, as well as industrial experts active in this field will profit from this valuable compilation, giving account beside the most up-to-date theories also of several practical problems. The Editorial Board has done a careful work. A rich collection of photographs and figures is included in the volume.

The first paper was read by SZEKÉR, Deputy Minister, discussing extensively the past, present and future of corrosion research in Hungary.

CORTON dealt with the formation and deterioration of surface layers, reviewing the achievements of the last 20 years in this field. GERISCHER discussed the corrosion of semiconductors, and emphasized the novel character of these corrosion phenomena.

LA COMBE showed the possibilities of the potentio static and dynamic methods of investigation, in the detection of intragranular corrosion, pitting, etc., and in studying passivation.

Several authors, *e.g.* VAGRAMYAN, DETTKE, EÖLLŐS and GERVIS, read papers on the deposition of galvanic coatings and on the properties of these coats. HASKO investigated the effect of electrolyte composition on the structure of the coats.

LÄSER described several automatic processes used in electrooxidation plants.

BRUSSIG reported on experiments for the protection of chromium plated parts, while EÖLLŐS and coworkers investigated the cause of whisker formation on electro-plated coats. ORGOVÁNY studied the effect of organic additives on electro-plating baths, while MORISSET discussed the evaluation of the standard methods of testing of coatings.

ABÁDI, VOLLY and GÁL investigate embrittlement and its diminution. A similar topic is treated by KUNZE and DRUCKER, who also discussed the importance of various acids used in pickling.

FRANKOV and FARKAS developed a new method for the removal of chromium impurities from plating baths.

WÉBER and ZAK studied the improvement of the corrosion resistance of sintered iron. VESZLÉNYI investigated the behaviour of various metallic and non-metallic coatings on springs. The advantages of chromium coatings applied for the protection of props used in mines is the theme of BRUGGER.

The papers by HECK, CAUCHETIER, TRAGAN and SIMO deal also with the properties of metal coatings. MITTENBERGER investigated the properties of paints applied on metal coatings. DÉKÁNY, KONKOLY and VARGA reported on experiments in connection with nitridation. MÉSZÁROS described laboratories equipped with metal pulverizers. TURI studies furnace enamel coatings, of importance in chemical industries. Results achieved in cathodic protection were reported by MAKÁRY, while KÜHN gave a survey of the possible applications of platinum-titanium anodes in cathodic protection.

ORLOWSKI stressed the importance of plastics. Several papers deal with possible applications of epoxy coatings on various bases (VALERIANCZYK, SZEREC, SIMON, JÜSTL, etc.). The same problem was investigated from the aspect of bacterial corrosion by KOLTAI and FARKAS.

ROSENFELD tried to improve the protective action of varnish coatings by means of inhibitors. MASSERA discussed the treatment of iron surfaces before painting, with a particular view to the importance of their proper selection. GÖNNEL investigated rust by means of X-ray analysis, and studied the importance of rust transformation, active primary and sand blasting.

Experiences gained by the combined application of paint coats and cathodic protection were reported by DOMÁNSKI.

BIRN described a new method for the application of paints, GÖNNEL the automation of application.

PERÉNYI investigated the corrosion of structural steel in the building industry. OETEREN studied problems of transitory protection, while MACHU described different methods for the chemical surface treatment of iron, and aluminium.

Electrostatic painting deserves particular attention. Painting is the subject of papers by BUREAU, MITTENBERGER, DEMÉNDY, PALLANEK, HAUSKA, SALMEN, etc. HÄRTEL presented non-metallic construction materials resistant to acids. MENRÁTH reported on the shipment of various machines to tropical countries and on their protection against corrosion. ROVÓ dealt with cavitation in the field of surface preparation. IVÁNFI investigated the properties of aqueous dispersions combined with aromatic oxycaroxyl acids, and their possible application as primers ones. HÜNECKE discussed the advantages and disadvantages of dip varnishing. VALKONY dealt with rubber linings, KUTASI and SOMODI with the reparation of enamel faults. HUISZ and HORKAY investigated the role of pigmentation. ZAKAR, TAKÁCS and JANÁSZIK made comparative laboratory tests on various coatings. BUCSI *et al.* investigated the adhering power of various organic coats. CHROMY took electron microscopic pictures of processes occurring on the paint coatings.

WAGNER described organic coatings which can be applied in the liquid form, and solidify on thermal or catalytic action. HORVÁTH, RAUSCHER, etc. investigated the inhibitor dicyclohexylamine, of great importance in corrosion prevention, in aqueous media containing hydrogen sulfide. LUNYEVA, JAKOBS, BAXTER, POMPOWSKY, COMELLE, LEVIN, VINOGRADOV, TRESL and HOFER studied inhibition of oils and fats, and investigated the products obtained. POUTILOVA and CHISLOVA reported on inhibitors used in acid media. KLENOWICZ studied mixed inhibitors, while LOHONYAI investigated the corrosion of lead in the presence of inhibitors. Inhibitors used in connection with the salting of roads in winter were discussed by KIRNER. The combined effect of detergents and inhibitors was investigated by SZÉPLAKY, YEFIMOVA, WLODARCZYK and WIEKIERA discussed inhibitors suitable for the elimination of corro-

sion in oil refineries. VÁMOS and PFEIFER reported the derivatographic analysis of inhibitors used in fats and oils. Among the theoretical problems discussed, the paper of SCHWABE on the theory of inhibition and passivation, the paper of VINKLER and GOTTFRIED dealing with similar problems, and the galvanostatic and potentiostatic investigation of the formation of oxide layers on iron by MOSHTEV are of particular interest.

PRAZAK and coworkers studied pitting of nickel, and draw conclusions on the mechanism of the process. HACKL and MÁRTA investigated the properties of the layer formed on copper. KÓNYA investigated the system silver-platinum from the aspect of corrosion current, comparing calculated and measured values. Using radioactive sulfur, PÉTERFI, SÁRVÁRI and VARGA studied, by tracer techniques, the corrosion caused by sulfur. WINCKLER and NÉMETH elaborated a new method for stadying corrosion phenomena in moist gases. VASVÁRI investigated the relationship between cavitation and corrosion. SHALNEV and SHALOBASOV dealt also with cavitation problems.

PHILIPP, D'AMBROGIO, CSERNY and GÁNCS studied the economic aspects of corrosion in various fields. RÓNAY, SZÜCS and KÖRMÖCZI investigated various possibilities for the protection of underground storage tanks. BÁCSKAI improved the corrosion resistance of chromium steel by chemical surface treatment, and drew conclusions on the observed passivation. RÉDEY, TASCHOW and BURDA studied the corrosion of steel. The corrosion of silver was discussed by MARALES and BOUCHER. KLINOV's paper dealt with plastics used in the chemical industry. EÖLLŐS, LIPOVETZ, etc. reported on the surface treatment of aluminium.

LIPOVETZ and LOHONYAI studied, in solutions containing aluminium, the effect of aluminium deposited on the lead cathode during corrosion. FARR and GREEN made an attempt to explain the corrosion of lead batteries. The paper of KÉRI dealt also with batteries. DÉKÁNY investigated the corrosive effect of substances of various types, emitted by plastics. KISS examined the atmospheric behaviour of paints used in nitrogen fertilizer plants. RÁDAY, ERDŐS and SZEKOWSZKY described methods of testing recently developed by them. LENGYEL and DÉVAY investigated layers developed on the surface of silver by anodic polarization. SZALAY studied the adhesive strength of coats prepared by electrolysis. VADÁSZ discussed friction corrosion. GÖRÖG, VÁMOS and RÓNAY dealt with corrosion occurring in oil storage tanks, etc. Investigations concerning cooling and lubricating oils were also undertaken. GOLUBYEV and KADYROV studied the relationship between atmospheric corrosion and climatic conditions. BOZSÓ and coworkers studied the corrosion in melts. DÉKÁNY and FEKETE investigated the contact corrosion of coated galvanic pairs of iron-aluminium and copper. BLEUER and LABODY studied the role of ion exchangers in corrosion. The paper of KOZYREV dealt with the relationship between sound velocity and the erosive properties of liquids.

GY. BÁCSKAI

Jack LOADER: *Basic Laser Raman Spectroscopy*

pp. 105. Heyden and Son Lts., London, Sadtler Research Laboratories Inc. New York, 1970

The author is a coworker of Dr. P. J. HENDRA, the head of one of the best schools in this field.

The book is a very useful introduction for spectroscopists who are thoroughly familiar with the theory and classical practice of Raman spectroscopy and desire to switch over to a laser light source.

A very short survey of Raman effect is followed by the essential parts of the book. The first part deals with the technics of laser Raman spectroscopy. There is a great difference between sample handling in classical and laser Raman spectrometers. The author describes in detail the laser Raman spectrometers CARY 81, CODBERG CH1 (and PH1) and the PERKINELMER LR1 being most widely used in the United Kingdom.

The subsequent chapters analyze the problems of calibration, resolution check and accuracy of the recorded intensities.

Approximately half of the volume (50 pages) comprises a collection of laser Raman spectra in various solvents together with the conditions of recording.

The book includes shorter chapters and appendices dealing with the types of laser sources and other laser Raman spectrometers, supplying a list of the most important basic literature (only books, review papers are not given).

In summary, the book is a good manual for the use of laser Raman spectrometers, especially of the instruments mentioned, but nothing more. The material is well selected and clearly presented.

F. BILLES

INDEX

INORGANIC AND ANALYTICAL CHEMISTRY – ANORGANISCHE UND ANALYTISCHE CHEMIE – НЕОРГАНИЧЕСКАЯ И АНАЛИТИЧЕСКАЯ ХИМИЯ

HAUFFE, K. und HEGEDŰS, A. J.: Über die Beeinflussung der Verdampfungsgeschwindigkeit von Zinkoxid durch kurzwelliges Licht. (The Effect of Shortwave Light on the Volatility of ZnO) 123

INCZÉDY, J., KLATSMÁNYI-GÁBOR, P. and ERDEY, L.: The Use of Complex Forming Agents in Ion Exchange Chromatography, V. Adsorption of Metal Ions on Cation Exchange Resin in the Presence of Pyridine, Ethylenediamine and Triethanolamine 137

FLÓRA, T. und MENYHÁRT, M.: Untersuchung der beim Erhitzen zwischen den Komponenten von N—P—K-Düngern verlaufenden Vorgänge, I. Im System Ammoniumnitrat–Kaliumchlorid verlaufende Prozesse. (Investigation of the Processes Occurring on Heating Between the Components of N—P—K-Fertiliziers, I. Processes Proceeding in the System Ammonium Nitrate–Potassium Chlorid 145

LÉGRÁDI, L.: Mechanism of a Adsorption Indication, IX. Phthaleins as Adsorption Indicators 157

HAVÍŘ, J. and FIDLER, A.: The Reaction of Ferrocyanide Ion With Silver Nitrate (Short Communication) 163

PHYSICAL CHEMISTRY – PHYSIKALISCHE CHEMIE – ФИЗИЧЕСКАЯ ХИМИЯ

KISS, L. und FARKAS, J.: Untersuchung der Ionisation von Metallen und Metallionenneutralisation mit der rotierenden Ring-Scheibenelektrode, VIII. Allgemeine Behandlung der an der Ringelektrode meßbaren Parameter. (Investigation of the Ionisation of Metals and the Neutralisation of Metal Ions at the Rotary Ring and Disc Electrode, VIII. General Discussion of the Parameters Measurable at the Ring Electrode) 167

WOJNÁROVITS, L. and FEJES, P.: Radiation Chemistry of Saturated–Unsaturated Hydrocarbon Systems, III. Kinetic Study of Hydrogen Formation 177

ERDEY-GRÚZ, T., GALLYAS, M. und SZETEY, É.: Abhängigkeit der Sauerstoffüberspannung von der Aktivität des Wassers, II. Wirkung der Alkalimetallionen in schwefelsaurer Lösung. (Dependence of the Oxygen (Over) Voltage on the Activity of Water, II. The Effect of Alkali Metal Ions in Sulfuric Acid Solution) 203

ERDEY-GRÚZ, T. und LÉVAY, B.: Bestimmung des Selbstdiffusionskoeffizienten des Dioxans in den Systemen Dioxan–Wasser und Dioxan–Methanol. (Determination of the Self-Diffusion Coefficient of Dioxane in the Systems Dioxane–Water and Dioxane–Methanol) 215

ORGANIC CHEMISTRY – ORGANISCHE CHEMIE – ОРГАНИЧЕСКАЯ ХИМИЯ

TOLDY, L., SÓLYOM, S., KOCKA, I., TÓTH, G. und TÓTH, I.: Thiocarbamidderivate mit Tuberkulostatischer Wirkung, II. Acylthiocarbamide. (Thiourea Derivatives with Tuberculostatic Action, II. Acyl Thiourea) 221

VINKLER, P., KLIVÉNYI, F., VINKLER, E., STÁJER, G. und SZABÓ, A. E.: Untersuchungen über aromatische Sulfenylchloride, II. Reaktionen des Sulfenylchlorids mit Thiocarbamiden und Thiosemicarbaziden. (Investigations in the Field of Aromatic Sulfenyl Chlorides, II. The Reaction of Sulfenyl Chloride with Thioureas and Semi-Thioureas) 229

ZSADON, B. and KAPOSI, P.: Tabersonine from Ripen Seeds of *Vinca Rosea L.* (Preliminary Communication) 241

RECENSIONES 243

Printed in Hungary

A kiadásért felel az Akadémiai Kiadó igazgatója — Műszaki szerkesztő: Várhelyi Tamás

A kézirat nyomdába érkezett: 1971. III. 15. — Terjedelem: 11,25 (A/5) ív, 65 ábra, 2 melléklet

71.71373 Akadémiai Nyomda, Budapest — Felelős vezető: Bernát György

ACTA CHIMICA

ТОМ 69 — ВЫП. 2

РЕЗЮМЕ

Влияние коротковолнового света на летучесть ZnO

К. ХАУФФЕ и Й. А. ХЕГЕДЮШ

Термогравиметрически, с помощью вакуумикровесов измерялась скорость испарения металлического цинка и его окиси. Наиболее удобная для измерений этим методом область скоростей $2 \div 20 \cdot 10^{-11}$ (г-моль или г-атом/сек · см^2, соответственно) соответствует следующим условиям: при давлении $1 \div 2 \cdot 10^{-5}$ торр 450 + 525 °C в случае ZnO, а в случае Zn 140—200°C. Выше этой температуры в случае обоих веществ наблюдается сильное образование Zn-сублимата вследствие слишком интенсивного испарения. В случае ZnO не удалось обнаружить влияние УФ-облучения, в случае же Zn наблюдается сильный эффект с температурным гистерезисом. Облучение ускоряет испарение Zn. Энергии активации испарения ZnO и Zn, а также реакции ZnO + H_2 оказались практически одинаковыми. Присутствие H_2O, по всей вероятности, ускоряет испарение ZnO и замедляет испарение Zn.

Применение комплексообразователей в ионообменной хроматографии, V

Закрепление ионов металлов на ионообменной смоле в присутствии пиридина, триэтаноламина и этилендиамина

Я. ИНЦЕДИ, П. ГАБОР-КЛАЧМАНИ и Л. ЭРДЕИ

Определялось распределение некоторых двухвалентных, комплексообразующих ионов металлов на катионообменной смоле из растворов с различным содержанием пиридина, триэтаноламина и этилендиамина. Приводятся приближенные значения констант ионообменных равновесий отдельных комплексов и ионов металлов. На основе результатов измерений были разработаны методы ионообменного хроматографического разделения ионов меди и цинка.

Изучение процессов, протекающих между компонентами тройных искусственных удобрений при их нагреве, I

Процессы, протекающие в системе нитрат аммония — хлорид калия

Т. ФЛОРА и М. МЕНЬХАРТ

Дериватографическим методом изучались процессы, протекающие при нагреве системы нитрат аммония — хлорид калия. Термические исследования в отдельных случаях дополнялись рентгеновским и элементарным анализом остатков после нагрева.

На основе результатов исследований было установлено, что: 1. под влиянием механического истирания при комнатной температуре между нитратом аммония и хлоридом калия протекает обменное разложение без количественного выхода; 2. часть непрореагировавшего нитрата аммония образует смешанный кристалл с образовавшимся нитратом калия; 3. другая часть его вступает в термическое взаимодействие с образовавшимся хлоридом аммония; 4. смешанный кристалл нитрат аммония — нитрат калия при температуре около 90°C вступает в реакцию с еще непрореагировавшим хлоридом калия.

Механизм адсорбционной индикации, IX

Фталеины как адсорбционные индикаторы

Л. ЛЕГРАДИ

Среди фталеиновых индикаторов, α-нафтолфталеин пригоден в аргентометрическом титровании хлористых, бромистых и роданистых ионов, фенолфталеин — для бромидов и йодидов, а тимолфталеин — для хлоридов, бромидов и йодидов. В качестве адсорбционных индикаторов может быть использована и смесь тимолфталеина с α-нафтолфталеином, а также тимолфталеина с фенолфталеином. Применение этих индикаторов при титровании должно происходить в слабо щелочных средах (pH = 7—9), а α-нафтолфталеин может быть использован и без подщелачивания. Фталеиновые индикаторы действуют по принципу поверхностной адсорбции на осадке. Серебряная соль красителя может быть обнаружена цветной реакцией с фильтровальной бумагой, а также может быть препарирована в виде осадка.

Изучение ионизации металлов и восстановления ионов металлов с помощью вращающегося дискового электрода с кольцом, VIII

Обобщенное обсуждение параметров, измеряемых на кольцевом электроде

Л. КИШ и Й. ФАРКАШ

Выведено уравнение, выражающее концентрацию ионов на поверхности кольцевого электрода, ионов, возникших или реагировавших на поверхности дискового электрода, для случая, когда через кольцевой электрод не пропускается ток, и концентрация вышеуказанных ионов в растворе не очень мала.

Даны также зависимости для измеряемого электродного потенциала на кольцевом электроде и для предельного тока, измеряемого на кольцевом электроде.

Изучение образования водорода при радиолизе смесей насыщенных-ненасыщенных углеводородов, III

Кинетическое изучение образования водорода

П. ФЕЙЕШ и Л. ВОЙНАРОВИЧ

Изучались реакции, приводящие к образованию водорода при радиолизе смесей насыщенных-ненасыщенных и линейных-разветвленных углеводородов. Было установлено, что многочисленные возможные ступени реакций, при сокращении процессов одинакового характера и кинетически не отличающихся друг от друга, могут быть сгруппированы и помещены в реакционную схему, пригодную для кинетических исследований. Эта схема содержит начальные процессы поглощения энергии, реакции разложения насыщенных и ненасыщенных молекул, приводящие к образованию атома водорода, произвольный способ передачи энергии от насыщенных к ненасыщенным молекулам, потерю энергии ненасыщенной молекулой в процессах кроме разложения, приводящего к образованию атома водорода, «бимолекулярное» выделение водорода при столкновении атомов водорода с насыщенными и ненасыщенными молекулами, а также реакции захвата водородных атомов ненасыщенными молекулами. Были составлены программы оптимализации и с помощью электронной вычислительной машины были определены некоторые характерные относительные константы скоростей вышеупомянутых реакций, которые открывают возможность для более глубокого понимания т. наз. «защитного влияния». Одна из относительных констант скоростей реакций может быть использована для численного характеризования отдельных типов связей.

Зависимость перенапряжения кислорода от активности воды, II

Эффект, оказываемый ионами щелочных металлов в растворах серной кислоты

Т. ЭРДЕИ-ГРУЗ, М. ГАЛЬЯШ и З-не СЕТЭИ

Изучалось повышение перенапряжения при электрохимическом выделении кислорода под влиянием ионов Li^+, Na^+, K^+ и Cs^+ в 0,1 N растворе серной кислоты. Активность воды изменялась с помощью растворения ε-капролактама в пределах $a_w = 0{,}998 \div 0{,}738$. Изученные ионы повышают перенапряжение, однако, не изменяют вид кривой поляризации, и наклон прямых Тафеля (δ-постоянная) лишь слегка изменяется.

В растворах с высокой активностью воды ($a_w = 0{,}998$), в случае одинаковых концентраций ионов, увеличение перенапряжения происходит согласно следующему ряду: $Cs^+ < Li^+ < Na^+ < K^+$, а в растворах с относительно низкой активностью воды ($a_w = 0{,}778$ и 0,738) этот ряд имеет следующий вид: $K^+ < Na^+ < Li^+ < Cs^+$.

В растворах с активностью воды, равной $a_w = 0{,}906$ и при концентрации ионов металлов 0,005 N имеем следующий ряд: $Cs^+ < Na^+ < Li^+ < K^+$. Однако, при увеличении концентрации ионов K^+ его эффект увеличения перенапряжения падает и, начиная с концентраций 0,065 N, был получен следующий ряд: $K^+ < Cs^+ < Na^+ < Li^+$.

Согласно проведенным исследованиям, ионы щелочных металлов, не превышающие по своим размерам молекулу воды, ведут себя в этом отношении иначе, чем большие ионы, и их влияние зависит также и от того, в какой области состава проводится измерение, а именно, падает или возрастает активность воды с уменьшением концентрации.

Определение коэффициента самодиффузии в системах диоксан—вода и диоксан—метанол

Т. ЭРДЕИ-ГРУЗ и Б. ЛЕВАИ

Коэффициент самодиффузии измерялся в смесях диоксан—вода и диоксан—метанол при 25 и 35°C.

Зависимость коэффициента самодиффузии от состава смеси диоксан—вода имеет минимум при 20 мол%-ном содержании диоксана, а энергия активации самодиффузии обладает максимумом при 15 мол%-ном содержании. Произведение $D^* \cdot \eta_r$ является приблизительно постоянным в интервале содержания диоксана от 100 до 40 мол%, а в смеси с большим содержанием воды уменьшается.

Коэффициент самодиффузии в системе диоксан—метанол монотонно и сильно возрастает с увеличением содержания метанола, а произведение $D^* \cdot \eta_r$ изменяется лишь в относительно узких пределах и при концентрации 40 мол % имеет минимум. Энергия активации имеет максимум в 20 мол%-ной смеси.

Производные тиокарбамида с туберкулостатической активностью, II

Ацил-тиокарбамиды

Л. ТОЛДИ, Ш. ШОЙОМ, И. КОЦКИ, Г. ТОТ и И. ТОТ

Исходя из зависимости, наблюдаемой между строением производных тиокарбамида, содержащих 2-тиохидантоиновую и N-карбалкокси-пиперазиновую группы, и их активностью, синтезировались 1-Q-3-ацил- и 1-Q-1-ацил-тиокарбамиды.

Если 1-Q-3-ацил-тиокарбамиды образуются однозначно при реакции соответствующих аминов с ацил-изотиоцианатом, то 1-Q-1-ациловые производные удалось получить через ацилирование S-метокси-метил-изотиокарбамидов с помощью галогенидов кислот с последующим гидролизом защитной группы. В последней реакции, в зависимости от ацилирующего агента и заместителей в тиокарбамиде, иногда наблюдалось 3-ацилирование. Вследствие этого исследовались факторы, влияющие на направление ацилирования.

1-(4-алкоксифенил)-3-карбалкокси-тиокарбамиды обладают значительным противотуберкулезным действием in vitro и in vivo и оказались нетоксичными. Наиболее ценным среди них является 1-(4-изоамилоксифенил)-3-карбетокси-тиокарбамид, который обладает также и благоприятными условиями рассасывания.

Исследования в области ароматических сульфенилхлоридов, II

Реакция сульфенилхлорида с тиокарбамидами и тиосемикарбазидами

П. ВИНКЛЕР, Ф. КЛИВЕНИ, Э. ВИНКЛЕР, Г. ШТАЙЕР и А. Е. САБО

Изучалось строение соединений, образующихся в реакциях тиокарбамида и тиосемикарбазида, а также их некоторых N-арил-замещенных производных с толилсульфенилхлоридом. На основе ИК-спектроскопических исследований было установлено, что в каждом случае замещение производных тиокарбамида и тиосемикарбазида происходит на атоме серы и в результате реакции образуется связь сера-сера.

Далее было доказано, что в случае семикарбазида и N^4-замещенных производных основным центром является атом азота N^1.

The Acta Chimica publish papers on chemistry in English, German, French and Russian.

The Acta Chimica appear in volumes consisting of four parts of varying size, 4 volumes being published a year.

Manuscripts should be addressed to

Acta Chimica
Budapest 112/91 Műegyetem

Correspondence with the editors should be sent to the same address.

The rate of subscription is $16.00 a volume.

Orders may be placed with "*Kultúra*" Foreign Trade Company for Books and Newspapers (Budapest I., Fő utca 32. Account No. 43-790-057-181) or with representatives abroad.

Les Acta Chimica paraissent en français, allemand, anglais et russe et publient des mémoires du domaine des sciences chimiques.

Les Acta Chimica sont publiés sous forme de fascicules. Quatre fascicules seront réunis en un volume (4 volumes par an).

On est prié d'envoyer les manuscrits destinés à la rédaction à l'adresse suivante:

Acta Chimica
Budapest 112/91 Műegyetem

Toute correspondance doit être envoyée à cette même adresse.

Le prix de l'abonnement est de $16.00 par volume.

On peut s'abonner à l'Entreprise pour le Commerce Extérieur de Livres et Journaux «*Kultúra*» (Budapest I., Fő utca 32. Compte-courant No. 43-790-057-181) ou à l'étranger chez tous les représentants ou dépositaires.

«*Acta Chimica*» издают трактаты из области химической науки на русском, французском, английском и немецком языках.

«*Acta Chimica*» выходят отдельными выпусками разного объема. 4 выпуска составляют один том. 4 тома публикуются в год.

Предназначенные для публикации рукописи следует направлять по адресу:

Acta Chimica
Budapest 112/91 Műegyetem

По этому же адресу направлять всякую корреспонденцию для редакции.

Подписная цена — $16.00 за том.

Заказы принимает предприятие по внешней торговле книг и газет «*Kultúra*» (Budapest I., Fő utca 32. Текущий счет № 43-790-057-181) или его заграничные представительства и уполномоченные.

Reviews of the Hungarian Academy of Sciences are obtainable at the following addresses:

ALBANIA

Drejtorija Qändrone e Pärhapjes dhe Propagandimit tä Librit
Kruga Konferenca e Päzes
Tirana

AUSTRALIA

A. Keesing
Box 4886, GPO
Sydney

AUSTRIA

GLOBUS
Höchstädtplatz 3
A-1200 Wien XX

BELGIUM

Office International de Librairie
30, Avenue Marnix
Bruxelles 5
Du Monde Entier
5, Place St. Jean
Bruxelles

BULGARIA

HEMUS
11 pl Slaveikov
Sofia

CANADA

Pannonia Books
2, Spadina Road
Toronto 4, Ont.

CHINA

Waiwen Shudian
Peking
P. O. B. 88

CZECHOSLOVAKIA

Artia
Ve Smečkách 30
Praha 2
Poštovní Novinová Služba
Dovoz tisku
Vinohradská 46
Praha 2
Mad'arská Kultura
Václavské nám. 2
Praha 1
SLOVART A. G.
Gorkého
Bratislava

DENMARK

Ejnar Munksgaard
Nörregade 6
Copenhagen

FINLAND

Akateeminen Kirjakauppa
Keskuskatu 2
Helsinki

FRANCE

Office International de Documentation et Librairie
48, rue Gay Lussac
Paris 5

GERMAN DEMOCRATIC REPUBLIC

Deutscher Buch-Export und Import
Leninstraße 16
Leipzig 701
Zeitungsvertriebsamt
Fruchtstraße 3—4
1004 Berlin

GERMAN FEDERAL REPUBLIC

Kunst und Wissen
Erich Bieber
Postfach 46
7 Stuttgart S.

GREAT BRITAIN

Blackwell's Periodicals
Oxenford House
Magdalen Street
Oxford
Collet's Subscription import Department
Dennington Estate
Wellingsborough. Northants.
Robert Maxwell and Co. Ltd.
4—5 Fitzroy Square
London W. 1

HOLLAND

Swetz and Zeitlinger
Keizersgracht 471—487
Amsterdam C
Martinus Nijhof
Lange Voorhout 9
The Hague

INDIA

Hind Book House
66 Babar Road
New Delhi 1

ITALY

Santo Vanasia
Via M. Macchi 71
Milano
Libreria Commissionaria Sanso
Via La Marmora 45
Firenze
Techna
Via Cesi 16.
40135 Bologna

JAPAN

Kinokuniya Book-Store Co. Ltd.
826 Tsunohazu 1-chome
Shinjuku-ku
Tokyo
Maruzen and Co. Ltd.
P. O. Box 605
Tokyo-Central

KOREA

Chulpanmul
Phenjan

NORWAY

Tanum-Cammermeyer
Karl Johansgt 41—43
Oslo 1

POLAND

RUCH
ul. Wronia 23
Warszawa

ROUMANIA

Cartimex
Str. Aristide Briand 14—18
Bucureşti

SOVIET UNION

Mezhdunarodnaya Kniga
Moscow G—200

SWEDEN

Almquist and Wiksell
Gamla Brogatan 26
S—101 20 Stockholm

USA

F. W. Faxon Co. Inc.
15 Southwest Park
Westwood Mass. 02090
Stechert Hafner Inc.
31. East 10th Street
New York, N. Y. 10003

VIETNAM

Xunhasaba
19, Tran Quoc Toan
Hanoi

YUGOSLAVIA

Forum
Vojvode Mišića broj 1
Novi Sad
Jugoslovenska Knjiga
Terazije 27
Beograd

18. VIII. 1971 **Index: 26.007**

547.214

V.

ACTA CHIMICA

ACADEMIAE SCIENTIARUM HUNGARICAE

ADIUVANTIBUS
V. BRUCKNER, GY. DEÁK, K. POLINSZKY,
E. PUNGOR, G. SCHAY, Z. G. SZABÓ

REDIGIT
B. LENGYEL

TOMUS 69 FASCICULUS 3



AKADÉMIAI KIADÓ, BUDAPEST
1971

2

ACTA CHIMICA

A MAGYAR TUDOMÁNYOS AKADÉMIA KÉMIAI TUDOMÁNYOK OSZTÁLYÁNAK IDEGEN NYELVŰ KÖZLEMÉNYEI

SZERKESZTI

LENGYEL BÉLA

TECHNIKAI SZERKESZTŐK

DEÁK GYULA és HARASZTHY-PAPP MELINDA

Az Acta Chimica német, angol, francia és orosz nyelven közöl értekezéseket a kémia tudományok köréből.

Az Acta Chimica változó terjedelmű füzetekben jelenik meg, egy-egy kötet négy füzetből áll. Évente átlag négy kötet jelenik meg.

A közlésre szánt kéziratok a szerkesztőség címére (Budapest 112/91 Műegyetem) küldendők.

Ugyanerre a címre küldendő minden szerkesztőségi levelezés. A szerkesztőség kéziratokat nem ad vissza.

Megrendelhető a belföld számára az „Akadémiai Kiadó"-nál (Budapest V., Alkotmány utca 21. Bankszámla 05-915-111-46), a külföld számára pedig a „Kultúra" Könyv- és Hírlap Külkereskedelmi Vállalatnál (Budapest I., Fő utca 32. Bankszámla: 43-790-057-181) vagy annak külföldi képviseleteinél és bizományosainál.

Die Acta Chimica veröffentlichen Abhandlungen aus dem Bereiche der chemischen Wissenschaften in deutscher, englischer, französischer und russischer Sprache.

Die Acta Chimica erscheinen in Heften wechselnden Umfanges. Vier Hefte bilden einen Band. Jährlich erscheinen 4 Bände.

Die zur Veröffentlichung bestimmten Manuskripte sind an folgende Adresse zu senden:

Acta Chimica
Budapest 112/91 Műegyetem

An die gleiche Anschrift ist auch jede für die Redaktion bestimmte Korrespondenz zu richten. Abonnementspreis pro Band: $16.00.

Bestellbar bei dem Buch- und Zeitungs-Außenhandels-Unternehmen »*Kultúra*« (Budapest I., Fő utca 32. Bankkonto No. 43-790-057-181) oder bei seinen Auslandsvertretungen und Kommissionären.

Acta Chimica Academiae Scientiarum Hungaricae, Tomus 69 (3), pp. 249—264 (1971)

INVESTIGATIONS ON A CHROMIUM PHOSPHATE ION EXCHANGER

L. ZSINKA and L. SZIRTES

(Institute of Isotopes of the Hungarian Academy of Sciences, Budapest)

Received February 25, 1970

Following our recent work on zirconium and titanium phosphate, chromium phosphate was investigated. In the course of this study, the solubility, the ion exchange and thermochemical properties of the prepared material were examined.

Based on the data found (solubility, thermochemical, etc.) it is assumed that during the synthesis various phosphates were formed, depending on the ratio of the materials used. These phosphates, depending on the PO_4/Cr ratio, may be classified as one of the three main types of phosphate polymers, having different specific surface areas due to significant adsorption effects.

Based on the results of the determination of ion exchange properties, we supposed that, regardless of the composition, exchangeable hydrogen ions may be formed by dissociation of the hydrogen phosphate groups.

Summarizing the experimental data, the samples which can be most successfully used as ion exchangers are those in which the PO_4/Cr ratio is about 0.75—1.0 (for example CP–1); *i.e.* those materials which can be classified as linear phosphate polymers

In recent years chromium phosphate became widely used as an anticorrosive pigment and as a colloidal solution in medical practice [1—8]. Besides the initial interest in phosphate containing materials, this fact could have been the reason for numerous detailed studies on the structure of chromium phosphate [9—14]. Based on these works a more or less unified picture emerges about this material according to which various types of polymers are formed, depending on the chromium to phosphate ratio.

Among the papers found in the literature only in the work by LUKASZEWSZKI, REDFERN and SALMON [15] are mentioned some preliminary data about the ion exchange properties of chromium arsenate.

Following our recent work on zirconium and titanium phosphates [16], chromium phosphate was also investigated. In this paper we present data concerning the preparation of chromium phosphate and its properties as an ion exchanger.

In the present study the solubility, the ion exchange and the thermochemical properties of the prepared material were examined. The resistance against radiation and the possibility of its use in practical separations have been described [17—18].

Experimental

1. *Chromium phosphate* was prepared as follows. To a 5% aqueous solution of chromium-(VI) oxide, 85% solution of phosphoric acid was added in excess, then the necessary amount of a 10% aqueous solution of hydrazine hydrate was added. The precipitations were carried

MAGYAR TUDOMÁNYOS AKADÉMIA KÖNYVTÁRA

out in the temperature interval 20—95 °C. The precipitates were washed as a rule up to pH = 4 (the pH determinations were carried out using a Radiometer PHM–4 type pH meter; error of the pH measurement being ±0.02 pH units), and dried at 70 °C. Fractions of the exchangers with 0.4—0.315 mm grain size were selected.

Samples CP–1 through CP–4, CP–6 and CP–7 were precipitated with various amounts of phosphoric acid.

Samples CP–1 through CP–4 were not washed after precipitation and the pH of the solution varied between 4.5 (CP–1) and 2.5 (CP–4). Samples CP–6 and CP–7 were washed with redistilled water until reaching pH = 4.

Sample CP–5 was precipitated with the same amount of phosphoric acid as sample CP–2, but it was washed until reaching pH = 4.

Samples CP–8 and CP–9 were precipitated with the same amount of phosphoric acid as sample CP–2, but at temperatures 70° and 95°, and were washed until reaching pH = 4.5 (CP–8) and 3.5 (CP–9), respectively.

2. *X-ray measurements* were carried out with a CuK_{alpha} source and a Guinier type focusing cell.

3. *The chromium and the phosphate contents* of the samples were determined as follows. The samples (100 mg) were dissolved in hot concentrated nitric acid. The solution was evaporated to 5—10 ml and afterwards washed with redistilled water into a 500 ml volumetric flask.

From these stock solutions the samples for the determinations of chromium and phosphate were obtained by dilution. The concentration of chromium or phosphate in these solutions was 1—25 μg/ml. The chromium content of the samples was determined with a Zeiss Q–24 type spectrograph. Equal volumes (30 μl) of the chromium phosphate solution (containing 1—25 μg Cr/ml) and the ammonium molybdate solution (containing 25 μg Mo/ml) were carried on a pair of specpure copper electrodes (diameter 6 mm).

The spectra of standard solution containing 1, 5, 10 and 25 μg/ml of chromium were determined under similar conditions in parallel. The spectrum (Cr = 2835.6 Å and Mo = = 2775.4 Å) was evaluated with a Zeiss G–II type photometer.

The phosphate content of the samples was determined spectrophotometrically as phosphorus molybdenum blue, by measuring the extinction of the solution at 830 mμ. For calibration, solutions of KH_2PO_4 with concentrations 0.1, 0.2, 0.5, 1.0 and 1.5 μgP/ml, respectively, were used.

The data given in Table I are the results of five parallel determinations.

Table I

Phosphate/chromium ratio in various samples

Sample	Ratio PO_4/Cr
CP–1	0.76
CP–5	0.91
CP–9	1.04
CP–2	1.10
CP–8	1.10
CP–7	1.13
CP–6	1.45
CP–3	1.51
CP–4	2.14

4. *The solubility* of the samples was studied in H_2O, 0.1 *N* NH_4Cl, and 0.2 *N* HCl under non-stationary conditions. The soluble phosphate content was determined as follows. 100 mg of the exchanger (after removing the fine grains adhered onto the surface) was brought into contact with 10 ml solution at 25±2 °C. The mixture was shaken for 8 hours, followed by

centrifugation. 5 ml solution was selected for determination of the amount of phosphate. Beside this, the variation of the amount of dissolved phosphate was determined as a function of the pH. In these cases the five ml portions of the solutions for the determination of capacity were used (time of shaking 2 hours, concentration of K^+ 0.03—0.2 mval/ml).

For the determination of the soluble amount of phosphate the previously described method was used. The results of the analyses are shown in Table II, and in Figs 1—3.

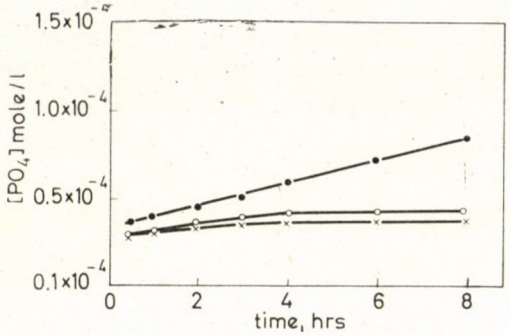


Fig. 1. Dependence of the dissolved quantity as a function of time in the case of sample CP–1. × — in H_2O; ○ — in 0.1 *N* NH_4Cl; ● — in 0.2 *N* HCl

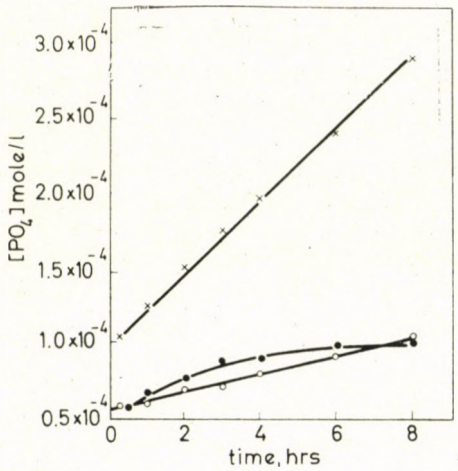


Fig. 2. Dependence of the dissolved quantity as a function of time in the case of sample CP–9. ● — in H_2O; ○ — in 0.1 *N* NH_4Cl; × — in 0.2 *N* HCl

5. *The exchange capacity* measurements were carried out with the static method using a radioactive tracer technique. A solution was prepared containing the tracers (counter-ions: generally K^+) in an amount 5—6 times higher than the expected exchange capacity value. To 10 ml of this solution 100 mg of ion exchanger was added and the system was shaken until attaining equilibrium. Afterwards the radioactivities of the original and the equilibrium solution (two parallels, 5 ml each) have been measured by a scintillation technique. The exchange capacity of the samples was calculated using the formula

$$Q = \frac{(I_0 - I_e)\, B}{(I_0 - I_{bg})\, A} \qquad (1)$$

where

Q — the exchange capacity (mval/g);
A — the weight of the ion exchanger (g);
B — the amount of the carrier (mval);
I_0 — the count rate for the initial solution;
I_e — the count rate for the solution after equilibration;
I_{bg} — the background.

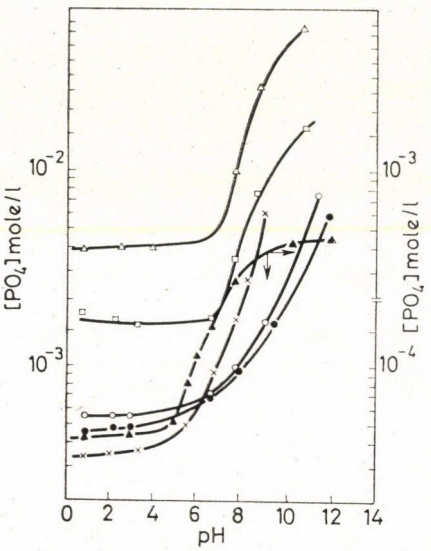


Fig. 3. Amount of soluble PO_4^{3-} as a function of the pH. ▲ — CP–1; ● — CP–8, × — CP–9; □ — CP–6, ○ — CP–2; △ — CP–3

Table II

Amount of soluble phosphates in various solutions

Sample	$[PO_4] \times 10^4$ mole/litre at 25 °C			$[PO_4] \times 10^4$ mole/litre at 80 °C		
	H_2O	0.1 *N* NH_4Cl	0.2 *N* HCl	H_2O	0.1 *N* NH_4Cl	0.2 *N* HCl
CP–1	0.38	0.46	0.85	6.5	6.9	8.9
CP–5	0.72	0.63	0.95	—	—	—
CP–9	1.0	1.0	2.8	47	51	67
CP–2	0.92	0.97	0.98	64	67	86
CP–8	0.95	0.82	1.30	—	—	—
CP–7	0.93	0.96	1.8	—	—	—
CP–6	8.8	6.6	13	—	—	—
CP–3	16	14	13	—	—	—
CP–4	53	51	87	—	—	—

The error of the measurements was evaluated by the method of least squares and found to be $\pm 5\%$.

As a first step the time being necessary to attain equilibrium and the influence of loading of the ion exchanger were determined (Table III).

Table III

Capacity values as a function of equilibration time and load

(amount of resin: 100 mg; volume of the solution: 10 ml)

Load (mval)	Time of equilibration (hrs)	CP–1		CP–2	
		capacity (mval/g)	pH	capacity (mval/g)	pH
1.0	0.25	0.25	2.8	0.40	2.9
	0.50	0.28		0.48	
	1.0	0.30		0.52	
	2.0	0.29		0.52	
	4.0	0.27		0.49	
3.0	0.25	0.24	2.8	0.42	2.8
	0.5	0.27		0.52	
	1.0	0.26		0.57	
	2.0	0.28		0.56	
	4.0	0.26		0.54	
6.0	0.5	0.24	2.8	0.53	2.8
	1.0	0.29		0.58	
	2.0	0.25		0.58	
	4.0	0.32		0.54	
20.0	0.25	4.10	12.4	5.10	12.2
	0.50	4.30		5.23	
	1.0	4.28		5.37	
	2.0	4.23		5.46	
	4.0	4.40		5.28	
30.0	1.0	4.48	12.3	5.22	12.2
	2.0	4.31		5.27	
	4.0	4.30		5.38	

In order to check the data obtained by the tracer method, the capacity was also determined by measuring the change of H^+ ion concentration in the solution; in the given case the pH values of the initial and the equilibrated solutions were measured.

The exchange capacity was calculated from the formulae:

$$Q' = \frac{[H^+]_e - [H^+]_0}{A} \cdot V \; ; \; \text{pH} < 7 \tag{2}$$

$$Q' = \frac{\frac{10^{-14}}{[H^+]_0} - \frac{10^{-14}}{[H^+]_e}}{A} \cdot V; \; \text{pH} > 7 \tag{3}$$

where

Q' — the capacity calculated from the change of H^+ ion concentration (mval/g);
$[H^+]_e$ — the H^+ ion concentration of the equilibrated solution (mval/ml);
$[H^+]_0$ — the H^+ ion concentration of the initial solution (mval/ml);
V — the volume of solution (ml);
A — the weight of the ion exchanger (g).

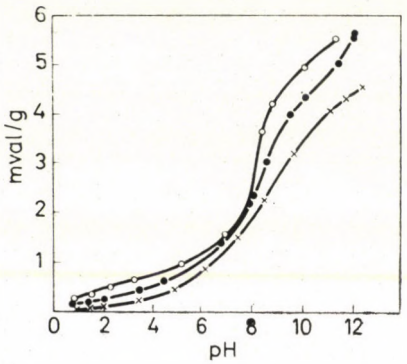


Fig. 4. Exchange capacity as a function of the pH. × — CP–1; ● — CP–5 and CP–9, ○ — CP–2, CP–8 and CP–7

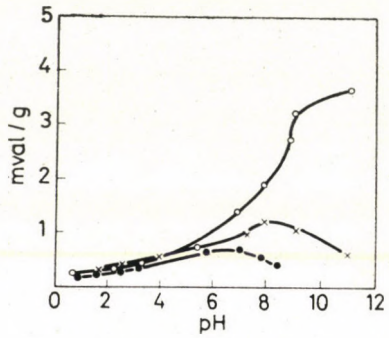


Fig. 5. Exchange capacity as a function of the pH. ○ — CP–6; × — CP–3; ● — CP–4

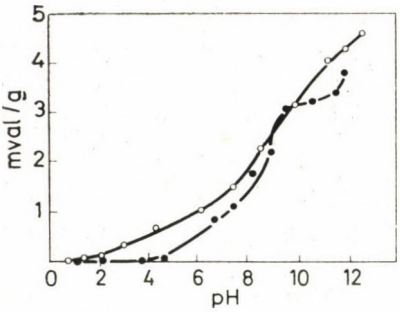


Fig. 6. Exchange capacity as a function of the pH for sample CP–1. ○ — saturated with K^+ ions; ● — saturated with Na^+ ions

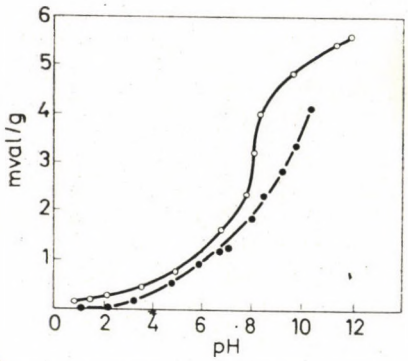


Fig. 7. Exchange capacity as a function of the pH for sample CP–8. ○ — saturated with K^+ ions; ● — saturated with Na^+ ions

The results of these two measurements are summarized in Table IV.

The change of capacity as a function of pH was determined also by the tracer method (Figs 4—7). The pH was measured as described previously; in the course of measurements KCl + HCl and KCl + KOH solutions were used. In case of sodium ion (labelled with ^{24}Na) the measurements were carried out under the same conditions, but NaCl + HCl and NaCl + + NaOH solutions were used, respectively.

6. *The thermochemical behaviour* of the samples was investigated by a thermogravimetric method. The measurements were carried out with the PAULIK—PAULIK—ERDEY type derivatograph which permitted the parallel determination of the weight change as a function of temperature (TG curve), the rate of the weight change (DTG curve) and the rate of the enthalpy change (DTA curve).

Table IV

Capacity data determined by two different methods

Sample	pH of the solution		Capacity (mval/g)	
	initial	equilibrium	by tracer technique	calcd. from $[H^+]$-change
CP–1	5.39	2.85	0.14	0.19
	11.52	5.82	0.31	0.43
	12.02	7.50	1.04	1.25
	12.29	8.33	1.95	2.40
	12.50	8.65	3.17	3.52
	12.68	11.10	4.65	4.10
	12.76	12.15	4.50	4.00
CP–5	5.39	2.93	0.47	0.12
	11.52	4.60	0.55	0.33
	12.02	6.90	1.40	1.04
	12.29	7.80	2.18	1.95
	12.50	9.34	3.75	3.17
	12.68	11.14	4.80	4.66
	12.76	11.97	5.40	4.81
CP–9	5.39	3.00	0.55	0.10
	11.52	5.23	0.85	0.33
	12.02	6.69	1.30	1.04
	12.29	7.87	1.95	1.95
	12.50	9.35	3.70	3.17
	12.68	9.89	4.20	4.81
	12.76	11.87	5.45	5.03
CP–2	5.39	2.94	0.40	0.11
	11.52	4.94	0.71	0.33
	12.02	6.75	1.60	1.04
	12.29	7.85	2.20	1.95
	12.50	8.33	3.54	3.17
	12.68	9.86	4.85	4.81
	12.76	11.85	5.46	5.06
CP–8	5.39	2.99	0.40	0.11
	11.52	4.87	0.75	0.33
	12.02	6.47	1.55	1.04
	12.29	7.95	2.33	1.95
	12.50	8.44	3.94	3.17
	12.68	10.20	5.30	4.78
	12.76	11.84	5.50	5.04

Table IV (continued)

Sample	pH of the solution		Capacity (mval/g)	
	initial	equilibrium	by tracer technique	calcd. from $[H^+]$-change
CP–7	5.39	3.25	0.60	0.06
	11.52	5.26	0.93	0.33
	12.02	7.02	1.54	1.04
	12.29	8.10	2.45	1.95
	12.50	8.47	3.67	3.17
	12.68	9.70	4.81	4.81
	12.76	11.34	5.52	5.50
CP–6	5.39	3.27	0.05	0.47
	11.52	5.31	0.33	0.75
	12.02	6.88	1.04	1.44
	12.29	7.78	1.95	2.00
	12.50	8.75	3.17	2.80
	12.68	8.83	3.81	3.28
	12.76	10.91	4.06	3.70
CP–3	5.39	3.97	0.50	0.62
	11.52	5.69	0.73	0.66
	12.02	7.21	1.04	1.00
	12.29	7.84	1.25	1.28
	12.50	8.96	1.10	1.08
	12.68	9.66	0.90	1.30
	12.76	10.82	0.68	0.66
CP–4	5.39	3.08	0.25	0.43
	11.52	5.37	0.50	0.49
	12.02	7.00	0.64	0.70
	12.29	7.70	0.15	0.58
	12.50	8.38	—	0.46
	12.68	9.12	—	—
	12.76	9.09	—	—

In order to make possible the comparison of various samples, the conditions of the measurements were chosen as follows:

sample weight:	500 mg
weight of Al_2O_3:	500 mg
end-point of heating:	900 °C (on a 1200 °C scale)
TG sensitivity:	200 mg
DTG sensitivity:	1/10
DTA sensitivity:	1/10
heating rate:	12 °C/min
particle size:	powdered sample

In Fig. 8 the data concerning samples CP–1, CP–2 and CP–5 are shown. Samples CP–7, CP–8 and CP–9 were fully analogous to these, therefore they are not represented in the Figure. The data shown in Fig. 9 refer to samples CP–3 and CP–6.

In Fig. 10 the data concerning sample CP–9 (initial, partly and fully saturated with K^+ ions) are shown.

From the thermochemical investigations certain valuable information about the structure of the examined samples could be obtained. On the other hand, using the weight

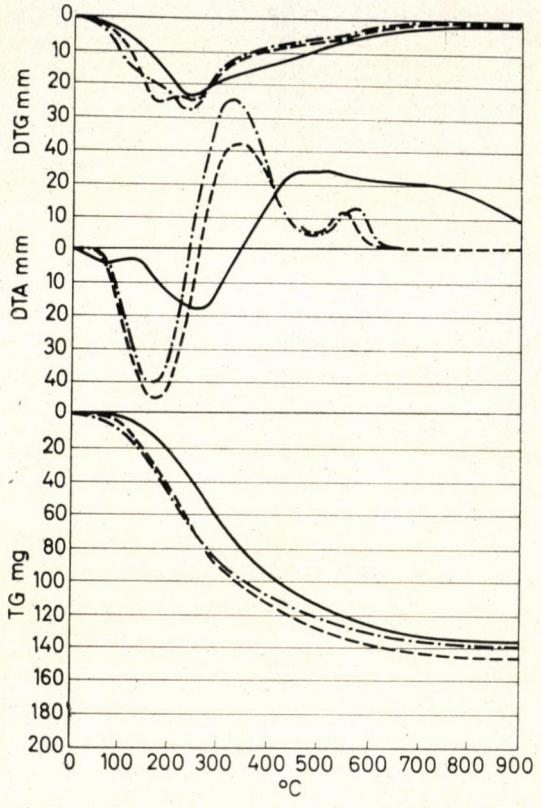


Fig. 8. Thermograms of samples CP–1, CP–5 and CP–2.
—— CP–1; ---- CP–5; ····· CP–2

loss data, the capacity of the samples has been calculated (these data are comparable with those calculated from the amount of exchangeable H^+ ions).

Based on the thermogravimetric data the capacity of the samples can be calculated in three ways.

a) By comparing the weight losses of the initial and the saturated (in our case with K^+ ions) samples. In the calculations we assumed that one molecule of structural water (originating from the dissociation of the phosphate groups) can be exchanged by two moles of potassium ions. In agreement with this, during the saturation each 18 mg of lost water corresponds to 78.2 mg of K^+, *i.e.* the observed weight increase (60.2 mg) in the case of a fully saturated sample corresponds to the loss of one mole of structural water which represents a capacity of 2 mval.

b) By calculation from the weight loss of the initial sample above 480 °C.

c) By calculation from the assumed molecular composition. On the basis of the PO_4/Cr ratio and the thermoanalytical data, the amount of crystalline and/or adsorbed water (in mole) per one mole chromium was determined. If the stoichiometric composition of the molecule

is known, the capacity can be calculated in the usual way in spite of the fact that the detailed structure is unknown.

The capacity data obtained by these methods are collected in Table V.

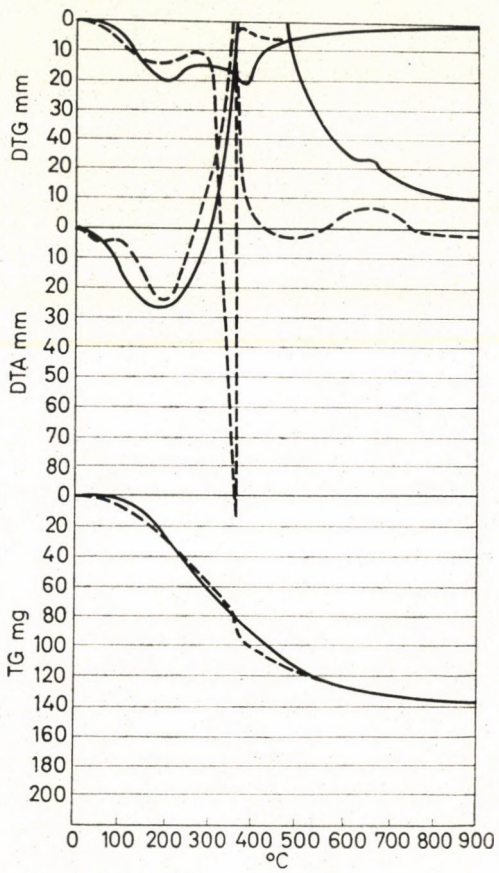


Fig. 9. Thermograms of samples CP–3 and CP–4.
—— CP–3; ---- CP–4

7. *The specific surface areas* of the samples were determined by the krypton adsorption method. The measurements were carried out on a volumetric gas adsorption apparatus at liquid nitrogen temperature and were analyzed by the BET method, using a computer program (computer type ICT–1905). The samples were pre-treated before the measurements at the same temperatures at which they were dried during the syntheses. The results of the measurements are given also in Table V.

ACTA CHIMICA

ТОМ 69 — ВЫП. 3

РЕЗЮМЕ

Изучение хромофосфатного ионообменника

Л. ЖИНКА и Л. СИРТЕШ

Настоящая работа является продолжением ранее начатых исследований, проведенных на фосфатах циркония и титана. Данные исследования, помимо выяснения условий получения, ставили своей целью также определение растворимости материала, а также его термохимических и ионообменных свойств.

На основе полученных данных (по растворимости, термохимическому поведению и т. д.) полагалось, что при приготовлении материала, в зависимости от соотношения исходных веществ, образуются фосфаты с различным составом. Последние, в зависимости от найденного отношения PO_4/Cr, могут быть отнесены к одной из 3 основных групп фосфатных полимеров. Рассматривая влияние отношения PO_4/Cr на величины удельной поверхности, можно заключить, что в данном случае необходимо считаться со значительным адсорбционным эффектом.

На основе результатов исследований ионообменных свойств можно полагать, что, независимо от состава, ионы H^+, способные к обмену, образуются в результате диссоциации кислофосфатных групп.

Суммируя экспериментальные данные, можно заключить, что в качестве ионообменников наиболее успешно могут быть применены образцы с отношением PO_4/Cr, равным 0,75 + 1,0 (напр. CP-1), т. е. вещества, которые могут быть отнесены в группу линейных полимеров.

Применение комплексообразователей в ионообменной хроматографии, VI

Разделение органических оснований на катионообменной колонке

Я. ИНЦЕДИ

Было определено отношение распределений пиридина, *п*-толуидина и бензиламина на катионообменной смоле в форме натрия или никеля(II) из растворов 50%-ого этанола, содержащих хлористый натрий или хлорид никеля(II). Концентрация ионов натрия и никеля в растворах была одинаковой, в то время как их pH отличались.

Были выведены уравнения, с помощью которых с хорошим приближением могут быть рассчитаны коэффициенты распределений органических оснований. Были разработаны методы хроматографического разделения оснований. Определение выделенных оснований производилось спектрофотометрическим методом.

Термическое разложение метил-полисилоксанов с разветвленной целью, II

Изучение разделения и идентификации продуктов пиролиза с помощью газовой хроматографии и масс-спектрометрии

Г. ГАРЗО, Й. ТАМАШ, Т. СЕКЕИ и К. УЙСАСИ

Полимеры, указанные в заглавии получили техническое применение как силиконовые смолы. С точки зрения химического строения, они состоят из звеньев Me_2SiO (D) и $Me_2SiO_{3/2}$ (T).

Пиролитическая газовая хроматография (ПГХ) позволяет идентифицировать качественно и измерять количественно летучие продукты терморазложения, и тем самым позволяет изучение химических превращений, происходящих в течение термообработки. Природа изученного полимера поставила необходимостью сочетание ПГХ с масс-спектрометрией и препаративной газовой хроматографией.

С помощью вышеупомянутого метода в пиролитической хроматограмме трехмерного полимера метилсилоксана было найдено 17 компонентов, которые химически были идентифицированы как следующие: D_3, D_4, D_5, D_6 — циклы, T_2D_3, T_2D_4, T_2D_5 — бициклы и T_4D_2, T_4D_3, T_6D, T_6D_2 — полициклы. Соединения T_2D_4, T_2D_5 и T_4D_5 фигурируют в пирограмме в форме трех-трех изомерной модификации

Программы регистрируют результаты микро-пиролитических-газово-хроматографических (ПГХ) измерений. Измерения проводились с помощью металлического микрореактора, собственного производства, присоединенного к входу на колонку.

Измеряя индекс ретенции перечисленных выше продуктов пиролиза на колонке, содержащей три различных жидких фазы, была получена информация относительно строения изомеров, образующихся при терморазложении.

Знание продуктов пиролиза вместе с масс-спектрометрическими схемами разложения позволяет составить картину о характере процессов терморазложения.

Изучение процессов, протекающих между компонентами тройных искусственных удобрений при их нагреве, II

Процессы, протекающие в системах нитрат аммония – первичный фосфат аммония, нитрат аммония – двузамещенный фосфорнокислый кальций, первичный фосфат аммония – двузамещенный фосфорнокислый кальций, первичный фосфат аммония – хлорид калия, двузамещенный фосфорнокислый кальций – хлорид калия

Т. ФЛОРА и М. МЕНЬХАРТ

Проводились дериватографические исследования двойных систем: нитрат аммония — первичный фосфат аммония, нитрат аммония — двузамещенный фосфорнокислый кальций, первичный фосфат аммония — хлорид калия, двузамещенный фосфорнокислый кальций — хлорид калия, первичный фосфат аммония — двузамещенный фосфорнокислый кальций. Было установлено, что во всех системах за исключением системы двузамещенный фосфорнокислый кальций — хлорид калия, компоненты вступают в термическое взаимодействие друг с другом. Далее было установлено, что двузамещенный фосфорнокислый кальций вступает в реакцию обменного разложения с хлористым калием. В остальных системах полагалось образование координационных связей между компонентами.

Уравнения состояний граничного поверхностного слоя в системе твердое тело – газ

Й. ТОТ

Уравнения состояний адсорбционных фаз, образующихся на поверхности твердого тела, определяются из интегральной формы зависимости Гиббса:

$$\pi = \frac{RT}{a^s} \int_0^p \frac{n^s}{p}\, dp$$

где π — тангенциальное давление слоя, a^s — удельная поверхность адсорбента, $\varphi = a^s/n^s$ — поверхность, занимаемая пленкой одного адсорбированного моля. Правильный расчет уравнения состояний возможен лишь в том случае, если в вышеприведенном уравнении интегрируется такое точное уравнение изотермы $n^s = f(p)$, которое, в самом полном смысле,

принимает в учет характер поверхности. Уравнения состояний одно- и многослойных адсорбционных фаз на энергетически гомогенных или приближающихся к ним поверхностях могут быть рассмотрены на основе единых физических и математических представлений. Это единство демонстрируется возможностью формулировки теоремы приводимых состояний, согласно которой идеальное состояние адсорбированного количества (n_u^s), соответсвующего полному монослою, означает такое основное состояние, при отношении к которому любого реального состояния, получаем безразмерное уравнение состояния, не содержащее индивидуальных констант. Для энергетически негомогенных поверхностей могут быть выведены безразмерные уравнения состояний, специфические для адсорбентов, которые в пределах справедливости теоремы приводимых состояний характеризуют также строение адсорбента.

Вывод уравнений транспорта неизотермичной гидродинамики, выраженных в разных формах, исходя из принципа Дьярмати

С. БЁРЁЦ

Исходя из вариационного принципа Дьярмати неравновесной термодинамики, были выведены дифференциальные уравнения транспорта импульса и внутренней энергии в изотопных, однокомпонентных, неизотермичных гидротермодинамических системах. Выводы заключают в себе многочисленные парциальные результаты, полученные раньше, а также освещают вопрос о связи, между вышеупомянутымы уравнениями транспорта (особенно уравнением транспорта внутренней энергии) в случае использования различных форм. Что касается «обратимой части» уравнения Навиера-Стокса, описывающего транспорт импульса, было установлено, что несмотря на то, что принцип Дьярмати по каким-то особенным и удачным обстоятельствам справедлив формально и в этом случае, но эта не может быть рассмотрена как действительный вариационный принцип для случая обратимых движений.

Окисление на окисно-никелевом электроде, IV

Кинетика окисления первичных спиртов

Дь. ВЕРТЕШ, Дь. ХОРАНИ и Ф. НАДЬ

Изучалась скорость окисления первичных спиртов на окисно-никелевом электроде. Было установлено, что помимо найденной ранее пропорциональности между скоростью и количеством NiOOH на электроде (Q), скорость зависит также и от концентрации спирта:

$$w = k_0 \cdot Q \cdot c_a$$

Рассматривая полученную таким образом константу скорости реакции второго порядка (k_0) было установлено, что ее величина не зависит от основности смеси.

При изучении роли электродного потенциала было доказано, что между потенциалом окисно-никелевого электрода и содержанием активного кислорода не наблюдается однозначной зависимости.

Было доказано экспериментально, что к различным электродным потенциалам могут относиться одинаковые скорости окисления. Это означает, что константа скорости, фигурирующая в уравнении k_0, не зависит от потенциала электрода.

Изучение совместного нитрования некоторых ароматических соединений

А. УЙХИДИ, О. РЕПАШИ и Й. ТАКАЧ

Относительные скорости нитрования в сернокислых гомогенных растворах отличаются от значений, приводимых в литературе для органических растворителей. Поэтому стало необходимым выяснение этого вопроса.

При совместном нитровании гомогенных растворов бензола, толуола и их некоторых нитропроизводных с различной концентрацией в серной и уксусной кислотах, а также в уксусной кислоте, содержащей серную кислоту, было установлено, что относительные скорости уменьшаются с увеличением содержания серной кислоты и температуры. Отношения констант скоростей в серной кислоте меньше, чем в уксусной. Это означает, что относительные реакционные способности различных ароматических соединений не могут быть заданы в виде общесправедливых значений, а при их задании необходимо принимать во внимание влияние растворителя, температуры, а в некоторых случаях даже и концентрации.

Использование хлористых амидов в реакции циклизации, III

Синтез амидразонов нового типа и изучение процесса замыкания кольца

З. ЧЮРЁШ, Р. ШОШ, И. БИТТЕР, и Й. ПАЛИНКАШ

Из метилового эфира антраниловой кислоты и хлорида диметилформамида был синтезирован гидрохлорид N,N-диметил-N'-(2-карбометоксифенил)-формамидина. Амидин подвергался взаимодействию с 4-замещенными фенилгидразонами, и, таким образом, были получены новые, до сих пор еще не описанные N_1-(4-замещенный фенил)-N_3-(2-карбометоксифенил)-формамидразоны. Исследовалась циклизация амидразонов в 3-[N-(4-замещенный фенил)-амино]-4(3H)-хиназолины.

Термическая диссоциация карбамидов, II

З. ЧЮРЁШ, Р. ШОШ, И. БИТТЕР, З. БЕНЦЕ и М. ЭЦЕТ

Изучались особенности термического разложения десяти различных диарилкарбамидов. Кинетические характеристики разложения рассчитывались методом, основанным на термоаналитических исследованиях, разработанных в последние годы. Были определены порядок и энергия активации реакции разложения симметричного дифенилкарбамида и его замещенных производных с симметричными группами: хлор-, метил- и нитрогруппы.

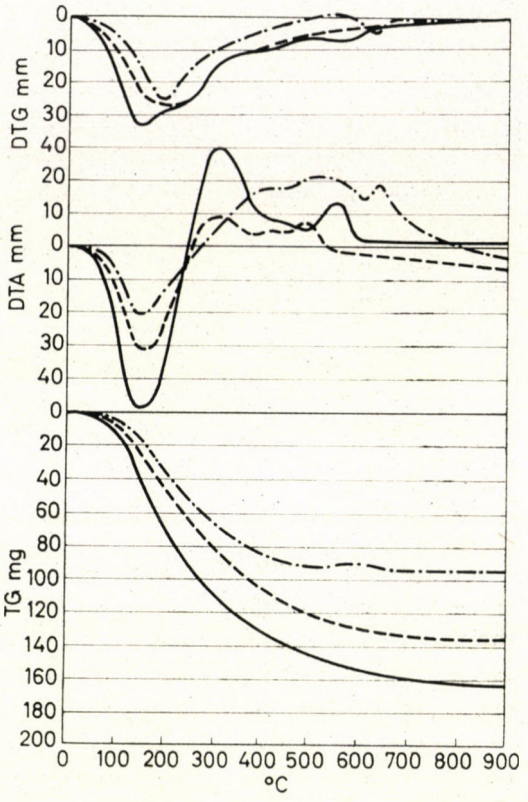


Fig. 10. Thermogram of sample CP–9, saturated with various amounts of K^+ ions. —— initial sample; ---- partly saturated sample; ····· fully saturated sample

Table V

Capacity data determined by various methods

Sample	PO_4/Cr ratio	Capacity (mval/g exchanger)					Specific surface area (m^2/g)
		by tracer technique	from change of $[H^+]$ concentration	from the thermogram by saturation with K^+	from the weight loss above 480 °C	calculated from the assumed molecular composition	
CP–1	0.76	4.5	4.0	4.0	4.2	4.2	134.2
CP–5	0.91	5.4	4.8	4.9	4.9	4.7	112.7
CP–9	1.04	5.5	4.9	4.8	4.9	5.5	136.0
CP–2	1.10	5.5	5.1	4.9	5.1	5.7	110.0
CP–8	1.10	5.5	5.0	4.9	5.1	5.7	26.8
CP–7	1.13	5.5	5.5	5.3	5.5	5.8	5.9
CP–6	1.45	4.0	3.7	—	—	—	0.6
CP–3	1.51	0.7	0.7	—	—	—	—
CP–4	2.14	>0.1	>0.1	—	—	—	—

Discussion

With the exception of CP–3 and CP–4, the samples had good mechanical stability, but sample CP–9 showed the best characteristics from this point of view.

The X-ray diffraction measurements have unambiguously proved that the samples precipitated with various excesses of phosphoric acid have amorphous character.

As it will be shown below, the capacity *vs.* pH curve indicates a microcrystalline character. This fact is in agreement with the data of EARNSHAW [19] who gives an example of chromium phosphate which behaves as an amorphous material according to X-ray measurements, but electron diffraction studies have proved that it has a microcrystalline structure.

The PO_4/Cr ratio of the samples prepared varied in accordance with the above mentioned conditions of the syntheses, but as it will be shown further, the PO_4/Cr ratio has a strong influence on the behaviour of the material. The time of digestion did not influence the PO_4/Cr ratio of the samples produced under the same conditions, therefore, in the course of further measurements this factor was not taken into consideration.

From the solubility data it was established that the equilibrium in the aqueous system was attained within 4 hrs (CP–1) and 6 hrs (CP–9), while in the 0.1 *N* NH_4Cl system, this required 6 hrs (CP–1) and 8 hrs (CP–9). In 0.2 *N* HCl solution the equilibrium was not reached within 8 hrs and the variation of the amount of soluble phosphate with time had a nearly linear character (Figs. 1 and 2). Based on the data of Table II, it can be established that the soluble amounts of phosphates were 10^{-3}—10^{-5} PO_4 mole/litre. The amounts of soluble phosphates increase in the order:

$$H_2O \leqslant 0.1\ N\ NH_4Cl \ll 0.2\ N\ HCl,$$

and for the various samples

$$CP\text{–}1 < CP\text{–}5 < CP\text{–}9 \leqslant CP\text{–}7 \leqslant CP\text{–}2 \leqslant CP\text{–}8 < CP\text{–}6 < CP\text{–}3 \ll CP\text{–}4$$

(in the case of all examined systems); *i.e.* the amount of soluble phosphate increases with increasing PO_4/Cr ratio. These data indicate that from the point of view of solubility those methods of syntheses are promising which result in a sample with a PO_4/Cr ratio < 1.5.

The control measurements were carried out at 80 °C with three samples. The data show that the amount of soluble phosphate increases in case of sample CP–1 by one, and in the case of samples CP–2 and CP–9, by about two orders of magnitude.

Concerning the determination of soluble phosphates as a function of pH it was found that the solubility of the samples increased by one order of magnitude upon increasing the pH from 1 to 12.

A closer examination of the solubility curves reveals the existence of two processes, one below and another above pH = 7. Such a character of the curves was found for all samples examined, *i.e.* the solubility process was found greater and more rapid in acidic than in basic media. This observation is in good agreement with data of other authors [9, 10] quoted in the foregoing. This supports our assumption (see below) about the types of polymers forming in the syntheses.

Results concerning ion exchange behaviour

The measurements performed have shown that in case of K^+ ion the equilibrium was attained in 30 min., and this time proved to be independent of the pH and the composition of the ion exchanger. Based on the data of Table III, it seems to be verified that the loading of the exchanger with 3—6-fold amounts of the expected capacity yields optimum results. Increasing loads result in a larger error of the measurements (because of the error in the count rate).

Based on the data of Table V, it was established that the capacity of the sample increases with increasing PO_4/Cr ratio. Moreover it was found that the samples with the PO_4/Cr ratio around 1 had identical capacity values ($\sim$5 mval/g).

The exchange capacities of the samples (CP–3, CP–4 and CP–6) with a PO_4/Cr ratio higher than 1.4 are decreased by the increase in this ratio. On the basis of solubility and capacity data, these samples can be regarded as being less suitable for practical use.

The change of the capacity with pH showed a single step character. On comparing the pH curves with the dissociation curve of phosphoric acid it can be established that the change of slope corresponds to the second dissociation step of phosphoric acid. Consequently, exchangeable H^+ ions may be formed by the dissociation of mono-hydrogen phosphates. This assumption may be checked by observing the change in H^+ ion concentration of a solution contacted with the ion exchanger.

The fairly good agreements in case of CP–1, CP–2, CP–5, CP–7, CP–8 and CP–9 between the capacity data calculated from the changes in the H^+ ion concentration of the solution and those measured by tracer techniques at high pH (Table V) support our assumption about the mechanism of the exchange process.

Below pH 7 the capacity data of the samples obtained by tracer methods show a difference from the data of the dissociation curve and from the capac-

ity data calculated on the basis of the changes in the H^+ ion concentration of the solution.

In our opinion these differences can be explained partly by the adsorption behaviour of the samples examined, and partly by the presence of various amounts of $H_2PO_4^-$ groups in the samples (in accordance with the structure of the molecule).

Thermochemical properties

On the thermograms (Fig. 8) of the initial samples endothermic processes were found at 175 °C for samples CP–5 and CP–2, and at 75 °C and 250 °C for sample CP–1. Exothermic processes were observed for samples CP–5 and CP–2 at 310 °C and about 560 °C, and for sample CP–1 at 450 °C and 510 °C respectively. The DTA curve of sample CP–1, which has the lowest PO_4/Cr ratio, is different in character from the others. The other curves belong to samples with PO_4/Cr ratios around or above 1.

Furthermore it can be seen that the areas under the peaks increase with increasing PO_4/Cr ratio.

The character of both the DTA and DTG curves seems to indicate that partly overlapping processes take place during the heating.

The change in the character of the curves (DTA, DTG and TG) for the sample with $PO_4/Cr \cong 1$ as a function of the saturation rate is demonstrated in Fig. 10. With increasing saturation rate the peak values decrease and are generally shifted to lower temperatures. On the DTA curve of the fully saturated sample a new exothermic peak appears at 620 °C wich may be due to the large content of K^+ ions in the sample.

Upon examining the DTA curves of various samples, certain differences in their character can be observed. On the basis of this the following three types of samples can be distinguished.

a) Linear phosphate polymers with various lengths of the chain. They may exist at $PO_4/Cr < 1$ and the chain length depends on the value of the PO_4/Cr ratio. The content of $H_2PO_4^-$ groups in polymers of this type is very low or they are completely absent. The content of these groups increases if the phosphate/chromium ratio is around one. This type of polymer can be described by the general formula $[—Cr—(HPO_4—Cr—)_x]_n$; from the chromium phosphate samples examined the CP–1 may be ranged in this type of polymers.

b) Cross-linked linear phosphate polymers with various lengths of the chain. They may exist around $PO_4/Cr = 1.0—1.4$. The cross-linking of these polymers increases with increasing PO_4/Cr ratio, and simultaneously the amount of $H_2PO_4^-$ groups also increases as expressed by the increase of the DTA peak height at 320 °C with increasing PO_4/Cr ratio.

This type of polymer can be described by the general formula:

$$\left[\begin{array}{l} -Cr-(HPO_4-Cr-)_x \\ \quad | \\ H_2PO_4 \end{array}\right]_n .$$

Among the examined samples the CP–5, CP–9, CP–2, CP–8 and the CP–7 may be classified as belonging to this type.

c) Cyclic phosphate polymers formed at about $PO_4/Cr \cong 2$. In the case of this type, an additional increase in the content of the $H_2PO_4^-$ groups was observed, as seen in Fig. 9 (DTA curve for the samples CP–3 and CP–4).

Both the solubility data reported in the literature and those found by us seem to support the above assumptions about the structure of the polyphosphates examined.

From the data given in Table V it can be seen that the capacity values increase with the increase of the phosphate/chromium ratio up to about 1.0—1.2. The capacity values determined by tracer techniques are higher than those obtained by thermochemical methods, except for sample CP–7 which has the lowest specific surface area. Taking into consideration the deviation of the specific surface area (more than one order of magnitude), we have to reckon with a significant adsorption effect. It should be mentioned that this problem requires further, more detailed studies.

The capacity data calculated from the weight loss above 480 °C (DTA curve) are in good agreement with both the measured and theoretical values; *i.e.* this method can be successfully used for predicting the capacity value of the sample examined. The data calculated from the assumed molecular composition of the exchanger are in good agreement with the measured values, but the results can be further refined by taking into account the soluble amount of phosphates (at about pH = 12).

In connection with the above described evaluation, it can be stated that during the synthesis various substances are formed depending on the amount of the initial materials. These phosphates can be classified as belonging to one of three main types of phosphate polymers.

On the basis of the capacity values and the solubility data, the samples that can be most successfully used as ion exchanger are those in which the PO_4/Cr ratio is about 0.75—1.0 (for example CP–1); *i.e.* such substances which can be classified as linear phosphate polymers.

Based on the results of the other studies we assume that, regardless of the molecular composition, the exchangeable H^+ ions are formed by the dissociation of the hydrogen phosphate groups.

REFERENCES

1. ALFREMOW, L. C., VANDEBERG, J. T.: J. Paint. Techn. **38,** 169 (1966)
2. STERN, M. A., DANYUSHEVSKAYA, N. E., ALEKSEEVA, O. V.: Lakokrasochnie materialy i ikh primenenie **1,** 32 (1964)
3. MAYER, G.: Schweiz. Arch. Angew. Wiss. Techn. **29,** 82 (1963)
4. ALLEN, E. R., OJAKAA, L., HILLER, N., JAKOB, F.: Am. Chem. Soc. Div. Paint, Preprints **18,** 289 (1958)
5. MAYER, G.: Farbe und Lack **68,** 315 (1962)
6. BIEDERMAN, C.: Nem. Nat. Sci. Soc. Vondois **14,** 37 (1965)
7. LERCH, P.: Minerva Nucl. **7,** 446, 451 (1963)
8. DOBSON, E. L., FIRKELSTEIN, L. J., FERNEY, C. R., KELLY, L. S.: USAEC Symp. Sec. No. 6, 477 (1966)
9. VAN WAZER, J. R.: Phosphorus and its Compounds. Interscience, New York, 1958
10. GIMBLETT, F. G. R.: Inorganic Polymer Chemistry. Butterworths and Co. London, 1963
11. CORBRIDGE, D. E. C., LOWE, E. J.: J. Chem. Soc. **1954,** 493
12. JAMESON, R. F., SALMON, J. E.: J. Chem. Soc. **1955,** 360
13. LUKASZEWSKI, G. M., REDFERN, J. P.: Nature **190,** 805 (1961)
14. LUKASZEWSKI, G. M., REDFERN, J. P.: J. Chem. Soc. 3790 (1963)
15. LUKASZEWSKI, G. M., REDFERN, J. P., SALMON, J. E.: J. Chem. Soc. **1961,** 39
16. SZIRTES, L., ZSINKA, L., ZABORENKO, K. B., IOFA, B. Z.: Acta Chim. Acad. Sci. Hung. **54,** 215 (1967)
17. ZSINKA, L., SZIRTES, L.: Radiochem. Radioanal. Letters **2,** 257 (1969)
18. ZSINKA, L., SZIRTES, L., STENGER, V.: Radiochem. Radioanal. Letters **4,** 257 (1970)
19. EARNSHAW, A., LAKWORTHY, L. F., PATEL, K. S.: J. Chem. Soc. **1965,** 3267

László ZSINKA
László SZIRTES } Budapest 114., P.O.B. 77.

Acta Chimica Academiae Scientiarum Hungaricae, Tomus 69 (3), pp. 265–271 (1971)

THE USE OF COMPLEX FORMING AGENTS IN ION EXCHANGE CHROMATOGRAPHY, VI

SEPARATION OF ORGANIC BASES ON A CATION-EXCHANGE COLUMN

J. INCZÉDY

(Institute of General and Analytical Chemistry, Technical University, Budapest)

Received March 5, 1970

The distribution coefficients of pyridine, *p*-toluidine and benzylamine were determined on Na-form and Ni-form cation-exchange resins from 50% ethanolic sodium chloride and nickel(II) chloride solutions, respectively. The concentration of the metal ion was kept constant and the pH of the solution varied. Equations were derived for informatory calculation of the distribution coefficients of organic bases. The side reaction functions introduced by RINGBOM were used. The chromatographic separation of the bases was also performed. The bases were determined spectrophotometrically.

In a system consisting of a solution of a monoacidic base B, sodium chloride and a cation-exchange resin of the Na form, the following reactions take place:

$$B + H^+ \overset{K}{\rightleftharpoons} BH^+ \tag{1}$$

$$BH^+ + R{-}Na \overset{K^X}{\rightleftharpoons} R{-}BH + Na^+ \tag{2}$$

where K is the protonation constant of the base; R denotes the equivalent amount of the ion-exchange resin, while K^X the ion-exchange equilibrium constant:

$$K^X = \frac{(BH^+)\,[Na^+]}{[BH^+]\,(Na^+)} . \tag{3}$$

The terms in parentheses are concentrations in the resin, while those in brackets are concentrations in the solution.

Denoting the total concentration of the base in solution by C_B, one obtains

$$C_B = [B] + [BH^+] = [BH^+]\left(1 + \frac{1}{[H^+]\,K}\right) . \tag{4}$$

The concentration of the protonated base can be expressed as follows:

$$[BH^+] = \frac{C_B}{\left(1 + \dfrac{1}{[H^+]\,K}\right)} = \frac{C_B}{\alpha_{(BH)H}} . \tag{5}$$

According to the widely used concept of RINGBOM [1] instead of the term in parenthesis the side reaction function $\alpha_{BH(H)}$ may be inserted. Inserting (5) into Eq. (3), and considering that in chromatographic separations the total amount of the base is small compared to the resin capacity, the latter may be substituted for the concentration of sodium ions in the resin phase, *i.e.* $(Na^+) \approx Q$, thus the distribution coefficient of the base can be approximated with the following equation:

$$D_B = \frac{(BH^+)}{C_B} = \frac{K^X}{\alpha_{BH(H)}} \cdot \frac{Q}{[Na^+]} . \tag{6}$$

If the concentration of sodium ions in the solution is kept constant, D_B varies with the value of $\alpha_{BH(H)}$ or rather with the pH of the solution only. Considering that K^X is not far from unity and Q is cca 2 meq/ml, the distribution coefficient will be lower than 1, *i.e.* the base practically will not be absorbed if $[Na^+] \geq 0.02\ M$ and $pH > 2 + \log K$, since the value of $\alpha_{BH(H)}$ will be greater than 10^2. The maximum value of D can be obtained in the range, where $pH < 2 + \log K$, since the value of $\alpha_{BH(H)} \approx 1$, and $C_B \approx [BH^+]$. The value of D_{max} does not change with decreasing pH until hydrogen ions do not displace sodium ions in the resin appreciably (*i.e.* $pH < 1 - \log[Na^+]$). Eq. (6) may not be used without change in the case of acidic solutions since a new ion exchange process will proceed between the protonated base and hydrogen ion. Thus a modified value of K^X must be used.

If the difference between the logarithm of the protonation constants of two bases is greater than 2, separation of the bases can be achieved using an eluent of suitable pH.

If the protonation constants of the bases are close each other, the separation can be performed with complexation. If the resin is loaded with a complex-forming divalent metal ion M, the non-protonated base is absorbed as a ligand:

$$R_2{=}M + B \overset{K^L}{\rightleftharpoons} R_2{=}MB \tag{7}$$

The principle of this method (so-called "ligand exchange") was first introduced and recommended for separation of ligands by HELFFERICH [2].

For calculating the distribution coefficient of the bases the following equation can be written:

$$D_B = \frac{(MB)+(B)}{C_B} = \frac{(M)(B)\,\beta_1+(B)}{[M][B]\,\beta_1+[B]} . \tag{8}$$

If ligand absorption takes place (*i.e.* $Q \cdot \beta_1 \gg 1$), Eq. (8) may be simplified:

$$D_B \approx Q \cdot d_B \frac{\bar{\beta}_1}{\alpha_{B(M)}} \qquad (pH > 1 + \log K) \tag{9a}$$

where $\alpha_{B(M)}$ is the side reaction function, according to RINGBOM [1]:

$$\alpha_{(BM)} = 1 + [M^{2+}]\,\beta_1.$$

Thus the ligand absorption constant is $K^L \approx d_B \bar{\beta}_1$. It was assumed that the base is practically not protonated in the solution, it forms only one complex of 1 : 1 composition since the total amount of nickel(II)ions is much larger than that of the base, and the resin capacity may be substituted for (M^{2+}). $\bar{\beta}_1$ denotes the stability constant of the 1 : 1 complex in the resin phase; $d_B = (B)/[B]$ is the partition coefficient of the free base.

In the case where complex formation does not occur, Eq. (8) reduces to

$$D_B = d_B \tag{9b}$$

According to Eq. (9a), the distribution coefficient of the base can be controlled by the concentration of the complex-forming metal ion in the solution only if $[M^{2+}] > 1/\beta_1$.

Two bases of similar proton affinity can be separated on the basis of their different complex-forming tendencies if a suitable metal-ion containing resin and eluent are used.

In the pH range where the protonated base exists (*i.e.* $pH < 1 + \log K$), an ion exchange reaction proceeds instead of ligand absorption and the distribution coefficient is calculated from an equation similar to (6):

$$D_B = \left(\frac{K^X}{\alpha^2_{BH(H)}} \cdot \frac{Q}{2\,[M^{2+}]} \right)^{1/2}. \tag{10}$$

(This equation may be used also in the whole pH range when complex formation does not occur.)

Here K^X is the ion-exchange constant of the BH^+ ion, referring to the divalent metal ion.

The distribution coefficients of pyridine, *p*-toluidine and benzylamine were determined by the batch method, first on a sodium-form cation exchange resin from sodium chloride solutions of varying pH. As solvent, a 1 : 1 water–ethanol mixture was used and the concentration of sodium ions was kept constant in each series. The distribution coefficients obtained are plotted as a function of pH in Fig. 1. Using similar measurements, the distribution coefficients of pyridine and *p*-toluidine were also determined on a nickel(II)-form resin, from nickel(II) chloride solutions of varying pH. The values obtained are plotted as a function of pH in Fig. 2.

The logarithm of the protonation constants of the bases investigated are as follows: pyridine: 5.2; *p*-toluidine: 5.3; benzylamine: 9.3.

The shapes of the obtained curves in Fig. 1 correspond to Eq. (6), but the inflection points are shifted in all cases towards lower pH values. According to Eq. (6), the distribution coefficients should be equal to $D_{max}/2$ at pH = = log K, whereas they were found at pH 4.7, 4.8 and 8.3, respectively. The

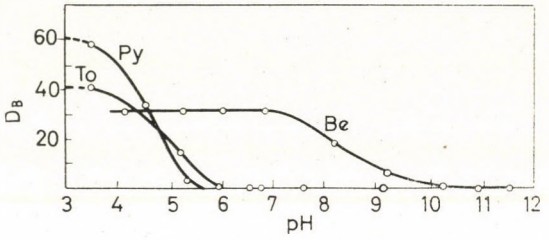


Fig. 1. Distribution coefficients of pyridine, *p*-toluidine and benzylamine on Lewatit SP 100 Na-form resin, from 50% ethanolic solution of sodium chloride, as a function of pH. $[Na^+] = 2 \times 10^{-2}$ *M*

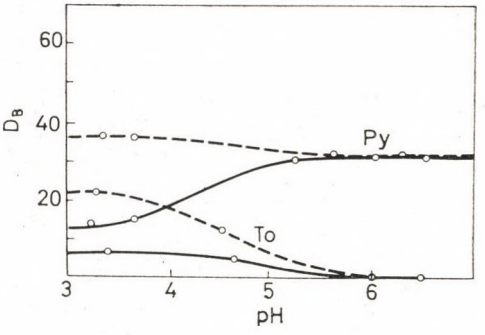


Fig. 2. Distribution coefficients of pyridine and *p*-toluidine on Lewatit SP 100 Ni-form resin from the solution of nickel(II) chloride, containing 50% ethanol, as a function of pH. —— $[Ni^{2+}] = 10^{-2}$ *M*; ----- $[Ni^{2+}] = 10^{-3}$ *M*

difference between the calculated and found D values may be explained by the reasonable assumption that the proton activity in the sodium-form resin phase is lower than that in the solution at equilibrium with it.

Using the D_{max} values found, the K^X ion-exchange constants of the protonated bases, referred to sodium ion, were calculated and presented in Table I. As can be seen, the order of the absorption strengths of the protonated bases corresponds to the reverse order of their base strengths or proton affinities.

Distribution experiments were carried out also with sodium chloride solutions of pH 3.5 and varying concentration. The results obtained support the reliability of Eq. (6).

Table I

Volume ion-exchange constants of protonated organic bases referred to sodium and nickel(II) ions

Base	K^X_{BH-Na}	K^X_{BH-Ni}
Pyridine	0.68	1.4
p-Toluidine	0.45	0.5
Benzylamine	0.34	—

According to literature data, nickel(II) ions form complexes with pyridine, but not with *p*-toluidine to any appreciable extent. The stability constant of the 1 : 1 nickel(II)—pyridine complex $\beta_1 = 60$ according to BJERRUM [3].

As seen from Fig. 2, pyridine is absorbed by the nickel(II)-form resin quite strongly and nearly independently of the nickel(II) ion concentration if the pH of the solution is higher than 5. Under the same conditions *p*-toluidine is practically not absorbed.

Assuming that $\bar{\beta}_1 \approx \beta_1$, the partition coefficient of free pyridine was calculated and found to be $d_{Py} = 0.26$.

At low pH values the ion exchange reaction of the protonated bases predominates. Accordingly, the distribution coefficients of the bases are controlled by the concentration of the competing nickel(II) ions. The ion-exchange constants of the protonated bases referred to nickel(II) ions have been calculated and are presented in Table I.

The ratio of the K^X values of protonated pyridine and *p*-toluidine on the Na-form resin is very near the square root of the ratio of the corresponding K^X values on the Ni-form resin. This is also an evidence that at lower pH values pure ion-exchange processes predominate.

On the basis of the obtained results, chromatographic separations of the bases were planned and performed. The chromatograms are shown in Figs 3 and 4. Pyridine and benzylamine could be separated utilizing the effect of the eluent pH on the absorption of the bases mentioned, but in the separation of pyridine and *p*-toluidine, an eluent containing nickel(II) as complex-forming ion had to be used. The separations proved to be clear and quantitative.

In the separation using the Ni-form resin column, the eluent volumes found were in good agreement with those calculated using the data obtained by static measurements. However, in the separation on a Na-form resin column, deviation was observed between the calculated and found peak positions since the pH required in the column was reached only with certain delay due to the low buffer capacity of the eluent.

For calculation of eluent volumes, GLUECKAUF's equation [4] was used: $v_{max} = X(D + a)$, where X denotes the column volume (ml), while

a is the void fraction of the column. The eluent volumes calculated on the Ni-form resin column are as follows

$$v_{max}, \text{ To} = 2.5 \ (0.4) = 1 \text{ ml} \qquad \text{(Fraction 1)}$$
$$v_{max}, \text{ Py} = 2.5 \ (31 + 0.4) = 78.5 \text{ ml} \qquad \text{(Fraction 22)}$$

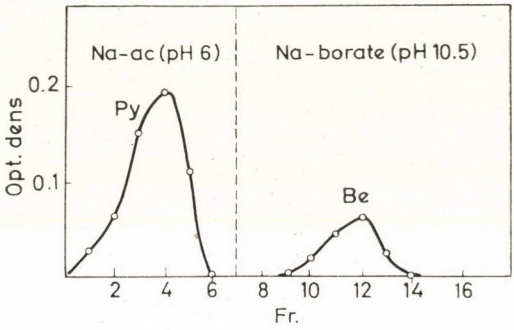


Fig. 3. Separation of pyridine and benzylamine on a Na-form resin column, using 2×10^{-2} *M* sodium acetate (pH 6) and sodium borate (pH 10.5) in 50% ethanol as eluents. Ion-exchange resin: Lewatit SP 100 (0.2—0.4 mm); Column 6.5×70 mm. Flow rate: 0.3 ml/min; fraction volume 3.5 ml

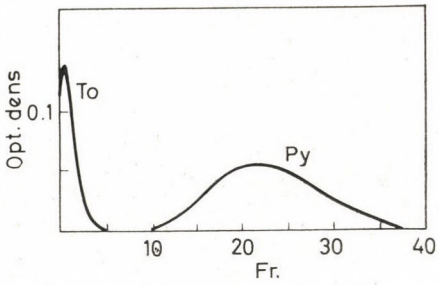


Fig. 4. Separation of *p*-toluidine and pyridine on a Ni-form cation-exchange column, using 10^{-2} *M* nickel(II) chloride (pH 6.6) in 50% ethanol as eluent. Ion-exchange resin: Lewatit SP 100 (0.2—0.4 mm). Column: 6.5×76 mm; flow rate: 0.3 ml/min; fraction volume: 3.5 ml.

Experimental

Reagents. Analytical grade solvents and reagents were used. Pyridine used for the preparation of stock solutions was freshly distilled. From *p*-toluidine a 0.1 *M* alcoholic solution was prepared and purified with carbon black. For the preparation of the solvent mixture and of aqueous stock solutions [sodium chloride, nickel(II) chloride, etc.] ion free water was used.

Ion-exchange resin. Macroporous strong acid cation exchange resin, Lewatit SP 100 (Farbenfabriken Bayer, G. F. R.) was sieved and the fraction with the particle diameter of 0.2—0.4 mm treated in the usual manner. Finally the resin in Na-form was extracted with ethanol in a Soxhlet apparatus to remove the coloured soluble impurities. After extraction, part of the resin was converted to the Ni-form and washed with a 1 : 1 ethanol–water mixture.

The air-dry resins were stored in glass-stoppered bottles and tested for capacity and column volume. The data of the sodium- and nickel-form resins were as follows: $Q_{Na} = 1.82$ meq/ml; 2.74 ml/g and $Q_{Ni} = 1.98$ meq/ml; 2.52 ml/g, respectively.

Instruments. The pH measurements were performed with a Universal pH-meter (Radelkis, Hungary). The photometric determination of the bases in solution was carried out using a Spectromom 201 (MOM, Hungary) spectrophotometer. In the chromatographic separations the effluent fractions were collected by means of a fraction collector, Fractomat Y–2 (Hako, G. F. R.).

Distribution measurements. For the determination of the distribution coefficients of the bases from solutions of different pH, sample solutions of 50 ml were prepared using ethanol, 0.1 *M* aqueous sodium chloride [or nickel(II) chloride], 10^{-3} *M* pyridine, 10^{-2} *M* alcoholic *p*-toluidine, and 10^{-2} *M* benzylamine stock solutions. The pH was adjusted roughly by addition of dilute hydrochloric acid or sodium hydroxide before the last dilution to 50 ml. The solutions contained 50% ethanol in the final volume in each experiment. The 50 ml solutions were shaken periodically with 0.50 g of air-dry resin (in the required form) in glass-stoppered flasks, for 24 hours. After equilibration, the pH was measured, 20 ml of the solutions was acidified with 5 ml of 1 *M* hydrochloric acid solution and the optical density measured at 256 nm against a blank. The concentration of the base in the solution was evaluated by means of a calibration graph, then the volume distribution coefficient was calculated.

Separation experiments. A column was filled with the pretreated ion-exchange resin in the required form, and washed with water–ethanol mixture. 0.5 μmole pyridine, and 5 μmole of benzylamine was added on to the sodium-form resin column (6.5 × 70 mm) by means of a micropipette and the pyridine eluted with 2×10^{-2} *M* sodium acetate in 50% ethanol, containing acetic acid (pH 6). For the elution of benzylamine a sodium borate solution was prepared in 50% ethanol: to the solution containing the required amount of sodium hydroxide and ethanol, boric acid solution was added to achieve pH 10.5. Finally the volume of the solution was adjusted with some water. The concentration of the sodium ions was 2×10^{-2} *M* in both eluents. Acetate and borate ions were added to the eluents to increase the buffer capacity of the solutions.

For the elution of *p*-toluidine and pyridine from the Ni-form resin column, a 10^{-2} *M* nickel(II) chloride solution of pH 6.6 in 50% ethanol was used. The pH of the solution was adjusted by adding a few drops of dilute sodium hydroxide. The total amounts of the bases separated were 5 and 1 μmole respectively.

The effluent was collected in 3.5 ml fractions, and after addition of 0.5 ml 1 *M* hydrochloric acid, their optical density was measured at 256 nm.

*

Acknowledgement. The author wishes to express his thanks to Miss J. MARÓTHY and Miss J. GAÁL for their valuable help in carrying out the measurements.

REFERENCES

1. RINGBOM, A.: Complexation in Analytical Chemistry. Interscience Publ., New York, 1963
2. HELFFERICH, F.: Nature **189**, 1001 (1961); Angew. Chem. **73**, 446 (1961)
3. BJERRUM, J.: Chem. Rev., **46**, 384 (1950)
4. GLUECKAUF, E.: Ion exchange and its applications p. 34., Soc. Chem. Ind. London, 1954

János INCZÉDY; Veszprém, Schönherz Z. u. 10.

Acta Chimica Academiae Scientiarum Hungaricae, Tomus 69 (3), pp. 273–299 (1971)

THERMAL DECOMPOSITION OF BRANCHED-CHAIN METHYLPOLYSILOXANES, II.

SEPARATION AND IDENTIFICATION OF THE PYROLYSIS PRODUCTS BY GAS CHROMATOGRAPHY AND MASS SPECTROMETRY

G. GARZÓ, J. TAMÁS, T. SZÉKELY and K. UJSZÁSZI

(Research Group for Inorganic Chemistry of the Hungarian Academy of Sciences, Budapest, and Center for Study of Chemical Structures, Hungarian Academy of Sciences, Budapest)

Received March 9, 1970

Branched-chain methylpolysiloxanes are the main constituents of silicone resins and are chemically composed of Me_2SiO (D) and $Me_2SiO_{3/2}$ (T) structural units.

Thermal decomposition of such polymeric systems has been investigated using pyrolysis gas chromatography (PGC). Compounds isolated from the product of large-scale pyrolysis served as standards in the identification of peaks in the micro-pyrograms. Mass spectra gave information on the isolated volatile pyrolysis products.

PGC experiments have been carried out in an all-metal micro-pyrolysis apparatus made in our laboratory. Seventeen pyrolysis products have been identified, each of them being a low molecular weight methylsiloxane with cyclic, bicyclic or polycyclic structure.

Some of the bi- and polycyclic compounds are represented by several isomers in the pyrograms. Retention indices of seventeen molecules have been determined on three different stationary phases. The index values allow hypotheses concerning the structure of the individual decomposition products.

On the basis of these results conclusions have been drawn on the degradation processes of the polymers and their original structural properties.

Knowledge of the mechanism of thermal decomposition of polymers is of interest both from the theoretical and practical points of view. It may afford information on the chemical structure and steric conformations of the original polymers.

Pyrolysis gas chromatography (PGC) seems to be a very promising method for studying the mechanism of thermal decomposition. Separation, chemical identification and determination of the relative amounts of decomposition products have become possible in this way.

Thermal decomposition of branched-chain methyl-polysiloxanes has not been investigated thoroughly so far. Thermal rearrangement of cohydrolysis products of dimethyldichlorosilane (D) and mehyltrichlorosilane (T) or D and silicon tetrachloride (Q) mixtures has been reported by SCOTT as early as 1946 [1]. Owing to the chosen monomer ratio, the value of carbon–silicon ratio (R = C/Si) was 1.5 in the hydrolysate investigated by SCOTT. Six different methylpolycyclopolysiloxanes and four different methylspirocyclopolysiloxanes were isolated from the cleavage products; their elementary compositions were obtained by elemental analysis and molecular weight determination, and the melting points were reported. According to SCOTT, a considerable part of the isolated products could not be characterized by definite structural

formulas, because several isomeric structures corresponded to the empirical formulas found for these compounds. All reported compounds were obtained by fractional crystallization procedures from distillation cuts of the large-scale pyrolysis product.

Octamethyloctasilsesquioxane (T_8) and dodecamethyldodecasilsesquioxane (T_{12}) were formed in the course of the alkali-catalyzed cracking of a crude polymer system prepared from methyl-T [2]. Based on X-ray diffraction data, the crystal structures of these compounds were also discussed in the same paper. These investigations were continued by VOGT *et al.* [3]. In one of their papers published in 1963 the isolation of T_6, T_8, T_{10}, T_{12}, T_{14} and T_9OR (R = = methyl or ethyl group) silsesquioxanes was announced, the preceding chemical conditions and manipulations being similar to those of BARRY *et al.* [2]. Nuclear magnetic resonance (NMR) and infrared (IR) spectroscopy, further gas chromatography (GC) were equally used for the investigation of the isolated compounds. According to the skeletal arrangements proposed by VOGT *et al.* [3], the T_6—T_{14} molecules appear to constitute a homologous series of prismatic cage-like polycycles, which may be regarded as the cyclic analogues of the linear double-chain polymers found in the phenylsilsesquioxane series. According to their experiments, T_{10} is characterized in this series by maximum thermodynamic stability.

A previous report from our laboratory deals with the PGC investigations of methylsilicone T—D polymers [4]. The primary aim of this paper was the description of a pyrolysis equipment constructed for the special purpose of these investigations. Results concerning the pyrolysis of these branched-chain methylpolysiloxanes have been discussed mainly to demonstrate the possibilities of the method.

The purpose of the present investigations has been to collect more complete and reliable information on the thermal degradation than it was possible earlier. With a definite type of branched-chain methylpolysiloxanes and within a definite interval (the Si_2—Si_7 range) of the rather complex pyrogram, we tried to identify as many peaks as possible with the available techniques.

For this purpose, several compounds were isolated from the product of large-scale pyrolysis. Distillation, preparative GC and crystallization were used as separation methods. Molecular weights and elementary compositions were determined using mass spectrometry. These compounds served then as "standards" in the identification of peaks in the PGC chromatograms.

Experimental

Investigations were carried out with a hydrolysate prepared in our laboratory from a D—T monomeric mixture. The crude polymer system was characterized by R = C/Si = 1.3, as calculated from the monomer ratio of the original mixture. Hydrolysis was effected in

the presence of butyl acetate. Under these conditions hydrolysis proceeded only in the boundary region of the aqueous butyl acetate phases, and only at an inhibited rate [5]. The average molecular weight in the hydrolysate, remaining after the removal of butyl acetate, was lower than 10,000. This hydrolysate consisted of a network-type methylpolysiloxane system still containing considerable amounts of reactive OH groups and soluble in various organic solvents.

From previous experiments, the following facts have been known concerning the thermal behaviour of the polymer system investigated.

(1) Thermal decomposition becomes measurable by GC methods at 240 °C. On raising the temperature up to 400 °C, new decomposition products appear gradually, but the spectrum of peaks in the pyrogram remains unchanged between 400 °C and 800 °C.

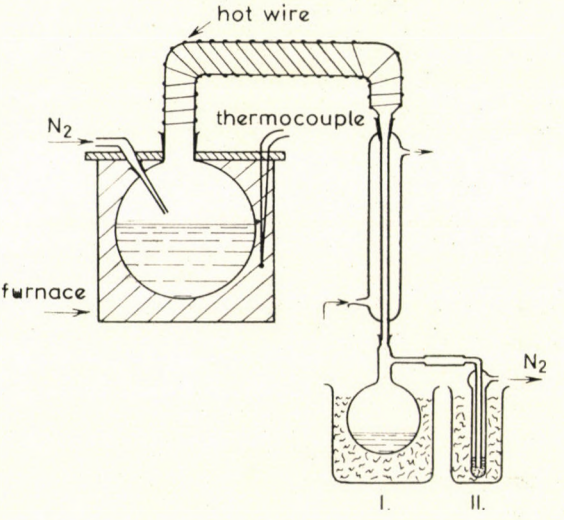


Fig. 1. Equipment for the macro-scale pyrolysis. Cold trap I: ice; Cold trap II: dry ice

(2) The hydrolysate has to be freed from the volatile components by heating it to 200 °C for a short time before the beginning of thermal decomposition. In the course of this procedure butyl acetate, cyclic dimethylsiloxanes (D_4, D_5, etc.) and some of the components which reappear in the decomposition spectra are evaporated.

(3) Chromatograms produced by micro- or macro-scale pyrolysis (from 1 mg to 100 g material) qualitatively consist of the same decomposition products.

Pyrolysis and gas chromatographic analysis

The equipment used for the thermal decomposition of 100 g polymer material in one batch is illustrated in Fig. 1. The total quantity of the sample (weighed in subsequent batches) amounted to about 400 g. It was introduced into the flask at room temperature, following previous drying at 100 °C in vacuum. The reaction flask was flushed with an argon stream and maintained at 600 °C maximum temperature. The heating of the furnace was interrupted at 200 °C for several hours, and the products which had vaporized were separated from the subsequent pyrolysis products. Ice and dry ice were used for cooling the cold traps.

Micropyrolysis was carried out in a stainless steel microreactor (*cf.* Fig. 2) which is a slightly modified duplicate of the microreactor described in our previous paper [4]. Needle valves 1, 2, 3 are used partly for the removal of some of the volatile components without contaminating the column, partly for flushing the microreactor with different reactive gases. Thermal degradation is achieved either by prolonged heating of the polymer sample in a closed chamber and in an inert atmosphere, or by heating it instantaneously (flash pyrolysis)

in an inert gas stream. Stopcock L and needle valve 1 in Fig. 2 are to be set in proper positions in order to realize either of the two possibilities. The entire free space of the microreactor is 1 ml. It is surrounded by a small furnace kept at constant temperatures sufficient to provide a temperature of 250 °C in the boat. Previous results have shown that components with KOVATS indices up to 2000 leave the microreactor without any loss if the above mentioned conditions are ensured.

Gas chromatographic analyses were carried out with a Carlo Erba Fractovap Model C, Type CID/ff dual FID instrument. An APL coated capillary column of 50 m length was used, operated with a linear temperature program of 3.5 °C/min. in the temperature range between 60 °C and 250 °C.

Nitrogen was used as carrier gas with an inlet pressure of 1.8 atm. and with a flow-rate of 2 ml/min. A splitting ratio 150 : 1 was used before the column inlet.

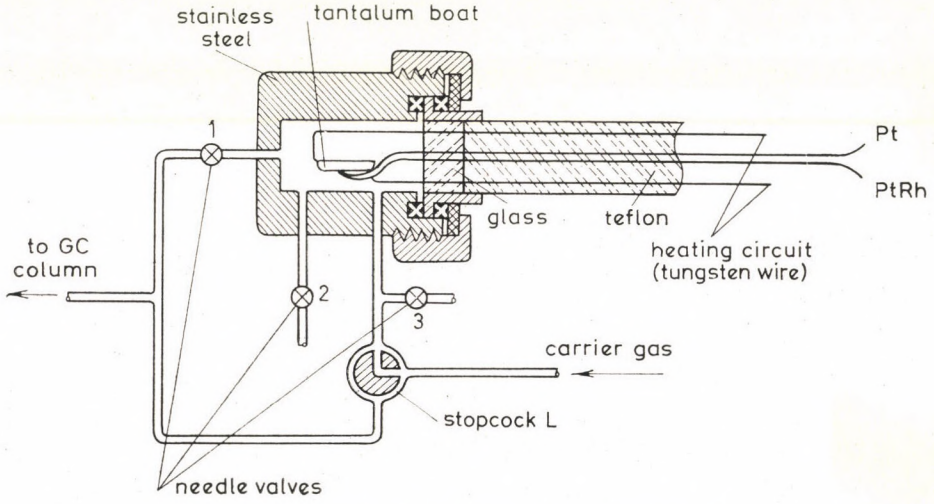


Fig. 2. Micro-pyrolysis assembly (Microreactor)

Preparative procedures

The bulk of the macro-scale pyrolysis products was collected in a cold trap cooled with ice. Small amounts of liquid condensed in the trap cooled with dry ice, but this material has not been processed so far.

The amount of volatile decomposition products obtained in the pyrolysis was about 25% of the polymeric material.

The bulk of the pyrolysate was distilled under reduced pressure (20 torr), and the fraction boiling between 85 and 155 °C, which was a transparent colourless liquid of 100 ml volume, was fractionated further by means of preparative GC.

The analytical chromatogram of the pyrolysate fraction is shown in Fig. 3 to give an impression on the complexity of the system. (The diagram will be discussed later.)

An automatic preparative gas chromatograph (Carlo Erba, Fractovap Model P) was used for the isolation of chemically pure compounds from the pyrolysate. It was provided with a 4 m long column with a clover leaf type cross-section (great diameter: 25 mm) filled with Celite 545 coated by a liquid methylsilicone polymer. Further conditions of the gas chromatographic separation were as follows: a TC detector was used and the temperature of the detector thermostat was 240 °C. Evaporator temperature: 270 °C; collector temperature: 140 °C; temperature program of the column thermostat: initial isothermic period: 240 °C — 8 min.: speed of heating: 5° C/min.; cooling and preconditioning: 4 min. each. Inlet pressure of carrier gas (H_2): 2.5 atm; outlet pressure: 0.4 atm. 2.5 ml pyrolysate was administered to the column in each run.

The pyrolysate was fractionated to give five subfractions. All five fractions were transparent, colourless liquids, in the following approximate quantitative distribution:

Fraction, No.	Volume, ml
1	16
2	10
3	15
4	8
5	2
transitory fractions	30 (total volume)

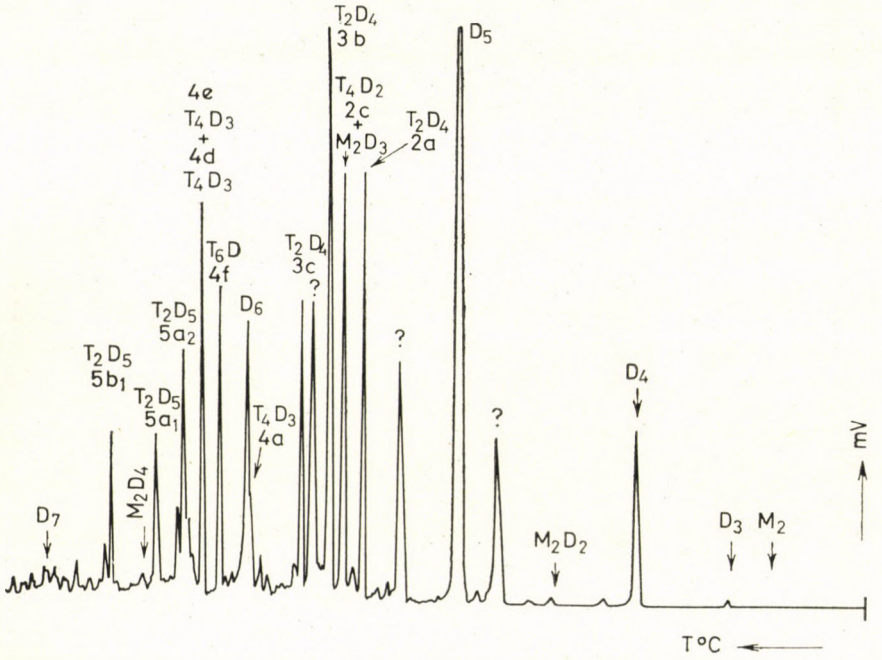


Fig. 3. Chromatogram of the 85—115 °C distillation cut (20 torr) of the macro-scale pyrolysis product. Column: APL capillary operated with a linear temperature program of 3.5 °C/min. in the temperature range 60°—250 °C

Although all these fractions appeared in the form of well resolved peaks in the preparative gas chromatogram, they were not chemically homogeneous. Analyses were carried out on a column coated with Tween 80, which was the most selective of several partition liquids tested. The analytical chromatogram of fraction No. 4 at 110 °C is shown in Fig. 4 in order to demonstrate this circumstance. It may be seen that in addition to some trace contaminants and D_6, this fraction could be resolved into six main components which were designated as fractions No. 4a, 4b, etc.

There were two possibilities to achieve further separation of the subfractions in order to obtain chemically homogeneous products.

One of them was based on our observation that a crystalline deposit was formed on storage in subfractions No. 3 and 4. The crystals were separated by filtration and purified by repeated recrystallization or washing.

Gas chromatographic microseparation of the individual peaks on columns containing Tween 80 as the liquid phase offered another possibility. This approach was realized using

a Fractovap Model C, Type ATC/f (Carlo Erba) apparatus with a TC detector attached to a 3 mm × 6 m column filled with Tween 80 on Chromosorb A. 30 to 60 μl samples were administered repeatedly.

The five fractions mentioned above were processed combining the two methods.

Fraction 1 contained 90% D_5 according to analysis at 100 °C using the Tween 80 column. This fraction could not be processed further with the method described.

Two components, approximately in equal amounts, were isolated from Fraction 2 using micropreparative gas chromatographic techniques at 120 °C column temperature. These fractions are referred to as No. 2a and 2c.

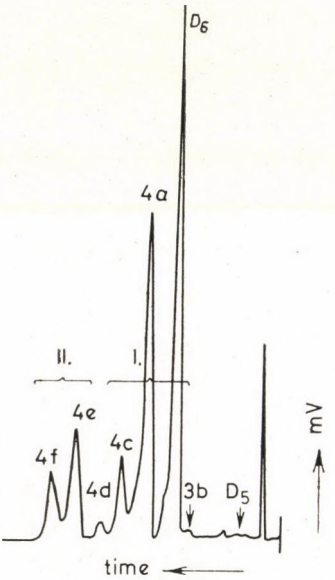


Fig. 4. Analytical chromatogram of the pyrolysate Subfraction 4. Column: 2 m × 2 mm; 3% Tween 80 on Chromosorb W. Temperature: 110 °C

Fraction 3 was cooled in ice-water when it partially crystallized. After filtration and drying 3 g dry material of 99% purity was obtained. It was found identical with one of the main components of the four peaks in the Tween 80 chromatogram of Fraction 3. (This component is referred to as No. 3b.) The other main component (3c) was isolated from the mother liquor at 134 °C column temperature by means of gas chromatographic micropreparation in 99% purity.

Crystals which could be filtered off easily separated from Fraction 4 on longer storage at room temperature. Repeated, careful washing of the surface of the crystalline material with ethanol and drying between sheets of filter paper gave a substance of 94% purity as checked by gas chromatography. This was found identical with component No. 4d in the chromatogram shown in Fig. 4. The mother liquor was resolved at 134 °C column temperature into fractions I and II as indicated in Fig. 4.

A further crystalline fraction formed in Fraction 4I in the course of a few days. After filtration and drying it was analyzed by gas chromatography and found identical with component No. 4a (Fig. 4). The purity of this product was 99% after washing with ethanol.

Fraction 4II consisted of two main components as seen in Fig. 4. After microseparation at 134 °C column temperature, one of these components was obtained as a homogeneous liquid at room temperature (referred to as No. 4e), and the other (4f) was crystalline under the same circumstances. The gas chromatographic purity of component No. 4e was, however, only 70%.

We tried to resolve Subfraction No. 5 into its pure chemical components with the help of gas chromatographic micropreparation; however, both fractions (5a and 5b) separated

by a Tween 80 column were found to be of insufficient purity. Fraction 5b consisted of two main components present in almost equal amounts.

Starting with Fraction 1, which turned out to be practically homogeneous as tested by the Tween 80 column, it was possible to prepare a further chemically pure component designated as No. 1a. Experimental conditions in this special micro-preparative procedure were the following: a 7 m × 10 mm column packed with Chromosorb A, coated with 15% QF–1; temperature: 120° C. The purity of this product was 80%.

Characterization of the products

The 12 products of the preparative procedure described above contained 13 different compounds. These were characterized on the basis of the following data:

1. Purity, determined with gas chromatography;
2. Retention indices, measured on columns coated with Tween 80 at 110 °C and with SE–30 at 125 °C;
3. Melting point;
4. Data obtained by mass spectrometry giving the molecular weight, stoichiometric composition and indicating the characteristic fragmentation of these molecules under electron bombardment;
5. Results of elemental analysis (in some cases) in order to check the stoichiometric composition determined with mass spectrometry.

Of the methods used, the mass spectrometric procedures and evaluation seem to deserve description in detail.

Mass spectrometry

The mass spectrometric investigation of the samples isolated by gas chromatographic techniques was carried out with a MH–1303 single-focusing mass spectrometer. The temperature of the all-metal inlet system was 100 °C, that of the ionization chamber 200 °C. The spectra were obtained within a wide ionization energy range. The investigation of metastable ions served for the detection of the ways of decomposition of the fragment ions formed as a result of electron bombardment [6].

Mass spectra obtained at 50 eV are shown in Fig. 5. The chemical formulas found for the individual ion peaks, the ways of their formation and decomposition, and formulas of the neutral parts emitted during decomposition, are indicated in the same diagram. All individual (not isotopic) peaks indicating an abundance exceeding 2% of the value of the base peak (the largest peak in the spectrum) are summarized in the spectrum ($m/e > 50$).

Completely identical mass spectra were obtained in the case of several preparations. Not only the mass numbers of the fragment ions and their relative intensities (within the range of 5% relative error) were found identical, but the same held true in the case of the metastable peaks. This type of congruency was obtained even with small ionization energies (12—15 eV). Thus, samples No. 3b, 3c and 2a (Fig. 5b), further 5a and 5b (Fig. 5c) and 4a, 4d and 4e (Fig. 5e) proved to be indistinguishable by mass spectrometric methods.

The practical absence of molecular ions (parent ions) in the mass spectra of methylsiloxanes is a general phenomenon. At the same time, intense single- and double-charged ion peaks representing $(P–15)^+$ and $(P–30)^{++}$ fragment ions, respectively (where P means the mass number of the parent ion) were present among the fragment peaks [7, 10]. Therefore, the molecular weights of these compounds could be calculated, even without direct observation of the molecular ion peaks, by adding fifteen to the maximum mass number observed in the given mass spectrum. In checking the correctness of the chemical gross formulas attributed to a substance in question, we relied on the measured and calculated relative intensity values of the first and second isotope peaks of the $(P–15)^+$ type ion peaks of the sample. The difference between the estimated isotope ratios and those calculated on basis of the accepted chemical formulas was always within the limits of reproducibility (±2%).

Results

Pyrolysis products

Results of purity investigations have been already reported.

The empirical formulas calculated on the basis of mass spectrometric data were checked in two cases (3b and 4b) by means of elemental analysis and were found to be completely identical.

The methylsiloxane character was established unequivocally from the mass spectra of Fig. 5 for all the 13 compounds prepared from the pyrolysate. This conclusion was based mainly on experiences gained in the mass spectrometry of other organosilicon compounds [6—10]. The presence of Si—H bonds was excluded by the mass spectra in each case.

The molecular weights and empirical formulas determined by mass spectrometry, the retention indices and, in the case of some samples, data of melting point determinations, are presented in Table I. For the purpose of drawing conclusions to be discussed later, the retention indices of several known methylsiloxanes are also included in Table I.

Various conclusions on the chemical structure of the detected pyrolysis products have become possible from the data reported in Table I.

It follows from the methylsiloxane character of all investigated substances that compounds with the formulas $Si_5O_6C_8H_{24}$ referred to as Sample 1a and $Si_6O_7C_{10}H_{30}$ referred to as samples 3b, 3c and 2a, as well as $Si_7O_8C_{12}H_{36}$ referred to as samples $5a_1$, $5a_2$ and $5b_1$, were polycyclic methylsiloxanes containing necessarily two rings (bicycles), while all the other isolated molecules contained more than two cycles (polycycles).

Each organosiloxane molecule may be regarded as a definite combination of the following four structural units:

Functionality	*Symbol*	*Unit formula*
Monofunctional	M	$R_3SiO_{1/2}$
Difunctional	D	$R_2SiO_{2/2}$
Trifunctional	T	$RSiO_{3/2}$
Tetrafunctional	Q	$SiO_{4/2}$

Assuming that all the molecules isolated in the course of this work consisted solely of T and D units, it follows that the symbols shown in the fifth column of Table I serve for a further characterization of the molecular structures. Permitting namely the participation of M and Q structural units in addition to T and D, a great variety of further symbols attains reality. Thus, *e.g.*, in addition to T_4D_2 seven further isomeric formulas may be attributed to $Si_6O_8C_8H_{24}$. These are the following: T_5M, QT_2D_3, QT_3DM, Q_2D_4, Q_2TD_2M, $Q_2T_2M_2$ and Q_3DM_2. Disregarding the detailed list of symbols possible without any restriction, the total number of theoretically possible isomers, each characterized by different symbols in terms of unit formulas, are calculated and shown in the eleventh column of Table I. On the other hand, the total number of theoretically possible isomer modifications realized in our preparations (restricted to molecules characterized by identical symbols in terms of unit formulas, *i.e.* by T—D symbols) is presented in Column 10 of Table I.

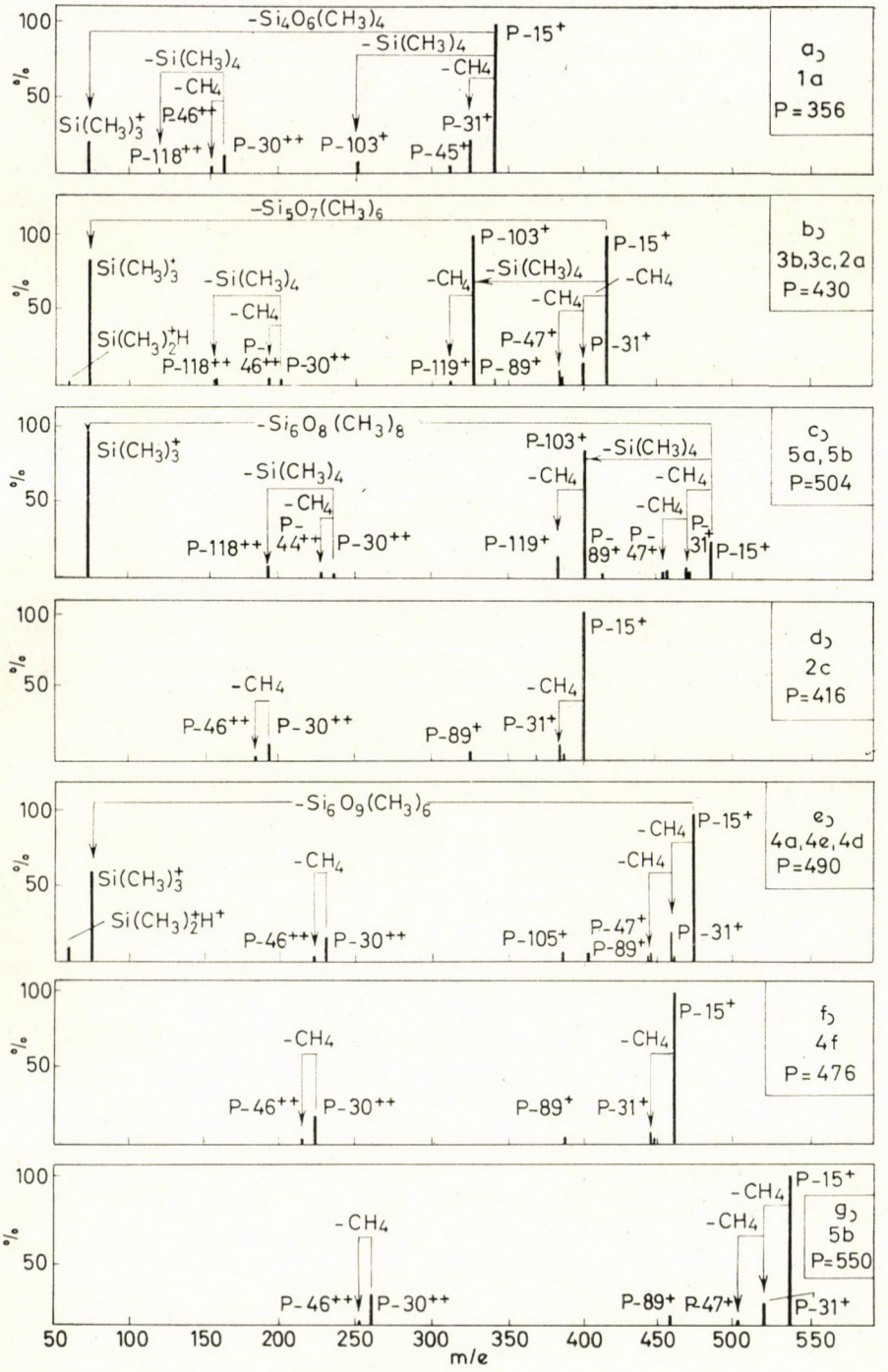


Fig. 5. Mass spectra of substances isolated from the pyrolysate. $m/e = P/z$, where m/e = mass to charge ratio; P = mass number of the parent ion; z = number of electric charge

Table I

Fraction index on prep. chromatogram	Peak index on TW—80 chromatogram	Mol. weight	Molecular formula	Symbol of compound	C/Si	Retention index SE-30; 125 °C	Retention index TW—60; 110 °C	Melting point, °C	Total number of isomeric T—D molecules with different ring combinations	Total number of isomers with different combinations of Q, M, T, D units
1	a	356	$Si_5O_6C_8H_{24}$	T_2D_3	1.6	—	—	—	2	6
2	c	416	$Si_6O_8C_8H_{24}$	T_4D_2	1.335	1246.5	1188	35.3	6 (5)	8
2	a	430	$Si_6O_7C_{10}H_{30}$	T_2D_4	1.67	1254	1103.5	54.5	4	8
			$Si_5O_4C_{12}H_{36}$	M_2D_3	2.4	1256	1078	—	—	—
3	b	430	$Si_6O_7C_{10}H_{30}$	T_2D_4	1.67	1285	1150	44	4	8
3	c	430	$Si_6O_7C_{10}H_{30}$	T_2D_4	1.67	1293	1181.5	—		
			$Si_6O_6C_{12}H_{36}$	D_6	2.00	1350	1171	—	—	—
4	f	476	$Si_7O_{10}C_8H_{24}$	T_6D	1.145	1359	1313	—	2	9
4	a	490	$Si_7O_9C_{10}H_{30}$	T_4D_3	1.43	1363	1216	49		
4	d	490	$Si_7O_9C_{10}H_{30}$	T_4D_3	1.43	1393	1263	148.5	10	10
4	e	490	$Si_7O_9C_{10}H_{30}$	T_4D_3	1.43	1395.5	1289	—		
5	a_2	504	$Si_7O_8C_{12}H_{36}$	T_2D_5	1.71	1416	—	—		
5	a_1	504	$Si_7O_8C_{12}H_{36}$	T_2D_5	1.71	1437	1270	—		
			$Si_6O_5C_{14}H_{42}$	M_2D_4	2.34	1442.5	1261	—	—	—
5	b_1	504	$Si_7O_8C_{12}H_{36}$	T_2D_5	1.71	1464.5	1332	—	6	10
5	b_2	550	$Si_8O_{11}C_{10}H_{30}$	T_6D_2	1.25	—	—	—	9	12
			$Si_7O_7C_{14}H_{42}$	D_7	2.00	1510	1346	—	—	—

Evidence for the assumption that no isomers except those constructed of T and D units were present among the compounds dealt with in this paper will be discussed later.

Data in Column 10 of Table I indicate the simultaneous existence of multiple geometrically isomeric structures even on those occasions when a given material consists merely of T and D structural units. The existence of these isomeric configurations is explained by the different possible modes of

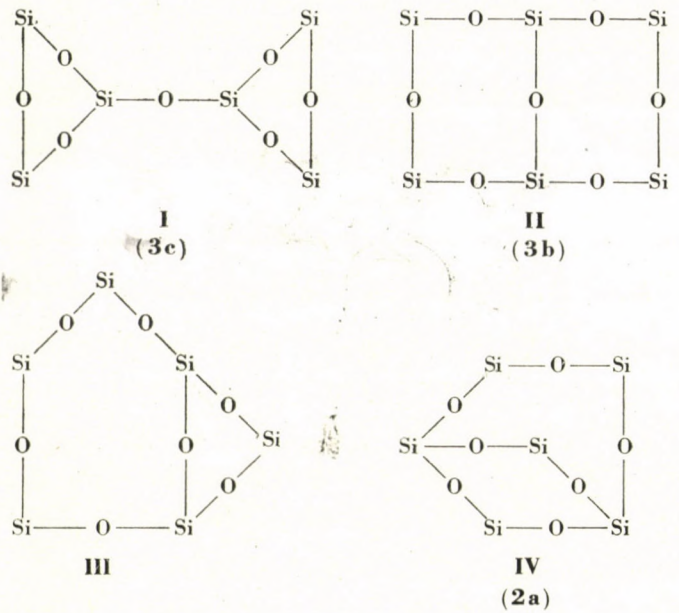


Fig. 6. Schematic structural patterns of the theoretically possible T_2D_4 isomers

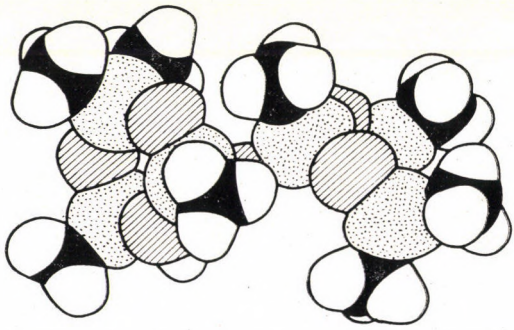
adding further rings to methylsiloxane cycles. Coupling by a T—T axis may take place leading both to isolated or fused ring systems. Coupling of separate rings may also be achieved by T—D_n—T connections, leading to highly extended separate ring connections. On the other hand, the fusion of cycles *via* T—D_n—T bridging (as another possibility) would lead to cage-like structures, more compact than the relatively extended ladder-like forms constructed of fused rings connected by a T—T axis.

These combinations in the case of the T_2D_4 molecule are shown in Fig. 6. From these structural patterns it is evident that differences in the number of siloxane units per cycle can give rise to structural differences even in the case of identical symbols in terms of unit formulas and identical coupling principles (*cf.* Formulas II and III).

Pictures of the space-filling atom calotte models ("EUGON", Hungary) of the isomers, I, II and IV are shown in Figs 7, 8 and 9.

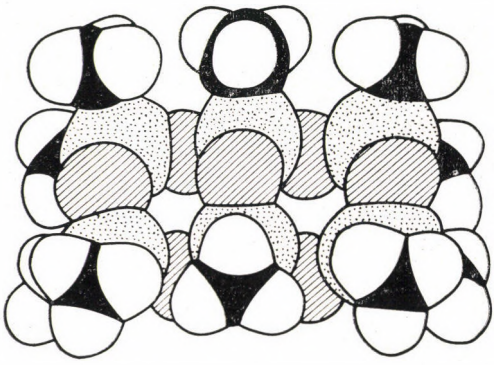
Characteristic data of the calotte models were the following:

Atom	Valency angle	Van der Waals atomic radius, Å	Covalent bond radius, Å
Si	$\alpha = \beta = \gamma = \delta = 109.5°$	1.85	R = 1.17
O	112°	1.30	R = 0.66
C	$\alpha = \beta = \gamma = \delta = 109.5°$	1.30	R = 0.77
H	—	0.95	R = 0.30



I.

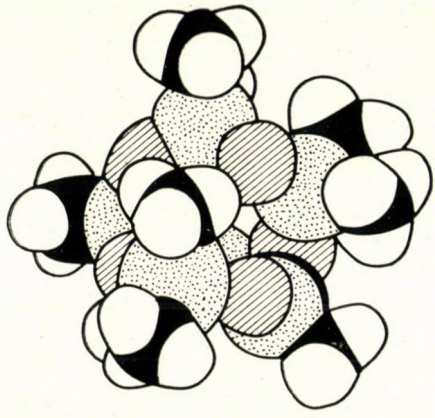
Fig. 7. Space-filling atom calotte model for isomer variation I of the T_2D_4 molecule (*cf.* Fig. 6)



II.

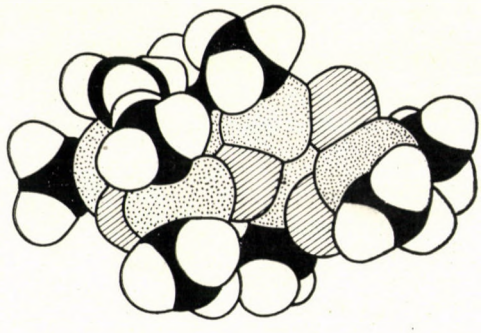
Fig. 8. Calotte model for isomer variation II

The pictures are demonstrative in pointing to the wide varieties in the closeness of packing of the different T_2D_4 isomers. However, distortions of the Si—O—Si valency angles — which are, in general, known to be comparatively flexible — are not shown by these models. It is not evident either, how far rotations are inhibited in the various isomeric structures.



IV.

Fig. 9. Calotte model for isomer variation IV



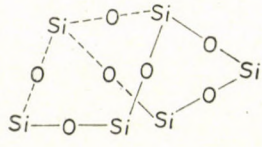


Fig. 10. Calotte model for a further conformation of the T_2D_4 molecule; isomeric modification II (*cf.* Figs 6 and 8)

Among the molecular structures presented, IV is characterized by a high degree of strain and rotational inhibition. There are no conformational or stereoisomeric modifications of this structure. Molecule II is just an opposite extreme: due to rotations along the Si—O axis, it may exist in several conformations different from that illustrated in Fig. 8. One of these possibilities is modelled in Fig. 10.

Based on the molecular models shown in Figs 6—10, it seems evident that apart from the conformational variations discussed above, the existence of stereoisomeric structures can by all means be taken for granted among the reviewed molecular species. This is especially true when compounds containing more than two cycles are considered, as the highly strained siloxane skeleton together with the inhibitory effect of the substituents leads to enhanced activation energies for the individual rotations in these compact polycyclic structures.

It is worth mentioning that while the sum of all isomers theoretically possible on the basis of the stoichiometric compositions is well above 80, the number of components indicated in the chromatograms, obtained even with columns of the highest resolution, was only 22 in the range of retention indices covering all the isolated molecular species (*cf.* Table I and Fig. 3).

It is evident from Table I that the molecular weights and empirical formulas of preparations 2a, 3b and 3c were identical. The same was found for preparations 4a, 4d and 4e, further for $5a_1$, $5a_2$ and $5b_1$. However, gas chromatographic retention indices determined on two different liquid phases and differences in the melting points proved in a convincing manner that the components in question were chemically different isomeric molecular species. At the same time, as mentioned in the description of mass spectrometry, the decomposition schemes of these isomers were practically identical. This extraordinarily similar behaviour of the isomeric structures was surprising. Investigation of model compounds of exactly known structures would be necessary for a detailed explanation of this problem.

Owing to the lack of direct experimental data in establishing the structural details of the isomeric compounds prepared, the gas chromatographic retention data were analyzed which may afford indirect and approximate information.

The retention indices, listed in Column 7 of Table I (SE–30, 125 °C) are plotted against the C/Si ratios in Fig. 11. The numerical values of the C/Si ratios indicate the average functionality of a definite molecule and are at the same time characteristic of structural features, such as the relative compactness or extended nature of the molecules in question. Higher C/Si values mean higher relative D contents accompanied by an increasing looseness of the molecular structure and its ability to occupy large surface areas.

Inspection of the position of plots in the diagram indicates the following

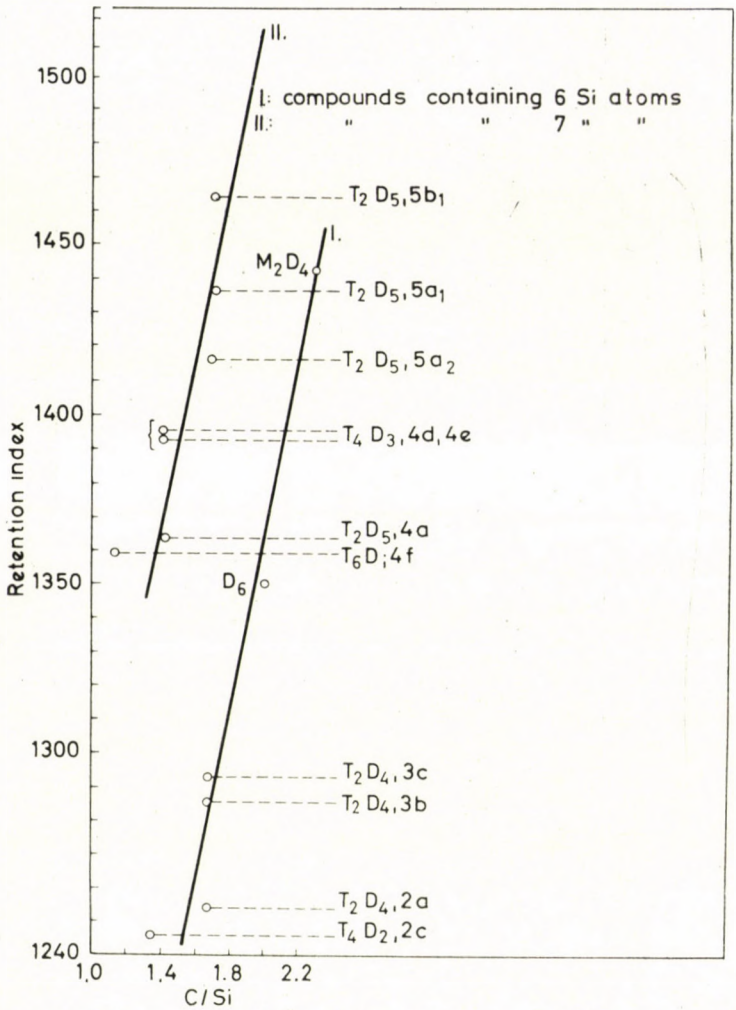


Fig. 11. Retention index *vs.* C/Si diagrams for various methylsiloxanes containing 6 and 7 Si atoms, respectively. Stationary phase: SE–30; column temperature: 125 °C

tendency: in compounds with identical silicon content, the retention indices are increasing whenever the average functionality decreases (increasing C/Si ratios). Consequently, molecules with high T contents and, consequently, having more compact structures (polycycles), are eluted with maximal speed from the GC column.

Data determined on APL coated capillaries are plotted in the same manner in Fig. 12. These data were not included in Table I because of their limited accuracy, which is due to the fact that they were calculated from the results of temperature-programmed chromatograms. On the other hand, this circumstance has offered some advantages, too: the tendency that plotting

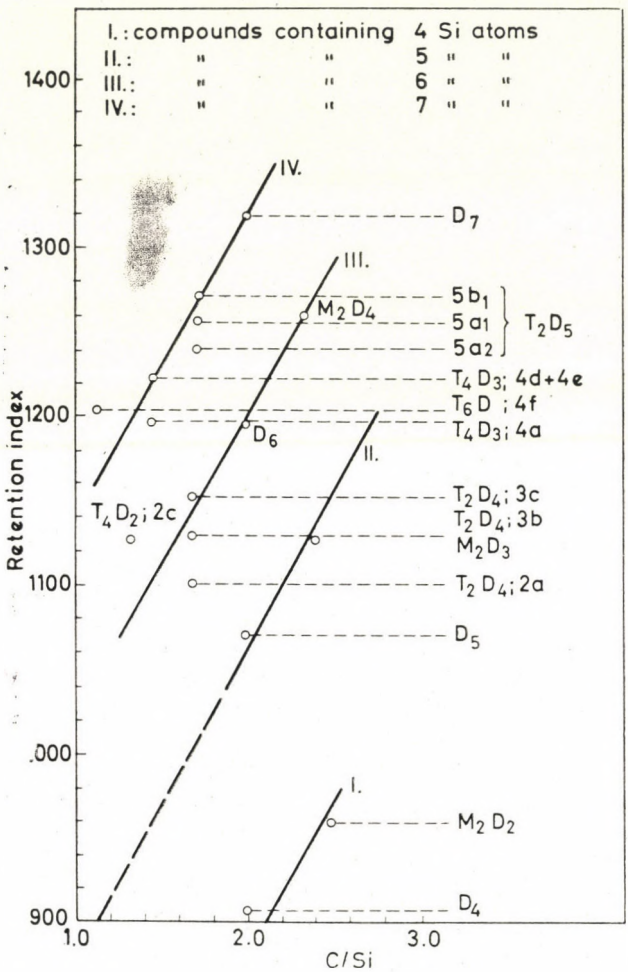


Fig. 12. Retention index *vs.* C/Si diagrams for various methylsiloxanes containing 4, 5, 6 and 7 Si atoms, respectively. Stationary phase: APL; column temperature: programmed in the temperature range 60—250 °C; heating rate: 3.5 °C/min.

of the retention indices of molecules containing the same number of silicon atoms *vs.* the C/Si ratios gives a straight line, was evidenced with index data of several further compounds containing 4, 5, 6 and 7 silicone atoms in known chemical structure (D_4, M_2D_2; D_5; M_2D_3; D_6, M_2D_4 and D_7). The slopes of the parallel lines belonging to compounds with different silicon contents may be considered characteristic of the retention increment per one carbon atom. This seems to be independent of the number of silicon atoms for the compounds investigated. Axial sections of the retention index *vs.* C/Si plots depend on the number of silicon atoms in the molecule. Differences in the molecular

structure seem to became manifest in the deviations of certain data around the straight lines.

It is known [11] that the effect of molecular shape, in general, is reflected by the fact that a higher degree of planarity (*e.g.*, in the case of fused ring systems) causes an increase in the retention time when a non-selective phase is used. Therefore, regarding compounds with identical silicon contents and C/Si ratios, *i.e.* isomers with different retention characteristics, it follows that species of more compact arrangements should have lower, and those with an extended structure should have higher retention indices. Similar index values of molecules having different empirical formulas, or even containing different numbers of Si atoms, indicate similarities in the compactness of their chemical structures.

Relative molecular stability of pyrolysis products

Mass spectrometric investigations of the isolated polycyclic methylsiloxanes have given interesting information concerning the relative stabilities of the pyrolysis products and their characteristic decomposition mechanisms. The relative abundance values of ions containing the intact siloxane skeleton were compared in the mass spectra of linear, cyclic, bicyclic and polycyclic methylsiloxanes. The results are summarized in Table II including data of an earlier communication [7] dealing with the properties of linear and cyclic methylsiloxanes. The relative abundances of doubly charged ions were com-

Table II

Relative stability of the siloxane skeleton and relative abundance of double-charged ions in different methylsiloxanes after electron impact

Chain molecules			Monocyclic molecules			Bicyclic molecules			Polycyclic molecules					
	S %	D %		S %	D %		S %	D %		S %	D %		S %	D %
M_2	80	4.1	—	—	—	—	—	—	—	—	—	—	—	—
M_2D	48	1.5	D_3	80	3.2	—	—	—	—	—	—	—	—	—
M_2D_2	23	1.1	D_4	73	2.6	—	—	—	—	—	—	—	—	—
M_2D_3	11	0.2	D_5	34	1.3	T_2D_3	68	2.2	—	—	—	—	—	—
M_2D_4	7	0.07	D_6	23	0.2	T_2D_4	40	0.7	T_4D_2	88	3	—	—	—
M_2D_5	4	0.05	—	—	—	T_2D_5	17	0.8	T_4D_3	67	6	T_6D	94	8
—	—	—	—	—	—	—	—	—	—	—	—	T_6D_2	>90	~9

S% = Relative abundance of ions with complete siloxane skeleton, in percentage of the total numbers of ions.

D% = Relative abundance of double-charged ions in percentage of the total numbers of ions.

pared, too. Data are presented in percentages of the total numbers of ions. From Table II it is evident that the stability of the silicon-oxygen skeleton is markedly increased against electron bombardment with decreasing C/Si ratios, *i.e.* with the increasing number of cycles; at the same time, the relative abundance of doubly charged ions increases as well.

The most striking characteristics of the decomposition patterns demonstrated in Fig. 5 are the very intense trimethylsilyl ion peaks of some molecules. The same peak is completely absent in some other cases. Its appearance in the mass spectrum by no means constitutes proof for the presence of trimethylsiloxi (M) groups in the molecule. Working with linear and cyclic methylsiloxanes it has been observed [7] that methyl group migration followed by rearrangement of the Si—O—Si skeleton, *i.e.* intramolecular scrambling reaction accompanied by the formation of a new cycle in the molecule, is indicated by the appearance of an intense trimethylsilyl peak. This phenomenon is demonstrated in Fig. 13, compound D_5 serving as an example.

Skeletal rearrangement and migration of the methyl radical on electron bombardment have been proved in the cases of samples with the empirical formulas $Si_6O_7C_{10}H_{30}$ (T_2D_4) and $Si_7O_8C_{12}H_{36}$ (T_2D_5) (both of bicyclic character) by a very intense $(P-103)^+$-type ion peak, whose formation is accompanied by the simultaneous expulsion of tetramethylsilane (*cf.* Fig. 5). This can be interpreted — similarly to the case of linear and cyclic methylsiloxanes — by further cyclization (*e.g.* $(T_2D_4-15)^+ - Si(CH_3)_4 \rightarrow (T_4D-15)^+$ transition). Further evidence for the cyclization process is furnished by the abundance of the $(P-103)^+$ ion peak, whose value is significant even at low ionization energies (12 to 15 eV), showing that the energy requirement of the process is small.

Trimethylsilyl ions, or ions of the $(P-103)^+$ type, were absolutely absent in the mass spectra of polycyclic compounds of $Si_6O_8C_8H_{24}$ (T_4D_2), $Si_7O_{10}C_8H_{24}$ (T_6D) and $Si_8O_{11}C_{10}H_{30}$ (T_6D_2) compositions. It follows that these compounds do not contain any M groups and they may not undergo skeletal rearrangements accompanied by methyl group migrations.

Polycyclic compounds with the empirical composition $Si_7O_9C_{10}H_{30}$ (T_4D_3) give rise to trimethylsilyl peaks of significant abundance. At the same time, no ion peaks of the $(P-103)^+$ type are present in the mass spectra (*cf.* Fig. 5). This observation can be interpreted either by the assumption of methyl group migration occurring to a limited extent, or by the presence of M groups.

Pyrolysis chromatogram

Knowledge of the character of the pyrolysis products facilitates the interpretation of the pyrolysis gas chromatograms.

The chromatogram shown in Fig. 3 demonstrates the results in identifying the pyrogram peaks, while using the separated pyrolysis products as

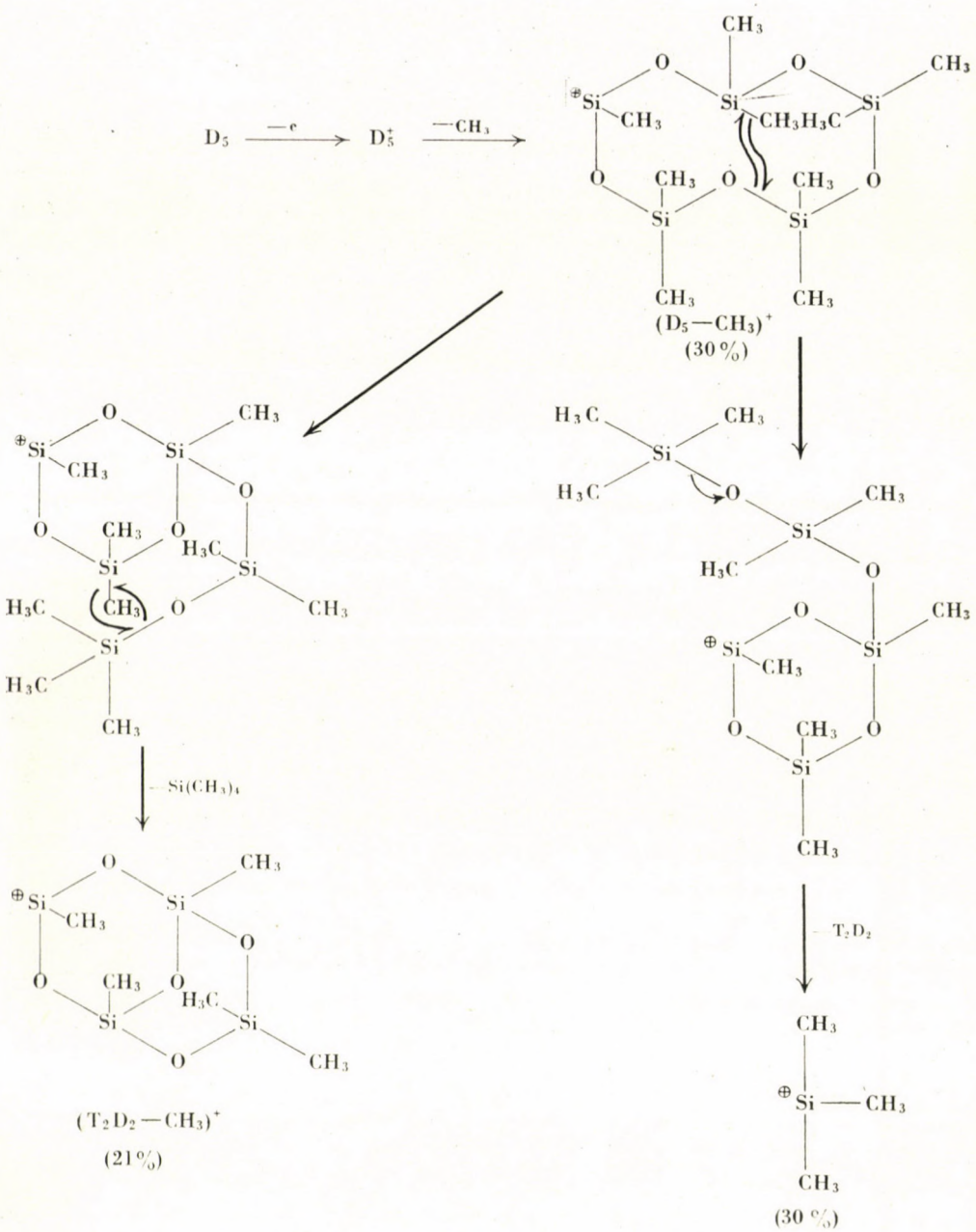


Fig. 13. Decomposition of decamethylcyclopentasiloxane (D_5) on electron impact in the mass spectrometer

internal standards. As can be seen, the significant peaks of the complex pyrogram could be identified with the exception of three peaks. It is evident that two compounds among the large-scale pyrolysis products (D_5 and one of the T_2D_4 isomers) occur in strikingly high quantities.

Discussion

In the previous discussions all the different sorts of molecules recovered from the pyrolysate have been supposed to consist solely of structural units T and D, irrespective of the fact that their molecular weights and stoichiometric compositions could correspond — in principle at least — to various combinations of Q, M, T and D units as well.

Exclusion of these combinations is justified because the original polymer was prepared by the hydrolysis of a $(CH_3)_2SiCl_2$–CH_3SiCl_3 monomeric mixture.

Nevertheless, it has to be considered that in the course of pyrolysis the structural units may change on account of scrambling reactions, according to the following equations:

$$(1) \quad 2T \rightarrow D + Q$$
$$(2) \quad 2D \rightarrow M + T \qquad (N = Si(CH_3)_4)$$
$$(3) \quad 2M \rightarrow N + D$$

An interpretation of the trimethylsilyl and $(P–103)^+$ peaks present in mass spectrographic decomposition patterns has been given in a previous chapter of this paper, and it has been pointed out that these peaks refer to fragmentations of mono- and bicyclic compounds accompanied by cyclization processes *via* Reaction (2) (*cf.* Fig. 13).

There is no direct evidence for intramolecular scrambling processes according to Eq. (1) in the mass spectrometer.

The possibility of scrambling reactions was investigated also in the course of pyrolysis. It has been proved [12] that changes in functionality take actually place, according to Eqs (2) and (3), under definite conditions in the pyrolysis of methylpolysiloxanes with network structure. If pyrolysis is carried out in the presence of mixed KOH and dimethyl sulfoxide (DMSO) catalyst at temperatures higher than 300 °C, high amounts of M_2, D_3, M_2D, M_2D_2 and D_4 are found in the pyrolysate, while N is only detectable in traces.

At the same time, molecules containing M units were completely absent in the pyrograms taken after non-catalyzed pyrolysis.

According to recent results of BROWN *et al.* [13], the compounds mentioned above are not formed even during equilibration (rearrangement at reflux temperatures) of T—D hydrolysates in the presence of KOH + DMSO.

Therefore, it may be concluded that neither the use of the mixed catalyst KOH + DMSO, nor the comparatively high temperatures employed

in our experiments are sufficient alone to give rise to scrambling reactions according to Eqs (2) and (3). Presumably the simultaneous effect of both factors is necessary to transform branched-chain methylpolysiloxanes not only into T—D polycyclics, but also to bring about structural variations which contain M and N units as well.

There is one common feature in the two widely different sets of experimental conditions leading to functionality changes that deserves attention: scrambling reaction in the mass spectrometer is produced as a consequence of ionization; similarly, the ionic mechanism of thermal decomposition is very probably promoted by the pronounced polar character of DMSO.

These observations — similarly to the results of mass spectrometry — do not exclude the existence of scrambling reactions according to Eq. (1), *i.e.* the formation of molecules containing Q, produced from the original T-containing material during pyrolysis. Nevertheless, the occurrence of Reaction (1) may be considered impossible if Reactions (2) and (3) are experimentally excluded.

This statement is further supported by mass spectrometric evidence. Data in Table II are instructive in this respect, showing that stability of the siloxane skeleton and the abundance of doubly charged ions in the mass spectrogram are both markedly increased with the growing number of cycles, *i.e.* the T-content pro molecule. This experience lowers the probability of Eq. (1) compared with Eqs (2) and (3), and is in accordance with earlier findings [7] and theoretical considerations.

The behaviour of siloxanes and other silicon compounds is markedly affected by atoms attached to the silicon atom and possessing lone electron pairs that are able to produce p_π—d_π interactions with the participation of the empty *d*-orbitals of silicon. This π-contribution of lone pairs partly stabilizes the doubly charged ions owing to delocalization of charge. Its effect on the siloxane skeleton is similar to that of conjugation: it results in stabilization because of rapid delocalization of the energy transferred, *e.g.* by the bombarding electrons. Thus the stability of the siloxane skeleton is expected to increase if the proportion of trifunctional units (three Si—O bonds per silicon atom) increases within the molecule.

Our assumption, according to which the isolated materials are regarded to be composed of T and D structural units, is based on these facts and considerations.

The experimental results reported in this paper also allow some conclusions on the structures of the isolated T and D isomers. As seen from the data in Figs 11 and 12, the only T_4D_2-type molecule prepared so far shows an extraordinarily high retention compared to its functionality. Therefore it is assumed that its structure — as pictured in Fig. 14, No. 1 — represents the highest steric extension possible for molecules characterized by the same

elemental compositions. It follows that of the three T_2D_4-type molecules (with retentions similar to that of T_4D_2), 2a should possess the most compact structure, as indicated by its lowest retention value on both columns. Of the four possible variants of T_2D_4 molecules, we have succeeded in isolating three representatives. The four isomeric variants are schematically shown in

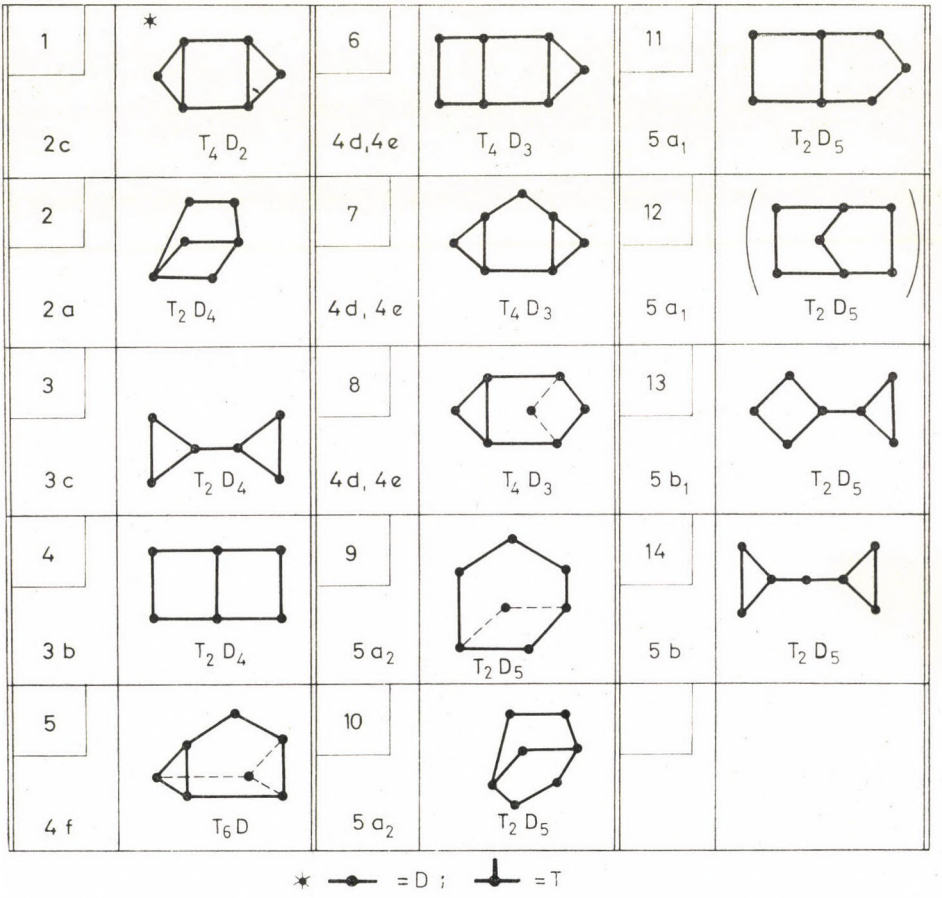


Fig. 14. Assignments of structures to molecules isolated from the pyrolysis product

Fig. 6 discussed above, and it is readily seen that structure IV is the one having the highest degree of close-packing. The schematic structure No. 2 in Fig. 14 refers to our assumption according to which structure IV corresponds to preparation 2a. There remain only three possibilities for the identification of preparations 3b and 3c with respect to their spatial arrangements.

Correct selection is facilitated by an empirical rule [13] concerned with the retention behaviour of methylsiloxane polycycles. According to this, the increase in retention produced by an increment of three D units is nearly

the same as that produced by four T units. Thus a peak for a species of composition T_mD_n is found in the same peak range as that for $T_{m+4}D_{n-3}$.

In view of our own experimental results, according to which molecules having identical formulas in terms of structural units may exist in various isomeric forms, and the retention indices of these forms may differ, the rule in its original and quoted form does not hold true. The conclusion cited has been drawn evidently on the basis of comparing molecules of analogous spatial arrangements. With this restriction the rule seems to be applicable, and casts some light on further connections. It emerges that if this rule is valid in respect of two compounds, this means that the compounds are analogues of each other, The interpretation of the concept of analogous spatial arrangements follows from Fig. 14 and its discussion.

The correctness of this finding becomes evident as the peaks of D_6 and one of the T_4D_3 isomers, and similarly, the peaks of T_6D_2 and one of the T_2D_5 isomers coincide in our pyrograms.

Starting with this observation, structure III in Fig. 6 can be excluded with high probability in the case of the T_2D_4-type molecules designated as 3c and 3b. According to similarities between structures III in Fig. 6 and No. 5 in Fig. 14, the retention of a molecule with structure III is expected to be in the retention range of T_6D. As the retentions of species 3c and 3b differ significantly from that of T_6D (4f), it follows unambiguously that II in Fig. 6 with a more compact structure has to be ordered to 3b (retention index on Tween 10 : 1150), while I in Fig. 6 with a more extended arrangement (index number 1881.5) belongs to 3c.

This pairing seems to be reasonable from another point of view, too. Preparation 3b is the dominant component among the products of the large-scale pyrolysis, and thus it is presumably a very stable molecule. Its proposed structure (III in Fig. 6) has been described above as a very flexible arrangement which may exist in many forms (*cf.* Figs 8 and 10). Its preference is evident considering that it can be regarded as a characteristic type of structures for polymers composed of trifunctional units, namely as an elementary cell of the double-chain ladder structure. Thermodynamic stability of this structure is explained mainly by the fact that the preferred Si—O—Si angle which is nearly 155° in methylsiloxanes, further the most separated arrangement of methyl groups are attained without difficulty in this configuration.

Some further well-founded assumptions concerning structural identification of the prepared isomers are due to an earlier observation of this working group [14]. According to this, addition of one Me_2SiO unit to various methylsiloxane molecules is accompanied by a retention index increment of about 160 on SE–30 column. The validity of this rule, similarly to that discussed above, is expected only if molecules with analogous steric arrangements are considered. Compounds obeying this rule may be regarded as homologues.

It follows from Table I that of the T_4D_3 molecules, preparations 4d and 4e may be regarded as homologues of the species 2c with symbol T_4D_2. Nevertheless, this circumstance alone does not determine the structures of the two substances designated as 4c and 4e, because three different homologous structures (6, 7 and 8) may be derived from structure 1 in Fig. 14. Actually, the number of imaginable conformations is doubled considering that, similarly to 1, structures 4, 5 and 6 may equally occur in *cis* and *trans* forms.

Possibilities for outlining the spatial arrangements for the three various T_2D_5 molecules are more favorable. From calculations based on the retention indices determined on SE–30 columns it appears that the relations between 2a and $5a_2$, 3b and $5a_1$, and between 3c and $5b_1$ are of "homologous" character, the members of the 5-series being enlarged by one Me_2SiO (D) unit. Considering Figs 6 and 14 simultaneously, the isomeric variations 9 and 10 for $5a_2$, further 11, 12 and 13, 14 as structures for $5a_1$ and $5b_1$, respectively are to be taken into account. Isomers 10 and 12 are identical and may be derived both from structures corresponding to 3b and 2a; however, considering the relatively high compactness of this conformation it is attributed rather to $5a_2$, characterized by a relatively low retention value. The retention data alone do not allow to decide which of the two possible structures of both $5a_2$ and $5b_1$ molecules of the T_2D_5 group is correct.

Structural considerations based on retention data and summarized in Fig. 14 do not give information about the molecules 4a of the T_4D_3 and $5b_2$ of the T_6D_2 series.

Finally, we should like to review some conclusions concerning the character of thermal decomposition processes and the structure of the original network system.

According to BROWN *et al.* [13, 15], silicone network polymer systems, in general, may have highly ordered double-chain ladder structures, or moderately ordered 'bead chain' structures composed of polycyclic blocks (cages) linked by single oxygen atoms or occasionally by D_n chains.

The same investigations led to the conclusion that equilibrated difunctional-trifunctional methylsiloxane network polymers should show beaded structures in which the individual polycyclic blocks may possess any out of a variety of structural forms (*e.g.*, structure I in Fig. 15).

This conclusion was based on the experimental isolation and identification of low molecular weight fractions of the equilibrated D—T methylsilicone polymer system [13]. These proved to consist mainly of polycycles in addition to some species of cycles and bicycles. On basis of infrared spectroscopic results it has been established that the basic structure of this molecular population is a cage-like block structure. In order to illustrate the statements of BROWN *et al.*, possible 'ladder-type' and 'cage-like' structures of the T_6D_2 molecule are presented by the schematic structures II and III in Fig. 15.

In our opinion, results of this paper also support the idea that the origin of the decomposition products obtained may be a polymer system, most probably with a 'bead chain' structure.

This view is corroborated in the first place by our experience that the elimination of decomposition products in methylsiloxane systems is accompanied by cyclization processes. Cyclization may occur according to two mechanisms: (1) cleavage of definite Si—O bonds, followed by recombination of the same type of linkages resulting in new molecular configurations.

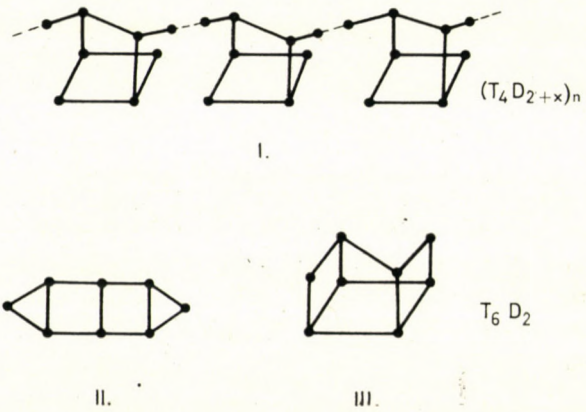


Fig. 15. Polycyclic structural configurations. I: 'bead-chain' structure composed of polycyclic T_4D_2 blocks. II and III: ladder-type and cage-like structure of the polycycle T_6D_2

This is the process which takes place in the course of siloxane chain polymer degradation [16] and does not involve any change in functionality: (2) intramolecular scrambling reactions, which are accompanied by functionality changes; as a consequence, bicyclic compounds are formed from monocyclic ones, and the formation of poly- or possibly spirocyclic components (cyclic systems containing Q elements) is also likely.

Our results seem to support the opinion that the latter mechanism has to be disregarded when the decomposition of branched-chain methylsilicone polymers is initiated only by heat. This means that the originally cyclic structures remain essentially unchanged during pyrolysis (accidentally various small independent rings are formed from a bigger one) and degradation will take place only in the chain fragments coupling the cycles or even the polycycles. These fragments may sometimes be comparatively long, owing to incomplete co-condensation (Fig. 15). This process may lead either to a breakdown of independent cyclic molecules, or to elimination of polycyclic blocks originally present in the system. However, as the number of T units in these blocks remains unchanged, the separated polycyclic products become neces-

sarily enlarged by one ring at least at the expense of the connecting chain-type section of the polymeric system. According to our present knowledge this mechanism of degradation (involving cleavage of Si—O bonds and their recombination by cycling) is determined by two factors.

One of them is the mutual repulsion of the methyl substituents [17]. As a consequence, the degradation of chain structures consisting merely of D units results in the preferred development of coplanar trisiloxane rings, because — although the Si—O—Si valence angle is somewhat strained — mutual repulsion of the methyl groups is diminished to a minimum in this way. Configurations in Fig. 14 may be rationalized in this respect, namely several structures contain definitely trisiloxane rings as constituents, while the other structures are most probably also characterized by low repulsion between the methyl groups.

A further factor which has to be taken into consideration is the well-known fact that the siloxane skeleton is made up of highly polar covalent bonds. A rather high flexibility of the valence angles — as compared with carbon-chain compounds — is one of the important consequences of the polarity of the Si—O bond. (As it is also known, if the bonds were completely ionized, orientation determining the valence-like preferential directions of the chemical bond would cease, giving place to spatial arrangements fixed only by the ratios of ionic radii.)

The highly polar character of the Si—O bond is reflected by the appearance of considerable Coulomb forces between segments of one siloxane chain. This leads to the formation of spirals and subsequent degradation involving decyclization reactions of the siloxane chains and similar oxane-type polymers. The latter process may be regarded as an intramolecular transfer reaction [19].

Therefore, the structures of the polycyclic compounds isolated from the pyrolysate are determined partly by the most favourable rotational position of the methyl substituents, and partly by possibilities for spontaneous re-coupling of the bead-chain (*cf.* Fig. 15).

These considerations, which have been used to furnish evidence for the concept of bead-chain structure proposed by J. F. Brown, may be supported by two further experimental results.

According to Table I and Fig. 4, it is obvious that the average C/Si value of the pyrolysis product is significantly higher than that of the original polymer, *i.e.* a loss of methyl groups (D units) is observed on heating the T—D polymeric system. This is, of course, evidence for the assumption that decomposition proceeds *via* cyclization of the chain part of the bead-chain. It follows from this fact that D units separating the polycyclic cages are the preferred regions for Si—O bond cleavage and recombination.

A further argument for the discussed hypothesis is that, according to PGC experiments, the lowest temperature of thermal decomposition of a

dimethylsiloxane high polymer (detected by FID) is nearly equal to that found for network polymers characterized in this paper (240 °C). Obviously, in the case of a ladder-like polymeric structure, cleavage and recombination of the Si—O bond must take place simultaneously at least on two adjacent or very closely situated Si atoms, in order to give rise to the formation of polycyclic decomposition products. The theoretical probability of a process of that type is very low [18]. The possibility of measuring the same decomposition temperatures in the cases of a ladder-like and a chain-like polymeric system may be ruled out with certainty.

REFERENCES

1. Scott, D. W.: J. Am. Chem. Soc. **68,** 356 (1946)
2. Barry, A. J., Daudt, W. H., Domicone, J. J., Gilkey, J. W.: J. Am. Chem. Soc. **77,** 4248 (1955)
3. Vogt, L. H., Brown, J. F.: Inorg. Chem. **2,** 189 (1964)
4. Garzó, G., Székely, T.: Acta Chim. Acad. Sci. Hung. **41,** 269 (1964)
5. Lengyel, B., Halmos, T., Székely, T.: Acta Chim. Acad. Sci. Hung. **44,** 378 (1965)
6. Tamás, J., Ujszászi, K., Székely, T., Bujtás, Gy.: Magy. Kém. Foly. **75,** 148 (1969)
7. Tamás, J., Ujszászi, K., Bujtás, Gy.: Acta Chim. Acad. Sci. Hung. (In press)
8. Tamás, J., Ujszászi, K., Bujtás, Gy.: Acta Chim. Acad. Sci. Hung. (In press)
9. Aulinger, F., Reering, W.: Z. anal. Chem. **197,** 24 (1963)
10. Orlov, V. Yu.: Zhur. Obshch. Khim. **37,** 2300 (1967); Zhur. Fiz. Khim. **43,** 28 (1969)
11. Giddings, J. C.: Advances in Chromatography. Vol. 1, Chapter 5, p. 157. M. Dekker Ed., New York, 1965
12. Pehrsson, K.: Doctoral Dissertation, Budapest, Eötvös L. Univ., 1969
13. Brown, J. F., Slusarczuk, G. M. J.: J. Am. Chem. Soc. Div. Polym. Chem. Preprint 8/1/157 (1967)
14. Garzó, G., Fekete, J., Blazsó, M.: Acta Chim. Acad. Sci. Hung. **51,** 359 (1967)
15. Brown, J. F.: J. Polym. Sci. Part C 1 83 (1963)
    Brown, J. F., Vogt, L. H.: J. Am. Chem. Soc. **87,** 4313 (1965)
    Brown, J. F., Vogt, D. H.: J. Am. Chem. Soc. **87,** 4317 (1965)
16. Székely, T.: Doctoral Dissertation, Budapest, (in preparation)
17. Allcock, H. R.: J. Polym. Sci. Part A—1 **5,** 355 (1967)
18. Tessler, M. M.: J. Polym. Sci. Part A—1 **4,** 2521 (1966)
19. Thomas, T. H., Kendrick, T. C.: J. Polym. Sci. Part A—2 **7,** 537 (1969)

Gabriella Garzó
József Tamás
Tamás Székely
Kálmán Ujszászi

Budapest VIII., Múzeum krt. 6—8.

MAGYAR
TUDOMÁNYOS AKADÉMIA
KÖNYVTÁRA

Acta Chimica Academiae Scientiarum Hungaricae, Tomus 69 (3), pp. 301–309 (1971)

UNTERSUCHUNG DER BEIM ERHITZEN ZWISCHEN DEN KOMPONENTEN VON N-P-K-DÜNGERN VERLAUFENDEN VORGÄNGE, II

SYSTEME: AMMONIUMNITRAT–AMMONIUMDIHYDROPHOSPHAT, AMMONIUMNITRAT–CALCIUMHYDROPHOSPHAT, AMMONIUMDIHYDROPHOSPHAT–CALCIUMHYDROPHOSPHAT, AMMONIUMDIHYDROPHOSPHAT–KALIUMCHLORID UND CALCIUMHYDROPHOSPHAT–KALIUMCHLORID

T. Flóra und M. Menyhárt

(Forschungsinstitut für die Schwerchemikalienindustrie, Veszprém)

Eingegangen am 18. März 1970

Die binären Systeme Ammoniumnitrat–Ammoniumdihydrophosphat, Ammoniumnitrat–Calciumhydrophosphat, Ammoniumdihydrophosphat–Calciumhydrophosphat, Ammoniumdihydrophosphat–Kaliumchlorid und Calciumhydrophosphat–Kaliumchlorid wurden derivatographisch untersucht. Die Untersuchungen ergaben, daß — mit Ausnahme des Systems Calciumhydrophosphat–Kaliumchlorid — die Komponenten der untersuchten Systeme miteinander in thermische Wechselwirkungen treten. Es wurde festgestellt, daß das Calciumhydrophosphat mit dem Kaliumchlorid eine Austauschreaktion eingeht. Bei den übrigen Systemen wurde angenommen, daß koordinative Bindungen zwischen den Komponenten gebildet werden.

Um die mannigfaltig zusammengesetzten Vorgänge zu erkennen, die sich beim Erhitzen von Dreinährstoffdüngern abspielen, wurden derivatographische Untersuchungen durchgeführt. Um die Auswertung der Ergebnisse zu erleichtern, wurde die Arbeit mit der Untersuchung von binären Systemen begonnen. In unserer vorangegangenen Mitteilung [1] haben wir über die thermischen Vorgänge im System Ammoniumnitrat–Kaliumchlorid berichtet. Als Fortsetzung dieser Arbeit wurden — unter den in [1] beschriebenen Versuchsbedingungen — die thermischen Eigenschaften der binären Systeme Ammoniumnitrat–Ammoniumdihydrophosphat, Ammoniumnitrat–Calciumhydrophosphat, Ammoniumdihydrophosphat–Kaliumchlorid und Calciumhydrophosphat–Kaliumchlorid untersucht. Über die Ergebnisse dieser Untersuchungen wird in der vorliegenden Arbeit berichtet.

Unter den Komponenten der Dreinährstoffdünger wurden die thermischen Eigenschaften des Ammoniumdihydrophosphats von Erdey und Mitarbeiter [2] derivatographisch, von Nabiew und Mitarbeiter [3] differentialthermoanalytisch untersucht. Die Eigenschaften des Calciumhydrophosphats mit 2 Molekülen Kristallwasser wurden von Petschkowsky und Mitarbeiter [4] mittels DTA, TG, IR-Spektrophotometrie und Elektronspinresonanzmessungen untersucht.

Ergebnisse über die thermischen Eigenschaften einiger binären Systeme wurden auf thermogravimetrischem oder differentialthermoanalytischem

Wege erhalten. MARINELA MAN [5] stellte bei der thermogravimetrischen Untersuchung des Systems Ammoniumnitrat–Ammoniumdihydrophosphat fest, daß im Gemisch aus gleichen Gewichtsteilen in erster Reihe das Ammoniumnitrat und im 1 : 2-Gemisch das Ammoniumdihydrophosphat zersetzt wird. NABIEW und Mitarbeiter [6] gelangten aufgrund differentialthermoanalytischer Messungen zu der Schlußfolgerung, daß das Ammoniumdihydrophosphat und das Kaliumchlorid beim Erhitzen miteinander in Reaktion treten.

Versuchsergebnisse und ihre Diskussion

Abb. 1 zeigt das Derivatogramm des Gemisches aus gleichen Gewichtsteilen *Ammoniumnitrat und Ammoniumdihydrophosphat* bei einer Aufheizgeschwindigkeit von 4 °C/Minute bis 900 °C, sowie die Derivatogramme der Komponenten.

Zur Herstellung des Gemisches wurde Ammoniumdihydrophosphat technischer Qualität (ein Produkt, welches in der Praxis zur Herstellung von N–P–K-Düngern verwendet wurde) benützt, welches mit Diammoniumhydrophosphat verunreinigt war. Je nach den Versuchsbedingungen zersetzte sich das Diammoniumhydrophosphat bei 145 °C (Abb. 1, DTG-Kurve 1) bzw. bei 136 °C (Abb. 2, DTG-Kurve 1) zu Ammoniumdihydrophosphat und Ammoniak [2]. Das demgemäß aus zwei Quellen stammende Ammoniumdihydrophosphat spaltete in drei Stufen, undzwar beim schnelleren Aufheizprogramm bei DTG-Spitzentemperaturen von 165, 185 und 235 °C (Abb. 1, DTG-Kurve 1), beim langsameren Aufheizprogramm bei 148, 169 und 180 °C (Abb. 2, DTG-Kurve 1) 0,5 Moleküle Wasser ab und es blieb Diammoniumdihydrogen–Pyrophosphat $(NH_4)_2H_2P_2O_7$ zurück. Parallel mit der Zersetzung schmolz die Probe bei 165 °C (Abb. 1, DTA-Kurve 1) bzw. bei 176 °C (Abb. 2, DTA-Kurve 1). Unter dem Mikroskop mit heizbarem Objekttisch wurde der Schmelzpunkt bei 180 °C beobachtet. Durch weitere Wasserabspaltung in den Zersetzungsstufen bei 245 und 280 °C entstand Ammoniummetaphosphat NH_4PO_3, welches sich zu Ammoniak, Wasser und Phosphorpentoxyd zersetzte. Bei 740 °C wurde die Sublimation des Phosphorpentoxyds beobachtet [2] (Abb. 1, DTG-Kurve 1). Wie aus den Derivatogrammer ersichtlich ist, überdecken sich die einzelnen Zersetzungsvorgänge.

Aus den Derivatogrammen des Gemisches (Abb. 1 und 2, Kurven 2) kann festgestellt werden, daß die thermischen Eigenschaften des Ammoniumnitrats in Gegenwart von Ammoniumdihydrophosphat verändert werden: die Phasenumwandlungstemperaturen verschieben sich (Abb. 1 und 2, DTA-Kurven 2) und die Zersetzung erfolgt in zwei Stufen (Abb. 1, DTG-Kurve 2). Die erste Zersetzungsstufe erfolgt bei einer niedrigeren Temperatur (230 °C)

als die Zersetzung des reinen Ammoniumnitrats (240 °C), während die zweite Stufe bei einer höheren Temperatur (250 °C) auftritt. Dennoch kann im

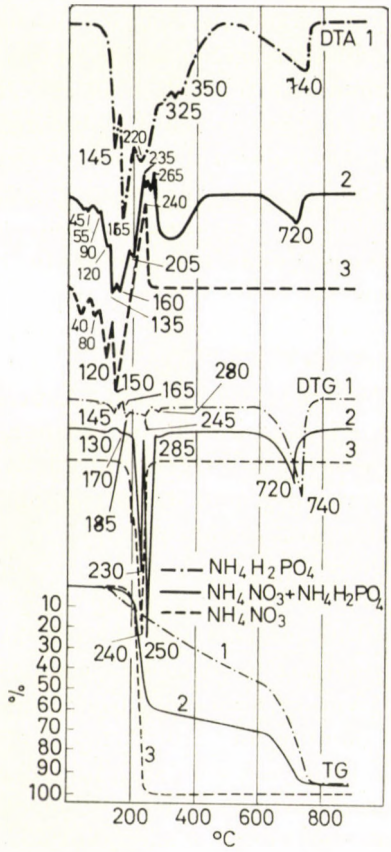


Abb. 1. Derivatographische Kurven des Systems Ammoniumnitrat–Ammoniumdihydrophosphat. Aufheizgeschwindigkeit 4 °C/Minute. 1 — Ammoniumdihydrophosphat; 2 — Gemisch aus gleichen Gewichtsteilen Ammoniumnitrat und Ammoniumdihydrophosphat; 3 — Ammoniumnitrat

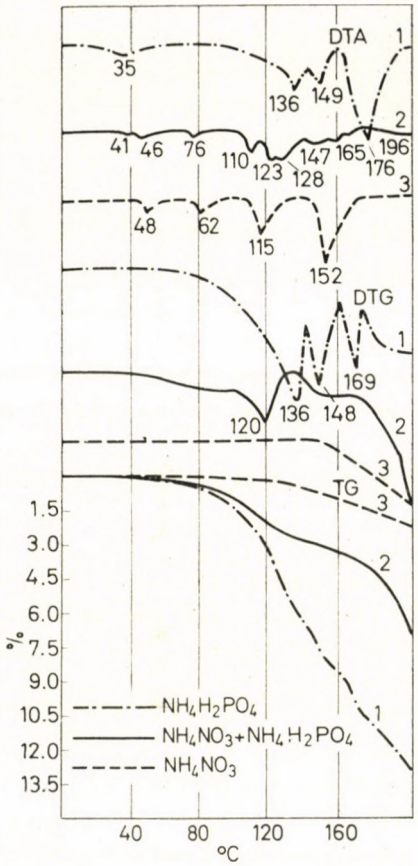


Abb. 2. Derivatographische Kurven des Systems Ammoniumnitrat–Ammoniumdihydrophosphat. Aufheizgeschwindigkeit 1 °C/Minute. 1 — Ammoniumdihydrophosphat; 2 — Gemisch aus gleichen Gewichtsteilen Ammoniumnitrat und Ammoniumdihydrophosphat; 3. — Ammoniumnitrat

Röntgenogramm des bis 130 °C vorerwärmten Gemisches kein Hinweis auf das Erscheinen einer neuen Phase beobachtet werden. Aus dem Röntgenogramm konnte nur festgestellt werden, daß die Probe — neben viel Ammoniumdihydrophosphat — wenig Ammoniumnitrat enthält; eine ähnliche

Erscheinung ist bereits beim System Ammoniumnitrat–Ammoniumchlorid beobachtet worden [1].

Unserer Annahme nach wird zwischen einem Teil des Ammoniumnitrats und dem Ammoniumdihydrophosphat bei dem Erhitzen eine lockere koordinative Bindung gebildet, die eventuell zu keiner Änderung der Lage der Röntgenlinien führt, sondern nur ihre Intensität verändert. Die thermische Stabilität des in der entstandenen Komplexverbindung gebundenen Ammoniumnitrats ist geringer, als die des reinen Ammoniumnitrats, deshalb erfolgt ihre Zersetzung bei niedrigerer Temperatur, als die der reinen Verbindung.

Nach der Zersetzung des Ammoniumnitrats verlaufen die Zersetzungsvorgänge des Ammoniumdihydrophosphats auf die oben beschriebene Weise.

Aus den Derivatogrammen des 1 : 1-Gemisches von *Ammoniumnitrat und Calciumhydrophosphat* (Abb. 3 und 4, Kurven 2) kann auf eine ähnliche thermische Wechselwirkung der Komponenten gefolgert werden, wie bei dem vorangehenden System. Auch hier tritt eine Verschiebung der Phasenumwandlungstemperaturen und des Schmelzpunktes im Vergleich zu den betreffenden DTA-Spitzentemperaturen des reinen Ammoniumnitrats auf. Außerdem erfolgt die Zersetzung des Ammoniumnitrats in Gegenwart von Calciumhydrophosphat in zwei Stufen, bei Spitzentemperaturen von 210 und 250 °C (Abb. 3, DTG-Kurve 2). Bei 400 °C wurde erwartungsgemäß die Zersetzung des Calciumhydrophosphats zu Calciumpyrophosphat beobachtet [4].

Aus den Gewichtsverlustangaben der Derivatogramme, die sich auf das 1 : 1-Gemisch von *Ammoniumdihydrophosphat und Calciumhydrophosphat* beziehen (Abb. 5 und 6, Kurven 2) kann bis 230 °C auf keinerlei thermische Wechselwirkung zwischen den Komponenten gefolgert werden. Wie ersichtlich, steht der Gewichtsverlust, der auf den Derivatogrammen des Gemisches beobachtet wird, bei schnellem Aufheizen (4 °C/Minute) bis 230 °C, bei langsamem Aufheizen (1 °C/Minute) bis 170 °C in Einklang mit dem aufgrund der Gewichtsverlustangaben der Komponenten zu erwartenden Wert. Jedoch weist die Form der thermischen Kurven, besonders auf den bei einer Aufheizgeschwindigkeit von 1 °C/Minute aufgenommenen Derivatogrammen (Abb. 6, Kurven 2) darauf, hin, daß auch in diesem Temperaturbereich thermische Reaktionen verlaufen. So verschwinden z. B. im Derivatogramm des Gemisches (Abb. 6, Kurven 2) die thermischen Spitzentemperaturen 148—149 °C (Abb. 6, Kurven 3), die sich auf die Wasserabspaltung des Ammoniumdihydrophosphats beziehen; zugleich tritt bei 180 °C eine DTG- und DTA-Spitze auf, die einen neuen Vorgang anzeigt.

Über 230 °C sprechen auch die Gewichtsverluststufen im Derivatogramm des Gemisches (Abb. 5, Kurven 2) dafür, daß eine Reaktion zwischen den Komponenten verläuft. Die Spitze um 400 °C, die der Zersetzung des Calciumhydrophosphats entspricht, wird am Derivatogramm bei 410 °C beobachtet, jedoch wird die Sublimation des aus der Zersetzung des Ammoniumdihydro-

phosphats stammenden Phosphorpentoxyds bei 740 °C durch das Derivatogramm nicht angezeigt. Dies bedeutet, daß ein Produkt in der Reaktion gebildet

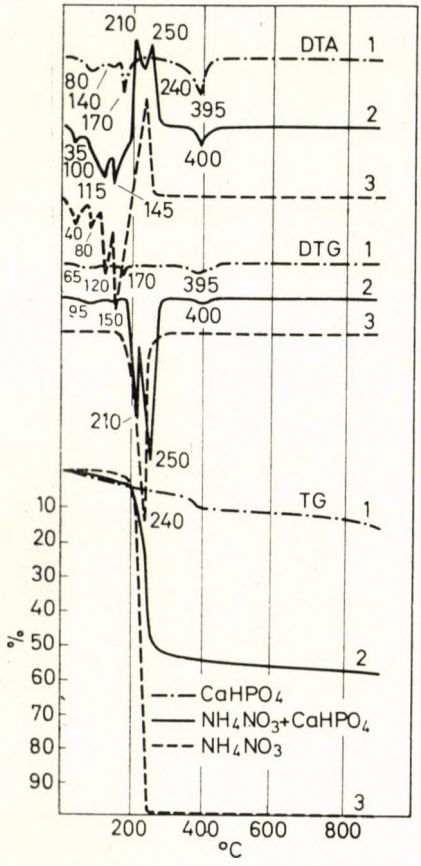


Abb. 3. Derivatographische Kurven des Systems Ammoniumnitrat–Calciumhydrophosphat. Aufheizgeschwindigkeit 4 °C/Minute. 1 — Calciumhydrophosphat; — 2 Gemisch aus gleichen Gewichtsteilen Ammoniumnitrat und Calciumhydrophosphat; 3 — Ammoniumnitrat

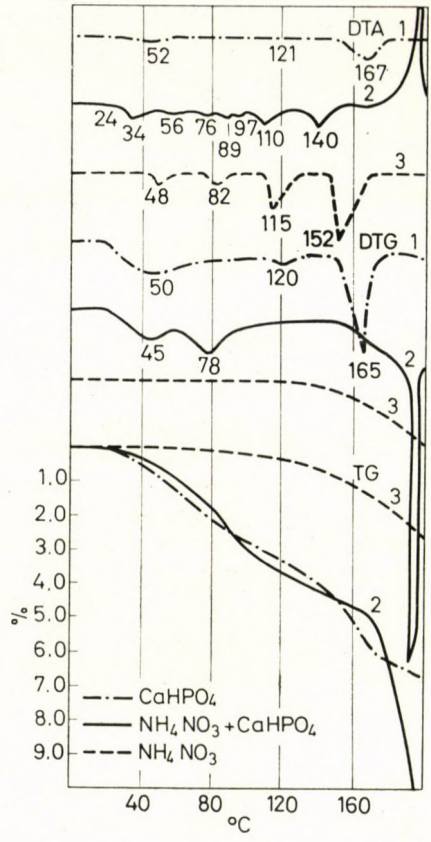


Abb. 4. Derivatographische Kurven des Systems Ammoniumnitrat–Calciumhydrophosphat. Aufheizgeschwindigkeit 1 °C/Minute. 1 — Calciumhydrophosphat; 2 — Gemisch aus gleichen Gewichtsteilen Ammoniumnitrat und Calciumhydrophosphat; 3 — Ammoniumnitrat

wird, in dem das Phosphorpentoxyd des Ammoniumdihydrophosphats in gebundenem Zustand vorliegt.

Aufgrund der Derivatogramme des Gemisches aus gleichen Gewichtsteilen *Ammoniumdihydrophosphat und Kaliumchlorid* (Abb. 7 und 8, Kurven 2) kann bis 260 °C allein aus der Form der Kurven auf eine Wechselwir-

kung zwischen den Komponenten gefolgert werden. Der Verdacht auf eine thermische Reaktion ergibt sich daraus, daß die Spitze bei 145 °C im Derivatogramm mit der Aufheizgeschwindigkeit von 4 °C/Minute (Abb. 7, Kurven

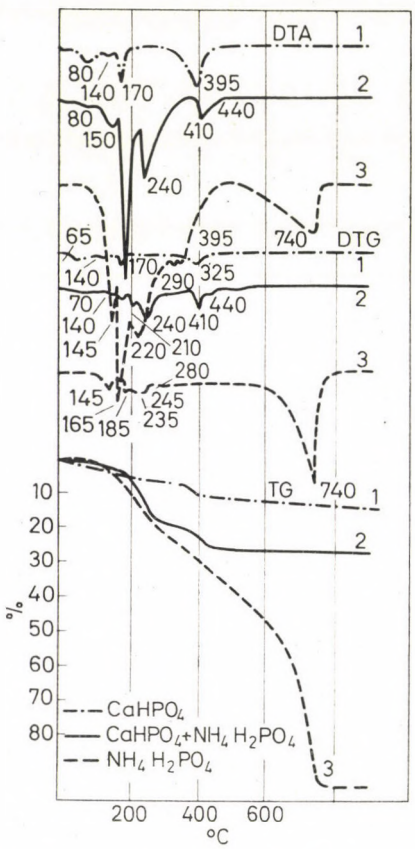


Abb. 5. Derivatographische Kurven des Systems Ammoniumdihydrophosphat–Calciumhydrophosphat. — Aufheizgeschwindigkeit 4 °C/Minute. 1 — Calciumhydrophosphat; 2 — Gemisch aus gleichen Gewichtsteilen Calciumhydrophosphat und Ammoniumhydrophosphat; 3 — Ammoniumdihydrophosphat

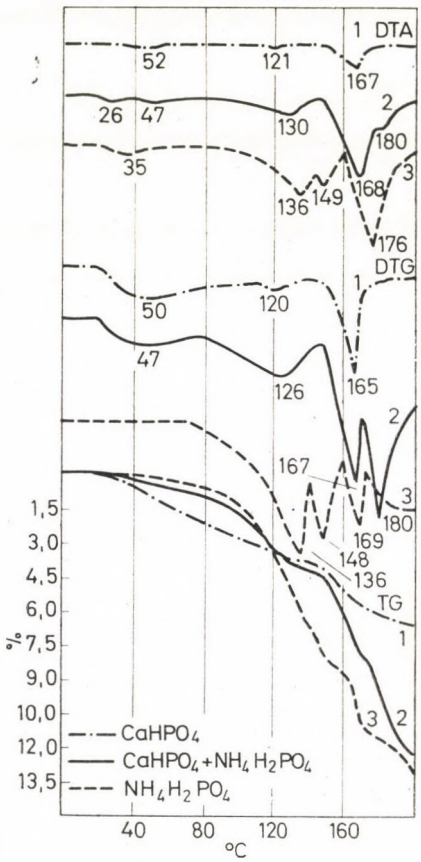


Abb. 6. Derivatographische Kurven des Systems Ammoniumdihydrophosphat–Calciumhydrophosphat. Aufheizgeschwindigkeit 1 °C /Minute. 1 — Calciumhydrophosphat; 2 — Gemisch aus gleichen Gewichtsteilen Calciumhydrophosphat und Ammoniumdihydrophosphat; 3 — Ammoniumdihydrophosphat

2 und 3), sowie die Spitzen bei 148 und 149 °C im Derivatogramm mit der Aufheizgeschwindigkeit von 1 °C/Minute (Abb. 8, Kurve 2), die für das Ammoniumdihydrophosphat charakteristisch wären, verschwinden. Im Bereich oberhalb von 260 °C wird dann völlig klar, daß sich eine Austauschreaktion abspielt.

Die DTG-Spitze bei 335° C (Abb. 7, Kurve 2) zeigt die Sublimation des gebildeten Ammoniumchlorids an. Unsere Analysenergebnisse zeigten, daß nur 36,8% des anwesenden Kaliumchlorids an der Austauschreaktion teilgenommen hat. Der unreagierte Teil tritt mit dem anderen Produkt der

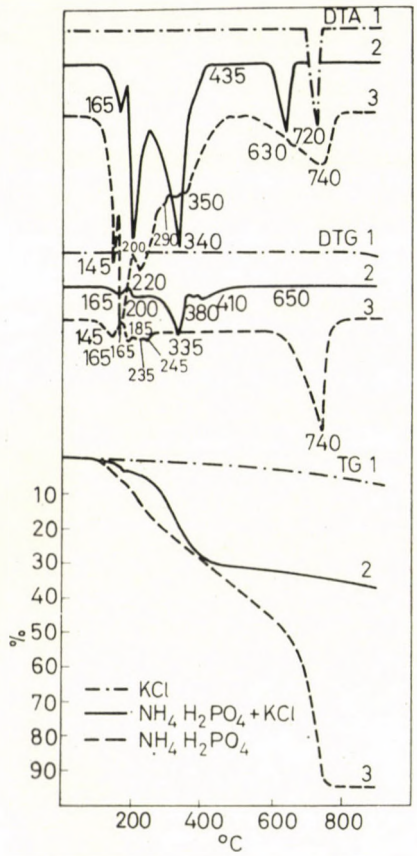


Abb. 7. Derivatographische Kurven des Systems Ammoniumdihydrophosphat–Kaliumchlorid. Aufheizgeschwindigkeit 4 °C/Minute. 1 — Kaliumchlorid; 2 — Gemisch aus gleichen Gewichtsteilen Kaliumchlorid und Ammoniumdihydrophosphat; 3 — Ammoniumdihydrophosphat

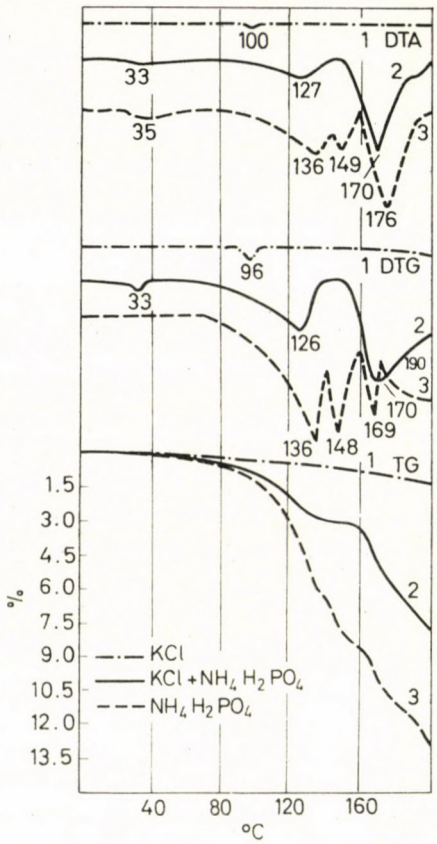


Abb. 8. Derivatographische Kurven des Systems Ammoniumdihydrophosphat–Kaliumchlorid. Aufheizgeschwindigkeit 1 °C/Minute. 1 — Kaliumchlorid; 2 — Gemisch aus gleichen Gewichtsteilen Kaliumchlorid und Ammoniumdihydrophosphat; 3 — Ammoniumdihydrophosphat

Austauschreaktion, mit dem Kaliumdihydrophosphat, in eine thermische Wechselwirkung. Demzufolge wird auf der DTA-Kurve des 1 : 1-Gemisches anstelle des Schmelzpunktes des Kaliumchlorids (720 °C) und der DTA-Spitze des Kaliumdihydrophosphats bei 770 °C (Abb. 9, DTA-Kurve 3) bei 630 °C

die für das System Kaliumchlorid–Kaliumdihydrophosphat charakteristische, mit keiner Gewichtsänderung verbundene endotherme Spitze gefunden (Abb. 7 und 9, DTA-Kurven 2).

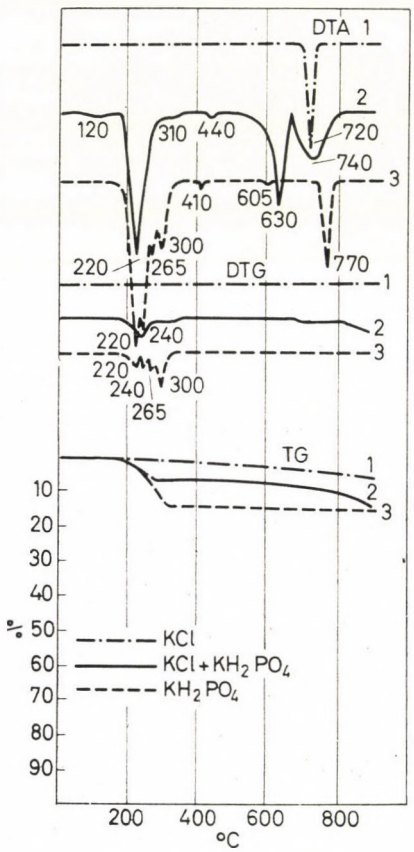


Abb. 9. Derivatographische Kurven des Systems Kaliumchlorid–Kaliumdihydrophosphat. Aufheizgeschwindigkeit 4 °C/Minute. 1 — Kaliumchlorid; 2 — Gemisch aus gleichen Gewichtsteilen Kaliumchlorid und Kaliumdihydrophosphat; 3 — Kaliumdihydrophosphat

Die derivatographischen Kurven des Gemisches aus gleichen Gewichtsteilen *Calciumhydrophosphat und Kaliumchlorid* (Abb. 10 und 11, Kurven 2) zeigen keinerlei Reaktion zwischen den Komponenten an. Im Vergleich zu den Derivatogrammen der Komponenten treten auf den Derivatogrammen des Gemisches keine wesentlichen neuen Spitzen auf. Die erwarteten und gefundenen Gewichtsverluste stimmen annähernd überein.

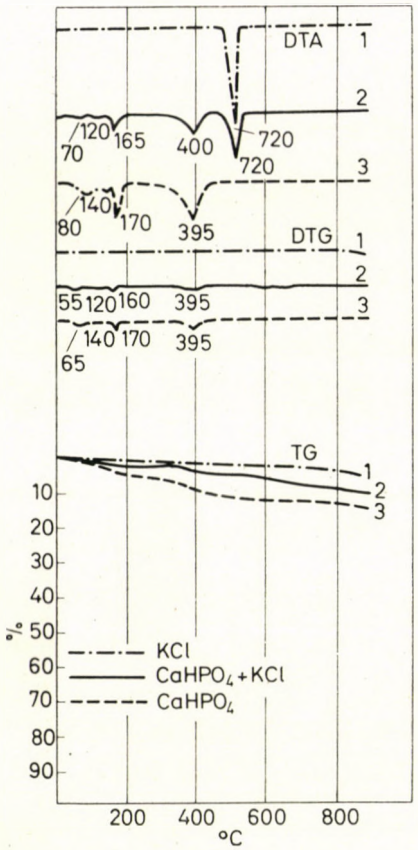


Abb. 10. Derivatographische Kurven des Systems Calciumhydrophosphat–Kaliumchlorid. Aufheizgeschwindigkeit 4 °C/Minute. 1 — Kaliumchlorid; 2 — Gemisch aus gleichen Gewichtsteilen Calciumhydrophosphat und Kaliumchlorid; 3 — Calciumhydrophosphat

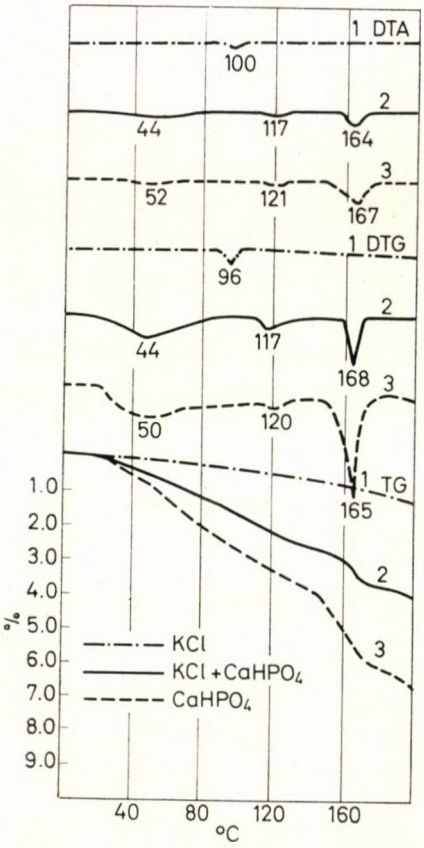


Abb. 11. Derivatographische Kurven des Systems Calciumhydrophosphat–Kaliumchlorid. Aufheizgeschwindigkeit 1 °C/Minute. 1 — Kaliumchlorid; 2 — Gemisch aus gleichen Gewichtsteilen Calciumhydrophosphat und Kaliumchlorid; 3 — Calciumhydrophosphat

LITERATUR

1. Flóra, T., Menyhárt, M.: Acta Chim. Acad. Sci. Hung. (Im Druck)
2. Erdey, L., Gál, S., Liptay, G.: Talanta **11,** 913 (1964)
3. Nabiew, M. N., Sajbowa, M. T., Boruchow, J. A., Parpiew, N. A.: Zhurn. Neorg. Chim. **14,** 2950 (1969)
4. Petschkowsky, W. W., Schtschegrow, L. N., Schulman, A. S., Melnikowa, R. Ya., Motschalina, M. D.: Zhurn. Neorg. Chim. **13,** 2360 (1968)
5. Marinela Man: Revista de Chimie, **18,** 145 (1967)
6. Nabiew, M. N., Sajbowa, M. T., Boruchow, J. A., Parpiew, N. A.: Dokl. Akad. Nauk. SSSR **25,** 28 (1968)

Teréz Flóra
Miklós Menyhárt } Veszprém, Wartha V. u. 1—3. Ungarn.

Acta Chimica Academiae Scientiarum Hungaricae, Tomus 69 (3), pp. 311–328 (1971)

STATE EQUATIONS OF THE SOLID–GAS INTERFACE LAYERS

J. TÓTH

(Petroleum Engineering Research Laboratory of the Hungarian Academy of Sciences, Miskolc)

Received February 15, 1970

The state equations of adsorption phases formed upon solid surfaces can be determined from the integral form of the Gibbs relationship:

$$\pi = \frac{RT}{a^s} \int_0^p \frac{n^s}{p}\, dp$$

where π is the spreading pressure of layers, a^s is the specific surface area of the adsorbent, $\varphi = a^s/n^s$ is the surface area required for 1 mole of adsorbed film. Correct state equations can be obtained only in the case when the explicit isotherm equations, $n^s = f(p)$, integrated in the above equation, take into account the character of the surface. State equations of mono- and multilayer adsorption phases formed upon energetically homogeneous or similar surfaces can be discussed within a uniform mathematical and physical conception. This unity is expressed by the fact that the theorem of referable states can be formulated. According to this theorem, the ideal state of the adsorbed amount n_u^s corresponding to the complete monolayer coverage comprises a reference state with respect to which any real state can be described by dimensionless state equations.

Adsorbent-specific dimensionless state equations can be derived for surfaces of inhomogeneous energy, by which the adsorbent structure, within the validity of the theorem of referable states, is also characterized.

The earlier literature concerning the state equations of adsorption layers formed on solid–gas interfaces (*i.e.* the so-called two-dimensional state equations) can be summarized according to two basic aspects. The first of them is based upon the mobility or rather the immobility of the layer, while the other can be related to the character of molecular interactions within the mobility or immobility.

According to YOUNG and CROWELL [1], the condition of mobility is that the activation energy of the translational motion along the surface should be, of necessity, less than the energy of desorption. If the former is greater, only an immobile, localized phase can be formed.

In most cases the studies were concerned with mobile phases and the existence of van der Waals type interactions was supposed between the molecules; consequently, the two-dimensional, or a more or less modified, form of the van der Waals equation was applied.

Thus MAGNUS [2], SEMENOFF [3], BAND [4], HILL [5—6] and more recently GOTTWALD [7] have shown the definite — though, limited — validity of the two-dimensional van der Waals equation.

Several authors have successively attempted the interpretation and description of molecular interactions in terms of statistical mechanics and have derived state equations containing, usually, virial coefficients [1, 8]. These relationships pointed unambiguously to the fact that two-dimensional layers can be regarded as compressible fluids.

In theories of localized (immobile) phases, too, the possible molecular interactions are taken into account by means of statistical mechanics [9—13]. A common feature of all the theories is that the adsorption isotherms relating to state equations obtained in different ways are calculated from the Gibbs equation, and the practical applicability of the given isotherm serves as a means of checking the validity of the state equation.

The Gibbs equation can, naturally, play a reverse role, namely the state equation can be obtained from known adsorption isotherm. We prefer this method of determining state equations since the applicability of the given isotherm is known and, on the other hand, the molecular interactions with the solid phase can be taken into account more easily during the deduction of isotherm equations. For example, deriving the Langmuir isotherm equation on the basis of statistical mechanics, SCHAY [14—15] has established that no conclusion can be drawn from the applicability of the equation about whether or not the adsorption is localized. Consequently, the state equation corresponding to the Langmuir equation — contrary to classical interpretation — is not necessarily valid for immobile layers, only.

Another common feature of the two-dimensional state equations is that they do not allow the formulation of the theorem of corresponding states, which is known in three dimensions and which would have the same physical meaning although a number of such attempts have been made. This failure is due to the experimental difficulties related to the determination of two-dimensional critical state parameters, and to the fact that the theoretical definition of these parameters led to very different results. For proof the reader is referred to theoretical considerations described by DEVONSHIRE [16], CASSEL [17], HILL [5] and GOTTWALD [7]. The ratio of the two-dimensional critical temperature to the three-dimensional one for a given adsorptive varies, according to the mentioned authors, between 0.53—0.30. In contrast to this according to the rather dubious measurements of ROSS and CLARK [18] this ratio varies in the range of 0.47—0.37. This means that the critical temperature of an adsorptive with respect to a given adsorbent can be given only with an uncertainty of ± 20—30 °K. Therefore, the formulation of the two-dimensional analogue of the three-dimensional theorem of corresponding states should be given up for the time being. This statement involves that

the generalization of, or the construction of a common physico-mathematical approach for, the briefly mentioned but extremely ramified and diverse research achievements have not been possible, as yet. This paper has, therefore, been prepared in sign of this attempt.

1. State equations for energetically homogeneous surfaces

1.1. State equation of monomolecular layers

In agreement with the generally accepted and correct basic principle, the Gibbs equation was used as starting point in our calculations:

$$d\gamma = -RT\frac{n^s}{a^s}\frac{dp}{p} \tag{1}$$

where γ is the specific free energy of the surface, n^s is the specific adsorbed amount (mole/g), a^s is the specific surface (m^2/g), and p is the equilibrium pressure. The free energy change $d\gamma$ figuring on the left-hand side of the equation is interpreted by assuming that the adsorbed film exerts a spreading pressure upon the surface; accordingly, the state equation can be obtained from the integrated form of Eq. (1), provided that the isotherm equation, $n^s = f(p)$, is known either graphically or in explicit form:

$$\pi = \frac{RT}{a^s}\int_0^p \frac{n^s}{p}\,dp \tag{2}$$

Since the free energy of the boundary surface is lowered by localized layers, too, Eq. (2) can be extended also to the latter with the only limitation that π should stand for the free energy decrease for unit surface area.

For the description of the monomolecular adsorption taking place upon a homogeneous surface the Langmuir equation can be applied, the form and the physical content of which are commonly known,

$$n^s = \frac{n_u^s\, p}{b+p} \tag{3}$$

where n_u^s is the adsorbed quantity corresponding to complete (monolayer) coverage. At low equilibrium pressures when $b \gg p$, the equation is linear

$$n^s = Hp; \quad \left(H \approx \frac{n_u^s}{b}\right) \tag{4}$$

and, accordingly, the state equation obtained from (2)

$$\pi\varphi = RT \tag{5}$$

is a relationship analogous with the three-dimensional gas law, if the quantity

$$\varphi = \frac{a^s}{n^s} \tag{6}$$

having an area/mole dimension, *i.e.* the surface occupied by one mole of the adsorbed species (film), is regarded as a two-dimensional volume.

The state function valid according to the Langmuir concept can be obtained by solution of the following integral

$$\pi = \frac{RT\, n_u^s}{a^s} \int_0^p \frac{dp}{b+p} \tag{7}$$

originating from the comparison of (2) and (3). To calculate (7), a new variable should be introduced

$$\xi = \frac{n_u^s}{n^s} = bp^{-1}+1 \tag{8}$$

so that Eq. (7) take the following form

$$\pi = -RT \frac{n_u^s}{a^s} \int_\infty^\xi \frac{d\xi}{\xi(\xi-1)} \tag{9}$$

Its solution is

$$\pi = RT \frac{n_u^s}{a^s} \ln \frac{\xi}{\xi-1} \tag{10}$$

It is easy to see that the expression $RT\ n_u^s/a^s$ on the right-hand side of Eq. (10) is that spreading pressure (π_u) which the adsorbed amount n_u^s would exert, if it were in the ideal state. It is clear, too, that the variable ξ introduced in (8) is the ratio of the value of φ and the two-dimensional volume corresponding to $n_u^s(\varphi_u)$. Thus (10) takes the following general form

$$\pi_d = \ln \frac{\xi}{\xi-1} \tag{11}$$

where

$$\pi_d = \frac{\pi}{\pi_u}\,;\quad \xi = \frac{\varphi}{\varphi_u} = \frac{n_u^s}{n^s} \tag{12}$$

and

$$\pi_u = RT\frac{n_u^s}{a^s} = \frac{RT}{\varphi_u} \tag{13}$$

Thus in relationship (11) the state parameters π and φ are related to the state parameters of the amount n_u^s, in the ideal state, corresponding to complete coverage; in this way a dimensionless state equation containing no individual constants was derived.

1.2. State equation of multimolecular layers

Multilayer adsorption occurring on homogeneous surfaces, or on surfaces which can be regarded practically homogeneous from a relative pressure value of $p_r \approx 0.03$, can be interpreted and described by the commonly known BET equation:

$$n^s = \frac{n_u^s\, c p_r}{[1+(c-1)\,p_r]\,[1-p_r]} \tag{14}$$

where c is the net desorption heat (the difference between the desorption heat of the first layer and the evaporation heat) defined as follows:

$$RT \ln c = Q_d - \lambda \tag{15}$$

The limited scope of application (the upper limit being $p_r = 0.4$) of Eq. (14) initiated several attempts for its modification or improvement. In an earlier paper [19] we have shown that isotherms of type II can be interpreted and described almost in the entire pressures range (*i.e.* very effectively up to $p_r = 0.95$—0.98 but not at $p_r = 1$) if, in contrast to the original BET assumption, starting from the adsorption of the second layer, the identity of the desorption and evaporation heats is not assumed. The difference of the above two heats, k, was defined by the following equation

$$RT \ln k = Q_{pl} - \lambda \tag{16}$$

Thus Eq. (14) is modified as follows

$$n^s = \frac{n_u^s\, c p_r}{[1+(c-k)p_r][1-kp_r]} \tag{17}$$

Using (17) and (2), the integral state equation of the multilayer adsorption phase, which is valid in a broad range, can be written as follows:

$$\pi = RT \frac{n_u^s}{a^s} \int_0^{p_r} \frac{c dp_r}{[1+(c-k)\,p_r]\,[1-kp_r]} \tag{18}$$

$$(p_r < 1)$$

To accomplish the above integration using the variable ξ introduced in (8), it is necessary that the overall quantity of substance adsorbed only in the *first* layer (n_1^s) be known. In our earlier paper [19] we have shown that k can be determined and, at the same time, the following expression is valid:

$$n_1^s = \frac{n_u^s\, c p_r}{1+(c-k)\,p_r} \tag{19}$$

$$(p_r < 1)$$

the amount adsorbed in the second, etc. layers is given by

$$n_t^s = \frac{n_1^s\, p_r}{1/k - p_r} \tag{20}$$

$$(p_r < 1)$$

Naturally, the sum of (19) and (20) gives (17). If (19) is known, one can write a variable with a meaning identical to that of (8):

$$\xi = \frac{n_u^s}{n_1^s} = \frac{1+(c-k)\,p_r}{cp_r} \tag{21}$$

Upon performing the mathematical operations which are necessary in connection with the introduction of a new variable, Eq. (9) can be obtained from Eq. (18) and, consequently, the dimensionless state equation of the multilayer phase remains unchanged:

$$\pi_d = \ln \frac{\xi}{\xi - 1} \tag{22}$$

It is obvious, too, that state equation (14) belonging to the original BET isotherm is also identical with (22), with the only restriction that quantities n_1^s and n_u^s are calculated from (17) and (19) with $k = 1$.

1.3. Formulation of the theorem of referable states

By deriving Eqs (11) and (22) the fact has been registered that in the case of adsorptions described by the Langmuir, BET or modified BET equations the fictive ideal state of the adsorbed amount n_u^s has a meaning of a reference state, with respect to which any real state can be described by dimensionless state equations (11) and (22) containing no individual constants explicitly. Reference has been accomplished using the state parameters of the ideal state of n_u^s

$$\pi_u = \frac{RT}{\varphi_u} \tag{23}$$

and

$$\varphi_u = \frac{a^s}{n_u^s} \tag{24}$$

These parameters have been named reference state-parameters and the existence of Eqs (11) and (12) in the above form has been called the theorem of referable states. With this name we have tried to point out the *formal* similarity to the three-dimensional theorem of corresponding states, but, naturally, there is no physical correspondence between these two concepts. That the systematizing value of this theorem is significant is shown by the fact that the state of the above mentioned adsorption layers can be characterized by the same equation independently of any factor (nature of the adsorbent and adsorptive, temperature, type of isotherm, etc.). In other words, within the above mentioned validity limits, an identical state equation is obtained for any adsorption layer whose state has been defined by parameters π_d and ξ. This important consequence of the theorem of referable states was also proved experimentally.

In Table I isotherms of various adsorptives recorded on various adsorbents are listed. According to the BET classification, these isotherms belong to groups I—II—III. The spreading pressure π of these layers was calculated from Eq. (2) by graphical integration. State parameter $\xi = n_u^s/n_1^s$ was determined using the data obtained from either the Langmuir, BET, or the modified BET equation depending on the type and character of the isotherm in question.

In Fig. 1 the values obtained by graphic integration from the isotherms listed in Table I are marked by circles, while the function calculated from Eq. (22) is shown by a continuous line. Since the total number of adsorptions which can be described by the Langmuir, BET or the modified BET equation is extremely large, the theorem of referable states expressed by Eq. (22) is also of rather extensive validity.

Table I

Data on some adsorption layers which can be described by the state equation $\pi_d = ln\ \xi/\xi - 1$

Adsorbed substance	Adsorbent	Temperature (°C)	Type of isotherm	Method of calculation of ξ	Reference
Carbon dioxide	Mica	−118	I	Langmuir equation	[20]
Carbon dioxide	Silica gel	−78	II	Modified BET equation	[21]
Sulfur dioxide	Silica gel	0	II	Modified BET equation	[21]
Oxygen	Silica gel	−183	II	Modified BET equation	[21]
Argon	Silica gel	−183	II	Modified BET equation	[21]
Nitrogen	Silica gel	−195.8	II	Modified BET equation	[21]
Methane	Glass	−205.8	II	Modified BET equation	[22]
Iodine vapour	Silica gel	158.3	III	Original BET equation	[23]
Iodine vapour	Silica gel	198.5	III	Original BET equation	[23]
Bromine vapour	Silica gel	58	III	Original BET equation	[23]
Bromine vapour	Silica gel	79	III	Original BET equation	[23]

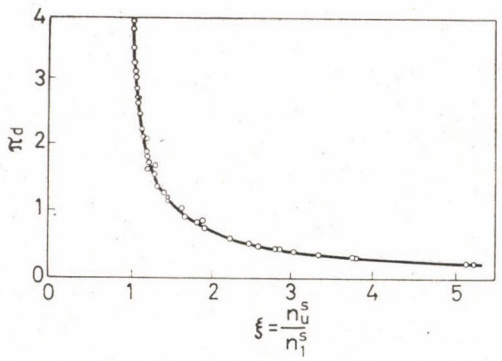


Fig. 1. State function of mono- and multilayer adsorption phases formed on a homogeneou surface. This function can be described by the equation $\pi_d = \ln\ \xi/\xi - 1$

2. State equations on energetically inhomogeneous surfaces

2.1. Characterization of the inhomogeneity of adsorbents

The common basis of theories aimed at taking into account the energetic inhomogeneity of surfaces is that the surface is theoretically divided into a large number of homogeneous regions with finite areas. Thus *e.g.* EUCKEN [24] applied the usual form (3) of the Langmuir equation to these finite homogeneous regions and then summed up the equations. In this treatment of surface inhomogeneity, finite dimensions of surface elements are assumed. This method is, however, arbitrary in choosing the number and

place (*i.e.* in which coverage region) of surface elements to be considered. Another difficulty is that no real physical meaning can be attributed to the n_u^s constants figuring in the Langmuir equations for they are simply empirical values.

The above errors in the consideration of inhomogeneity can be avoided if the surface is divided into such small elements (so-called macrodifferentials) which can already be considered to be of homogeneous energy. Consequently, the *differential equation of the Langmuir-isotherm* can be applied to these elements. This latter fact is emphasized because on the basis of mathematical considerations differential equations would rather be applicable to macrodifferentials, while at the same time the differential equations written for the totality, or at least the majority, of the surface elements determine the character of energetic inhomogeneity of the surface. This, however, requires that the above mentioned differential equation could be calculated from the adsorption isotherm data and be exactly defined by a measurable physical quantity. These two conditions are satisfied by the following differential form of the Langmuir equation (3):

$$\frac{n^s}{p}\frac{dp}{dn^s} - 1 = \frac{1}{b}p \tag{25}$$

The differential expression on the left-hand side of Eq. (25) can be calculated from the adsorption isotherm. Denoting this expression by ψ, Eq. (25) can be written in a simple form:

$$\psi = \frac{1}{b}p \tag{26}$$

It has been shown [25] that the net desorption heat can be generally defined by the following equation

$$\Delta\lambda = RT \ln\left[\psi \frac{1}{p_r}\right] \tag{27}$$

In the case of a Langmuir-isotherm, (26) can be substituted into (27) to give the following expression

$$\Delta\lambda = RT \ln \frac{p_0}{b} = \text{const.} \tag{28}$$

according to which the desorption energy is constant for a homogeneous surface. Consequently ψ is proportional to p on a Langmuir surface. The reverse is also true: if the experimental function ψ *vs.* p is a straight line

starting from the origin, then the adsorption is undoubtedly of the Langmuir type and the slope of this line is equal to $1/b$.

If the surface is energetically inhomogeneous, then different values of $1/b$ (*i.e.* adsorption heats) will belong to coverage regions (surface elements) of different energy. Accordingly, a separate differential equation similar to (25) or, in a ψ *vs.* p representation, a straight line can be assigned to each of the coverages. There is a point on each of these lines which is determined by

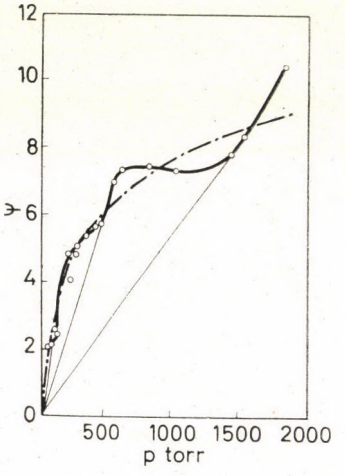


Fig. 2. The function ψ *vs.* p of the propane isotherm measured on Nuxit-Al charcoal at 20 °C

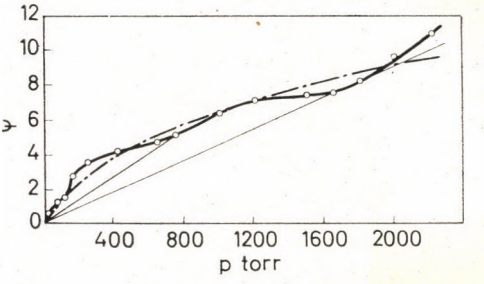


Fig. 3. The function ψ *vs.* p of the propane isotherm measured upon Columbia-L charcoal at 37.8 °C

the ψ value of the isotherm obtained by graphical differentiation. The set of these points gives the function ψ *vs.* p, depending upon the character of the surface. This function is generally denoted by the following symbol:

$$\psi = f(p) \tag{29}$$

Several functions of this type were examined on microporous adsorbents (charcoal) and the conclusion was drawn that the energetic inhomogeneity of charcoal is not continuous but rather of a 'stepwise' character. The $\psi = f(p)$ functions were calculated for all the isotherms determined by SZEPESY and ILLÉS [26], and LEWIS and co-workers [27], and all of them were found similar to the relationships shown in Figs 2 and 3. According to Eq. (26), the intervals which fall on the straight line starting from the origin can be qualified as coverage regions of homogeneous energy. These Langmuir-intervals are separated by intervals of inhomogeneous energy in which the relation $\psi = \text{const.}$

is approximately valid. It can be noticed too that the homogeneous coverage regions follow the order of decreasing energies, corresponding to the fact that with increasing p the slopes $1/b$ of these intervals decrease.

If the 'steps' of functions ψ *vs.* p are averaged in the way shown in Figs 2 and 3, the explicit form of the function can be written as follows:

$$\psi = \frac{1}{b''} p^m \tag{30}$$

where b'' is a constant and the relation $0 < m < 1$ is valid. The permissibility of this averaging is proved by the fact that the adsorption isotherms can be described with high accuracy [29] by the isotherm equation

$$n^s = \frac{n^s_\infty p}{(b'' + p^m)^{1/m}} \tag{31}$$

obtained by solving differential equation (30), or by its linearized form

$$\left(\frac{p}{n^s}\right)^m = \frac{p^m}{(n^s_\infty)^m} + \frac{b''}{(n^s_\infty)^m} \tag{32}$$

The definition of the constant n^s_∞ figuring in Eqs (31) and (32) is given by (33)

$$n^s_\infty = n^s_u \frac{(b'' + p^m_u)^{1/m}}{p_u} \tag{33}$$

which follows from the solution of differential equation (30). In Eq. (33), p_u is the equilibrium pressure attributed to the adsorbed amount n^s_u on condition that in the course of the solution of (30), integration was performed between the limits $n^s - n^s_u$ and $p - p_u$, respectively. If, by comparing (27) and (30), b'' is defined by $\Delta\lambda$, then the following relationship is valid:

$$b'' = p_0 p^{m-1} \exp\left(\frac{-\Delta\lambda}{RT}\right) \tag{34}$$

It can be seen from (34) that at sufficiently high values of $\Delta\lambda$ the existence of inequality

$$b'' \ll p^m_u \tag{35}$$

is possible. By this condition and Eq. (33), the value of n^s_∞ is given as follows:

$$n^s_\infty \approx n^s_u \tag{36}$$

The application of Eq. (31) to isotherm data measured on various charcoals has unambiguously confirmed that the value of m is characteristic of the adsorbent only, irrespective of the temperature and the nature of the adsorptive. This fact was proved by the following procedure: several hundred data on isotherms obtained by SZEPESY and ILLÉS [26] on Nuxit-Al and by LEWIS *et al.* [27] on Columbia-L charcoal were processed and the value of m was determined from the slope of the straight line corresponding to the equation

$$\log \psi = \log \frac{1}{b''} + m \log p \tag{37}$$

which was derived from (30). In this procedure values of $m = 0.42$ and $m = 0.60$ were obtained for the Nuxit-Al and the Columbia-L charcoal, respectively. These values show a deviation of $\pm 15\%$ which reflects only the accuracy of the calculations. The result does not depend upon the nature and temperature of the adsorptive the isotherm of which was used in the calculations with (37). If the values of m are those shown above, all the isotherms measured on both adsorbents can be accurately described by Eq. (32) in the entire pressure range of the experiments (*e.g.* this range for the Nuxit charcoal was 10 mm Hg — 7 atm). The deviation calculated by the least-squares method did never exceed the uncertainties of the adsorption measurement amounting to ± 2—3%. Thus m can be regarded as a factor (of inhomogeneity) characterizing the adsorbent; the physical meaning of its constancy can be formulated as follows. There are coverage regions of homogeneous energy in various intervals of p on the adsorbent surface, the existence of which is indicated by the value $m = 1$ regardless of their energy level (the b value) and the p-interval. The extreme, 'most inhomogeneous' transition between these homogeneous regions is possible in the form where $m = 0$, *i.e.* $\psi = \text{const}$. In this case, too, the zero value of m is independent of p and the energy level characterized by b''. The possible values of m in the process of averaging (according to Eq. (30)) of an inhomogeneous region occurring between two or more homogeneous intervals are $0 < m < 1$, again irrespective of the above mentioned factors. The structure of the adsorbent is a given property therefore the distribution of homogeneous and inhomogeneous regions does not depend upon the energy level at which it is determined *i.e.* on the adsorptive used. Consequently, it is necessary that the value of m should be constant, regardless of the energy level. Accordingly, the homogeneous and inhomogeneous regions can be averaged at any energy level by means of m. Thus m is a dimensionless characteristic of the adsorbent structure ($m = 1$ represents the completely homogeneous adsorbent, $m = 0$ indicates zero homogeneity or an 'infinitely' inhomogeneous adsorbent) in correspondence with the fact that the structure of an adsorbent, without

indicating the energy level and the distribution, does not involve dimensions. The characterization of the adsorbent structure by the constant m offers the only possibility for the state equations of layers formed upon inhomogeneous surfaces to be calculated from Eq. (2).

2.2. The integral of state equation for monomolecular layers formed upon inhomogeneous surfaces and the theorem of referable states

With the physical meaning of all the constants in Eq. (31) being clear, it seems to be a purely mathematical task to obtain the state equations by solving the following integral

$$\pi = \frac{RT\, n^s}{a^s} \int_0^p \frac{dp}{(b'' + p^m)^{1/m}} \tag{38}$$

obtained by substitution of (31) into (2). However, the integral is irrational since the exponent has values $0 < m < 1$, therefore, the solution of (38) cannot be given in a simple analytical form and at the same time the physical meaning hidden in the mathematical solution should be examined, too. Integrals of the type (38) can be solved only by the Chebyshev transformation. The first step of this procedure is to write m in the following form

$$m = \frac{L}{K} \tag{39}$$

where L and K are relative primes.

The essence of the transformation is the introduction of the new variable

$$\eta = \left(\frac{n^s_\infty}{n^s}\right)^{1/K} = (b'' \bar{p}^{L/K} + 1)^{1/L} \tag{40}$$

Performing all the necessary mathematical transformations connected to and required by the introduction of a new variable, the following rational integral equation is obtained:

$$\pi = - RT \frac{n^s_\infty}{a^s} K \int_\infty^\eta \frac{d\eta}{\eta^{K-L+1}(\eta^L - 1)} \tag{41}$$

Applying the theorem of referable states, (41) can be written as follows

$$\pi_{d,\infty} = - K \int_\infty^\eta \frac{d\eta}{\eta^{K-L+1}(\eta^L - 1)} \tag{42}$$

where

$$\pi_{d,\infty} = \frac{\pi}{\pi_\infty}; \quad \pi_\infty = \frac{RT}{\varphi_\infty}; \quad \varphi_\infty = \frac{a^s}{n^s_\infty} \tag{43}$$

According to Eq. (42), if the ideal state of the adsorbed amount n^s_∞ is taken as the reference state, the reference state-parameters upon an inhomogeneous surface will be as follows:

$$\pi_{d,\infty} \text{ and } \eta = \left(\frac{\varphi}{\varphi_\infty}\right)^{1/K} = \left(\frac{n^s_\infty}{n^s}\right)^{1/K} \tag{44}$$

The integral state equation (42) constructed with state parameters (44) is already dimensionless and its solution — the explicit form of the state equation — depends only upon the value of m, *i.e.* the nature of the adsorbent. In other words, the state of monomolecular layers of any nature and temperature, formed upon an adsorbent with known characteristics, can be described by an identical state equation if $\pi_{d,\infty}$ and η are chosen as state parameters. The above formulation of the theorem of referable states, which is valid for surfaces of inhomogeneous energy, differs from the statements valid for homogeneous surfaces — besides the adsorbent-specificity of the theorem — with respect to other features, too. First of all it is not only the state equation that is adsorbent-specific, but, as a result of the exponent $1/K$, also the state parameter η. Another difference from the homogeneous surfaces is that if conditions (35) and (36) are not satisfied, the relations $n^s_\infty > n^s_u$ and, consequently, $n_s/n^s_\infty < \Theta$ are valid owing to (33), thus in some cases the basis of the $1/K$-th power, which is a function of the adsorbent's nature, can be not only the reciprocal coverage $(1/\Theta)$ but a greater number, too.

The only possible mathematical solution of equation (38) was pointed out earlier. This emphasizes the remarkable fact that the introduction of the new variable defined by (40) not only represents the only mathematical solution to the calculation of state equations but this procedure offers the only possibility for the physical interpretation of this problem.

This specific possibility becomes evident in the formulation of the theorem of referable states for homogeneous and inhomogeneous surfaces. The homogeneous surface can be included into the scope of the above two statements since in the case of $m = 1$, *i.e.* $L = K = 1$, we obtain in (40)

$$\eta = \xi = \frac{1}{\Theta} \tag{45}$$

i.e. Eq. (40) also contains the statements of the theorem of referable states valid for homogeneous surfaces.

2.3. *The explicit form of state equations valid upon inhomogeneous surfaces and the experimental confirmation of the theorem of referable states*

The solution of integral (42) for various values of $m = L/K$, *i.e.* for various adsorbents, is now a purely mathematical problem. Details of the procedure performed by known methods and giving rise to certain difficulties in some cases will not be given here. In the following only those solutions will be presented which are valid for the intervals of m appearing among industrial adsorbents. As a consequence of the integration procedure applied the equations can be classified according to the values of L:

$$L = 1$$

$$\pi_{d,\infty} = K\left[\ln\frac{\eta}{\eta - 1} - \sum_{i=1}^{i=K-L}\frac{1}{i\eta^i}\right]_{i=1,\,1+L,\,1+2L\ldots\,K-L} \tag{46}$$

$$L = 2$$

$$\pi_{d,\infty} = K\left[\ln\frac{\eta+1}{\eta-1} - \sum_{i=1}^{i=K-L}\frac{1}{i\eta^i}\right]_{i=1,\,1+L,\,1+2L\ldots\,K-L} \tag{47}$$

$$L = 3$$

$$\pi_{d,\infty} = K\left[\frac{1}{3}\ln\frac{(\eta^2+\eta+1)^{1/2}}{\eta-1} \mp \frac{1}{\sqrt{3}}\operatorname{arc\,tg}\left(\frac{2\eta+1}{3}\right) \pm \frac{3.1\cdot 4}{2\sqrt{3}} - \sum_{\substack{i=1\\ i=2}}^{i=K-L}\frac{1}{i\eta^i}\right]_{\substack{i=1,\,1+L,\,1+2L\ldots\,K-L\\ i=2,\,2+L,\,2+2L\ldots\,K-L}} \tag{48}$$

Of the double sign and the double lower limit of summation, the upper one should be used for the values $K = 4,\ 4 + L,\ 4 + 2L,\ 4 + 3L, \ldots$ and the lower one for the values $K = 5,\ 5 + L,\ 5 + 2L,\ 5 + 3L, \ldots$ etc.

$$L = 4$$

$$\pi_{d,\infty} = K\left[\frac{1}{4}\ln\frac{\eta+1}{\eta-1} \mp \frac{1}{2}\operatorname{arc\,tg}\eta \pm \pm\frac{3.1\cdot 4}{4} - \sum_{\substack{i=1\\ i=3}}^{i=K-L}\frac{1}{i\eta^i}\right]_{\substack{i=1,\,1+L,\,1+2L\ldots\,K-L\\ i=3,\,3+L,\,3+2L\ldots\,K-L}} \tag{49}$$

According to the above, the double signs and subscripts should be used for the values of $K = 5,\ 5 + L,\ 5 + 2L,\ 5 + 3L, \ldots$ or $K = 7,\ 7 + L,\ 7 + 2L,\ 7 + 3L, \ldots$ respectively.

$$L = 5$$

$$\pi_{d,\infty} = K \left[\frac{1}{5} \ln \frac{\left[\eta^2 + \left(\frac{1-\sqrt{5}}{2}\right)\eta + 1\right]^{\frac{\sqrt{5}+1}{4}}}{\left[\eta^2 + \left(\frac{1+\sqrt{5}}{2}\right)\eta + 1\right]^{\frac{\sqrt{5}-1}{4}} [\eta - 1]} + \right.$$

$$+ \frac{1}{5}\left(\frac{10}{5 \pm \sqrt{5}}\right)^{1/2} \text{arc tg} \frac{4\eta + 1 \pm \sqrt{5}}{(10 \mp 2\sqrt{5})^{1/2}} - \frac{1}{5}\left(\frac{10}{5 \pm \sqrt{5}}\right)^{1/2} \text{arc tg} \frac{4\eta + 1 \mp \sqrt{5}}{(10 \pm 2\sqrt{5})^{1/2}} +$$

$$\left. + 0.314\left(\frac{10}{5 \pm \sqrt{5}}\right)^{1/2} - 0.314\left(\frac{10}{5 \mp \sqrt{5}}\right)^{1/2} - \sum_{\substack{i=2 \\ i=3}}^{i=K-L} \frac{1}{i\eta^i} \right]_{\substack{i=2,\ 2+L,\ 2+2L \ldots\ K-L \\ i=2,\ 3+L,\ 3+2L \ldots\ K-L}} \tag{50}$$

The upper sign and subscript refer to the values $K = 7,\ 7 + L, \ldots$, while the lower sign and subscript to the values $K = 8,\ 8 + L, \ldots$

Using Eqs (46)—(50) the appropriate state function can be written for practically every adsorbent in the interval $m = 0.83$—0.17. Furthermore, the possible structural changes, which are, of necessity, reflected in the m

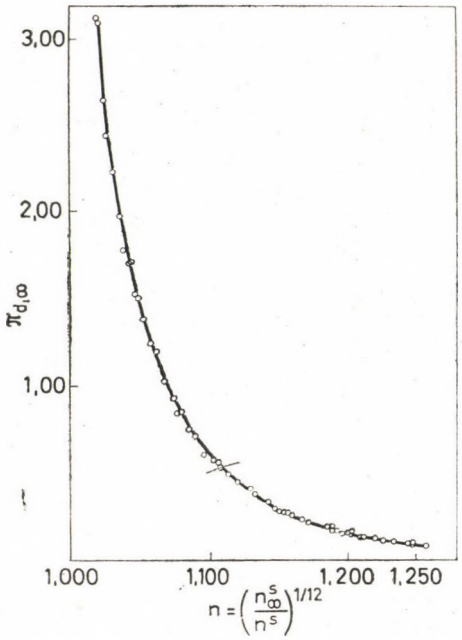


Fig. 4. State equations of adsorption layers of methane, ethane, propane, *n*-butane, ethylene, propylene, acetylene, carbon dioxide formed on Nuxit-Al charcoal

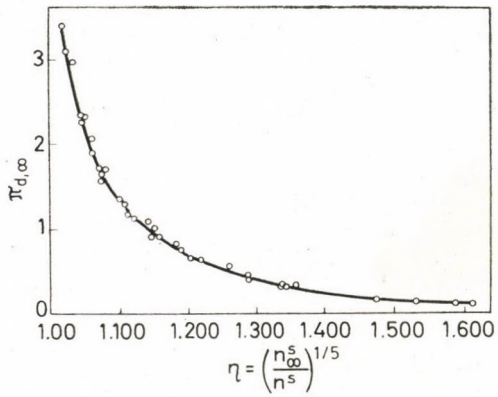


Fig. 5. State equations of adsorption layers of ethane, ethylene, propane, *n*-butane, carbon dioxide formed on Columbia-L charcoal

value of the adsorbent, too, can be instantly followed by choosing a new state equation.

The experimental confirmation of the theorem of referable states was accomplished on the basis of data relating to isotherms measured upon Nuxit-Al [26] and Columbia-L [27] charcoals. In Figs 4 and 5 the results of graphical integration of the isotherms according to Eq. (2) are marked by circles, whereas the continuous lines represent the state functions obtained by Eq. (50) for the Nuxit-Al charcoal ($m = 0.42$, $L = 5$, $K = 12$), and by Eq. (48) for the Columbia-L charcoal ($m = 0.60$, $L = 3$, $K = 5$). The data necessary for the calculation of the state functions, and the isotherms evaluated by graphical integration are collected in Table II.

Table II

Data of isotherms measured on Nuxit-Al and Columbia-L charcoals [26—27], on the basis of which the theorem of referable states can be confirmed

Nuxit-Al			Columbia-L		
$M = 0.42$	$L = 5$	$K = 12$	$M = 0.60$	$L = 3$	$K = 5$
$a^s = 989.5$ m²/g			$a^s = 1195$ m²/g		
Adsorbed substance	Temperature of isotherm °C	n^S_∞ nml/g	Adsorbed substance	Temperature of isotherm °C	n^S_∞ nml/g
Methane	20	237.7	Ethane	37.8	161.6
Methane	40	343.1	Ethane	121.1	134.1
Ethane	20	175.8	Propane	37.8	144.3
Ethane	60	191.3	Propane	148.9	110.9
Ethane	90	223.8	*n*-Butane	93.3	104.6
Propane	40	133.8	*n*-Butane	148.9	85.6
Propane	90	134.3	Ethylene	37.8	178.5
n-Butane	40	99.9	Ethylene	148.9	157.3
n-Butane	90	113.2	Carbon dioxide	37.8	144.2
Ethylene	20	195.7	Carbon dioxide	65.5	216.7
Ethylene	60	202.4			
Propylene	40	132.1			
Propylene	90	147.7			
Acetylene	20	263.5			
Acetylene	60	274.2			
Carbon dioxide	20	423.0			
Carbon dioxide	90	442.9			

Figures 4 and 5 and the data in Table II fully confirm the most important statement of the theorem of referable states, according to which the state of a monomolecular layer with any characteristics, formed upon a given adsorbent can be characterized by a single state equation.

REFERENCES

1. YOUNG, D. M. and CROWELL, A. D.: Physical Adsorption of Gases, pp. 13—18. Butterworths, London, 1962
2. MAGNUS, A.: Z. Phys. Chem. A **142,** 401 (1929)
3. SEMENOFF, N.: Z. Phys. Chem. B **7,** 471 (1930)
4. BAND, W.: J. Chem. Phys. **8,** 116 (1940)
5. HILL, T. L.: J. Chem. Phys. **14,** 441 (1946)
6. HILL, T. L.: Advan. Catalysis **4,** 211 (1952)
7. GOTTWALD, B. A.: Z. Physik. Chem. Neue Folge **62,** 213 (1968)
8. BERING, B. P., SERPINSKI, V. V.: Dokl. Akad. Nauk. S.S.S.R. **79,** 273 (1951)
9. FOWLER, R. H.: Proc. Camb. Phil. Soc. **32,** 144 (1936)
10. PEIERLS, R.: Proc. Camb. Phil. Soc. **32,** 471 (1936)
11. WANG, J. S.: Proc. Roy. Soc. A **161,** 127 (1937)
12. GRAHAM, D.: J. Phys. Chem. **57,** 665 (1953)
13. BETHE, H. A.: Proc. Roy. Soc. A **150,** 552 (1935)
14. SCHAY, G.: Acta Chim. Acad. Sci. Hung. **3,** 511 (1953)
15. SCHAY, G.: J. Chim. Phys. **53,** 691 (1956)
16. DEVONSHIRE, A. F.: Proc. Roy. Soc. **163,** 132 (1937)
17. CASSEL, H. M.: J. Phys. Chem. **48,** 195 (1944)
18. ROSS, S., CLARK, H.: J. Amer. Chem. Soc. **76,** 4291 (1954)
19. TÓTH, J.: Acta Chim. Acad. Sci. Hung. **48,** 27 (1966)
20. LANGMUIR, J.: J. Amer. Chem. Soc. **40,** 1369 (1918)
21. EMMETT, P. H., BRUNAUER, J.: J. Amer. Chem. Soc. **59,** 2682 (1937)
22. ITTERBECK, A.: Z. Phys. Chem. **48,** 131 (1941)
23. REYERSON, L. H., CAMERON, A. E.: J. Phys. Chem. **39,** 181 (1935)
24. EUCKEN, A.: Lehrbuch der chemischen Physik. II. 1209 (1949)
25. TÓTH, J.: Acta Chim. Acad. Sci. Hung. **30,** 415 (1962)
26. SZEPESY, L., ILLÉS, V.: Acta Chim. Acad. Sci. Hung. **35,** 53 (1963)
27. LEWIS, W. K., GILLILAND, E. R., CHERTOV, B., CADOGAN, W. P.: Ind. Eng. Chem. **42,** 1319 (1950)
28. TÓTH, J.: Acta Chim. Acad. Sci. Hung. **48,** 57 (1966)
29. TÓTH, J.: Acta Chim. Acad. Sci. Hung. **32,** 39 (1962)

József TÓTH; Miskolc-Egyetemváros, Hungary.

Acta Chimica Academiae Scientiarum Hungaricae, Tomus 69 (3) pp. 329—340 (1971)

DERIVATION OF THE TRANSPORT EQUATIONS OF NON-ISOTHERMAL HYDRODYNAMICS FROM THE GYARMATI PRINCIPLE IN DIFFERENT PICTURES

Sz. Böröcz

(Department of Physical Chemistry, Technical University, Budapest)

Received April 16, 1970

Differential equations governing the transport of momentum and internal energy in isotropic and non-isothermal hydrodynamic systems have been derived from Gyarmati's variational principle of non-equilibrium thermodynamics. The derivations contain several earlier results and clarify the relations among the different forms of the transport equations in question, particularly the transport equation of internal energy. It has been found that though Gyarmati's principle is formally also valid in a peculiar manner for the reversible part of the Navier–Stokes equation, it cannot be considered as a genuine variational principle for reversible motions.

1. Introduction

It is well known that in 1957 the Onsager principle of the least dissipation of energy was formulated by Gyarmati in a local form valid also for continua and in such a new representation [1], by which he was able to formulate the general variational (integral) principle of thermodynamics in 1965 [2, 3]. As has been proved in several works of Gyarmati *et al.* (*cf.* [3—9], and particularly [10]) the differential equations describing irreversible transport processes can be derived from the variational principle of Gyarmati. The main purpose of the author of this paper is to derive the differential equations describing the transport of mass, energy and momentum taking place in isotropic and non-isothermal fluid systems, and at the same time to formulate the above mentioned differential equations in — sometimes misleadingly used — different pictures. The differential equations in question can be directly obtained, if in addition to the mass balance equation

$$\dot{\varrho} = -\varrho \nabla . \boldsymbol{v} \tag{1}$$

or

$$\dot{v} = v \nabla . \boldsymbol{v}$$

(where ϱ is the substantial time derivative of the density of the continuum, $\boldsymbol{v}$ is the velocity of the convective motion, $V = \varrho^{-1}$ is the specific volume, and ∇ is the nabla operator), in the following balance equations of the momentum and internal energy [10, 11], we also introduce the actual linear laws (Newton's law, Fourier's law) into the substantial current densities of the momentum **P** and internal energy (heat) $\boldsymbol{Jq}$

$$\varrho\dot{\boldsymbol{v}} = -\nabla . \mathbf{P} + \varrho \boldsymbol{F} \tag{2}$$

and

$$\varrho u = -\nabla . \boldsymbol{J}_q - \mathbf{P} : (\nabla \boldsymbol{v})^s \tag{3}$$

In the above equations $\dot{\boldsymbol{v}}$ and $\dot{u}$ are the substantial time derivatives of the velocity and the specific internal energy, $\mathbf{P}$ is the pressure tensor (which is assumed to be symmetric) and $(\nabla \boldsymbol{v})^s$ is the symmetric part of the gradient of the velocity. The more general case, when the stress tensor is not symmetrical is not dealt with now (*cf.* [8, 11, 10]). Taking into account the well-known splitting of the tensors $\mathbf{P}$ and $(\nabla \boldsymbol{v})^s$, *i.e.*

$$\mathbf{P} = p\delta + \mathbf{P}^\nu = (p + p^\nu)\,\delta + \mathring{\mathbf{P}}^\nu \tag{4}$$

and

$$(\nabla \boldsymbol{v})^s = \frac{1}{3}(\nabla \cdot \boldsymbol{v})\delta + (\mathring{\nabla \boldsymbol{v}})^s$$

[where $\mathbf{P}$ is the hydrostatic pressure, $\mathbf{P}^\nu$ is the viscous pressure tensor which can be split as $\mathbf{P}^\nu = p^\nu\delta + \mathring{\mathbf{P}}^\nu$ into the sum of the viscous pressure p^ν and of the tensor of zero trace $\mathring{\mathbf{P}}^\nu$, further on $\nabla . \boldsymbol{v}$ and $(\mathring{\nabla \boldsymbol{v}})^s$ are the parts of the $(\nabla \boldsymbol{v})^s$ tensor split in a similar way, finally δ is the unity tensor] the linear laws

$$p^\nu = -\eta_v \nabla . \boldsymbol{v}, \quad \mathring{\mathbf{P}}^\nu = -2\eta(\mathring{\nabla \boldsymbol{v}})^s, \quad \boldsymbol{J}_q = -\lambda \nabla T \tag{5}$$

convert the balance equations (2) and (3) into the following linear transport equations:

$$\varrho\dot{\boldsymbol{v}} = -\nabla p + \eta \Delta \boldsymbol{v} + \left(\frac{1}{3}\eta + \eta_v\right) \nabla \cdot \nabla \boldsymbol{v} + \varrho \boldsymbol{F} \tag{6}$$

$$\varrho\dot{u} = \nabla \cdot (\lambda \nabla T) = p \nabla . \boldsymbol{v} + 2\eta(\mathring{\nabla \boldsymbol{v}})^s : (\mathring{\nabla \boldsymbol{v}})^s + \eta_v (\nabla . \boldsymbol{v})^2 \tag{7}$$

When substituting the linear laws, decompositions (4) have been taken into consideration and it has been assumed that the coefficient of the volume η_v and the shear viscosity η as well as the ordinary heat conductivity coefficient λ are constant.

Differential equations (6) and (7) governing momentum and energy transport and continuity equation (1) provide 5 scalar equations for the unknown quantities. If these are completed with the following equations of state

$$P = (\varrho, T) \quad \text{and} \quad u = u(\varrho, T) \tag{8}$$

the space-time behaviour of isotropic non-isothermal fluid systems is given by the equations in question, for specified initial and boundary conditions. In

other words Eqs (1), (7) and (8) are the basic equations of one-component hydro-thermodynamic systems.

It can be easily seen that owing to the following alternative forms of linear law (5), referring to heat conduction [9, 10]:

$$\boldsymbol{J}_q = -\lambda \nabla T = -L_{qq} \nabla \ln T = L_{qq} \nabla T^{-1} \tag{9}$$

where the following relations are valid between the coefficients

$$\lambda = T^{-1} L_{qq}^* = T^{-2} L_{qq} \tag{10}$$

differential equations (7) can also be given in the following alternative forms

$$\varrho \dot{u} = \nabla . (L_{qq}^* \nabla \ln T) - p \nabla . \boldsymbol{v} + 2\eta (\mathring{\nabla} \boldsymbol{v})^s : (\mathring{\nabla} \boldsymbol{v})^s + \eta_v (\nabla . \boldsymbol{v})^2 \tag{11}$$

$$\varrho \dot{u} = -\nabla . (L_{qq} \nabla T^{-1}) - p \nabla . \boldsymbol{v} + 2\eta (\mathring{\nabla} \boldsymbol{v})^s : (\mathring{\nabla} \boldsymbol{v})^s + \eta_v (\nabla . \boldsymbol{v})^2 \tag{12}$$

These equations are equivalent to (7) in every respect. According to GYARMATI, who has introduced the three 'pictures' in question for the case of heat conduction in solids ([3, 4, 10], *cf.* also [9]), the transport equations of internal energy (7), (11) and (12) are called Fourier, energy and entropy 'pictures'.

For the determination of the actual form of the entropy balance, playing a central role in irreversible thermodynamics, let us start from the substantial time derivative

$$T\dot{s} = \dot{u} + p\dot{v} \tag{13}$$

of the special form of the Gibbs relation

$$T ds = du + p dv \tag{14}$$

where $\dot{s}$ is the substantial time derivative of the specific entropy. Substituting into (13) balance equations (1), (3) and taking into consideration relation (4), the following form of the entropy balance is obtained

$$\varrho \dot{s} + \nabla \left(\frac{\boldsymbol{J}_q}{T} \right) = \boldsymbol{J}_q . \nabla T^{-1} - \frac{P_v}{T} \nabla . \boldsymbol{v} - \frac{\mathring{\mathbf{P}}^v}{T} : (\mathring{\nabla} \boldsymbol{v})^s = \sigma \tag{15}$$

where σ is the entropy production per unit volume and unit time. The following forms of Eq. (15) obtained by multiplication by the temperature T, and T^2, respectively

$$T\sigma = -\boldsymbol{J}_q . \nabla \ln T - p^v \nabla . \boldsymbol{v} - \mathring{\mathbf{P}}^v : (\mathring{\nabla} \boldsymbol{v})^s \tag{16}$$

$$T^2 \sigma = -\boldsymbol{J}_q . \nabla T - T p^v \nabla . \boldsymbol{v} - T \mathring{\mathbf{P}}^v : (\mathring{\nabla} \boldsymbol{v})^s \tag{17}$$

correspond to the description in the energy and in the Fourier 'picture', respectively. The quantity $T\sigma$ is the energy dissipation per unit volume and unit time.

From the form (15) of the entropy balance it can be seen that the entropy production σ is determined by bilinear expressions of the current densities of the transport processes $\boldsymbol{J}_q$, p^ν/T and $\mathring{\mathbf{P}}^\nu/T$, by the thermodynamic forces ∇T^{-1}, $\nabla . \boldsymbol{v}$ and by $(\mathring{\nabla}\boldsymbol{v})^S$ conjugated to them. The situation is similar in the case of energy dissipation $T\sigma$ and the corresponding quantity of the Fourier 'picture' $T^2\sigma$. The current densities and the thermodynamic forces conjugated to them are summarized in different 'pictures' :

	Currents	Forces
Entropy 'picture':	$\boldsymbol{J}_q, J_v \equiv p^\nu/T, \mathring{\mathbf{J}}_v \equiv \mathring{\mathbf{P}}^\nu/T$	$\boldsymbol{X}_q \equiv \nabla T^{-1}, \; X_v \equiv -\nabla . \boldsymbol{v}, \; \mathring{\mathbf{X}}_v \equiv -(\mathring{\nabla}\boldsymbol{v})^S$
Energy 'picture':	$\boldsymbol{J}_q, J_v^* \equiv p^\nu, \mathring{\mathbf{J}}_v^* \equiv \mathring{\mathbf{P}}^\nu$	$\boldsymbol{X}_q^* \equiv -\nabla \ln T, X_v \equiv -\nabla . \boldsymbol{v}, \mathring{\mathbf{X}}_v \equiv -(\mathring{\nabla}\boldsymbol{v})^S$ (18)
Fourier 'picture':	$\boldsymbol{J}_q, J_v^{**} \equiv Tp^\nu, \; \mathring{\mathbf{J}}_v^{**} \equiv T\mathring{\mathbf{P}}^\nu$	$\boldsymbol{X}_q^{**} \equiv -\nabla T, \; X_v \equiv -\nabla . \boldsymbol{v} \; \mathring{\mathbf{X}}_v \equiv -(\mathring{\nabla}\boldsymbol{v})^S$

It should be noted that the heat current density $\boldsymbol{J}_q$ as well as the viscous forces $X_v \equiv -\nabla \boldsymbol{v}$ and $\mathring{\mathbf{X}}_v \equiv -(\mathring{\nabla}\boldsymbol{v})^S$ are identical in each 'picture', furthermore, the impulse current densities p^ν and $\mathring{\mathbf{P}}^\nu$ are identical with their form in the energy balance equation only in the energy 'picture' which is natural. If we introduce the following new quantities for the viscosity coefficients

$$L \equiv T^{-1}\eta, \; \mathring{L} \equiv 2T^{-1}\eta_v, \; L^* \equiv \eta, \; \mathring{L}^* \equiv 2\eta_v, \; L^{**} \equiv T\eta, \; L^{**} \equiv 2T\eta_v \quad (19)$$

then, using the notations of (18), linear laws (5) can be written in the following form:

Entropy 'picture':

$$J_v = -L\nabla . \boldsymbol{v}, \quad \mathring{\mathbf{J}}_v = -\mathring{L}(\mathring{\nabla}\boldsymbol{v})^S, \quad \boldsymbol{J}_q = L_{qq}\nabla T^{-1} \quad (20)$$

Energy 'picture':

$$J_v^* = -L^*\nabla . \boldsymbol{v}, \quad \mathring{\mathbf{J}}_v^* = -\mathring{L}^*(\mathring{\nabla}\boldsymbol{v})^S, \quad \boldsymbol{J}_q^* = -L_{qq}^*\nabla \ln T \quad (21)$$

Fourier 'picture':

$$J_v^{**} = -L^{**}\nabla . \boldsymbol{v}, \; \mathring{\mathbf{J}}_v^{**} = -\mathring{L}^{**}(\mathring{\nabla}\boldsymbol{v})^S, \; \boldsymbol{J}_q^{**} = -\lambda\nabla T \quad (22)$$

Generally, if we use the linear laws of Onsager's irreversible thermodynamics in the entropy 'picture' as

$$J_i = \sum_{k=1}^{f} L_{ik} X_k \quad (i = 1, 2, \ldots f) \tag{23}$$

where Onsager's reciprocal relations are valid for the conductivity coefficients, *i.e.*

$$L_{ik} = L_{ki} \quad (i = 1, 2, \ldots f) \tag{24}$$

then we may write linear laws (23) in the energy and Fourier 'picture' by appropriately transformed current densities, forces and conductivity coefficients, so that the linear laws in the energy and Fourier 'pictures'

$$J_i^* = \sum_{k=1}^{f} L_{ik}^* X_k^* \quad \text{and} \quad J_i^{**} = \sum_{k=1}^{f} L_{ik}^{**} X_k^{**} \tag{25}$$

be equivalent to (23) with respect to the description of the phenomena. Important subcases of the mentioned general transformation are the following. 1) The current densities are invariant, *i.e.* $J_i^* = J_i^{**} = J_i$ which is valid in our example for the term describing heat conduction. Naturally, the invariance of the current densities involves the transformation of L_{ik} and X_k. 2) The forces are invariant, *i.e.* $X_i^* = X_i^{**} = X_i$ which is valid in our example for the case of viscous forces. Naturally the invariance of forces involves the transformation of L_{ik} and J_k.

It is possible to find such 'pictures' for the description of the phenomena in which each quantity is transformed upon transformation from one 'picture' to another. However, such 'pictures' are generally not 'pure' and they have not yet been used in practice.

2. Formulation of Gyarmati's integral principle of thermodynamics

The variational principle of non-equilibrium thermodynamics has been formulated by GYARMATI in 1965 in the following general form (*cf.* [2, 3] and particularly [10]). Denoting by Γ_i the scalar parameters, the gradients of which are the thermodynamic forces ($X_i = \nabla \Gamma_i$), in the case of independent scalar parameters the Lagrangian density for dissipative phenomena will be $L = L(\Gamma_i, \nabla \Gamma_i)$. The explicit form of the Lagrangian is given by the difference between the entropy production σ and the dissipational potential depending on the forces [10]:

$$\mathfrak{L} = \sigma - \psi = \sum_{i=1}^{f} J_i X_i - \frac{1}{2} \sum_{i,k=1}^{f} L_{ik} X_i X_k \tag{26}$$

where σ is the bilinear functional of the independent currents J_i and forces X_i. The dissipational potential (at least in the case of the linear theory) is a positive definite quadratic functional. According to GYARMATI, the following variational principle is valid for a dissipative continuum

$$\delta \int_V \mathfrak{L} \alpha V = 0 \tag{27}$$

since the Euler–Lagrange equations

$$\frac{\partial \mathfrak{L}}{\partial \Gamma_i} - \sum_{\alpha=1}^{3} \frac{\partial}{\partial x_\alpha} \frac{\partial \mathfrak{L}}{\partial \left(\frac{\partial \Gamma_i}{\partial x_\alpha} \right)} = 0 \quad (i = 1, 2, \ldots, f) \tag{28}$$

belonging to it are identical with the partial differential equations (Fourier, Fick, Navier–Stokes, etc.) of irreversible transport processes [2—10]. In order to derive the transport equations from variational principle (27), the following variational restrictions must be used:

1. Variation involves only the parameters Γ_i, from which the dissipative forces X_i can be derived by gradient operations.

2. No variation is done with respect to the currents occurring in Lagrangian density (26), $\delta J_i = 0$ or those quantities which are connected by the balance equations with the divergency of the current densities.

3. No variation is done along the boundary surface of the continuum unless we wish to obtain the transversality conditions.

Beyond the formulation of the Gyarmati principle, (27), in the entropy 'picture', it can be formulated both in the energy 'picture' and in the Fourier 'picture', moreover completely general formulations equivalent to (27) are also possible. Denoting by $\mathfrak{L}^*$ and $\mathfrak{L}^{**}$ the dissipative Lagrangian densities in the energy and Fourier 'picture' respectively, the general forms of which are

$$\mathfrak{L}^* = T\sigma - \psi^* = \sum_{i=1}^{f} J_i^* X_i^* - \frac{1}{2} \sum_{i,k=1}^{f} L_{ik}^* X_i^* X_k^* \tag{29}$$

$$\mathfrak{L}^{**} = T^2\sigma - \psi^{**} = \sum_{i=1}^{f} J_i^{**} X_i^{**} - \frac{1}{2} \sum_{i,k=1}^{f} L_{ik}^{**} X_i^{**} X_k^{**} \tag{30}$$

the following variational conditions represent the Gyarmati principle in energy and in the Fourier 'picture':

$$\delta \int_V \mathfrak{L}^* \, dV = 0 \quad \text{and} \quad \delta \int_V \mathfrak{L}^{**} \, dV = 0 \tag{31}$$

In the following it will be demonstrated that from variational principles (27) and (31), with the restrictions mentioned in paragraphs 1, 2, and 3, one can

derive the differential equations governing the transport of internal energy and momentum in non-isothermal, isotropic, viscous fluid media.

3. The derivation of transport equations in different 'pictures'

The first terms of the Lagrangian densities $\mathfrak{L}$, $\mathfrak{L}^*$ and $\mathfrak{L}^{**}$ are already determined by expressions (15), (16) and (17) referring to the entropy production σ, the energy dissipation $T\sigma$, and the quantity $T^2\sigma$ respectively. The second terms of Lagrangian densities (26), (29) and (30) are the adequate dissipational potentials: ψ, ψ^* and ψ^{**}, which, considering linear laws (20), (21) and (22), are the following:

Entropy 'picture':

$$\psi = \frac{L_{qq}}{2}(\nabla T^{-1})^2 + \frac{L}{2}(\nabla . \boldsymbol{v})^2 + \frac{\overset{\circ}{L}}{2}[(\nabla \overset{\circ}{\boldsymbol{v}})^s : (\nabla \overset{\circ}{\boldsymbol{v}})^s] \tag{32}$$

Energy 'picture':

$$\psi^* = \frac{L^*_{qq}}{2}(\nabla \ln) + \frac{L^*}{2}(\nabla . \boldsymbol{v})^2 + \frac{\overset{\circ}{L}{}^*}{2}[(\nabla \overset{\circ}{\boldsymbol{v}})^s : (\nabla \overset{\circ}{\boldsymbol{v}})^s] \tag{33}$$

Fourier 'picture':

$$\psi^{**} = \frac{\lambda}{2}(\nabla T)^2 + \frac{L^{**}}{2}(\nabla . \boldsymbol{v})^2 + \frac{\overset{\circ}{L}{}^{**}}{2}[(\nabla \overset{\circ}{\boldsymbol{v}})^s : (\nabla \overset{\circ}{\boldsymbol{v}})^s] \tag{34}$$

From expressions (15), (16) and (17), and (32), (33) and (34) the actual forms of the Gyarmati principle, (26) and (31), are:

$$\delta \int_V \left\{ J_q . \nabla T^{-1} - J_v \nabla . \boldsymbol{v} - \overset{\circ}{J}_v : (\nabla \overset{\circ}{\boldsymbol{v}})^s - \frac{L_{qq}}{2}(\nabla T^{-1})^2 - \right.$$
$$\left. - \frac{L}{2}(\nabla . \boldsymbol{v})^2 - \frac{\overset{\circ}{L}}{2}[(\nabla \overset{\circ}{\boldsymbol{v}})^s : (\nabla \overset{\circ}{\boldsymbol{v}})^s] \right\} dV = 0 \tag{35}$$

$$\delta \int_V \left\{ -J_q . \nabla \ln T - J^*_v \nabla . \boldsymbol{v} - \overset{\circ}{J}{}^*_v : (\nabla \overset{\circ}{\boldsymbol{v}})^s - \frac{L^*_{qq}}{2}(\nabla \ln T)^2 - \right.$$
$$\left. - \frac{L^*}{2}(\nabla . \boldsymbol{v})^2 - \frac{\overset{\circ}{L}{}^*}{2}[(\nabla \overset{\circ}{\boldsymbol{v}})^s : (\nabla \overset{\circ}{\boldsymbol{v}})^s] \right\} dV = 0 \tag{36}$$

$$\delta \int_V \left\{ -J_q . \nabla T - J^{**}_v \nabla . \boldsymbol{v} - \overset{\circ}{J}{}^{**}_v : (\nabla \overset{\circ}{\boldsymbol{v}})^s - \frac{\lambda}{2}(\nabla T)^2 - \right.$$
$$\left. - \frac{L^{**}}{2}(\nabla . \boldsymbol{v})^2 - \frac{\overset{\circ}{L}{}^{**}}{2}[(\nabla \overset{\circ}{\boldsymbol{v}})^s : (\nabla \overset{\circ}{\boldsymbol{v}})^s] \right\} dV = 0 \tag{37}$$

First, let us consider the energy 'picture' that seems to be the simplest one in our actual example according to scheme (18). It should be noted that the earlier derivations of the Navier–Stokes equation or its generalized form from the GYARMATI principle have always been carried out in the energy 'picture' [6, 8, 10]. Let us transform the first term of (36) by means of the vector-analytical identity

$$-\boldsymbol{J}_q \cdot \nabla \ln T = -\nabla \cdot (\boldsymbol{J}_q \ln T) + \ln T \nabla \cdot \boldsymbol{J}_q \tag{38}$$

and the equation

$$\nabla \cdot \boldsymbol{J}_q = -\varrho \dot{u} - p \nabla \cdot \boldsymbol{v} - \mathbf{J}_\nu^* : (\nabla \boldsymbol{v})^s \tag{39}$$

which is identical with the balance of internal energy (3), and where $\mathbf{J}_\nu^* = \mathbf{P}^\nu = p^\nu \delta + \mathring{\mathbf{P}}^\nu$. Hence

$$-\boldsymbol{J}_q \cdot \nabla \ln T = -\nabla \cdot (\boldsymbol{J}_q \ln T) - \ln T \left[\varrho \dot{u} + p(\nabla \cdot \boldsymbol{v}) + \mathbf{J}_\nu^* : (\nabla \boldsymbol{v})_s\right] \tag{40}$$

Let us now consider the second and third terms of expression (36) which can be given in the following form according to Eqs (4) and (18):

$$-\mathbf{J}_\nu^* : (\nabla \boldsymbol{v})^s = -\nabla \cdot (\mathbf{J}_\nu^* \cdot \boldsymbol{v}) + \boldsymbol{v} \cdot (\nabla \cdot \mathbf{J}_\nu^*) \tag{41}$$

By writing the balance of momentum, (2), multiplied scalarly by the velocity V, in the form

$$\boldsymbol{v} \cdot (\varrho \dot{\boldsymbol{v}} + \nabla p - \varrho \boldsymbol{F}) = -\boldsymbol{v} \cdot (\nabla \cdot \mathbf{J}_\nu^*) \tag{42}$$

($\mathbf{J}_\nu^* = \mathbf{P}^\nu$), then with the aid of Eqs (40), (41), (42), and applying the Gauss theorem to the divergencies, variational task (36) can be formulated as

$$\delta \int_\nu \left\{ -\left\{ \ln T \left[\varrho \dot{u} + p \nabla \cdot \boldsymbol{v} + \mathbf{J}_\nu^* : (\nabla \dot{\boldsymbol{v}})^s\right] - \boldsymbol{v} \cdot (\varrho \dot{\boldsymbol{v}} + \nabla p - \varrho \boldsymbol{F}) - \right.\right.$$
$$\left.\left. - \frac{L_{qq}^*}{2} (\nabla \ln T)^2 - \frac{L^*}{2} (\nabla \cdot \boldsymbol{v})^2 - \frac{\mathring{L}^*}{2} [(\nabla \mathring{\boldsymbol{v}})^s : (\nabla \mathring{\boldsymbol{v}})^s] \right\} \right\} dV - \tag{43}$$
$$- \delta \oint_\Omega [\boldsymbol{J}_q \ln T + \mathbf{J}_\nu^* \cdot \boldsymbol{v}] \, d\Omega = 0$$

Considering Gyarmati's parameters $\Gamma_q = \ln T$ and $\Gamma_\alpha = \mathbf{v}_\alpha$ ($\alpha = x, y, z$) as variational parameters, and taking into consideration the variational restriction according to which the irreversible current densities are not varied, *i.e.*

$$\delta \boldsymbol{J}_q = 0 \quad \text{and} \quad \delta \mathbf{J}_\nu^* \equiv \delta \mathbf{P}^\nu = 0 \tag{44}$$

the variational task (43) becomes equivalent to differential equations (6) and (11) governing the transport of momentum and internal energy. It can be seen that, owing to balance equations (2) and (3), conditions (44) lead to the following variational restrictions

$$\delta \nabla . \mathbf{P}^v = \nabla . \delta \mathbf{P}^v = - \delta(\varrho \dot{\boldsymbol{v}} + \nabla p - \varrho \boldsymbol{F}) = 0 \tag{45}$$

and

$$\delta \nabla . \boldsymbol{J}_q = \nabla . \delta \boldsymbol{J}_q = - \delta(\varrho \dot{u} + p \nabla . \boldsymbol{v} + \mathbf{J}_v^* : (\nabla \boldsymbol{v})^s) \tag{46}$$

because δ and ∇ are commutative operators.

The derivation of the transport equations can be easily repeated in the entropy 'picture'. Let us transform the first term of the variational problem into the expression

$$\boldsymbol{J}_q . \nabla T^{-1} = \nabla . (\boldsymbol{J}_q T^{-1}) + T^{-1} [\varrho \dot{u} + p \nabla \boldsymbol{v} + \mathbf{J}_v^* : (\nabla \boldsymbol{v})^s] \tag{40'}$$

which is analogous to expression (40). The analogues of relations (41) and (42) in the entropy 'picture' are

$$- \mathbf{J}_v : (\nabla \boldsymbol{v})^s = - \nabla . (\mathbf{J}_v . \boldsymbol{v}) + \boldsymbol{v} . (\nabla . \mathbf{J}_v) \tag{41'}$$

and

$$\boldsymbol{v} \cdot \left(\frac{\varrho \dot{\boldsymbol{v}} + \nabla p - \varrho \boldsymbol{F}}{T} \right) = - \frac{\boldsymbol{v}}{T} \cdot (\nabla \mathbf{J}_v^*) - \boldsymbol{v} . (\mathbf{J}_v^* . \nabla T^{-1}) \tag{42'}$$

Variational problem (35) in the entropy 'picture' can be given in the following manner with the aid of relations (40') and (42')

$$\delta \int_V \left\{ T^{-1} [\varrho \dot{u} + p \nabla . \boldsymbol{v} + \mathbf{J}_v T : (\nabla \boldsymbol{v})^s] - \boldsymbol{v} \cdot \left[\frac{\varrho \dot{\boldsymbol{v}} + \nabla p - \varrho \boldsymbol{F}}{T} \right] - \right.$$
$$\left. - \boldsymbol{v} \cdot \left(\mathbf{J}_v \cdot \frac{\nabla T}{T} \right) - \frac{L_{qq}}{2} (\nabla T^{-1})^2 - \frac{L}{2} (\nabla \boldsymbol{v})^2 - \frac{\mathring{L}}{2} [(\Delta \boldsymbol{v})^s : (\nabla \boldsymbol{v})^s] \right\} dV + \tag{43'}$$
$$+ \delta \oint_\Omega [\boldsymbol{J}_q T^{-1} - \mathbf{J}_v . \boldsymbol{v}] \, d\boldsymbol{\Omega} = 0$$

Now Gyarmati's variational parameters will be $\Gamma_q \equiv T^{-1}$ and $\Gamma_\alpha \equiv \mathbf{v}_\alpha$; and from the balance equations and variational conditions $\delta \boldsymbol{J}_q = 0$ and $\delta \mathbf{J}_v = 0$ the following restrictions are obtained

$$- \delta \nabla . \boldsymbol{J}_q = \delta [\varrho \dot{u} + p \nabla . \boldsymbol{v} + \mathbf{J}_v T : (\nabla \boldsymbol{v})^s] = 0 \tag{45'}$$

and

$$\delta \left[\frac{\varrho \dot{\boldsymbol{v}} + \nabla p - \varrho \boldsymbol{F}}{T} \right] + \mathbf{J}_v \cdot \delta \left(\frac{\nabla T}{T} \right) = 0 \tag{46'}$$

which, in the entropy 'picture' are analogous to restrictions (45) and (46).

It is clear that variational problem (43′) under the restrictions (45′) and (46′), is equivalent to differential equation (6) governing the momentum transport and to equation (11) referring to the transport of internal energy in the entropy 'picture'.

Finally let us briefly repeat the derivation of the transport equations in the Fourier 'picture'. Starting from the formulation of the Gyarmati principle in the Fourier 'picture' and making use of the relations

$$-\boldsymbol{J}_q \cdot \nabla T = -\nabla \cdot (\boldsymbol{J}_q T) - T[\varrho \dot{u} + p \nabla \cdot \boldsymbol{v} + \mathbf{J}_\nu^* : (\nabla \boldsymbol{v})^s] \tag{40″}$$

$$-\mathbf{J}_v^{**} \nabla \cdot \boldsymbol{v} = -\nabla (\mathbf{J}_\nu^{**} \cdot \boldsymbol{v}) + \boldsymbol{v} (\nabla \cdot \mathbf{J}_\nu^{**}) \tag{41″}$$

$$\boldsymbol{v} \cdot T(\varrho \dot{\boldsymbol{v}} + \nabla p - \varrho \boldsymbol{F}) = -\boldsymbol{v} T (\nabla \cdot \mathbf{J}_\nu^*) = -\boldsymbol{v} \cdot (\nabla \cdot \mathbf{J}_\nu^{**}) + \boldsymbol{v} \cdot (\mathbf{J}_\nu^{**} \cdot \nabla T/T) \tag{42″}$$

which are similar to relations (40′), (41′), (42′) in the energy 'picture', the following variational problem is obtained:

$$\begin{aligned} \delta \int_V \Big\{ & -T[\varrho \dot{u} + p \nabla \cdot \boldsymbol{v} + \mathbf{J}_\nu^{**} T^{-1} : (\nabla \boldsymbol{v})^s] - \boldsymbol{v} \cdot T[\varrho \dot{\boldsymbol{v}} + \Delta p - \varrho \boldsymbol{F}] - \\ & - \boldsymbol{v} \cdot \left(\mathbf{J}_\nu^{**} \cdot \frac{\nabla T}{T} \right) - \frac{\lambda}{2} (\nabla T)^2 - \frac{L^{**}}{2} (\nabla \cdot \boldsymbol{v})^2 - \frac{\mathring{L}^{**}}{2} [(\nabla \boldsymbol{v})^s : (\mathring{\nabla \boldsymbol{v}})^s] \Big\} dV + \\ & + \delta \oint_\Omega [-\boldsymbol{J}_q T - \mathbf{J}_\nu^{**} \cdot \boldsymbol{v}] \cdot d\boldsymbol{\Omega} = 0 \end{aligned} \tag{43″}$$

The restrictions

$$-\delta \nabla \cdot \boldsymbol{J}_q = \delta [\varrho \dot{u} + p \nabla \cdot \boldsymbol{v} + \mathbf{J}_\nu^{**} T^{-1} : (\nabla \boldsymbol{v})^s] = 0 \tag{45″}$$

$$\delta [T(\varrho \dot{\boldsymbol{v}} + \nabla p - \varrho \boldsymbol{F})] - \mathbf{J}_\nu^{**} \cdot \delta \left(\frac{\nabla T}{T} \right) = 0 \tag{46″}$$

following from the momentum and internal energy balance owing to the non-variation of the current densities, ensure unambiguously that variational problem (43″) in the case of the variation of Gyarmati's parameters $\Gamma_q = \boldsymbol{T}$ and $\Gamma_\alpha = V_\alpha$ ($\alpha = x, y, z$) leads directly to transport equations (6) and (12).

4. Remarks concerning the reversible part of the momentum transport equation

In the foregoing we saw that the application of the Gyarmati principle in different 'pictures' influences the form of the transport equation of the internal energy only. The Navier–Stokes equation governing momentum transport is invariant in all 'pictures'. Though this equation has already been

derived from the Gyarmati principle for isothermal systems [6, 8, 10], the clarification of an important problem is yet to be done. This problem refers to the fact that though the integral principle of GYARMATI is equivalent to the differential equations governing the dissipative processes, *i.e.* it is a genuine variational principle only for dissipative phenomena, yet, it involves also the equations describing reversible motions. Indeed, if we are considering variational problem (43) exclusively for momentum transport, then its Lagrangian density

$$\mathfrak{L} = \boldsymbol{v} \cdot (\varrho \dot{\boldsymbol{v}} + \nabla p - \varrho \boldsymbol{F}) + \frac{L^*}{2} (\nabla \cdot \boldsymbol{v})^2 + \frac{\mathring{L}^*}{2} (\mathring{\nabla \boldsymbol{v}})^S : (\mathring{\nabla \boldsymbol{v}})^S \tag{47}$$

can be considered as the sum of a Lagrangian containing 'dissipative terms'

$$\mathfrak{L}_d \equiv \frac{L^*}{2} (\nabla \cdot \boldsymbol{v})^2 + \frac{\mathring{L}^*}{2} [(\mathring{\nabla \boldsymbol{v}})^S : (\mathring{\nabla \boldsymbol{v}})^S] \tag{48}$$

and of another one containing only 'reversible terms':

$$\mathfrak{L}_{\text{rev.}} \equiv \boldsymbol{v} \cdot (\varrho \dot{\boldsymbol{v}} + \nabla p - \varrho \boldsymbol{F}) \tag{49}$$

As for the physical meaning of the last quantity, it is the expression of the kinetic energy belonging to the Eulerian equation of motion of ideal fluid systems, *i.e.*

$$\varrho \dot{\boldsymbol{v}} + \nabla p - \varrho \boldsymbol{F} = 0 \tag{50}$$

since it is obtained as the scalar product of (50) and the velocity v. A forma 'variational principle'

$$\delta \int_V \mathfrak{L}_{\text{rev.}} dV = 0 \tag{51}$$

can be given for the 'reversible part' describing the pure mechanical motion if variation is done only with respect to the velocity according to the restrictions under points 1, 2, and 3. In this case the Euler equation (50) governing the pure reversible motion can be considered as the differential equation belonging to variational principle (51). However, Eq. (51) is not a genuine variational principle because the real principle for reversible motion is represented by a Hamilton type principle valid for the time integral of an adequate Lagrangian. Therefore 'variational principle' (51) can be considered only as a 'quasi-variational problem' for ideal fluid systems (or for the reversible motion of real systems) which is also suitable for a formal derivation of the equation of motion (50), *i.e.* for a formal deduction of the reversible part of the Navier–Stokes equation. Consequently, though formula (51)

does not represent a genuine variational principle, it permits to derive formally the equation of motion for purely mechanical processes by means of an adequate variational formalism. It should be noted that our statements are in agreement with those made by SERRIN concerning Herivel's variational principle for ideal fluid systems [12].

Clearly the integral principle formulated by GYARMATI for dissipative processes represents a genuine variational principle for irreversible processes and, at the same time, it is suitable for a formal treatment of reversible motions within the framework of this variational formalism. Considering that the dissipative processes occurring in a real medium are superimposed on the reversible motions, the outlined feature of the Gyarmati principle becomes evident immediately.

REFERENCES

1. GYARMATI, I.: On the Principles of Thermodynamics, manuscript, 1957; Dissertation, Budapest, 1958
2. GYARMATI, I.: Zhurn. Fiz. Khim. (Moscow) **39**, 1489 (1965)
3. GYARMATI, I.: Acta Chim. Acad. Sci. Hung. **43**, 353 (1965)
4. GYARMATI, I.: Acta Chim. Acad. Sci. Hung. **47**, 63 (1966)
5. VERHÁS, J.: Zhurn. Fiz. Khim. **40**, 1213 (1966)
6. VERHÁS, J.: Z. Phys. Chem. **234**, 226 (1967)
7. VERHÁS, J.: Ann. Phys. **7**, 90 (1967)
8. BÖRÖCZ, SZ.: Z. Physik. Chem. **234**, 26 (1967)
9. FARKAS, H.: Z. Physik. Chem. **239**, 124 (1968)
10. GYARMATI, I.: Non-equilibrium Thermodynamics. Field Theory and Variational Principles. Springer Verlag, Berlin—Heidelberg—New York, 1970
11. DE GROOT, S. R., MAZUR, P.: Non-equilibrium Thermodynamics. North-Holland Publ. Co., Amsterdam, 1962
12. SERRIN, J.: Mathematical Principles of Classical Fluid Mechanics. Handbuch der Physik. Band VIII/1 125. Springer Verlag, 1959

Szilárd BÖRÖCZ; Budapest XI., Budafoki út 8.

Acta Chimica Academiae Scientiarum Hungaricae, Tomus 69 (3), pp. 341–347 (1971)

OXIDATION ON THE NICKEL HYDROXIDE ELECTRODE, IV

KINETICS OF OXIDATION OF PRIMARY ALCOHOLS

G. VÉRTES, G. HORÁNYI and F. NAGY

(Central Research Institute for Chemistry of the Hungarian Academy of Sciences, Budapest)

Received April 22, 1970

The rates of oxidation of primary alcohols were studied on a nickel hydroxide electrode. It was found that besides the earlier found proportionality between the rate and the amount of NiOOH (Q) on the electrode, the rate is proportional to the alcohol concentration:

$$w = k_0 Q\, c_a$$

It was found that the second order rate constant, k_0, does not depend on the alkalinity of the medium.

It was proved that there is no unambiguous connection between the potential of the nickel hydroxide electrode and the active oxygen content.

It was proved experimentally that identical oxidation rates can relate to different electrode potentials, which means that the rate constant, k_0, appearing in the equation does not depend on the electrode potential.

In a previous communication [1] we dealt with the possibility of the electrochemical study of the oxidation reaction of primary alcohols on nickel(III) oxide hydroxide according to the overall reaction:

$$4\ \mathrm{NiOOH} + \mathrm{OH^-} + \mathrm{RCH_2OH} \rightarrow 4\ \mathrm{Ni(OH)_2} + \mathrm{RCOO^-}$$

It was shown that with the help of electrochemical methods the possibility arises for a relatively simple and rapid determination of oxidation rates and for the study of some parameters of the oxidation.

In addition, those experimental conditions were analyzed which are necessary for the clear-cut determination of oxidation rates on a nickel hydroxide electrode. Apart from these, the most significant finding was that it is expedient to use cathodic polarization simultaneously with the discharge process occurring in the presence of the alcohol. Under such conditions the variation with time of the amount of nickel(III) oxide hydroxide in an alcohol solution of given concentration is given by the following relation:

$$-\frac{dQ}{d\tau_r} = I + kQ \qquad (1)$$

where Q is the charge which may be used for oxidation equivalent to the amount of nickel(III) oxide hydroxide on the electrode at time τ_r (*e.g.* in Coulombs), I is the cathodic polarizing current, and k is the apparent rate constant of the oxidation. Thus it may be seen that the rate of oxidation of the alcohol is proportional to the amount of nickel(III) oxide hydroxide on the electrode.

The elucidation of the physical meaning of the apparent rate constant defined by Eq. (1) must be considered a fundamental question from the point of view of understanding the mechanism of oxidation. For this, both the role of the concentrations of the substances in the overall equation for the reaction and also (since also electrochemical processes occur in the system) the effect of the electrode potential on the reaction rate must be examined.

Dependence of the reaction rate on the alcohol concentration

The effect of the alcohol concentration on the rate of oxidation on the nickel hydroxide electrode was studied in detail for methanol and ethanol. Apart from this, some studies of informative character were also made in the case of alcohols which display properties differing from those of aliphatic alcohols. In addition to the fact that the reactivity of aromatic alcohols and especially of aldehydes conceivable as intermediates makes possible special processes in certain cases, in the interest of the generalization of the kinetic picture the kinetic study of the oxidation of some other alcohols, *e.g.* aromatic and heteroaromatic alcohols, seems expedient. In the second communication of this series [2] it was shown that these too may be oxidized in good yield to carboxylic acids.

Using a method described in detail in the previous communication we determined for each alcohol the value of the apparent rate constant k in alcohol solutions of different concentrations. The values calculated from the results are given in Table I.

Table I

Apparent rate constants of the oxidation of alcohols on nickel hydroxide at 25.0 °C

Alcohol concentration, M	Apparent rate constant, $k \times 10^3$ (sec^{-1})			
	methanol	ethanol	benzyl alcohol	furfuryl alcohol
0.01	—	0.6	3.9	7.8
0.03	1.0	1.8	—	—
0.10	3.5	6	45	—
0.30	12	17	—	—
1.00	35	—	—	—

From the data in Table I it may be seen directly, and may be proved beyond doubt by the usual logarithmic plot that the apparent rate constant is proportional to the alcohol concentration. This proves that the reaction is first order with respect to both nickel(III) oxide hydroxide and the alcohol. That is, the rate equation for the oxidation of the alcohol is of the following form:

$$w = k_0 Q c_a . \tag{2}$$

Accordingly, the rate constants k_0 for alcohol oxidations on nickel hydroxide can be calculated. These are listed in Table II.

Table II

Rate constants of the oxidation of various alcohols

	k_0 $M^{-1} \times \sec^{-1}$
Methanol	0.04
Ethanol	0.06
Benzyl alcohol	0.4*
Furfuryl alcohol	0.8**

* from two measurements
** from one measurement, taking the order with respect to the alcohol as one

In addition to the wide applicability over several orders of magnitude of the second order kinetics given by Eq. (2), it must be mentioned that with higher reaction rates ($c_a > 1\ M$) observations show that this is no longer valid. With regard to this, only qualitative statements can be made because the determination of rate constants at such high concentrations is a still unsolved problem. With a view to ensuring approximately equilibrium conditions, the study of the kinetics is carried out on a thin nickel hydroxide layer and this means a small Q_0 [Q_0 is the amount of charge (NiOOH) which can be brought into the electrode]. At high concentrations, however, the discharge rate is already so large that the reaction is completed in a short time because of the small Q_0, and so the values of the rate constant k can be determined only with an extremely large error. Another difficulty is that the electrochemical behaviour of a more concentrated solution (conductivity, degree of dissociation, activities) differs significantly from that of a weaker solution, and therefore complications can arise the analysis of which would far exceed the scope of the present work.

The effect of hydroxide ion concentration on the reaction rate

The roles of the amount of nickel hydroxide and the alcohol concentration have been elucidated above. In addition to these the hydroxide ion also

appears among the starting materials in the reaction equation. Thus in order to complete the kinetic picture, it is necessary to examine the effect of pH on the reaction rate. In connection with this it must be taken into consideration that the nickel hydroxide electrode is stable only in a definite pH range, and trivalent nickel is not stable in aqueous solution in an acidic medium. In addition, the reaction of the hydroxide ion during the oxidation of alcohols increases the acidity in the vicinity of the surface, and thus the pH of the solution can be decreased only to such an extent that the acidification occurring during reaction could still be compensated for. Accordingly the pH can vary over only a rather narrow range, but a change of the hydroxide ion concentration by two orders of magnitude is sufficient to establish certain tendencies.

Studies were made using a solution containing 0.1 *M* ethanol. The measurement conditions were somewhat different from those given earlier; the background solution then contained 1 *N* NaOH, but in the present case the concentrations were 0.01, 0.1 and 1.0 *N* NaOH. The results of this series of experiments are given in Table III. The apparent rate constants k calculated from the results appear in the last row of the Table.

Table III

The effect of pH on the oxidation rate of 0.1 M ethanol

I μA	τ_r* sec		
	0.01 *N* NaOH	0.1 *N* NaOH	1.0 *N* NaOH
200	40	50	48
100	76	85	83
60	111	116	107
40	150	155	156
25	202	207	210
20	228	234	231
15	267	273	267
12.5	291	297	282
10	321	333	300
$k\times10^3$ (sec^{-1})	6.2	5.2	6.1

From the data it may be seen that within experimental error the reaction rate for a hydroxide ion concentration change of two orders of magnitude agrees with the value measured for 1 *N* NaOH. This means that the oxidation reaction is zero order with respect to the hydroxide ion concentration. Thus rate equation (2) is complete and k_0 can be considered a true rate constant, *i.e.* it does not contain factors depending on the concentration.

The role of the electrode potential

So far during our work connected with the study of oxidation processes taking place on the nickel hydroxide electrode the measurement of electrode potential has primarily been used with a view to observing the end-point of the reaction, the complete disappearance of NiOOH. Since the electrode potential changes monotonously during the reaction and at the same time the reaction rate too decreases monotonously, in principle it is possible that there is a connection between the two quantities.

In the course of describing the technique of measurement we have already commented that in the vicinity of the end-point the electrode potential is not characteristic of the amount of NiOOH to be found on the electrode and this is why it was necessary to elaborate the reported measurement procedure [1]. In addition it appears from the literature connected with the NiOOH electrode that there is no clear-cut connection between the electrode potential and the amount of NiOOH on the electrode [3—12]. On the other hand we found earlier that there is a forced relation between the reaction rate and the amount of unreacted NiOOH. Thus during the change of the electrode potential there is a clear-cut connection between the rate and the amount of NiOOH while there is no well-defined relation between the electrode potential and the amount of NiOOH. On this basis it can scarcely be expected that there should be a functional connection between the rate and the potential.

The following experimental observations serve as illustration.

The electrochemical capacity of a nickel hydroxide electrode with not too thin a layer was determined by charging for 5 min. with a 30 mA current and then discharging with constant current in 1 N NaOH. The value of Q_0 was found to be 235 mC. After this the charging of the electrode was carried out not in the previous manner but with an electronic potentiostat. After discharge the electrode potential was adjusted with the help of a potentiostat to 1350 mV (relative to a 1 atmosphere hydrogen electrode immersed in the same solution) and maintained at that value for 10 min. Within about 10 min. the current decreased by two orders of magnitude, that is presumably the residual current arising from the decomposition of the nickel hydroxide has been reached. After this the amount of charge on the electrode was determined by the normal electrochemical method. With discharges carried out with a constant (0.5 mA) current, an average value of 52 mC was obtained. If the charging was carried out at 1400 mV, a charge of 170 mC could be be brought onto the electrode. However, if the electrode was kept at 1400 mV for 2 min. after discharge and we then switched over to 1350 mV which was maintained for another 10 min., then at the discharge following this, a charge of 160 mC was found on the electrode. This measurement shows directly that,

depending on the pre-treatment of the electrode, different active oxygen contents can be ascribed to one given electrode potential.

The relation of the electrode potential and the reaction rate are shown in Fig. 1 for two parallel experiments. Both curves show the phenomena observed during the discharge of an electrode containing 30 mC/10 cm^2 nickel(III) oxide hydroxide for a solution containing 1 *N* NaOH and 1 *M* ethanol. Since the cathodic polarizing currents were identical in the two measurements, the cause of the difference is merely the pre-treatment of the electrode. It should be noted that differences of such a nature occur relatively rarely but this is not an isolated phenomenon; on the basis of the observations it must be considered characteristic for the system. From

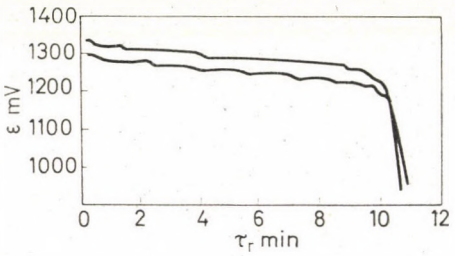


Fig. 1. Dependence of the potential interval of the discharge curve on the pre-treatment of the electrode

Fig. 1 it may be seen that the discharge periods are the same but the potential interval is displaced by nearly 50 mV which means that despite a difference of 50 mV in the two cases there was no difference between the discharge rates, *i.e.* as a consequence of the identical cathodic polarizing currents there was no difference between the rates of oxidation of ethanol. Since the discharge of the electrode takes place in a 100 mV range but the position of this may be displaced by 50 mV without change of the reaction rate, it may be stated that the rate of oxidation of alcohols cannot be affected by the potential of the nickel hydroxide electrode.

Without going into a detailed discussion of the mechanism of oxidation (which will be the basis of a subsequent paper), it is now possible to state from the experiment shown in Fig. 1 that the rate constant for the reaction, which can be said to be second order from the kinetic picture, does not depend on the electrode potential. For the explanation of the identical reaction rates measured in the individual cases at different electrode potentials, that property of the nickel hydroxide electrode may serve, that different electrode potentials can belong to identical active oxygen contents, *i.e.* to identical $NiOOH/Ni(OH)_2$ ratios on one electrode. Thus the electrode potential on the nickel hydroxide electrode is not a measure of the oxidizing ability.

REFERENCES

1. VÉRTES, G., HORÁNYI, G., NAGY, F.: Acta Chim. Acad. Sci. Hung. **67,** 145 (1971)
2. HORÁNYI, G., VÉRTES, G., NAGY, F.: Acta Chim. Acad. Sci. Hung. **67,** 357 (1971)
3. BODE, H., DEHMELT, K., WITTE, J.: Z. anorg. allg. Chem. **366,** 1 (1969)
4. VÉRTES, GY., NAGY, F.: Magy. Kém. Foly. **76,** 260 (1970)
5. KUCHINSKII, E. N., ERSHLER, P. V.: Zh. Fiz. Khim. **20,** 539 (1946)
6. BOURGAULT, P., CONWAY, B. E.: Canad. J. Chem. **38,** 1557 (1960)
7. CONWAY, B. E., GILEADI, E.: Canad. J. Chem. **40,** 1933 (1962)
8. BRIGGS, G. W. D., STOTT, G. W., WYNNE-JONES, W. F. K.: Electrochim. Acta **7,** 249 (1962)
9. TUOMI, D.: J. Electrochem. Soc. **112,** 1 (1965)
10. YOSHIZAWA, S., TAKEHARA, Z.: CITCE Meeting, Tokyo—Kyoto, 1966
11. BODE, H., DEHMELT, K., WITTE, J.: Electrochim. Acta **11,** 1079 (1966)
12. KRONENBERG, M. L.: J. Electroanal. Chem. **13,** 120 (1967)

György VÉRTES
György HORÁNYI
Ferenc NAGY
Budapest II., Pusztaszeri út 59—67.

Acta Chimica Academiae Scientiarum Hungaricae, Tomus 69 (3), pp. 349—359 (1971)

THE COMPETITIVE NITRATION OF SOME AROMATIC COMPOUNDS

A. UJHIDY*, O. RÉPÁSY** and J. TAKÁCS*

*(*Research Institute for Technical Chemistry of the Hungarian Academy of Sciences, Veszprém, and **Hungarian Research Institute for Oil and Gas, Veszprém)*

Received February 25, 1970

The relative nitration rates obtained in homogeneous solutions containing sulfuric acid differed from the values published in the literature, which so far were determined only in organic solvents, so that it was thought necessary to clarify this problem.

Combinations of benzene, toluene and some of their nitro derivatives were nitrated competitively in homogeneous solutions at various sulfuric acid and acetic acid concentrations, and in acetic acid solutions containing sulfuric acid. It has been shown that the relative rate constants decrease with increasing sulfuric acid concentration and temperature. The ratio of the rate constants is smaller in sulfuric acid medium than in acetic acid. This means that no values of general validity can be given for the relative reactivities of the various aromatic compounds, because the effects of the solvent, temperature, and in certain cases of the concentration must also be considered.

Introduction

During heterogeneous-phase nitration in a film reactor [1] it has become evident that when two compounds are allowed to react simultaneously, in the competitive manner, the ratio of the rate constants depends both on the sulfuric acid concentration and on the reaction temperature. Experiments were carried out in homogeneous sulfuric acid medium on the competitive nitration of the following pairs of compounds: *p*-nitrotoluene–nitrobenzene, toluene–benzene, *p*-nitrotoluene–*p*-nitroethylbenzene, nitrobenzene–*o*-nitrotoluene, nitrobenzene–*p*-nitrochlorobenzene and benzene–*p*-nitrotoluene. The nitration of these compounds in mixed acid alone has not been described in the literature. Our investigations also included the competitive nitration of toluene–benzene and benzene–*p*-nitrotoluene in acetic acid and acetic anhydride solutions, in order to check the data reported in the literature and our method, and to allow comparison with the results obtained in sulfuric acid medium.

Survey of the literature

The competitive (simultaneous) method was first used by FRANCIS [2]. The method consists essentially in reacting a mixture of two different compounds with less than the stoichiometric amount of the reaction partner;

the relative reaction rates, *i.e.* the ratio of the rate constants is determined from the degrees of conversion. This method can be used in the case when the two compounds react according to the same mechanism. The method has the advantage that it is easy to ensure completely identical reaction conditions and, according to DEWAR [3], an exact knowledge of the kinetics is not necessary for the calculations.

The first competitive nitration in homogeneous phase (benzene–toluene and halobenzene mixtures) was reported by INGOLD in 1927 [4]. He found that toluene was nitrated 15.7-times as quickly as benzene, and modified this value in a later publication [5] to 27. BIRD and INGOLD [6] compared the nitration rate of halobenzenes with that of benzene. It was found that the solvents acetic anhydride, acetonitrile, or nitromethane did not affect the ratio of the rate constants, whereas the ratio approached unity with increasing the temperature. BORDWELL and ROHDE [7], INGOLD and SMITH [8], and KNOWLES *et al.* [9] did not study the effect of either the solvents or the temperature in the competitive nitration.

STOCK [10] nitrated a mixture of toluene and *t*-butylbenzene in acetic anhydride and nitromethane. He found the ratio of the rate constants to be independent of the concentration of nitric acid, of the solvents investigated and, in the range between 0 and 40 °C, of temperature. According to SUHR *et al.* [11] the ratio of the rate constants for toluene–benzene is 35.

The relative nitration rates of nitrotoluene isomers in sulfuric acid solution was investigated by TILLETT [12] by the competitive method. He found in 84% sulfuric acid the relative rate 395, on the basis of the rate constants of *m*-nitrotoluene and nitrobenzene which were determined separately, while *p*-nitrotoluene was nitrated about 430-times as rapidly as nitrobenzene. This is not considered by TILLETT a too large deviation from the value of 330 found by BRAND and PATTON [13] in 99% sulfuric acid.

Similarly to TILLETT and BRAND, BONNER *et al.* [14] found that the relative nitration rate was practically independent of the composition of the reaction mixture and of temperature.

The use of nitronium salts for preparative nitration has been described by OLÁH *et al.* [15, 16]. Subsequently, they investigated the kinetics and the reaction mechanism of the nitration of aromatic compounds by means of such salts [17, 18].

Competitive nitrations with various nitronium salts have shown that the relative nitration rate depends also on the nitrating agent [19]. Thus, the rate of toluene referred to benzene varied between 1.4 and 1.65 in tetramethylene sulfone solution (TMS), while in nitromethane solution it varied from 0.91 to 1.19.

OLÁH *et al.* [20, 21] also investigated the nitration of alkylbenzenes in the presence of benzene with nitric acid and with mixed acid in nitromethane,

acetic acid, acetic anhydride and TMS solutions. In this latter solvent, they also tried $NO_2^+BF_4^-$ as the nitrating agent. Some of the results obtained are summarized in Table I.

Table I

Effect of the reaction medium on the ratio of the rate constants in the competitive nitration of toluene and benzene

Nitrating agent	Solvent	$\frac{k_T}{k_B}$
HNO_3	Nitromethane	26.40
HNO_3	Acetic acid	28.80
HNO_3	TMS	17.00
Mixed acid (30% of the total solution)	TMS	28.00
	Acetic acid	21.00
Mixed acid (75% of the total solution)	TMS	1.60
	Acetic acid	2.10
$NO_2^+BF_4^-$	TMS	1.52

These authors assume that the mechanism of nitration changes depending on the solvent.

Similarly, TÖLGYESI [22] nitrated simultaneously benzene and toluene with $NO_2^+BF_4^-$ in TMS solution. He established that the product ratio increased with increasing intensity of stirring and with decreasing concentration of the solution. At low product ratios dinitrotoluene could be detected.

Competitive nitration in sulfuric acid medium

Though the irreversibility of the nitration reaction has been proved earlier [23, 24], it was thought advisable to check this known fact using more advanced methods of analysis gas chromatography available today. In the case of the given experimental method the fact to be proved unequivocally was that no 'transnitration' can occur when compounds with different numbers of nitro groups and possessing different reactivities are heated in sulfuric acid solution in the presence of each other. If there is no 'transnitration', the irreversibility of the nitration reaction, though indirectly, is proved again.

In these investigations 1 : 1 molar mixtures of *p*-nitrotoluene and dinitrobenzene (Mixture I) and of 2,4-dinitrotoluene and nitrobenzene (Mixture II) were agitated in 85 and 91% sulfuric acid, respectively, for 15—60 minutes. After work-up, the samples were analyzed with a gas chromatograph. After sulfuric acid treatment, the composition (1 : 1 molar ratio) of the single pairs of compounds was the same as the initial composition. Thus, no 'transnitration' took place, which proved that for the compounds investigated and under the given conditions the nitration reaction was irreversible.

Table II

Effect of the change of temperature and sulfuric acid concentration on the ratio of the rate constants of p-nitrotoluene and nitrobenzene

°C	DVS*	3.0	3.5	4.55	5.67	7.0	8.56	13.7	27.5
	H_2SO_4%	75.0	77.5	82.0	85.0	87.5	89.6	93.0	96.5
24		329	259	235	191	144	76	104	126
69		208	208	115	100	70.5	10.8	4.7	15.8
80		150	127	83	50.5	48	5	3.3	7.6

As can be seen from Table II, the value of the ratios decreases with increasing sulfuric acid concentration up to 89—93%, to increase then again. Moreover, the ratio of the rate constants decreases unequivocally with increasing temperature (the values 167 and 133 obtained for 4.5 DVS at 45 and 56 °C, respectively, fit well into the series) [25].

From the results comprised in Table III, it may be seen that the changes in sulfuric acid concentration and in temperature have a similar effect in the competitive nitration of *o*-nitrotoluene and nitrobenzene as in the case of *p*-nitrotoluene and benzene.

Table III

Effect of the change of temperature and sulfuric acid concentration on the ratio of the rate constants of nitration of o-nitrotoluene and nitrobenzene

°C	DVS	3.0	3.5	4.55	5.67	7.0	8.56	13.7	27.5
	H_2SO_4 %	75.0	77.5	82.0	85.0	87.5	89.6	93.0	96.5
24		1292	624	583	475	234	142.5	129	234
69		448	253	167	133	86	37.0	20	30
80		274	184	160	96	40	18.0	13	17

In the nitration of *o*-nitrotoluene the isomers 2,4-dinitrotoluene and 2,6-dinitrotoluene were formed. The increase in sulfuric acid concentration and the decrease in temperature seemed to have a diminishing effect on the quantity of 2,6-dinitrotoluene. In order to clarify the isomer distribution, *o*-nitrotoluene was nitrated alone in a homogeneous solution. The results are comprised in Table IV; they are in agreement with the values obtained in the competitive nitration [26].

According to TILLETT [12], the distribution of the isomers for the nitration of *o*-nitrotoluene in 97% sulfuric acid at 25 °C is 66.6% 2,4-dinitrotoluene and 33.33% 2,6-dinitrotoluene.

Table IV

Isomer distribution for the nitration of o-nitrotoluene

Experiment, No.	Temperature, °C	DVS	o-NT, mole %	2,6-DNT, mole %	2,4-DNT, mole %	2,6-DNT, %, referred to the total DNT
460	69	3.0	73.00	8.37	18.63	31.10
461	69	5.7	52.25	13.21	34.54	27.63
462	69	8.5	51.76	11.54	36.70	23.95
463	80	5.7	51.15	14.50	34.35	29.70
464	24	5.7	54.81	11.81	33.38	26.15

TILLETT found further that *o*-nitrotoluene is 2.02-times more reactive than *p*-nitrotoluene in 97% sulfuric acid. The ratios obtained in our experiments are shown in Table V (solvent: 96.5% sulfuric acid).

Table V

Ratio of the reactivity of o-nitrotoluene and p-nitrotoluene

Temperature, °C	$\frac{k_{p-NT}}{k_{NB}}$	$\frac{k_{o-NT}}{k_{NB}}$	$\frac{k_{o-NT}}{k_{p-NT}}$
24	126	234	1.84
69	15.8	30	1.90
80	7.6	17	2.20

An investigation of the dependence of the ratio of the rate constant on the concentration of the aromatic compound showed that in the range investigated the value of this ratio is not influenced, within the limits of experimental error, by the concentrations of the aromatic compounds.

Depending on the sulfuric acid concentration and on temperature, the change of the ratio of the rate constants of *p*-nitrotoluene and *p*-nitroethylbenzene and that of nitrobenzene and *p*-nitrochlorobenzene has the same character as in the case of *p*-nitrotoluene and nitrobenzene (Tables VI and VII).

Table VI

Effect of the change in temperature and sulfuric acid concentration on the ratio of the rate constants of nitration of p-nitrotoluene and p-nitroethylbenzene

°C	DVS	3	3.5	4.5	8.56
	H_2SO_4 %	75.0	77.5	82.0	89.60
24		2.33	2.18	1.16	1.81
69		2.08	1.81	1.00	1.49
80		1.70	1.65	1.00	1.00

Table VII

Effect of the change in temperature and sulfuric acid concentration on the ratio of the rate constants of nitration of nitrobenzene and p-nitrochlorobenzene

°C	DVS	4.5	5.67	7.0	17.7
	H_2SO_4 %	82.0	85.0	87.5	93.0
24		14.9	13.8	11.4	13.2
69		9.5	8.35	7.3	8.4
80		8.5	7.7	6.5	6.65

In the nitration of toluene–benzene mixture, the change of the ratio of the rate constants shows regularities similar to the results contained in Table VIII.

Table VIII

Effect of the change in temperature and sulfuric acid concentration on the ratio of the rate constants of nitration of toluene and benzene

°C	DVS	1.8	2.4	3.0
	H_2SO_4 %	64.3	71.0	75.0
25		unmeasurable, owing to poor solubility		1.24
40		4.1	2.0	1.15
50		3.5	1.55	1.07
60		2.78	1.24	1.03

In the isomer distribution of nitrotoluene, no dependence on the sulfuric acid concentration or on temperature can be observed (the average isomer distribution is 59—60% *o*-nitrotoluene, 36—37% *p*-nitrotoluene, and 2—5% *m*-nitrotoluene). In both mononitration and dinitration, the isomer distribution is very slightly dependent on, or independent of, the reaction temperature, contrary to sulfonation, where the temperature often influences the quantity of the isomers formed.

With the pairs of compounds investigated, a decrease in the rate ratios can be observed on increasing the absolute nitration rate. Therefore, it seems justified to raise the question, whether this effect may be due to some 'non-kinetic' factor. In this case, notwithstanding the homogeneous reaction mixture, this 'non-kinetic' factor can be due to inadequate mixing. Indeed, if the nitrating acid is not mixed into the reaction mixture after addition, a local temporary deficiency in the more reactive compound may occur. If the time required for the meeting of the more reactive compound and the nitrating agent is larger than the reaction rate of the less reactive partner, the relative rate will be of necessity smaller than the true value.

The batch experiments shown in Table IX illustrate extreme cases, where the nitrations of *p*-nitrotoluene–nitrobenzene and *o*-nitrotoluene–nitrobenzene are compared under heterogeneous and homogeneous conditions at various speeds of the stirrer.

Table IX

The effect of the intensity of stirring on the ratio of the rate constants in batch nitration experiments

Experiment, No.	Temperature, °C	DVS	Reaction conditions				Speed of the stirrer, rpm
			homogeneous		heterogeneous		
			$\frac{k_{p-NT}}{k_{NB}}$	$\frac{k_{o-NT}}{k_{NB}}$	$\frac{k_{p-NT}}{k_{NB}}$	$\frac{k_{o-NT}}{k_{NB}}$	
E 206	69	4.5	119	—	—	—	800
E 207	69	4.5	113	—	—	—	1400
E 217	69	4.5	—	—	3.3	—	without mix.
E 219	69	4.5	—	—	3.7	—	200
E 285	69	8.5	10.8	—	—	—	1400
E 470	69	8.5	10.5	—	—	—	2800
E 282	69	13.7	4.7	—	—	—	1400
E 271	69	13.7	4.3	—	—	—	2800
E 456	69	3.0	—	—	—	11.74	1400
+ E $\frac{316}{317}$	69	3.0	—	448	—	—	1400
E 457	69	7.0	—	—	—	2.09	1400
E 323	69	7.0	—	86	—	—	1400
E 458	24	7.0	—	—	—	2.91	1400
E 309	24	7.0	—	243	—	—	1400

It can be seen that the ratio of the rate constants obtained under heterogeneous conditions is for both pairs of compounds considerably lower than in homogeneous solution, that is to say, hindrance of diffusion has played an important role. On the other hand, in the nitrations carried out in homogeneous phase, the ratio of the rate constants remained unchanged when the speed of the stirrer was doubled; it follows that a speed of 1400 rpm has been sufficient. These experimental results prove that the decrease in the ratio of the rate constants was not due to the 'non-kinetic' factor mentioned.

Competitive nitration in glacial acetic acid and in acetic anhydride solutions

When the pair toluene–benzene is nitrated in acetic anhydride and glacial acetic acid solutions, the ratio of the rate constants varies between 22.0 and 38.0, depending on the solvent used [27]. The value of 27.4 obtained

in acetic anhydride is in good agreement with the value 27 measured by INGOLD [4]. The value of about 35, obtained in glacial acetic acid at 24 °C, agrees with the result given by SUHR [11] for nitromethane solution. The addition of acetyl chloride to the reaction mixture containing acetic anhydride does not produce substantial changes in the value of the ratio of the rate constants, as can be seen from Table X.

Table X

Ratio of the rate constants for the competitive batch nitration of a toluene–benzene mixture in glacial acetic acid and in acetic anhydride solution

Molar ratio, nitrating agent–hydrocarbon: 0.45

Exp. No.	Solvent	Temperature, °C	Composition of the product, mole-%				Conversion, %		$\frac{k_T}{k_B}$
			B	T	NB	*o*-NT + *o*-NT	B	T	
427/1	AcOH	24	48.26	14.35	1.74	35.65	3.48	71.3	35.2
427/2	AcOH	24	48.50	17.80	1.50	32.20	3.00	64.4	34.1
427/3	AcOH	24	48.56	18.36	1.44	31.65	2.88	63.3	34.2
428/1	AcOH	45	48.55	16.52	1.45	33.48	2.90	67.1	37.6
428/2	AcOH	45	48.82	19.95	1.18	30.05	2.36	60.1	38.4
428/3	AcOH	45	48.56	16.48	1.44	33.52	2.88	67.2	38.0
433	Ac_2O+AcOH	30	47.55	17.00	2.45	33.00	4.90	66.0	21.4
434	Ac_2O+AcOH	45	47.72	18.25	2.28	31.75	4.56	63.5	21.6
435	Ac_2O+5 v/v% AcCl	30	48.16	18.80	1.84	31.20	3.68	62.4	26.0
436	Ac_2O	30	46.95	8.90	3.05	41.10	6.01	82.2	27.4

The difference between the ratio of the rate constants found in acetic anhydride or glacial acid medium on the one hand, and in sulfuric acid solution on the other, prompted us to carry out a series of experiments in which various amounts of sulfuric acid were added to the acetic anhydride solvent. As little as 0.4% of sulfuric acid reduced the ratio of the rate constants to 10.5, and this value decreased to 1.09, when the concentration of sulfuric acid was increased in the solvent, as shown in Table XI.

These experiments prove again that the concentration of sulfuric acid in the solvent is of decisive importance from the viewpoint of reactivity.

In the experimental series mentioned above, consideration was given to the observation of FISCHER *et al.* [28, 29], according to which aromatic hydrocarbons containing a side-chain undergo besides nitration a so-called acetoxidation reaction, if acetyl nitrate is used as the nitrating agent in acetic anhydride medium. Thus, in the nitration of toluene, *p*-cresol acetate can be detected besides the nitrotoluene isomers; *p*-cresol acetate was found only in acetic anhydride medium, in an amount of 1—2%, referred to nitrotoluene.

Table XI

Competitive batch nitration of toluene and benzene in acetic anhydride solutions containing various amounts of sulfuric acid

Molar ratio, nitrating agent–hydrocarbon: 0.42

Exp. No.	% H_2SO_4 in the solvent	Temperature, °C	Composition of the product, mole-%				Conversion, %		$\frac{k_T}{k_B}$
			B	T	NB	NT	B	T	
442	48.0	30	34.2	33.0	15.8	17.0	31.6	34.0	1.09
443	30.0	30	21.2	12.5	28.8	37.5	57.6	75.0	1.61
444	23.0	30	34.2	6.8	15.8	43.2	31.6	86.6	5.25
445	8.0	30	41.9	10.4	8.1	39.6	16.2	79.3	9.0
446	4.0	30	43.65	14.0	6.35	36.0	12.7	72.2	9.5
447	0.4	30	47.18	26.95	2.82	23.05	5.64	46.0	10.5

Experiments were carried out for the comparison of the rates of mono- and dinitration reactions. A 1 : 1 molar mixture of benzene and *p*-nitrotoluene was nitrated in an acetic anhydride–glacial acetic acid solution. The values obtained for the rate constant ratios can be regarded only as semi-quantitative. As can be seen from Table XII, benzene is 1500—1970-times more reactive than *p*-nitrotoluene.

Table XII

Competitive nitration of a benzene–nitrotoluene mixture in 1:1 solution of acetic anhydride and glacial acetic acid

Experiment, No.	Temperature, °C	Composition of the product, mole-%				Conversion, %		$\frac{k_B}{k_{NT}}$
		B	*p*-NT	NB	2,4-DNT	B	*p*-NT	
417	20	25.50	49.98	24.50	0.02	49.0	0.04	1620
414	30	26.00	49.98	24.00	0.02	48.0	0.04	1578
418	30	25.90	49.98	24.10	0.02	48.2	0.04	1590
416	45	22.10	49.98	27.90	0.02	55.8	0.04	1970
419	45	22.60	49.98	27.40	0.02	54.8	0.04	1920

No conversion of nitrobenzene could be detected when a mixture of *p*-nitrotoluene and nitrobenzene was allowed to react with nitric acid in acetic anhydride. When the same mixture was treated with a 2 : 1 v/v mixture of Ac_2O—H_2SO_4, both hydrocarbons were nitrated. A ratio of the rate constants round 100 can be taken in the temperature range from 20 to 69 °C (Table XIII). If this ratio is compared with the average ratio of 1800 obtained for the mixture benzene–*p*-nitrotoluene, it appears that the nitration of benzene proceeds $1.8 \cdot 10^{-5}$ times quicker than that of nitrobenzene.

Table XIII

Competitive batch nitration of p-nitrotoluene and nitrobenzene in 2 : 1 v/v Ac_2O–H_2SO_4 *solution*

Nitrating agent: acetyl nitrate; nitrating agent—hydrocarbon molar ratio: 0.45

Experiment, No.	Temperature, °C	Composition of the product, mole-%				Conversion, %		$\frac{k_{NT}}{k_{NB}}$
		NB	NT	DNB	2,4-DNT	NB	*p*-NT	
401	20	49.97	47.34	0.03	2.66	0.06	5.33	88.0
402	30	49.81	36.40	0.16	13.60	0.32	27.20	97.8
403	45	49.72	29.00	0.28	21.00	0.56	42.00	98.0
404	69	49.80	19.90	0.40	30.10	0.80	60.20	114.0
408*	30	49.98	48.62	0.32	1.38	0.04	2.76	67.6

* The Ac_2O solvent contained 0.5% of H_2SO_4

Experimental method

The experiments were carried out in a 250-ml three-necked flask, equipped with a thermometer, a separatory funnel and an agitator.

A 1 : 1 molar mixture of the hydrocarbons to be nitrated (0.0092 mole) was poured into the flask, and sulfuric acid of the required concentration (150 g) was added, using one part of it for washing quantitatively the starting nitro compounds from the weighing bottle into the flask. The mixture was homogenized by stirring, and after it had attained the required temperature, nitrating acid containing 0.0041—0.0045 mole of nitric acid was added. These nitrating acids contained 5% of nitric acid, and their DVS values corresponded to the apparent DVS value of the sulfuric acid used as solvent. The reaction time sufficient to attain optimum conversion varied between 10 and 45 minutes, depending on the sulfuric acid concentration and temperature. The mixture was then poured into a flask containing about 80 g of ice and cooled externally with ice. Next, the acidity of the solution was reduced by the addition of 30% sodium hydroxide solution. This was necessary in order to decrease the solubility of the nitro compounds.

Table XIV

Composition of the mixed acids used for competitive nitration

DVS	Composition of the acid						Initial NO_2^+ concentration g-mole/1000 g	NO_2^+ concentration at 50% conversion g-mole/1000 g
	H_2SO_4		HNO_3		H_2O			
	%	mole-%	%	mole-%	%	mole-%		
1.8	62.00	24.30	5.00	3.42	33.0	72.20	—	—
2.4	68.00	30.50	5.00	3.495	27.0	66.00	—	—
3.0	72.30	35.50	5.00	3.82	22.7	60.75	—	—
3.5	75.00	39.10	5.00	4.06	20.0	56.80	—	—
4.4	78.30	44.50	5.32	4.71	16.38	50.75	—	—
4.5	78.90	45.25	5.00	4.46	16.1	50.40	—	—
5.7	82.00	50.90	5.00	4.86	13.0	44.25	0.14	0.080
7.0	84.30	56.00	5.00	5.16	10.7	38.80	0.34	0.235
8.5	86.30	60.90	5.00	5.49	8.7	33.50	0.48	0.350
13.7	89.90	71.80	5.00	6.21	5.1	22.15	0.70	0.460
27.5	93.00	83.30	5.00	6.97	2.0	9.76	0.90	0.485

The mixture was then transferred into a separatory funnel, and shaken with chloroform to extract the aromatic hydrocarbons (in the case of the toluene–benzene mixture, ether was used for the extraction). The adequacy of product processing and the completeness of the extraction were verified experimentally. The combined extracts were dried overnight with anhydrous calcium chloride, and analyzed on a gas chromatograph Carlo Erba Model Fractovap C.

The ratio of the relative rate constants was calculated by means of the following equation [4, 5, 6]:

$$\frac{k_T}{k_B} = \frac{\log \frac{x_0}{x_v}}{\log \frac{y_0}{y_v}}$$

where:

x_0, y_0 = concentrations of the hydrocarbons to be nitrated, in mole-%,
x_v, y_v = concentrations of the unreacted hydrocarbons, in mole-%.

The values listed in the tables represent average values of two, if necessary of three, parallel experiments. The composition of the nitrating acids used in the experiments is given in Table XIV.

REFERENCES

1. UJHIDY, A., BABOS, B., HEIL, B., MARKÓ, L.: Conference on Some Aspects of Physical Chemistry, Vol. 2, pp. 179—187. Budapest, April 25—27, 1966
2. FRANCIS, A. W.: J. Am. Chem. Soc. **48,** 655 (1926)
3. DEWAR, M. J. S., MOLE, T., WARFORD, E. W. T.: J. Chem. Soc. **1950,** 2400
4. INGOLD, C. K., SHAW, F. R.: J. Chem. Soc. **1927,** 2918
5. INGOLD, C. K., LAPWORTH, A., ROTHSTEIN, E., WARD, D.: J. Chem. Soc. **1931,** 1959
6. BIRD, M. L., INGOLD, C. K.: J. Chem. Soc. **1938,** 918
7. BORDWELL, F. G., ROHDE, K.: J. Am. Chem. Soc. **70,** 1191 (1948)
8. INGOLD, C. K., SMITH, M. S.: J. Chem. Soc. **1938,** 905
9. KNOWLES, J. R., NORMAN, R. O. C., RADDA, G. E.: J. Chem. Soc. **1960,** 4885
10. STOCK, L. M.: J. Org. Chem. **26,** 4120 (1961)
11. SUHR, H., ZOLLINGER, H.: Helv. Chim. Acta **44,** 1011 (1961)
12. TILLETT, J. G.: J. Chem. Soc. **1962,** 5142
13. BRAND, J. C. D., PATTON, L. T.: J. Chem. Soc. **1952,** 281
14. BONNER, T. C., JAMES, M. E., LOWER, A. M., WILLIAMS, G.: Nature **163,** 955 (1949)
15. OLÁH, G., KUHN, J. S., MLINKO, A.: J. Chem. Soc. **1956,** 4257
16. KUHN, J. S., OLÁH, G. A.: J. Am. Chem. Soc. **83,** 4564 (1961)
17. OLÁH, G. A., KUHN, J. S., FLOOD, S. H.: J. Am. Chem. Soc. **83,** 4571 (1961)
18. OLÁH, G. A., KUHN, J. S., FLOOD, S. H.: J. Am. Chem. Soc. **83,** 4581 (1961)
19. OLÁH, G. A., KUHN, J. S.: J. Am. Chem. Soc. **84,** 3684 (1962)
20. OLÁH, G. A., KUHN, J. S., FLOOD, S. H., EVANS, J. C.: J. Am. Chem. Soc. **84,** 3687 (1962)
21. OLÁH, G. A., KUHN, J. S.: J. Am. Chem. Soc. **86,** 1067 (1964)
22. TÖLGYESI, W. S.: Can. J. Chem. **43,** 343 (1965)
23. SPINDLER, P.: Ber. **16,** 1252 (1883)
24. SUEN, T. J.: Mass. Inst. Tech. Sc. D. thesis, 1937
25. UJHIDY, A., BABOS, B., HEIL, B.: Vegyészkonferencia kiadványa, p. 130. Publication of the Conference of the Hungarian Chemical Society, Pécs, 1967
26. TAKÁCS, J.: Diploma thesis, 1966
27. RÉPÁSY, O.: Diploma thesis, 1965
28. FISCHER, A., PACKER, J., VAUGHAN, J., WRIGHT, G. J.: J. Chem. Soc. **1964,** 3587
29. FISCHER, A., READ, A. J., VAUGHAN, J.: J. Chem. Soc. **1964,** 3691

Aurél UJHIDY, József TAKÁCS — Veszprém, Schönherz Z. u. 10, Hungary.

Ottó RÉPÁSY — Veszprém, Wartha V. u. 2/6, Hungary.

Acta Chimica Academiae Scientiarum Hungaricae, Tomus 69 (3), pp. 361—366 (1971)

THE USE OF AMIDE CHLORIDES IN RING CLOSURE REACTIONS, III

SYNTHESIS AND RING CLOSURE OF NOVEL AMIDRAZONES

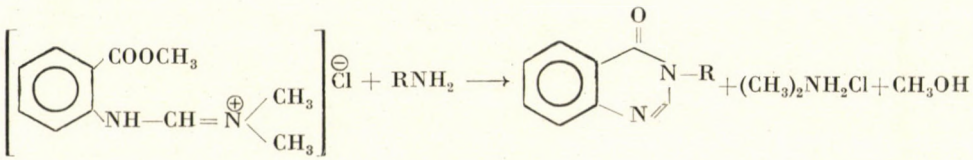
Z. CSŰRÖS, R. SOÓS, I. BITTER and J. PÁLINKÁS

(Department of Organic Chemical Technology, Technical University, Budapest)

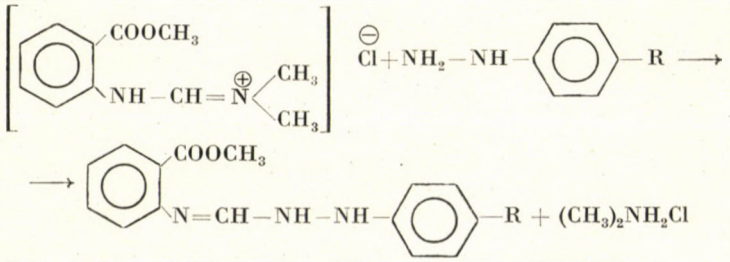
Received April 19, 1970

N,N-dimethyl-*N'*-(2-carbomethoxyphenyl)formamidine hydrochloride has been prepared from anthranilic acid mehyl ester and dimethylformamide hydrochloride. This amidine was reacted with 4-substituted phenylhydrazines to produce N_1-(4-R-phenyl)-N_3-(2-carbomethoxyphenyl)formamidrazones. The formation of 3-[N_1-(4-R-phenyl)amino]-4(3H)-quinazolines through ring closure in the amidrazones has been studied.

In a former communication [1] we reported a new synthesis of 4(3H)-quinazoline derivatives. This method proved suitable for the synthesis of 4(3H)-thieno (2,3-d)-pyrimidones [2], too. From aromatic or heteroaromatic *o*-amino-carboxylic acid derivatives and amide chlorides we prepared trisubstituted amidines which were converted by cyclization into condensed pyrimidones.



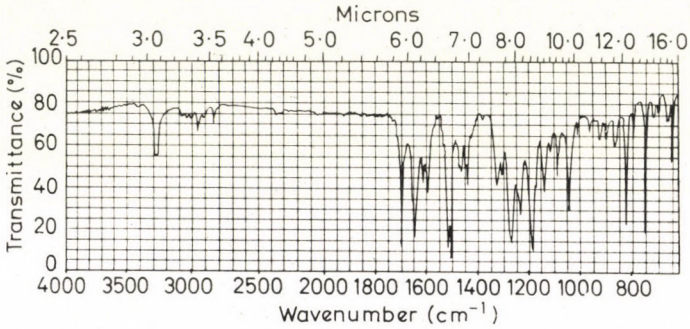
The amidine base, assumed to be an intermediate, could not be isolated. However, we succeeded in the isolation of the intermediate of the ring closure reaction with phenylhydrazine: N_1-phenyl-N_3-(2-carbomethoxyphenyl)form-amidrazone. Since this offered a possibility for elucidating the reaction mechanism, the ring closure was attempted also with other 4-R-phenyl-hydrazines. Using this method of synthesis, 7 different formamidrazones have been prepared.



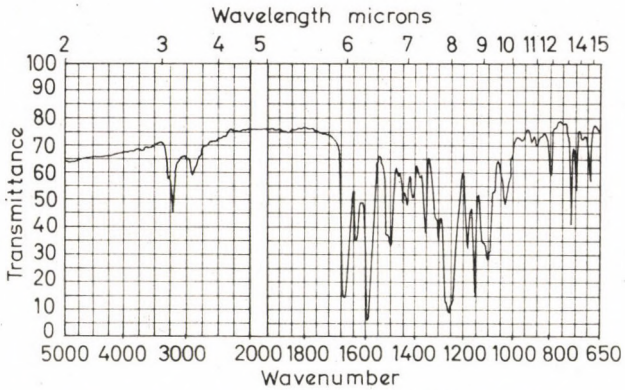
where R = —H, —CH_3, —OCH_3, —Cl, —NO_2, —COOH, —$COOC_2H_5$

Equimolar amounts of the components were brought together and kept at room temperature in methanol.

We have found the reaction rate to be dependent on the nature of substituent R. Electron donor substituents which enhance the basicity of phenylhydrazine accelerate, while electron acceptors retard the reaction. In the first case a few minutes suffice, in the second several hours are needed to complete the reaction and to precipitate the product.



Spectrum 1. IR spectrum of N_1-(4-methoxyphenyl)-N_3-(2-carbomethoxyphenyl)formamidrazone



Spectrum 2. IR spectrum of N_1-(4-carbethoxyphenyl)-N_3-(2-carbomethoxyphenyl)formamidrazone

The compounds thus produced are coloured ranging from pale yellow to dark red. Most of these compounds are rather unstable: the methyl, methoxy and chloro derivatives decompose within a few hours, the others within a few days. Only the nitro and the carboxyl compounds are stable.

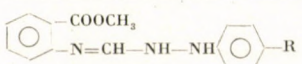
Also the hydrochloric salts of the formamidrazones have been prepared: the chloride content of these was determined by titration with silver nitrate; the amounts calculated and found were in good agreement.

The formamidrazones were identified by elemental analysis and infrared spectroscopy. The IR spectra of two typical derivatives are given here.

All formamidrazones synthesized here show two intense bands between 1640 and 1700 cm^{-1}. The >C=O band of the carbomethoxy group is found between 1693 and 1699 cm^{-1}, the absorption of the >C=N-bond occurs at 1643 and 1648 cm^{-1}. Upon salt formation the latter is shifted towards higher wave-numbers. In the infrared spectrum of the hydrochloride of N_1-phenyl-N_3-(2-carbomethoxyphenyl)formamidrazone absorption by the >C=N bond is shifted to 1680 cm^{-1}. The stretching vibration bands of the two NH groups present in the compound are in the 3200—3300 cm^{-1} range, sometimes these bands overlap.

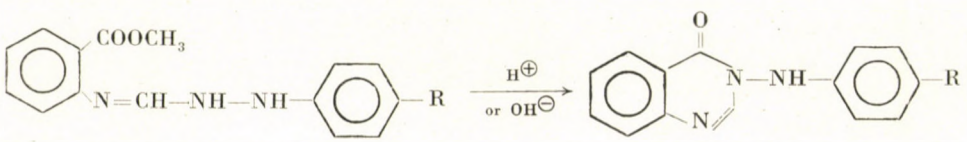
Table I contains the most important data about these compounds and the wave-numbers of the >C=N- and the ester carbonyl group.

Table I

	Method	M. p. (°C)	Yield %	>C=O cm^{-1}	>C=N— cm^{-1}
R = —H	a	105—108 (decomp.)	88.2	1699	1648
R = —CH_3	a	98—103 (decomp.)	90.1	1693	1645
R = —OCH_3	a	92—97 (decomp.)	86.9	1699	1647
R = —Cl	a	103—107 (decomp.)	91.7	1693	1645
R = —NO_2	b	153—161 (decomp.)	98.7	1696	1643
R = —COOH	b	271—272 (decomp.)	94.2	1693	1646
R = —$COOC_2H_5$	b	173—176 (decomp.)	91.3	1695	1643

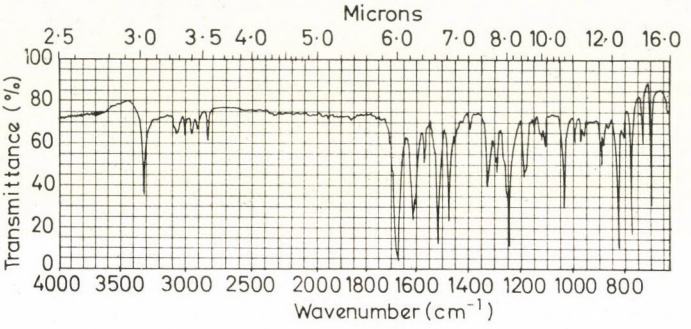
In our first communication dealing with this subject [1] we reported that no ring closure of N_1-phenyl-N_3-(2-carbomethoxyphenyl)formamidrazone can be brought about even by boiling its solution in absolute alcohol for several hours. However, in the presence of an acid-type catalyst, ring closure in the dimethylamine hydrochloride obtained as a by-product of the reaction could be effected by boiling for a short time.

Ring closure was accomplished also in the formamidrazone compounds described.

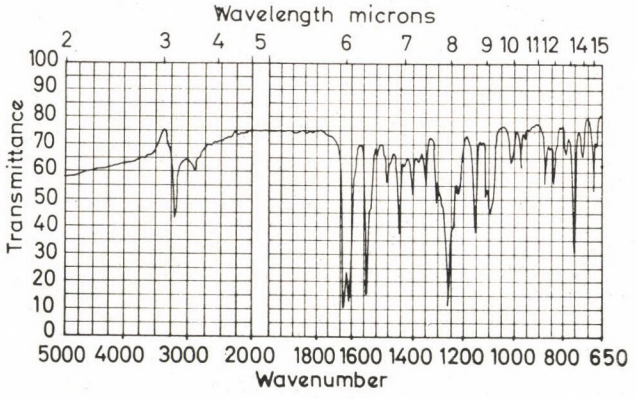


In the presence of an equimolar quantity of dimethylamine hydrochloride, the amidrazones were boiled in absolute alcohol. We found that, as in the case of hydrazinolyses, the rate of ring closure depends strongly on the nature of substituent R. While first order substituents increased the reaction rate,

second order substituents retarded the reaction. 30 minutes were needed for ring closure in the case of R = methyl and methoxy, one hour was required if R = H and Cl, and boiling for 4 to 6 hours was necessary in the case of R = COOH and $COOC_2H_5$. Solubility problems added to the difficulty of the cyclization of the nitro derivative: its suspension in alcohol had to be kept boiling for 10 to 12 hours in order to effect reaction.



Spectrum 3. IR spectrum of 3-[*N*-(4-methoxyphenyl)amino]-4(3H)-quinazolinone



Spectrum 4. IR spectrum of 3-[*N*-(4-carbethoxyphenyl)amino]-4(3H)-quinazolinone

If we tried to help ring closure with protonic catalysts stronger than dimethylamine hydrochloride, which form salts with the formamidrazones, reaction was slowed down or stopped altogether. In a hydrochloric acid medium no ring closure occurred even after boiling for several hours.

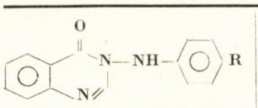
On the other hand, basic catalysts strongly accelerated the reaction. The carbethoxy derivative, for instance, formed a ring within a few minutes when some 0.1 *N* sodium hydroxide was added to its hot alcoholic solution.

Our studies have led to the conclusion that the reaction rate depends upon the basicity of the nitrogen at position 2 (N_2), and that bases and weak acids act as catalysts. The infrared spectra of the cyclic derivatives are shown here.

Comparison with the corresponding formamidrazone spectra demonstrates that the bands assigned to the >C=N— bond, to one of the NH groups, and to the carbethoxy group are absent and the maxima characteristic of the 4(3H)-quinazolines appear [1].

In Table II are listed the most important data for the 3-[*N*-(4-R-phenyl)amino]-4(3H)-quinazolines; the methods used for the synthesis of these compounds are also indicated.

Table II

	Method	M. p. (°C)	Yield %	Analysis					
				Calculated			Found		
				C %	H %	N %	C %	H %	N %
R = —H	c	168—170	93.1	70.89	4.64	17.72	70.92	4.61	17.75
R = —Cl	c	193—194	94.2	61.87	3.68	15.46	61.95	3.87	15.41
R = —CH_3	d	141—143	90.9	71.71	5.17	16.73	71.60	5.02	16.70
R = —OCH_3	d	157—159	91.4	64.98	4.69	15.16	70.09	4.65	15.37
R = —COOH	e	198—201	94.1	64.05	3.91	14.94	63.92	4.90	13.56
R = —$COOC_2H_5$	e	165—166	90.5	66.01	4.85	13.59	66.11	4.90	13.50
R = —NO_2	f	197—216	98.1	59.58	3.54	19.85	59.62	3.21	19.54

Identification was carried out by elemental analysis, occasionally by the determination of melting points, and by infrared spectroscopy. IR spectra were recorded in KBr pellets on a Perkin-Elmer Type 237 and a Unicam SP 200 instrument.

Experimental

1) N,N-dimethyl-N'-(2-carbomethoxyphenyl)formamidine hydrochloride [1]

2) p subst. phenylhydrazine

The following phenylhydrazines substituted at position 4 were prepared from the corresponding aromatic amines by diazotization and subsequent reduction of the diazonium salt:

a) *p*-tolylhydrazine [3],
b) 4-methoxyphenylhydrazine [4],
c) 4-chlorophenylhydrazine [5],
d) 4-carboxyphenylhydrazine [6],
e) carbethoxyphenylhydrazine [7],

4-Carbethoxyphenylhydrazine was prepared from the carboxyl derivative through esterification with ethanol in the presence of sulfuric acid as the catalyst.

These phenylhydrazines are rather easily decomposed; for a longer time only their salts can be stored, consequently the bases were set free immediately before use. Due to this instability, the elemental analyses of formamidrazones could not be carried out.

3) N_1-(4-methoxyphenyl)-N_3(2-carbomethoxyphenyl)formamidrazone (a)

N-*N*-dimethyl-*N'*-(2-carbomethoxyphenyl)formamidine hydrochloride (24.25 g, 0.1 mole) is dissolved in methanol (100 ml) and mixed with 4-methoxyphenylhydrazine (13.8 g, 0.1 mole). After standing for 10 minutes the yellow precipitate is collected on a filter, rinsed with some alcohol, and dried. Yield 24.1 g (86.9%), m. p. 92—97 °C (decomp.).

4) N_1-(4-carbethoxyphenyl)-N_3-(2-carbomethoxyphenyl)-formamidrazone (b)

N,*N*-dimethyl-*N*'-(2-carbomethoxyphenyl)-formamidine hydrochloride (24.25 g, 0.1 mole), dissolved in methanol (100 ml) is mixed with 4-carbethoxyphenylhydrazine (18.9 g, 0.1 mole). After standing for 4 hours the pale yellow precipitate produced is collected by filtration, washed with some alcohol, and dried. Yield 31.1 g (91.3%), m. p. 173—176 °C (decomp.).

5) 3-[N-(4-chlorophenyl)-amino]-4(3H)-quinazolinone (c)

N_1-(4-chlorophenyl)N_3-(2-carbomethoxyphenyl)-formamidrazone (30.35 g, 0.1 mole) dissolved in hot methanol (100 ml) is mixed with dimethylamine hydrochloride (8.15 g, 0.1 mole), refluxed for one hour, and then cooled. The white precipitate is filtered off, washed with some alcohol, and dried. Yield 25.55 g (94.2%), m. p. 193—194 °C.

Processes (d) and (e) were the same as that described in (c). The reaction time for (d) was 1/2 hour and for (e) six hours.

6) 3-[N-(4-nitrophenyl)amino]-4(3H)-quinazolinone (f)

Dimethylamine hydrochloride (8.15 g, 0.1 mole) in methanol (500 ml) is mixed with finely powdered N_1-(4-nitrophenyl)-N_3(2-carbomethoxyphenyl)formamidrazone (31.4 g, 0.1 mole). The resulting suspension is boiled for 12 hours under stirring to produce a yellow precipitate which is filtered after cooling, washed repeatedly with alcohol, and dried. Yield 27.7 g (98.1%), m. p. 197—216 °C.

REFERENCES

1. CSŰRÖS, Z., SOÓS, R., PÁLINKÁS, J., BITTER, I.: Acta Chim. Acad. Sci. Hung. **63**, 215 (1970)
2. CSŰRÖS, Z., SOÓS, R., PÁLINKÁS, J., BITTER, I.: Acta Chim. Acad. Sci. Hung. (In press)
3. FISCHER, E.: Ber. **9**, 890 (1876)
4. ALTSCHUL, J.: Ber. **25**, 1849 (1892)
5. WILLGERADT, C., BÖHM, A.: J. Prakt. Chem. **43**, 482 (1891)
6. FISCHER, E.: Ann. **212**, 337 (1882)
7. HELLER, G.: J. Prakt. Chem. (2) **111**, 371 (1925)

Zoltán CSŰRÖS
Rudolf SOÓS
István BITTER
János PÁLINKÁS
Budapest XI., Műegyetem-rkp. 3.

Acta Chimica Academiae Scientiarum Hungaricae, Tomus 69 (3). pp. 367—371 (1971)

КАРБОЛИНЫ, II

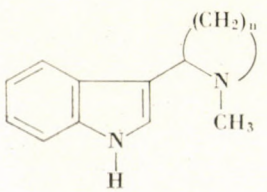
ПОЛНЫЙ СИНТЕЗ АЛКАЛОИДА БРЕВИКАРИНА И ЕГО НИЗШЕГО ГОМОЛОГА

К. И. КУЧКОВА, А. А. СЕМЕНОВ и И. В. ТЕРЕНТЬЕВА
(Институт химии АН Молд. ССР, Кишинев, СССР)

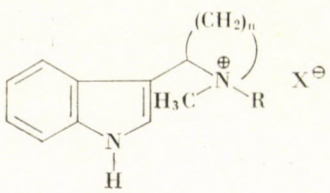
Поступило: 8. V. 1970 г.

Реакцией четвертичной соли пиперидилиндола III с калиевым производным бензилсульфинилацетона и последующим расщеплением образовавшегося β-кетосульфоксида получен аминокетон VI. Оксим этого кетона циклизован в 3,4-дигидро-β-карболин XI, который при дегидрировании дал продукт XIII, идентичный природному алкалоиду бревикарину. По аналогичной схеме из пирролидилиндола II получен низший гомолог бревикарина XIV.

Для алкалоида бревикарина, выделенного из Carex brevicollis CD была предложена структура 1-метил-4(ω-метиламинобутил)-β-карболина (XIII) (1). В настоящем сообщении мы описываем полный синтез этого природного продукта, а также его низшего гомолога — 1-метил-4-(ω-диметиламинопропил)-β-карболина (XIV).



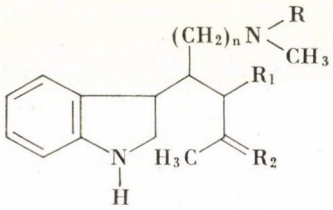
I n = 4
II n = 3



III R = $CH_2C_6H_5$, X = Br, n = 4
IV R = CH_3, X = J, n = 3

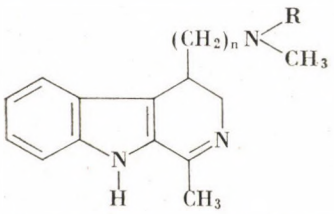
Пиперидилиндол 1, полученный из индола и 1-метилпиперидона-2 по (4), обработкой бромистым бензилом в теплом нитрометане был превращен в бромбензилат III. Как аналог четвертичной соли грамина III, реагируя с калиевым производным бензилсульфинилацетона по (2), образовал β-кетосульфоксид V, который без очистки обработали амальгамированным алюминием в водном тетрагидрофуране и получили аминокетон VI. Это жидкое вещество давало аморфный динитрофенилгидразон, который охарактеризован в виде перхлората, кристаллизующегося с одной молекулой бензола. При перемешивании метанольного раствора кетона VI с солянокислым гидроксиламином и гидроокисью бария получили оксим VII. По методу, описанному в первом сообщении этой серии (3), VII обработали теплым

раствором пятихлористого фосфора в нитробензоле. При этом происходила бекмановская перегруппировка с одновременной циклизацией в 3,4-дигидро-β-карболин XI, который выделен и охарактеризован в виде дипикрата. Для дегидрирования гидрохлорид XI перемешивали с палладиевой чернью в горячем этиленгликоле, причем ароматизация дигидропиридинового цикла сопровождалась отщеплением защитной бензильной группы. Подобное сочетание гидрогенолиза с дегидрированием отмечалось ранее в работе (5). Полученное в результате этих реакций основание XIII и его дигидрохлорид по данным ИК- и масс-спектрометрии, а также по температурам плавления смешанных проб, полностью идентичны природному алкалоиду беревикарину и его хлористоводородной соли.

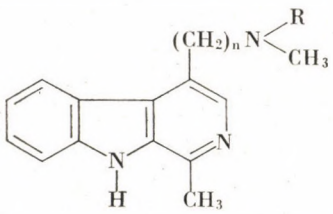


V–VIII n = 4, R = $CH_2C_6H_5$, **V** R_1 = $SOCH_2C_6H_5$, R_2 = O, **VI** R_1 = H, R_2 = O, **VII** R_1 = H, R_2 = NOH

VIII–X n = 3, R = CH_3, **VIII** R_1 = $SOCH_2C_6H_5$, R_2 = O, **IX** R_1 = H, R_2 = O, **X** R_1 = H, R_2 = NOH



XI n = 4, R = $CH_2C_6H_5$, **XII** n = 3, R = CH_3,



XIII n = 4, R = H, **XIV** n = 3, R = CH_3

Низший гомолог бревикарина XIV синтезирован по аналогичной схеме. Пирролидинилиндол II (6) перевели в йодметилат IV и конденсировали с калиевым производным бензилсульфинилацетона. Кристаллический кетосульфоксид VIII реакцией с алюминием в тетрагидрофуране превратили в кетон IX, оксим которого подвергли бекмановской перегруппировке и циклизации. Образовавшийся при этом 3,4-дигидро-β-карболин XII дегидрировали в XIV, выделенный и охарактеризованный в форме дипикрата и дигидрохлорида.

Экспериментальная часть

Все температуры плавления определены на приборе Кофлера и неисправлены. ИК-спектры сняты на приборе UR-10 в таблетках KBr, УФ-спектр — в спирте на спектрофотометре СФ-4. Масс-спектр получен на приборе МХ-1303 с системой ввода непосредственно в ионный источник при температуре ионизационной камеры 150° и ионизационном излучении 70 eV.

Бромбензилат 3-(1-метилпиперидил-2) индола (III)

К 8,79 г (41 ммол) I в 14 мл нитрометана при охлаждении и перемешивании за 15 мин. приливают 7,2 г (0,51 ммол) бромистого бензила в 12,4 мл нитрометана. При нагревании на теплой бане выпадают кристаллы, которые отфильтровывают и промывают спиртом. Из маточника добавлением эфира осаждают еще некоторое количество вещества, которое объединяют с основной порцией. Перекристаллизацией из спирта, подкисленного уксусной кислотой, получают 11,42 г III с температурой плавления 138—139°. Выход 72,2%. $C_{21}H_{25}N_2Br \cdot 1/2\ H_2O$. Вычислено: C 63,95; H 6,67; N 7,10; Br 20,26. Найдено: C 63,98; H 6,90; N 7,04; Br 20,34. ИК-спектр, $см^{-1}$: 3415(NH), 3500(H_2O).

8-Метилбензиламино-4-(индолил-3)-октанон-2 (VI)

0,59 г (5,26 ммол) трет-бутилата калия и 1,03 г (5,26 ммол) бензилсульфинилацетона в 10 мл безводного диметилсульфоксида перемешивают до образования прозрачного раствора и затем несколькими порциями присыпают 2,03 г (5,26 ммол) III. Раствор выдерживают 2,25 часа при комнатной температуре, выливают в 100 мл воды и экстрагируют эфиром. Экстракт промывают водой, сушат слуьфатом натрия и упаривают досуха. Получают 1,69 г 8-метилбензиламино-4-(индолил-3)-3-бензилсульфинилоктанона-2 (V). Его растворяют в 101 мл водного тетрагидрофурана (9 : 1) и перемешивают с 0,91 г амальгамированной алюминиевой фольги. Через 1,3 часа реакционную смесь фильтруют, отгоняют тетрагидрофуран, а остаток обрабатывают эфиром. Водный слой отделяют, а эфирный раствор сушат и упаривают в вакууме. Остаток хроматографируют на окиси алюминия III степени активности. Смесью бензола с петролейным эфиром (9 : 1) элюируют 0,82 г (43,6%) VI в виде вязкой жидкости. ИК-спектр, $см^{-1}$: 3430 (NH), 1710 (CO). Перхлорат динитрофенилгидразона, полученного по (7), кристаллизуется из смеси ацетон-бензол с одной молекулой бензола. Т. пл. 126—134°. $C_{30}H_{34}N_6O_4 \cdot HClO_4 \cdot C_6H_6$. Вычислено: C 59,95; H 5,73; N 11,67; Cl 4,91. Найдено: C 59,98; H 5,98; N 11,86; Cl 4,15.

7-Диметиламино-4-(индолил-3)-3-бензилсульфинилгептанон-2 (VIII)

К 9,58 г (48 ммол) II в 48 мл нитрометана добавляют 7,6 мл йодистого метила и через 2 часа упаривают досуха. Полученный йодметилат IV растворяют в 48 мл диметилсульфоксида и за 1 час добавляют к калиевому производному бензилсульфинилацетона (49 ммол) в 48 мл диметилсульфоксида. Через 2,5 часа обрабатывают, как описано для V и получают кристаллический сульфоксид VIII. После перекристаллизации из спирта отфильтровывают 3,95 г (21,6%) бесцветных кристаллов. Т. пл. 162—163°. $C_{24}H_{30}N_2O_2S$. Вычислено: C 70,21; H 7,37; N 6,82; S 7,81. Найдено: C 70,52; H 7,66; N 6,80; S 7,82. ИК-спектр, $см^{-1}$. 3450 (NH), 1700 (CO), 1050 (SO).

7-Диметиламино-4-(индолил-3)-гептанон-2 (IX)

Из 3,7 г VIII аналогично VI получено 1,29 г (53,8%) IX в виде вязкой жидкости. ИК-спектр, $см^{-1}$. 3420 (NH), 1728 (CO). Гидрохлорид динитрофенилгидразона, т. пл. 122—123° (из этанола). $C_{23}H_{28}N_6O_4 \cdot HCl \cdot C_2H_5OH$. Вычислено: C 56,12; H 6,69; N 15,71; Cl 6,63. Найдено: C 35,73; H 6,59; N 15,92; Cl 6,85.

Оксим 8-метилбензиламино-4(индолил-3)-октанона-2 (VII)

0,75 г (2,07 ммол) VI, 0,215 г (3,1 ммол) солянокислого гидроксиламина и 1,9 г (6 ммол) $Ba(OH)_2 \cdot 8H_2O$ в 7,5 мл метилового спирта перемешивают в течение 4 часа, фильтруют, промывают метанолом и фильтрат выливают в 150 мл воды. Выделившийся оксим экстрагируют эфиром, экстракт тщательно промывают водой, высушивают сульфатом натрия и после удаления эфира получают 0,81 г (100%) маслообразного VII.

Для анализа 100 мг продукта хроматографируют на 6 г окиси алюминия (IV степень активности), производя элюирование смесью бензола с эфиром (5 : 1).

$C_{24}H_{31}N_3O$. Вычислено: C 76,35; H 8,28; N 11,13. Найдено: C 76,87; H 8,24; N 11,09%. ИК-спектр, $см^{-1}$: 3430 (NH), 3250 (OH), 1650 (C = N).

Оксим 7-диметиламино-4-(индолил-3)-гептанона-2 (X)

Получен из IX аналогично VII с выходом 63%. Т. пл. 134—135° (из изопропилового спирта).

$C_{17}H_{25}N_3O$. Вычислено: C 71,04; H 8,77; N 14,62. Найдено: C 71,05; H 8,74; N 14,38%

1-Метил-4-(4-метилбензиламинобутил)-3,4-дигидро-β-карболин (XI)

К 6,8 г (32,8 ммол) PCl_5 в 40 мл нитробензола при 65—70° и энергичном перемешивании за 1,5 мин. приливают раствор 4,11 г (10,9 ммол) VII в 41 мл нитробензола и перемешивают еще 0,5 минуты. Затем реакционную смесь быстро охлаждают и разлагают избыток PCl_5, добавляя кусочки льда. Органический слой разбавляют эфиром и экстрагируют несколько раз 5%-ной соляной кислотой. Объединенные кислые экстракты промывают органическим растворителем, подщелачивают и экстрагируют эфиром. Эфирную вытяжку высушивают сульфатом натрия, фильтруют и подкисляют эфирным раствором HCl. Растворитель сливают с маслянистого слоя дигидрохлорида, полученную соль высушивают в вакуум эксикаторе и растворяют в минимальном количестве кипящего изопропилового спирта. При охлаждении окрашенного раствора выпадают кристаллы, которые отфильтровывают и отбрасывают. Фильтрат разбавляют водой, подщелачивают NaOH и извлекают эфиром. Экстракт высушивают и приливают к раствору 5,7 пикриновой кислоты в 600—700 мл эфира. Выпавшие кристаллы отделяют и кристаллизуют из ацетона. Получают 2,5 г дипикрата XI (22,5%) с т. пл. 178—180°.

$C_{24}H_{29}N_3 \cdot 2C_6H_3O(NO_2)_3 \cdot CH_3COCH_3$. Вычислено: C 53,48; H 4,72; N 14,39. Найдено: C 53,76; H 4,57; N 14,50%. ИК-спектр, $см^{-1}$: 3400 (NH), 1700 (CO ацетона), 1630 (C = N), 1570, 1330 (NO_2).

Бревикарин (XIII)

Палладиевый катализатор готовят по Брауну (8), а затем отфильтровывают в атмосфере инертного газа. К раствору 1,42 г аморфного дигидрохлорида XI (получен из дипикрата обычным образом) в 16 мл этиленгликоля добавляют 1,8 г палладия и перемешивают 15 мин. при 155° в атмосфере азота. Затем реакционную смесь охлаждают, фильтруют, разбавляют водой, подщелачивают и экстрагируют хлороформом. Твердое вещество, оставшееся после удаления растворителя, кристаллизуют из ацетона, растворяют в спирте и спиртовый раствор подкисляют эфирным HCl. Выпавшие кристаллы перекристаллизовывают из спирта и получают 0,32 г (27,6%) дигидрохлорида XIII с т. пл. 192—193°. (По литературным данным (1) т. пл. 195—196°). Образец не дает депрессии температуры плавления с хлористоводородной солью природного алкалиода. ИК-спектры природного и синтетического образцов идентичны во всех деталях.

Основание XIII, полученное из дигидрохлорида, имело т. пл. 60° (кристаллогидрат) и 110° (безводное вещество), масс-спектр: m/e: 267 (M^+), 252, 237, 223, 209, 196, 183, 44 (max), 29; что согласуется с лит. данными (1).

1-Метил-4-(3-диметиламинопропил)-β-карболин (XIV)

К перемешиваемому раствору 1,63 г (7,83 ммол) PCl_5 в 7,5 мл нитробензола при 70° за 2—3 минуты приливают раствор 0,75 г (2,61 ммол) X в 7,5 мл нитробензола. Полученный раствор немедленно обрабатывают, как описано для XI и получают 0,48 г сырого дигидрохлорида XII. Эту соль дегидрируют при 155° в течение 1,5 часа аналогично XI и получают 0,24 г сырого основания XIV. Его очищают хроматографированием на 10 г окиси алюминия (IV степени активности), вымывая смесью бензола с эфиром (3 : 7). Получают 105 мг бесцветных кристаллов. Выход 15,2% в расчете на X.

Дипикрат, т. пл. 220—222° (из метанола).

$C_{17}H_{21}N_3 \cdot 2C_6H_3O(NO_2)_3$. Вычислено: C 48,00, H 3,75, N 17,37. Найдено: C 47,67, H 3,71, N 17,06.

Дигидрохлорид, т. пл. 270—271° (из этанола, в запаянном капилляре). ИК-спектр, $см^{-1}$: 3400 (NH), 2650 (=NH), 1645 (C = N). УФ-спектр. λ_{max} ммк(log ε): 250 (4.50), 301 (4.12), 370 (3.06); λ_{min} ммк (log ε): 220 (4.02), 275 (3.62), 320 (3.06).

SUMMARY

By reacting the quaternary salt of piperidylindole (**III**) with the potassium derivative of benzylsulfinylacetone, and by the subsequent decomposition of the β-ketosulfoxide formed, we have prepared aminoketone **VI**. The oxime of this ketone was cyclized to give 3,4-dihydro-β carboline (**XII**) which upon dehydrogenation, afforded product **XIII** identical with the naturally occurring alkaloid brevicarine. In an analogous manner, the lower homologue of brevicarine (**XIV**) has been obtained from pyrrolidylindole (**II**).

ЛИТЕРАТУРА

1. И. В. Терентьева, Г. В. Лазурьевский, Т. И. Ширшова: Хим. природн. соед., *1969*, 397.
2. К. И. Кучкова, А. А. Семенов: Хим. гетероцикл. соед., 1970, 1069.
3. К. И. Кучкова, А. А. Семенов, И. В. Терентьева: Хим. гетероцикл. соед., (в печати).
4. Powers, J.: J. Org. Chem., **30**, 2534 (1965).
5. Buu-Hoi, N. P., Russel, O., Jacquinon, P.: J. Chem. Soc., **1964**, 708.
6. Yongdale, G. A., Anger, D. G. at all: J. Med. Chem., **7**, 415 (1964).
7. Parrick, J., Rasburn, J. W.: Can. J. Chem. **43**, 3453 (1965).
8. Brown, H. C.: Tetrahedron, **22**, suppl. 8, p. 1, 149 (1966).

К. И. Кучкова
А. А. Семенов
И. В. Терентьева

Институт химии АН Молд. ССР, Кишинев, СССР.

Acta Chimica Academiae Scientiarum Hungaricae, Tomus 69 (3), pp. 373—381 (1971)

THERMAL DISSOCIATION OF UREA DERIVATIVES, II

Z. CSŰRÖS, R. SOÓS, I. BITTER, Z. BENDE and M. ECET

(Institute of Organic Chemical Technology, Technical University, Budapest)

Received January 8, 1970; in revised form June 25, 1970

Characteristics of the thermal decomposition of ten different diarylureas were investigated. Kinetic characteristics of the decomposition were calculated by procedures based on thermoanalytical measurements, developed in the last years. Reaction orders and activation energies of symmetrical diphenylurea and its symmetrically substituted chloro, methyl and nitro derivatives were determined.

In our previous paper [1], the kinetic characteristics of some urea derivatives were discussed on the basis of measurements in various solvents by means of conventional isothermal kinetic methods. This method, however, is not of general applicability, owing to analytical problems and inadequate solubility of the substances to be examined. The effect of some important substituents with respect to the discussed mechanism could not be determined because of this fact.

In the last decade some new methods of investigation and calculation have been developed which make possible the calculation of kinetic data from the thermoanalytical curves (DTA, DTG, TG) of solids.

FREEMANN and CARROL [2] derived the following relationship for decomposition reactions involving at least one volatile product, based on thermoanalytical data:

$$\frac{\Delta E^{\ddagger}/2.3R}{\Delta \lg Wr} \cdot \frac{(\Delta T)^{-1}}{\Delta \lg Wr} = -n + \frac{\lg (dw/dt)}{\Delta \lg Wr} \quad (1)$$

where:

Wr = $We - W$;
We = weight loss determined at the end of the reaction (mg);
W = weight loss measured at time t (mg);
T = absolute temperature (K);
dw/dt = rate of weight loss (mg/time);
n = reaction order;
$\Delta E^{\ddagger}$ = energy of activation (kcal/mole).

Graphical representation of this equation permits calculation of the reaction order and the activation energy.

PFEIFER-FLÓRA [3] inserted into Eq. (1) quantities obtained directly from the derivatograms.

SELMECZI [4] developed a method for the determination of the kinetic parameters (activation energy, frequency factor, rate constant) of solid → solid + gas type reactions taking place at high temperatures. The calculations were carried out according to the following relationship:

$$\lg h - n \lg \frac{(B-m)}{M} = \lg Q + \lg A - \frac{\Delta E^{\ddagger}}{RT} \lg e. \qquad (2)$$

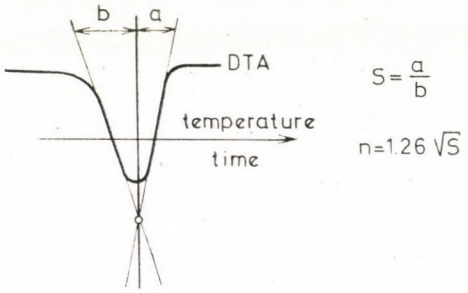


Fig. 1. Determination of the reaction order, according to KISSINGER

Plotting the left-hand side of Eq. (2) against $1/T$, a straight line is obtained. The value of the activation energy ($\Delta E^{\ddagger}$) and the pre-exponential factor (A) can be calculated from its slope and intercept, respectively.

The values to be substituted into Eq. (2) can be read from the derivatograms.

h = deflection of the DTG curve (cm);
B = weight of the sample (mg);
m = quantity of the decomposed material at the actual value of h (mg);
Q = proportionality factor containing the maximum rate of decomposition and the corresponding deflection of the DTG curve;
M = molecular weight;
n = reaction order.

KISSINGER's graphical procedure [5] was recommended by SELMECZI for determination of the reaction order, n, required for the calculations. According to this, the reaction order can easily be determined by making use of the asymmetry of DTA curves in derivatograms; this simple construction method is shown in Fig. 1.

In order to determine the kinetic characteristics of monomolecular decomposition reactions producing gaseous products exclusively, a simple

integration approximation procedure is proposed by HOROWITZ and METZGER [6]. The relationship applied for calculation of the activation energy of first-order reactions is:

$$\ln \ln \frac{W_0}{W} = \frac{\Delta E^{\ddagger}}{RT_s^2} \tag{3}$$

where:

W_0 = initial weight of the sample (mg);
W = weight of the sample at a given temperature (mg);
$\Delta E^{\ddagger}$ = activation energy (kcal/mole);
T_s = that temperature (in K) at which $W = \frac{W_0}{e}$
Θ = $T - T_s$.

Plotting $\lg \lg W_0/W$ against Θ a line with a slope of $\Delta E^{\ddagger}/2.3\ RT_s^2$ is obtained, and this value can be used for calculating the activation energy.

Kinetics of the thermal decomposition of symmetrically substituted diphenylurea derivatives

Thermoanalytical methods developed for kinetic analysis of processes taking place under non-isothermal conditions are not of general character. Their main field of application is special decomposition processes of inorganic compounds producing water vapour, carbon dioxide and ammonia as decomposition products.

In the thermal decomposition of all diarylureas, an aromatic amine and isocyanate are formed, the boiling points of which are far higher than those of the above substances [1]. Under the conditions of thermoanalytical investigations, diarylureas show a considerably more complicated behaviour than the substances used as models in the development of calculation methods published in the literature. Thus, the correctness of similar calculations based on the derivatograms of diphenylurea and its derivatives should be verified first.

The activation energy values given in Table I, calculated from the derivatograms of diphenylurea obtained at various heating rates, show good agreement.

Other, less important characteristics of the derivatograms (DTA and DTG sensitivity, inert atmosphere or use of special sample holder) have practically no effect on the kinetic data.

Table I

Rate of heating (°C/min)	Activation energy $\Delta E^{\ddagger}$ (kcal/mole)	
	by SELMECZI's method	by the HOROWITZ—METZGER method
5.4	62.0	59.6
7.1	60.7	63.0
10.4	65.4	59.7

Derivatograms of the various derivatives indicate decomposition reactions of identical type. The only difference between the individual decomposition processes appeared in the degree of separation of the melting and decomposition periods.

In the case of some substances (diphenylurea, its *p*-nitro and -chloro derivatives) the two processes are not separated (Fig. 2).

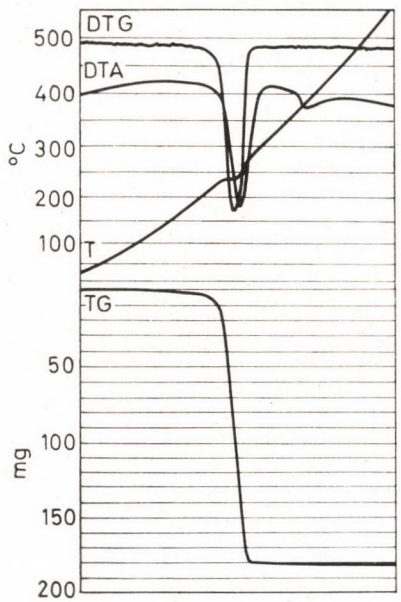


Fig. 2. Derivatogram of diphenylurea

The activation energy calculated from a diagram (Fig. 3) based on the derivatogram constructed according to the method of HOROWITZ and METZGER is 59.7 kcal/mole.

Calculations based on the same derivatogram, carried out according to SELMECZI's method (Fig. 4), resulted in an activation energy of 62 kcal/mole.

On the DTA curve in the derivatogram of *N*,*N*'-di(*m*-tolyl)urea (Fig. 5), the two processes appear distinctly, however, most of the substances give derivatograms similar to that of the *o*-nitro derivative (Fig. 6). In this case a double peak on the DTA curve indicates two different processes, however, separation of the melting and decomposition periods cannot be achieved.

The kinetic data calculated from the derivatograms of urea derivatives are summarized in Table II.

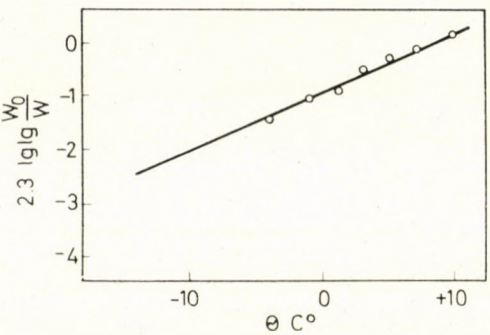


Fig. 3. Plot of the decomposition of diphenylurea, according to HOROWITZ and METZGER

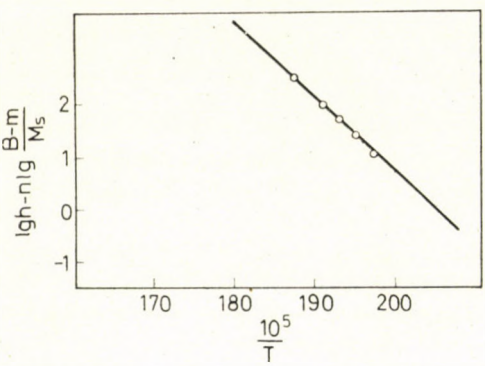


Fig. 4. Plot of the decomposition of diphenylurea, according to SELMECZI

Evaluation of results

In first approximation, the data calculated from derivatograms are found to be realistic. This fact supports our assumption that the calculation of the kinetic data of decomposition can be carried out by use of the relationship derived for decomposition reactions of the solid → gas (vapour) type, based on thermoanalytical data of symmetrical diarylureas. Since very few

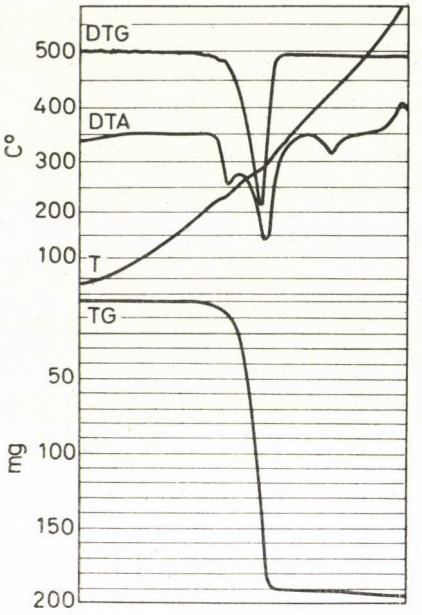


Fig. 5. Derivatogram of *N,N'*-di(*m*-tolyl)urea

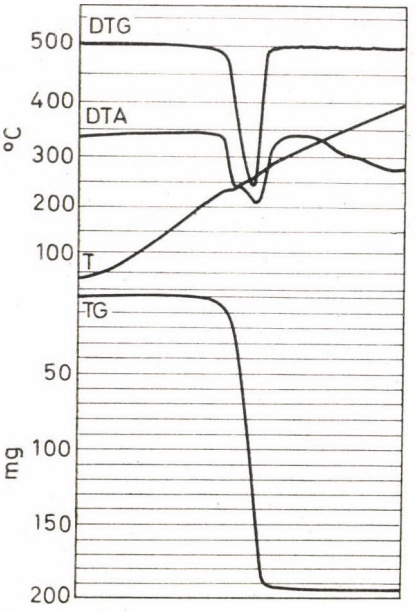


Fig. 6. Derivatogram of *N,N'*-di (*o*-nitrophenyl)urea

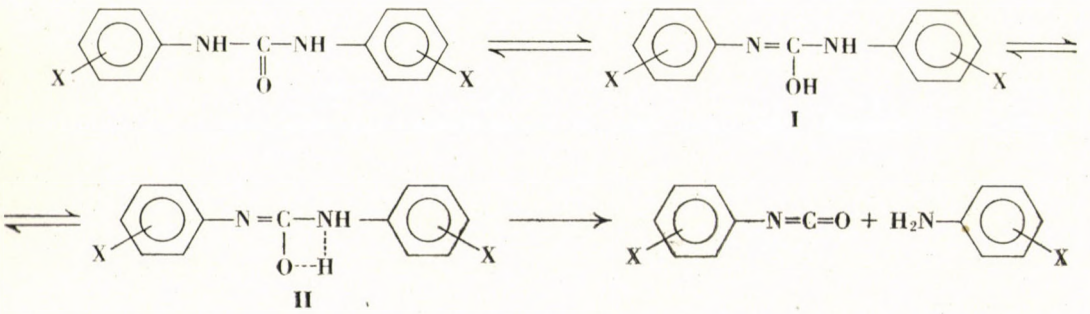
literature data have been found regarding the kinetic evaluation of non-isothermal decomposition of organic compounds, the check of the applied method and obtained results can be carried out on the basis of our own investigations on the kinetics of isothermal decomposition reactions in solvents and on general kinetic principles only.

Table II

Compound	M.p. (°C)	Temperature of the DTA peak (°C)	T_s (K)	Activation energy (kcal/mole)	
				by SELMECZI's method	by the HOROWITZ—METZGER method
N,N'-di(*m*-nitrophenyl)urea	242	290	554	46.2	39.0
N,N'-di(*m*-chlorophenyl)urea	245	255	524	50.1	52.4
N,N'-di(*m*-tolyl)urea	221	290	555	52.8	57.2
N,N'-di(*o*-chlorophenyl)urea	238	250	521	53.3	61.0
N,N'-di(*o*-tolyl)urea	250	275	552	55.0	57.0
N,N'-di(*o*-nitrophenyl)urea	225	260	527	57.1	57.2
N,N'-diphenylurea	238	245	516	62.0	59.7
N,N'-di(*p*-chlorophenyl)urea	275	308	579	62.5	65.5
N,N'-di(*p*-tolyl)urea	260	285	555	64.5	71.5
N,N'-di(*p*-nitrophenyl)urea	312	320	591	67.5	71.6

KISSINGER's graphical method was used for the determination of the reaction order, resulting in values between 0.8 and 1.1. The thermal decomposition of the examined compounds is considered to be of the first order, owing to the fact that the activation energy values obtained by means of the HOROWITZ—METZGER method, involving a relationship applicable for first-order decompositions only, were in excellent agreement with those calculated according to SELMECZI's method under the condition that $n = 1$.

The following decomposition mechanism can be supposed:



Critical steps of the decomposition mechanism are tautomeric transformation and subsequent attachment of the hydroxyl hydrogen of the isomeric molecule to the nitrogen atom. Of the substituents of the aromatic ring, those increasing the basicity of the nitrogen atom, activate and promote the second step of the decomposition process; these simultaneously reduce the mobility of the hydrogen attached to the nitrogen atom, thus hindering tautomerism. Groups of deactivating effect (increasing the mobility of the hydrogen atom and decreasing the basicity of the nitrogen atom) promote the first (tautomeric) step and hinder the second one. Since the diphenylurea derivatives examined are compounds substituted symmetrically, substituents of either activating or deactivating action influence the two steps of the decomposition in opposite directions.

In Table II the sequence of listing the compounds is that of increasing activation energies. Only the activation energies of *p*, *p'* disubstituted derivatives are greater than that of diphenylurea. On the basis of values calculated by SELMECZI's method, the activation energies increase in the order of *meta* → → *ortho* → *para* substitution, irrespective of the nature of the substituents. However, the values calculated by the HOROWITZ—METZGER method are practically the same from *N*,*N*'-di(*m*-tolyl)urea up to and including *N*,*N*'-diphenylurea. Further on, as the estimated accuracy of these measurements is about 10—12% and the difference between the values of the neighbouring activation energies is 1—8%, establishment of a strict order of these activation energies would be unjustified. It can be established, however, that *meta*, *ortho* and *para* substitutions can be characterized by average values of 50, 55 and 65 kcal/mole, respectively. This tendency indicates a greater activation energy requirement of the overall decomposition process involving two steps, when a substituent exerts extreme activation or deactivation on the carbon atom of urea attached to the nitrogen atom. In the case of strong activation (*e.g.* methyl substituent in *para* position), the effect promoting the second step will be exceeded by that hindering the first step of decomposition (*i.e.* tautomerism). In the case of strong deactivation (*e.g.* nitro substituent in *para* position), the decrease in the proton-binding ability of the nitrogen atom is greater than the increase in the mobility of the hydrogen atom.

In derivatives carrying substituents in *meta* positions, their $+I$ or $-I$ effects alter the electron density on the nitrogen atoms to a relatively small extent. The low activation energies measured for these compounds indicate that such small changes in the electron distribution give rise to activation effects greater than the opposing tendencies. With respect to these facts, in our opinion, the appearance of the activation energies of derivatives containing substituents in the *ortho* position, between those of *para* and *meta* substituted derivatives representing extreme cases (in terms of the proposed mechanism) is evident.

Establishment of an order with various groups of derivatives containing different substituents in the same position is not considered reasonable because of the slight differences occurring between the corresponding activation energy values.

As shown by the results of our experiments and calculations, the thermoanalytical investigation of diphenylurea derivatives is a suitable method for kinetic evaluation of their thermal decomposition processes. In each case, decomposition of the examined diarylureas starts with melting and — since decomposition proceeds at a greater rate in the liquid than in solid state — the process as a whole should be regarded as decomposition taking place in the melt. This type of decomposition differs from the one taking place without formation of a liquid phase, used in the development of SELMECZI's calculation method. However, the relationship derived can also be applied for the compounds examined by us. The comparison of the results with our isothermal kinetic data in solvents supports the assumption that the decomposition is faster in solvents and has a lower activation energy. (Activation energy values given here are nearly twice as high as those measured in solvents.) A more accurate determination of the decomposition mechanism and the elucidation of some phenomena not yet explored in our experiments is planned in further studies of other types of urea derivatives containing substituents of unequivocal influence on the two steps of the proposed decomposition mechanism. The rate-determining step of the decomposition will be determined from these investigations.

REFERENCES

1. CSŰRÖS, Z., SOÓS, R., BITTER, I., BENDE, Z.: Acta Chim. Acad. Sci. Hung. (In the press)
2. FREEMANN, E. S., CAROLL, B.: J. Phys. Chem. **62,** 394 (1958)
3. PFEIFER-FLÓRA, T.: Acta Chim. Acad. Sci. Hung. **48,** 225 (1966)
4. SELMECZI, B.: Magy. Kém. Foly. **74,** 461 (1968)
5. KISSINGER, H. E.: J. Research Natl. Bur. Standards **57,** 217 (1956)
6. HOROWITZ, H. H., METZGER, G.: Anal. Chem. **35,** 1464 (1963)

Zoltán CSŰRÖS
Rudolf SOÓS
István BITTER
Zoltán BENDE
Mihály ECET
Budapest XI., Műegyetem-rkp. 3.

MAGYAR
FÖLDRAJZI TÁRSASÁG
KÖNYVTÁRA

INDEX

INORGANIC AND ANALYTICAL CHEMISTRY – ANORGANISCHE UND ANALYTISCHE CHEMIE – НЕОРГАНИЧЕСКАЯ И АНАЛИТИЧЕСКАЯ ХИМИЯ

ZSINKA, L. and SZIRTES, L.: Investigations on a Chromium Phosphate Ion Exchanger 249

INCZÉDY, J.: The Use of Complex Forming Agents in Ion Exchange Chromatography, VI. Separation of Organic Bases on a Cation-Exchange Column 265

GARZÓ, G., TAMÁS, J., SZÉKELY, T. and UJSZÁSZI, K.: Thermal Decomposition of Branched-Chain Methylpolysiloxanes, II. Separation and Identification of the Pyrolysis Products by Gas Chromatography and Mass Spectrometry 273

FLÓRA, T. und MENYHÁRT, M.: Untersuchung der beim Erhitzen zwischen den Komponenten von N–P–K-Düngern verlaufenden Vorgänge, II. Systeme: Ammoniumnitrat–Ammoniumdihydrophosphat, Ammoniumnitrat–Calciumhydrophosphat, Ammoniumdihydrophosphat–Calciumhydrophosphat, Ammoniumdihydrophosphat–Kaliumchlorid und Calciumhydrophosphat–Kaliumchlorid (Investigation of the Processes Occurring on Heating between the Components of N–P–K-Fertilizers, II. Systems: Ammonium Nitrate–Ammonium Dihydrogen Phosphate, Ammonium Nitrate–Calcium Hydrogen Phosphate, Ammonium Dihydrogen Phosphate–Calcium Hydrogen Phosphate, Ammonium Dihydrogen Phosphate–Potassium Chloride and Calcium Hydrogen Phosphate–Potassium Chloride) 301

PHYSICAL CHEMISTRY – PHYSIKALISCHE CHEMIE – ФИЗИЧЕСКАЯ ХИМИЯ

TÓTH, J.: State Equations of the Solid–Gas Interface Layers 311

BÖRÖCZ, SZ.: Derivation of the Transport Equations of Non-Isothermal Hydrodynamics from the Gyarmati Principle in Different Pictures 329

VÉRTES, G., HORÁNYI, G. and NAGY, F.: Oxidation on the Nickel Hydroxide Electrode, IV. Kinetics of Oxidation of Primary Alcohols 341

ORGANIC CHEMISTRY – ORGANISCHE CHEMIE – ОРГАНИЧЕСКАЯ ХИМИЯ

UJHIDY, A., RÉPÁSY, O. and TAKÁCS, J.: The Competitive Nitration of Some Aromatic Compounds 349

CSŰRÖS, Z., SOÓS, R., BITTER, I. and PÁLINKÁS, J.: The Use of Amide Chlorides in Ring Closure Reactions, III. Synthesis and Ring Closure of Novel Amidrazones 361

Кучкова, К. И., Семенов, А. А. и Терентьева, И. В.: Карболины, II. Полный синтез Алкалоида бревикарина и его гомолога (KUCHKOVA, K. I., SEMENOV, A. A., TERENTJEVA, I. V.: Carbolines, II. Total Synthesis of Alkaloid Brevicarine and Its Inferior Homologue) 367

CSŰRÖS, Z., SOÓS, R., BITTER, I., BENDE, Z. and ECET, M.: Thermal Dissociation of Urea Derivatives, II 373

MAGYAR
TUDOMÁNYOS AKADÉMIA
KÖNYVTÁRA

Printed in Hungary

A kiadásért felel az Akadémiai Kiadó igazgatója — Műszaki szerkesztő: Várhelyi Tamás

A kézirat nyomdába érkezett: 1971. III. 19. — Terjedelem: 11 (A/5) ív, 59 ábra

71.71455 Akadémiai Nyomda, Budapest — Felelős vezető: Bernát György

The Acta Chimica publish papers on chemistry in English, German, French and Russian.

The Acta Chimica appear in volumes consisting of four parts of varying size, 4 volumes being published a year.

Manuscripts should be addressed to

Acta Chimica
Budapest 112/91 Műegyetem

Correspondence with the editors should be sent to the same address.

The rate of subscription is $16.00 a volume.

Orders may be placed with "*Kultúra*" Foreign Trade Company for Books and Newspapers (Budapest I., Fő utca 32. Account No. 43-790-057-181) or with representatives abroad.

Les Acta Chimica paraissent en français, allemand, anglais et russe et publient des mémoires du domaine des sciences chimiques.

Les Acta Chimica sont publiés sous forme de fascicules. Quatre fascicules seront réunis en un volume (4 volumes par an).

On est prié d'envoyer les manuscrits destinés à la rédaction à l'adresse suivante:

Acta Chimica
Budapest 112/91 Műegyetem

Toute correspondance doit être envoyée à cette même adresse.

Le prix de l'abonnement est de $16.00 par volume.

On peut s'abonner à l'Entreprise pour le Commerce Extérieur de Livres et Journaux «*Kultúra*» (Budapest I., Fő utca 32. Compte-courant No. 43-790-057-181) ou à l'étranger chez tous les représentants ou dépositaires.

«*Acta Chimica*» издают трактаты из области химической науки на русском, французском, английском и немецком языках.

«*Acta Chimica*» выходят отдельными выпусками разного объема. 4 выпуска составляют один том. 4 тома публикуются в год.

Предназначенные для публикации рукописи следует направлять по адресу:

Acta Chimica
Budapest 112/91 Műegyetem

По этому же адресу направлять всякую корреспонденцию для редакции.

Подписная цена — $16.00 за том.

Заказы принимает предприятие по внешней торговле книг и газет «*Kultúra*» (Budapest I., Fő utca 32. Текущий счет № 43-790-057-181) или его заграничные представительства и уполномоченные.

Reviews of the Hungarian Academy of Sciences are obtainable at the following addresses:

ALBANIA

Drejtorija Qändrone e Pärhapjes dhe Propagandimit tä Librit
Kruga Konferenca e Päzes
Tirana

AUSTRALIA

A. Keesing
Box 4886, GPO
Sydney

AUSTRIA

GLOBUS
Höchstädtplatz 3
A-1200 Wien XX

BELGIUM

Office International de Librairie
30, Avenue Marnix
Bruxelles 5
Du Monde Entier
5, Place St. Jean
Bruxelles

BULGARIA

HEMUS
11 pl Slaveikov
Sofia

CANADA

Pannonia Books
2, Spadina Road
Toronto 4, Ont.

CHINA

Waiwen Shudian
Peking
P. O. B. 88

CZECHOSLOVAKIA

Artia
Ve Směčkách 30
Praha 2
Poštovní Novinová Služba
Dovoz tisku
Vinohradská 46
Praha 2
Mad'arská Kultura
Václavské nám. 2
Praha 1
SLOVART A. G.
Gorkého
Bratislava

DENMARK

Ejnar Munksgaard
Nörregade 6
Copenhagen

FINLAND

Akateeminen Kirjakauppa
Keskuskatu 2
Helsinki

FRANCE

Office International de Documentation et Librairie
48, rue Gay Lussac
Paris 5

GERMAN DEMOCRATIC REPUBLIC

Deutscher Buch-Export und Import
Leninstraße 16
Leipzig 701
Zeitungsvertriebsamt
Fruchtstraße 3—4
1004 Berlin

GERMAN FEDERAL REPUBLIC

Kunst und Wissen
Erich Bieber
Postfach 46
7 Stuttgart S.

GREAT BRITAIN

Blackwell's Periodicals
Oxenford House
Magdalen Street
Oxford
Collet's Subscription import Department
Dennington Estate
Wellingsborough. Northants.
Robert Maxwell and Co. Ltd.
4—5 Fitzroy Square
London W. 1

HOLLAND

Swetz and Zeitlinger
Keizersgracht 471—487
Amsterdam C
Martinus Nijhof
Lange Voorhout 9
The Hague

INDIA

Hind Book House
66 Babar Road
New Delhi 1

ITALY

Santo Vanasia
Via M. Macchi 71
Milano
Libreria Commissionaria Sanso
Via La Marmora 45
Firenze
Techna
Via Cesi 16.
40135 Bologna

JAPAN

Kinokuniya Book-Store Co. Ltd.
826 Tsunohazu 1-chome
Shinjuku-ku
Tokyo
Maruzen and Co. Ltd.
P. O. Box 605
Tokyo-Central

KOREA

Chulpanmul
Phenjan

NORWAY

Tanum-Cammermeyer
Karl Johansgt 41—43
Oslo 1

POLAND

RUCH
ul. Wronia 23
Warszawa

ROUMANIA

Cartimex
Str. Aristide Briand 14—18
Bucureşti

SOVIET UNION

Mezhdunarodnaya Kniga
Moscow G—200

SWEDEN

Almquist and Wiksell
Gamla Brogatan 26
S—101 20 Stockholm

USA

F. W. Faxon Co. Inc.
15 Southwest Park
Westwood Mass. 02090
Stechert Hafner Inc.
31. East 10th Street
New York, N. Y. 10003

VIETNAM

Xunhasaba
19, Tran Quoc Toan
Hanoi

YUGOSLAVIA

Forum
Vojvode Mišića broj 1
Novi Sad
Jugoslovenska Knjiga
Terazije 27
Beograd

ACTA CHIMICA

ACADEMIAE SCIENTIARUM HUNGARICAE

ADIUVANTIBUS

V. BRUCKNER, GY. DEÁK, K. POLINSZKY,
E. PUNGOR, G. SCHAY, Z. G. SZABÓ

REDIGIT

B. LENGYEL

TOMUS 69 FASCICULUS 4

AKADÉMIAI KIADÓ, BUDAPEST

1971

ACTA CHIM. (BUDAPEST)

ACTA CHIMICA

A MAGYAR TUDOMÁNYOS AKADÉMIA KÉMIAI TUDOMÁNYOK OSZTÁLYÁNAK IDEGEN NYELVŰ KÖZLEMÉNYEI

SZERKESZTI

LENGYEL BÉLA

TECHNIKAI SZERKESZTŐK

DEÁK GYULA és HARASZTHY-PAPP MELINDA

Az Acta Chimica német, angol, francia és orosz nyelven közöl értekezéseket a kémiai tudományok köréből.

Az Acta Chimica változó terjedelmű füzetekben jelenik meg, egy-egy kötet négy füzetből áll. Évente átlag négy kötet jelenik meg.

A közlésre szánt kéziratok a szerkesztőség címére (Budapest 112/91 Műegyetem) küldendők.

Ugyanerre a címre küldendő minden szerkesztőségi levelezés. A szerkesztőség kéziratokat nem ad vissza.

Megrendelhető a belföld számára az „Akadémiai Kiadó"-nál (Budapest V., Alkotmány utca 21. Bankszámla 05-915-111-46), a külföld számára pedig a „Kultúra" Könyv- és Hírlap Külkereskedelmi Vállalatnál (Budapest I., Fő utca 32. Bankszámla: 43-790-057-181) vagy annak külföldi képviseleteinél és bizományosainál.

Die Acta Chimica veröffentlichen Abhandlungen aus dem Bereiche der chemischen Wissenschaften in deutscher, englischer, französischer und russischer Sprache.

Die Acta Chimica erscheinen in Heften wechselnden Umfanges. Vier Hefte bilden einen Band. Jährlich erscheinen 4 Bände.

Die zur Veröffentlichung bestimmten Manuskripte sind an folgende Adresse zu senden:

Acta Chimica
Budapest 112/91 Műegyetem

An die gleiche Anschrift ist auch jede für die Redaktion bestimmte Korrespondenz zu richten. Abonnementspreis pro Band: $16.00.

Bestellbar bei dem Buch- und Zeitungs-Außenhandels-Unternehmen »*Kultúra*« (Budapest I., Fő utca 32. Bankkonto No. 43-790-057-181) oder bei seinen Auslandsvertretungen und Kommissionären.

Acta Chimica Academiae Scientiarum Hungaricae, Tomus 69 (4), pp. 383—396 (1971)

RECTIFICATION OF MULTICOMPONENT MIXTURES, I

TOPOLOGICAL ANALYSIS OF LIQUID–VAPOUR PHASE EQUILIBRIUM DIAGRAMS

L. A. SERAFIMOV,* V. T. ZHAROV** and V. S. TIMOFEYEV*

*(*Lomonosov Institute of Fine Chemical Technology, Moscow, and **Zhdanov University, Leningrad)*

Received November 1, 1969

The fundamental problems of the classification of liquid–vapour phase equilibrium diagrams are discussed on the basis of the azeotropy rule. It is demonstrated that each type of diagram is characterized by the specific behaviour of the components during phase transformations. The concept of distillation and rectification regions is defined. The fundamental principles of designing technological schemes for the rectification of non-ideal, multicomponent mixtures are discussed on the basis of the qualitative thermodynamical-topological analysis of the structure of liquid–vapour phase equilibrium diagrams. The principle of concentration field redistribution between the regions of rectification is described and an example is given for the separation of a heteroazeotropic mixture.

In the industrial practice of separating multicomponent mixtures an important role is played by azeotropic mixtures. As a rule, the rectification of such mixtures requires special techniques and methods, the application of which brings into the foreground the physico-chemical features of the process. In contrast to nonazeotropic mixtures in which the order of removal of the fractions is solely determined by the boiling points of the components, in azeotropic mixtures this order is governed by the properties of the phase equilibrium diagram. Of importance here are the number, mutual position, and type of azeotropic points.

The following is a short summary of the principles involved in the classification and analysis of the liquid–vapour equilibrium diagrams for multicomponent systems.

A primary basis for the classification of phase equilibrium diagrams is the number of azeotropic points and their position on the concentration simplex. Using these characteristics, in Ref. [1] a classification scheme has been proposed for the phase equilibrium diagrams. According to this, a given class of diagrams is characterized by a consecutive series of numbers, each corresponding to the number of azeotropic mixtures with different dimensions:

$$\left[\frac{n!}{2!(n-2)!} - A_1\right]\left[\frac{n!}{3!(n-3)!} - A_2\right] \ldots \left[\frac{n!}{(n-2)!2!} - A_{n-2}\right][1 - A_{n-1}] \tag{1}$$

where n is the number of components in the mixture, A_i is the number of

elements in the concentration simplex not occupied by azeotropic points, and i is the dimension of the element.

The dimension of the azeotropic mixture corresponds to the dimension of the concentration simplex element on which the azeotropic point is situated. Thus, a binary azeotropic mixture has a dimension of unity, while a ternary one is two-dimensional, etc. The terms in parentheses determine the number of azeotropic mixtures with the given dimension, beginning from binary mixtures.

A detailed analysis has shown that the number of different diagram classes increases with the increasing number of components. Thus for binary mixtures the number of classes is equal to 2, for ternary mixtures it is already 7, for four-component systems it reaches 51, while in the case of 5 components, the number of classes equals 899.

This classification is, however, not satisfactory since the character of azeotropic points and, consequently, that of the rectification process itself may be quite different within a given class of diagrams. Therefore, the following more detailed classification is based on internal criteria of phase equilibrium diagrams, *viz.* on the type of singular points on the diagram, corresponding to various azeotropic mixtures and various components of the multicomponent system.

The types of singular points on phase equilibrium diagrams have been studied in detail [2—7] in connection with the local regularities of open evaporation processes. It has been shown that the singular points of the dynamic system of differential equations for open evaporation may be either nodes or saddles with various structures [2, 5].

Thus, within a given class of diagrams, there may be types differing in the relative number of nodal and saddle-type singular points. This raises the important question of permissible combinations of various singular point types on the state diagram. To answer this question, it is necessary to perform a topological analysis of liquid–vapour phase equilibrium diagrams. This problem was treated in independent papers [8—11] which have led to results supplementing each other.

In papers [8, 9] the topological theory of vector fields (theorems of KRONECKER and HOPPF) was used to show that the numbers of singular points of various types on two-phase equilibrium diagrams of n-component systems must be governed by the following relationship:

$$\sum_{K=1}^{n} 2^K (N_K^+ + C_K^+ - N_K^- - C_K^-) = (-1)^{n-1} + 1 \qquad (2)$$

where N_K^+ (N_K^-) is the number of K-component nodal singular points with indices $+1$ (1); C_K^+ (C_K^-) is the number of K-component saddle-type singular

points with indices +1 (-1). The notion of index refers to the known concept of singular point index of a vector field. It should be noted that in the present case the singular point index is defined by the following simple rule: the index is equal to +1 (-1) if the number of negative roots of the characteristic equation (*cf.* [2—7]) determining the type of the singular point is even (odd). This rule permits the determination of the index from the type of the singular point without any calculations. A characteristic feature of relationship (2) is the presence in it of all internal and boundary singular points of the concentration simplex, regardless of how these were introduced into the concentration space.

In papers [10, 11] a different relationship has been derived, *viz.*

$$2(N^+_{n-1} + C^+_{n-1} - N^-_{n-1} - C^-_{n-1}) + \sum_0^{n-2} (N^+_B + C^+_B - N^-_B - C^-_B) = (-1)^{n-1} + 1 \tag{3}$$

where B refers to the boundary singular points on edges, faces and hyperfaces of the concentration simplex.*

This equation involves only singular points determined from the difference:

$$N^+_B + C^+_B - N^-_B - C^-_B = G_B - G^0_B \tag{4}$$

where G_B is the overall number of boundary singular points in the concentration space; G^0_B is the number of those singular points which are introduced into the concentration space in such a manner that they are complex relative to the vicinity of the boundary space and have an index equal to zero. The points of this type include node-saddle points CN^0_0, CN^0_1, CN^0_2, etc., the positive-negative node N^0_0, N^0_1, N^0_2, etc., and the positive-negative saddle C^0_0, C^0_1, C^0_2, etc.

Equations (2) and (3) considered above constitute the basis for the complete classification and analysis of phase equilibrium diagrams. More specifically, Eqs (2) and (3) permit to determine all the possible combinations of saddle-type and nodal singular points and, consequently, to find the thermodynamically possible types of liquid–vapour equilibrium diagrams for multicomponent systems. For example, in the case of ternary mixtures Eqs (2) and (3) lead to the following relationship obtained first in Ref. [2]:

$$2\,N_2 + N_1 + N_0 = 2\,C_2 + C_1 + 2 \tag{5}$$

By means of this equation, it has been established that ternary mixtures are subdivided into 16 types. Among these a number of types with the same relation of saddle type and nodal singular points may have them in different

* From here on, the numerical lower index of the symbols for singular points refers to the dimension of the element of the concentration simplex on which the given point is located.

positions. The diagrams which possess this property are sub-types of the same general class and are denoted in Fig. 1 by an additional letter, retaining also the type number [9].

With each one of the types shown in Fig. 1, the distillation lines may be oriented, *e.g.* in the direction of increasing boiling point of the liquid. In this

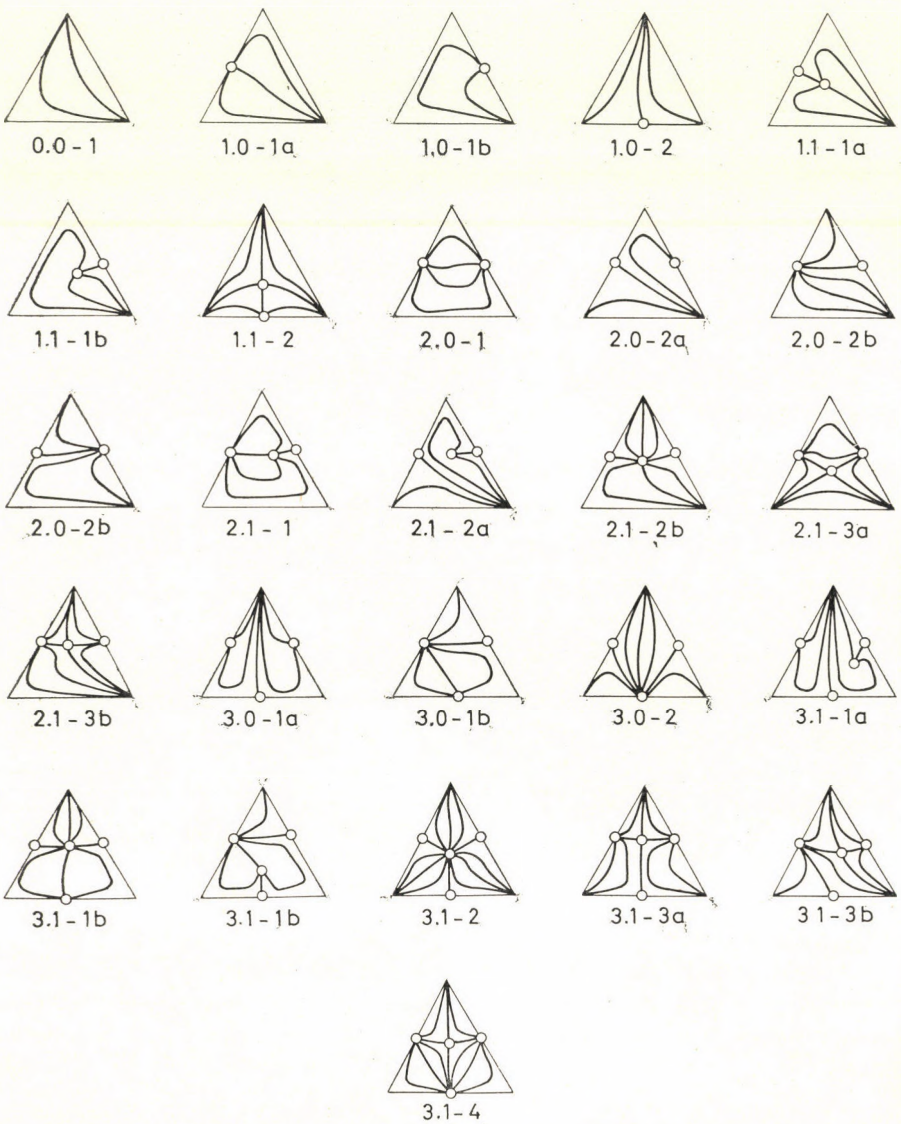


Fig. 1. Liquid–vapour phase equilibrium diagrams for ternary mixtures differing in the form of the distillation lines. The first two numbers refer to the class of the diagram, the next number specifies the type, and the letter gives the sub-type

case, with the exception of the diagrams of zero-th class and type 1 (00—1), of 2nd class and type 1 (2.0—1), of 2.1-th class and type 3a (2.1—3a), each diagram may be oriented in two ways, depending on whether it is characterized by azeotropic mixtures of minimum or maximum boiling temperature. The diagrams belonging to the same class and type, but differing in the orientation of the distillation lines, are referred to as antipodes.

It may be seen from Fig. 1 that a given mixture belonging to one or another type or sub-type is characterized by the specific behaviour of its components in each column, while upon going from one column to another, by a specific order of fractions which does not, in general, depend on the column efficiency. The fractions going into the distillate or the residual products may consist of pure substances, azeotropic mixtures or mixtures containing all the components but in a composition different from the initial. The process trajectories divide the diagram of the n-component mixture into a number of distillation regions. Each region includes its own process trajectories with a common starting and terminal point. The points of the nodal type constitute such points. Thus the distillation region on the diagram of an n-component mixture, which is an n — 1-dimensional simplex, is that closed space of the same dimension which is uniformly filled by the family of distillation lines. The initial point of each family is a singular point of the unstable node type from which the evaporation trajectories start, while the terminal singular point of the stable node type is one to which the trajectories converge.

In the case of antipodes, the stable and unstable nodes are interchanged.

The distillation regions are separated from one another by n — 2-dimensional sub-spaces which, depending on the dimension of the full concentration space of lines, may be surfaces and hyper-surfaces. The distillation lines of these sub-spaces have the property of remaining within their boundaries, *i.e.* they do not egress into the full concentration space. A dividing sub-space of the first order separates families of distillation lines with different starting points, while that of the second order — families with different terminal points. Each family of distillation curves is oriented. The distillation region may collapse into several regions of continuous rectification. Upon variation of the composition of the initial mixture, each rectification region will be characterized by a specific set of continuous rectification lines. These lines correspond to the distribution of the components of the mixture to be separated along the height of the continuous rectification column.

For apparatuses of the still-head or film type, the equation of such a line may be written either in the integral or in the differential form [12].

In the case of plate type columns in which the composition of the vapour and liquid phases varies in a discreet manner, the points corresponding to compositions in one of the phases may be formally joined by a line [13, 14]. The line of continuous rectification is always interlaced by the straight line

of mass balance. Various cases of such interlacing are shown in Fig. 2. At a given composition of the initial mixture subjected to rectification, the possible limiting compositions of the product will be those corresponding to the distillate and the residue belonging to the boundary sub-space of the rectification region which, at the same time, is also a sub-space of the distillation region. Since

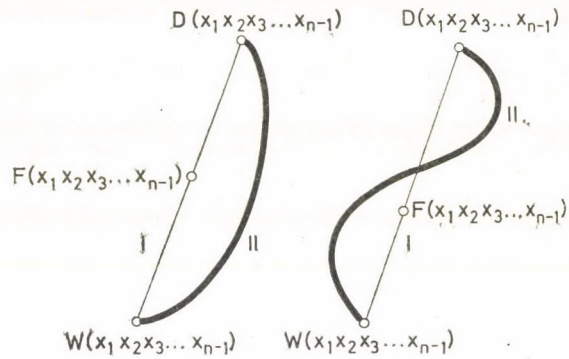


Fig. 2. Various cases of interlacing of the line of continuous rectification by the straight line of material balance. $F(x_1, x_2, \ldots x_{n-1})$ is the point corresponding to the composition of the initial mixture; $D(x_1, x_2, \ldots x_{n-1})$ is the composition point of the distillate; $W(x_1, x_2, \ldots x_{n-1})$ is the composition point of the residue

the composition point of the initial mixture $F(x_1, x_2, \ldots x_{n-1})$ is fixed, the possible product compositions in proper rectification form two conjugated sets in the opposite domains of the boundary sub-space including the given region.

At a constant reflux number and a sufficient plate number for good separation, the variation of the ratio of final products removed leads to the rotation of the line corresponding to the material balance with respect to point $F(x_1, x_2, \ldots x_{n-1})$, referring to the initial composition of the mixture. The intersections of this line with the dividing boundary sub-spaces form two curves, one of which corresponds to the possible distillate compositions and the other, to the possible compositions of the residue (*cf.* Fig. 3). The length of these lines is determined by the limiting compositions, one of which (N^-) has a minimum boiling temperature and lies on the $D(x_1, x_2, \ldots x_{n-1}) = 0$ line. The other composition (N^+) has the maximum boiling temperature in the given region and lies on the line $W(x_1, x_2, \ldots x_{n-1}) = 0$. These compositions correspond to singular-points of the node type. Since the points $D(x_1, x_2, \ldots \ldots x_{n-1})$ and $W(x_1, x_2, \ldots x_{n-1})$ are mutually conjugated, in the case when the compositions having the maximum and the minimum boiling temperature do not lie on the same straight line, to each one of these there would correspond a second limiting point, thus the lines $D(x_1, x_2, \ldots x_{n-1}) = 0$ and $W(x_1, x_2, \ldots \ldots x_{n-1}) = 0$ will be limited from both ends. If the initial composit ion point is

situated in such a manner that the points of minimum and maximum boiling temperature can be connected by the line of material balance, then the variation of the ratio of end products is excluded because this would upset the conditions of good rectification. This is so because the line of material balance coincides with the separation line or lies in the plane or hyper-plane separating the two regions of continuous rectification belonging to one and the same distillation region.

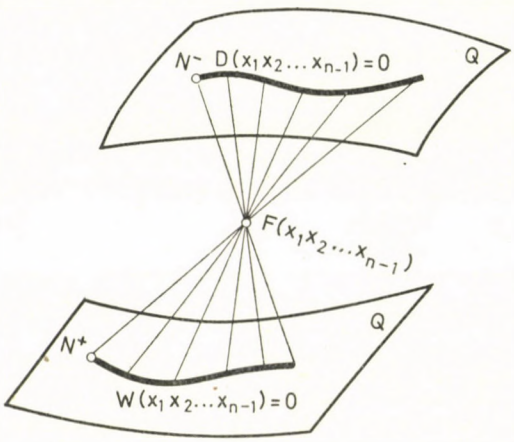


Fig. 3. The lines representing the variation of the final compositions, $D(x_1, x_2, \ldots x_{n-1}) = 0$ and $W(x_1, x_2, \ldots x_{n-1}) = 0$, as a function of the given separation in the case of full rectification. N^- is the minimum boiling temperature point; N^+ is the maximum boiling temperature point; Q is the boundary sub-space of the given rectification region; $F(x_1, x_2, \ldots \ldots x_{n-1})$ is the composition point of the initial mixture

The analysis of the topological structure of liquid–vapour phase equilibrium diagrams has shown that the points of maximum and minimum boiling temperatures characteristic of the region of continuous rectification are the only extrema with respect to the temperature during the variation of the end-product compositions along the curves $D(x_1, x_2, \ldots x_{n-1}) = 0$ and $W(x_1, x_2, \ldots \ldots x_{n-1}) = 0$. Thus, upon the variation of the ratio of end products, W/D, the temperature of the distillate and the residue will either continuously increase or decrease, *i.e.* they will change in parallel.

The variation of the initial composition together with the reflux number gives a family of curves lying at the boundary of the rectification region and completely filling that part of the boundary sub-space which is at the same time also the boundary region of distillation including the rectification region under consideration. As for the separating planes within the distillation region, the $D(x_1, x_2, \ldots x_{n-1}) = 0$ and $W(x_1, x_2, \ldots x_{n-1}) = 0$ positions are excluded.

The above analysis permits to give a precise definition for the region of continuous rectification. This region in the $(n - 1)$-dimensional concentration simplex is that closed concentration sub-space of the same dimension which, under conditions of clear separation, has its own consecutive set of given separations, *i.e.* possible distillate and residue compositions.

The first given separation is that to which there corresponds a distillate with a minimum boiling temperature relative to the temperature range characteristic of the given rectification region. The second given separation is that associated with a maximum boiling temperature residue in the temperature range of the given rectification region. The differential transition from the first to the second separation may be brought about by a single route only, changing continuously the residue to distillate ratio, W/D.

It follows from the above definition of the region of continuous rectification that a given separation in the general case is determined by the configuration of the given region, *i.e.* by the mutual position of the boundary surfaces or hyper-surfaces. As a consequence, the end-products of rectification may often contain all the components of the mixture subjected to separation even if the composition is not azeotropic.

The above definitions include, as a special case, the definition of the given separation proposed by Lvov for azeotropic mixtures [15]. In fact, for non-azeotropic mixtures the boundaries of the continuous rectification region fully coincide with the boundaries of the concentration simplex and, consequently, in the case of first separation, the first component to appear in the distillate will be the most volatile one with the lowest boiling temperature, while in the case of second separation, the residue will contain only the most non-volatile component with the highest boiling point. All regions of continuous rectification may be subdivided into two groups. To the first group belong those regions which have the same compositions corresponding to the minimum and maximum boiling temperatures. Each one of this set of regions is a distillation region by itself. The second group which, as shown below, is of special interest to the technologist, consists of those continuous rectification regions lying in different distillation regions. These regions have only one common point, corresponding to the maximum and the minimum boiling temperatures. As an example, in Fig. 4 are shown two limiting separations for the different regions of continuous rectification, for all types of ternary mixtures.

As seen from Fig. 4, in the great majority of cases, separation into fractions consisting of the pure components is impossible even under the conditions of full rectification. Due to this fact special importance is attached to the detailed study of the topological structure of the diagram for the mixture to be separated. In the first stage of design, during the selection of the technological set-up for rectification, it is sufficient to know the types and mutual position of singular points, *i.e.* the class and type of the diagram for the mixture to be

separated. This permits to reckon with all the limitations introduced by the presence of continuous rectification regions, and to choose the most suitable special technique for the separation of the given mixture. At this stage, of special assistance are the above generalized relationships between singular points of various types.

Taking into account the topological regularities, it is now possible to classify all the special rectification methods of separation.

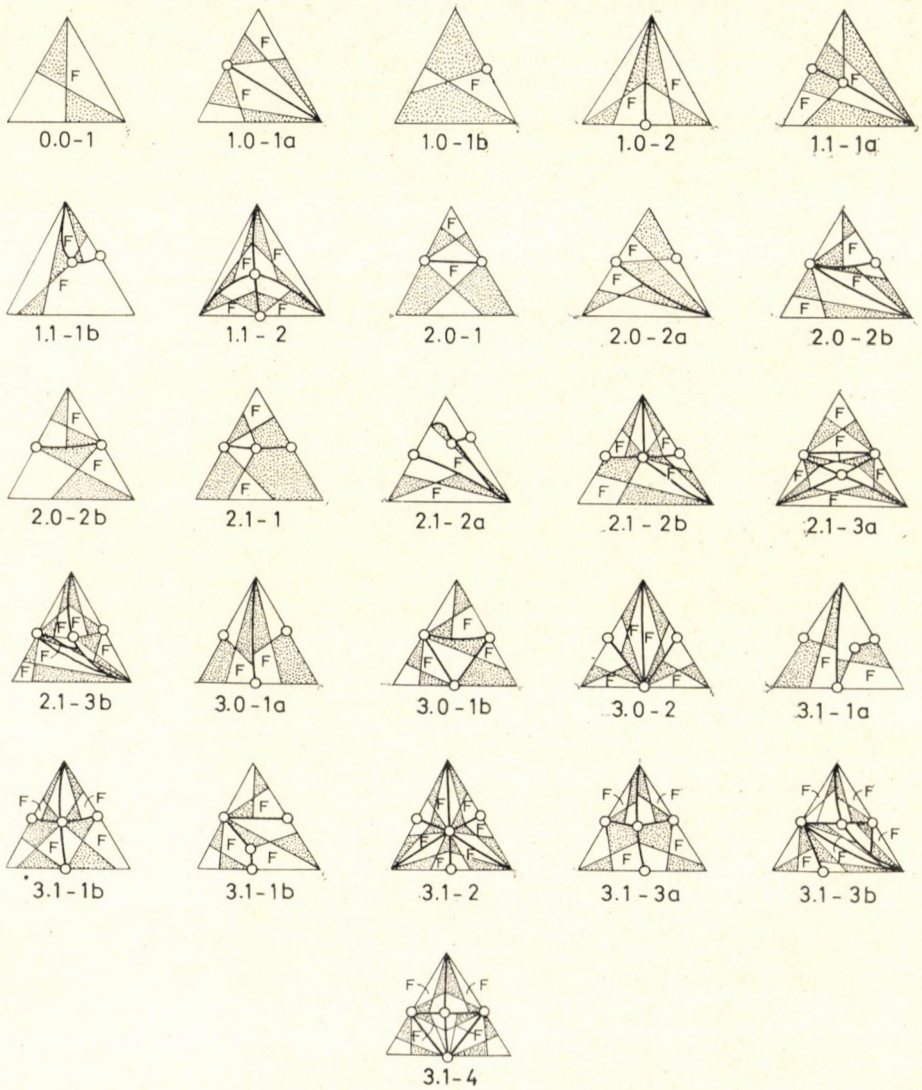


Fig. 4. Limiting cases of a given separation (I and II) for arbitrary initial compositions F, located in different rectification regions. The hatched regions correspond to possible compositions of distillate and residue. The lines mark the boundaries between regions

In the first group are included those methods which employ the introduction of a second component either into the initial mixture or to a given point of the rectification column. As a consequence of this, the dimension of the concentration simplex is increased by one with the simultaneous formation of new continuous rectification regions in which the separation of the target products becomes possible at acceptable levels of energy and operating costs. The methods belonging to this group include extractive and azeotropic rectifications which have lately become widely used in industry. Naturally, when selecting the extracting azeotropic agents, it is necessary to take into account the topological structure of the diagram for both the initial and the resulting mixture.

The second group includes methods in which one of the target products is recycled, ensuring that the rectification process takes place in a more suitable region with respect to the given objectives. It is appropriate here to mention autoextractive rectification in which an agent is utilized that is present in the initial mixture.

The third group consists of methods in which the liquid–vapour phase equilibrium diagram is modified on purpose by means of external influence on the system. This method is based on the known property of azeotropic points to change their position, *e.g.* as a result of changes in the pressure. The variation of the position of singular points on the diagram at a given stage of separation brings about a shift in the boundaries between rectification regions. Thus the composition points obtained at a given stage of rectification, and lying in one of the rectification regions, are transferred into other regions due to the shift in the inter-regional boundaries [11]. In other words, the concentration fields are redistributed between the rectification regions, to each one of which corresponds a specific set of given separations. The realization of this principle involves the presence of recycling, the amount of which is usually small in the case of mixtures with 3 and more components [16, 17].

Often the redistribution principle may be successfully applied when the liquid compositions are situated in different regions of continuous rectification, belonging to the second group.

As an example of such application, we consider the rectification of the four-component mixture water–isobutyraldehyde–butyraldehyde–toluene. This mixture is involved in the production of butyraldehydes by means of the oxo synthesis.

It follows from mutual solubility data [18] that this mixture is heterogeneous in a large region of the concentration tetrahedron. The boundary space of the given tetrahedron is evolved in Fig. 5, where also the distillation lines are shown for each of the three-component constituents. The mixture under consideration is characterized also by the presence of three binary heteroazeotropic mixtures, *viz.* water–isobutyraldehyde (N_1), water–butyral-

dehyde (CN_1), and water–toluene (C_1). The boiling points of these heteroazeotropic mixtures are in the order

$$t_{N_1} < t_{CN_1} < t_{C_1} .$$

The regions (volumes) of continuous rectification, of which there are 4, are shown in Fig. 6. The first rectification region $N_1 - CN_1 - C_1 - 1$, coincides

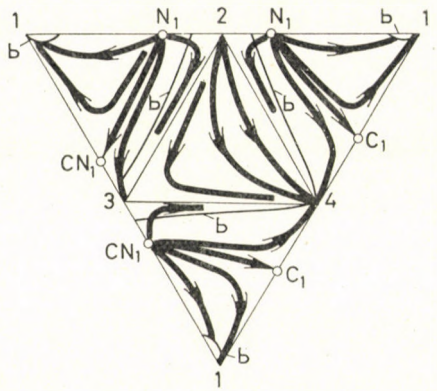


Fig. 5. The evolvent of the concentration tetrahedron for the mixture water (1)–isobutyraldehyde (2)–butyraldehyde (3)–toluene (4). b are the traces of binodal surfaces on the tetrahedron planes; N_1 is a singular point (binary azeotropic mixture isobutyraldehyde–water) of the unstable node type; CN_1 is a singular point (binary azeotropic mixture butyraldehyde–water) of the saddle-node type relative to the boundary sub-space; C_1 is a singular point (binary azeotropic mixture toluene–water) of the saddle type. The direction of the distillation line is indicated by arrows

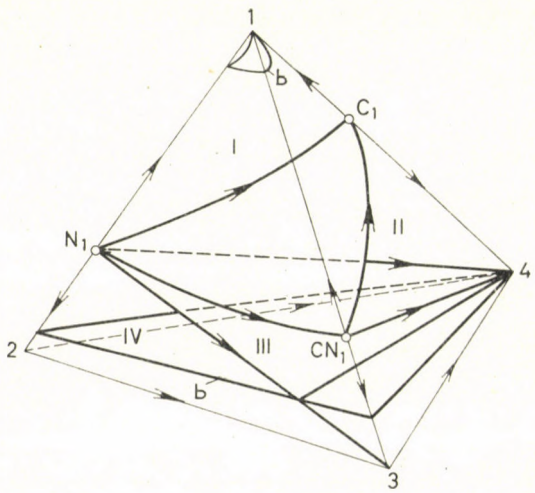


Fig. 6. Rectification regions (I, II, III, IV) in the diagram of the 4-component mixture water–isobutyraldehyde–butyraldehyde–toluene. b are binodal surfaces. The main directions of distillation are indicated by arrows

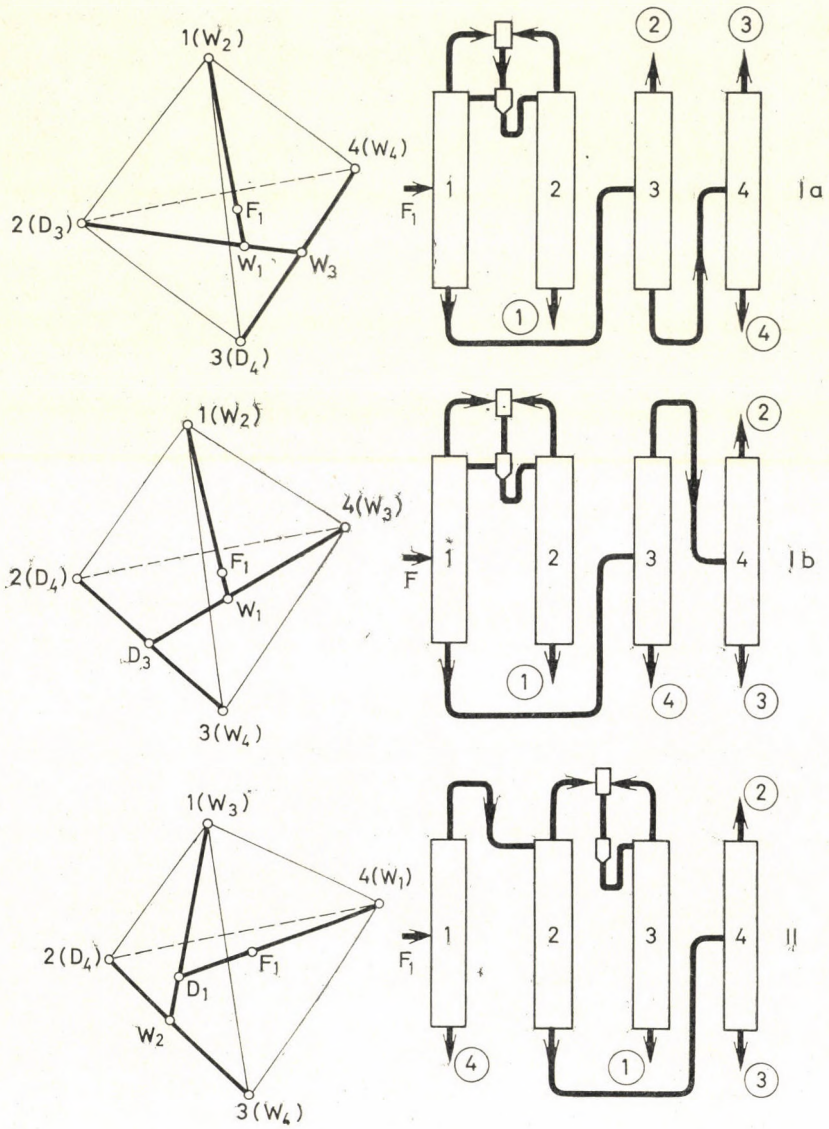


Fig. 7. Theoretically possible technological schemes for the separation of the 4-component mixture water–isobutyraldehyde–butyraldehyde–toluene into pure components. In the tetrahedrons are shown the material balance lines for a 2-column arrangement and for separate columns. F, D, W are the fluxes of initial mixture, distillate and residue, respectively. The subscripts of these letters refer to a given column. The component numbers are encircled. 1 = water, 2 = isobutyraldehyde, 3 = butyraldehyde, and 4 = toluene

with the distillation region and has a maximum boiling temperature in the point corresponding to pure water. In this region, the minimum boiling temperature corresponds to the binary azeotropic mixture water–isobutyral-

dehyde. The second distillation region which, in contrast to the first, has a maximum boiling point corresponding to pure toluene, includes 3 rectification regions belonging to the first group, *viz.* 2) $N_1 - CN_1^0 - C_1 - 4$; 3) $N_1 - - CN_1 - 3 - 4$; 4) $N_1 - 2 - 3 - 4$.

Obviously rectification region 1 forms pairs with each one of the regions 2, 3 and 4, which belong to the second group and have a common point of minimum boiling temperature corresponding to the binary azeotropic mixture isobutyraldehyde–water. Assume that the initial composition is in the fourth region. In the general case, there are two given separations corresponding to this region.

1) The distillate may be the binary heteroazeotropic mixture isobutyraldehyde–water, and the residue may be a 3-component mixture containing isobutyraldehyde, butyraldehyde and toluene.

2) The distillate may be the water–isobutyraldehyde–butyraldehyde ternary mixture, and the residue toluene.

Considering that the boundary plane $N_1 - 3 - 4$ of rectification region 4 is almost completely within the heterogeneous region, either one of the two possible separations will lead to a heterogeneous distillate and, consequently, after condensation, the latter will be separated into two layers with compositions in the first and fourth rectification region, respectively. This permits the separation of the organic components from water in a 2-column apparatus closed with respect to the upper product. Suitable variants of the corresponding technological scheme with prior dehydration of the mixtures Ia and Ib, are shown in Fig. 7.

It is easy to see that in both variants the first given separation occurs in column 1. In the same Figure is shown also variant II for the second given separation.

As shown by technological and economic analysis, the most convenient scheme is Ia.

The proposed topological analysis of the structure of liquid–vapour phase equilibrium diagrams permits to find the separation schemes which are possible in principle, and to determine the possible limits for the composition of the distillate and the residue in the case of the rectification of a given, non-ideal, multicomponent initial mixture for all the possible separation variants.

REFERENCES

1. SERAFIMOV, L. A.: Zhurn. Fiz. Khim. **41,** II, 2972 (1967)
2. GURIKOV, YU. V.: Zhurn. Fiz. Khim. **32,** 9, 1980 (1958)
3. STORONKIN, A. V.: Thermodynamics of Heterogeneous Systems (in Russian). Izd. LGU, Leningrad, 1967
4. ZHAROV, V. T.: Zhurn. Fiz. Khim. **41,** II, 2865 (1967)
5. ZHAROV, V. T.: Zhurn. Fiz. Khim. **42,** I, 121 (1968)

6. ZHAROV, V. T.: Zhurn. Fiz. Khim. **42**, 2, 364 (1968)
7. SERAFIMOV, L. A.: Zhurn. Fiz. Khim. **42**, I, 248 (1968)
8. ZHAROV, V. T., RUSANOV, A. I., LEVICHEV, S. A.: Koll. Zhurn. **6**, 819 (1968)
9. ZHAROV, V. T.: Zhurn. Fiz. Khim. **43**, II, 2784 (1969)
10. SERAFIMOV, L. A.: Zhurn. Fiz. Khim. **42**, I, 284 (1968)
11. SERAFIMOV, L. A.: D. Sc. Thesis, Lomonosov MITKhT, Moscow, 1968
12. SERAFIMOV, L. A.: Chapter 21 in V. V. SVENTOSLAVSKI: Azeotropy and Polyazeotropy .(in Russian), p. 202. Izd. Khimia, 1968
13. ZHAROV, V. T.: Zhurn. Prikl. Khim. **41**, 12, 2688 (1968)
14. ZHAROV, V. T.: Zhurn. Prikl. Khim. **42**, I, III (1969)
15. LVOV, S. V.: Problems of the Rectification of Binary and Multicomponent Mixtures (in Russian). Izd. AN USSR, Moscow, 1960
16. GVOZDOVSKI, G. N., KUSHNER, T. M., LVOV, S. V., MUSHENKO, D. V., SERAFIMOV, L. A., TATSIEVSKAYA, G. I.: Patent No. 188953, 1965; Bull. Izobret. No. **23**, 1966, USSR
17. KUSENER, T. M., TATSIEVSKAYA, G. I., SERAFIMOV. L. A., LVOV, S. V.: Khim. Prom. No. I, 20 (1968)
18. SERAFIMOV, L. A., TIMOFEYEV, V. S., BALASHOV, M. I., MEZHEVITCH, G. V.: Izv. Vysshih Utch. Zav., Khimia i Khimicheskaya Technologia, **5**, 722 (1962)

L. A. SERAFIMOV; Lomonosov Institute of Fine Chemical Technology, Moscow
V. T. ZHAROV; Zhdanov University, Leningrad
V. S. TIMOFEYEV; Lomonosov Institute of Fine Chemical Technology, Moscow, USSR.

Acta Chimica Academiae Scientiarum Hungaricae, Tomus 69 (4), pp. 397—409 (1971)

STUDY OF THE MOLECULAR STRUCTURE OF ALKYL- AND ARYL-ALKOXYSILANES, II

DIELECTRIC STUDY OF MONO-, DI- AND TRIALKOXYSILANES

J. NAGY, S. FERENCZI-GRESZ, R. FARKAS, I. BARTA and A. BORBÉLY-KUSZMANN

(Department of Inorganic Chemistry, Technical University, Budapest)

Received July 22, 1969

Revised manuscript received November 2, 1970

1. The dipole moment values of the homologous series of methylalkoxysilanes of general formula $(CH_3)_n Si(OR)_{4-n}$ ($n = 1, 2, 3$; R = CH_3, C_2H_5, C_3H_7, iso-C_3H_7, C_4H_9, *sec*-C_4H_9, C_6H_{13}) were determined by the ONSAGER method.

2. A linear correlation was found by the comparative calculation method of KARAPETIANTS between the dipole moments of the individual members of the homologous methylalkoxysilane series of different functionalities.

3. In the case of alkyl groups of low spatial requirements free rotation was observed for the monofunctional silanes, while the rotation of the di-, tri- and tetrafunctional alkoxysilanes was restricted, the extent of this increasing in the direction of the tetrafunction.

Very many contradictory data can be found in the literature regarding the molecular structure of alkylalkoxysilanes. In an earlier communication [1] we attempted to clear up the relevant problems using as examples the tetraalkoxysilanes; in the present work our studies have been extended to mono-, di- and trialkoxysilanes. Dielectric studies were carried out to investigate the steric effects in these compounds.

The methylalkoxysilanes of general formula $(CH_3)_n Si(OR)_{4-n}$ were selected as model compounds, where

$n = 1, 2, 3;$

R = CH_3, C_2H_5, C_3H_7, C_4H_9, C_6H_{13}, i-C_3H_7, *sec*-C_4H_9 .

Some of these were prepared from chlorosilanes by sodium alkoxide condensation and esterification, some by *trans*-esterification of alkoxysilanes and by alcoholysis of silazanes. The purity of the compounds was checked gas-chromatographically, similarly as in our earlier work, and by the comparison of measured and calculated molar refraction values.

The dielectric constants were determined at a frequency of 10^4 Hz at 25 °C using a bridge of our own design [2]. Values of the dipole moments were calculated by the method of ONSAGER [3]. The atom polarizations necessary for the calculations were determined from the values of the ALTSCHULLER

Table I

Compound	$(CH_3)_3SiOCH_3$	$(CH_3)_3SiOC_2H_5$	$(CH_3)_3SiO_nC_3H_7$	$(CH_3)_3SiO_nC_4H_9$	$(CH_3)_3SiOC_6H_{13}$	$(CH_3)_3SiO\,i\text{-}C_3H_7$	$(CH_3)_3SiO sec\text{-}C_4H_9$
d, g/ml	0.75340	0.75341	0.76355	0.77336	0.78561	0.75009	0.76650
ε	3.248	3.013	2.850	2.758	2.690	2.851	2.722
n_D	1.3658	1.3721	1.3819	1.3915	1.4035	1.3749	1.3870
$MR_{D\ \text{calcd}}$, ml	31.04	35.67	40.30	44.93	54.19	40.30	44.93
$MR_{D\ \text{measd}}$, ml	30.97	35.68	40.31	44.99	54.22	40.36	44.93
V	138.34	156.96	173.24	189.18	221.94	176.35	190.88
$n_F - n_C$	0.00705	0.00720	0.00740	0.00762	0.00755	0.00718	0.00745
n_∞	1.35514	1.36121	1.37026	1.38002	1.39216	1.36411	1.37579
P_e, ml	30.160	34.744	39.208	43.817	52.863	39.319	43.786
P_A, ml	3.006	3.082	3.158	3.234	3.386	3.158	3.234
$R = P_A + P_e$	33.166	37.826	42.366	47.051	56.249	42.477	47.020
ε_{eff}	1.9460	1.9525	1.9711	1.9930	2.0184	1.9519	1.9804
P^*	30.066	28.224	25.984	24.682	25.395	27.253	24.354
μ [D]	1.213	1.175	1.128	1.099	1.115	1.155	1.092

Table II

Compound	$(CH_3)_2Si(OCH_3)_2$	$(CH_3)_2Si(OC_2H_5)_2$	$(CH_3)_2Si(OC_3H_{7\ 2}$	$(CH_3)_2Si(OC_4H_9)_2$	$(CH_3)_2Si(O\,i\text{-}C_3H_7)_2$	$(CH_3)_2Si(O\,sec\text{-}C_4H_9)_2$	$(CH_3)_2(O\,i\text{-}C_4H_9)_2$
d, g/ml	0.85714	0.83440	0.83554	0.83693	0.81580	0.83105	0.81996
ε	3.663	3.216	2.992	2.836	3.050	2.966	2.795
n_D	1.3692	1.3791	1.3926	1.4034	1.3838	1.3981	1.3952
$MR_{D\ calcd}$, ml	31.80	41.06	50.32	59.58	50.32	59.58	59.58
$MR_{D\ measd}$, ml	31.67	41.08	50.32	59.65	50.51	59.37	59.78
V	140.26	177.71	211.04	244.21	216.15	245.94	249.27
$n_F - n_C$	0.00665	0.00677	0.00688	0.00715	0.00680	0.00718	0.00717
n_∞	1.35918	1.36896	1.38223	1.39262	1.37348	1.38729	1.38440
P_e, ml	30.893	40.092	49.140	58.235	49.301	57.938	58.333
P_A, ml	3.138	3.290	3.442	3.594	3.442	3.594	3.594
$R = P_A + P_e$	34.031	43.382	52.582	61.829	52.743	61.532	61.927
ε_{eff}	1.9611	1.9689	1.9965	2.0170	1.9683	2.0010	1.9920
P^*	38.582	36.752	34.912	33.602	39.010	39.648	34.082
μ [D]	1.374	1.341	1.307	1.282	1.385	1.393	1.292

Table III

Compound	$CH_3Si(OCH_3)_3$	$CH_3Si(OC_2H_5)_3$	$CH_3Si(OC_3H_7)_3$	$CH_3Si(OC_5H_9)_3$	$CH_3Si(OC_6H_{13})_3$	$CH_3Si(OiC_3H_7)_3$	$CH_3Si(OsecC_4H_9)_3$
d, g/ml	0.94920	0.88796	0.87920	0.87438	0.86611	0.84938	0.86321
ε	4.900	3.845	3.339	3.138	2.853	3.255	2.950
n_D	1.3686	1.3813	1.3972	1.4089	1.4241	1.3849	1.4037
$MR_{D\ calcd}$, ml	32.56	46.45	60.34	74.23	102.01	60.34	74.23
$MR_{D\ measd}$, ml	32.35	46.66	60.39	74.20	102.14	60.76	74.32
V	143.51	200.80	250.67	300.18	400.21	259.33	304.06
$n_F - n_C$	0.00613	0.00638	0.00695	0.00705	0.00728	0.00657	0.00693
n_∞	1.35937	1.37170	1.38675	1.39829	1.41310	1.37498	1.39328
P_e, ml	31.623	45.604	58.979	72.493	99.816	59.363	72.579
P_A, ml	3.270	3.498	3.564	3.954	4.410	3.564	3.954
$R = P_A + P_e$	34.893	49.102	62.543	76.447	104.226	62.927	76.533
ε_{eff}	1.9637	1.9710	1.9973	2.0251	2.0564	1.9611	2.0091
P^*	64.388	59.956	54.677	54.561	52.715	55.319	48.171
μ [D]	1.777	1.713	1.636	1.634	1.606	1.645	1.536

and ROSENBLUM [4] bond increments, and the electron polarizations with the aid of the refractive index n calculated from the anomalous dispersion formula. A detailed description of the measurement methods was given in our previous paper [1].

The results of our measurements and calculations are listed in Tables I to III where

n_D = the refractive index referred to the Na D line,
ε = the measured dielectric constant,
d = density,
$n_F - n_C$ = dispersion,
MR_D = molar refraction,
n_∞ = the refractive index relating to the electron polarization,
P_e = electron polarization,
P_A = atom polarization,
ε_{eff}, P^* = the effective dielectric constant and molar polarization calculated from the formula given in the previous paper,
μ = the value of the dipole moment, D, calculated from the ONSAGER formula,
V = molar volume.

From these Tables it can be established that in the case of all the functions the dipole moment decreases with the increasing number of methylene groups in the alkoxy group. A similar tendency can also be observed in the case of the decrease of the functional groups. The first comparative method of KARAPETIANTS [14] for the two observed relations was used in part to determine more accurate values, in part to find the dipole moments of the compounds missing from some homologous series.

The correlation of the dipole moments for the normal homologous series of methylalkoxysilanes of various functionalities are given in Fig. 1. The equations of the straight lines thus obtained were calculated with the help of the least squares principle to be:

$$\mu_M = 1.29054\,\mu_D - 0.56030$$

$$\mu_M = 0.73521\,\mu_T - 0.08838$$

$$\mu_M = 0.52127\,\mu_Q + 0.26368$$

$$\mu_D = 0.77487\,\mu_M + 0.43416$$

$$\mu_D = 0.60479\,\mu_T + 0.30231$$

$$\mu_D = 0.40397\,\mu_Q + 0.63810$$

$$\mu_T = 1.26770\,\mu_M + 0.23323$$

$$\mu_T = 1.64893\,\mu_D - 0.49364$$

$$\mu_T = 0.65698\,\mu_Q + 0.57379$$

$$\mu_Q = 1.91839\,\mu_M - 0.50584$$

$$\mu_Q = 2.47543\,\mu_D - 1.57957$$

$$\mu_Q = 1.45707\,\mu_T - 0.76623$$

$$\mu_{(OC_6H_{13})_{4-n}} = 1.00218\,\mu_{(OC_4H_9)_{4-n}} - 0.002817$$

These regressed dipole moment values were determined from these s raight lines.

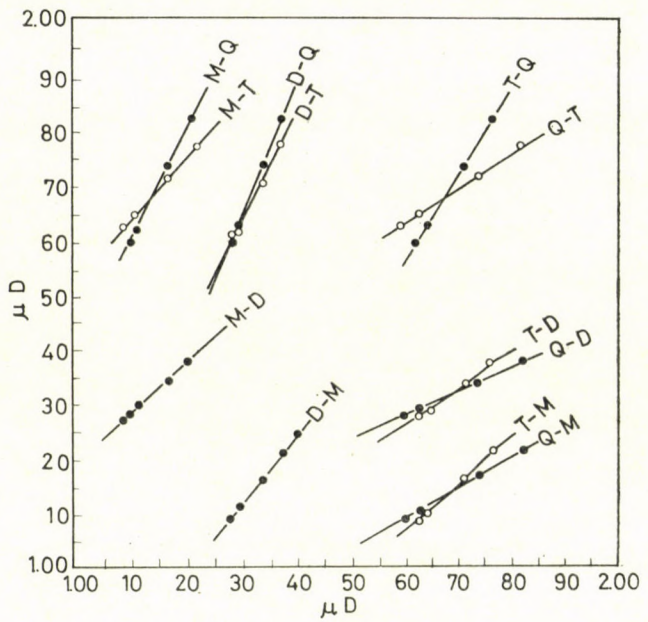


Fig. 1. Correlation diagrams for the dipole moments of individual methylalkoxysilanes of different functionalities

The correlation was also determined for the compounds containing various alkoxy groups, as a result of which it was possible to calculate the missing dipole moments of di- and tetrahexoxysilane. This is shown in Fig. 2.

The dipole moment values of the branched-chain alkoxysilanes were also calculated from a similar correlation.

Since the dipole moments of the compounds studied by us had been determined by other authors too, it appeared of interest to compare their results with our values calculated according to ONSAGER and regressed on the

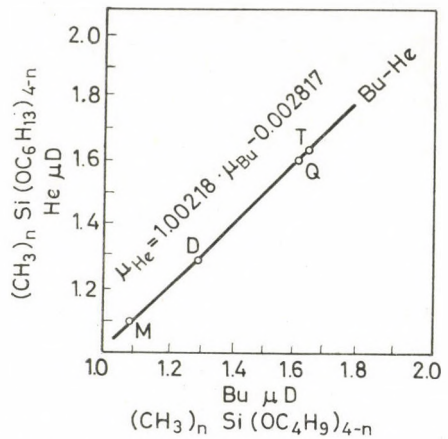


Fig. 2. Correlation diagram for the dipole moments of the methylbutoxy- and methylhexoxysilanes of different functionalities

basis of the first comparative method of KARAPETIANTS. The data are collected in Table IV.

From Table IV it is clear that the values of the dipole moments calculated from the measurement data and from the equations of the correlation lines are in good agreement; this confirms the correctness of our experimental method and the correlation calculations.

It may be seen that the measured values differ from the literature data for certain compounds by up to 0.5 *D*.

With modern experimental techniques, under identical conditions the accuracy of the determination of dipole moments is $+0.05$ *D*. (Our measured values were given to three decimal places so that comparison with the regressed values would be easier.) Under different conditions the derivation of the dipole moment values can be explained by the following causes:

1. the error arising from the degree of purity of the compound;

2. the error arising from the applied measurement method (ONSAGER, HEDESTRAND, etc.);

3. the error arising from the calculation technique pertaining to the measurement method;

4. a solvent error; cyclohexane was used as solvent thereby decreasing this to a minimum, whilst the literature values were measured most often in benzene or carbon tetrachloride solutions where the solvent error is substantially larger;

5. the error arising from the calculation of the atom polarization; since the total of the electron and atom polarizations is generally taken as 5% of the molar polarization in the calculation of the literature values, this can be a source of serious error.

Table IV

Compound	μ_{measd} [D]	μ_{corr} [D]	$\lvert\Delta\mu\rvert$ [D]	μ_{lit} [D]
$(CH_3)_3SiOCH_3$	1.213	1.214	0.001	1.18 [7]
$(CH_3)_2Si(OCH_3)_2$	1.374	1.375	0.001	1.33 [7]; 1.29 [12]
$CH_3Si(OCH_3)_3$	1.776	1.773	0.003	1.60; 1.62 [7]; 1.70 [8]; 1.68 [12]
$Si(OCH_3)_4$	1.832	1.825	0.007	1.62 [9]; 1.78; 1.80 [7]; 1.71; 1.65; 1.40; 2.00 [10]
$(CH_3)_3SiOC_2H_5$	1.175	1.172	0.003	1.146 [5]; 1.18 [6]; 1.39 [12]
$(CH_3)_2Si(OC_2H_5)_2$	1.341	1.340	0.001	1.358 [5]; 1.36 [6]; 1.39 [12]
$CH_3Si(OC_2H_5)_3$	1.713	1.717	0.004	1.678 [5]; 1.72 [8]; 1.72 [12]
$Si(OC_2H_5)_4$	1.728	1.736	0.008	1.736 [5]; 1.72 [11]; 1.84 [8]; 1.70 [9]; 1.75 [12]; 1.63; 1.34; 1.54; 1.84 [10]
$(CH_3)_3SiOC_3H_7$	1.128	1.116	0.012	
$(CH_3)_2Si(OC_3H_7)_2$	1.307	1.296	0.011	
$CH_3Si(OC_3H_7)_3$	1.636	1.643	0.007	
$Si(OC_3H_7)_4$	1.623	1.628	0.005	1.66 [9]; 1.48; 1.36; 1.04; 1.54 [10]; 1.83 [8]
$(CH_3)_3SiOC_4H_9$	1.099	1.103	0.004	
$(CH_3)_2Si(OC_4H_9)_2$	1.282	1.285	0.003	1.34 [12]
$CH_3Si(OC_4H_9)_3$	1.634	1.626	0.008	
$Si(OC_4H_9)_4$	1.610	1.603	0.007	1.66 [9]; 1.80 [8]; 1.44; 1.69; 1.82 [10]; 1.63 [5]; 1.78 [11]
$(CH_3)_3SiOC_6H_{13}$	1.115	1.102	0.013	
$(CH_3)_2Si(OC_6H_{13})_2$	—	1.285	—	
$CH_3Si(OC_6H_{13})_3$	1.606	1.625	0.019	
$Si(OC_6H_{13})_4$	—	1.602	—	
$(CH_3)_3SiO$ i-C_3H_7	1.155	1.143	0.012	
$(CH_3)_2Si(O$ i-$C_3H_7)_2$	1.385	1.366	0.019	
$CH_3Si(O$ i-$C_3H_7)_3$	1.645	1.613	0.032	
$Si(O$ i-$C_3H_7)_4$	1.573	1.599	0.026	1.69; 1.58; 1.16; 1.57 [10]; 1.80 [8]
$(CH_3)_3SiO$*sec*C_4H_9	1.092	1.170	0.078	
$(CH_3)_2Si(O$*sec*$C_4H_9)_2$	1.393	1.264	0.129	
$CH_3Si(O$ *sec*-$C_4H_9)_3$	1.536	1.436	0.100	
$Si(O$ *sec*-$C_4H_9)_4$	1.277	1.427	0.150	1.57; 1.44; 1.10; 1.50 [10]

Finally it may be stated that the differences of our measured dipole moments from the literature values are not greater than the differences among values to be found in the literature.

The methylethoxysilanes were chosen for the investigation of the steric effect because the steric hindrance observed in these shows up to an even more pronounced extent than in alkoxysilanes containing more carbon atoms. The dipole moment value relating to free rotation was calculated from a vector diagram of methylethoxysilanes of all functionalities. According to derivations reported in an earlier paper [5], the following equations can be written for the free rotational state of the compounds examined:

$(CH_3)_3SiOC_2H_5$ $\quad \bar{\mu}^2_{rot} = m_1^2 + m_2^2 + 3\,m_3^2 + [3\,m_3 \cos\vartheta\,(m_1 \cos\Theta + m_3 + m_2) + m_1 m_2 \cos\Theta]$

$(CH_3)_2Si(OC_2H_5)_2$ $\quad \bar{\mu}^2_{rot} = 2(m_1^2 + m_2^2 + m_3^2) + 2[m_1^2 \cos\vartheta \cdot \cos^2\Theta + 2\,m_1 m_2 \cos\Theta\,(1 + \cos\vartheta) + 4\,m_3 \cos\Theta\,(m_2 + m_1 \cos\Theta) + \cos\vartheta\,(m_2^2 + m_3^2)]$

$CH_3Si(OC_2H_5)_3$ $\quad \bar{\mu}^2_{rot} = 3\,m_1^2\,(1 + 2\cos^2\Theta \cdot \cos\vartheta) + (3\,m_2^2 + 6\,m_1 m_2 \cos\Theta)\,(1 + 2\cos\vartheta) + m_3^2 + 6\,m_3 \cos\vartheta\,(m_2 + m_1 \cos\Theta)$

$Si(OC_2H_5)_4$ $\quad \bar{\mu}^2_{rot} = 4\,m_1^2(1 + 3\cos^2\alpha \cdot \cos\vartheta)$

The following bond angle and bond moment values were substituted into the above equations:

$m_1 = m_{C-O} = 1.12\ D$ [6]; $\quad \Theta = O\begin{matrix}\diagup C \\ \diagdown Si\end{matrix} \sphericalangle = 113°$ [13]

$m_2 = m_{Si-O} = 1.22\ D$ [5]; $\quad \vartheta = Si\begin{matrix}\diagup O \\ \diagdown O\end{matrix} \sphericalangle = 109°\,28'$

$m_3 = m_{Si-CH_3} = 0.2\ D$ [4]; $\quad \alpha = 180° - \Theta = 67°$

The free rotational dipole moment values thus calculated are compared with the values obtained from the measurement data in Table V.

Table V

Compound	μ_{exp} [D]	μ_{rot} [D]	$\lvert\Delta\mu\rvert$ [D]
$(CH_3)_3SiOC_2H_5$	1.175	1.190	0.015
$(CH_3)_2Si(OC_2H_5)_2$	1.341	1.605	0.264
$CH_3Si(OC_2H_5)_3$	1.713	1.878	0.165
$Si(OC_2H_5)_4$	1.728	2.062	0.334

From Table V it can be seen that the experimental and calculated dipole moment values for trimethylethoxysilane are almost identical; this permits the conclusion that in the case of a rotator we can speak of free rotation. With the increase of the number of alkoxy groups, the difference between the experimental and calculated values, that is the hindrance to rotation, also increases. It can be established from the Table that the rotational hindrance is greatest for the tetrafunction, the decreases through the difunction to the trifunction. This finding is confirmed by the dipole moment measurements in the temperature region between 0 and 80 °C for methylethoxysilanes of different functionalities.

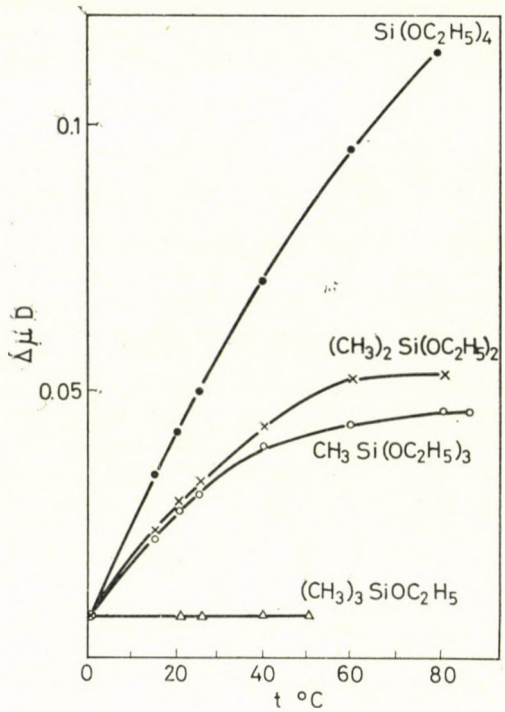


Fig. 3. Increase of the dipole moments of methylethoxysilanes of different functionalities as a function of temperature

If the difference of the measured dipole moments from the values measured at 0 °C are plotted as a function of temperature (Fig. 3), it is readily seen that whilst the observed dipole moment values in the case of the monofunction can be considered as constant within the experimental error, the dipole moments of the other compounds examined are functions of the temperature. These plots differ from each other in slope; within a given temperature interval the change of dipole moment is greatest for the tetrafunction,

next largest for the difunction, and then follows the trifunction. The data given in Table V and Fig. 3 together prove the assumption that free rotation is only possible in the case of silanes containing alkyl groups with low spatial requirements; in the other compounds the alkoxy group can only move fanwise about the Si—O bond axis.

In our further work we wish to study the restricted rotation of alkylalkoxysilanes on a thermodynamic basis. We succeeded in finding a generally valid equation similar to the Arrhenius expression for the description of the phenomenon; according to this there is a linear relationship between the reciprocal of the absolute temperature and the logarithm of the temperature-dependent dipole moment:

$$\bar{\mu} = \mu_{rot}\, e^{\Delta S/R}\, e^{-\Delta E^*/RT}$$

where $\bar{\mu}$ = the measured dipole moment;
μ_{rot} = the free rotation value obtained as a result of vectorial calculations;
ΔS = the rotational activation entropy;
ΔE^* = the rotational activation energy.

We shall deal with this in detail in a forthcoming paper.

Experimental

Preparation of trimethylalkoxysilanes

Trimethylmethoxysilane

250 ml abs. toluene, 32 g (1 mole) abs. methanol and 95 g (1.2 mole) abs. pyridine were placed in a flask fitted with a mercury-seal stirrer, a reflux condenser and a dropping funnel. A mixture of 150 ml abs. toluene and 109 g (1 mole) trimethylchlorosilane was slowly added with stirring, and then the mixture was heated in a water-bath for 2—3 hours. Ice-water was added to the cooled mixture in order to remove the precipitated pyridine hydrochloride, and washing was continued in a separatory funnel until the toluene phase showed a neutral reaction. The toluene solution was dried with $CaCl_2$, filtered and fractionated using a Raschig-ring column.

B.p. 56—57 °C/760 mm Hg.

Trimethylethoxysilane

Commercial trimethylethoxysilane was rectified on a column corresponding to 6—7 theoretical plates.

B.p. 75.5 °C/760 mm Hg.

Trimethylpropoxysilane

80.5 g (1.35 mole) abs. propanol was placed in a flask fitted with a mercury-seal stirrer, a reflux condenser, a dropping funnel and a gas inlet, and then 120 g (0.75 mole) hexamethyldisilazane was added. With stirring and the passage of N_2, the mixture was boiled until the cessation of NH_3 evolution. The product was fractionated using a Raschig-ring column.

B.p. 99—99.5 °C/760 mm Hg.

Trimethyl-n-hexoxysilane

115 g (1.1 mole) abs. hexanol was placed in a flask fitted with a mercury-seal stirrer, a reflux condenser and a dropping funnel, and in this was dissolved 23 g (1 mole) metallic sodium. After dissolution was complete, 109 g (1 mole) trimethylchlorosilane was slowly added to the alkoxide and the mixture boiled for about 2 hours. The product was fractionated on a column equivalent to 6—7 theoretical plates.

B.p. 171—172 °C/760 mm Hg.

The compounds listed below were prepared by the following general procedure:

1.16 mole metallic sodium granulated in xylene was placed in a flask fitted with a mercury-seal stirrer, a reflux condenser and a dropping funnel (in the preparation of trimethyl-butoxysilane and trimethyl-*sec*-butoxysilane the xylene was exchanged for benzene after granulation), and 1 mole of the appropriate abs. alcohol was slowly added. After the addition was complete the mixture was boiled for about 2 hours. A xylene solution of 1 mole trimethyl-chlorosilane was slowly added dropwise to the cold alkoxide. The mixture was again boiled for about 2 hours, then distilled from the precipitated NaCl, and fractionated using a Raschig-ring column.

Trimethyl-iso-propoxysilane

60 g (1 mole) abs. iso-propanol and then 109 g (1 mole) trimethylchlorosilane was added to 26 g (1.16 mole) metallic sodium granulated in xylene.

B.p. 89—90.5 °C/760 mm Hg.

Trimethyl-n-butoxysilane

74 g (1 mole) abs. butanol and then 130 ml (1 mole) trimethylchlorosilane was added to 26 g (1.16 mole) metallic sodium granulated in xylene.

B.p. 123.5 °C/763 mm Hg.

Trimethyl-sec-butoxysilane

76 g (1 mole) abs. *sec*-butanol and then 109 g (1 mole) trimethylchlorosilane was added to 26 g (1.16 mole) metallic sodium granulated in xylene.

B.P. 112—113 °C/760 mm Hg.

Preparation of dimethyldialkoxysilanes

The compounds were prepared according to the following procedure with the exception of the commercially available dimethyldiethoxysilane:

2 moles of abs. pyridine was placed in a flask fitted with a mercury-seal stirrer, a reflux condenser and a dropping funnel, and with efficient ice-cooling 1 mole dimethyldichlorosilane was slowly added. 2 moles of the appropriate abs. alcohol was added dropwise. When this addition was complete the mixture was boiled for 1 day. When cold, the precipitated pyridine hydrochloride was filtered off under a stream of N_2 and the mixture fractionated using a Raschig-ring column.

Dimethyldimethoxysilane

129 g (1 mole) dimethyldichlorosilane and then 64.1 g (2 moles) abs. methanol was added to 158.2 g (2 moles) abs. pyridine.

B.p. 82 °C/760 mm Hg.

Dimethyldi-n-propoxysilane

129 g (1 mole) dimethyldichlorosilane and then 120 g (2 mole) abs. *n*-propanol was added to 158.2 g (2 mole) abs. pyridine.

B.p. 152 °C/760 mm Hg.

Dimethyldi-iso-propoxysilane

129 g (1 mole) dimethyldichlorosilane and then slowly 120 g (2 moles) abs. *iso*-propanol was added to 158.2 g (2 moles) abs. pyridine.
B.p. 133 °C/760 mm Hg.

Dimethyldi-n-butoxysilane

129 g (1 mole) dimethyldichlorosilane and then 148 g (2 moles) abs. *n*-butanol was added to 158.2 g (2 moles) abs. pyridine.
B.p. 190 °C/760 mm Hg.

Dimethyldi-isobutoxysilane

129 g (1 mole) dimethyldichlorosilane and then 148 g (2 moles) abs. *iso*-butanol was added to 158.2 g (2 moles) abs. pyridine.
B.p. 172 °C/760 mm Hg.

Dimethyldi-sec-butoxysilane

129 g (1 mole) dimethyldichlorosilane and then 148 g (2 moles) abs. *sec*-butanol was added to 158.2 g (2 moles) abs. pyridine.
B.p. 178—179 °C/760 mm Hg.

Preparation of methyltrialkoxysilanes

The following procedure was used for all compounds with the exception of methyltriethoxysilane which is commercially available:

In order to trap the HCl gas evolved, gaseous ammonia was passed over 3 moles of vigorously stirred methyltrichlorosilane in a 2 l flask fitted with a stirrer, a reflux condenser, a dropping funnel and a gas inlet, and with efficient external cooling 9.5 moles (0.5 mole excess) of the appropriate alcohol was added dropwise. The purity of the alcohol was earlier checked with a gas-chromatograph.

The reaction could be considered finished when the reaction mixture became alkaline. The precipitated ammonium chloride was filtered off and the reaction mixture fractionated on a column equivalent to 6—7 theoretical plates. The alcohols taken in excess were collected as headings. The headings were fractionated in 20 ml portions and the gas-chromatographically pure fractions were used for measurement. The gas-chromatographic examination could not be carried out for the high boiling point tri-*n*-propoxy-, tri-*n*-butoxy- and tri-*n*-hexoxysilanes.

Methyltrimethoxysilane

305 g (9.5 moles) methanol was added to 448.5 g (3 moles) methyltrichlorosilane under a stream of gaseous NH_3. After the reaction, the mixture was heated at the boiling point for 1 hour.
B.p. 102 °C/760 mm Hg.

Methyltri-n-propoxysilane

575 g (9.5 moles) *n*-propanol was added to 448.5 g (3 moles) methyltrichlorosilane similarly as in the preparation of methyltrimethoxysilane.
B.p. 84 °C/760 mm Hg.

Methyltri-iso-propoxysilane

448.5 g (3 moles) methyltrichlorosilane was esterified with 575 g (9.5 moles) *iso*-propanol.
B.p. 163 °C/760 mm Hg.

Methyltri-n-butoxysilane

The required product was obtained by the reaction of 448.5 g (3 moles) methyltrichlorosilane and 705 g (9.5 moles) *n*-butanol.
B.p. 123 °C/15 mm Hg.

Methyltri-sec-butoxysilane

448.5 g (3 moles) methyltrichlorosilane was reacted with 705 g (9.5 moles) *sec*-butanol.
B.p. 214 °C/760 mm Hg.

Methyltri-n-hexoxysilane

The product was obtained by the reaction of 370 g (2.5 moles) methyltrichlorosilane with 820 g (8 moles) *n*-hexanol.
B.p. 187 °C/15 mm Hg.

REFERENCES

1. NAGY, J., FERENCZI-GRESZ, S., FARKAS, R.: Acta Chim. Acad. Sci. Hung. **52,** 319 (1967)
2. NAGY, J., GRESZ, I., FERENCZI-GRESZ, S.: Periodica Polytechnica Ch **10,** 335 (1966)
3. ONSAGER, L.: J. Am. Chem. Soc. **58,** 1486 (1936)
4. ALTSHULLER, A. P., ROSENBLUM, L.: J. Am. Chem. Soc. **77,** 272 (1955)
5. NAGY, J.: C. S. Thesis 1960. Budapest
6. FREISER, H., EAGLE, M. V., SPEIER, J. R. JR.: J. Am. Chem. Soc. **75,** 2824 (1953)
7. MATSUMURA, L.: Bull. Chem. Soc. Japan **35,** 801—8 (1962)
8. LARSSON, E.: Trans. Chalmers Univ. Techn., Göteborg No. **115,** 15 (1951)
9. ARBUZOV, B. A., SAVSA, T. G.: Dokl. AN SSSR **68,** 859 (1949)
10. MAY, L. A., STRAUSZ, I. J.: Intern. Symp. on Organosilicon Chem., Prague, 1965, Comm. 245
11. SVIRBELY, W. J., LANDER, J. J.: J. Am. Chem. Soc. **67,** 2189 (1945)
12. CUMPER, C. W. N., MELNIKOFF, A. L., VOGEL, A. I.: J. Chem. Soc. (A) 242 (1966)
13. UEDA, Y., YOKOI, M., KOTERA, A., YAMASAKI, K.: J. Chem. Soc. Japan **72,** 544 (1951)
14. KARAPETIANTS, M. H.: Metodi sravnitelnovo raschota fizikokhimicheskih svoistv. "Nauka", Moscow, 1965

József NAGY
Sarolta FERENCZI-GRESZ
Renáta FARKAS
István BARTA
Anna BORBÉLY-KUSZMANN

Budapest XI., Gellért tér 4.

Acta Chimica Academiae Scientiarum Hungaricae, Tomus 69 (4), pp. 411—421 (1971)

INVESTIGATION OF THE DIPOLE MOMENTS AND INFRARED SPECTRA OF PHENOXYSILANES

J. NAGY, P. HENCSEI, S. FERENCZI-GRESZ and T. GÁBOR

(Department of Inorganic Chemistry, Technical University, Budapest)

Received December 20, 1969

The dipole moments and infrared spectra of several phenoxysilanes were determined. The m_{Si-O} bond moment was calculated and it has been established that the trimethylphenoxysilane and bis-(trimethylsiloxy)benzene molecules rotate freely, whereas the rotation of the other phenoxysilanes is hindered.

The infrared spectra have shown that the $\nu_s(SiO)$ value is higher for phenoxysilanes than for alkoxysilanes. From this we conclude that in phenoxysilanes a $d\pi—p\pi$ bond forms between the silicon and oxygen and this bond extends over the phenyl group, too.

In our earlier papers [1—4] we reported the preparation and ultraviolet spectra of several phenoxysilanes as well as the results of quantum-mechanical calculations on these compounds. It could be ascertained that the Si—O bond in phenoxysilanes has a partially double-bond character. A $d\pi—p\pi$ bond exists between the unshared electron pair of the oxygen and the 3 *d* orbital of the silicon. According to our calculations, the π-bond order is 0.26. In our present paper we describe the infrared spectra and the determination of the dipole moments of phenoxysilanes and evaluate the results.

The following compounds were investigated:

$(CH_3)_n\,Si(OC_6H_5)_{4-n}$ (where $n = 0, 1, 2, 3$) and
$C_6H_4[OSi(CH_3)_3]_2$ (the *ortho*, *meta* and *para* derivatives).

The compounds were obtained on the basis of the following reaction equations, in accordance with the literature:

$$(CH_3)_nSiCl_{4-n} + (4-n)\,C_6H_5OH = (CH_3)_n\,Si(OC_6H_5)_{4-n} + (4-n)\,HCl$$
(where $n = 0, 1, 2$) [5—7]

$$(CH_3)_3SiNHSi(CH_3)_3 + 2C_6H_5OH = 2(CH_3)_3SiOC_6H_5 + NH_3 \quad [1]$$

$$(CH_3)_3SiNHSi(CH_3)_3 + C_6H_4(OH)_2 = C_6H_4[OSi(CH_3)_3]_2 + NH_3 \quad [8]$$

The purity of the compounds obtained was checked by gas chromatography and by comparison of measured and calculated molar refraction values.

The dipole moments of the compounds were determined with a capacity measuring device described earlier [9]. The dielectric constant was calculated from the capacity values measured. The dipole moment was determined by the methods of ONSAGER [10] and HEDESTRAND [11].

In the method of ONSAGER, the dipole moments are calculated from the following relations:

$$R = P_A + P_e = 1.05 \cdot MR_D$$

$$\varepsilon_{\text{eff}} = \frac{2R + V}{V - R}$$

$$p^* = (\varepsilon_0 - \varepsilon_{\text{eff}}) \cdot V \frac{2\varepsilon_0 + \varepsilon_{\text{eff}}}{\varepsilon_0(\varepsilon_{\text{eff}} + 2)^2}$$

$$\mu = 0.0128 \sqrt{T} \cdot \sqrt{p^*}$$

where R — the sum of the atom and electron polarization,
MR_D — the molar refraction calculated from the refractive index (n_D) and density (d),
ε_{eff} — effective dielectric constant,
V — molar volume,
p^* — directional polarization,
ε_0 — measured dielectric constant,
T — temperature (in °K),
μ — dipole moment (in Debye).

According to HEDESTRAND, the dipole moment can be determined from the following equations:

$$P_\infty = \frac{\varepsilon_1 - 1}{\varepsilon_1 + 2} \cdot \left(\frac{M_2}{d_1} - \frac{M_1}{d_1^2} \beta \right) + \frac{3M_1}{(\varepsilon_1 + 2)^2 d_1} \alpha$$

$$\mu = 0.0128 \sqrt{T} \cdot \sqrt{P_\infty - R}$$

where P_∞, ε_1 and d_1 are the dielectric polarization extrapolated to infinite dilution, the dielectric constant and the density respectively. M_1 is the molecular weight of the solvent (cyclohexane), M_2 is the molecular weight of the solute, α is the slope of the dielectric constant (ε) *vs.* mole fraction (x_2) straight line and β is the slope of the density (d) *vs.* mole fraction (x_2) straight line.

The dipole moment of tetraphenoxysilane was — because of the low melting point (47—48 °C) — determined in melt at 60 °C. The R value for the dipole moment of *para*-bis(trimethylsiloxy)benzene was calculated from the molar refraction obtained theoretically from the increments.

The dipole moments of dimethyldiphenoxysilane and methyltriphenoxysilane were determined by the methods of ONSAGER and HEDESTRAND. The difference between the results is rather small (0.062 and 0.029 *D*, respectively), *i.e.* in our case both methods can be applied.

The measured data and dipole moments of the compounds are listed in Tables I and II.

Table I

Dipole moments of phenoxysilanes obtained by the method of ONSAGER *and the data necessary for the calculations*

Compound	t (°C)	n_D	d_4 (g/ml)	ε_0	μ (*D*)
$(CH_3)_3SiOC_6H_5$	25	1.4753	0.9192	3.3953	1.215
$(CH_3)_2Si(OC_6H_5)_2$	0	1.5421	1.0821	3.5600	1.212
	15	1.5351	1.0695	3.5136	1.246
	25	1.5299	1.0608	3.5000	1.278
	40	1.5223	1.0463	3.4440	1.309
	60	1.5123	1.0283	3.3806	1.353
	80	1.5021	1.0104	3.3220	1.399
$CH_3Si(OC_6H_5)_3$	25	1.5575	1.1297	3.6280	1.417
$Si(OC_6H_5)_4$	60	1.5508	1.1412	3.4915	1.586
o-$C_6H_4[OSi(CH_3)_3]_2$	25	1.4679	0.9380	2.9767	1.228
	50	1.4552	0.9144	2.8971	1.273
m-$C_6H_4[OSi(CH_3)_3]_2$	25	1.4724	0.9456	3.7847	1.703
	50	1.4588	0.9196	3.5816	1.726

From the values of the dipole moments, the following conclusions can be drawn about the molecular structure and stereo-chemistry of phenoxysilanes.

From the dipole moment of the diphenylether and the COC angle, the $m_{C_6H_5-O}$ bond moment was calculated using the following relationship

$$\mu = m_{C_6H_5-O} \cdot \sqrt{2(1 + \cos \omega)}$$

where $\mu = 1.14\ D$, and $\omega = 118°$ [12]. Hence

$$m_{C_6H_5-O} = 1.107\ D$$

The Si—O bond moment was determined from the dipole moment of trimethylphenoxysilane. The vectorial structure of trimethylphenoxysilane is

Table II

Dipole moments of phenoxysilanes obtained by the method of HEDESTRAND *and the measured and calculated data necessary for the calculations ($t = 25$ °C)*

Compound	x_2	$\varepsilon_{1,2}$	$d_{1,2}$		$\overset{\mu}{(D)}$
$(CH_3)_2Si(OC_6H_5)_2$	0.011044	2.0402	0.77805	$\alpha = 2.2250$	1.216
	0.019638	2.0617	0.78319	$\beta = 0.5732$	
	0.037710	2.1020	0.79290	$\varepsilon_1 = 2.0182$	
	0.050146	2.1252	0.80111	$d_1 = 0.77177$	
	0.080845	2.1982	0.81767		
$CH_3Si(OC_6H_5)_3$	0.010738	2.0522	0.78110	$\alpha = 3.0736$	1.446
	0.048920	2.1702	0.81232	$\beta = 0.8036$	
	0.078414	2.2535	0.83545	$\varepsilon_1 = 2.0180$	
				$d_1 = 0.77254$	
$p\text{-}C_6H_4[OSi(CH_3)_3]_2$	0.009831	2.0435	0.78052	$\alpha = 2.8990$	1.606
	0.015956	2.0621	0.78187	$\beta = 0.2700$	
	0.027473	2.0967	0.78493	$\varepsilon_1 = 2.0157$	
	0.031464	2.1075	0.78612	$d_1 = 0.77767$	
	0.048555	2.1543	0.79060		

shown in Fig. 1. Assuming free rotation, the resultant dipole moment can be calculated from the bond-moments according to NAGY [13] as follows:

$$\mu^2 = m_1^2 + [m_2^2 + 3 m_3^2 + 2 [3 m_3 \cdot \cos\beta(m_1 \cos\alpha + m_2 + m_3) + m_1 m_2 \cos\alpha]$$

where $m_3 = m_{Si-CH_3} = 0.2\ D$ after ALTSHULLER and ROSENBLUM [14],
$m_1 = 1.107\ D$,
$\mu = 1.215\ D$,
$\beta = 109°28'$, the bond angle corresponding to the sp^3 hybrid state of silicon
$\alpha = 120°$.

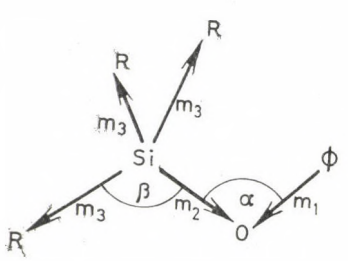


Fig. 1. Vectorial structure of trimethylphenoxysilane

In hydroquinonedimethylether the COC bond angle is $121 \pm 2°$ [15]. Accordingly, the value of the SiOC angle was taken as 120°. Our supposition was proved by electron diffraction investigations of GLIDEWELL *et al.* [21]. With these data the m_{Si-C} bond moment is 1.500 *D*. With the help of the m_{Si-O} bond moment determined, the free-rotation dipole moments were calculated for the other phenoxysilanes. The vectorial picture of tetraphenoxysilane is shown in Fig. 2.

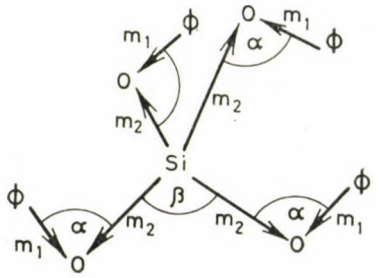


Fig. 2. Vectorial structure of tetraphenoxysilane

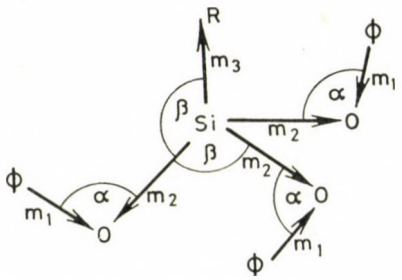


Fig. 3. Vectorial structure of methyltriphenoxysilane

The free-rotation dipole moment is

$$\mu^2 = 4\, m_1^2\, (1 + 3 \cos^2 \alpha \cdot \cos \beta)$$

Hence

$$\mu_{rot} = 1.917\ D$$

The vectorial structure of methyltriphenoxysilane is shown in Fig. 3. The free-rotation dipole moment is

$$\mu^2 = 3\, m_1^2\, (1 + \cos^2 \alpha \cdot \cos \beta) + (3\, m_2^2 + 6\, m_1 m_2 \cos \alpha) \cdot$$

$$\cdot\, (1 + 2 \cos \beta) + m_3^2 + 6\, m_3 \cdot \cos \beta\, (m_2 + m_1 \cos \alpha)$$

Hence

$$\mu_{rot} = 1.820\ D$$

The vectorial structure of the dimethyldiphenoxysilane molecule is shown in Fig. 4.

The free-rotation dipole moment is

$$\mu^2 = 2(m_1^2 + m_2^2 + m_3^2) + 2[m_1^2 \cdot \cos\beta \cdot \cos^2\alpha +$$

$$+ 2\, m_1 m_2 \cos\alpha \cdot (1 + \cos\beta) + 4\, m_3 \cos\beta(m_2 + m_1 \cos\alpha) + \cos\beta(m_2^2 + m_3^2)].$$

Hence

$$\mu_{\text{rot}} = 1.607\ D$$

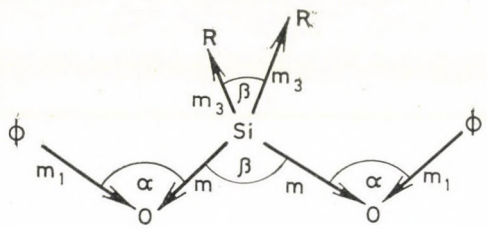


Fig. 4. Vectorial structure of dimethyldiphenoxysilane

The free-rotation dipole moment of the *p*-bis(trimethylsiloxy)benzene is

$$\mu_{\text{rot}} = \sqrt{2} \cdot m \cdot \sin 60^\circ \qquad m = m_2 - m_3$$

$$\mu_{\text{rot}} = 1.592\ D$$

The free-rotation dipole moments of *ortho*- and *meta*-bis(trimethylsiloxy)-benzene were calculated from the relation of FUCHS [16] and TIGANIK [17]. If a molecule contains two polar groups with moments μ_1 and μ_2, rotating freely about the respective axes, the angles between the direction of the rotation axes and the vectors of the group moment are Θ_1 and Θ_2, and the angle between the axes is ω_{12}, then the resultant dipole moment is:

$$\mu = (\mu_1^2 + \mu_2^2 + 2\,\mu_1\mu_2 \cos\Theta_1 \cos\Theta_2 \cos\omega_{12})^{1/2}$$

$\mu_1 = \mu_2 = 1.215\ D$ and equal to the dipole moment of trimethylphenoxysilane.

ω_{12} is 60° for the *ortho*-compound, 120° for the *meta*- and 180° for the *para*-derivative.

The angle Θ was calculated from the experimental dipole moment of *p*-bis(trimethylsiloxy)benzene (which compound rotates freely) in the following way:

$$\sin\Theta = \frac{\mu}{\mu_1\sqrt{2}} = \frac{1.606}{1.4142 \times 1.215} = 0.9347$$

hence

$$\Theta = 69°11'$$

On the basis of these data, the free-rotation dipole moments are:
o-bis(trimethylsiloxy)benzene:

$$\mu = \sqrt{2\mu_1^2 \left(1 + \frac{\cos^2 \Theta}{2}\right)} = 1.772\ D$$

m-bis(trimethylsiloxy)benzene:

$$\mu = \sqrt{2\mu_1^2 \left(1 - \frac{\cos^2 \Theta}{2}\right)} = 1.663\ D$$

The calculated free-rotation dipole moments and the experimental values are compared in Table III.

From the data in Table III, it can be ascertained that the *p*-bis(trimethylsiloxy)benzene molecule rotates freely, while the rotation of the other phenoxysilanes is hindered. This is proved by the difference between the calculated and measured dipole moments. Hindered rotation is also shown by the fact that the dipole moments of dimethyldiphenoxysilane, *o*-bis(trimethylsiloxy)benzene and the *m*-bis(trimethylsiloxy)benzene change with the temperature. At the same time our results indicate that it was correct to suppose free rotation in the case of trimethylphenoxysilane and to take 120° as the SiOC angle because the m_{Si-O} bond moment calculated from this proved to be realistic in our subsequent calculation and gave the expected results.

Table III

Calculated and experimental dipole moments of phenoxysilanes

	μ_{rot} (*D*)	μ_{exp} (*D*)	Deviation (*D*)
$(CH_3)_3SiOC_6H_5$	1.215	1.215	—
$Si(OC_6H_5)_4$	1.917	1.586	0.331
$CH_3Si(OC_6H_5)_3$	1.820	1.417	0.403
$(CH_3)_2Si(OC_6H_5)_2$	1.607	1.278	0.329
o-$C_6H_4[OSi(CH_3)_3]_2$	1.772	1.228	0.544
m-$C_6H_4[OSi(CH_3)_3]_2$	1.663	1.703	0.040
p-$C_6H_4[OSi(CH_3)_3]_2$	1.592	1.606	0.014

The infrared spectra of the phenoxysilanes were recorded on a UR-20 type instrument. In the case of liquids we used 0.02 mm KBr tubes, between two plates, and approximately 1% solutions in CCl_4. The spectra of solids were recorded in KBr pellets.

The infrared spectra of the compounds are shown in Figs 5—9. (The dotted line represents the liquid-film spectrum.) The results are summarized in Table IV.

On examining the results we may conclude that the ν_s value of the

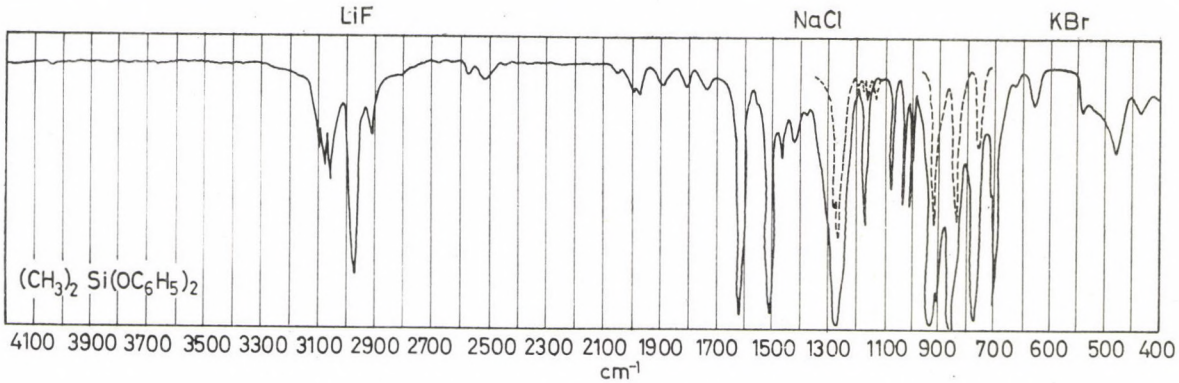


Fig. 5. Infrared spectrum of dimethyldiphenoxysilane

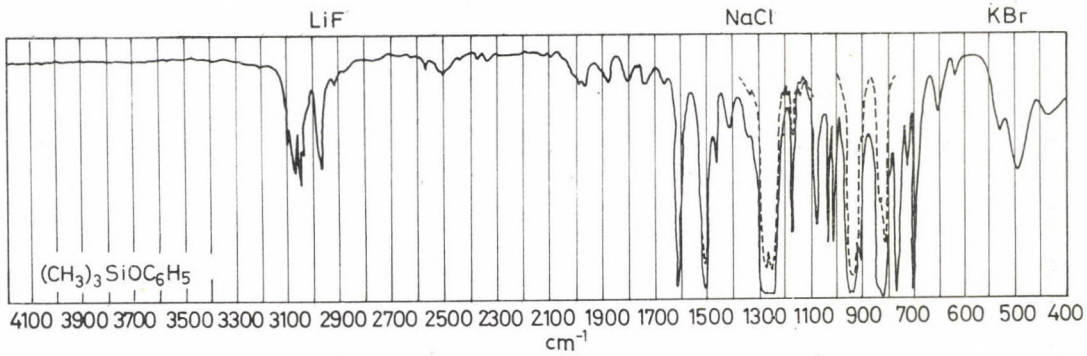


Fig. 6. Infrared spectrum of trimethylphenoxysilane

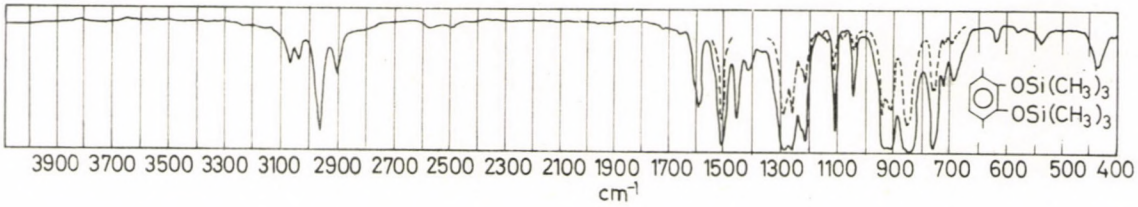


Fig. 7. Infrared spectrum of *o*-bis(trimethylsiloxy)benzene

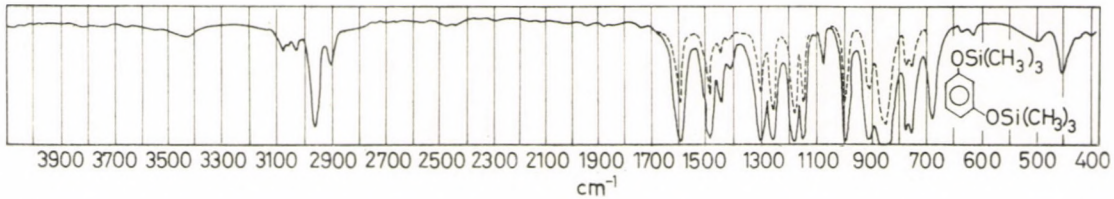


Fig. 8. Infrared spectrum of *m*-bis(trimethylsiloxy)benzene

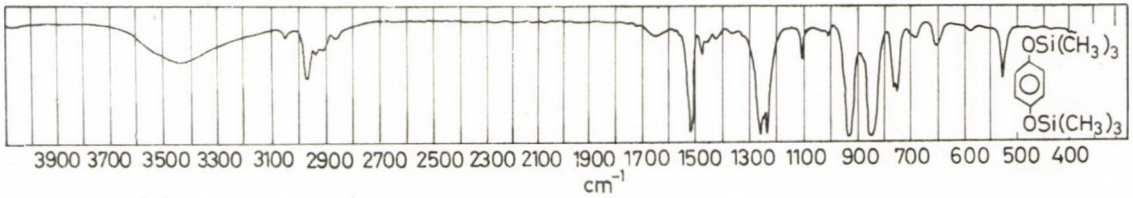


Fig. 9. Infrared spectrum of *p*-bis(trimethylsiloxy)benzene

Table IV

Infrared data spectra of phenoxysilanes

	SiOC		Si—CH_3							C_6H_5			
	ν_s	ν_{as}	ν_s	ν_{as}	δ_s	Si—CH_3	δ_{as}	Rocking	νSi(C_3)	ν = CH	νC—C	γC—C	γ = CH
										3021 *w*	1425 *w*		
$(CH_3)_3SiOC_6H_5$	925 *ss*	1176 *m*	2912 *w*	2982 *m*	1380 *vw*	1268 *ss*	1472 *w*	780 *s*	626 *vw*	3038 *m*	1515 *s*	700 *s*	852 *ss*
								852 *ss*	714 *m*	3052 *m*	1580 *w*		
										3077 *m*	1585 *w*		
										3102 *m*	1620 *s*		
										3038 *m*	1418 *w*		
$(CH_3)_2Si(OC_6H_5)_2$	940 *ss*	1176 *m*	2918 *w*	2978 *m*		1259 *ss*		764 *s*	622 *w*	3050 *m*	1470 *m*	695 *s*	862 *s*
								812 *ss*	652 *ss*	3075 *m*	1512 *s*		
										3100 *m*	1615 *s*		
								752 *s*		3040 *w*	1452 *m*		752 *s*
o-$C_6H_4[OSi(CH_3)_3]_2$	938 *ss*	1120 *m*	2905 *m*	2965 *m*	1365 *vw*	1256 *s*		845 *ss*	618 *w*	3070 *m*	1508 *s*	694 *w*	
										3110 *vw*	1588 *w*		763 *s*
											1598 *m*		
										3034 *w*	1440 *w*		778 *m*
m-$C_6H_4[OSi(CH_3)_3]_2$	998 *s*	1180 *s*	2906 *w*	2968 *m*		1258 *s*		765 *s*	618 *w*	3058 *vw*	1484 *m*	692 *m*	
								850 *ss*		3080 *w*	1596 *s*		910 *m*
		1108 *m*						845 *s*			1450 *w*		
p-$C_6H_4[OSi(CH_3)_3]_2$	930 *s*		2860 *w*	2982 *m*		1260 *s*		758 *m*		3050 *w*	1473 *w*	695 *w*	845 *s*
		1235 *s*									1518 *s*		
											1640—		
											—70 *w*		

Si—O—C bond varies between 940—925 cm^{-1} with the exception of the *meta* derivative. This agrees with the 970—920 cm^{-1} interval given in the literature for phenoxysilanes [18] and with the results of FÖLDESI and TÖRÖK [19]. The frequency of the Si—O bond is 719 cm^{-1} in trimethylmethoxysilane [20], 870 cm^{-1} in trimethylbenzyloxysilane and 925 cm^{-1} in trimethylphenoxysilane. The frequency values increase, because in the phenoxysilanes the π electrons of the oxygen atom are delocalized over the —Si—O—C_6H_5 system. Therefore the electronegativity of the oxygen shifts the ν_S for the Si—O bond to higher frequencies.

On comparing the results of infrared and dielectric measurements it should be taken into account that in alkoxysilanes the oxygen atom is in sp^3 hybrid state, while the sterics tructure of phenoxysilanes corresponds to an sp^2 oxygen. Because of the different hybrid state, the atom dipole moment of oxygen is different and the $m_{Si—O}$ bond moment is also higher in phenoxysilanes than in alkoxysilanes. The ultraviolet, infrared and dipole moment data can be interpreted accurately only on the basis of quantum chemical calculations which will be described in a forthcoming paper.

REFERENCES

1. NAGY, J., HENCSEI, P.: J. Organometal. Chem. **9**, 57 (1967)
2. HENCSEI, P.: T. D. Thesis. Department of Inorganic Chemistry, Technical University, Budapest, 1968 (in Hungarian)
3. HENCSEI, P., NAGY, J.: Periodica Polytechn. **13**, 351 (1969)
4. NAGY, J., HENCSEI, P., BORBÉLY-KUSZMANN, A., FARKAS, R.: Periodica Polytechn. **15**, 83, (1971)
5. Gmelins Handbuch der Anorganischen Chemie: Silicium. Verlag Chemie, Weinheim, 1958
6. JÖRG, H., STETTER, J.: J. Prakt. Chemie, **117**, 305 (1927)
7. RHONE-POULENC, S. A.: French Patent 1311, 158 (1962)
8. ANDRIANOV, K. A., ASTAKHIN, V. V., NIKIFOROV, B. P.: Zh. Obshch. Khim. (USSR) **34**, 914 (1964)
9. NAGY, J., GRESZ, I., FERENCZI-GRESZ, S.: Periodica Polytechn. **10**, 335 (1966)
10. ONSAGER, L.: J. Am. Chem. Soc. **58**, 1486 (1936)
11. HEDESTRAND, G.: Z. physik. Chem. **2**, 428 (1929)
12. MAXWELL, I. R., HENDRICKS, S. B., MOSLEY, V. M.: J. Chem. Phys. **3**, 699 (1935)
13. NAGY, J.: C. S. Thesis. Department of Inorganic Chemistry, Technical University, Budapest, 1960 (in Hungarian)
14. ALTSHULLER, A. P., ROSENBLUM, R.: J. Am. Chem. Soc. **77**, 272 (1955)
15. GOODWIN, T. H., PRZYBYLSKA, M., ROBERTSON, J. M.: Acta Cryst. **3**, 279 (1950)
16. FUCHS, O.: Z. physik. Chem. **B 14**, 339 (1931)
17. TIGANIK, L.: Z. physik. Chem. **B 14**, 135 (1932)
18. HOLLY, S., SOHÁR, P.: Infrared Spectroscopy. Budapest, Műszaki Kiadó, 1968 (in Hungarian)
19. FÖLDESI, I., TÖRÖK, F.: Acta Chim. Acad. Sci. Hung. **53**, 1 (1967)
20. FORNERIS, R., FUNCK, E.: Z. Electrochem. **62**, 1130 (1958)
21. GLIDEWELL, C., RANKIN, D. W. H., ROBIETTE, A. G., SHELDRICK, G. M., BEAGLEY, B. FREEMAN, J. M.: J. Mol. Structure **5**, 417 (1970)

József NAGY
Pál HENCSEI
Sarolta FERENCZI-GRESZ
Tamás GÁBOR

Budapest XI., Gellért tér 4.

Acta Chimica Academiae Scientiarum Hungaricae, Tomus 69 (4), pp. 423—431 (1971)

SELBSTDIFFUSIONSKOEFFIZIENTEN DES SYSTEMS METHANOL–WASSER–KALIUMCHLORID

T. ERDEY-GRÚZ, P. FODOR-CSÁNYI, B. LÉVAY und E. SZILÁGYI-GYŐRI

(Lehrstuhl für physikalische Chemie und Radiologie, Eötvös Loránd Universität, Budapest)

Eingegangen am 24. März 1970

Der Selbstdiffusionskoeffizient des Methanols in den Systemen Methanol–Wasser, Methanol–Wasser–Kaliumchlorid und Methanol–Wasser–Salzsäure, in Abhängigkeit von der Zusammensetzung, durchläuft bei 15—20 Mol% Methanolgehalt ein Minimum. Das Produkt $D^*\eta$ durchläuft bei ungefähr 45 Mol% ein Maximum und weist bei niedrigerer Temperatur ein geringes Minimum bei 8 Mol% auf.

Die Aktivierungsenergie der Selbstdiffusion besitzt bei ungefähr 15 Mol% Methanolgehalt ein Maximum.

Die Selbstdiffusionskoeffizienten der beiden Ionen des in Gemischen von Methanol und Wasser gelösten Kaliumchlorids unterscheiden sich kaum. Ausgehend vom reinen Wasser bzw. Methanol, nimmt der Selbstdiffusionskoeffizient der Ionen durch Zugabe der anderen Komponente ab und durchläuft bei 35—40 Mol% ein flaches Minimum. Die Produkte $D^*\eta$ der K^+- bzw. Cl^--Ionen besitzen keinen Extremwert, sondern steigen mit zunehmender Wasserkonzentration monoton an.

Zur Ergänzung unserer früheren Bestimmungen von Leitfähigkeiten und Überführungszahlen [1—8], deren Ziel die Untersuchung des Mechanismus der Ionenwanderung und der Struktur der Lösungsmittelgemische war, haben wir die Selbstdiffusionskoeffizienten einer Komponente des Lösungsmittelgemisches und der darin gelösten Ionen in Abhängigkeit von der Zusammensetzung bzw. der Temperatur bestimmt.

In der Literatur finden sich zahlreiche Angaben über die Eigenschaften von Alkohol–Wasser bzw. Alkohol–Wasser–Elektrolyt-Systemen und es wurde mehrfach versucht, ihre Struktur mit Modellen zu beschreiben [9]. Über die Selbstdiffusionskoeffizienten dieser Systeme liegen jedoch wenig Hinweise vor [10—15].

In dieser Arbeit wird über unsere Versuchsergebnisse mit in Methanol–Wasser-Gemischen gelöstem Kaliumchlorid bzw. Salzsäure berichtet.

Der Selbstdiffusionskoeffizient von Methanol wurde in Gemischen aus Methanol und Wasser im gesamten Konzentrationsbereich bei 10, 25 und 35 °C, der Selbstdiffusionskoeffizient des Kaliumions bzw. des Chloridions von Kaliumchlorid, welches im Methanol–Wasser-Gemisch gelöst war, bei 25 °C bestimmt. Aus den Meßergebnissen wurde auch die Aktivierungsenergie der Selbstdiffusion des Methanols berechnet.

Versuchsverfahren

Zur Messung des Selbstdiffusionskoeffizienten wurde das Offenend-Kapillarverfahren [16—18] und zwar dessen Variante ohne Rühren [19—20] angewendet. Dieses Verfahren besteht darin, daß eine am unteren Ende geschlossene Kapillare bekannter Länge und mit gleichmäßigem Querschnitt mit einer Lösung bekannter Zusammensetzung gefüllt wird, welche die zu

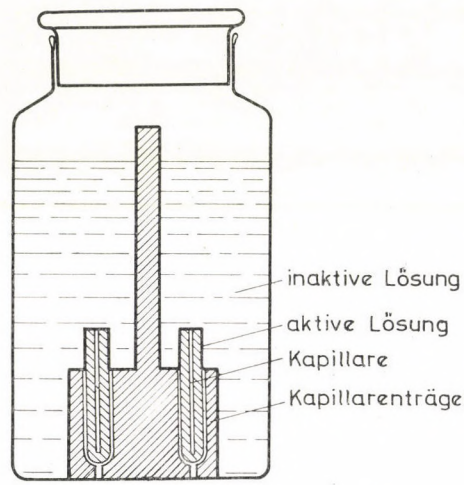


Abb. 1. Skizze des Diffusionsgefäßes

bestimmende Komponente in einer z. B. mit radioaktivem Isotop markierten Form enthält. Die Kapillare wird dann in eine Lösung gleicher Zusammensetzung getaucht, die jedoch keine markierten Teilchen enthält und deren Volumen (einige 100 cm^3) im Verhältnis zum inneren Volumen der Kapillare (einige Hundertstel cm^3) sehr groß ist (Abb. 1). Die Konzentration des markierten Stoffes wird vor Beginn der Diffusion und nach Verlauf einer bestimmten Zeit gemessen, woraus — unter Berücksichtigung der Länge der Kapillare — der Selbstdiffusionskoeffizient berechnet werden kann.

Bei Kapillaren mit kleinem inneren Durchmesser wird die Diffusion des markierten Stoffes durch die lineare Form des zweiten Fickschen Gesetzes beschrieben:

$$\frac{\partial c}{\partial t} = D^* \frac{\partial^2 c}{\partial x^2} \tag{1}$$

Bei den Grenzbedingungen

$$c(P, t) = 0, \quad \frac{\partial c(0, t)}{\partial x} = 0 \qquad (t > 0) \tag{2}$$

und der Anfangsbedingung

$$c(x, 0) = c_0 \qquad (0 < x < l) \tag{3}$$

ist die Lösung der Gleichung (1) [21, 22]:

$$\bar{c}(t) = \frac{8}{\pi^2} \sum_{n=0}^{\infty} \frac{c_0}{(2n+1)^2} \exp\left[-\pi^2(2n+1)^2 \frac{D^* t}{4l^2} \right]. \tag{4}$$

Ist der Wert von D^*t/l^2 genügend groß ($>0{,}2$), so liefert bereits das erste Glied der Summe auf der rechten Seite der Gl. (4) eine ausreichend genaue Näherung. Unter diesen Bedingungen ist der Selbstdiffusionskoeffizient

$$D^* = \frac{4l^2}{\pi^2 t} \cdot \ln\left(\frac{8}{\pi^2} \cdot \frac{c_0}{\bar{c}} \right). \tag{5}$$

In den Gleichungen (1)—(5) ist $c = c(x, t)$ die Konzentration des markierten Stoffes im Punkt x der Kapillare im Zeitpunkt t; c_0 die Anfangskonzentration des markierten Stoffes in der Kapillare; $\bar{c} = \bar{c}(t)$ die durchschnittliche Konzentration des markierten Stoffes in der Kapillare im Zeitpunkt t; l die Länge der Kapillare, t die Dauer der Diffusion und D^* der Selbstdiffusionskoeffizient des markierten Moleküls oder Ions.

Die Hauptschwierigkeit des Verfahrens ist die Sicherung der Grenzbedingung $c(l, t)=0$, d.h., daß die Konzentration des markierten Stoffes am offenen Ende der Kapillare im Laufe des Versuches stets gleich Null bleibt. Einige Verfasser versuchten, diese Bedingung durch Rühren der Lösung zu erreichen. In diesem Fall muß jedoch die optimale Rührgeschwindigkeit — in Abhängigkeit von der Viskosität der Lösung — recht sorgfältig gewählt werden, wodurch viel Unsicherheit entsteht.

Deswegen führten TAMÁS, LENGYEL und GIBER [19] ihre Versuche ohne Rühren aus und erhielten auf diese Weise besser reproduzierbare Ergebnisse. Es kann nachgewiesen werden [20], daß unter diesen Bedingungen ein nicht ganz strenges Einhalten der Grenzbedingung nur einen geringen Fehler verursacht.

In unserer Arbeit wurde die letztere Variante angewendet, d. h. es wurde nicht gerührt.

Die Kapillaren müssen äußerst vorsichtig in die Lösung eingetaucht werden, da die Konvektion in der Umgebung der Öffnung einen ähnlichen Fehler verursacht, wie das Rühren. Am besten reproduzierbare Werte und Verringerung dieses Fehlers konnten erreicht werden, indem ein Tropfen der markierten Lösung, mit der die Kapillare gefüllt war, am oberen, offenen Ende der Kapillare gelassen und die Kapillare im Kapillarenträger mitsamt diesem Tropfen in das Gefäß eingetaucht wurde, in dem sich die inaktive Lösung befand. Durch diese Anordnung wurde erreicht, daß der Rühreffekt der Konvektion in erster Reihe auf diesen Tropfen einwirkt, während auf die Lösung in der Kapillare keine Wirkung ausgeübt wird.

Die 40 mm langen Kapillaren mit inneren Durchmessern von ungefähr 0,8 mm wurden auf Länge und Volumen kalibriert. Je Versuch wurden gleichzeitig sechs Kapillaren in das Diffusionsgefäß eingetaucht. Letzteres war eine 250 cm^3-Pulverflasche mit gut schließendem eingeschliffenem Stopfen. Die Kapillaren waren vertikal in den aus Aluminium angefertigten Kapillarenträger eingesetzt (Abb. 1). Die Diffusionsgefäße befanden sich in einem Thermostaten mit einer Regelgenauigkeit von $\pm 0{,}01$ °C.

Zur Bestimmung der Selbstdiffusionskoeffizienten wurde mit ^{14}C markiertes Methanol ($T_{1/2} = 5568$ Jahre, $E_{\beta max} = 0{,}158$ MeV) und mit ^{36}Cl ($T_{1/2} = 2{,}6 \cdot 10^5$ Jahre, $E_{\beta max} = 0{,}714$ MeV) bzw. mit ^{42}K ($T_{1/2} = 12{,}46$ Stunden, $E_\gamma = 1{,}53$ und 0,309 MeV) markiertes Kaliumchlorid verwendet.

Die Diffusionszeit wurde bei Methanol und beim Chloridion so gewählt, daß der Wert von D^*t/l^2 genügend hoch war, um Gl. (5) zur Berechnung des Selbstdiffusionskoeffizienten anwenden zu können.

Wegen der kurzen Halbwertszeit von ^{42}K mußte die Diffusionszeit kurz bemessen

werden. Demgemäß wurde der Selbstdiffusionskoeffizient aufgrund von Gl. (4), unter Einbeziehung der ersten beiden Glieder berechnet.

Die Konzentration des markierten Stoffes in den Kapillaren bzw. seine dieser proportionale Radioaktivität wurde beim Gamma-Strahler ^{42}K durch Messung der γ-Aktivität der Kapillaren mit der Lösung bestimmt. Zur Bestimmung der Konzentration der Isotopen ^{14}C und ^{36}Cl, die weiche β-Strahlen emittieren, wurde die Lösung aus den Kapillaren entfernt und ihre Aktivität mit dem Flüssigkeitszintillationsverfahren für ^{14}C gemessen, über welches in unseren früheren Mitteilungen [23, 24] ausführlich berichtet wurde. ^{36}Cl wurde auf ähnliche Weise bestimmt, nachdem durch Bestimmen der absoluten Aktivität von Proben mit verschiedenem KCl-Gehalt festgestellt wurde, daß die Gegenwart von KCl unter den gegebenen Versuchsbedingungen die Bestimmung nicht stört.

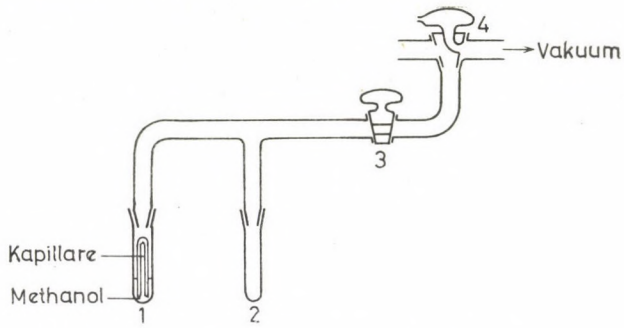


Abb. 2. Skizze des Destillationsgerätes

Die $K^{36}Cl$-haltige Lösung wurde aus den Kapillaren unter Anwendung einer Ultrazentrifuge unmittelbar in die zur Messung der Aktivität verwendeten Glasküvetten zentrifugiert und dort im Flüssigkeitscintillator gelöst.

Bei mit ^{14}C markiertem Methanol konnte diese Arbeitsweise wegen des Verdampfens des Methanols nicht angewendet werden. Deshalb wurden die methanolhaltigen Lösungen unter Anwendung des in Abb. 2 dargestellten Gerätes aus den Kapillaren herausdestilliert. Die Kapillaren wurden mit ihrer Öffnung nach unten in das Gefäß 1 eingesetzt, welches bereits 0,5 cm^3 inaktives Methanol enthielt. (Dieses »Trägermaterial« war notwendig, um die Adsorption der geringen Menge an aktivem Stoff an der Wand des Destillationsgefäßes zu verhindern.) Anschließend wurde der Inhalt des Gefäßes — nach Schließen der Hähne 3 und 4 — mit flüssigem Stickstoff zum Gefrieren gebracht, wonach die Hähne geöffnet und das Gerät der mit Vakuum abgesaugt wurde. Dann wurden die Hähne erneut geschlossen und der Inhalt Kapillare mitsamt dem Trägermaterial durch Erwärmen des gefrorenen Teils und gleichzeitiges Tiefkühlen der Vorlage 2 in letztere überdestilliert. Die gewonnene Probe wurde unmittelbar im Flüssigkeitszintillator gelöst.

Die Anfangskonzentration c_0 wurde in sämtlichen Fällen auf die gleiche Art bestimmt, wobei die aktive Ausgangslösung ebenfalls in Kapillaren gefüllt wurde.

Es wurden analytisch reine Reagenzien verwendet. Der Wassergehalt des Methanols wurde mit dem Fischer-Reagens bestimmt. Die Gemische wurden durch Wägen zusammengestellt.

Jede einzelne Lösung gegebener Zusammensetzung wurde mit zweimal sechs Kapillaren geprüft. Der Fehler der Bestimmung der Selbstdiffusionskoeffizienten nach dem beschriebenen Verfahren beträgt $\pm 0{,}05 \cdot 10^{-5}$ $cm^2 s^{-1}$.

Versuchsergebnisse

Der Selbstdiffusionskoeffizient D^* des Methanols nimmt vom reinen Methanol ausgehend bei Wasserzugabe bei allen drei geprüften Temperaturen anfangs ab und nimmt in den Gemischen mit hohem Wassergehalt nach Durch-

laufen eines ziemlich flachen Minimums zu (Abb. 3). Das Minimum entspricht einem Methanolgehalt von etwa 15—20 Mol% und ändert sich nicht merklich mit der Temperatur.

Bei der Beurteilung der Änderung des Selbstdiffusionskoeffizienten mit der Zusammensetzung der Lösung muß in Betracht gezogen werden, daß die Viskosität des Systems Methanol–Wasser sich mit der Zusammensetzung

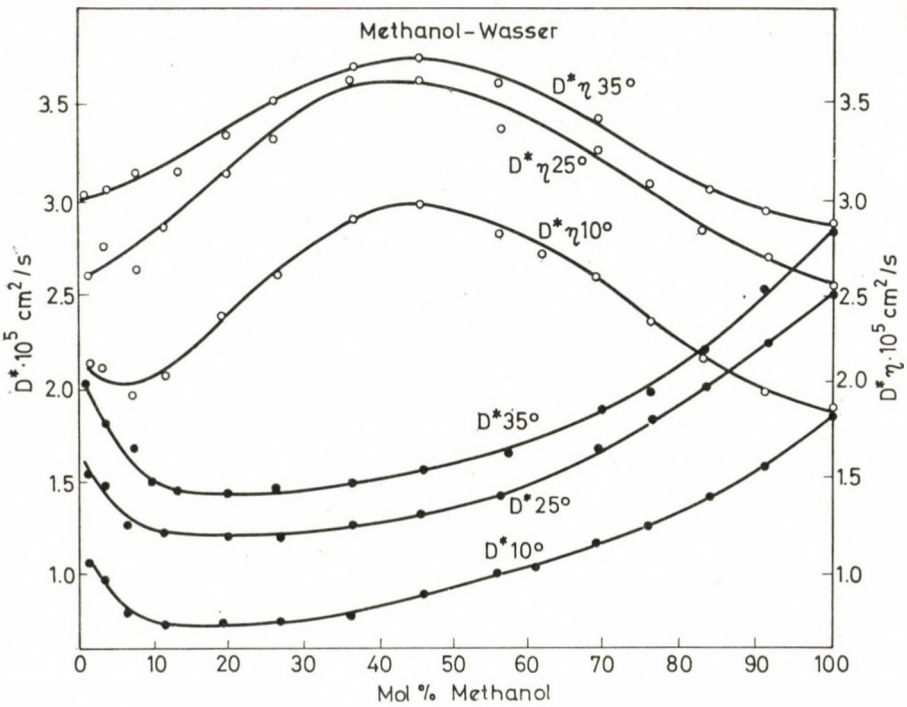


Abb. 3. Selbstdiffusionskoeffizient D^* und Produkt $D^*\eta$ von Methanol in Methanol–Wasser-Gemischen bei 10, 25 und 35 °C

wesentlich ändert [26]. Unter solchen Bedingungen ist das Produkt $D\eta$ für Vergleichszwecke besser geeignet als D. Unter den einfachsten Bedingungen sollte es — dem Stokesschen Gesetz gemäß — konstant sein. Im geprüften System ist jedoch das Produkt $D^*\eta$ des Selbstdiffusionskoeffizienten und der auf reines Methanol bezogenen relativen Viskosität ebenfalls von der Zusammensetzung der Flüssigkeit abhängig, jedoch auf andere Art als D^* (Abb. 3). Bei Wasserzugabe steigt der Wert des Produktes $D^*\eta$ bei allen drei Temperaturen, durchläuft bei etwa 45 Mol% Methanolgehalt ein Maximum und nimmt dann ab. Bei 10 °C tritt bei 8 Mol% Methanolgehalt ein Minimum auf, das aber bei höheren Temperaturen verschwindet.

Bei der Prüfung der Temperaturabhängigkeit des Selbstdiffusionskoeffizienten konnte festgestellt werden, daß lg D^* sich in guter Näherung linear mit $\frac{1}{T}$ ändert. Aus der Neigung der Geraden wurde die mittlere Aktivierungsenergie der Selbstdiffusion E_{D^*}, bezogen auf den Temperaturbereich 10—35 °C, berechnet. Mit steigendem Wassergehalt nimmt die Aktivierungsenergie anfangs zu und durchläuft bei etwa 15 Mol% Methanolgehalt ein deutliches Maximum (Abb. 4).

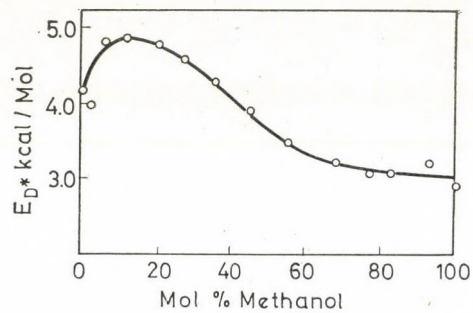


Abb. 4. Durchschnittliche Aktivierungsenergie E_{D^*} der Selbstdiffusion des Methanols in Methanol–Wasser-Gemischen

Der Selbstdiffusionskoeffizient des Methanols bei 25 °C wurde auch in Methanol–Wasser-Gemischen untersucht, die 0,215 Mol% KCl bzw. 0,215 Mol% Salzsäure enthielten. Dabei wurden keine die Versuchsfehler übertreffenden Abweichungen gegenüber den Werten gefunden, die in den entsprechenden, jedoch keinen Elektrolyten enthaltenden Lösungen gemessen wurden.

Die Meßergebnisse der Selbstdiffusionskoeffizienten der Ionen von in Methanol–Wasser-Gemischen gelöstem Kaliumchlorid sind in Abb. 5 dargestellt. Vom reinen Methanol ausgehend, nimmt der Selbstdiffusionskoeffizient beider Ionen an Wasserzugabe anfänglich ab, durchläuft bei 35—40 Mol% Methanol ein flaches Minimum und nimmt danach relativ steil bis zum reinen Wasser zu. Im Bereich von 15—80 Mol% Methanolgehalt ist der Selbstdiffusionskoeffizient des Kaliumions etwas höher als der des Chloridions, während unterhalb und oberhalb dieses Bereichs das Verhältnis umgekehrt ist.

Da das Minimum des Selbstdiffusionskoeffizienten im Konzentrationsbereich liegt, der ungefähr dem Maximum der Viskosität entspricht, besitzen die Produkte $D^*\eta$ der Ionen des Kaliumchlorids in Abhängigkeit von der Zusammensetzung keinen Extremwert. Die $D^*\eta$ Produkte beider Ionen steigen monoton mit zunehmender Wasserkonzentration an und auch ihr Relativwert zueinander ändert sich mit der Konzentration ähnlich wie D^* (Abb. 5).

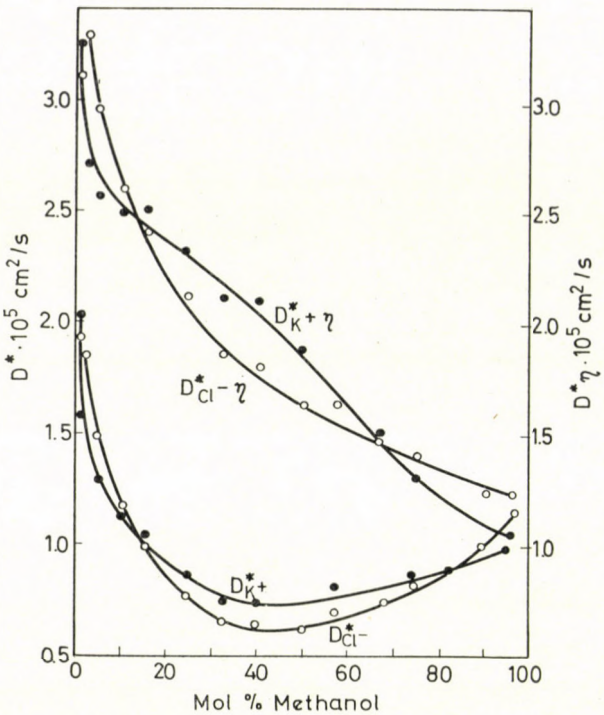


Abb. 5. Selbstdiffusionskoeffizienten D^*_{K+} und D^*_{Cl-}–und Produkte $D^*\eta$ der Kalium- und Chloridionen in Methanol–Wasser-Gemischen bei 25 °C und einer KCl-Konzentration von 0,215 Mol%

Diskussion der Ergebnisse

Ähnlich der äquivalenten Leitfähigkeit der entsprechenden Lösungen [1], verläuft die Änderung der Selbstdiffusionskoeffizienten der Ionen des Kaliumchlorids mit der Zusammensetzung über ein Minimum. Dagegen weicht der Verlauf des Produktes $D^*\eta$ in Abhängigkeit von der Zusammensetzung wesentlich vom Verlauf des entsprechenden Produktes $\Lambda\eta$ ab. Dieser Befund zeigt, daß die Änderung der Zusammensetzung des Mediums auf die thermische Bewegung und auf die durch das elektrische Feld hervorgerufene Wanderung der Ionen des Kaliumchlorids unterschiedlich wirkt.

Aus den $D^*\eta$-Kurven der Ionen geht — in Übereinstimmung mit anderen Beobachtungen — hervor, daß die Änderung ihrer Beweglichkeiten nicht allein durch das Stokes - Einsteinsche hydrodynamische Modell gedeutet werden kann. Wird angenommen, daß die hydrodynamischen Radien der diffundierenden Ionen mit zunehmendem Wassergehalt in stärkerem Maße ansteigen, als die durch Solvatation mit Alkohol bedingte Abnahme, so wäre eine Abnahme des Produktes $D^*\eta$ mit steigendem Wassergehalt zu erwarten. Die Erfahrung

zeigt jedoch das Gegenteil. Dies dürfte auch damit zusammenhängen, daß die Struktur der Lösung in der unmittelbaren Umgebung der Ionen stärker verändert wird, als makroskopisch zu beobachten ist, sodaß dort die Mikroviskosität wesentlich von dem makroskopischen Wert abweicht.

Erwähnenswert ist, daß sich die Aktivierungsenergie der Selbstdiffusion des Methanols mit der Zusammensetzung des Lösungsmittels auf ähnliche Weise ändert, wie die elektrolytische Leitfähigkeit [1]. Kurvenverlauf und Ort der Maxima sind beinahe gleich. In dieser Beziehung scheinen also dieselben Faktoren einflußnehmend zu sein.

Der Konzentrationsbereich des Maximums der Aktivierungsenergie der Selbstdiffusion stimmt mit der Theorie von SAMOJLOW [27] überein. Gemäß dieser Theorie wird die Struktur des Wassers durch das Ausfüllen der Strukturhohlräume in Wasser mit eisartigem Strukturbereich durch Nichtelektrolyte, z. B. durch Alkoholmoleküle verstärkt. Um sämtliche Hohlräume mit Nichtelektrolytmolekülen auszufüllen, werden etwa 17 Mol% Nichtelektrolyt benötigt; dies entspricht der maximalen Verstärkung der Struktur. Für Methanol, d. h. für den Alkohol mit den kleinsten Molekülen, fand SAMOJLOW auf experimentellem Wege die relativ stabilste Struktur bei 19 Mol%.

Nach Literaturangaben befindet sich das Minimum des partiellen Molvolumens des Methanols im System Methanol–Wasser ebenfalls bei dieser Zusammensetzung [28, 29]. Unsere Versuche zeigen, daß das Minimum des Selbstdiffusionskoeffizienten des Methanols und das Maximum der Aktivierungsenergie der Selbstdiffusion ebenfalls bei ungefähr dieser Methanolkonzentration liegen. Es kann also angenommen werden, daß diese Befunde ebenfalls auf eine Stabilisierung der Wasserstruktur hinweisen. Mit zunehmendem Methanolgehalt scheint die strukturzerstörende Wirkung des Methanols zu dominieren. Demzufolge nimmt der Selbstdiffusionskoeffizient zu, während die Aktivierungsenergie abnimmt.

Das Minimum des Produktes $D^*\eta$ für Methanol, welches bei 10 °C und etwa 8 Mol% Methanolgehalt beobachtet wurde, weist auf eine Wechselwirkung hin, die die Bewegung der Moleküle hindert. Das Maximum des Produktes $D^*\eta$ bei ungefähr 50 Mol% deutet auf eine Lockerung der Struktur.

*

Den Technikern Frau B. JANKÓ und L. LÉB sei für ihre Hilfe in der experimentellen Arbeit auch an dieser Stelle gedankt.

LITERATUR

1. ERDEY-GRÚZ, T., KUGLER, E., REICH, A.: Acta Chim. Acad. Sci. Hung. **13,** 428 (1958)
2. ERDEY-GRÚZ, T., MAJTHÉNYI, L.: Acta Chim. Acad. Sci. Hung. **16,** 417 (1958)
3. ERDEY-GRÚZ, T., KUGLER, E., HIDVÉGI, J.: Acta Chim. Acad. Sci. Hung. **19,** 89 (1959)
4. ERDEY-GRÚZ, T., KUGLER, E., HIDVÉGI, J.: Acta Chim. Acad. Sci. Hung. **19,** 363 (1959)
5. ERDEY-GRÚZ, T., MAJTHÉNYI, L.: Acta Chim. Acad. Sci. Hung. **20,** 73 (1959)
6. ERDEY-GRÚZ, T., MAJTHÉNYI, L.: Acta Chim. Acad. Sci. Hung. **20,** 175 (1959)

7. ERDEY-GRÚZ, T., MAJTHÉNYI, L., NAGY-CZAKÓ, I.: Acta Chim. Acad. Sci. Hung. **53,** 28 (1967)
8. ERDEY-GRÚZ, T., KUGLER, E.: Acta Chim. Acad. Sci. Hung. **57,** 301 (1968)
9. Zusammenfassend siehe z. B. FRANKS, F., IVES, D. J. G.: Quarterly Reviews, **20,** 1 (1966)
10. PARTINGTON, J. R., HUDSON, R. F., BAGNALL, K. W.: Nature, **169,** 583 (1952)
11. PARTINGTON, J. R., HUDSON, R. F., BAGNALL, K. W.: J. Chim. Phys. **55,** 77 (1958)
12. RATHBUM, R. E., BABB, A. L.: J. Phys. Chem. **65,** 1072 (1961)
13. GARY-BOBO, C. M., WEBER, H. W.: J. Phys. Chem. **73,** 1155 (1969)
14. KULKARNI, M. V., LYONS, P. A.: J. Phys. Chem. **69,** 2336 (1965)
15. MARCINOWSKY, A. E., PHILLIPS, H. O., KRAUS, K. A.: J. Phys. Chem. **69,** 3968 (1965)
16. ANDERSON, J., SADDINGTON, K.: J. Chem. Soc. **1949,** 381
17. WANG, J.: J. Am. Chem. Soc. **73,** 510 (1951)
18. TYRREL, H. J. V.: Diffusion and Heat Flow in Liquids. Butterworth Inc., Washington, 1961
19. TAMÁS, J., LENGYEL, S., GIBER, J.: Acta Chim. Acad. Sci. Hung. **38,** 225 (1963)
20. GERGELY, J., TAMÁS, J., VÉRTES, A., LENGYEL, S.: Acta Chim. Acad. Sci. Hung. **39,** 423 (1963)
21. CRANK, J.: The Mathematics of Diffusion. Oxford, 1957
22. JOST, W.: Diffusion in Solids, Liquids, Gases. New York, 1960
23. LÉVAY, B., FODOR-CSÁNYI, P.: Magy. Kém. Foly. **71,** 356 (1965)
24. FODOR-CSÁNYI, P., LÉVAY, B.: Acta Chim. Acad. Sci. Hung. **47,** 343 (1965)
25. FODOR-CSÁNYI, P., SZILÁGYI-GYŐRI, E.: Int. J. Appl. Rad. Isotopes **19,** 712 (1968)
26. TIMMERMANS, J.: The Physico-chemical Constants of Binary Systems in Concentrated Solutions, Vol. 4. Interscience Publ. Inc. New York, 1960, p. 163
27. BULAEWA, M. N., SAMOJLOW, O. JA.: Zhur. Strukt. Chim. **4,** 502 (1963)
28. MATJASCH, I. W., JASCHKITSCHEW, W. I.: Zhur. Strukt. Chim. **5,** 13 (1964)
29. HEIDIG, H. A., YINGLING, R. T., LOCKWOOD, K. L., TEATES, T. G.: J. Chem. Educ. **42,** 309 (1965)

Tibor ERDEY-GRÚZ
Piroska FODOR-CSÁNYI
Béla LÉVAY
Erzsébet SZILÁGYI-GYŐRI

Budapest VIII., Puskin u. 11—13.

Acta Chimica Academiae Scientiarum Hungaricae, Tomus 69 (4), pp. 433—443 (1971)

ABHÄNGIGKEIT DER SAUERSTOFFÜBERSPANNUNG VON DER AKTIVITÄT DES WASSERS, III

WIRKUNG DES pH IN SULFATLÖSUNGEN

T. ERDEY-GRÚZ, M. GALLYAS und É. SZETEY

(Lehrstuhl für Physikalische Chemie und Radiologie der Eötvös Loránd Universität, Budapest)

Eingegangen am 22. April 1970

Es wurde die Überspannung der anodischen Sauerstoffentwicklung in wäßrigen 0,1 *n* Sulfationenlösungen mit annähernd konstanter Ionenstärke, bei verschiedenen Stromdichten, in Abhängigkeit vom pH und von der Aktivität des Wassers untersucht.

Die Polarisationskurve in Abhängigkeit von der Stromdichte setzt sich in saurer Lösung aus drei, in alkalischer Lösung aus zwei Tafelschen Geraden mit verschiedenen Neigungswinkeln zusammen.

In rein wäßrigen Lösungen ($a_w = 0{,}998$) nimmt die Stromstärke bei konstanter Stromdichte mit steigendem pH linear zu, und zwar in Gegenwart von Na^+-Ionen (bei Veränderung des pH mit NaOH, ausgehend aus reiner Schwefelsäurelösung) bis pH = 12, in Gegenwart von K^+-Ionen bis pH = 10. Mit weiter steigendem pH nimmt die Überspannung linear ab. Im sauren Gebiet beträgt der Wert von $\frac{d\eta}{d\,\mathrm{pH}}$ in Gegenwart von K^+-Ionen in Abhängigkeit von der Stromdichte ≈0,006—0,009, in Gegenwart von Na^+-Ionen ≈0,002—0,003. Im alkalischen Bereich ist $\frac{d\eta}{d\,\mathrm{pH}}$ annähernd unabhängig von der Art des Kations. Aus den Versuchsergebnissen kann gefolgert werden, daß die K^+-Ionen in der Doppelschicht auf der Elektrodenoberfläche die Aktivierungsenergie der Sauerstoffentwicklung aus Wassermolekülen in höherem Maße steigern, als die Na^+-Ionen; folglich ändert sich in Gegenwart letzterer der Reaktionsmechanismus nur in Lösungen mit höherem pH, in der Weise, daß der Sauerstoff anstelle von Wassermolekülen aus Hydroxydionen entwickelt wird.

Auch in Lösungen mit geringeren Wasseraktivitäten ($a_w = 0{,}906$, 0,778 bzw. 0,738) nimmt die Überspannung im pH-Bereich von 1 bis 10 linear mit steigendem pH zu, jedoch erscheint in der Geraden $\eta = f(\mathrm{pH})$ bei pH 7 ein Knickpunkt, der Wert von $\frac{d\eta}{d\,\mathrm{pH}}$ nimmt zu. Diese Änderung ist in den Lösungen mit $a_w = 0{,}906$ am stärksten und am geringsten in den Lösungen mit $a_w = 0{,}738$; in den meisten Fällen ist die Richtungsänderung der Geraden $\eta = f(\mathrm{pH})$ bei hohen Stromdichten geringer, als bei niedrigen Stromdichten.

Als Fortsetzung unserer früheren Untersuchungen [1] wurde die Wirkung des pH auf die Überspannung der elektrolytischen Sauerstoffentwicklung in Lösungen untersucht, in denen die Aktivität des Wassers im Bereich $a_w =$ $= 0{,}998$—$0{,}738$ verändert wurde.

Über die Abhängigkeit der Überspannung der Sauerstoffentwicklung vom pH findet man in der Literatur nur wenige und teilweise miteinander in Widerspruch stehende Angaben. HICKLING und HILL [2] stellten fest, daß die Überspannung an einer Platinanode, in 2 *n* H_2SO_4-Lösung, in Phosphatpuffer (pH = 6,8) bzw. in 1 *n* KOH-Lösung gemessen, mit dem pH zunimmt.

Aus den Messungen von BOCKRIS und HUQ [3] geht dagegen hervor, daß die Überspannung im Bereich pH = 1,5—3,7 anfangs mit steigendem pH-Wert ab und von ungefähr pH 2,4 angefangen, zunimmt. Nach DAMJANOVIC, DEY und BOCKRIS [4] nimmt die Überspannung in perchlorationhaltigen Lösungen mit steigendem pH im Bereich pH=10—13 bis etwa pH=12 zu und dann ab. VETTER und BERNDT untersuchten den Aufbau der Oxydschicht an Pt-Anoden und fanden, daß die charakteristischen Punkte der Ladungskurven mit steigendem pH in negativer Richtung verschoben werden [5].

Demgemäß ist der Zusammenhang zwischen der Sauerstoffüberspannung und dem pH zur Zeit noch ziemlich unklar, um so mehr, als die Überspannung in alkalischen Lösungen — aufgrund des wahrscheinlichen Reaktionsmechanismus, der aus sonstigen Erscheinungen folgt — mit steigendem pH abnehmen sollte, während einige Beobachtungen das Entgegengesetzte zeigen. Wir hielten es daher begründet, die Abhängigkeit der Überspannung vom pH weiter zu untersuchen.

Das Versuchsverfahren

Die Polarisationskurven, welche die Abhängigkeit der Überspannung von der Stromdichte darstellen, sowie die Aktivität des Wassers wurden in der bereits früher beschriebenen Versuchseinrichtung [6, 7] bei 25 °C in Sulfatlösungen mit verschiedenen pH und bei den Wasseraktivitätswerten a_w = 0,998, 0,906, 0,778 bzw. 0,738 bestimmt. Die Aktivität des Wassers wurde durch Lösen von 0, 5, 10, bzw. 15 Mol/Liter Kaprolactam eingestellt.

Die Wirkung der pH-Änderung auf Überspannung bei konstanter Alkalimetallionenkonzentration wurde derart untersucht, daß NaOH bzw. KOH in 0,1 *n* Schwefelsäurelösung aufgelöst wurden, undzwar in solchen Verhältnissen, daß der pH-Wert zwischen 1 und 10 verändert wurde. Die gesamte Alkalimetallionenkonzentration wurde in sämtlichen Fällen durch Zugabe des entsprechenden Alkalimetallsulfats auf 0,05 *n* ergänzt und die durch den Salzzusatz verursachte Zunahme der Überspannung als Korrektion in Betracht gezogen. Es wurde ferner angenommen, daß diese Elektrolyte — neben dem in hoher Konzentration vorliegenden Kaprolactam — die Aktivität des Wassers hinsichtlich der Überspannung nicht wesentlich verändern, sodaß die Änderungen der Kurven $\eta - \lg i$ im wesentlichen auf die Änderungen des pH zurückgeführt werden können. Der pH der Lösungen wurde mit einer Glaselektrode gegen eine gesättigte Kalomelelektrode gemessen.

Versuchsergebnisse

Die zu verschiedenen pH-Werten gehörenden Überspannungen wurden unter Berücksichtigung der Korrektionen für die durch die Salzzugabe verursachte Zunahme der Überspannung berechnet. In Lösungen mit gegebener Aktivität des Wassers, in Gegenwart von 0,05 *n* Salz wurde von den bei den untersuchten Stromdichten gemessenen Überspannungswerten der in Lösungen ohne Zusatz gemessene betreffende Wert abgezogen. Das arithmetische Mittel der erhaltenen Differenzen (wobei die Abweichungen der einzelnen Werte den Meßfehler, $\pm$ 10 mV, nicht überstiegen) wurde bei sämtlichen Stromdichten von jenen Überspannungswerten abgezogen, welche in Lösungen gemessen

wurden, in denen die Zusatzkonzentration nach dem Einstellen des pH auf 0,05 *n* ergänzt wurde.

Die auf die beschriebene Weise korrigierte Überspannung zeigt bei sämtlichen pH-Werten, in Übereinstimmung mit der Tafelschen Gleichung, eine lineare Abhängigkeit vom Logarithmus der Stromdichte. Wird jedoch der pH mit NaOH eingestellt, so setzt sich die Tafelsche Gerade in dem durch uns untersuchten Stromdichtebereich (10^{-8}—10^{-3} A/cm^2) aus zwei bzw. drei

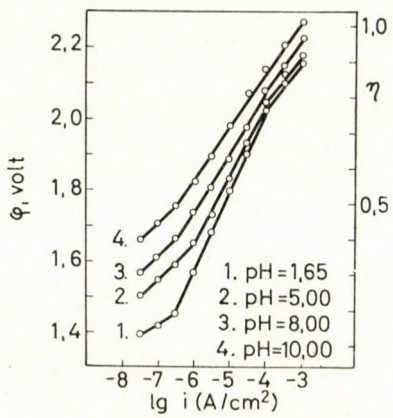


Abb. 1. Polarisationskurven in 0,1 *n* Sulfationenlösungen mit der Wasseraktivität $a_w = 0{,}778$ bei verschiedenen pH-Werten. (Die Änderung des pH erfolgte durch Zusatz von NaOH)

Teilen verschiedener Neigung zusammen, die sich bei ungefähr 10^{-6} bzw. 10^{-4} A/cm^2 aneinander anschließen (siehe z. B. Abb. 1 für $a_w = 0{,}778$). Der dritte, weniger steile Abschnitt zeigt sich nur in Lösungen mit niedrigem pH. Die Überspannung nimmt mit steigendem pH zu, wogegen sich die Form und Neigung der Kurven nur wenig ändert. Aus den Meßergebnissen bei den übrigen drei Wasseraktivitäten erhielten wir ähnliche Kurvenscharen. Wurde der pH mit KOH eingestellt, so waren die Verhältnisse ähnlich, jedoch zeigte sich der dritte Abschnitt bei niedrigen pH-Werten und hohen Stromdichten in diesem Fall nicht. Die Neigungen der Tafelschen Kurven, die in Lösungen erhalten wurden, deren pH mit verschiedenen Alkalimetallhydroxyden eingestellt wurde, sind in Tab. I angeführt.

Aus der Tabelle ist ersichtlich, daß sich die Neigung keines Abschnittes der Tafelschen Kurven monoton ändert; der Wert von b_1 liegt zwischen 0,04 und 0,09, der von b_2 zwischen 0,15 und 0,19. Bei Einstellung des pH-Wertes mit KOH liegen die unter gleichen Bedingungen gemessenen Werte etwas niedriger.

Die Abhängigkeit des Polarisationspotentials bzw. der Überspannung vom pH, in Lösungen mit 0,1 *n* Sulfationengehalt und einer Wasseraktivität $a_w = 0{,}998$ ist in Abb. 2a und 2b dargestellt. Der pH wurde — ausgehend

Tabelle I

b-Werte der Tafelschen Gleichung in Lösungen mit verschiedenen Wasseraktivitäten (a_w), deren pH mit Natrium- bzw. Kaliumhydroxyd eingestellt wurde.
(Die Angaben in Klammern beziehen sich auf Lösungen, deren pH mit KOH eingestellt wurde)

a_w	pH = 3		pH = 5		pH = 7		pH = 8		pH = 10	
	b_1	b_2	b_1	b_2	b_1	b_2	b_1	b_2	b_1	b_2
0,998	0,06	0,17	0.06	0,17	0,07	0,16	—	—	0,07	0,17
	(0,04)	(0,16)	(0,04)	(0,16)	(0,05)	(0,16)	(—)	(—)	(0,05)	(0,16)
0,906	0,09	0,15	0,09	0,19	0,09	0,17	0,09	0,16	0,07	0,16
	(0,08)	(0,17)	(0,07)	(0,17)	(0,06)	(0,15)	(0,07)	(0,15)	(0,06)	(0,15)
0,778	0,09	0,17	0,08	0,17	0,09	0,17	0,10	0,16	0,10	0,16
	(0,08)	(0,16)	(0,06)	(0,16)	(0,06)	(0,15)	(0,06)	(0,16)	(0,06)	(0,15)
0,738	0,09	0,17	0,07	0,17	0,11	0,18	0,10	0,16	0,10	0,16
	(0,08)	(0,16)	(0,07)	(0,16)	(0,07)	(0,15)	(0,07)	(0,15)	(0,07)	(0,14)

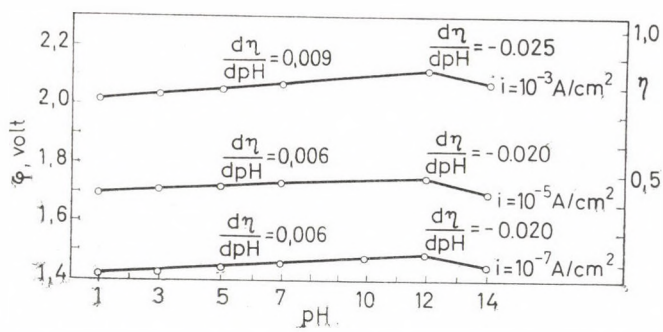


Abb. 2a. Abhängigkeit des Polarisationspotentials vom pH in 0,1 *n* Sulfationenlösungen (Einstellung des pH mit NaOH) bei der Wasseraktivität $a_w = 0{,}998$

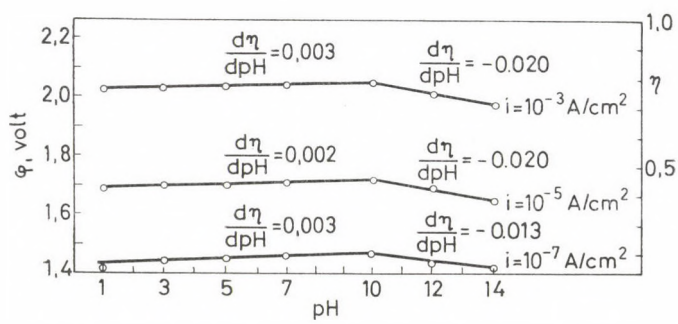


Abb. 2b. Abhängigkeit des Polarisationspotentials vom pH in 0,1 *n* Sulfationenlösungen (Einstellung des pH mit KOH) bei der Wasseraktivität $a_w = 0{,}998$

aus reiner wäßriger Schwefelsäurelösung — durch Zugabe von NaOH bzw. KOH eingestellt. Wie ersichtlich, nimmt unter den untersuchten Bedingungen die Überspannung von den sauren Lösungen an (pH = 1) bis zu schwach alkalischen Lösungen linear mit steigendem pH zu. In stärker alkalischen Lösungen ändert sich jedoch die Richtung der η—pH Kurve.

In Na^+-ionenhaltigen Lösungen erfolgt eine Abnahme der Überspannung mit steigendem pH von pH = 12, bei K^+-haltigen Lösungen von pH = 10 angefangen. In den drei Stromdichtebereichen, die den drei verschiedenen Tafelschen Koeffizienten b entsprechen (siehe unsere vorangegangene Mitteilung), weichen die Verhältnisse in dieser Beziehung kaum voneinander ab. Die Steilheit der Kurven η—pH hängt jedoch merklich davon ab, ob Na^+- oder K^+-Ionen in der Lösung konstanter Ionenstärke vorliegen (siehe Tab. II). Im steigenden Abschnitt der Kurven ändert sich die Überspannung in Gegenwart von Na^+-Ionen stärker mit dem pH, als in Gegenwart von K^+-Ionen, während in den Lösungen mit hohem pH kaum ein Unterschied vorliegt.

Tabelle II

Neigungen m_1 und m_2 (mV/pH) der Kurven $\varphi(\eta)$—pH in Lösungen mit verschiedenen Wasseraktivitäten (a_W), deren pH mit Natrium- bzw. Kaliumhydroxyd eingestellt wurde.
(Die Angaben in Klammern beziehen sich auf Lösungen, deren pH mit KOH eingestellt wurde)

a_W	10^{-3} A/cm²		10^{-5} A/cm²		10^{-7} A/cm²	
	m_1	m_2	m_1	m_2	m_1	m_2
0,998	9	—25	6	—20	6	—20
	(3)	(—20)	(2)	(—20)	(3)	(—13)
0,906	8	42	8	42	8	40
	(4)	(38)	(9)	(33)	(10)	(35)
0,778	17	22	11	42	14	45
	(10)	(27)	(13)	(37)	(20)	(33)
0,738	19	20	14	38	20	32
	(13)	(27)	(23)	(58)	(23)	(40)

Die Abnahme der Aktivität des Wassers infolge des darin gelösten Kaprolactams übt einen starken Einfluß auf den Zusammenhang zwischen dem pH und der Überspannung der elektrolytischen Sauerstoffentwicklung aus (Abb. 3a, 3b, 3c und 4a, 4b, 4c). In den untersuchten Lösungen mit $a_W = 0{,}906$, 0,778 bzw. 0,738 reicht der erste, linear ansteigende Abschnitt der Kurve η—pH nur bis pH = 7; hier erfolgt ein Bruch und der Anstieg wird steiler, bis pH = 10. In Lösungen mit höherem pH konnten keine Messungen in Gegenwart von Kaprolactam durchgeführt werden. Die Wert evon $m = \frac{d\eta}{d\ \mathrm{pH}}$ unterscheiden

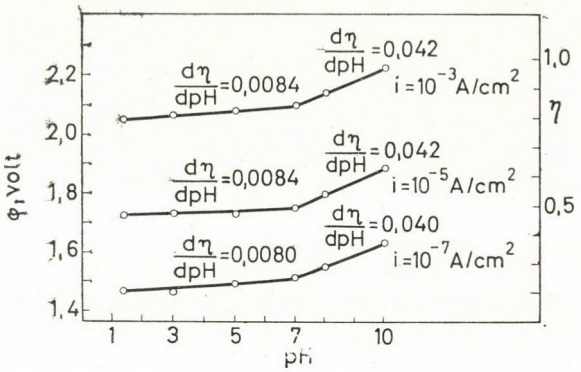


Abb. 3a. Abhängigkeit des Polarisationspotentials vom pH in 0,1 *n* Sulfationenlösungen (Einstellung des pH mit NaOH) bei der Wasseraktivität $a_w = 0{,}906$

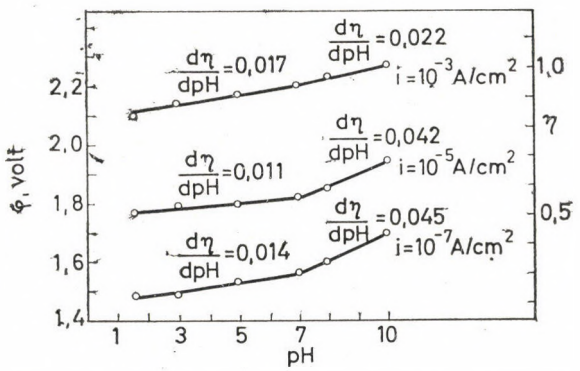


Abb. 3b. Abhängigkeit des Polarisationspotentials vom pH in 0,1 *n* Sulfationenlösungen (Einstellung des pH mit NaOH) bei der Wasseraktivität $a_w = 0{,}778$

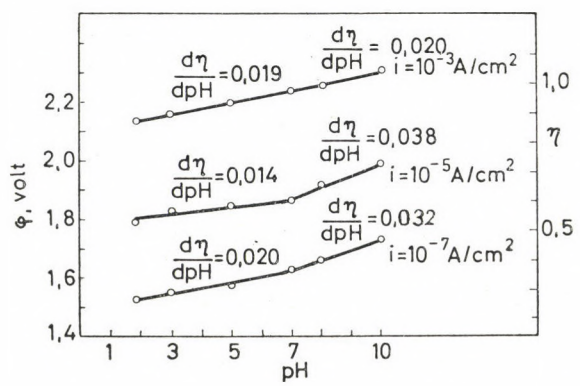


Abb. 3c. Abhängigkeit des Polarisationspotentials vom pH in 0,1 *n* Sulfationenlösungen (Einstellung des pH mit NaOH) bei der Wasseraktivität $a_w = 0{,}738$

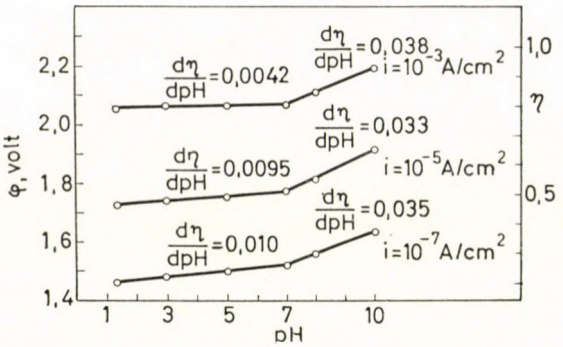


Abb. 4a. Abhängigkeit des Polarisationspotentials vom pH in 0,1 *n* Sulfationenlösungen (Einstellung des pH mit KOH) bei der Wasseraktivität $a_w = 0{,}906$

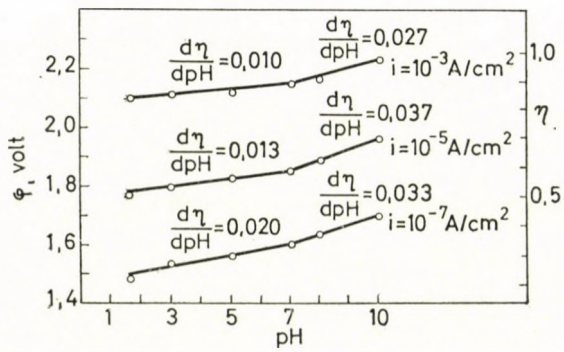


Abb. 4b. Abhängigkeit des Polarisationspotentials vom pH in 0,1 *n* Sulfationenlösungen (Einstellung des pH mit KOH) bei der Wasseraktivität $a_w = 0{,}778$

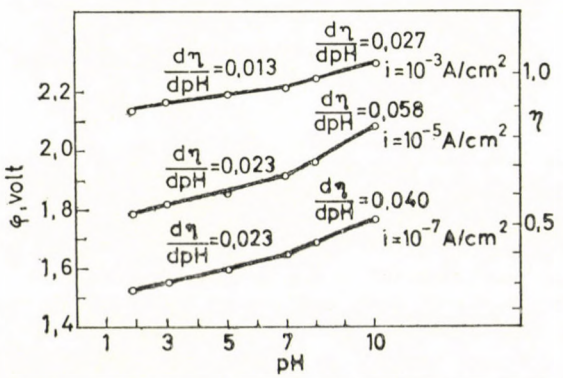


Abb. 4c. Abhängigkeit des Polarisationspotentials vom pH in 0,1 *n* Sulfationenlösungen (Einstellung des pH mit KOH) bei der Wasseraktivität $a_w = 0{,}738$

sich in den drei geprüften Stromdichtebereichen verhältnismäßig wenig voneinander (siehe Tab. II), sind jedoch im sauren Bereich um so höher, je niedriger die Aktivität des Wassers ist. Im pH Bereich von 7 bis 10 ändert sich dagegen die Steilheit der Kurve $\eta - \mathrm{pH}$ $\left(\frac{d\eta}{d\,\mathrm{pH}}\right)$ in allen drei Stromdichtebereichen der Lösungen mit $a_w = 0{,}906$ und in den beiden niedrigeren Stromdichtebereichen der Lösungen mit $a_w = 0{,}778$ nur wenig, nimmt jedoch in den letzteren Lösungen im Stromdichtebereich 10^{-3} A/cm² etwa um die Hälfte ab. In den Lösungen mit $a_w = 0{,}738$ sind die Steilheiten der Kurven merklich flacher.

Diskussion der Ergebnisse

Aus dem Umstand, daß die Polarisationskurven in den Lösungen mit verschiedenen Wasseraktivitäten und verschiedenen pH-Werten ebenfalls meistens aus drei Tafelschen Geraden zusammengesetzt sind (Abb. 1), kann gefolgert werden, daß der Mechanismus der Elektrodenreaktion im niedrigsten, im mittleren und im höchsten Stromdichtebereich unterschiedlich ist bzw., daß zumindest ein anderer Reaktionsschritt geschwindigkeitsbestimmend ist, ähnlich wie in reiner Schwefelsäurelösung. Es scheint jedoch, als sei der Reaktionsmechanismus in jenen Lösungen, in denen die Aktivität des Wassers verhältnismäßig gering und der pH-Wert hoch ist, im mittleren und hohen Stromdichtebereich nicht unterschiedlich bzw. der etwaige Unterschied zeigt sich im Neigungswinkel nicht.

In reinen wäßrigen Lösungen, in denen die Sulfationenkonzentration — und zugleich annähernd auch die Ionenstärke — konstant ist, nimmt die Überspannung bei einer gegebenen Stromdichte im sauren bzw. schwach alkalischen Gebiet mit steigendem pH zu; dies steht in Einklang damit, daß der Sauerstoff in diesem Bereich aus Wassermolekülen entwickelt wird [3, 4]. Die Abhängigkeit vom pH wird jedoch durch die Art des in der Lösung anwesenden Kations wesentlich beeinflußt (Abb. 2). Aus der Tatsache, daß der Wert von $\frac{d\,\eta}{d\,\mathrm{pH}}$ in diesem Bereich in der Gegenwart von Na^+-Ionen zwei- bis dreimal so hoch ist, als in Gegenwart von K^+-Ionen (siehe Tab. II) und anderseits, daß der linear ansteigende Teil der Kurve $\eta = f(\mathrm{pH})$ in Gegenwart von Na^+-Ionen bis zum pH = 12, in Gegenwart von K^+-Ionen dagegen nur bis zum pH = 10 reicht, kann geschlossen werden, daß die Gegenwart bzw. Adsorption dieser Metallkationen an der Pt-Anode den Elektrodenvorgang wesentlich beeinflußt. (Einige frühere, widersprechende Beobachtungen dürften mit dem Außerachtlassen dieses Umstandes zu erklären sein.)

Die Richtungsänderung der Funktion $\eta = f(\mathrm{pH})$ in alkalischer Lösung

ist die Folge der Änderung des Elektrodenvorgangs, da unter solchen Bedingungen der entwickelte Sauerstoff aus den in der Lösung bereits in ausreichender Konzentration gegenwärtigen OH^--Ionen stammt; die Konzentration dieser Ionen nimmt mit steigendem pH zu, während die Überspannung abnimmt. Die Änderung des Mechanismus erfolgt offensichtlich bei jenem pH-Wert, bei dem der Diffusionsstrom der OH^--Ionen und demgemäß ihre Oberflächenkonzentration hoch genug ist, um die Abscheidung des Sauerstoffs aus OH^--Ionen — mit Berücksichtigung der Aktivierungsenergie — günstiger zu gestalten, als aus den in relativ höherer Konzentration vorliegenden Wassermolekülen. Daß diese Grenze im schwach alkalischen Bereich liegt, steht in Einklang mit den Untersuchungen von SATO und OKAMOTO [8] über Nickelelektroden, in denen gefunden wurde, daß der Mechanismus der anodischen Sauerstoffentwicklung sich an dieser Anode bei ungefähr $pH = 11$ ändert.

Daß die OH^--Ionen die Rolle der Quelle für den elektrolytisch entwickelten Sauerstoff in K^+-haltigen Lösungen bereits bei $pH = 10$, in Na^+-haltigen dagegen erst bei $pH = 12$ übernehmen, kann mehrere Ursachen haben. Es muß in Betracht gezogen werden, daß — nach unseren früheren Untersuchungen [1] — die Überspannung der Sauerstoffentwicklung in reinen wäßrigen Schwefelsäurelösungen durch Zugabe von K^+-Ionen, unter vergleichbaren Bedingungen, in höherem Maße gesteigert wird, als durch Na^+-Ionen; mit anderen Worten, daß die Aktivierungsenergie des geschwindigkeitsbestimmenden Schrittes der Sauerstoffentwicklung aus Wassermolekülen in Gegenwart von Na^+-Ionen geringer ist als in Gegenwart von K^+-Ionen. Daraus kann geschlossen werden, daß der »saure Mechanismus« in Gegenwart von Na^+-Ionen deshalb um zwei pH-Einheiten tiefer in das alkalische Gebiet hineinreicht, weil — infolge der geringeren Aktivierungsenergie der Sauerstoffentwicklung aus Wassermolekülen in Gegenwart von Na^+-Ionen — der Diffusionsstrom der OH^--Ionen nur in Lösungen mit höherer OH^--Konzentration ausreichend ist, um eine so hohe OH^--Konzentration in der mit der Elektrode in Berührung stehenden Lösungsschicht aufrechtzuerhalten, welche die Sauerstoffentwicklung aus OH^--Ionen energetisch günstiger gestaltet.

Die Tatsache, daß der Wert von $\frac{d\eta}{d\,\mathrm{pH}}$ im sauren Bereich stark von der Art der in der Lösung vorhandenen Metallkationen abhängig, dagegen im alkalischen Bereich davon fast unabhängig ist, weist darauf hin, daß die Absorption der Na^+- bzw. K^+-Ionen an der Anode nur auf die Sauerstoffentwicklung aus Wasser einen merklichen Einfluß ausübt, auf den Mechanismus der aus Hydroxydionen ausgehenden Reaktion dagegen nicht merklich wirkt.

Wird die Aktivität des Wassers in der Lösung durch Auflösen von Kaprolactam verringert, so werden zwei wesentliche Änderungen im Bereich des

»sauren Mechanismus« beobachtet (Abb. 3 und 4). Einerseits nimmt der Wert von $\frac{d\eta}{d\,\mathrm{pH}}$ — sowohl in Gegenwart von Na^+- als auch in Gegenwart von K^+-Ionen — zu, und zwar in um so höherem Maße, je geringer die Aktivität des Wassers ist. Anderseits tritt bei pH = 7 ein Bruch in der Geraden $\eta = f(\mathrm{pH})$ auf. Dieser Bruch ist um so weniger scharf, je geringer die Aktivität des Wassers in der Lösung und je höher die Stromdichte ist. Zwischen der Wirkung der Na^+- und K^+-Ionen besteht in dieser Hinsicht kein wesentlicher Unterschied, der Bruch der Geraden tritt bei demselben pH auf. In Gegenwart von K^+-Ionen ist die Gerade $\eta = f(\mathrm{pH})$ bei geringen Stromdichten und im Bereich pH < 7 meistens etwas steiler als in Gegenwart von Na^+-Ionen unter sonst gleichen Bedingungen. Im Bereich pH > 7 dagegen ist dies nur bei $a_w = 0{,}738$ der Fall, während bei den sonstigen Wasseraktivitätswerten die Steilheit in Gegenwart von K^+-Ionen etwas geringer ist. Die *b*-Werte der Tafelschen Gleichung (Tab. I) sind nur wenig vom pH abhängig.

Der Knickpunkt der Funktion $\eta = f(\mathrm{pH})$ bei pH = 7 in Lösungen, deren Wasseraktivität durch Kaprolactam herabgesetzt wurde, zeigt eine Änderung des Mechanismus des Anodenvorgangs in diesem Punkt an; jedoch stammt der entwickelte Sauerstoff in beiden pH-Bereichen aus Wassermolekülen, da die Überspannung mit steigendem pH zunimmt. Der Wert von $\frac{d\eta}{d\,pH}$ ist im Bereich pH < 7 im allgemeinen um so höher und im Bereich pH > 7 um so niedriger, je geringer die Aktivität des Wassers ist. Die diesen beiden Bereichen entsprechenden Neigungswinkel nähern sich also mit abnehmender Aktivität des Wassers und zugleich meistens auch mit zunehmender Stromdichte.

Diese Beobachtungen zeigen, daß das Überwiegen der Hydroxydionen über die Wasserstoffionen eine ähnliche Wirkung ausübt, wie die Abnahme der Wasseraktivität. Auch eine Änderung der Adsorption der Kaprolactam-Moleküle kann eine Rolle spielen. Die Änderung des Mechanismus der Elektrodenreaktion kann offensichtlich auf eine Zustandsänderung jener Moleküle in der Doppelschicht an der Elektrodenoberfläche zurückgeführt werden, aus denen unter Aufwand der geringsten Aktivierungsenergie Sauerstoff entwickelt werden kann. Auf die Einzelheiten dieser Änderung können jedoch aus den zu Verfügung stehenden Versuchsergebnissen keine zuverlässigen Schlüsse gezogen werden.

LITERATUR

1. Erdey-Grúz, T., Gallyas, M., Szetey, É.: Acta Chim, Acad. Sci. Hung. **69**, 203 (1971)
2. Hickling, A., Hill, S.: Trans. Faraday Soc., **46**, 550 (1950)
3. Bockris, J. O'M., Huq, A. K. M. S.: Proc. Roy. Soc. **A 237**, 277 (1956)
4. Damjanovic, A., Dey, A., Bockris, J. O'M.: Electrochim. Acta, **11**, 791 (1966)

5. VETTER, K. J., BERNDT, D.: Z. Elektrochemie, **62,** 378 (1958)
6. ERDEY-GRÚZ, T., GOLOPENCZA-BAJOR, O.: Acta Chim. Acad. Sci. Hung., **34,** 281 (1962)
7. ERDEY-GRÚZ, T., GOLOPENCZA-BAJOR, O., GALLYAS, M.: Acta Chim. Acad. Sci. Hung., **50,** 179 (1966)
8. SATO, N., OKAMOTO, G.: Electrochim. Acta, **10,** 495 (1965)

Tibor ERDEY-GRÚZ
Miklós GALLYAS
Éva SZETEY
Budapest VIII., Puskin u. 11—13.

Acta Chimica Academiae Scientiarum Hungaricae, Tomus 69 (4) pp. 445—457 (1971)

ХИМИЯ 1,3-БИФУНКЦИОНАЛЬНЫХ СИСТЕМ, X*

КАТАЛИТИЧЕСКИЕ ПРЕВРАЩЕНИЯ 4-ЗАМЕЩЕННЫХ 1,3-ДИОКСАНОВ. ЦИКЛИЧЕСКИЕ АЦЕТАЛИ И КЕТАЛИ

Й. АПЬОК, М. БАРТОК и К. КОВАЧ

(Университет им. Йожефа Аттилы, Кафедра Органической Химии г. Сегед)

Поступило: 9. II. 1969

Изучались превращения 2,2,4-замещенных 1,3-диоксанов с различным строением на катализаторах $Pt/_T$ в токе водорода. При исследовании 13 соединений сравнивались отдельные скорости протекающих процессов, а также определялось влияние числа и природы заместителей на отдельные направления реакций. Экспериментально было доказано, что и в случае 2,4-дизамещенных 1,3-диоксанов протекает процесс, уже ранее обнаруженный авторами, а именно, процесс изомеризации в соответствующие сложные эфиры.

Введение

В предыдущих сообщениях авторов были опубликованы некоторые результаты о контактно-каталитических превращениях 1,3-диоксанов на металлических катализаторах [1—8].

Эти опыты проводились в импульсном режиме. В этих опытах было изучено влияние числа и характера алкильных заместителей 1,3-диоксанов на степень и направления превращений в зависимости от температуры. В качестве катализатора использовалась в большинстве случаев платина, нанесенная на термолит** ($Pt/_T$).

Опыты проводились в токе водорода. Водород играет решающую роль при превращении 1,3-диоксанов, в результате чего происходят следующие основные процессы: изомеризация в сложные эфиры, расщепление кольца, изомеризация в алкоксиальдегиды, гидрогенолиз в моноэфиры диолов и другие вторичные процессы.

Процентное соотношение образующихся продуктов зависит от расположения и характера заместителей и от температуры.

В настоящей статье рассматриваются превращения 2,4-ди-, 2,2,4-тризамещенных 1,3-диоксанов на катализаторе $Pt/_T$ (платина на термолите) в токе водорода. Изучение превращений настоящих 13 соединений позволяло сравнивать относительные скорости происходящих процессов и установить

* Сообщение IX: Acta Chim. Hung. **66**, 319 (1970)

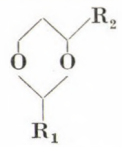
** Термолит — огнеупорный кирпич, содержащий в основном силикаты кальция и магния. Изготовление катализатора описано в сообщениях [7, 9].

закономерности изменения направлений реакций в зависимости от числа и характера заместителей. По опытам было доказано, что и в случае 2,4-диалкилзамещенных-1,3-диоксанов имеет место изомеризация в соответствующие сложные эфиры, открытая авторами раньше.

Обсуждение экспериментальных результатов

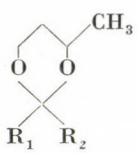
В настоящем сообщении рассматриваются превращения следующих 2,4-ди- и 2,2,4-тризамещённых 1,3-диоксанов*:

Ацетали:



$R_1 = R_2 = CH_3$ (I)
$R_1 = C_2H_5$, $R_2 = CH_3$ (II)
$R_1 = C_3H_7$, $R_2 = CH_3$ (III)
$R_1 =$ изо-C_3H_7, $R_2 = CH_3$ (IV)
$R_1 = C_6H_5$, $R_2 = CH_3$ (V)
$R_1 = CH_3$, $R_2 = C_6H_5$ (VI)
$R_1 =$ 2-фурил, $R_2 = CH_3$ (VII)
$R_1 =$ 2-тиенил, $R_2 = CH_3$ (VIII)

Кетали:

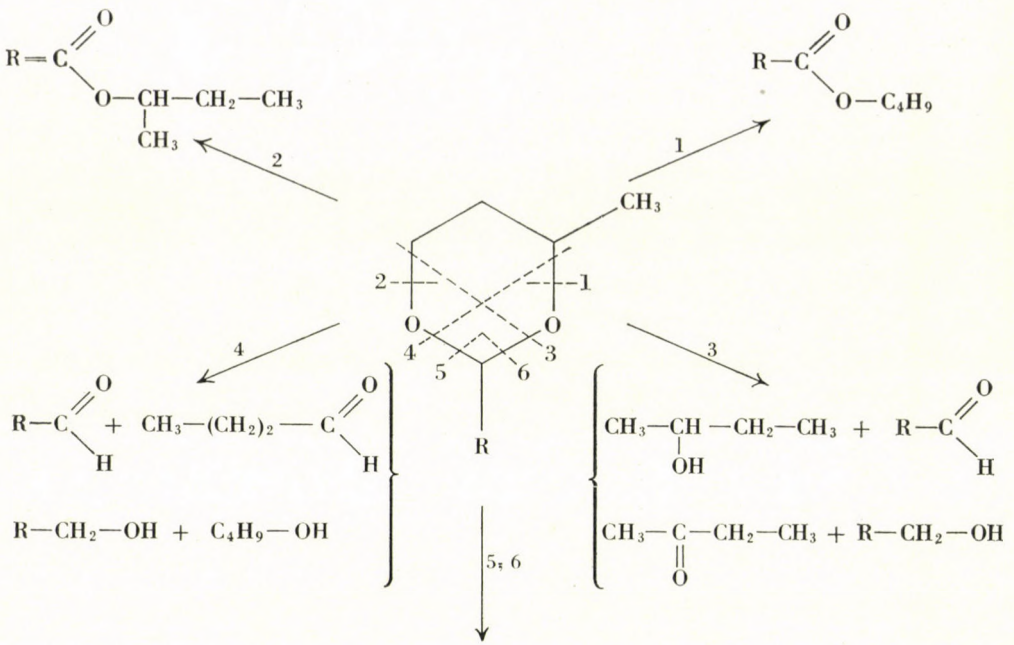


$R_1 = R_2 = CH_3$ (IX)
$R_1 = R_2 = C_2H_5$ (X)
$R_1 = CH_3$, $R_2 = C_3H_7$ (XI)
R_1, $R_2 = -(CH_2)_4-$ (XII)
R_1, $R_2 = -(CH_2)_5-$ (XIII)

1. *Превращения 2,4-дизамещенных циклических ацеталей*

Превращения циклических ацеталей (I—VIII) были исследованы на катализаторе $Pt/_T$ в токе водорода. В катализате кроме исходных метадиоксанов были найдены соответствующие сложные эфиры первичных и вторичных спиртов, гидрокси- и оксосоединения, производные эфиров и углеводороды. Анализ катализата и проведенные дальнейшие каталитические исследования продуктов превращения позволяют составлять общую схему превращений 2,4-диалкил-1,3-диоксанов:

*Синтез и физические константы 1,3-диоксанов описаны в статье [10].
Физические константы 2-метил-4-фенил-1,3-диоксана (VI) Т. к.: 133 °C (22 мм рт. ст.), n_D^{22} : 1, 5128.



Гидрогенолиз в моноэфир диола
Изомеризация в алкокси-оксосоединения

Как видно из схемы, главные направления превращения — изомеризация в сложные эфиры (напр. 1,2), расщепление (напр. 3,4), гидрогенолиз в моноэфиры диола и изомеризация в алкокси-оксосоединения (напр. 5,6).

Процентное соотношение разных направлений превращения (т. е. проценты продуктов) изменяются в зависимости от характера заместителей во втором положении кольца при прочих равных экспериментальных условиях, однако в случаях алкильных и арильных заместителей (I—VI) изомеризация в сложные эфиры (напр. 1,2) станет преобладающим процессом с повышением температуры.

а) *Алкилзамещенные 1,3-диоксаны*

2,4-Диметил-1,3-диоксан (I). Превращение диоксана (I) на $Pt/_T$ в присутствии водорода показывает, что каталитические процессы происходят в соответствии с предыдущей схемой. Следует отметить, что главный продукт изомеризации (напр. I) н-бутиловый эфир уксусной кислоты на примененных нами колонках не разделялся с исходным диоксаном. Вследствие этого не определялись количественные соотношения образующихся продуктов и изменения степени превращения в зависимости от температуры.

2-Этил-4-метил-1,3-диоксан (II). Превращение диоксана (II) было

Таблица I

Изменения степени превращения и процентного соотношения продуктов превращения 2-этил-4-метил-1,3-диоксана (II) на $Pt/_T$ в присутствии водорода

1. Температура °C	190	235	265	270	295	330
2. Степень превращения диоксана, %	29	52,3	74,1	80,4	84,7	97,1
3. Образовавшиеся жидкие продукты, %	28,5	46,8	59,4	61,2	51,4	48,1
4. Образовавшиеся газы %	0,5	5,5	14,7	19,2	33,3	49,7
5. втор. бутил-пропионат, %	6,7	12,5	14,3	14,3	10,0	3,7
6. перв. бутил-пропионат, %	13,6	27,3	34,5	36,3	24,5	23,1
7. Гидрогенолиз + изомеризация в алкоксиальдегид, %	2,0	3,0	5,5	5,0	4,5	2,0
8. Пропионовый альдегид, %	0,4	1,2	1,0	1,6	3,7	5,3
9. Масляный альдегид, %	1,4	0,4	0,7	0,7	1,6	2,5
10. Метилэтилкетон, %	1,8	0,8	1,0	0,8	1,8	3,5
11. Пропиловый спирт, %	1,0	0,6	0,6	0,7	2,3	4,9
12. Бутиловый спирт, %	1,6	1,0	1,8	1,8	3,0	3,1

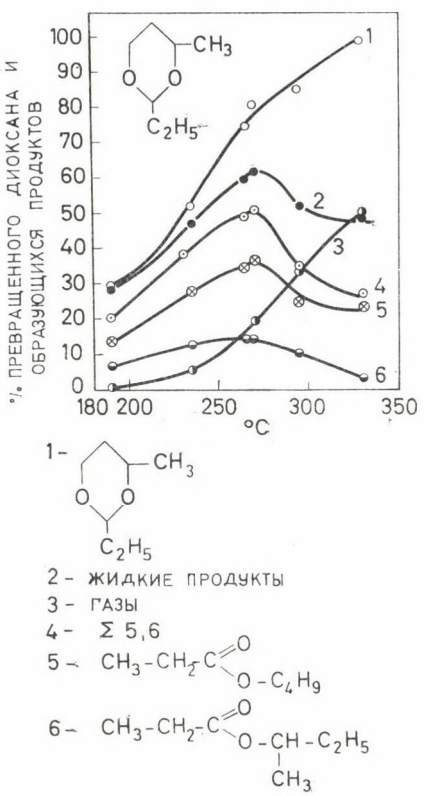


Рис. 1. Изменение степени превращения диоксана и процентного соотношения главных продуктов при превращении 2-этил-4-метил-1,3-диоксана (II)

изучено нами более подробно среди 2,4-диалкилзамещенных-1,3-диоксанов на катализаторе $Pt/_T$.

Состав катализата и изменение процентного соотношения продуктов в зависимости от температуры приведены в таблице I и на рис. 1.

Из таблицы I и рисунка 1 видно, что главными продуктами превращения являются сложные эфиры, причем их суммарное количество при температуре 270 °C достигает 50% от исходного диоксана (II). Как видно из рис. 1, количество жидких продуктов при комнатной температуре возрастает вплоть до 270 °C, потом падает, причем количество газов монотонно возрастает. Это явление свидетельствует о том, что скорость расщепления диоксанового кольца (направл. 3,4) резко возрастает наряду с повышением скорости вторичных процессов (декарбонилирование, дегидратация и т. п.), эти два процесса совместно ведут к образованию газообразных продуктов.

Типичная хроматограмма катализата превращения соединения II приведена на рис. 2.

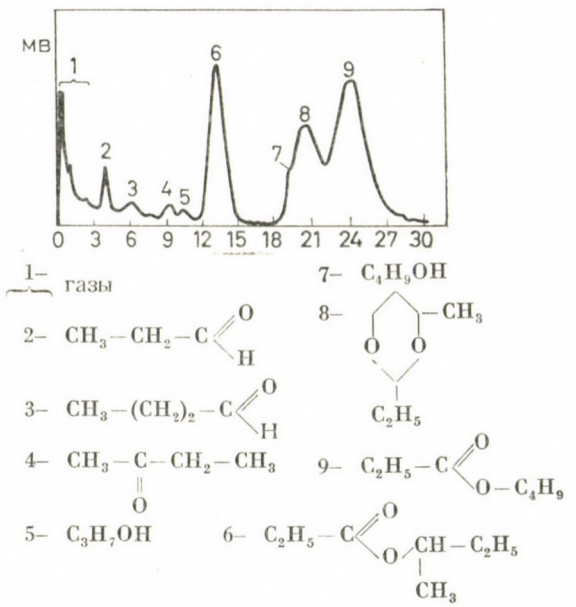


Рис. 2. Типичная хроматограмма превращения 2-этил-4-метил-1,3-диоксана (II)
Экспериментальные условия: а) 1 мл $Pt/_T$, H_2, 270°C, б) 1 м, 20% β,β'-оксидипропионитрил, 72°C, 60 мл/мин H_2, 160 мА

Нами были проведены опыты и для изучения влияния термолита, использованного в качестве носителя для платины.

При термическом превращении II в присутствии термолита не наблюдается образования сложных эфиров, а степень превращения II при температуре 300 °C составляет всего лишь 47%, и в то же время в присутствии $Pt/_T$ — 87%. Среди продуктов реакции кроме газообразных продуктов и

непревращенного диоксана наблюдается значительное количество оксосоединений (пропионовый и масляный альдегиды, метилэтилкетон).

Состав катализата термического разложения II на поверхности кварца оказался аналогичным, как в случае термолита. Следовательно, превращение II в сложные эфиры путем изомеризации является специальной функцией платинового катализатора на носителе, и присутствующего водорода.

Таблица 2

Изменения степени превращения 2-изопропил-4-метил-1,3-диоксана (IV) и процентного соотношения образовавшихся сложных эфиров на $Pt/_T$ в присутствии водорода

Температура °C	165	180	2	220
Степень превращения диоксана %	50	65,5	82,5	97,8
втор. бутил-изобутират %	6,8	13,5	26,5	32
перв. бутил-изобутират %	7,1	14,5	28,5	33

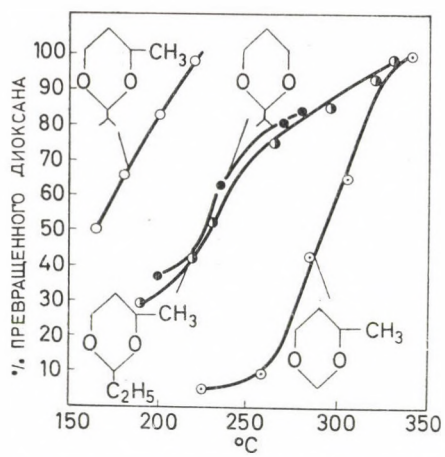


Рис. 3. Изменение степени превращения некоторых 1,3-диоксанов* на катализаторе $Pt/_T$ в зависимости от температуры

2-Пропил-4-метил-1,3-диоксан (III). Каталитическое превращение III было исследовано на катализаторе $Pt/_T$. Для разделения образующихся продуктов мы использовали двухметровые хроматографические колонки, наполненные неподвижными фазами: β,β'-оксидипропионитрилом, динонильфталатом, полипропиленгликольадипатом, но главный продукт изомеризации — н-бутылбутират не разделялся с исходным диоксаном, поэтому не было возможности провести количественное определение состава катализата и степени превращения в зависимости от температуры. Качест-

*Изменение степени превращения 2-изопропил и 4-метил-1,3-диоксанов дано по лит. [7, 11].

венная оценка продуктов превращения указывает на то, что главные направления реакции те же самые, как и в случае I, II.

2-Изопропил-4-метил-1,3-диоксан (IV). Скорость превращения IV в присутствии контакта $Pt/_T$ оказалась самой высокой среди изученных 2-моноалкил-1,3-диоксанов (таблица 2, рис. 3).

Это можно объяснить совместным электронодонорным (+ I) влиянием изопропильного и метильного заместителей, облегчающим размыкание диоксанового кольца. Соответственно этому, IV превосходит по своей реакцион-

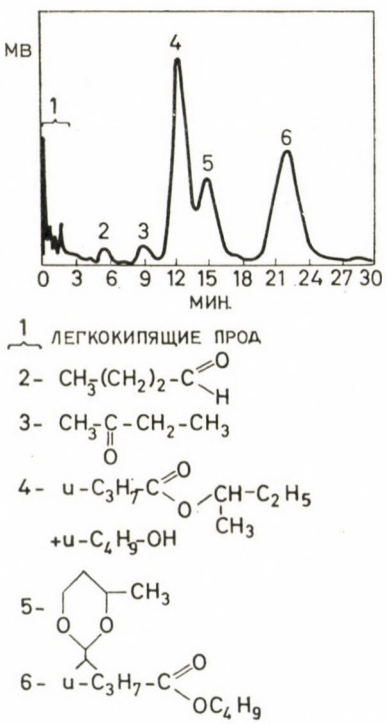


Рис. 4. Типичная хроматограмма превращения 2-изопропил-4-метил-1,3-диоксана (IV) Экспериментальные условия: а) 1 мл $Pt/_T$, H_2, 200°C, б) 1 м, 20% β,β'-оксидипропионитрил, 72°C, 60 мл/мин H_2, 160 мА

ной способности 2-изопропил-1,3-диоксан и другие 2,4-диалкилзамещенные-1,3-диоксаны (рис. 3). В то же время при превращении IV заметно возрастает склонность к гидрогенолизу диоксанового кольца (направл. 5,6), что наблюдается и в случае 2-изопропил-1,3-диоксана [11].

Образовавшийся при расщеплении диоксана изомасляный альдегид либо декарбонилируется, либо гидрируется в изобутиловый спирт. Поэтому в катализате присутствуют только следы этого альдегида, но другие оксосоединения, как масляный альдегид и метилэтилкетон присутствуют в за-

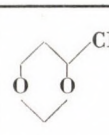
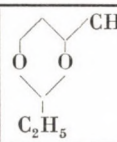
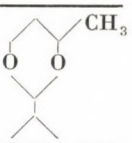
метных количествах. Наблюдаемые в катализате количества бутиловых спиртов невелики. Можно установить, что при более высокой температуре главным процессом превращения IV является изомеризация в сложные эфиры (направл. 1,2).

Типичная хроматограмма превращения IV приведена на рис. 4.

*Сравнение реакционной способности и соотношения образовавшихся продуктов 2,4-диалкилзамещенных 1,3-диоксанов и 4-метил-1,3-диоксана**. При контактно-каталитическом превращении диоксанов на $Pt/_T$ в присутствии водорода наблюдаемое соотношение образовавшихся сложных эфиров первичных и вторичных спиртов сильно изменяется в ряду 4-метил-, 2-этил-4-метил-(II), 2-изопропил-4-метил-1,3-диоксан (IV) при переходе от первого члена к двум последующим и сближается один к одному (см. таблицу 3)

Таблица 3

Сравнение степени превращения и процентного соотношения главных направлений реакции при превращении некоторых 4-метил-1,3-диоксанов

Диоксан			
Температура °C	305	270	200
Степень превращения в %-ах от исходного диоксана	65,5	80,3	82,5
Первичные сложные эфиры в %-ах от исходного диоксана	11	36	28,5
Вторичные сложные эфиры в %-ах от исходного диоксана	1	14	26,5
Суммарное количество сложных эфиров в %-ах от исходного диоксана	12	50	55
Гидрогенолиз в моноэфир диола в %-ах от исходного диоксана	следы	5	13

Как видно из таблицы 3, степень превращения диоксана и суммарное количество образовавшихся сложных эфиров в катализате с увеличением молекулярного веса и разветвленности алкильных заместителей во 2-ом положении возрастает и в том случае, если температура превращения, принятая в качестве примера понижается. Склонность метадиоксанов к гидрогенолизу также возрастает в данном порядке.

При обсуждении настоящих результатов надо иметь в виду, что наряду с влиянием заместителей во 2-ом положении [2,8], присутствие метильного заместителя в 4-ом положении, как правило, способствует общему увеличению скорости превращения диоксанов (рис. 3). Разницы выходов первич-

* Превращение 4-метил-1,3-диоксана обсуждается по лит. [7].

ных и вторичных сложных эфиров имеют частично вторичное происхождение, потому что сложные эфиры карбоновой кислоты, в частности муравьиной кислоты, претерпевают вторичное превращение при этой температуре. Однако, данные специальных опытов * [11] свидетельствуют о том, что заместитель в 4-ом положении играет при превращении 4-алкилзамещенных-1,3-диоксанов на $Pt/_T$ в присутствии водорода направляющую роль в определении места размыкания диоксанового кольца.

Так выход первичных сложных эфиров всегда превышает вторичных при изомеризации 4-метил-1,3-диоксанов, т. е. раскрытие диоксанового кольца по связи O(3) — C(4) более вероятно, чем по связи O(1) — C(6). Эти данные соответствуют результатам, полученным при каталитической изомеризации 4-метил-1,3-диоксанов в жидкой фазе [12].

б) *Арилзамещенные 1,3-диоксаны*

2-Фенил-4-метил-1,3-диоксан (V). При превращении диоксанов, содержащих ароматические заместители во втором положении, активность катализатора $Pt/_T$ падает быстрее, чем в случае алкильных заместителей. Поэтому импульсный метод в данном случае позволяет получить лишь качественные результаты. При превращении *V* на $Pt/_T$ в присутствии водорода наряду с образованием сложных эфиров диоксан *V* претерпевает также значительное расщепление. В присутствии активного катализатора степень превращения уже при невысокой температуре велика и среди продуктов изомеризации выход н-бутилбензоата превышает выход втор.-бутилбензоата. Так, например при температуре 245° C, степень превращения — 90% с образованием бутилбензоата 30% и втор.-бутилбензоата 10% (напр. 1 и 2).

2-метил-4-фенил-1,3-диоксан (VI). Диоксан VI подвергался превращению на $Pt/_T$ в присутствии водорода. Однако не удалось установить изменение степени превращения VI в зависимости от температуры, потому что диоксан и образующийся сложный эфир уксусной кислоты с 1-фенилпроранол-3-ом не разделялись на использованных хроматографических колонках.

Образование упомянутого сложного эфира было доказано специальными опытами. С одной стороны была установлена высокая устойчивость

* Наши экспериментальные результаты по определению степени превращения первичных и вторичных формиатов показали на разницу, что имеется между скоростями их превращения. Степень превращения вторичных формиатов при такой же температуре значительно превышает величину, наблюдавшуюся в случае первичных эфиров. В то же время, разница по выходам формиатов при превращении 4-метил-1,3-диоксана значительно отличается от того, что должно было ожидать в предполагаемом случае образования смеси, состоящейся по 50 процентов из первичных и вторичных формиатов и последующего их вторичного разложения. Следовательно, разница по выходам формиатов получается уже по первичному образованию сложных эфиров из диоксана, а далее лишь углубляется вследствие различия реакционной способности изомерных формиатов.

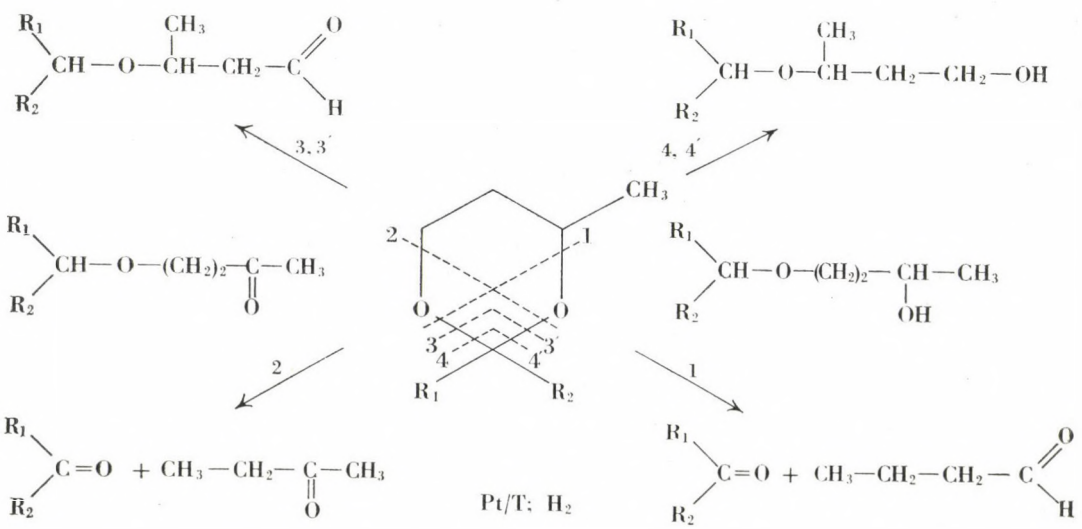
1-фенил-3-ацетоксипропана на $Pt/_T$ в широком интервале температуры. С другой стороны в пределах температуры 260—320° С суммарное количество диоксана VI и сложного эфира (высота хроматографического пика) существенно не изменялась. Эти факты свидетельствуют об образовании сложного эфира, причем выход сложного эфира, достигая определенного уровня температуры, существенно не меняется. В катализате имелись в небольшом количестве бензиловый спирт и бензальдегид.

в) *1,3-Диоксаны, содержащие гетероциклические заместители*

2-(2'-фурил)-4-метил-1,3-диоксан (VII); 2-(2'-тиенил)-4-метил-1,3-диоксан (VIII). При превращении диоксанов VII и VIII на $Pt/_T$ в присутствии водорода состав катализата довольно сложный. В обоих случаях наряду с превращениями диоксанового кольца происходит превращение и пятичленного кольца. В случае VIII активность катализатора быстро падает. Судя по хроматографическому анализу, продукты и направление процессов являются аналогичными: в обоих случаях преобладает сильное расщепление диоксанового кольца (направл. 3,4) и разнообразные превращения образовавшихся продуктов. Среди продуктов превращения VII найдены 2-бутил-фуроат в количестве 2—3%-а, что свидетельствует об изомеризации VII в сложный эфир (направл. 1).

2. *2,2,4-Алкилзамещенные 1,3-диоксаны (циклические кетали)*

2,2,4-триметил-1,3-диоксан (IX), 2,2-диэтил-4-метил-1,3-диоксан (X), 2-пропил-2,4-диметил-1,3-диоксан (XI). Превращение 2-гем.-диалкил-4-метил-1,3-диоксанов (IX, X, XI) не было изучено так подробно, как в случае ацеталей (I—VIII).



Эти представители диоксанов проявляют уже при низкой температуре большую реакционную способность. При этих температурах испарение впускаемых жидких проб происходит медленнее в микрореакторе — следовательно возрастает время контакта, и результаты негодны для количественного сравнения изменения степени превращения в зависимости от температуры.

Степень превращения в ряду диоксанов IX, X, XI достигает 90—95% при температуре 200—220° C. В случае циклических кеталей изомеризация в сложные эфиры не наблюдается, однако образуются ß-алкоксиоксосоединения путем изомеризации. Их количество понижается в упомянутом порядке, причем склонность диоксанового кольца к гидрогенолизу увеличивается в описанном же порядке.

Общие направления превращения для 2-гем.-замещенных 1,3-диоксанов на $Pt/_T$ в присутствии водорода приведены на следующей схеме на примере 2,2-диалкил-4-метил-1,3-диоксана.

Реакция гидрогенолиза (направл. 4, 4') становится преобладающим с повышением молекулярного веса заместителей во втором положении и с повышением температуры.

2-метил-1,5-диоксаспиробицикло-(5,4)-декан (XII), 2-метил-1,5-диоксаспиробицикло-(5,5)-ундекан (XIII). Превращения диоксанов XII и XIII исследовались на $Pt/_T$ в присутствии водорода. Несмотря на циклическое строение заместителей во втором положении диоксанового кольца, главные направления превращений такие же, как и на последней схеме. Реакция гидрогенолиза является преобладающим процессом по сравнению с расщеплением молекулы и изомеризацией в алкоксиальдегид и алкоксикетон. Из двух диоксанов — XII и XIII — последний оказался более реакционноспособным. При температуре 240° C и 260° C степень превращения диоксана XII составляет 45% и 53%, соответственно, а в случае XIII — 49% и 64%.

Согласно литературным данным, при жидкофазном гидролизе 2-тетраметилен- и 2-пентаметилен-производных 1,3-диоксанов, наоборот, повышенная реакционная способность приписывается присутствию пятичленного кольца [13]. Однако при контактно-каталитических реакциях существенно влияют на превращение стерические факторы, связанные с адсорбцией молекул. По-видимому, повышенная реакционная способность XIII связана с облегченной адсорбцией сочлененного циклогексаного кольца на поверхности платины. Среди 2-гем.-замещенных 1,3-диоксанов (IX—XIII) соединения, содержащие заместители с открытой цепью во втором положении (IX—XI), имеют повышенную способность к превращению, чем диоксаны с циклическими заместителями (XII, XIII).

На основании исследований по превращениям 4-замещенных 1,3-диоксанов на $P/_T$ в присутствии водорода можно сделать следующие выводы:

1. Алкильные заместители в 4-ом положении диоксанового кольца ускоряют превращения.

2. С ростом молекулярного веса заместителей скорость превращения возрастает.

3. Введение нового заместителя в кольцо диоксанов способствует ускорению превращения. Особенно сказывается это влияние при превращении гем.-замещенных производных диоксана.

4. Несимметричное строение 4-замещенных 1,3-диоксанов приводит к образованию продуктов 2-х рядов при размыкании кольца. В случае изомеризации в сложные эфиры, заместитель в 4-ом положении способствует разрыву по связи O(3) — C(4).

5. В случае 2,4-дизамещенных 1,3-диоксанов, главными направлениями превращений являются изомеризации с образованием сложных эфиров.

6. 2,2,4-Тризамещенные 1,3-диоксаны превращаются в моноэфир 1,3-диола путем гидрогенолиза и в β-алкоксиоксосоединения с изомеризацией кольца.

SUMMARY

The transformations of various 2,2,4-substituted 1,3-dioxanes over a Pt/T catalyst have been studied in a stream of hydrogen. By examination of the conversions of 13 compounds, it was possible to determine the relative rates of the occurring processes and to establish the dependence of directions of the reactions on the number and nature of substituents. It has been shown that a process recognized earlier by the authors, viz. isomerization into the corresponding esters, takes place also in the case of 2,4-disubstituted 1,3-dioxanes.

ЛИТЕРАТУРА

1. Апьок, И., Барток, М., Караханов, Р. А. и Шуйкин, Н. И.: Изв. АН СССР. Сер. Хим. **1968,** 2357
2. Апьок, Й., Барток, М., Караханов, Р. А. и Ковач, К.: Acta Phys. et Chem. Szeged, **14,** 99 (1968)
3. Апьок, Й., Барток, М., Караханов, Р. А. и Шуйкин, Н. И.: Усп. Химии **38,** 72 (1969)
4. Апьок, Й., Барток, М.: Acta. Phys. et Chem. Szeged, **16,** 39 (1970)
5. Караханов, Р. А., Блинов, Б. Б., Апьок, Й., Барток, М., Шуйкин, Н. И.: Всесоюзный Симпозиум, Рига, 1969
6. Апьок, Й., Барток, М., и Ковач, К.: Конференция Химиков, ОВХ, г. Сегед, 1969
7. Bartok, M., Apjok, J., Karakhanov, R. A., Kovács, K.: Acta Chim. Hung. **61,** 315 (1969)
8. Апьок, Й., Барток, М., Караханов, Р. А., Ковач, К.: Acta Phys. et Chem. Szeged, **15** 141, (1969)

9. Барток, М., Фени, С.: Acta Phys. et Chem. Szeged, **12,** 157 (1969)
10. Апьок, Й., Барток, М., Караханов, Р. А., Шуйкин, Н. И.: Изв. АН СССР., Сер. Хим. *1968*, 2352
11. Апьок, Й.: Кандидатская диссертация, Москва, 1969
12. Huyser, E. S., Garcia, Z.: J. Org. Chem., **27,** 2716 (1962)
13. Rondestvedt, Ch. S.: J. Org. Chem. **26,** 2247 (1961)

József Apjok
Mihály Bartók
Kálmán Kovács
Szeged, Dóm tér 8, Hungary.

Acta Chimica Academiae Scientiarum Hungariae, Tomus 69 (4), pp. 459—462 (1971)

CHEMISTRY OF 4*H*-1,3-BENZOTHIAZINE DERIVATIVES, II*

QUATERNIZATION OF 2-ARYL-4*H*-1,3-BENZOTHIAZINE DERIVATIVES**

J. SZABÓ, I. VARGA, E. VINKLER and É. BARTHOS

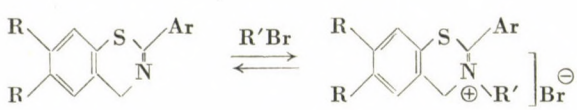
(Department for Pharmaceutical Chemistry, Medical University, Szeged)

Received April 10, 1970

On heating with alkyl- and arylalkyl halides, 2-aryl-4*H*-1,3-benzothiazines give the corresponding 3-alkyl- and 3-arylalkyl-4*H*-1,3-benzothiazinium halide derivatives, respectively.

It was reported by us [2, 3] that 2-aryl-4*H*-1,3-benzothiazine derivatives give salts with acids and the observation has been confirmed by other authors [4], too. In the course of studying the chemistry of the 4*H*-1,3-benzothiazine ring, the hydrolysis of 2-phenyl-6,7-dimethoxy-4*H*-1,3-benzothiazine was examined in this laboratory [2]. Since no data are available in the literature concerning the quaternization reaction of 4*H*-1,3-benzothiazine derivatives, the present publication deals with our results in this field.

Our first attempt to quaternize 2-phenyl-6,7-dimethoxy-4*H*-1,3-benzothiazine (**Ia**) consisted of the usual procedure, i.e. heating of compound **Ia** with ethyl bromide in ethanol solution. Contrary to expectation, the procedure failed to give the desired result. However, 2-phenyl-3-ethyl-6,7-dimethoxy-4*H*-1,3-benzothiazinium bromide (**IIa**) was obtained in excellent yield when

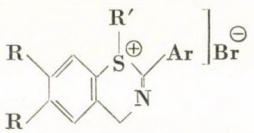


I **II**

a) $R=OCH_3$ $R'=C_2H_5$ $Ar=C_6H_5$
b) $R=OCH_3$ $R'=C_2H_5$ $Ar=3,4\text{-}(CH_3O)_2C_6H_3$
c) $R=OC_2H_5$ $R'=C_2H_5$ $Ar=3,4\text{-}(CH_3O)_2C_6H_3$
d) $R=H$ $R'=C_2H_5$ $Ar=C_6H_5$
e) $R=OCH_3$ $R'=CH_2C_6H_5$ $Ar=C_6H_5$

* Part I: SZABÓ, J., VINKLER, E., VARGA, I.: Acta Chim. Acad. Sci. Hung. **58,** 179 (1968).
** Presented in part at the Conference of the Hungarian Chemical Society, Pécs, 1967, and at the Session of the Committee of Organic Chemistry, Hungarian Academy of Sciences, February 22, 1966 [1].

compound **Ia** was heated with a large excess of ethyl bromide for long periods at 120 °C in a sealed tube. Under such conditions, the formation of the sulfonium salt (**III**), which might also be expected, was not observed.

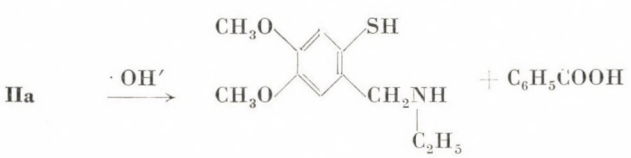


III

Quaternary salt **IIa** is an unstable compound, readily soluble in water. On standing for longer periods at room temperature, it is transformed to the original benzothiazine base (**Ia**) with the liberation of ethyl bromide. Compound **IIa** decomposes on heating in ethanol solution and this is the reason why the attempted quaternization of benzothiazine base **Ia** failed to give the expected results. The alcoholysis of quaternary salt **IIa** has not been examined as yet, but its hydrolysis was studied in detail. The results will be reported in a forthcoming paper of this series.

The IR spectrum of quaternary salt **IIa** revealed the following absorption bands: 1605, 1510, 775, 705, cm^{-1} (aromatic vibrations), 1580 cm^{-1} ($\nu C{=}N$), 2835, 1270, 1170 cm^{-1} (methoxy bands). The NMR spectrum had the following characteristics: δCH_3 (ethyl); 1.50 ppm, triplet (J = 7 Hz) (3 hydrogens); δOCH_3: 3.92 and 3.96 ppm, singlets (6 hydrogens); δCH_2 (ethyl): 4.35 ppm, quartet (J = 7 Hz) (2 hydrogens); δNCH_2 (ring): 5.66 ppm, singlet (2 hydrogens); δArH_8: 7.07 ppm, singlet (1 hydrogen); δArH_6 + $\delta ArHPh$: 450—490 Hz, multiplets (6 hydrogens).

The NMR spectrum of **IIa** is in accord with structure **III** as well. The IR spectrum could decide unambiguously for structure **IIa** only if compound **III**, too, were available and thus the two IR spectra could be compared. Therefore in order to prove the position of the ethyl group, compound **IIa** was subjected to alkaline hydrolysis. The reaction gave benzoic acid and *N*-ethyl-2-mercapto-4,5-dimethoxybenzylamine (**IV**), of which the latter was isolated as the hydrochloride salt. The *N*-ethyl-2-mercaptobenzylamine derivative



IV

(**IV**) gave a positive mercapto reaction. On treatment with lead acetate it gave the yellow lead mercaptide, while upon oxidation with air 2,2'-bis-

(methylaminoethyl)-4,4',5,5'-tetramethoxydiphenyldisulfide dihydrochloride was obtained. The formation of compound **IV** unequivocally proves the formation of compound **II** in the quaternization reaction. Alkaline hydrolysis of compound **III** would be expected to lead to the formation of other hydrolysis products.

The quaternization of some further 2-aryl-4*H*-1,3-benzothiazine derivatives was also examined. Thus, 2-(3',4'-dimethoxyphenyl)-6,7-dimethoxy-4*H*-1,3-benzothiazine (**Ib**) [3], 2-(3',4'-dimethoxyphenyl)-6,7-diethoxy-4*H*-1,3-benzothiazine (**Ic**) [3] and 2-phenyl-4*H*-1,3-benzothiazine (**Id**) [4] gave on heating with ethyl bromide as above 2-(3',4'-dimethoxyphenyl)-3-ethyl-6,7-dimethoxy-4*H*-1,3-benzothiazinium bromide (**IIb**), 2-(3',4'-dimethoxyphenyl)-3-ethyl-6,7-diethoxy-4*H*-1,3-benzothiazinium bromide (**IIc**) and 2-phenyl-3-ethyl-4*H*-1,3-benzothiazinium bromide (**IId**), respectively. Similarly, the reaction of benzothiazine base **Ia** with benzyl bromide gave 2-phenyl-3-benzyl-6,7-dimethoxy-4*H*-1,3-benzothiazinium bromide (**IIe**).

Experimental

(Melting points are uncorrected)

1) 2-Phenyl-3-ethyl-6,7-dimethoxy-4*H*-1,3-benzothiazinium bromide (IIa)

A mixture of 28.5 g (0.1 mole) of 2-phenyl-6,7-dimethoxy-4*H*-1,3-benzothiazine (**Ia**) and 86 ml ethyl bromide was heated for 12 hrs at 120 °C in a sealed tube. After cooling the excess ethyl bromide was removed by distillation, the crystalline residue was dissolved in 100 ml chloroform, the solution filtered and treated with 250 ml ether to precipitate compound **IIa.** The crystalline product was filtered, washed with ether and dried to give 37.4 g (94.7%) of the product; pale yellow prisms, m.p. 190.5—192 °C (decomposition).

$C_{18}H_{20}BrNO_2S$ (394.38). Calcd. C 54.83; H 5.11; N 3.55; Br 20.26. Found C 54.57; H 5.24; N 3.27; Br 19.85%.

2) Decomposition of 2-phenyl-3-ethyl-6,7-dimethoxy-4*H*-1,3-benzothiazinium bromide (IIa)

0.20 g (0.0005 mole) of 2-phenyl-6,7-dimethoxy-4*H*-1,3-benzothiazinium bromide decomposed in 6 months at room temperature to give 0.14 g of 2-phenyl-6,7-dimethoxy-4*H*-1,3-benzothiazine, m.p. 98—100 °C. The m.p. of a mixture with an authentic sample [3] was the same. The picrate crystallized from ethanol in the form of yellow needles melted at 178—179 °C (decomposition); no m.p. depression was observed with an authentic material [3].

3) Alkaline hydrolysis of 2-phenyl-3-ethyl-6,7-dimethoxy-4*H*-1,3-benzothiazinium bromide (IIa)

A mixture of 3.94 g (0.01 mole) of 2-phenyl-3-ethyl-6,7-dimethoxy-4*H*-1,3-benzothiazinium bromide (**IIa**) and a solution of 3 g of sodium hydroxide in 40 ml water was refluxed for 5 hrs, while a stream of nitrogen gas was passed through the apparatus. After cooling, the solution was acidified with concentrated hydrochloric acid. The benzoic acid which precipitated in crystalline form was filtered and the filtrate extracted with ether to remove traces of benzoic acid. The crystalline benzoic acid obtained on evaporation of the ethereal extract was combined with the precipitated benzoic acid fraction and crystallized from water to give 1.1 g of the product (90%); colourless plates, m.p. 121—122 °C, no m.p. depression with authentic benzoid acid.

The aqueous solution was evaporated to dryness in vacuum and the residue extracted with 100 ml hot ethanol. The ethanol solution was concentrated to 10 ml and treated with 25 ml ether to precipitate 2.3 g of *N*-ethyl-4,5-dimethoxy-2-mercaptobenzylammonium chloride (87%), colourless powdery crystals, m.p. 185—186 °C.

$C_{11}H_{18}ClNO_2S$ (263.78). Calcd. C 50.08; H 6.78; Cl 13.44. Found C 49.90; H 6.95; Cl 13.12%.

In order to prepare a characteristic derivative, 0.26 g (0.001 mole) of *N*-ethyl-2-mercapto-4,5-dimethoxybenzylamine hydrochloride was dissolved in 5 ml ethanol and the solution was exposed to air for a week. The 2,2'-bis(methylaminoethyl)-4,4',5,5'-tetramethoxydiphenyldisulfide dihydrochloride obtained by air oxidation was precipitated by the addition of 10 ml ether: 0.19 g of colourless powdery crystals, m.p. 217—218 °C.

$C_{22}H_{34}Cl_2N_2O_4S_2$ (525.56). Calcd. C 50.27; H 6.52; Cl 13.50. Found C 50.10; H 6.40; Cl 13.21%.

4) 2-(3',4'-Dimethoxyphenyl)-3-ethyl-6,7-dimethoxy-4*H*-1,3-benzothiazinium bromide (IIb)

1.52 g (0.005 mole) of 2-(3',4'-dimethoxyphenyl)-6,7-dimethoxy-4*H*-1,3-benzothiazine (**Ib**) and 5 ml ethyl bromide were reacted as described in experiment No. 1 to give 1.26 g of **IIb** (63%). Yellow prisms, m.p. 179—182 °C (decomposition).

$C_{20}H_{24}BrNO_4S$ (454.38). Calcd. N 3.08; Br 17.59. Found N 2.94; Br 17.10%.

5) 2-(3',4'-Dimethoxyphenyl)-3-ethyl-6,7-diethoxy-4*H*-1,3-benzothiazinium bromide (IIc)

3.73 g (0.01 mole) of 2-(3',4'-dimethoxyphenyl)-6,7-diethoxy-4*H*-1,3-benzothiazine (**Ic**) and 10 ml ethyl bromide were reacted similarly as in the first experiment to give 3.2 g (66.5%) of **IIc**; yellow prisms, m.p. 183—186 °C (decomposition).

$C_{22}H_{28}BrNO_4S$ (482.43). Calcd. C 54.77; H 5.85; N 2.90. Found C 54.10; H 6.05; N 3.02%

6) 2-Phenyl-3-ethyl-4*H*-1,3-benzothiazinium bromide (IId)

Reaction of 1.12 g (0.005 mole) of 2-phenyl-4*H*-1,3-benzothiazine and 5 ml ethyl bromide, under the conditions described in experiment No. 1 gave 0.8 g (47.9%) of the quaternary salt (**IId**); colourless prisms, m.p. 165—168 °C (decomposition).

$C_{16}H_{16}BrNS$ (334.28). Calcd. Br 23.91. Found Br 23.58%.

7) 2-Phenyl-3-benzyl-6,7-dimethoxy-4*H*-1,3-benzothiazinium bromide (IIe)

2.85 g (0.01 mole) of 2-phenyl-6,7-dimethoxy-4*H*-1,3-benzothiazine (**Ia**) and a solution of 1.2 ml benzyl bromide in 5 ml chloroform was heated for 2 hrs at 120 °C in a sealed tube. After cooling, the product was precipitated by addition of 15 ml ether: 2.6 g, yellow powdery crystals, m.p. 62—65 °C (decomposition).

$C_{23}H_{22}BrNO_2S$ (424.40). Calcd. Br 18.83. Found Br 18.54%.

*

The authors express their thanks to Dr. P. SOHÁR for recording the IR and NMR spectra and for his help in the interpretation.

REFERENCES

1. SZABÓ, J., VINKLER, E., VARGA, I., BARTHOS, É.: Kémiai Közl. **26,** 21 (1966)
2. SZABÓ, J., VINKLER, E., VARGA, I.: Acta Chim. Acad. Sci. Hung. **58,** 179 (1968)
3. VINKLER, E., SZABÓ, J.: Acta. Chim. Acad. Sci. Hung. **6,** 323 (1955)
4. BOURGOIN-LEGAY, D., BOUDET, R.: Compt. Rend. Ser. C, **263** (1), 77 (1966)

János SZABÓ
István VARGA
Elemér VINKLER
Éva BARTHOS
Szeged, Eötvös u. 2, Hungary

INDEX

PHYSICAL CHEMISTRY – PHYSIKALISCHE CHEMIE – ФИЗИЧЕСКАЯ ХИМИЯ

SERAFIMOV, L. A., ZHAROV, V. T. and TIMOFEYEV, V. S.: Rectification of Multicomponent Mixtures, I. Topological Analysis of Liquid–Vapour Phase Equilibrium Diagrams 383

NAGY, J., FERENCZI-GRESZ, S., FARKAS, R., BARTA, I. and BORBÉLY-KUSZMANN, A.: Study of the Molecular Structure of Alkyl- and Aryl-Alkoxysilanes, II. Dielectric Study of Mono-, Di- and Trialkoxysilanes 397

NAGY, J., HENCSEI, P., FERENCZI-GRESZ, S. and GÁBOR, T.: Investigation of the Dipole Moments and Infrared Spectra of Phenoxysilanes 411

ERDEY-GRÚZ, T., FODOR-CSÁNYI, P., LÉVAY, B. und SZILÁGYI-GYŐRI, E.: Selbstdiffusionskoeffizienten des Systems Methanol–Wasser–Kaliumchlorid. (Self-Diffusion Coefficients of the System Methanol–Water–Potassium Chloride) 423

ERDEY-GRÚZ, T., GALLYAS, M. und SZETEY, É.: Abhängigkeit der Sauerstoffüberspannung von der Aktivität des Wassers, III. Wirkung des pH in Sulfatlösungen. (Dependence of the Oxygen Overvoltage on the Activity of Water, III. The Effect of the pH Value in Sulfate Solutions) 433

ORGANIC CHEMISTRY – ORGANISCHE CHEMIE – ОРГАНИЧЕСКАЯ ХИМИЯ

Апьок, Й., Барток, М, и Ковач, К., Хнмия 1,3 бнфункцнональный систем, X, Каталитические превращенуя 4-замещенных 1,3-днкосанов. Циклаческие ацетали и катали (APJOK, J., BARTÓK, M. and KOVÁCS, K.: Chemistry of 1,3-Bifunctional Systems, X. Catalytic Transformations of 4-Substituted 1,3-Dioxanes. Cyclic Acetals and Ketals) 445

SZABÓ, J., VARGA, E., VINKLER, E. and BARTHOS, É.: Chemistry of 4*H*-1,3-Benzothiazine Derivatives, II. Quaternization of 2-Aryl-4*H*-1,3-Benzothiazine Derivatives ... 459

Printed in Hungary

A kiadásért felel az Akadémiai Kiadó igazgatója — Műszaki szerkesztő: Várhelyi Tamás

A kézirat nyomdába érkezett: 1971. IV. 21. — Terjedelem: 7,25 (A/5) ív, 63 ábra

71.71633 Akadémiai Nyomda, Budapest — Felelős vezető: Bernát György

The Acta Chimica publish papers on chemistry in English, German, French and Russian.

The Acta Chimica appear in volumes consisting of four parts of varying size, 4 volumes being published a year.

Manuscripts should be addressed to

Acta Chimica
Budapest 112/91 Műegyetem

Correspondence with the editors should be sent to the same address.

The rate of subscription is $16.00 a volume.

Orders may be placed with "*Kultúra*" Foreign Trade Company for Books and Newspapers (Budapest I., Fő utca 32. Account No. 43-790-057-181) or with representatives abroad.

Les Acta Chimica paraissent en français, allemand, anglais et russe et publient des mémoires du domaine des sciences chimiques.

Les Acta Chimica sont publiés sous forme de fascicules. Quatre fascicules seront réunis en un volume (4 volumes par an,.

On est prié d'envoyer les manuscrits destinés à la rédaction à l'adresse suivante:

Acta Chimica
Budapest 112/91 Műegyetem

Toute correspondance doit être envoyée à cette même adresse.

Le prix de l'abonnement est de $16.00 par volume.

On peut s'abonner à l'Entreprise pour le Commerce Extérieur de Livres et Journaux «*Kultúra*» (Budapest I., Fő utca 32. Compte-courant No. 43-790-057-181) ou à l'étranger chez tous les représentants ou dépositaires.

«*Acta Chimica*» издают трактаты из области химической науки на русском, французском, английском и немецком языках.

«*Acta Chimica*» выходят отдельными выпусками разного объема. 4 выпуска составляют один том. 4 тома публикуются в год.

Предназначенные для публикации рукописи следует направлять по адресу:

Acta Chimica
Budapest 112/91 Műegyetem

По этому же адресу направлять всякую корреспонденцию для редакции.

Подписная цена — $16.00 за том.

Заказы принимает предприятие по внешней торговле книг и газет «*Kultúra*» (Budapest I., Fő utca 32. Текущий счет № 43-790-057-181) или его заграничные представительства и уполномоченные.

Reviews of the Hungarian Academy of Sciences are obtainable at the following addresses:

ALBANIA
Drejtorija Qändrone e Pärhapjes dhe Propagandimit tä Librit
Kruga Konferenca e Päzes
Tirana

AUSTRALIA
A. Keesing
Box 4886, GPO
Sydney

AUSTRIA
GLOBUS
Höchstädtplatz 3
A-1200 Wien XX

BELGIUM
Office International de Librairie
30, Avenue Marnix
Bruxelles 5
Du Monde Entier
5, Place St. Jean
Bruxelles

BULGARIA
HEMUS
11 pl Slaveikov
Sofia

CANADA
Pannonia Books
2, Spadina Road
Toronto 4, Ont.

CHINA
Waiwen Shudian
Peking
P. O. B. 88

CZECHOSLOVAKIA
Artia
Ve Smečkách 30
Praha 2
Poštovní Novinová Služba
Dovoz tisku
Vinohradská 46
Praha 2
Mad'arská Kultura
Václavské nám. 2
Praha 1
SLOVART A. G.
Gorkého
Bratislava

DENMARK
Ejnar Munksgaard
Nörregade 6
Copenhagen

FINLAND
Akateeminen Kirjakauppa
Keskuskatu 2
Helsinki

FRANCE
Office Internationa de Documentation et Librairie
48, rue Gay Lussac
Paris 5

GERMAN DEMOCRATIC REPUBLIC
Deutscher Buch-Export und Import
Leninstraße 16
Leipzig 701
Zeitungsvertriebsamt
Fruchtstraße 3—4
1004 Berlin

GERMAN FEDERAL REPUBLIC
Kunst und Wissen
Erich Bieber
Postfach 46
7 Stuttgart S.

GREAT BRITAIN
Blackwell's Periodicals
Oxenford House
Magdalen Street
Oxford
Collet's Subscription Import Department
Dennington Estate
Wellingsborough. Northants.
Robert Maxwell and Co. Ltd.
4—5 Fitzroy Square
London W. 1

HOLLAND
Swetz and Zeitlinger
Keizersgracht 471—487
Amsterdam C.
Martinus Nijhof
Lange Voorhout 9
The Hague

INDIA
Hind Book House
66 Babar Road
New Delhi 1

ITALY
Santo Vanasia
Via M. Macchi 71
Milano
Libreria Commissionaria Sansoni
Via La Marmora 45
Firenze
Techna
Via Cesi 16.
40135 Bologna

JAPAN
Kinokuniya Book-Store Co. Ltd.
826 Tsunohazu 1-chome
Shinjuku-ku
Tokyo
Maruzen and Co. Ltd.
P. O. Box 605
Tokyo-Central

KOREA
Chulpanmul
Phenjan

NORWAY
Tanum-Cammermeyer
Karl Johansgt 41—43
Oslo 1

POLAND
RUCH
ul. Wronia 23
Warszawa

ROUMANIA
Cartimex
Str. Aristide Briand 14—18
Bucureşti

SOVIET UNION
Mezhdunarodnaya Kniga
Moscow G—200

SWEDEN
Almquist and Wiksell
Gamla Brogatan 26
S—101 20 Stockholm

USA
F. W. Faxon Co. Inc.
15 Southwest Park
Westwood Mass. 02090
Stechert Hafner Inc.
31. East 10th Street
New York, N. Y. 10003

VIETNAM
Xunhasaba
19, Tran Quoc Toan
Hanoi

YUGOSLAVIA
Forum
Vojvode Mišića broj 1
Novi Sad
Jugoslovenska Knjiga
Terazije 27
Beograd

29. X. 1971

Index: 26.007